Fluid mechanics, turbulent flow and turbulence modeling

Lars Davidson

Division of Fluid Dynamics
Department of Mechanics and Maritime Sciences
Chalmers University of Technology
SE-412 96 Göteborg, Sweden
http://www.tfd.chalmers.se/~lada
lada@chalmers.se

September 1, 2020

Abstract

This course material is used in two courses in the International Master's programme **Applied Mechanics** at Chalmers. The two courses are TME226 Mechanics of fluids (Chapters 1-10, part of Chapter 11), and MTF271 Turbulence Modeling (part of Chapter 9 and 10, Chapters 11-27). MSc students who follow these courses are supposed to have taken one basic course in fluid mechanics.

This eBook can be downloaded at
http://www.tfd.chalmers.se/~lada/postscript_files/solids-and-fluids_turbulent-flow_turbulence-modelling.pdf

The Fluid courses in the MSc programme are presented at
http://www.tfd.chalmers.se/~lada/msc/msc-programme.html

The MSc programme is presented at
http://www.chalmers.se/en/education/programmes/masters-info/Pages/Applied-Mechanics.aspx

Contents

TME226 Mechanics of fluids

L. Davidson

Division of Fluid Dynamics
Department of Mechanics and Maritime Sciences
Chalmers University of Technology, Göteborg, Sweden
http://www.tfd.chalmers.se/~lada, lada@chalmers.se

Please find the TME226 Lecture Notes

This eBook can be downloaded at
http://www.tfd.chalmers.se/˜lada/MoF/

Recorded lectures are found at http://www.tfd.chalmers.se/˜lada/MoF/recorded_lecture.html

Please find the TME226 Lecture Notes
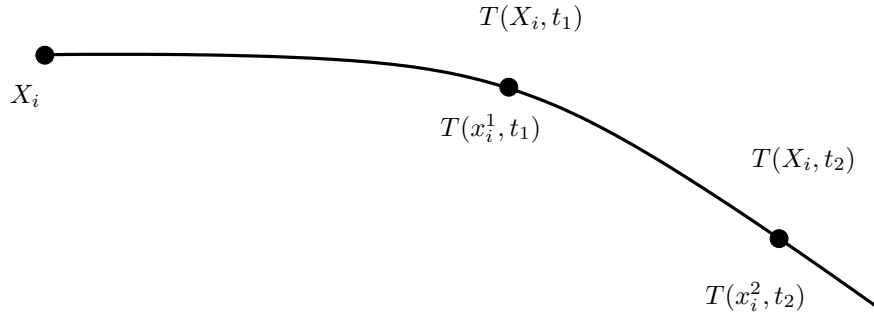
Figure 1.1: The temperature of a fluid particle described in Lagrangian, $T(X_i, t)$, or Eulerian, $T(x_i, t)$, approach.

1 Motion, flow

1.1 Eulerian, Lagrangian, material derivative

SEE also [1], Chapt. 3.2.

Assume a fluid particle is moving along the line in Fig. 1.1. We can choose to study its motion in two ways: Lagrangian or Eulerian. In the Lagrangian approach we keep track of its original position (X_i) and follow its path which is described by $x_i(X_i, t)$. For example, at time t_1 the temperature of the particle is $T(X_i, t_1)$, and at time t_2 its temperature is $T(X_i, t_2)$, see Fig. 1.1. This approach is not used for fluids because it is very tricky to define and follow a fluid particle. It is however used when simulating movement of particles in fluids (for example soot particles in gasoline-air mixtures in combustion applications). The speed of the particle is then expressed as a function of time and its position at time zero, i.e. $v_i = v_i(X_i, t)$.

In the Eulerian approach we pick a position, e.g. x_i^1, and watch the particle pass by. This approach is used for fluids. The temperature of the fluid, T, for example, is expressed as a function of the position, i.e. $T = T(x_i)$, see Fig. 1.1. It may be that the temperature at position x_i, for example, varies in time, t, and then $T = T(x_i, t)$.

Now we want to express how the temperature of a fluid particle varies. In the Lagrangian approach we first pick the particle (this gives its starting position, X_i). Once we have chosen a particle its starting position is fixed, and temperature varies only with time, i.e. $T(t)$ and the temperature gradient can be written dT/dt.

In the Eulerian approach it is a little bit more difficult. We are looking for the temperature gradient, dT/dt, but since we are looking at fixed points in space we need to express the temperature as a function of both time and space. From classical mechanics, we know that the velocity of a fluid particle is the time derivative of its space location, i.e. $v_i = dx_i/dt$. The chain-rule now gives

$$\frac{dT}{dt} = \frac{\partial T}{\partial t} + \frac{dx_j}{dt}\frac{\partial T}{\partial x_j} = \frac{\partial T}{\partial t} + v_j \frac{\partial T}{\partial x_j} \tag{1.1}$$

Note that we have to use partial derivative on T since it is a function of more than one (independent) variable. The first term on the right side is the **local rate of change**; by this we mean that it describes the variation of T *in time* at position x_i. The second term on the right side is called the **convective rate of change**, which means that it describes

local rate of change

Conv. rate of change

the variation of T *in space* when it passes the point x_i. The left side in Eq. 1.1 is called the **material derivative** and is in this text denoted by dT/dt.

Exercise 1 *Write out Eq. 1.1, term-by-term.*

1.2   What is the difference between $\dfrac{dv_2}{dt}$ and $\dfrac{\partial v_2}{\partial t}$?

Students sometimes get confused about the difference between $\dfrac{dv_2}{dt}$ and $\dfrac{\partial v_2}{\partial t}$. Here we give a simple example. Figure 1.2 shows a flow path of fluid particles which can be expressed in time as

$$x_1 = \exp(t), \quad x_2 = \exp(-t) \tag{1.2}$$

and hence $x_2 = 1/x_1$. The flow path is steady in time and it starts at $(x_1, x_2) = (0.5, 2)$ and ends at $(x_1, x_2) = (2, 0.5)$. The flow path is taken from stagnation flow, see Fig. 4.7. Equation 1.2 gives the velocities

$$v_1^L = \frac{dx_1}{dt} = \exp(t), \quad v_2^L = \frac{dx_2}{dt} = -\exp(-t) \tag{1.3}$$

and Eqs. 1.2 and 1.3 give

$$v_1^E = x_1, \quad v_2^E = -x_2 \tag{1.4}$$

(cf. Eq. 4.52). The superscripts E and L denote Eulerian and Lagrangian, respectively. Note that $v_1^L = v_1^E$ and $v_2^L = v_2^E$; the only difference is that v_i^E is expressed as function of (t, x_1, x_2) and v_i^L as function of t (and in general also starting location, X_1, X_2). Now we can compute the time derivatives of the v_2 velocity as

$$\begin{aligned}
\frac{dv_2^L}{dt} &= \exp(-t) \\
\frac{dv_2^E}{dt} &= \frac{\partial v_2^E}{\partial t} + v_1^E \frac{\partial v_2^E}{\partial x_1} + v_2^E \frac{\partial v_2^E}{\partial x_2} = 0 + x_1 \cdot 0 - x_2 \cdot (-1) = x_2
\end{aligned} \tag{1.5}$$

We find, of course, that $\dfrac{dv_2}{dt} = \dfrac{dv_2^E}{dt} = \dfrac{dv_2^L}{dt} = x_2 = \exp(-t)$.

Consider, for example, the point $(x_1, x_2) = (1, 1)$ in Fig. 1.2. The difference between $\dfrac{dv_2}{dt}$ and $\dfrac{\partial v_2}{\partial t}$ is now clearly seen by looking at Eq. 1.5. The velocity at the point $(x_1, x_2) = (1, 1)$ does not change in time and hence $\dfrac{\partial v_2^E}{\partial t} = 0$. However, if we sit on a particle which passes the location $(x_1, x_2) = (1, 1)$, the velocity, v_2^L, increases by time, $\dfrac{dv_2^L}{dt} = \dfrac{dv_2}{dt} = 1$ (the velocity, v_2, gets less negative) . Actually it increases all the time from the starting point where $\dfrac{dv_2}{dt} = 2$ and $v_2 = -2$ until the end point where $\dfrac{dv_2}{dt} = 0.5$ and $v_2 = -0.5$.

1.3   Viscous stress, pressure

See also [1], Chapts. 6.3 and 8.1.
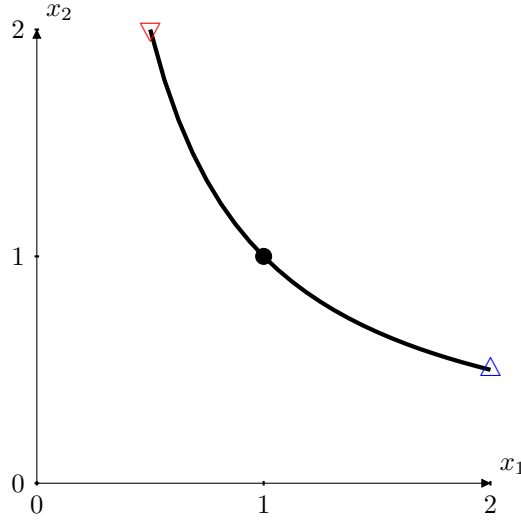
Figure 1.2: Flow path $x_2 = 1/x_1$. The filled circle shows the point $(x_1, x_2) = (1, 1)$. $\triangledown$: start $(t = \ln(0.5))$; $\triangle$: end $(t = \ln(2))$.

We have in Part I [2] derived the balance equation for linear momentum which reads

$$\boxed{\rho \dot{v}_i - \sigma_{ji,j} - \rho f_i = 0} \tag{1.6}$$

Switch notation for the material derivative and derivatives so that

$$\rho \frac{dv_i}{dt} = \frac{\partial \sigma_{ji}}{\partial x_j} + \rho f_i \tag{1.7}$$

where the first and the second term on the right side represents, respectively, the net force due to surface and volume forces (σ_{ij} denotes the stress tensor). Stress is force per unit area. The first term on the right side includes the viscous stress tensor, τ_{ij}. As you have learnt earlier, the first index relates to the surface at which the stress acts and the second index is related to the stress component. For example, on a surface whose normal is $n_i = (1, 0, 0)$ act the three stress components σ_{11}, σ_{12} and σ_{13}, see Fig. 1.3a; the volume force acts in the middle of the fluid element, see Fig. 1.3b.

In the present notation we denote the velocity vector by $\mathbf{v} = v_i = (v_1, v_2, v_3)$ and the coordinate by $\mathbf{x} = x_i = (x_1, x_2, x_3)$. In the literature, you may find other notations of the velocity vector such as $u_i = (u_1, u_2, u_3)$. If no tensor notation is used the velocity vector is usually denoted as (u, v, w) and the coordinates as (x, y, z).

The diagonal components of σ_{ij} represent the normal stresses and the off-diagonal components of σ_{ij} represent the shear stresses. In Part I [2] you learned that the pressure is defined as minus the sum of the normal stress, i.e.

$$P = -\sigma_{kk}/3 \tag{1.8}$$

The pressure, P, acts as a normal stress. In general, pressure is a thermodynamic property, p_t, which can be obtained – for example – from the ideal gas law. In that case the thermodynamics pressure, p_t, and the mechanical pressure, P, may not be the

(a) Stress components and stress vector on a surface. (b) Volume force, $f_i = (0, -g, 0)$, acting in the middle of the fluid element.
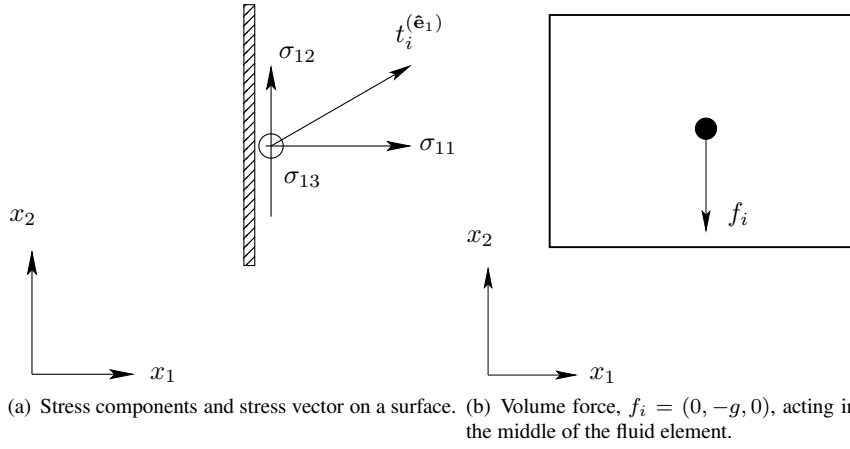
Figure 1.3: Stress tensor, volume (gravitation) force and stress vector, $t_i^{(\hat{e}_1)}$, see Eq. D.2.

same but Eq. 1.8 is nevertheless used. The *viscous* stress tensor, τ_{ij}, is obtained by subtracting the trace, $\sigma_{kk}/3 = -P$, from σ_{ij}; the stress tensor can then be written as

$$\sigma_{ij} = -P\delta_{ij} + \tau_{ij} \qquad (1.9)$$

τ_{ij} is the deviator of σ_{ij}. The expression for the viscous stress tensor is found in Eq. 2.4 at p. 26. The minus-sign in front of P appears because the pressure acts *into* the surface. When there is no movement, the viscous stresses are zero and then of course the normal stresses are the same as the pressure. In general, however, the normal stresses are the sum of the pressure and the viscous stresses, i.e.

$$\sigma_{11} = -P + \tau_{11}, \quad \sigma_{22} = -P + \tau_{22}, \quad \sigma_{33} = -P + \tau_{33}, \qquad (1.10)$$

Exercise 2 *Consider Fig. 1.3. Show how $\sigma_{21}, \sigma_{22}, \sigma_{23}$ act on a surface with normal vector $n_i = (0, 1, 0)$. Show also how $\sigma_{31}, \sigma_{32}, \sigma_{33}$ act on a surface with normal vector $n_i = (0, 0, 1)$.*

Exercise 3 *Write out Eq. 1.9 on matrix form.*

1.4 Strain rate tensor, vorticity

See also [1], Chapt. 3.5.3, 3.6.

We need an expression for the viscous stresses, τ_{ij}. They are needed in the momentum equations, Eq. 1.7 (see also Eq. 1.9). They will be expressed in the velocity gradients, $\frac{\partial v_i}{\partial x_j}$. Hence we will now discuss the velocity gradients.

The velocity gradient tensor can be split into two parts as

$$\frac{\partial v_i}{\partial x_j} = \frac{1}{2} \left(\underbrace{\frac{\partial v_i}{\partial x_j} + \frac{\partial v_i}{\partial x_j}}_{2\partial v_i/\partial x_j} + \underbrace{\frac{\partial v_j}{\partial x_i} - \frac{\partial v_j}{\partial x_i}}_{=0} \right)$$

$$= \frac{1}{2} \left(\frac{\partial v_i}{\partial x_j} + \frac{\partial v_j}{\partial x_i} \right) + \frac{1}{2} \left(\frac{\partial v_i}{\partial x_j} - \frac{\partial v_j}{\partial x_i} \right) = S_{ij} + \Omega_{ij} \qquad (1.11)$$

where

   S_{ij} is a *symmetric* tensor called the **strain-rate tensor**

   Ω_{ij} is a *anti-symmetric* tensor called the **vorticity tensor**

Strain-rate tensor vorticity tensor

The vorticity tensor is related to the familiar **vorticity vector** which is the curl of the velocity vector, i.e. $\boldsymbol{\omega} = \boldsymbol{\nabla} \times \mathbf{v}$, or in tensor notation

$$\omega_i = \epsilon_{ijk} \frac{\partial v_k}{\partial x_j} \tag{1.12}$$

where ϵ_{ijk} is the permutation tensor, see lecture notes of Ekh [2] and Table C.1 in Appendix C. If we set, for example, $i = 3$ we get

$$\omega_3 = \partial v_2 / \partial x_1 - \partial v_1 / \partial x_2. \tag{1.13}$$

The vorticity represents rotation of a fluid particle. Inserting Eq. 1.11 into Eq. 1.12 gives

$$\omega_i = \epsilon_{ijk}(S_{kj} + \Omega_{kj}) = \epsilon_{ijk}\Omega_{kj} \tag{1.14}$$

since $\epsilon_{ijk}S_{kj} = 0$ because the product of a symmetric tensor (S_{kj}) and an anti-symmetric tensor (ε_{ijk}) is zero. Let us show this for $i = 1$ by writing out the full equation. Recall that $S_{ij} = S_{ji}$ (i.e. $S_{12} = S_{21}$, $S_{13} = S_{31}$, $S_{23} = S_{32}$) and $\epsilon_{ijk} = -\epsilon_{ikj} = \epsilon_{jki}$ etc (i.e. $\varepsilon_{123} = -\varepsilon_{132} = \varepsilon_{231} \ldots, \varepsilon_{113} = \varepsilon_{221} = \ldots \varepsilon_{331} = 0$)

$$\begin{aligned}
\varepsilon_{1jk}S_{kj} &= \varepsilon_{111}S_{11} + \varepsilon_{112}S_{21} + \varepsilon_{113}S_{31} \\
&+ \varepsilon_{121}S_{12} + \varepsilon_{122}S_{22} + \varepsilon_{123}S_{32} \\
&+ \varepsilon_{131}S_{13} + \varepsilon_{132}S_{23} + \varepsilon_{133}S_{33} \\
&= 0 \cdot S_{11} + 0 \cdot S_{21} + 0 \cdot S_{31} \\
&+ 0 \cdot S_{12} + 0 \cdot S_{22} + 1 \cdot S_{32} \\
&+ 0 \cdot S_{13} - 1 \cdot S_{23} + 0 \cdot S_{33} \\
&= S_{32} - S_{23} = 0
\end{aligned} \tag{1.15}$$

Now let us invert Eq. 1.14. We start by multiplying it with $\varepsilon_{i\ell m}$ so that

$$\varepsilon_{i\ell m}\omega_i = \varepsilon_{i\ell m}\epsilon_{ijk}\Omega_{kj} \tag{1.16}$$

The ε-δ-identity gives (see Table C.1 at p. 327)

$$\varepsilon_{i\ell m}\epsilon_{ijk}\Omega_{kj} = (\delta_{\ell j}\delta_{mk} - \delta_{\ell k}\delta_{mj})\Omega_{kj} = \Omega_{m\ell} - \Omega_{\ell m} = 2\Omega_{m\ell} \tag{1.17}$$

This can easily be proved by writing out all the components, see Table C.1 at p. 327. Now Eqs. 1.16 and 1.17 give

$$\Omega_{m\ell} = \frac{1}{2}\varepsilon_{i\ell m}\omega_i = \frac{1}{2}\varepsilon_{\ell mi}\omega_i = -\frac{1}{2}\varepsilon_{m\ell i}\omega_i \tag{1.18}$$

or, switching indices

$$\Omega_{ij} = -\frac{1}{2}\varepsilon_{ijk}\omega_k \tag{1.19}$$

It turns out that is is much easier to go from Eq. 1.14 to Eq. 1.19 by writing out the components of Eq. 1.14 (here we do it for $i = 1$)

$$\omega_1 = \varepsilon_{123}\Omega_{32} + \varepsilon_{132}\Omega_{23} = \Omega_{32} - \Omega_{23} = -2\Omega_{23} \tag{1.20}$$

and we get

$$\Omega_{23} = -\frac{1}{2}\omega_1 \qquad (1.21)$$

which indeed is identical to Eq. 1.19.

Exercise 4 *Write out the second and third component of the vorticity vector given in Eq. 1.12 (i.e. ω_2 and ω_3).*

Exercise 5 *Complete the proof of Eq. 1.15 for $i = 2$ and $i = 3$.*

Exercise 6 *Write out Eq. 1.20 also for $i = 2$ and $i = 3$ and find an expression for Ω_{12} and Ω_{13} (cf. Eq. 1.21). Show that you get the same result as in Eq. 1.19.*

Exercise 7 *In Eq. 1.21 we proved the relation between Ω_{ij} and ω_i for the off-diagonal components. What about the diagonal components of Ω_{ij}? What do you get from Eq. 1.11?*

Exercise 8 *From your course in linear algebra, you should remember how to compute a vector product using Sarrus' rule. Use it to compute the vector product*

$$\boldsymbol{\omega} = \nabla \times \mathbf{v} = \left[\begin{array}{ccc} \hat{\mathbf{e}}_1 & \hat{\mathbf{e}}_2 & \hat{\mathbf{e}}_3 \\ \frac{\partial}{\partial x_1} & \frac{\partial}{\partial x_2} & \frac{\partial}{\partial x_3} \\ v_1 & v_2 & v_3 \end{array} \right]$$

Verify that this agrees with the expression in tensor notation in Eq. 1.12.

1.5 Product of a symmetric and antisymmetric tensor

In this section we show the proof that the product of a symmetric and antisymmetric tensor is zero. First, we have the definitions:

- A tensor a_{ij} is symmetric if $a_{ij} = a_{ji}$;

- A tensor b_{ij} is antisymmetric if $b_{ij} = -b_{ji}$.

It follows that for an antisymmetric tensor all diagonal components must be zero; for example, $b_{11} = -b_{11}$ can only be satisfied if $b_{11} = 0$.

The (inner) product of a symmetric and antisymmetric tensor is always zero. This can be shown as follows

$$a_{ij}b_{ij} = a_{ji}b_{ij} = -a_{ji}b_{ji},$$

where we first used the fact that $a_{ij} = a_{ji}$ (symmetric), and then that $b_{ij} = -b_{ji}$ (antisymmetric). Since the indices i and j are both dummy indices we can interchange them in the last expression ($-a_{ji}b_{ji} = -a_{ij}b_{ij}$), which gives

$$a_{ij}b_{ij} = -a_{ij}b_{ij}$$

This expression says that $A = -A$ which can be only true if $A = 0$ and hence $a_{ij}b_{ij} = 0$.

This can of course also be shown be writing out $a_{ij}b_{ij}$ on component form, i.e.

$$a_{ij}b_{ij} = \underbrace{a_{11}b_{11}}_{} + \underbrace{a_{12}b_{12}}_{I} + \underbrace{a_{13}b_{13}}_{II}$$
$$+ \underbrace{a_{21}b_{21}}_{I} + \underbrace{a_{22}b_{22}}_{} + \underbrace{a_{23}b_{23}}_{III}$$
$$+ \underbrace{a_{31}b_{31}}_{II} + \underbrace{a_{32}b_{32}}_{III} + \underbrace{a_{33}b_{33}}_{} = 0$$

$$\Delta x_1$$

$$\frac{\partial v_1}{\partial x_2}\Delta x_2 \Delta t = \Delta\alpha\Delta x_2$$

$$\Delta\alpha$$

$$\Delta x_2$$

$$\frac{\partial v_2}{\partial x_1}\Delta x_1 \Delta t = \Delta\alpha\Delta x_1$$

$$\Delta\alpha$$

$$x_2$$

$$x_1$$
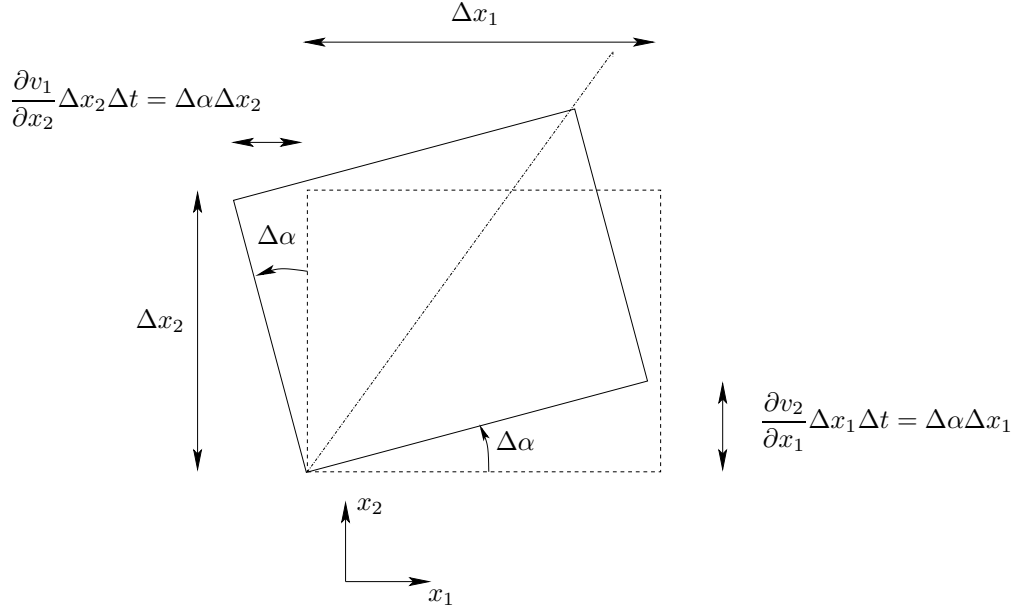
Figure 1.4: Rotation of a fluid particle during time Δt. Here $\partial v_1/\partial x_2 = -\partial v_2/\partial x_1$ so that $-\Omega_{12} = \omega_3/2 = \partial v_2/\partial x_1 > 0$. The distance of the upper-left corner is negative because the corner has moved with a negative v_1 velocity.

The underlined terms are zero ($b_{11} = b_{22} = b_{33} = 0$); terms I cancel each other ($a_{12} = a_{21}$, $b_{12} = -b_{21}$) as do terms II and III.

1.6 Deformation, rotation

See also [1], Chapt. 3.3.

The velocity gradient can, as shown above, be divided into two parts: S_{ij} and Ω_{ij}. We have shown that the latter is connected to *rotation* of a fluid particle. During rotation **rotation** the fluid particle is not deformed. This movement can be illustrated by Fig. 1.4. The vertical movement (v_2) of the lower-right corner ($x_1 + \Delta x_1$) of the particle in Fig. 1.4 is estimated as follows. The velocity at the lower-left corner is $v_2(x_1)$. Now we need the velocity at the lower-right corner which is located at $x_1 + \Delta x_1$. It is computed using the first term in the Taylor series as[1]

$$v_2(x_1 + \Delta x_1) = v_2(x_1) + \Delta x_1 \frac{\partial v_2}{\partial x_1}$$

It is assumed that the fluid particle in Fig. 1.4 is rotated the angle $\Delta\alpha$ during the time Δt. The angle rotation per unit time can be estimated as $\Delta\alpha/\Delta t \simeq d\alpha/dt = -\partial v_1/\partial x_2 = \partial v_2/\partial x_1$; if the fluid element does not rotate as a solid body, the rotation is computed as the average, i.e. $d\alpha/dt = (\partial v_2/\partial x_1 - \partial v_1/\partial x_2)/2$. The vorticity is computed as $\omega_3 = \partial v_2/\partial x_1 - \partial v_1/\partial x_2 = -2\Omega_{12} = 2d\alpha/dt$, see Eq. 1.13 and

---

[1]this corresponds to the equation for a straight line $y = kx + \ell$ where k is the slope which is equal to the derivative of y, i.e. dy/dx, and $\ell = v_2(x_1)$
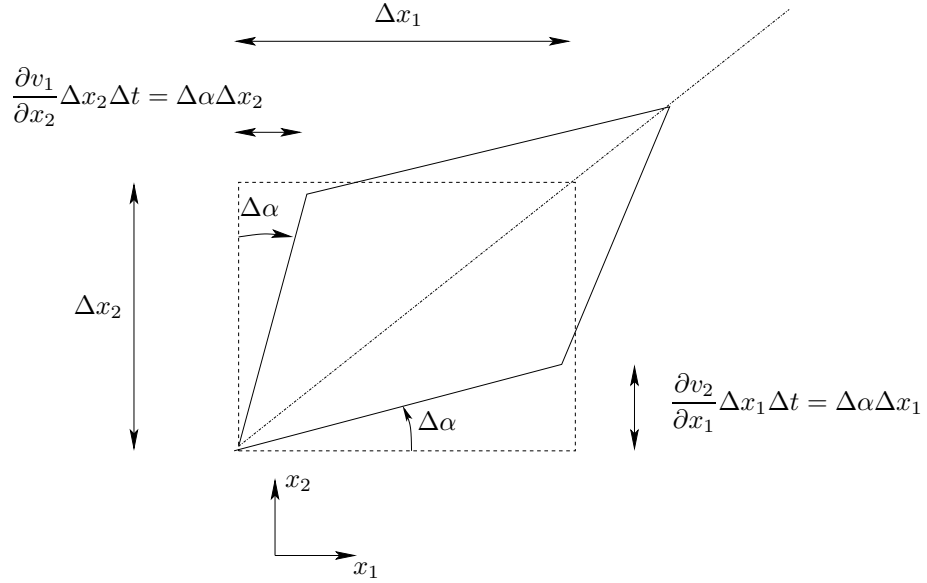
Figure 1.5: Deformation of a fluid particle by shear during time Δt. Here $\partial v_1/\partial x_2 = \partial v_2/\partial x_1$ so that $S_{12} = \partial v_1/\partial x_2 > 0$.

Exercise 4. Hence, the vorticity ω_3 can be interpreted as twice the average rotation per unit time of the horizontal edge $(\partial v_2/\partial x_1)$ and vertical edge $(-\partial v_1/\partial x_2)$.

Next let us have a look at the deformation caused by S_{ij}. It can be divided into two parts, namely shear and elongation (also called extension or dilatation). The deformation due to shear is caused by the off-diagonal terms of S_{ij}. In Fig. 1.5, a pure shear deformation by $S_{12} = (\partial v_1/\partial x_2 + \partial v_2/\partial x_1)/2$ is shown. The deformation due to elongation is caused by the diagonal terms of S_{ij}. Elongation caused by $S_{11} = \partial v_1/\partial x_1$ is illustrated in Fig. 1.6.

In general, a fluid particle experiences a combination of rotation, deformation and elongation as indeed is given by Eq. 1.11.

Exercise 9 *Consider Fig. 1.4. Show and formulate the rotation by ω_1.*

Exercise 10 *Consider Fig. 1.5. Show and formulate the deformation by S_{23}.*

Exercise 11 *Consider Fig. 1.6. Show and formulate the elongation by S_{22}.*

1.7 Irrotational and rotational flow

In the previous subsection we introduced different types of movement of a fluid particle. One type of movement was rotation, see Fig. 1.4. Flows are often classified based on rotation: they are *rotational* ($\omega_i \neq 0$) or *irrotational* ($\omega_i = 0$); the latter type is also called inviscid flow or potential flow. We will talk more about that later on, see Section 4.4. In this subsection we will give examples of one irrotational and one rotational flow. In potential flow, there exists a potential, Φ, from which the velocity components can be obtained as

$$v_k = \frac{\partial \Phi}{\partial x_k} \tag{1.22}$$
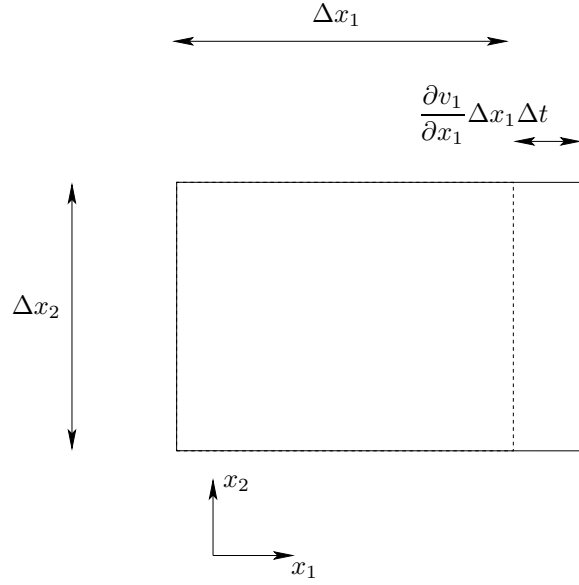
Figure 1.6: Deformation of a fluid particle by elongation during time Δt.
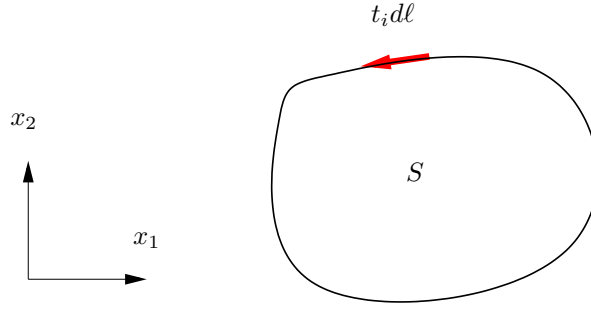
Figure 1.7: The surface, S, is enclosing by the line ℓ. The vector, t_i, denotes the unit tangential vector of the enclosing line, ℓ.

Before we talk about the ideal vortex line in the next section, we need to introduce the concept **circulation**. Consider a closed line on a surface in the $x_1 - x_2$ plane, see Fig. 1.7. When the velocity is integrated along this line and projected onto the line we obtain the circulation

$$\Gamma = \oint v_m t_m d\ell \tag{1.23}$$

Using Stokes's theorem we can relate the circulation to the vorticity as

$$\Gamma = \oint v_m t_m d\ell = \int_S \varepsilon_{ijk} \frac{\partial v_k}{\partial x_j} n_i dS = \int_S \omega_i n_i dS = \int_S \omega_3 dS \tag{1.24}$$

where $n_i = (0, 0, 1)$ is the unit normal vector of the surface S. Equation 1.24 reads in vector notation

$$\Gamma = \oint \mathbf{v} \cdot \mathbf{t} d\ell = \int_S (\nabla \times \mathbf{v}) \cdot \mathbf{n} dS = \int_S \boldsymbol{\omega} \cdot \mathbf{n} dS = \int_S \omega_3 dS \tag{1.25}$$

The circulation is useful in, for example, aeronautics and windpower engineering where the lift of a 2D section of an airfoil or a rotorblade is expressed in the circulation for that 2D section. The lift force is computed as (see Eqs. 4.85 and 4.86)

$$L = \rho V \Gamma \tag{1.26}$$

where V is the velocity around the airfoil (for a rotorblade it is the relative velocity, since the rotorblade is rotating). In an PhD project, an inviscid simulation method (based on the circulation and vorticity sources) is used to compute the aerodynamic loads for windturbine rotorblades [3].

Exercise 12 *In potential flow $\omega_i = \varepsilon_{ijk}\partial v_k/\partial x_j = 0$. Multiply Eq. 1.22 by ε_{ijk} and derivate with respect to x_k (i.e. take the curl of) and show that the right side becomes zero as it should, i.e. $\varepsilon_{ijk}\partial^2\Phi/(\partial x_k \partial x_j) = 0$.*

1.7.1 Ideal vortex line

The two-dimensional ideal vortex line is an irrotational (potential) flow where the fluid moves along circular paths, see Fig. 1.8. The governing equations are derived in Section 4.4.5. The velocity field in polar coordinates reads

$$v_\theta = \frac{\Gamma}{2\pi r}, \quad v_r = 0 \tag{1.27}$$

where Γ is the circulation. Its potential reads

$$\Phi = \frac{\Gamma \theta}{2\pi} \tag{1.28}$$

The velocity, v_θ, is then obtained as

$$v_\theta = \frac{1}{r}\frac{\partial \Phi}{\partial \theta} = \frac{\Gamma}{2\pi r} \tag{1.29}$$

To transform Eq. 1.27 into Cartesian velocity components, consider Fig. 1.9. The Cartesian velocity vectors are expressed as

$$
\begin{aligned}
v_1 &= -v_\theta \sin(\theta) = -v_\theta \frac{x_2}{r} = -v_\theta \frac{x_2}{(x_1^2 + x_2^2)^{1/2}} \\
v_2 &= v_\theta \cos(\theta) = v_\theta \frac{x_1}{r} = v_\theta \frac{x_1}{(x_1^2 + x_2^2)^{1/2}}
\end{aligned}
\tag{1.30}
$$

Inserting Eq. 1.30 into Eq. 1.27 we get

$$v_1 = -\frac{\Gamma x_2}{2\pi(x_1^2 + x_2^2)}, \quad v_2 = \frac{\Gamma x_1}{2\pi(x_1^2 + x_2^2)}. \tag{1.31}$$

To verify that this flow is a potential flow, we need to show that the vorticity, $\omega_i = \varepsilon_{ijk}\partial v_k/\partial x_j$ is zero. Since it is a two-dimensional flow ($v_3 = \partial/\partial x_3 = 0$), $\omega_1 = \omega_2 = 0$, we only need to compute $\omega_3 = \partial v_2/\partial x_1 - \partial v_1/\partial x_2$. The velocity derivatives are obtained as

$$\frac{\partial v_1}{\partial x_2} = -\frac{\Gamma}{2\pi}\frac{x_1^2 - x_2^2}{(x_1^2 + x_2^2)^2}, \quad \frac{\partial v_2}{\partial x_1} = \frac{\Gamma}{2\pi}\frac{x_2^2 - x_1^2}{(x_1^2 + x_2^2)^2} \tag{1.32}$$
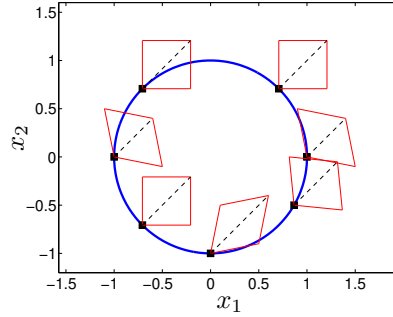
Figure 1.8: Ideal vortex. The fluid particle (i.e. its diagonal, see Fig. 1.4) does not rotate. The locations of the fluid particle is indicated by black, filled squares. The diagonales are shown as black dashed lines. The fluid particle is shown at $\theta = 0$, $\pi/4$, $3\pi/4$, π, $5\pi/4$, $3\pi/2$ and $-\pi/6$.
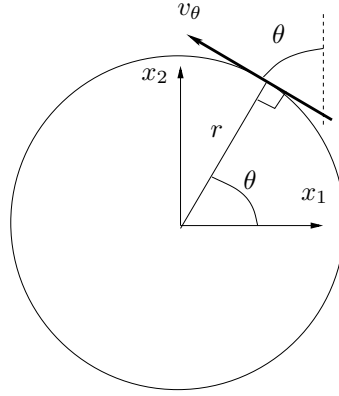
Figure 1.9: Transformation of v_θ into Cartesian components.

and we get

$$\omega_3 = \frac{\Gamma}{2\pi} \frac{1}{\left(x_1^2 + x_2^2\right)^2} (x_2^2 - x_1^2 + x_1^2 - x_2^2) = 0 \tag{1.33}$$

which shows that the flow is indeed a potential flow, i.e. *irrotational* ($\omega_i \equiv 0$). Note that the deformation is not zero, i.e.

$$S_{12} = \frac{1}{2}\left(\frac{\partial v_1}{\partial x_2} + \frac{\partial v_2}{\partial x_1}\right) = \frac{\Gamma}{2\pi} \frac{x_2^2}{\left(x_1^2 + x_2^2\right)^2} \tag{1.34}$$

Hence a fluid particle in an ideal vortex does deform but it does not rotate (i.e. its diagonal does not rotate, see Fig. 1.8).

It may be little confusing that the flow path forms a *vortex* but the flow itself has no *vorticity*. Thus one must be very careful when using the words "vortex" and "vorticity". By vortex we usually mean a recirculation region of the mean flow. That the flow has no vorticity (i.e. no rotation) means that a fluid particle moves as illustrated in Fig. 1.8. As a fluid particle moves from position a to b – on its counter-clockwise-rotating path – the particle itself is not rotating. This is true for the whole flow field, except at the center where the fluid particle does rotate. This is a singular point as is seen from Eq. 1.27 for which $v_\theta \rightarrow \infty$.

vortex vs. vorticity

Note that generally a vortex has vorticity, see Section 4.2. The ideal vortex is a very special flow case.
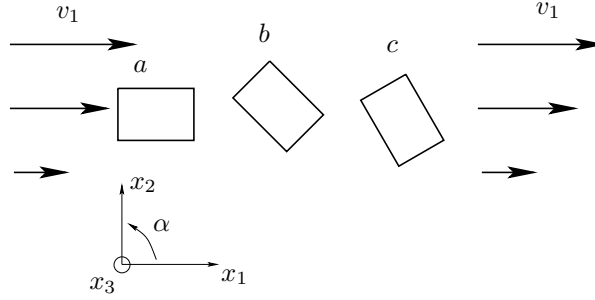
Figure 1.10: A shear flow. The fluid particle rotates. $v_1 = cx_2^2$.
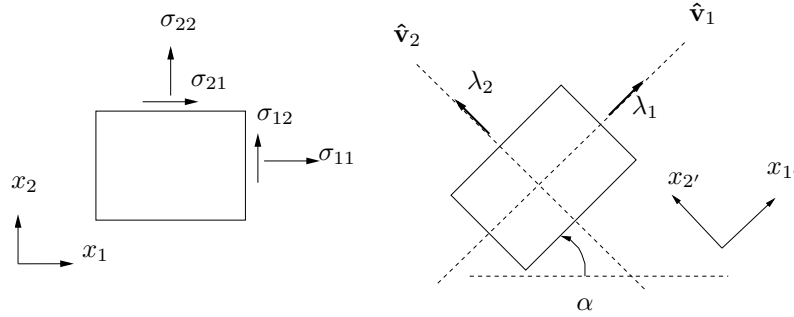
Figure 1.11: A two-dimensional fluid element. Left: in original state; right: rotated to principal coordinate directions. λ_1 and λ_2 denote eigenvalues; $\hat{\mathbf{v}}_1$ and $\hat{\mathbf{v}}_2$ denote unit eigenvectors.

1.7.2 Shear flow

Another example – which is rotational – is the lower half of fully-developed channel flow for which the velocity reads (see Eq. 3.28)

$$\frac{v_1}{v_{1,max}} = \frac{4x_2}{h}\left(1 - \frac{x_2}{h}\right), \quad v_2 = 0 \tag{1.35}$$

where $x_2 < h/2$, see Fig. 1.10. The vorticity vector for this flow reads

$$\omega_1 = \omega_2 = 0, \quad \omega_3 = \frac{\partial v_2}{\partial x_1} - \frac{\partial v_1}{\partial x_2} = -\frac{4}{h}\left(1 - \frac{2x_2}{h}\right) \tag{1.36}$$

When the fluid particle is moving from position a, via b to position c it is indeed rotating. It is rotating in clockwise direction. Note that the positive rotating direction is defined as the counter-clockwise direction, indicated by a in Fig. 1.10. This is why the vorticity, ω_3, in the lower half of the channel ($x_2 < h/2$) is negative. In the upper half of the channel the vorticity is positive because $\partial v_1/\partial x_2 < 0$.

1.8 Eigenvalues and eigenvectors: physical interpretation

See also [1], Chapt. 2.5.5.

Consider a two-dimensional fluid (or solid) element, see Fig. 1.11. In the left figure it is oriented along the $x_1 - x_2$ coordinate system. On the surfaces act normal stresses

(σ_{11}, σ_{22}) and shear stresses (σ_{12}, σ_{21}). The stresses form a tensor, σ_{ij}. Any tensor has eigenvectors and eigenvalues (also called principal vectors and principal values). Since σ_{ij} is symmetric, the eigenvalues are real (i.e. not imaginary). The eigenvalues are obtained from the characteristic equation, see [1], Chapt. 2.5.5 or Eq. 13.5 at p. 165. When the eigenvalues have been obtained, the eigenvectors can be computed. Given the eigenvectors, the fluid element is rotated α degrees so that its edges are aligned with the eigenvectors, $\hat{\mathbf{v}}_1 = \hat{x}_{1'}$ and $\hat{\mathbf{v}}_2 = \hat{x}_{2'}$, see right part of Fig. 1.11. Note that the sign of the eigenvectors is not defined, which means that the eigenvectors can equally well be chosen as $-\hat{\mathbf{v}}_1$ and/or $-\hat{\mathbf{v}}_2$. In the principal coordinates $x_{1'} - x_{2'}$ (right part of Fig. 1.11), there are no shear stresses on the surfaces of the fluid element. There are only normal stresses. This is the very definition of eigenvectors. Furthermore, the eigenvalues are the normal stresses in the principal coordinates, i.e. $\lambda_1 = \sigma_{1'1'}$ and $\lambda_2 = \sigma_{2'2'}$.

2 Governing flow equations

S EE also [1], Chapts. 5 and 8.1.

2.1 The Navier-Stokes equation

2.1.1 The continuity equation

The first equation is the continuity equation (the balance equation for mass) which reads [2]

$$\boxed{\dot{\rho} + \rho v_{i,i} = 0} \tag{2.1}$$

Change of notation gives

$$\frac{d\rho}{dt} + \rho \frac{\partial v_i}{\partial x_i} = 0 \tag{2.2}$$

For incompressible flow ($\rho = $ const) we get

$$\frac{\partial v_i}{\partial x_i} = 0 \tag{2.3}$$

2.1.2 The momentum equation

The next equation is the momentum equation. We have formulated the constitutive law for Newtonian viscous fluids [2]

$$\sigma_{ij} = -P\delta_{ij} + 2\mu S_{ij} - \frac{2}{3}\mu S_{kk}\delta_{ij}$$
$$\tau_{ij} = 2\mu S_{ij} - \frac{2}{3}\mu S_{kk}\delta_{ij} \tag{2.4}$$

Inserting Eq. 2.4 into the balance equations, Eq. 1.7, we get

$$\rho \frac{dv_i}{dt} = -\frac{\partial P}{\partial x_i} + \frac{\partial \tau_{ji}}{\partial x_j} + \rho f_i = -\frac{\partial P}{\partial x_i} + \frac{\partial}{\partial x_j}\left(2\mu S_{ij} - \frac{2}{3}\mu \frac{\partial v_k}{\partial x_k}\delta_{ij}\right) + \rho f_i \tag{2.5}$$

where μ denotes the dynamic viscosity. This is the *Navier-Stokes* equations (sometimes the continuity equation is also included in the name "Navier-Stokes"). It is also called the *transport equation for momentum*. Note that the stress tensor, σ_{ij}, depends only on the *symmetric* part (i.e. S_{ij}, see Eq. 1.11) of the velocity gradient. It is only the part of the velocity gradient that *deforms* the fluid (see Figs. 1.5 and 1.6) that appears in σ_{ij}. The part of the velocity gradient that rotates the fluid (i.e. Ω_{ij}, see Eq. 1.11 and Fig. 1.4) does not appear in σ_{ij}.

For incompressible flow, the last term in the diffusion term is zero because of the continuity equation (see Eq. 2.3) so that

$$\rho \frac{du_i}{dt} = -\frac{\partial P}{\partial x_i} + \frac{\partial}{\partial x_j}\left(\frac{\partial u_i}{\partial x_j} + \frac{\partial u_j}{\partial x_i}\right) + \rho f_i \tag{2.6}$$

Furthermore, if the viscosity, μ, is constant it can be moved outside the derivative. We can then re-write the first term in the parenthesis in Eq. 2.6 as

$$\frac{\partial}{\partial x_j}\left(\frac{\partial u_i}{\partial x_j} + \frac{\partial u_j}{\partial x_i}\right) = \mu\frac{\partial}{\partial x_j}\left(\frac{\partial u_i}{\partial x_j} + \frac{\partial u_j}{\partial x_i}\right) = \mu\frac{\partial^2 u_i}{\partial x_j \partial x_j} \tag{2.7}$$

because of the continuity equation, i.e.

$$\mu\frac{\partial}{\partial x_j}\left(\frac{\partial v_j}{\partial x_i}\right) = \mu\frac{\partial}{\partial x_i}\left(\frac{\partial v_j}{\partial x_j}\right) = 0. \tag{2.8}$$

Equation 2.5 can now – for constant μ and incompressible flow – be written

$$\rho\frac{dv_i}{dt} = -\frac{\partial P}{\partial x_i} + \mu\frac{\partial^2 v_i}{\partial x_j \partial x_j} + \rho f_i \tag{2.9}$$

The viscous stress tensor then reads

$$\tau_{ij} = 2\mu S_{ij} = \mu\left(\frac{\partial v_i}{\partial x_j} + \frac{\partial v_j}{\partial x_i}\right) \tag{2.10}$$

In inviscid (potential) flow, there are no viscous (friction) forces. In this case, the Navier-Stokes equation reduces to the *Euler equations*

Euler equations

$$\rho\frac{dv_i}{dt} = -\frac{\partial P}{\partial x_i} + \rho f_i \tag{2.11}$$

Exercise 13 *Equation 1.7 states that mass times acceleration is equal to the sum of forces forces (per unit volume). Write out the momentum equation (without using the summation rule) for the x_1 direction and show the surface forces and the volume force on a small, square fluid element (see lecture notes of Toll & Ekh [2]). Now repeat it for the x_2 direction.*

Exercise 14 *Formulate the Navier-Stokes equation for incompressible flow but non-constant viscosity.*

2.2 The energy equation

See also [1], Chapts. 6.4 and 8.1.

We have in Part I [2] derived the energy equation which reads

$$\boxed{\rho\dot{u} - v_{i,j}\sigma_{ji} + q_{i,i} = \rho z} \tag{2.12}$$

where u denotes internal energy (N.B.: in [2] it is denoted by e). q_i denotes the conductive heat flux and z the net radiative heat source. For simplicity, we neglect the radiation from here on. Change of notation gives

$$\rho\frac{du}{dt} = \sigma_{ji}\frac{\partial v_i}{\partial x_j} - \frac{\partial q_i}{\partial x_i} \tag{2.13}$$

In Part I [2] we formulated the constitutive law for the heat flux vector (Fourier's law)

$$q_i = -k\frac{\partial T}{\partial x_i} \tag{2.14}$$

Inserting the constitutive laws, Eqs. 2.4 and 2.14, into Eq. 2.13 gives

$$\rho\frac{du}{dt} = -P\frac{\partial v_i}{\partial x_i} + \underbrace{2\mu S_{ij}S_{ij} - \frac{2}{3}\mu S_{kk}S_{ii}}_{\Phi} + \frac{\partial}{\partial x_i}\left(k\frac{\partial T}{\partial x_i}\right) \tag{2.15}$$

where we have used $S_{ij}\partial v_i/\partial x_j = S_{ij}(S_{ij} + \Omega_{ij}) = S_{ij}S_{ij}$ because the product of a symmetric tensor, S_{ij}, and an anti-symmetric tensor, Ω_{ij}, is zero. The dissipation term, Φ, can be re-written as

$$\Phi = 2\mu \left(S_{ij}S_{ij} - \frac{1}{3}S_{kk}S_{ii} \right) = \left[2\mu \left(S_{ij} - \frac{1}{3}S_{kk}\delta_{ij} \right) \right]^2 > 0$$

which shows that Φ is positive. The dissipation represents irreversible viscous heating (i.e. transformation of kinetic energy into thermal energy); it is important at high-speed flow[2] (for example re-entry from outer space) and for highly viscous flows (lubricants). The first term on the right side represents reversible heating and cooling due to compression and expansion of the fluid. Equation 2.15 is the *transport equation for (internal) energy, u*.

Now we assume that the flow is incompressible (i.e. the velocity should be smaller than approximately $1/3$ of the speed of sound) for which

$$du = c_p dT \tag{2.16}$$

where c_p is the heat capacity (see Part I) [2] so that Eq. 2.15 gives (c_p is assumed to be constant)

$$\rho c_p \frac{dT}{dt} = \Phi + \frac{\partial}{\partial x_i} \left(k \frac{\partial T}{\partial x_i} \right) \tag{2.17}$$

The dissipation term is simplified to $\Phi = 2\mu S_{ij}S_{ij}$ because $S_{ii} = \partial v_i/\partial x_i = 0$. If we furthermore assume that the heat conductivity coefficient is constant and that the fluid is a gas or a common liquid (i.e. not an lubricant oil) so that the viscous dissipation is negligible (i.e. $\Phi = 0$), we get

$$\frac{dT}{dt} = \alpha \frac{\partial^2 T}{\partial x_i \partial x_i} \tag{2.18}$$

where $\alpha = k/(\rho c_p)$ is the *thermal diffusivity*. The Prandtl number is defined as

thermal diffusivity

$$Pr = \frac{\nu}{\alpha} \tag{2.19}$$

where $\nu = \mu/\rho$ is the kinematic viscosity. The physical meaning of the Prandtl number is the ratio of how well the fluid diffuses momentum to how well it diffuses internal energy (i.e. temperature).

The dissipation term, Φ, is neglected in Eq. 2.18 when one of two assumptions are valid:

1. The fluid is a gas with low velocity (lower than $1/3$ of the speed of sound); this assumption was made when we assumed that the fluid is incompressible

2. The fluid is a common liquid (i.e. not an lubricant oil). In lubricant oils the viscous heating (i.e. the dissipation, Φ) is large. One example is the oil flow in a gearbox in a car where the temperature usually is more than $100^o C$ higher when the car is running compared to when it is idle.

Exercise 15 *Write out and simplify the dissipation term, Φ, in Eq. 2.15. The first term is positive and the second term is negative; are you sure that $\Phi > 0$?*

---

[2]High-speed flows relevant for aeronautics will be treated in detail in the course "TME085 Compressible flow" in the MSc programme.

2.3 Transformation of energy

Now we will derive the equation for the kinetic energy, $k = v_i v_i/2$. Multiply Eq. 1.7 with v_i

$$\rho v_i \frac{dv_i}{dt} - v_i \frac{\partial \sigma_{ji}}{\partial x_j} - v_i \rho f_i = 0 \qquad (2.20)$$

Using the product rule backwards (Trick 2, see Eq. 8.4), the first term on the left side can be re-written

$$\rho v_i \frac{dv_i}{dt} = \frac{1}{2}\rho \frac{d(v_i v_i)}{dt} = \rho \frac{dk}{dt} \qquad (2.21)$$

$(v_i v_i/2 = k)$ so that

$$\rho \frac{dk}{dt} = v_i \frac{\partial \sigma_{ji}}{\partial x_j} + \rho v_i f_i \qquad (2.22)$$

Re-write the stress-velocity term so that (Trick 1, see Eq. 8.2)

$$\rho \frac{dk}{dt} = \frac{\partial v_i \sigma_{ji}}{\partial x_j} - \sigma_{ji} \frac{\partial v_i}{\partial x_j} + \rho v_i f_i \qquad (2.23)$$

This is the *transport equation for kinetic energy, k*. Adding Eq. 2.23 to Eq. 2.13 gives

$$\rho \frac{d(u+k)}{dt} = \frac{\partial \sigma_{ji} v_i}{\partial x_j} - \frac{\partial q_i}{\partial x_i} + \rho v_i f_i \qquad (2.24)$$

This is an equation for the sum of internal and kinetic energy, $u + k$. This is the *transport equation for total energy, $u + k$*.

Let us take a closer look at Eqs. 2.13, 2.23 and 2.24. First we separate the term $\sigma_{ji}\partial v_i/\partial x_j$ in Eqs. 2.13 and 2.23 into work related to the pressure and viscous stresses respectively (see Eq. 1.9), i.e.

$$\sigma_{ji} \frac{\partial v_i}{\partial x_j} = \underbrace{-P \frac{\partial v_i}{\partial x_i}}_{\textbf{a}} + \underbrace{\tau_{ji} \frac{\partial v_i}{\partial x_j}}_{\textbf{b}=\Phi} \qquad (2.25)$$

The following things should be noted.

- The physical meaning of the **a**-term in Eq. 2.25 – which includes the pressure, P – is heating/cooling by compression/expansion. This is a reversible process, i.e. no loss of energy but only transformation of energy.

- The physical meaning of the **b**-term in Eq. 2.25 – which includes the viscous stress tensor, τ_{ij} – is a dissipation, which means that kinetic energy is transformed to thermal energy. It is denoted Φ, see Eq. 2.15, and is called viscous dissipation. It is always positive and represents irreversible heating.

- The dissipation, Φ, appears as a sink term in the equation for the kinetic energy, k (Eq. 2.23) and it appears as a source term in the equation for the internal energy, u (Eq. 2.13). The transformation of kinetic energy into internal energy takes place through this source term. In incompressible flow for which the viscous term in Navier-Stokes can be simplified (see Eq. 2.9), the viscous term reads

$$\tau_{ji} \frac{\partial v_i}{\partial x_j} = \mu \frac{\partial v_i}{\partial x_j} \frac{\partial v_i}{\partial x_j} \qquad (2.26)$$

This quantity is very important in turbulent flow, cf. Eqs. 8.14 and 8.36.

- Φ does not appear in the equation for the total energy $u+k$ (Eq. 2.24); this makes sense since Φ represents a energy transfer between u and k and does not affect their sum, $u + k$.

Dissipation is very important in turbulence where transfer of energy takes place at several levels. First energy is transferred from the mean flow to the turbulent fluctuations. The physical process is called production of turbulent kinetic energy. Then we have transformation of kinetic energy from turbulence kinetic energy to thermal energy; this is turbulence dissipation (or heating). At the same time we have the usual viscous dissipation from the mean flow to thermal energy, but this is much smaller than that from the turbulence kinetic energy. For more detail, see Section 5.

2.4 Left side of the transport equations

So far, the left sides in transport equations have been formulated using the material derivative, d/dt. Let ψ denote a transported quantity (i.e. $\psi = v_i, u, T \ldots$); the left side of the equation for momentum, thermal energy, total energy, temperature etc reads

$$\rho\frac{d\psi}{dt} = \rho\frac{\partial\psi}{\partial t} + \rho v_j\frac{\partial\psi}{\partial x_j} \quad \textbf{non-conservative} \tag{2.27}$$

This is often called the *non-conservative* Using the continuity equation, Eq. 2.2, it can be re-written as

$$
\begin{aligned}
\rho\frac{d\psi}{dt} &= \rho\frac{\partial\psi}{\partial t} + \rho v_j\frac{\partial\psi}{\partial x_j} + \psi\underbrace{\left(\frac{d\rho}{dt} + \rho\frac{\partial v_j}{\partial x_j}\right)}_{=0} = \\
&\underline{\rho\frac{\partial\psi}{\partial t}} + \rho v_j\frac{\partial\psi}{\partial x_j} + \psi\left(\underline{\frac{\partial\rho}{\partial t}} + v_j\frac{\partial\rho}{\partial x_j} + \rho\frac{\partial v_j}{\partial x_j}\right)
\end{aligned}
\tag{2.28}
$$

The two underlined terms will form a time derivative term, and the other three terms can be collected into a convective term, i.e.

$$\rho\frac{d\psi}{dt} = \frac{\partial\rho\psi}{\partial t} + \frac{\partial\rho v_j\psi}{\partial x_j} \quad \textbf{conservative} \tag{2.29}$$

Thus, the left side of the temperature equation and the Navier-Stokes, for example, can be written in three different ways (by use of the chain-rule and the continuity equation)

$$
\begin{aligned}
\rho\frac{dv_i}{dt} &= \rho\frac{\partial v_i}{\partial t} + \rho v_j\frac{\partial v_i}{\partial x_j} = \frac{\partial\rho v_i}{\partial t} + \frac{\partial\rho v_j v_i}{\partial x_j} \\
\rho\frac{dT}{dt} &= \rho\frac{\partial T}{\partial t} + \rho v_j\frac{\partial T}{\partial x_j} = \frac{\partial\rho v_i}{\partial t} + \frac{\partial\rho v_j T}{\partial x_j}
\end{aligned}
\tag{2.30}
$$

The continuity equation can also be written in three ways (by use of the chain-rule)

$$\frac{d\rho}{dt} + \rho\frac{\partial v_i}{\partial x_i} = \frac{\partial\rho}{\partial t} + v_i\frac{\partial\rho}{\partial x_i} + \rho\frac{\partial v_i}{\partial x_i} = \frac{\partial\rho}{\partial t} + \frac{\partial\rho v_i}{\partial x_i} \tag{2.31}$$

The forms on the right sides of Eqs. 2.30 and 2.31 are called the *conservative* form. When solving transport equations (such as the Navier-Stokes) numerically using finite volume methods, the left sides in the transport equation are always written as the expressions on the right side of Eqs. 2.30 and 2.31; in this way Gauss law can be used

to transform the equations from a volume integral to a surface integral and thus ensuring that the transported quantities are *conserved*. The results may be inaccurate due to too coarse a numerical grid, but no mass, momentum, energy etc is lost (provided a transport equation for the quantity is solved): "what comes in goes out".

2.5 Material particle vs. control volume (Reynolds Transport Theorem)

See also lecture notes of Toll & Ekh [2] and [1], Chapt. 5.2.

In Part I [2] we initially derived all balance equations (mass, momentum and energy) for a collection of *material particles*. The conservation of mass, $d/dt \int \rho dV = 0$, Newton's second law, $d/dt \int \rho v_i = F_i$ etc were derived for a collection of particles in the volume V_{part}, where V_{part} is a volume that includes the same fluid particles all the time. This means that the volume, V_{part}, must be moving and it may expand or contract (if the density is non-constant), otherwise particles would move across its boundaries. The equations we have looked at so far (the continuity equation 2.3, the Navier-Stokes equation 2.9, the energy equations 2.15 and 2.23) are all given for a fixed control volume. How come? The answer is the Reynolds transport theorem, which converts the equations from being valid for a moving, deformable volume with a collection of particles, V_{part}, to being valid for a fixed volume, V. The Reynolds transport theorem reads (first line)

$$
\frac{d}{dt} \int_{V_{part}} \Phi dV = \int_V \left(\frac{d\Phi}{dt} + \Phi \frac{\partial v_i}{\partial x_i} \right) dV
$$

$$
= \int_V \left(\frac{\partial \Phi}{\partial t} + v_i \frac{\partial \Phi}{\partial x_i} + \Phi \frac{\partial v_i}{\partial x_i} \right) dV = \int_V \left(\frac{\partial \Phi}{\partial t} + \frac{\partial v_i \Phi}{\partial x_i} \right) dV \qquad (2.32)
$$

$$
= \int_V \frac{\partial \Phi}{\partial t} dV + \int_S v_i n_i \Phi dS
$$

where V denotes a fixed non-deformable volume in space. The divergence of the velocity vector, $\partial v_i / \partial x_i$, on the first line represents the increase or decrease of V_{part} during dt. The divergence theorem was used to obtain the last line and S denotes the bounding surface of volume V. The last term on the last line represents the net flow of Φ across the fixed non-deformable volume, V. Φ in the equation above can be ρ (mass), ρv_i (momentum) or ρu (energy). This equation applies to *any* volume at *every* instant and the restriction to a collection of a material particles is no longer necessary. Hence, in fluid mechanics the transport equations (Eqs. 2.2, 2.5, 2.13, ...) are valid both for a material collection of particles as well as for a *volume*; the latter is usually fixed (this is not necessary).
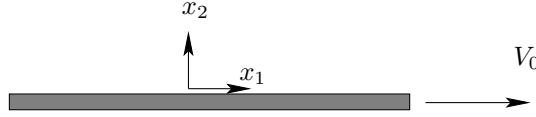
Figure 3.1: The plate moves to the right with speed V_0 for $t > 0$.
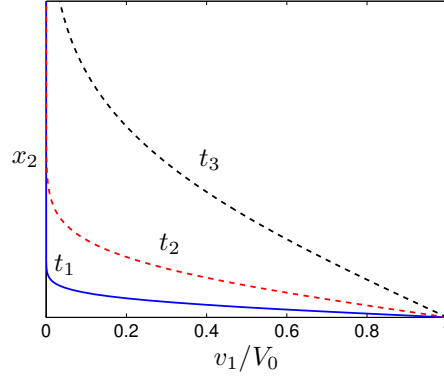
Figure 3.2: The v_1 velocity at three different times. $t_3 > t_2 > t_1$.

3 Solutions to the Navier-Stokes equation: three examples

3.1 The Rayleigh problem

IMAGINE the sudden incompressible motion of an infinitely long flat plate. For time greater than zero the plate is moving with the speed V_0, see Fig. 3.1. Because the plate is infinitely long, there is no x_1 dependency. Hence the flow depends only on x_2 and t, i.e. $v_1 = v_1(x_2, t)$ and $p = p(x_2, t)$. Furthermore, $\partial v_1/\partial x_1 = \partial v_3/\partial x_3 = 0$ so that the continuity equation gives $\partial v_2/\partial x_2 = 0$. At the lower boundary ($x_2 = 0$) and at the upper boundary ($x_2 \to \infty$) the velocity component $v_2 = 0$, which means that $v_2 = 0$ in the entire domain. So, Eq. 2.9 gives (no body forces, i.e. $f_1 = 0$) for the v_1 velocity component

$$\frac{\partial v_1}{\partial t} = \nu \frac{\partial^2 v_1}{\partial x_2^2} \qquad (3.1)$$

where we have divided the equation by density so that $\nu = \mu/\rho$. The boundary conditions for Eq. 3.1 are

$$v_1(x_2, t = 0) = 0, \quad v_1(x_2 = 0, t) = V_0, \quad v_1(x_2 \to \infty, t) = 0 \qquad (3.2)$$

The solution to Eq. 3.1 is shown in Fig. 3.2. For increasing time ($t_3 > t_2 > t_1$), the moving plate affects the fluid further and further away from the plate.

It turns out that the solution to Eq. 3.1 is a *similarity solution*; this means that the number of independent variables is reduced by one, in this case from two (x_2 and t) to one (η). The similarity variable, η, is related to x_2 and t as **similarity solution**

$$\eta = \frac{x_2}{2\sqrt{\nu t}} \qquad (3.3)$$

If the solution of Eq. 3.1 depends only on η, it means that the solution for a given fluid will be the same ("similar") for many (infinite) values of x_2 and t as long as the ratio $x_2/\sqrt{\nu t}$ is constant. Now we need to transform the derivatives in Eq. 3.1 from $\partial/\partial t$ and $\partial/\partial x_2$ to $d/d\eta$ so that it becomes a function of η only. We get

$$\frac{\partial v_1}{\partial t} = \frac{dv_1}{d\eta}\frac{\partial \eta}{\partial t} = -\frac{x_2 t^{-3/2}}{4\sqrt{\nu}}\frac{dv_1}{d\eta} = -\frac{1}{2}\frac{\eta}{t}\frac{dv_1}{d\eta}$$

$$\frac{\partial v_1}{\partial x_2} = \frac{dv_1}{d\eta}\frac{\partial \eta}{\partial x_2} = \frac{1}{2\sqrt{\nu t}}\frac{dv_1}{d\eta}$$

$$\frac{\partial^2 v_1}{\partial x_2^2} = \frac{\partial}{\partial x_2}\left(\frac{\partial v_1}{\partial x_2}\right) = \frac{\partial}{\partial x_2}\left(\frac{1}{2\sqrt{\nu t}}\frac{dv_1}{d\eta}\right) = \frac{1}{2\sqrt{\nu t}}\frac{\partial}{\partial x_2}\left(\frac{dv_1}{d\eta}\right) = \frac{1}{4\nu t}\frac{d^2 v_1}{d\eta^2}$$

$$(3.4)$$

We introduce a non-dimensional velocity

$$f = \frac{v_1}{V_0} \tag{3.5}$$

Inserting Eqs. 3.4 and 3.5 in Eq. 3.1 gives

$$\frac{d^2 f}{d\eta^2} + 2\eta\frac{df}{d\eta} = 0 \tag{3.6}$$

We have now successfully transformed Eq. 3.1 and reduced the number of independent variables from two to one. Now let us find out if the boundary conditions, Eq. 3.2, also can be transformed in a physically meaningful way; we get

$$\begin{aligned}
v_1(x_2, t = 0) = 0 &\Rightarrow f(\eta \to \infty) = 0 \\
v_1(x_2 = 0, t) = V_0 &\Rightarrow f(\eta = 0) = 1 \\
v_1(x_2 \to \infty, t) = 0 &\Rightarrow f(\eta \to \infty) = 0
\end{aligned} \tag{3.7}$$

Since we managed to transform both the equation (Eq. 3.1) and the boundary conditions (Eq. 3.7) we conclude that the transformation is suitable.

Now let us solve Eq. 3.6. Integration once gives

$$\frac{df}{d\eta} = C_1 \exp(-\eta^2) \tag{3.8}$$

Integration a second time gives

$$f = C_1 \int_0^\eta \exp(-\eta'^2)d\eta' + C_2 \tag{3.9}$$

The integral above is the error function

$$\mathrm{erf}(\eta) \equiv \frac{2}{\sqrt{\pi}} \int_0^\eta \exp(-\eta'^2)d\eta' \tag{3.10}$$

At the limits, the error function takes the values 0 and 1, i.e. $\mathrm{erf}(0) = 0$ and $\mathrm{erf}(\eta \to \infty) = 1$. Taking into account the boundary conditions, Eq. 3.7, the final solution to Eq. 3.9 is (with $C_2 = 1$ and $C_1 = -2/\sqrt{\pi}$)

$$f(\eta) = 1 - \mathrm{erf}(\eta) \tag{3.11}$$
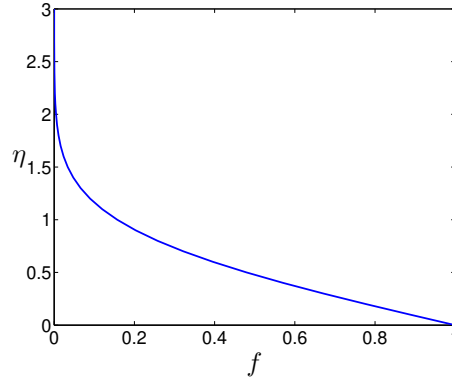
Figure 3.3: The velocity, $f = v_1/V_0$, given by Eq. 3.11.
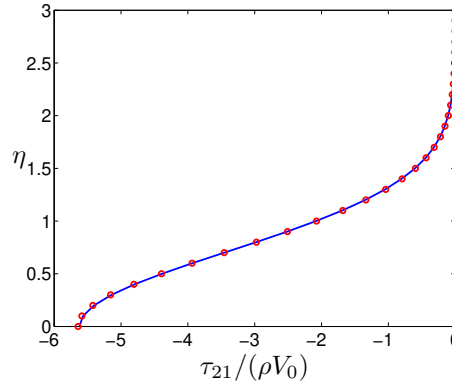
Figure 3.4: The shear stress for water ($\nu = 10^{-6}$) obtained from Eq. 3.12 at time $t = 100\,000$.

The solution is presented in Fig. 3.3. Compare this figure with Fig. 3.2 at p. 32; all graphs in that figure collapse into one graph in Fig. 3.3. To compute the velocity, v_1, we pick a time t and insert x_2 and t in Eq. 3.3. Then f is obtained from Eq. 3.11 and the velocity, v_1, is computed from Eq. 3.5. This is how the graphs in Fig. 3.2 were obtained.

From the velocity profile we can get the shear stress as

$$\tau_{21} = \mu\frac{\partial v_1}{\partial x_2} = \frac{\mu V_0}{2\sqrt{\nu t}}\frac{df}{d\eta} = -\frac{\mu V_0}{\sqrt{\pi\nu t}}\exp\left(-\eta^2\right) \tag{3.12}$$

where we used $\nu = \mu/\rho$. Figure 3.4 presents the shear stress, τ_{21}. The solid line is obtained from Eq. 3.12 and circles are obtained by evaluating the derivative, $df/d\eta$, numerically using central differences $(f_{j+1} - f_{j-1})/(\eta_{j+1} - \eta_{j-1})$. As can be seen from Fig. 3.4, the magnitude of the shear stress increases for decreasing η and it is largest at the wall, $\tau_w = -\rho V_0/\sqrt{\pi t}$

The vorticity, ω_3, across the boundary layer is computed from its definition (Eq. 1.36)

$$\omega_3 = -\frac{\partial v_1}{\partial x_2} = -\frac{V_0}{2\sqrt{\nu t}}\frac{df}{d\eta} = \frac{V_0}{\sqrt{\pi\nu t}}\exp(-\eta^2) \tag{3.13}$$

From Fig. 3.2 at p. 32 it is seen that for large times, the moving plate is felt further and further out in the flow, i.e. the thickness of the boundary layer, δ, increases. Often
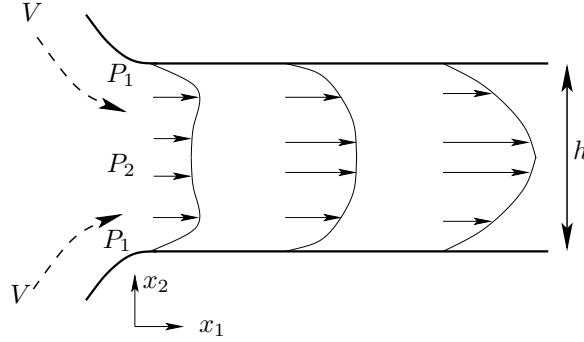
Figure 3.5: Flow in a horizontal channel. The inlet part of the channel is shown.

the boundary layer thickness is defined by the position where the local velocity, $v_1(x_2)$, reaches 99% of the freestream velocity. In our case, this corresponds to the point where $v_1 = 0.01V_0$. Find the point $f = v_1/V_0 = 0.01$ in Fig. 3.3; at this point $\eta \simeq 1.8$ (we can also use Eq. 3.11). Inserting $x_2 = \delta$ in Eq. 3.3 gives

$$\eta = 1.8 = \frac{\delta}{2\sqrt{\nu t}} \quad \Rightarrow \delta = 3.6\sqrt{\nu t} \tag{3.14}$$

It can be seen that the boundary layer thickness increases with $t^{1/2}$. Equation 3.14 can also be used to estimate the *diffusion length*. After, say, 10 minutes the diffusion length for air and water, respectively, are **diffusion length**

$$\begin{aligned} \delta_{air} &= 10.8cm \\ \delta_{water} &= 2.8cm \end{aligned} \tag{3.15}$$

The diffusion length can also be used to estimate the thickness of a developing boundary layer, see Section 4.3.1.

Exercise 16 *Consider the graphs in Fig. 3.3. Create this graph with Python/Matlab/Octave.*

Exercise 17 *Consider the graphs in Fig. 3.2. Note that no scale is used on the x_2 axis and that no numbers are given for t_1, t_2 and t_3. Create this graph with Python/Matlab/Octave for both air and engine oil. Choose suitable values on t_1, t_2 and t_3.*

Exercise 18 *Repeat the exercise above for the shear stress, τ_{21}, see Fig. 3.4.*

3.2 Flow between two plates

Consider steady, incompressible flow in a two-dimensional channel, see Fig. 3.5, with constant physical properties (i.e. $\mu = $ const).

3.2.1 Curved plates

Provided that the walls at the inlet are well curved, the velocity near the walls is larger than in the center, see Fig. 3.5. The reason is that the flow (with velocity V) following the curved wall must change its direction. The physical agent which accomplish this is the pressure gradient which forces the flow to follow the wall as closely as possible (if the wall is not sufficiently curved a separation will take place). Hence the pressure
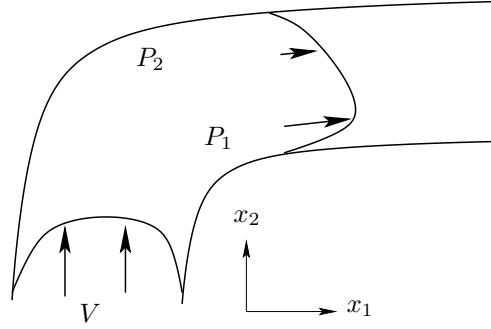
Figure 3.6: Flow in a channel bend.

in the center of the channel, P_2, is higher than the pressure near the wall, P_1. It is thus easier (i.e. less opposing pressure) for the fluid to enter the channel near the walls than in the center. This explains the high velocity near the walls.

The same phenomenon occurs in a channel bend, see Fig. 3.6. The flow V approaches the bend and the flow feels that it is approaching a bend through an increased pressure. The pressure near the outer wall, P_2, must be higher than that near the inner wall, P_1, in order to force the flow to turn. Hence, it is easier for the flow to sneak along the inner wall where the opposing pressure is smaller than near the outer wall: the result is a higher velocity near the inner wall than near the outer wall. In a three-dimensional duct or in a pipe, the pressure difference $P_2 - P_1$ creates secondary flow downstream the bend (i.e. a swirling motion in the $x_2 - x_3$ plane).

3.2.2 Flat plates

The flow in the inlet section (Fig. 3.5) is two dimensional. Near the inlet the velocity is largest near the wall and further downstream the velocity is retarded near the walls due to the large viscous shear stresses there. The flow is accelerated in the center because the integrated mass flow (from $x_2 = 0$ to h) at each x_1 must be constant because of continuity. The acceleration and retardation of the flow in the inlet region is "paid for " by a pressure loss which is rather high in the inlet region; if a separation occurs because of sharp corners at the inlet, the pressure loss will be even higher. For large x_1 the flow will be fully developed; the region until this occurs is called the *entrance region*, and the entrance length can, for moderately disturbed inflow, be estimated as [4]

$$\frac{x_{1,e}}{D_h} = 0.016 Re_{D_h} \equiv 0.016 \frac{V D_h}{\nu} \tag{3.16}$$

where V denotes the bulk (i.e. the mean) velocity, and $D_h = 4A/S_p$ where D_h, A and S_p denote the hydraulic diameter, the cross-sectional area and the perimeter, respectively. For flow between two plates we get $D_h = 2h$.

Let us find the governing equations for the fully developed flow region; in this region the flow does not change with respect to the streamwise coordinate, x_1 (i.e. $\partial v_1/\partial x_1 = \partial v_2/\partial x_1 = 0$). Since the flow is two-dimensional, it does not depend on the third coordinate direction, x_3 (i.e. $\partial/\partial x_3$), and the velocity in this direction is zero, i.e. $v_3 = 0$. Taking these restrictions into account the continuity equation can be simplified as (see Eq. 2.3)

$$\frac{\partial v_2}{\partial x_2} = 0 \tag{3.17}$$

Integration gives $v_2 = C_1$ and since $v_2 = 0$ at the walls, it means that

$$v_2 = 0 \tag{3.18}$$

across the entire channel (recall that we are dealing with the part of the channel where the flow is fully developed; in the inlet section $v_2 \neq 0$, see Fig. 3.5).

Now let us turn our attention to the momentum equation for v_2. This is the vertical direction (x_2 is positive upwards, see Fig. 3.5). The gravity acts in the negative x_2 direction, i.e. $f_i = (0, -g, 0)$. The momentum equation can be written (see Eq. 2.9 at p. 27)

$$\rho \frac{dv_2}{dt} \equiv \rho v_1 \frac{\partial v_2}{\partial x_1} + \rho v_2 \frac{\partial v_2}{\partial x_2} = -\frac{\partial P}{\partial x_2} + \mu \frac{\partial^2 v_2}{\partial x_2^2} - \rho g \tag{3.19}$$

Since $v_2 = 0$ we get

$$\frac{\partial P}{\partial x_2} = -\rho g \tag{3.20}$$

Integration gives

$$P = -\rho g x_2 + C_1(x_1) \tag{3.21}$$

where the integration "constant" C_1 may be a function of x_1 but not of x_2. If we denote the pressure at the lower wall (i.e. at $x_2 = 0$) as p we get

$$P = -\rho g x_2 + p(x_1) \tag{3.22}$$

Hence the pressure, P, decreases with vertical height. This agrees with our experience that the pressure decreases at high altitudes in the atmosphere and increases the deeper we dive into the sea. Usually the *hydrodynamic pressure*, p, is used in incompressible **hydrodynamic** flow. This pressure is zero when the flow is *static*, i.e. when the velocity field is zero. **pressure** However, when you want the *physical* pressure, the $\rho g x_2$ as well as the surrounding atmospheric pressure must be added.

We can now formulate the momentum equation in the streamwise direction

$$\rho \frac{dv_1}{dt} \equiv \rho v_1 \frac{\partial v_1}{\partial x_1} + \rho v_2 \frac{\partial v_1}{\partial x_2} = -\frac{dp}{dx_1} + \mu \frac{\partial^2 v_1}{\partial x_2^2} \tag{3.23}$$

where P was replaced by p using Eq. 3.22. Since $v_2 = \partial v_1 / \partial x_1 = 0$ the left side is zero so

$$\mu \frac{\partial^2 v_1}{\partial x_2^2} = \frac{dp}{dx_1} \tag{3.24}$$

Since the left side is a function of x_2 and the right side is a function of x_1, we conclude that they both are equal to a constant (i.e. Eq. 3.24 is independent of x_1 and x_2) . The velocity, v_1, is zero at the walls, i.e

$$v_1(0) = v_1(h) = 0 \tag{3.25}$$

where h denotes the height of the channel, see Fig. 3.5. Integrating Eq. 3.24 twice and using Eq. 3.25 gives

$$v_1 = -\frac{h}{2\mu} \frac{dp}{dx_1} x_2 \left(1 - \frac{x_2}{h}\right) \tag{3.26}$$

The minus sign on the right side appears because the pressure is decreasing for increasing x_1; the pressure is *driving* the flow. The negative pressure gradient is constant (see Eq. 3.24) and can be written as $-dp/dx_1 = \Delta p / L$.
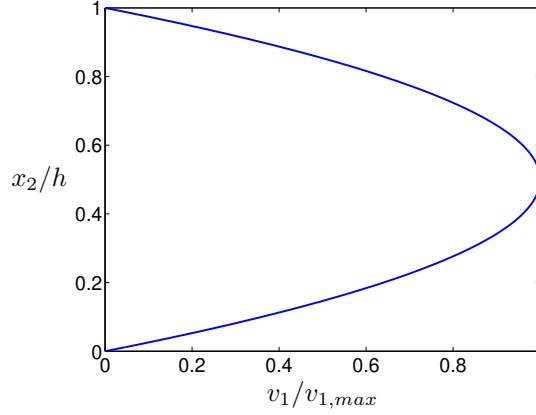
Figure 3.7: The velocity profile in fully developed channel flow, Eq. 3.28.

The velocity takes its maximum in the center, i.e. for $x_2 = h/2$, and reads

$$v_{1,max} = \frac{h}{2\mu}\frac{\Delta p}{L}\frac{h}{2}\left(1 - \frac{1}{2}\right) = \frac{h^2}{8\mu}\frac{\Delta p}{L} \tag{3.27}$$

We often write Eq. 3.26 on the form

$$\frac{v_1}{v_{1,max}} = \frac{4x_2}{h}\left(1 - \frac{x_2}{h}\right) \tag{3.28}$$

The mean velocity (often called the bulk velocity) is obtained by integrating Eq. 3.28 across the channel, i.e.

$$v_{1,mean} = \frac{v_{1,max}}{h}\int_0^h \frac{4x_2}{h}\left(1 - \frac{x_2}{h}\right)dx_2 = \frac{2}{3}v_{1,max} \tag{3.29}$$

The velocity profile is shown in Fig. 3.7

Since we know the velocity profile, we can compute the wall shear stress. Equation 3.26 gives

$$\tau_w = \mu\frac{\partial v_1}{\partial x_2} = -\frac{h}{2}\frac{dp}{dx_1} = \frac{h}{2}\frac{\Delta p}{L} \tag{3.30}$$

Actually, this result could have been obtained by simply taking a force balance of a slice of the flow far downstream.

This flow is analyzed in Appendix D.

3.2.3 Force balance, channel flow

We continue to consider fully developed flow between two parallel plates. To formulate a force balance in the x_1 direction, we start with Eq. 1.7 which reads for $i = 1$

$$\rho\frac{dv_1}{dt} = \frac{\partial \sigma_{j1}}{\partial x_j} \tag{3.31}$$

The left hand side is zero since the flow is fully developed. Forces act on a volume and its bounding surface. Hence we integrate Eq. 3.31 over the volume of a slice (length L), see Fig. 3.8

$$0 = \int_V \frac{\partial \sigma_{j1}}{\partial x_j}dV \tag{3.32}$$
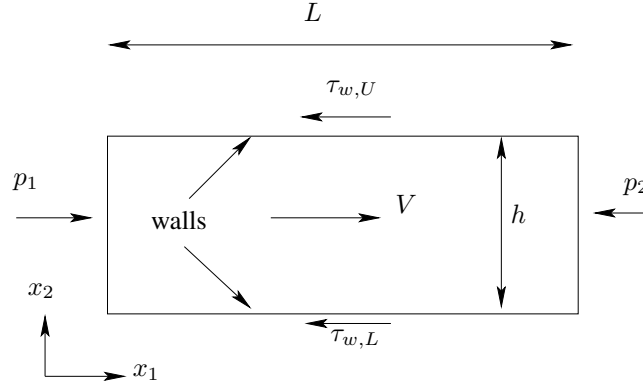
Figure 3.8: Force balance of the flow between two plates.

Recall that this is the form on which we originally derived the momentum balance (Newton's second law) in Part I. [2] Now use Gauss divergence theorem

$$0 = \int_V \frac{\partial \sigma_{j1}}{\partial x_j} dV = \int_S \sigma_{j1} n_j dS \qquad (3.33)$$

The bounding surface consists in our case of four surfaces (lower, upper, left and right) so that

$$0 = \int_{S_{left}} \sigma_{j1} n_j dS + \int_{S_{right}} \sigma_{j1} n_j dS + \int_{S_{lower}} \sigma_{j1} n_j dS + \int_{S_{upper}} \sigma_{j1} n_j dS \quad (3.34)$$

The normal vector on the lower, upper, left and right are $n_{i,lower} = (0, -1, 0), n_{i,upper} = (0, 1, 0), n_{i,left} = (-1, 0, 0), n_{i,right} = (1, 0, 0)$. Inserting the normal vectors and using Eq. 1.9 give

$$0 = -\int_{S_{left}} (-p + \tau_{11}) dS + \int_{S_{right}} (-p + \tau_{11}) dS - \int_{S_{lower}} \tau_{21} dS + \int_{S_{upper}} \tau_{21} dS \qquad (3.35)$$

$\tau_{11} = 0$ because $\partial v_1/\partial x_1 = 0$ (fully developed flow). The shear stress at the upper and lower surfaces, τ_{21}, have opposite sign because $\mu(\partial v_1/\partial x_2)_{lower} = -\mu(\partial v_1/\partial x_2)_{upper}$. Using this and Eq. 3.22 give ($p = p(x_1)$ and τ_w is constant and can thus be taken out in front of the integration)

$$0 = p_1 W h - p_2 W h - 2\tau_w L W \qquad (3.36)$$

where $\tau_w = \mu(\partial v_1/\partial x_2)_{lower}$ and W is the width (in x_3 direction) of the two plates (for convenience we set $W = 1$). With $\Delta p = p_1 - p_2$ we get Eq. 3.30.

3.2.4 Balance equation for the kinetic energy

In this subsection we will use the equation for kinetic energy, Eq. 2.23. Let us integrate this equation in the same way as we did for the force balance. The left side of Eq. 2.23

is zero because we assume that the flow is fully developed; using Eq. 1.9 gives

$$
\begin{aligned}
0 &= \frac{\partial v_i \sigma_{ji}}{\partial x_j} - \sigma_{ji}\frac{\partial v_i}{\partial x_j} + \underbrace{\rho v_i f_i}_{=0} \\
&= -\frac{\partial v_j p}{\partial x_j} + \frac{\partial v_i \tau_{ji}}{\partial x_j} + p\delta_{ij}\frac{\partial v_i}{\partial x_j} - \underbrace{\tau_{ji}\frac{\partial v_i}{\partial x_j}}_{\Phi}
\end{aligned}
\tag{3.37}
$$

On the first line $v_i f_i = v_1 f_1 + v_2 f_2 = 0$ because $v_2 = f_1 = 0$. The third term on the second line $p\delta_{ij}\partial v_i/\partial x_j = p\partial v_i/\partial x_i = 0$ because of continuity. The last term corresponds to the viscous dissipation term, Φ (i.e. loss due to friction), see Eq. 2.25 (term **b**). Now we integrate the equation over a volume

$$
0 = \int_V \left(-\frac{\partial p v_j}{\partial x_j} + \frac{\partial \tau_{ji} v_i}{\partial x_j} - \Phi \right) dV
\tag{3.38}
$$

Gauss divergence theorem on the two first terms gives

$$
0 = \int_S (-p v_j + \tau_{ji} v_i) n_j dS - \int_V \Phi dV
\tag{3.39}
$$

where S is the surface bounding the volume. The unit normal vector is denoted by n_j which points *out* from the volume. For example, on the right surface in Fig. 3.8 it is $n_j = (1, 0, 0)$ and on the lower surface it is $n_j = (0, -1, 0)$. Now we apply Eq. 3.39 to the fluid enclosed by the flat plates in Fig. 3.8. The second term is zero on all four surfaces and the first term is zero on the lower and upper surfaces (see Exercises below). We replace the pressure P with p using Eq. 3.22 so that

$$
\begin{aligned}
\int_{S_{left}\&S_{right}} (-p v_1 + \rho g x_2 v_1) n_1 dS &= -(p_2 - p_1)\int_{S_{left}\&S_{right}} v_1 n_1 dS \\
&= \Delta p v_{1,mean} W h
\end{aligned}
\tag{3.40}
$$

because $\rho g x_2 n_1 v_1$ on the left and right surfaces cancels; p can be taken out of the integral as it does not depend on x_2. Finally we get

$$
\Delta p = \frac{1}{W h v_{1,mean}} \int_V \Phi dV
\tag{3.41}
$$

3.3   Two-dimensional boundary layer flow over flat plate

The equations for steady, two-dimensional, incompressible boundary layer flow reads (x_1 and x_2 denote streamwise and wall-normal coordinates, respectively)

$$
\begin{aligned}
v_1 \frac{\partial v_1}{\partial x_1} + v_2 \frac{\partial v_1}{\partial x_2} &= \nu \frac{\partial^2 v_1}{\partial x_2^2} \\
\frac{\partial p}{\partial x_2} &= 0 \\
\frac{\partial v_1}{\partial x_1} + \frac{\partial v_2}{\partial x_2} &= 0
\end{aligned}
\tag{3.42}
$$

where the pressure gradient is omitted in the v_1 momentum equation because $\partial p/\partial x_1 = 0$ along a flat plate in infinite surroundings. The boundary conditions are

$$
\begin{aligned}
&x_2 = 0 : v_1 = v_2 = 0 \quad \text{(at the wall)} \\
&x_2 \to \infty : v_1 \to V_{1,\infty}, v_2 = 0 \quad \text{(far from the wall)}
\end{aligned}
\tag{3.43}
$$

Let's introduce the *streamfunction* Ψ, which is useful when re-writing the two-dimensional Navier-Stokes equations. It is defined as **stream-function**

$$v_1 = \frac{\partial \Psi}{\partial x_2}, \quad v_2 = -\frac{\partial \Psi}{\partial x_1} \tag{3.44}$$

With the velocity field expressed in Ψ, the continuity equations is automatically satisfied which is easily shown by inserting Eq. 3.44 into the continuity equation

$$\frac{\partial v_1}{\partial x_1} + \frac{\partial v_2}{\partial x_2} = \frac{\partial^2 \Psi}{\partial x_1 \partial x_2} - \frac{\partial^2 \Psi}{\partial x_2 \partial x_1} = 0 \tag{3.45}$$

Inserting Eq. 3.44 into the streamwise momentum equation gives

$$\frac{\partial \Psi}{\partial x_2} \frac{\partial^2 \Psi}{\partial x_1 \partial x_2} - \frac{\partial \Psi}{\partial x_1} \frac{\partial^2 \Psi}{\partial x_2^2} = \nu \frac{\partial^3 \Psi}{\partial x_2^3} \tag{3.46}$$

The boundary conditions for the streamfunction read

$$x_2 = 0 : \Psi = \frac{\partial \Psi}{\partial x_2} = 0 \quad \text{(at the wall)}$$
$$x_2 \to \infty : \frac{\partial \Psi}{\partial x_2} \to V_{1,\infty} \quad \text{(far from the wall)} \tag{3.47}$$

As in Section 3.1 we want to transform the partial differential equation, Eq. 3.46, into an ordinary differential equation. In Section 3.1 we replaced x_1 and t with the new non-dimensional variable η. Now we want to replace x_1 and x_2 with a new dimensionless variable, say ξ. At the same time we define a new dimensionless streamfunction, $g(\xi)$, as

$$\xi = \left(\frac{V_{1,\infty}}{\nu x_1}\right)^{1/2} x_2, \quad \Psi = (\nu V_{1,\infty} x_1)^{1/2} g \tag{3.48}$$

First we need the derivatives $\partial \xi / \partial x_1$ and $\partial \xi / \partial x_2$

$$\frac{\partial \xi}{\partial x_1} = -\frac{1}{2} \left(\frac{V_{1,\infty}}{\nu x_1}\right)^{1/2} \frac{x_2}{x_1} = -\frac{\xi}{2x_1}$$
$$\frac{\partial \xi}{\partial x_2} = \left(\frac{V_{1,\infty}}{\nu x_1}\right)^{1/2} = \frac{\xi}{x_2} \tag{3.49}$$

Now we express the first derivatives of Ψ in Eq. 3.46 as derivatives of g, i.e. (g' denotes $dg/d\xi$)

$$\begin{aligned}
\frac{\partial \Psi}{\partial x_1} &= \frac{\partial}{\partial x_1} \left((\nu V_{1,\infty} x_1)^{1/2}\right) g + (\nu V_{1,\infty} x_1)^{1/2} g' \frac{\partial \xi}{\partial x_1} \\
&= \frac{1}{2} \left(\frac{\nu V_{1,\infty}}{x_1}\right)^{1/2} g - (\nu V_{1,\infty} x_1)^{1/2} g' \frac{\xi}{2x_1} \\
&= \frac{1}{2} \left(\frac{\nu V_{1,\infty}}{x_1}\right)^{1/2} (g - \xi g') \\
\frac{\partial \Psi}{\partial x_2} &= \frac{\partial}{\partial x_2} \left((\nu V_{1,\infty} x_1)^{1/2}\right) g + (\nu V_{1,\infty} x_1)^{1/2} \frac{\partial \xi}{\partial x_2} g' = V_{1,\infty} g'
\end{aligned} \tag{3.50}$$

The second and third derivatives of Ψ read

$$\frac{\partial^2 \Psi}{\partial x_2^2} = V_{1,\infty} g'' \frac{\partial \xi}{\partial x_2} = V_{1,\infty} \left(\frac{V_{1,\infty}}{\nu x_1} \right)^{1/2} g'' = V_{1,\infty} \frac{\xi}{x_2} g''$$

$$\frac{\partial^3 \Psi}{\partial x_2^3} = V_{1,\infty} \left(\frac{V_{1,\infty}}{\nu x_1} \right)^{1/2} g''' \frac{\partial \xi}{\partial x_2} = V_{1,\infty} \frac{V_{1,\infty}}{\nu x_1} g''' = V_{1,\infty} \left(\frac{\xi}{x_2} \right)^2 g''' \quad (3.51)$$

$$\frac{\partial^2 \Psi}{\partial x_1 \partial x_2} = V_{1,\infty} g'' \frac{\partial \xi}{\partial x_1} = -\frac{\xi}{2x_1} V_{1,\infty} g''$$

Inserting Eqs. 3.50 and 3.51 into Eq. 3.46 gives

$$-V_{1,\infty} g' \frac{\xi}{2x_1} V_{1,\infty} g'' - \left(\frac{1}{2} \left(\frac{\nu V_{1,\infty}}{x_1} \right)^{1/2} (g - \xi g') \right) V_{1,\infty} \left(\frac{V_{1,\infty}}{\nu x_1} \right)^{1/2} g''$$

$$= \nu \frac{V_{1,\infty}^2}{\nu x_1} g''' \tag{3.52}$$

Divide by $V_{1,\infty}^2$ and multiply by x_1 gives

$$- g' \frac{\xi}{2} g'' - \frac{1}{2} (g - \xi g') g'' = g''' \tag{3.53}$$

so that

$$\frac{1}{2} g g'' + g''' = 0 \tag{3.54}$$

This equation was derived (and solved numerically!) by Blasius in his PhD thesis 1907 [5, 6]. The numerical solution is given in Table 3.1. The flow is analyzed in Appendix E.

Exercise 19 *For the fully developed flow, compute the vorticity, ω_i, using the exact solution (Eq. 3.28).*

Exercise 20 *Show that the first and second terms in Eq. 3.39 are zero on the upper and the lower surfaces in Fig. 3.8.*

Exercise 21 *Show that the second term in Eq. 3.39 is zero also on the left and right surfaces in Fig. 3.8 (assume fully developed flow).*

Exercise 22 *Using the exact solution, compute the dissipation, Φ, for the fully developed flow.*

Exercise 23 *From the dissipation, compute the pressure drop. Is it the same as that obtained from the force balance (if not, find the error; it should be!).*

3.3.1 Momentum balance, boundary layer

Let's make a momentum balance for the boundary layer in the same way as we did for fully-developed channel flow in Section 3.2.3. The left boundary (see Fig. 3.9) is located upstream of the plate, i.e. at $x < 0$, see Fig. E.1, Note that here – contrary to the channel flow – we do not have any pressure gradient. At the upper boundary we also have an outflow because the right boundary includes a boundary layer meaning

ξ	g	g$'$	g$''$
0	0.000000000E+00	0.000000000E+00	3.320573362E-01
0.2	6.640999715E-03	6.640779210E-02	3.319838371E-01
0.4	2.655988402E-02	1.327641608E-01	3.314698442E-01
0.6	5.973463750E-02	1.989372524E-01	3.300791276E-01
0.8	1.061082208E-01	2.647091387E-01	3.273892701E-01
1.0	1.655717258E-01	3.297800312E-01	3.230071167E-01
1.2	2.379487173E-01	3.937761044E-01	3.165891911E-01
1.4	3.229815738E-01	4.562617647E-01	3.078653918E-01
1.6	4.203207655E-01	5.167567844E-01	2.966634615E-01
1.8	5.295180377E-01	5.747581439E-01	2.829310173E-01
2.0	6.500243699E-01	6.297657365E-01	2.667515457E-01
2.2	7.811933370E-01	6.813103772E-01	2.483509132E-01
2.4	9.222901256E-01	7.289819351E-01	2.280917607E-01
2.6	1.072505977E+00	7.724550211E-01	2.064546268E-01
2.8	1.230977302E+00	8.115096232E-01	1.840065939E-01
3.0	1.396808231E+00	8.460444437E-01	1.613603195E-01
3.2	1.569094960E+00	8.760814552E-01	1.391280556E-01
3.4	1.746950094E+00	9.017612214E-01	1.178762461E-01
3.6	1.929525170E+00	9.233296659E-01	9.808627878E-02
3.8	2.116029817E+00	9.411179967E-01	8.012591814E-02
4.0	2.305746418E+00	9.555182298E-01	6.423412109E-02
4.2	2.498039663E+00	9.669570738E-01	5.051974749E-02
4.4	2.692360938E+00	9.758708321E-01	3.897261085E-02
4.6	2.888247990E+00	9.826835008E-01	2.948377201E-02
4.8	3.085320655E+00	9.877895262E-01	2.187118635E-02
5.0	3.283273665E+00	9.915419002E-01	1.590679869E-02
5.2	3.481867612E+00	9.942455354E-01	1.134178897E-02
5.4	3.680919063E+00	9.961553040E-0	1 7.927659815E-03
5.6	3.880290678E+00	9.974777682E-0	1 5.431957680E-03
5.8	4.079881939E+00	9.983754937E-0	1 3.648413667E-03
6.0	4.279620923E+00	9.989728724E-01	2.402039844E-03
6.2	4.479457297E+00	9.993625417E-01	1.550170691E-03
6.4	4.679356615E+00	9.996117017E-01	9.806151170E-04
6.6	4.879295811E+00	9.997678702E-01	6.080442648E-04
6.8	5.079259772E+00	9.998638190E-01	3.695625701E-04
7.0	5.279238811E+00	9.999216041E-01	2.201689553E-04
7.2	5.479226847E+00	9.999557173E-01	1.285698072E-04
7.4	5.679220147E+00	9.999754577E-01	7.359298339E-05
7.6	5.879216466E+00	9.999866551E-01	4.129031111E-05
7.8	6.079214481E+00	9.999928812E-01	2.270775140E-05
8.0	6.279213431E+00	9.999962745E-01	1.224092624E-05
8.2	6.479212887E+00	9.999980875E-01	6.467978611E-06
8.4	6.679212609E+00	9.999990369E-01	3.349939753E-06
8.6	6.879212471E+00	9.999995242E-01	1.700667989E-06
8.8	7.079212403E+00	9.999997695E-01	8.462841214E-07

Table 3.1: Blasius numerical solution of laminar flow along a flat plate.

L

$v_2(x_1)$

wall $\quad\longrightarrow\quad V$ $\qquad H$

τ_w

x_2

x_1
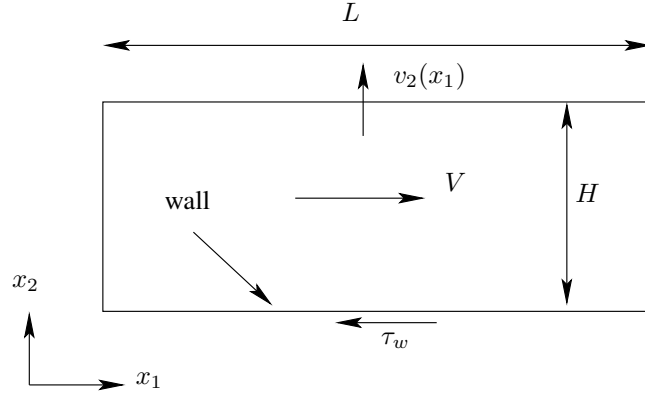
Figure 3.9: Force balance of boundary layer flow along a flat plate.

that the outflow here is smaller than the inflow at the left boundary. Hence, the right side of the momentum equation reads (cf. Eq. 3.34)

$$0 = \int_{S_{lower}} \sigma_{j1} n_j dS = -\int_{S_{lower}} \sigma_{21} = -\int_{S_{lower}} \tau_w dS \tag{3.55}$$

using Eq. 1.9 and $n_j = (0, -1, 0)$. Only the contribution from the lower boundary appears. The reason is that is no pressure forces on the left and right (or, rather, they cancel each other) and there is no shear stress on the top boundary since $\partial v_1 / \partial x_2 = 0$. The other difference compared to the channel flow in Section 3.2.3 is that the left side of Eq. 3.31 is not zero. It reads

$$\rho \frac{dv_1}{dt} \equiv \frac{\partial v_j v_1}{\partial x_j}. \tag{3.56}$$

Gauss divergence theorem gives

$$\int_V \frac{\partial v_j v_1}{\partial x_j} dV = \int_{S_{left}} v_j v_1 n_j dS + \int_{S_{right}} v_j v_1 n_j dS + \int_{S_{top}} v_j v_1 n_j dS \tag{3.57}$$

where the contribution at the lower boundary is zero since the velocity is zero at the walls. The unit normal vector at the left, right and top boundaries are $(1, 0, 0)$, $(-1, 0, 0)$ and $(0, 1, 0)$, respectively, which gives

$$\int_V \frac{\partial v_j v_1}{\partial x_j} dV = \int_{S_{right}} v_1^2 dS - \int_{S_{left}} v_1^2 dS + \int_{S_{top}} v_1 v_2 dS \tag{3.58}$$

At the left boundary $v_1 = V_\infty$ which gives

$$\int_V \frac{\partial v_j v_1}{\partial x_j} dV = \int_S \left(v_1^2 - V_{1,\infty}^2\right) dS + \int_{S_{top}} v_1 v_2 dS \tag{3.59}$$

Combining Eqs. 3.55 and 3.59 we can write (assuming that the extent of the integration domain in the third direction is one)

$$\tau_w = \frac{1}{L} \left[\int_S \left(V_{1,\infty}^2 - v_1^2\right) dx_2 + \int_{S_{top}} v_1 v_2 dx_1 \right] \tag{3.60}$$

We find one important difference between fully-developed channel flow and boundary layer flow: the flow in channel flow is driven by a pressure gradient (the pressure decreases) whereas in the boundary layer the "force" to overcome the opposing wall shear stress is achieved by decreasing momentum in the convective term. Making a balance of the mass flow and combining it with Eq. 3.60 the expression for the momentum thickness, E.2, is derived.
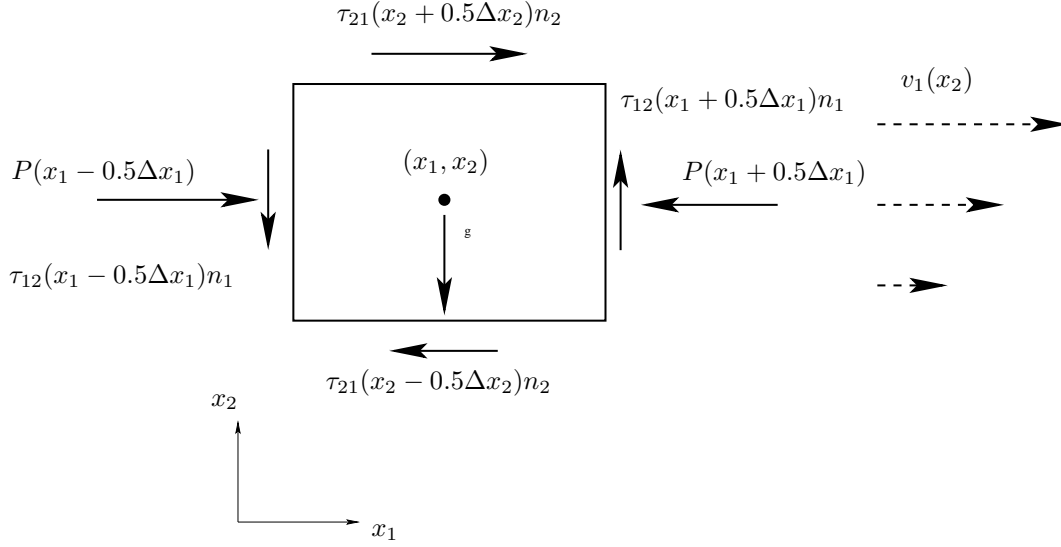
Figure 4.1: Surface forces acting on a fluid particle. The fluid particle is located in the lower half of fully developed channel flow. The v_1 velocity is given by Eq. 3.28 and $v_2 = 0$. Hence $\tau_{11} = \tau_{22} = \partial\tau_{12}/\partial x_1 = 0$ and $-\partial\tau_{21}/\partial x_2 > 0$. The v_1 velocity field is indicated by dashed vectors.

4 Vorticity equation and potential flow

4.1 Vorticity and rotation

$\mathbf{V}$ORTICITY, ω_i, was introduced in Eq. 1.12 at p. 17. As shown in Fig. 1.4 at p. 19, vorticity is connected to rotation of a fluid particle. Figure 4.1 shows the surface forces acting on a fluid particle in a shear flow. Looking at Fig. 4.1 it is obvious that only the shear stresses are able to rotate the fluid particle; the pressure acts through the center of the fluid particle and is thus not able to affect rotation of the fluid particle. Note that the v_2 momentum equation (see Eqs. 2.4 and 3.32) requires that the vertical viscous stresses in Fig. 4.1 are in balance. The v_1 momentum equation requires that the horizontal viscous stresses balance the pressure difference.

Let us have a look at the momentum equations in order to show that the viscous terms indeed can be formulated with the vorticity vector, ω_i. In incompressible flow the viscous terms read (see Eqs. 2.4, 2.5 and 2.7)

$$\frac{\partial \tau_{ji}}{\partial x_j} = \mu \frac{\partial^2 v_i}{\partial x_j \partial x_j} \tag{4.1}$$

The right side can be re-written using the tensor identity

$$\begin{aligned}\frac{\partial^2 v_i}{\partial x_j \partial x_j} &= \frac{\partial^2 v_j}{\partial x_j \partial x_i} - \left(\frac{\partial^2 v_j}{\partial x_j \partial x_i} - \frac{\partial^2 v_i}{\partial x_j \partial x_j} \right) \\ &= \underbrace{\frac{\partial}{\partial x_i} \left(\frac{\partial v_j}{\partial x_j} \right)}_{=0} - \varepsilon_{inm}\varepsilon_{mjk} \frac{\partial^2 v_k}{\partial x_j \partial x_n} = -\varepsilon_{inm}\varepsilon_{mjk} \frac{\partial^2 v_k}{\partial x_j \partial x_n}\end{aligned} \tag{4.2}$$

where the first on the second line is zero because of continuity. Let's verify that

$$\left(\frac{\partial^2 v_j}{\partial x_j \partial x_i} - \frac{\partial^2 v_i}{\partial x_j \partial x_j}\right) = \varepsilon_{inm}\varepsilon_{mjk}\frac{\partial^2 v_k}{\partial x_j \partial x_n} \tag{4.3}$$

Use the $\varepsilon - \delta$-identity (see Table C.1 at p. 327)

$$\varepsilon_{inm}\varepsilon_{mjk}\frac{\partial^2 v_k}{\partial x_j \partial x_n} = (\delta_{ij}\delta_{nk} - \delta_{ik}\delta_{nj})\frac{\partial^2 v_k}{\partial x_j \partial x_n} = \frac{\partial^2 v_k}{\partial x_i \partial x_k} - \frac{\partial^2 v_i}{\partial x_j \partial x_j} \tag{4.4}$$

which shows that Eq. 4.3 is correct. At the right side of Eq. 4.3 we recognize the vorticity, $\omega_m = \varepsilon_{mjk}\partial v_k/\partial x_j$, so that

$$\frac{\partial^2 v_i}{\partial x_j \partial x_j} = -\varepsilon_{inm}\frac{\partial \omega_m}{\partial x_n} \tag{4.5}$$

In vector notation the identity Eq. 4.5 reads

$$\nabla^2 \mathbf{v} = \nabla(\nabla \cdot \mathbf{v}) - \nabla \times \nabla \times \mathbf{v} = -\nabla \times \boldsymbol{\omega} \tag{4.6}$$

Using Eq. 4.5, Eq. 4.1 reads

$$\frac{\partial \tau_{ji}}{\partial x_j} = -\mu\varepsilon_{inm}\frac{\partial \omega_m}{\partial x_n} \tag{4.7}$$

Thus, there is a one-to-one relation between the viscous term and vorticity: no viscous terms means no vorticity and vice versa. An imbalance in shear stresses (left side of Eq. 4.7) causes a change in vorticity, i.e. generates vorticity (right side of Eq. 4.7). Hence, inviscid flow (i.e. friction-less flow) has no rotation. (The exception is when vorticity is transported *into* an inviscid region, but also in that case no vorticity is generated or destroyed: it stays constant, unaffected.) Inviscid flow is often called *irrotational* flow (i.e. no rotation) or *potential* flow. The vorticity is always created at **potential** *boundaries*, see Section 4.3.1.

The main points that we have learnt in this section are:

1. The viscous terms are responsible for creating vorticity; this means that the vorticity can not be created or destroyed in inviscid (friction-less) flow

2. The viscous terms in the momentum equations can be expressed in ω_i; considering Item 1 this was to be expected.

Exercise 24 *Prove the first equality of Eq. 4.5 using the ε-δ-identity.*

Exercise 25 *Write out Eq. 4.7 for $i = 1$ and verify that it is satisfied.*

4.2 The vorticity transport equation in three dimensions

Up to now we have talked quite a lot about vorticity. We have learnt that physically it means rotation of a fluid particle and that it is only the viscous terms that can cause rotation of a fluid particle. The terms inviscid (no friction), irrotational and potential flow all denote *frictionless flow* which is equivalent to zero (change in) vorticity. There **friction-** is a small difference between the three terms because there may be vorticity in inviscid **less** flow that is convected into the flow at the inlet(s); but also in this case the vorticity is not

affected once it has entered the inviscid flow region. However, usually no distinction is made between the three terms.

In this section we will derive the transport equation for vorticity in incompressible flow. As usual we start with the Navier-Stokes equation, Eq. 2.9 at p. 27. First, we re-write the convective term of the incompressible momentum equation (Eq. 2.9) as

$$v_j \frac{\partial v_i}{\partial x_j} = v_j(S_{ij} + \Omega_{ij}) = v_j \left(S_{ij} - \frac{1}{2}\varepsilon_{ijk}\omega_k \right) \tag{4.8}$$

where Eq. 1.19 on p. 17 was used. Inserting $S_{ij} = (\partial v_i/\partial x_j + \partial v_j/\partial x_i)/2$ and multiplying by two gives

$$2v_j \frac{\partial v_i}{\partial x_j} = v_j \left(\frac{\partial v_i}{\partial x_j} + \frac{\partial v_j}{\partial x_i} \right) - \varepsilon_{ijk}v_j\omega_k \tag{4.9}$$

The second term on the right side can be written as (Trick 2, see Eq. 8.4)

$$v_j \frac{\partial v_j}{\partial x_i} = \frac{1}{2}\frac{\partial(v_j v_j)}{\partial x_i} = \frac{\partial k}{\partial x_i} \tag{4.10}$$

where $k = v_j v_j/2$. Equation 4.9 can now be written as

$$v_j \frac{\partial v_i}{\partial x_j} = \underbrace{\frac{\partial k}{\partial x_i}}_{\text{no rotation}} - \underbrace{\varepsilon_{ijk}v_j\omega_k}_{\text{rotation}} \tag{4.11}$$

The last term on the right side is the vector product of $\mathbf{v}$ and $\boldsymbol{\omega}$, i.e. $\mathbf{v} \times \boldsymbol{\omega}$.

The trick we have achieved is to split the convective term into one term without rotation (first term on the right side of Eq. 4.11) and one term including rotation (second term on the right side). Inserting Eq. 4.11 into the incompressible momentum equation (Eq. 2.9) yields

$$\frac{\partial v_i}{\partial t} + \underbrace{\frac{\partial k}{\partial x_i}}_{\text{no rotation}} - \underbrace{\varepsilon_{ijk}v_j\omega_k}_{\text{rotation}} = -\frac{1}{\rho}\frac{\partial P}{\partial x_i} + \nu\frac{\partial^2 v_i}{\partial x_j \partial x_j} + f_i \tag{4.12}$$

The volume source is in most engineering flows represented by the gravity, i.e. $f_i = g_i$.

From Eq. 4.12 we get Crocco's theorem for steady inviscid flow

$$\varepsilon_{ijk}v_j\omega_k = \frac{\partial}{\partial x_i}\left(\frac{P}{\rho} + k \right) - f_i = \frac{\partial}{\partial x_i}\underbrace{\left(\frac{P}{\rho} + k + \phi \right)}_{P_0/\rho} \tag{4.13}$$

where $\partial\phi/\partial x_i = -f_i$ is the potential of the body force. In vector notation, Eq. 4.13 reads

$$\mathbf{v} \times \omega = \frac{1}{\rho}\nabla(P_0) \tag{4.14}$$

These equations states that the gradient of stagnation pressure, P_0, is orthogonal to both the velocity and vorticity vector.

Since the vorticity vector in Eq. 1.12 is defined by the cross product $\varepsilon_{pqi}\partial v_i/\partial x_q$ ($\nabla \times \mathbf{v}$ in vector notation, see Exercise 8), we start by applying the operator $\varepsilon_{pqi}\partial/\partial x_q$ to the Navier-Stokes equation (Eq. 4.12) so that

$$\begin{aligned}
\varepsilon_{pqi}\frac{\partial^2 v_i}{\partial t \partial x_q} + \varepsilon_{pqi}\frac{\partial^2 k}{\partial x_i \partial x_q} - \varepsilon_{pqi}\varepsilon_{ijk}\frac{\partial v_j\omega_k}{\partial x_q} \\
= -\varepsilon_{pqi}\frac{1}{\rho}\frac{\partial^2 P}{\partial x_i \partial x_q} + \nu\varepsilon_{pqi}\frac{\partial^3 v_i}{\partial x_j \partial x_j \partial x_q} + \varepsilon_{pqi}\frac{\partial g_i}{\partial x_q}
\end{aligned} \tag{4.15}$$

where the body force f_i was replaced by g_i. We know that ε_{ijk} is anti-symmetric in all indices, and hence the second term on line 1 and the first term on line 2 are zero (product of a symmetric and an anti-symmetric tensor). The last term on line 2 is zero because the gravitation vector, g_i, is constant (it is zero even if it is non-constant, because it can be expressed as a potential, see Eq. 4.31). The last term on line 1 is re-written using the ε-δ identity (see Table C.1 at p. 327)

$$\varepsilon_{pqi}\varepsilon_{ijk}\frac{\partial v_j \omega_k}{\partial x_q} = (\delta_{pj}\delta_{qk} - \delta_{pk}\delta_{qj})\frac{\partial v_j \omega_k}{\partial x_q} = \frac{\partial v_p \omega_k}{\partial x_k} - \frac{\partial v_q \omega_p}{\partial x_q}$$
$$= v_p \frac{\partial \omega_k}{\partial x_k} + \omega_k \frac{\partial v_p}{\partial x_k} - v_q \frac{\partial \omega_p}{\partial x_q} - \omega_p \frac{\partial v_q}{\partial x_q} \qquad (4.16)$$

Using the definition of ω_i we find that its divergence

$$\frac{\partial \omega_i}{\partial x_i} = \frac{\partial}{\partial x_i}\left(\varepsilon_{ijk}\frac{\partial v_k}{\partial x_j}\right) = \varepsilon_{ijk}\frac{\partial^2 v_k}{\partial x_j \partial x_i} = 0 \qquad (4.17)$$

is zero (product of a symmetric and an anti-symmetric tensor). Using the continuity equation $(\partial v_q/\partial x_q = 0)$ and Eq. 4.17, Eq. 4.16 can be written

$$\varepsilon_{pqi}\varepsilon_{ijk}\frac{\partial v_j \omega_k}{\partial x_q} = \omega_k \frac{\partial v_p}{\partial x_k} - v_k \frac{\partial \omega_p}{\partial x_k} \qquad (4.18)$$

The second term on line 2 in Eq. 4.15 can be written as

$$\nu\varepsilon_{pqi}\frac{\partial^3 v_i}{\partial x_j \partial x_j \partial x_q} = \nu\frac{\partial^2}{\partial x_j \partial x_j}\left(\varepsilon_{pqi}\frac{\partial v_i}{\partial x_q}\right) = \nu\frac{\partial^2 \omega_p}{\partial x_j \partial x_j} \qquad (4.19)$$

Inserting Eqs. 4.18 and 4.19 into Eq. 4.15 gives finally

$$\frac{d\omega_p}{dt} \equiv \frac{\partial \omega_p}{\partial t} + v_k \frac{\partial \omega_p}{\partial x_k} = \omega_k \frac{\partial v_p}{\partial x_k} + \nu\frac{\partial^2 \omega_p}{\partial x_j \partial x_j} \qquad (4.20)$$

We recognize the usual unsteady term, the convective term and the diffusive term. Furthermore, we have got rid of the pressure gradient term. That makes sense, because as mentioned in connection to Fig. 4.1, the pressure cannot affect the rotation (i.e. the vorticity) of a fluid particle since the pressure acts through its center. Equation 4.20 has a new term on the right-hand side which represents amplification and bending or tilting of the vorticity lines. If we write it term-by-term it reads

$$\omega_k \frac{\partial v_p}{\partial x_k} = \begin{cases} \omega_1 \dfrac{\partial v_1}{\partial x_1} & +\omega_2 \dfrac{\partial v_1}{\partial x_2} + \omega_3 \dfrac{\partial v_1}{\partial x_3}, & p=1 \\[2mm] \omega_1 \dfrac{\partial v_2}{\partial x_1} & +\omega_2 \dfrac{\partial v_2}{\partial x_2} + \omega_3 \dfrac{\partial v_2}{\partial x_3}, & p=2 \\[2mm] \omega_1 \dfrac{\partial v_3}{\partial x_1} & +\omega_2 \dfrac{\partial v_3}{\partial x_2} + \omega_3 \dfrac{\partial v_3}{\partial x_3}, & p=3 \end{cases} \qquad (4.21)$$

The diagonal terms in this matrix represent *vortex stretching*. Imagine a slender, cylindrical fluid particle with vorticity ω_i and introduce a cylindrical coordinate system with the x_1-axis as the cylinder axis and r_2 as the radial coordinate (see Fig. 4.2) so that $\omega_i = (\omega_1, 0, 0)$. We assume that a positive $\partial v_1/\partial x_1$ is acting on the fluid cylinder; it will act as a source in Eq. 4.20 increasing ω_1 and it will stretch the cylinder. The volume of the fluid element must stay constant during the stretching (the incompressible

Vortex stretching
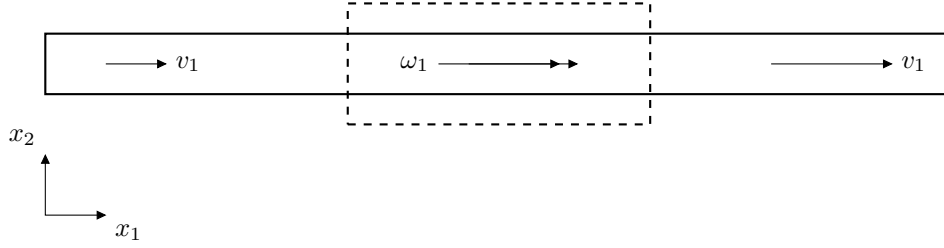
Figure 4.2: Vortex stretching. Dashed lines denote fluid element before stretching. $\dfrac{\partial v_1}{\partial x_1} > 0$.
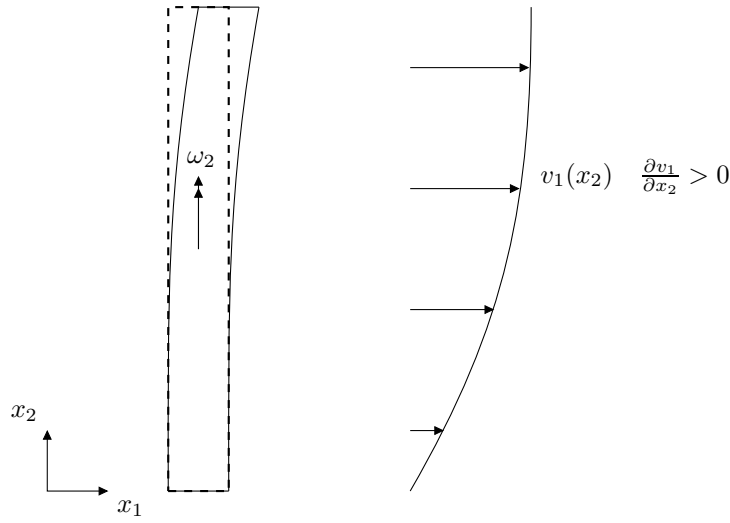
Figure 4.3: Vortex tilting. Dashed lines denote fluid element before bending or tilting.

continuity equation), which means that the radius of the cylinder will decrease. Hence vortex stretching will either make a fluid element longer and thinner (as in the example above) or shorter and thicker (when $\partial v_1/\partial x_1 < 0$).

The off-diagonal terms in Eq. 4.21 represent *vortex tilting*. Again, take a slender fluid particle, but this time with its axis aligned with the x_2 axis, see Fig. 4.3. Assume is has a vorticity, ω_2, and that the velocity surrounding velocity field is $v_1 = v_1(x_2)$. The velocity gradient $\partial v_1/\partial x_2$ will tilt the fluid particle so that it rotates in clock-wise direction. The second term $\omega_2 \partial v_1/\partial x_2$ in line one in Eq. 4.21 gives a contribution to ω_1. This means that vorticity in the x_2 direction, through the source term $\omega_2 \partial v_1/\partial x_2$, creates vorticity in the x_1 direction..

Vortex tilting

Vortex stretching and tilting are physical phenomena which act in three dimensions: fluid which initially is two dimensional becomes quickly three dimensional through these phenomena. Vorticity is useful when explaining why turbulence must be three-dimensional, see Section 5.4.

4.3 The vorticity transport equation in two dimensions

It is obvious that the vortex stretching/tilting has no influence in two dimensions; in this case the vortex stretching/tilting term vanishes because the vorticity vector is orthogonal to the velocity vector (for a 2D flow the velocity vector reads $v_i = (v_1, v_2, 0)$ and the vorticity vector reads $\omega_i = (0, 0, \omega_3)$ so that the scalar product is zero, i.e. $\omega_k \partial v_p / \partial x_k = 0$). Thus in two dimensions the vorticity equation reads

$$\frac{d\omega_3}{dt} = \nu \frac{\partial^2 \omega_3}{\partial x_\alpha \partial x_\alpha} \tag{4.22}$$

(Greek indices are used to indicate that they take values 1 or 2). This equation is exactly the same as the transport equation for temperature in incompressible flow, see Eq. 2.18. This means that vorticity is convected and diffused in the same way as temperature. In fully developed channel flow, for example, the vorticity and the temperature equations reduce to

$$0 = \nu \frac{\partial^2 \omega_3}{\partial x_2^2} \tag{4.23a}$$

$$0 = k \frac{\partial^2 T}{\partial x_2^2} \tag{4.23b}$$

For the temperature equation the heat flux is given by $q_2 = -k \partial T / \partial x_2$; with a hot lower wall and a cold upper wall (constant wall temperatures) the heat flux is constant for all x_2 and goes from the lower wall to the upper wall. We have the same situation for the vorticity. Its gradient, i.e. the vorticity flux, $\gamma_2 = -\nu \partial \omega_3 / \partial x_2$, is constant across the channel (you have plotted this quantity in TME226 Assignment 1). Equation 4.23 is turned into relations for q_2 and γ_2 by integration

$$\gamma_{wall} = \gamma_2 \tag{4.24a}$$

$$q_{wall} = q_2 \tag{4.24b}$$

If the wall-normal temperature derivative $\partial T / \partial x_2 = 0$ at both walls (*adiabatic walls*), the heat flux at the walls, q_{wall}, will be zero and the temperature will be equal to an arbitrary constant in the entire domain. It is only when the wall-normal temperature derivative at the walls are non-zero that a temperature field is created in the domain. The same is true for ω_3: if $\nu \partial \omega_3 / \partial x_2 = -\gamma_2 = 0$ at the walls, the flow will not include any vorticity. Hence, vorticity is – in the same way as temperature – generated at the walls.

4.3.1 Boundary layer thickness from the Rayleigh problem

In Section 3.1 we studied the Rayleigh problem (unsteady diffusion). As shown above, the two-dimensional unsteady temperature equation is identical to the two-dimensional unsteady equation for vorticity. The diffusion time, t, or the diffusion length, δ, in Eq. 3.14 can now be used to estimate the thickness of a developing boundary layer (recall that the limit between the boundary layer and the outer free-stream region can be defined by vorticity: inside the vorticity is non-zero and outside it is zero).

In a boundary layer, the streamwise pressure gradient is zero, see Eq. 3.42. This means that

$$\mu \frac{\partial^2 v_1}{\partial x_2^2}\bigg|_{wall} = 0$$
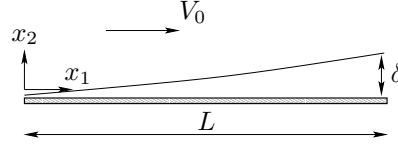
Figure 4.4: Boundary layer. The boundary layer thickness, δ, increases for increasing streamwise distance from leading edge ($x_1 = 0$).

because, at the wall, the only non-zero terms in the Navier-Stokes equation are the streamwise pressure gradient and the wall-normal diffusion term (see, for example, Eqs. 2.9 and 3.23). Hence, the flux of vorticity

$$\gamma_2 = -\nu \frac{\partial \omega_3}{\partial x_2}\bigg|_{wall} = \nu \frac{\partial^2 v_1}{\partial x_2^2}\bigg|_{wall} = 0 \qquad (4.25)$$

(recall that $(\partial v_2/\partial x_1)_{wall} = 0$) along the wall which means that no vorticity is created along the boundary. The vorticity in a developing boundary layer is created at the leading edge of the plate (note that in channel flow, vorticity is indeed created along the walls because in this case the streamwise pressure gradient is not zero). The vorticity generated at the leading edge is transported along the wall by convection and at the same time it is transported by diffusion away from the wall.

Below we will estimate the boundary layer thickness using the expression derived for the Rayleigh problem. In a boundary layer there is vorticity and outside the boundary layer it is zero (in the Rayleigh flow problem, the vorticity is created at time $t = 0^+$ when the plate instantaneously accelerates from rest to velocity V_0). Hence, if we can estimate how far from the wall the vorticity diffuses, this gives us an estimation of the boundary layer thickness.

Consider the boundary layer in Fig. 4.4. The boundary layer thickness at the end of the plate is $\delta(L)$. The time it takes for a fluid particle to travel from the leading edge of the plate to $x = L$ is L/V_0 (in the Rayleigh problem this corresponds to the flow field after time $t = L/V_0$). During this time vorticity will be transported by diffusion in the x_2 direction the length δ according to Eq. 3.14. If we assume that the fluid is air with the speed $V_0 = 3m/s$ and that the length of the plate $L = 2m$ we get from Eq. 3.14 that $\delta(L) = 1.2cm$.

Exercise 26 *Note that the estimate above is not quite accurate because in the Rayleigh problem we assumed that the convective terms are zero, but in a developing boundary layer, as in Fig. 4.4, they are not ($v_2 \neq 0$ and $\partial v_1/\partial x_1 \neq 0$). The proper way to solve the problem is to use Blasius solution, see Section 3.3. Blasius solution gives (see Eq. E.1)*

$$\frac{\delta}{L} = \frac{5}{Re_L^{1/2}}, \quad Re_L = \frac{V_0 L}{\nu} \qquad (4.26)$$

Compute what $\delta(L)$ you get from Eq. 4.26.

Exercise 27 *Assume that we have a developing flow in a pipe (radius R) or between two flat plates (separation distance h). We want to find out how long distance it takes for the the boundary layers to merge. Equation 3.14 can be used with $\delta = R$ or h. Make a comparison with this and Eq. 3.16.*

4.4   Potential flow

IN potential flow, the velocity vector can be expressed as the gradient of its potential Φ, see Eq. 1.22. The vorticity is then zero by definition since the curl of the divergence is zero. This is easily seen by inserting Eq. 1.22 ($v_i = \partial\Phi/\partial x_i$) into the definition of the vorticity, Eq. 1.12, i.e.

$$\omega_i = \epsilon_{ijk}\frac{\partial v_k}{\partial x_j} = \epsilon_{ijk}\frac{\partial^2\Phi}{\partial x_j\partial x_k} = 0 \tag{4.27}$$

since ϵ_{ijk} is anti-symmetric in indices j and k and $\partial^2\Phi/\partial x_j\partial x_k$ is symmetric in j and k. Inserting Eq. 1.22 into the continuity equation, Eq. 2.3, gives

$$0 = \frac{\partial v_i}{\partial x_i} = \frac{\partial}{\partial x_i}\left(\frac{\partial\Phi}{\partial x_i}\right) = \frac{\partial^2\Phi}{\partial x_i\partial x_i} \tag{4.28}$$

i.e. the potential satisfies the Laplace equation. This is of great important since many analytical methods exist for the Laplace equation.

4.4.1   The Bernoulli equation

The velocity field in potential flow is thus given by the continuity equation, Eq. 4.28 (together with Eq. 1.22). Do we have any use of the Navier-Stokes equation? The answer is yes: this equation provides the pressure field. We use the Navier-Stokes equation (Eq. 4.12) with the viscous term expressed as in Eq. 4.5

$$\frac{\partial v_i}{\partial t} + \frac{\partial k}{\partial x_i} - \varepsilon_{ijk}v_j\omega_k = -\frac{1}{\rho}\frac{\partial P}{\partial x_i} - \nu\varepsilon_{inm}\frac{\partial\omega_m}{\partial x_n} + f_i \tag{4.29}$$

Since $\omega_i = 0$ in potential (irrotational) flow, we get (with $f_i = g_i$) and using $k = v_iv_i/2 = v^2/2$

$$\frac{\partial}{\partial x_i}\left(\frac{\partial\Phi}{\partial x_i}\right) + \frac{1}{2}\frac{\partial v^2}{\partial x_i} = -\frac{1}{\rho}\frac{\partial P}{\partial x_i} + g_i \tag{4.30}$$

where v_i in the unsteady term was replaced by its potential (Eq. 1.22). The gravity force can be expressed as a force potential, $g_i = -\partial\mathcal{X}/\partial x_i$ (see Eq. 4.13), because it is *conservative*. The gravity force is conservative because when integrating this force, the work (i.e. the integral) depends only on the starting and ending points of the integral: in mathematics this is called an *exact* differential. **conservative force**

Inserting $g_i = -\partial\mathcal{X}/\partial x_i$ in Eq. 4.30 gives

$$\frac{\partial}{\partial x_i}\left(\frac{\partial\Phi}{\partial t} + \frac{v^2}{2} + \frac{P}{\rho} + \mathcal{X}\right) = 0 \tag{4.31}$$

Integration gives the famous Bernoulli equation

$$\frac{\partial\Phi}{\partial t} + \frac{v^2}{2} + \frac{P}{\rho} + \mathcal{X} = C(t) \tag{4.32}$$

where $\mathcal{X} = -g_ix_i$. In steady flow, we get

$$\frac{v^2}{2} + \frac{P}{\rho} - g_3x_3 = C \tag{4.33}$$

where $g_i = (0,0,g_3)$. Using the height, $gh = -g_3x_3$, we get the more familiar form

$$\frac{v^2}{2} + \frac{P}{\rho} + gh = C \tag{4.34}$$

4.4.2 Complex variables for potential solutions of plane flows

Complex analysis is a suitable tool for studying potential flow. We start this section by repeating some basics of complex analysis. For real functions, the value of a partial derivative, $\partial f/\partial x$, at $x = x_0$ is defined by making x approach x_0 and then evaluating $(f(x+x_0) - f(x))/x_0$. The total derivative, df/dt, is defined by approaching the point $x_{10}, x_{20}, x_{30}, t$ as a linear combination of all independent variables (cf. Eq. 1.1).

A complex derivative of a complex variable is defined as $(f(z + z_0) - f(z))/z_0$ where $z = x+iy$ and $f = u+iv$. We can approach the point z_0 both in the real coordinate direction, x, and in the imaginary coordinate direction, y. The complex derivative is defined only if the value of the derivative is independent of how we approach the point z_0. Hence

$$\frac{df}{dz} = \lim_{\Delta z \to 0} \frac{f(z_0 + \Delta z) - f(z_0)}{\Delta z}$$
$$= \lim_{\Delta x \to 0} \frac{f(x_0 + \Delta x, iy_0) - f(x_0, iy_0)}{\Delta x} = \lim_{\Delta y \to 0} \frac{f(x_0, iy_0 + i\Delta y) - f(x_0, iy_0)}{i\Delta y}.$$
(4.35)

The second line can be written as

$$\frac{\partial f}{\partial x} = \frac{1}{i}\frac{\partial f}{\partial y} = \frac{i}{i^2}\frac{\partial f}{\partial y} = -i\frac{\partial f}{\partial y} \tag{4.36}$$

since $i^2 = -1$. Inserting $f = u + iv$ and taking the partial derivative of f we get

$$\frac{\partial f}{\partial x} = \frac{\partial u}{\partial x} + i\frac{\partial v}{\partial x}$$
$$-i\frac{\partial f}{\partial y} = -i\frac{\partial u}{\partial y} - i^2\frac{\partial v}{\partial y} = -i\frac{\partial u}{\partial y} + \frac{\partial v}{\partial y}$$
(4.37)

Using Eq. 4.36 gives

$$\frac{\partial u}{\partial x} = \frac{\partial v}{\partial y}, \quad \frac{\partial u}{\partial y} = -\frac{\partial v}{\partial x} \tag{4.38}$$

Equations 4.38 are called the *Cauchy-Riemann* equations. Another way to derive Eq. 4.38 is to require that f should depend only on z but not on $\bar{z}$ [7] ($\bar{z}$ is the complex conjugate of z, i.e. $\bar{z} = x - iy$).

So far the complex plane has been expressed as $z = x+iy$. It can also be expressed in polar coordinates (see Fig. 4.5)

$$z = re^{i\theta} = r(\cos\theta + i\sin\theta) \tag{4.39}$$

Now we return to fluid mechanics and potential flow. Let us introduce a complex potential, f, based on the streamfunction, Ψ (Eq. 3.44), and the velocity potential, Φ (Eq. 1.22)

$$f = \Phi + i\Psi \tag{4.40}$$

Recall that for potential (i.e. inviscid, $\nu = 0$) two-dimensional, incompressible flow, the velocity potential satisfies the Laplace equation, see Eq. 4.28. The streamfunction also satisfies the Laplace equation in potential flow where the vorticity, ω_i, is zero. This is easily seen by taking the divergence of the streamfunction, Eq. 3.44

$$\frac{\partial^2 \Psi}{\partial x_1^2} + \frac{\partial^2 \Psi}{\partial x_2^2} = -\frac{\partial v_2}{\partial x_1} + \frac{\partial v_1}{\partial x_2} = -\omega_3 = 0 \tag{4.41}$$
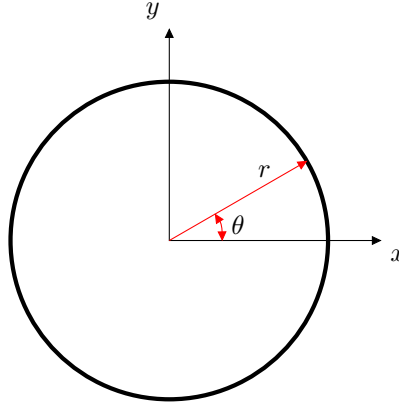
Figure 4.5: The complex plane in polar coordinates. Real and imaginary axes correspond to the horizontal and vertical axes, respectively.

see Eq. 1.13. Hence the complex potential, f, also satisfies the Laplace equation. Furthermore, f also satisfies the Cauchy-Riemann equations, Eq. 4.38, since

$$\frac{\partial \Phi}{\partial x} = \frac{\partial \Psi}{\partial y} = v_1 \quad \text{and} \quad \frac{\partial \Phi}{\partial y} = -\frac{\partial \Psi}{\partial x} = v_2 \tag{4.42}$$

see Eqs. 3.44 and 1.22. Thus we can conclude that f defined as in Eq. 4.40 is differentiable, i.e. df/dz exists. We have now defined a complex funtction, $f = \Phi + i\Psi$ which satisfies Laplace equation and which has a physical meaning in fluid dynamics.

4.4.3 $f \propto z^n$

Now we will give some examples of $f(z)$ which correspond to useful engineering flows. The procedure is as follows:

- assume that $f \propto z^n$ is complex potential

- verify that this is true (see, e.g, Eqs. 4.43-4.47)

- choose an n and find out what physical flow the complex potential describes

We can choose any exponent n in $f \propto z^n$ and multiply with any constant in order to get a physical, meaningful flow. The solution

$$f = C_1 z^n \tag{4.43}$$

is one example. Let's first verify that this is a solution of the Laplace equation (i.e. the continuity equation, 4.28 and thet the flow is inviscid, $\omega_3 = 0$, Eq. 4.41). We write it in polar coordinates

$$f = C_1 \left(r e^{i\theta} \right)^n = C_1 r^n e^{in\theta} = C_1 r^n (\cos(n\theta) + i \sin(n\theta)) \tag{4.44}$$

The Laplace operator in polar coordinates reads

$$\nabla^2 f = \frac{1}{r} \frac{\partial}{\partial r} \left(r \frac{\partial f}{\partial r} \right) + \frac{1}{r^2} \frac{\partial^2 f}{\partial \theta^2} \tag{4.45}$$
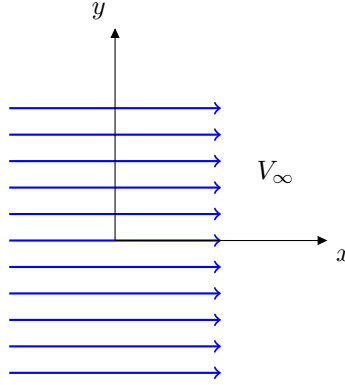
Figure 4.6: Parallel flow.

Taking the first and the second derivatives of Eq. 4.44 with respect to r and θ gives

$$
\begin{aligned}
\frac{\partial f}{\partial r} &= C_1 n r^{n-1}(\cos(n\theta) + i\sin(n\theta)) \\
\frac{1}{r}\frac{\partial}{\partial r}\left(r\frac{\partial f}{\partial r}\right) &= C_1 n^2 r^{n-2}(\cos(n\theta) + i\sin(n\theta)) \\
\frac{\partial f}{\partial \theta} &= C_1 n r^n(-\sin(n\theta) + i\cos(n\theta)) \\
\frac{\partial^2 f}{\partial \theta^2} &= -C_1 n^2 r^n(\cos(n\theta) + i\sin(n\theta))
\end{aligned}
\tag{4.46}
$$

When we divide the fourth line with r^2 and add it to the second line we find that the Laplace equation (Eq. 4.45) is indeed zero, i.e.

$$
\nabla^2 f = \frac{1}{r}\frac{\partial}{\partial r}\left(r\frac{\partial f}{\partial r}\right) + \frac{1}{r^2}\frac{\partial^2 f}{\partial \theta^2} = 0
\tag{4.47}
$$

4.4.3.1 *Parallel flow*

When we set $n = 1$ in Eq. 4.43 we get ($C_1 = V_\infty$)

$$
f = V_\infty z = V_\infty(x + iy)
\tag{4.48}
$$

The streamfunction, Ψ, is equal to the imaginary part, see Eq. 4.40. Equation 4.42 gives the velocity components

$$
v_1 = \frac{\partial \Psi}{\partial y} = V_\infty \quad \text{and} \quad v_2 = -\frac{\partial \Psi}{\partial x} = 0
\tag{4.49}
$$

The flow is shown in Fig. 4.6.

4.4.3.2 *Stagnation flow*

When we set $n = 2$ in Eqs. 4.43 and 4.44 we get (inviscid) stagnation flow onto a wall. The streamfunction, Ψ, corresponds to the imaginary part of f, see Eqs. 4.40 and 4.44, so that ($C_1 = 1$)

(a) Vector plot. (b) Streamlines. Colors represent Ψ.
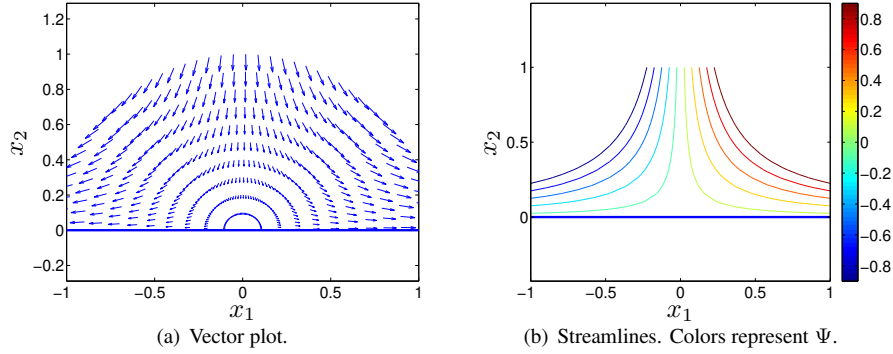
Figure 4.7: Potential flow. Stagnation flow.

$$\Psi = r^2 \sin(2\theta) \tag{4.50}$$

The solution in form of a vector plot and contour plot of the streamfunction is given in Fig. 4.7. The flow impinges at the wall at $x_2 = 0$. The streamfunction is zero along the symmetry line, $x_1 = 0$, and it is negative to the left and positive to the right. The polar velocity components are obtained as (see. Eq. 4.42)

$$
\begin{aligned}
v_r &= \frac{1}{r}\frac{\partial \Psi}{\partial \theta} = 2r\cos(2\theta) \\
v_\theta &= -\frac{\partial \Psi}{\partial r} = -2r\sin(2\theta)
\end{aligned}
\tag{4.51}
$$

and in Cartesian components (see Fig. 1.9)

$$
\begin{aligned}
v_1 &= v_r \cos\theta - v_\theta \sin\theta = 2r\cos\theta\cos(2\theta) + 2r\sin\theta\sin(2\theta) \\
&= 2r\cos\theta(1 - 2\sin^2\theta) + 4r\sin^2\theta cos\theta = 2r\cos\theta = 2x_1 \\
v_2 &= v_r \sin\theta + v_\theta \cos\theta = 2r\sin\theta\cos(2\theta) - 2r\cos\theta\sin(2\theta) \\
&= 2r\sin\theta(2\cos^2\theta - 1) - 4r\sin\theta\cos^2\theta = -2r\sin\theta = -2x_2
\end{aligned}
\tag{4.52}
$$

Recall that since the flow is inviscid (no friction), the boundary condition on the wall is slip, i.e. a frictionless wall (same as a symmetric boundary). Note that this flow is the same as we looked at in Section 1.2 except that the velocities are here twice as large because we chose $C_1 = 1$ (see Eq. 1.4).

Figure 4.7 was generated in Matlab by evaluating Eqs. 4.50, 4.51 and 4.52 on a polar grid.

4.4.3.3 *Flow over a wedge and flow in a concave corner*

Next we set $n = 6/5$ in Eqs. 4.43 and 4.44. This gives us (inviscid) flow over a wedge and flow over a concave corner (n should be in the interval $1 < n < 2$). The streamfunction, the imaginary part of f, is given by (Eqs. 4.40 and 4.44)

$$\Psi = r^{6/5}\sin(6\theta/5) \tag{4.53}$$

(a) Vector plot.

(b) Streamlines. Colors represent Ψ.
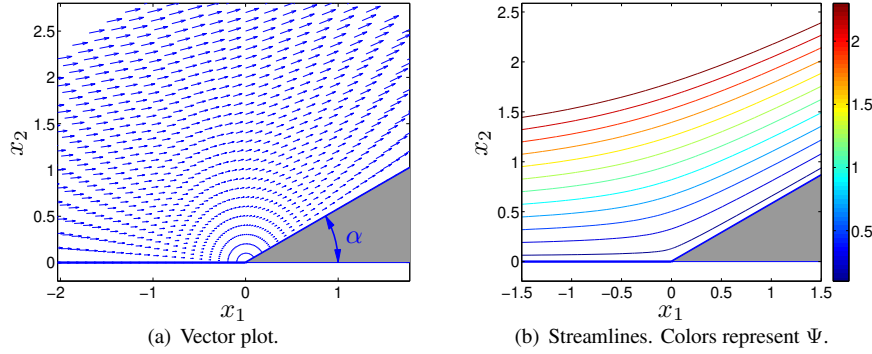
Figure 4.8: Potential flow. The lower boundary for $x_1 < 0$ can either be a wall (concave corner) or symmetry line (wedge).

($C_1 = 1$) and the velocity components read (see Fig. 4.51)

$$
\begin{aligned}
v_r &= \frac{1}{r}\frac{\partial \Psi}{\partial \theta} = \frac{6}{5} r \cos(6\theta/5) \\
v_\theta &= -\frac{\partial \Psi}{\partial r} = -\frac{6}{5} r \sin(6\theta/5)
\end{aligned}
\tag{4.54}
$$

The velocity vector field and the streamfunction are presented in Fig. 4.8. The stream-function is zero along the lower boundary. The angle, α, in Fig. 4.8a is given by

$$
\alpha = \frac{(n-1)\pi}{n} = \frac{\pi}{6}
\tag{4.55}
$$

4.4.4 Analytical solutions for a line source

The complex potential for a line source reads

$$
f = \frac{\dot{m}}{2\pi} \ln z
\tag{4.56}
$$

where $\dot{m}$ is the strength of the source; the physical meaning of $\dot{m}$ is volume flow assuming that the extent of the domain in the third coordinate direction, x_3, is one. Writing Eq. 4.56 on polar form gives

$$
f = \frac{\dot{m}}{2\pi} \ln\left(re^{i\theta}\right) = \frac{\dot{m}}{2\pi}\left(\ln r + \ln\left(e^{i\theta}\right)\right) = \frac{\dot{m}}{2\pi}\left(\ln r + i\theta\right)
\tag{4.57}
$$

First, we need to make sure that this solution satisfies the Laplace equation, Eq. 4.45. The first and second derivatives read

$$
\begin{aligned}
\frac{\partial f}{\partial r} &= \frac{\dot{m}}{2\pi r} \\
\frac{1}{r}\frac{\partial}{\partial r}\left(r\frac{\partial f}{\partial r}\right) &= 0 \\
\frac{\partial f}{\partial \theta} &= i\frac{\dot{m}}{2\pi} \\
\frac{\partial^2 f}{\partial \theta^2} &= 0
\end{aligned}
\tag{4.58}
$$
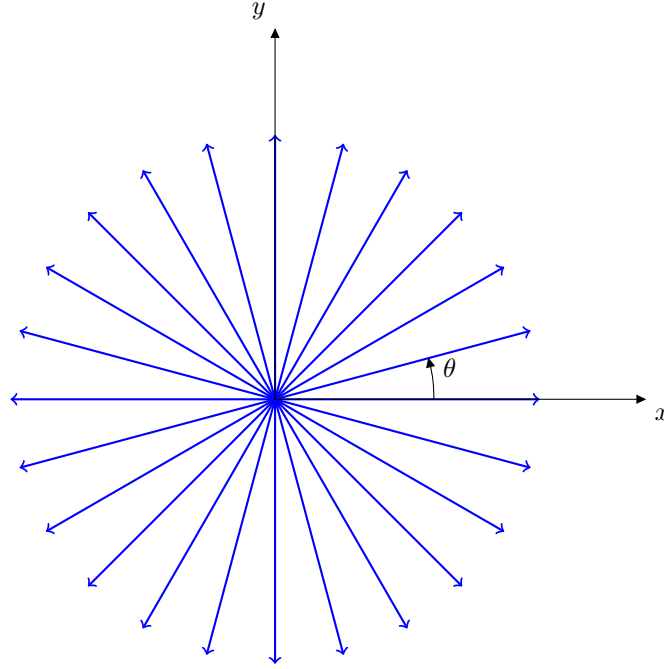
Figure 4.9: Line source. $\dot{m} > 0$

which shows that Eq. 4.47 is satisfied.

The streamfunction corresponds to the imaginary part of f and we get (see Eq. 4.51)

$$v_r = \frac{1}{r}\frac{\partial \Psi}{\partial \theta} = \frac{\dot{m}}{2\pi r}$$
$$v_\theta = -\frac{\partial \Psi}{\partial r} = 0 \tag{4.59}$$

We find that the physical flow is in the radial direction, see Fig. 4.9. If $\dot{m} > 0$, the flow is outwards directed and for $\dot{m} < 0$ it is going inwards toward origo. When origo is approached, the velocity, v_r, tends to infinity. Hence, Eq. 4.59 gives nonphysical flow near origo. The reason is that the inviscid assumption (zero viscosity) is not valid in this region.

It was mentioned above that the physical meaning of $\dot{m}$ is volume flow. This is easily seen by integrating v_r (Eq. 4.59) over a cylindrical surface as

$$\int_0^1 dx_3 \int_0^{2\pi} v_r r d\theta = \int_0^1 dx_3 \int_0^{2\pi} \frac{\dot{m}}{2\pi r} r d\theta = \frac{\dot{m}}{2\pi}\int_0^1 \int_0^{2\pi} dx_3 d\theta = \dot{m}. \tag{4.60}$$

4.4.5 Analytical solutions for a vortex line

A line vortex is another example of a complex potential; it is very similar to Eq. 4.56 and reads

$$f = -i\frac{\Gamma}{2\pi}\ln z \tag{4.61}$$

which on polar form reads (cf. Eq. 4.57)

$$f = -\frac{\Gamma}{2\pi}\left(i\ln r - \theta\right) \tag{4.62}$$
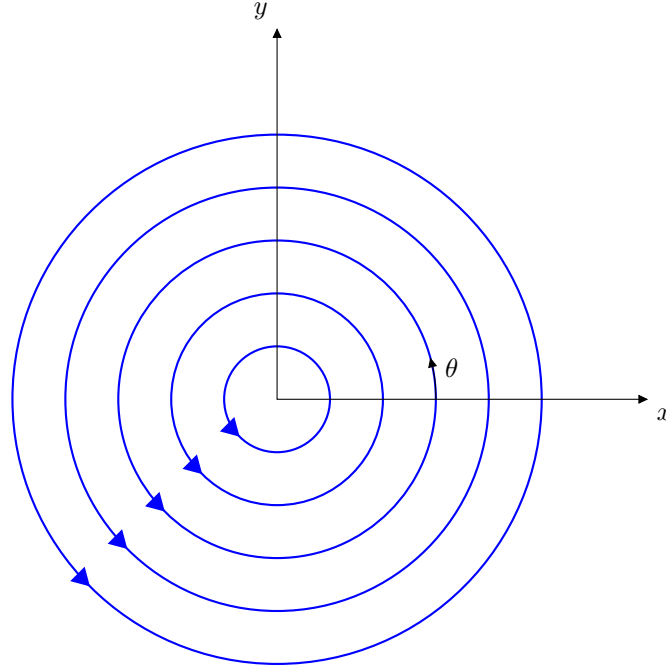
Figure 4.10: Vortex line.

From the streamfunction (the imaginary part of f) we get (cf. Eq. 4.59)

$$v_r = \frac{1}{r}\frac{\partial \Psi}{\partial \theta} = 0$$
$$v_\theta = -\frac{\partial \Psi}{\partial r} = \frac{\Gamma}{2\pi r}$$

$$(4.63)$$

This flow was introduced in Section 1.7.1 (where we called it an ideal vortex line) as an example of a flow with no vorticity. The flow is in the positive θ direction along lines of constant radius, see Fig. 4.10. The circulation, Γ, appears in the expression of v_θ. It was introduced in Section 1.7. It is defined as a closed line integral along line C, see Eq. 1.23 and can be expressed as an integral of the vorticity over surface S bounded by line C, see Eq. 1.25 and Fig. 1.7.

4.4.6 Analytical solutions for flow around a cylinder

The complex potential for the flow around a cylinder can be found by combining a doublet and a parallel flow. A doublet consists of a line source (strength $\dot{m}$) and sink (strength $-\dot{m}$) separated by a distance ε in the x_1 direction (line sources were introduced in Section 4.4.4). Imagine that we move the source and the sink closer to each other and at the same time we increase their strength $|\dot{m}|$ so that the product $\mu = \dot{m}\varepsilon$ stays constant. The resulting complex potential is

$$f = \frac{\mu}{\pi z}$$

$$(4.64)$$

When adding the complex potential of parallel flow, see Eq. 4.48, we get
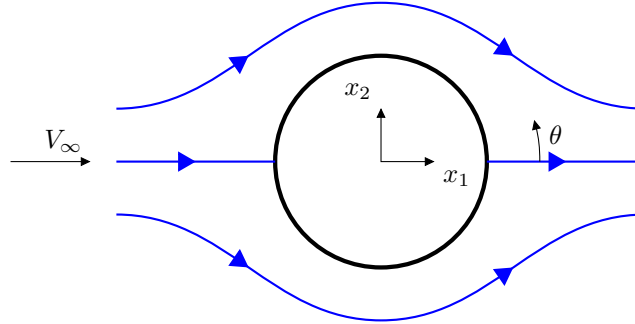
Figure 4.11: Flow around a cylinder of radius r_0.
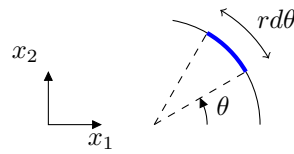
Figure 4.12: Flow around a cylinder of radius r_0. Integration of surface pressure.

(a) CFD of unsteady laminar flow [8]. The markers show the time-averaged location of separation.

(b) Potential flow, Eq. 4.73
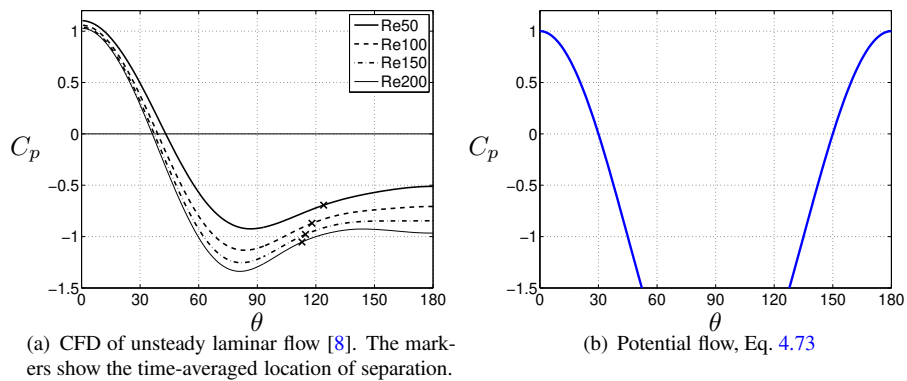
Figure 4.13: Pressure coefficients.

$$f = \frac{\mu}{\pi z} + V_\infty z \tag{4.65}$$

Now we define the radius of a cylinder, r_0, as

$$r_0^2 = \mu/(\pi V_\infty) \tag{4.66}$$

so that

$$f = \frac{V_\infty r_0^2}{z} + V_\infty z \tag{4.67}$$

On polar form it reads

$$\begin{aligned}
f &= \frac{V_\infty r_0^2}{re^{i\theta}} + V_\infty re^{i\theta} = V_\infty \left(\frac{r_0^2}{r} e^{-i\theta} + re^{i\theta} \right) \\
&= V_\infty \left(\frac{r_0^2}{r}(\cos\theta - i\sin\theta) + r(\cos\theta + i\sin\theta) \right)
\end{aligned} \tag{4.68}$$

The streamfunction reads (imaginary part)

$$\Psi = V_\infty \left(r - \frac{r_0^2}{r} \right) \sin\theta \tag{4.69}$$

Now we can compute the velocity components (see Eq. 4.51)

$$\begin{aligned}
v_r &= \frac{1}{r}\frac{\partial\Psi}{\partial\theta} = V_\infty \left(1 - \frac{r_0^2}{r^2} \right) \cos\theta \\
v_\theta &= -\frac{\partial\Psi}{\partial r} = -V_\infty \left(1 + \frac{r_0^2}{r^2} \right) \sin\theta
\end{aligned} \tag{4.70}$$

We find that $v_r = 0$ for $r = r_0$ as intended (thanks to the definition in Eq. 4.66). We are not interested in the solution inside the cylinder ($r < r_0$). Furthermore, we see that the tangential velocity is zero at $\theta = 0$ and π; hence these points correspond to the stagnation points, see Fig. 4.11. The velocity field at the cylinder surface, $r = r_0$, reads

$$\begin{aligned}
v_{r,s} &= 0 \\
v_{\theta,s} &= -2V_\infty \sin\theta
\end{aligned} \tag{4.71}$$

where index s denotes surface. Note that the local velocity gets twice as large as the freestream velocity at the top ($\theta = \pi/2$) and the bottom ($\theta = -\pi/2$) of the cylinder. The surface pressure is obtained from Bernoulli equation (see Eq. 4.34)

$$\frac{V_\infty^2}{2} + \frac{P_\infty}{\rho} = \frac{v_{\theta,s}^2}{2} + \frac{p_s}{\rho} \Rightarrow p_s = P_\infty + \rho\frac{V_\infty^2 - v_{\theta,s}^2}{2} \tag{4.72}$$

where we neglected the gravitation term. The surface pressure is usually expressed as a pressure coefficient

$$C_p \equiv \frac{p_s - P_\infty}{\rho V_\infty^2/2} = 1 - \frac{v_{\theta,s}^2}{V_\infty^2} = 1 - 4\sin^2\theta \tag{4.73}$$

using Eq. 4.71.

It should be stressed that although Eqs. 4.71 and 4.73 are exact they are not realistic because of the strict requirement that the flow should be inviscid. This requirement is

valid neither in the boundary layers nor in the wake; the boundary layers may be thin but the wake is a large part of the domain. Figure 4.13 presents the pressure coefficient for potential flow and accurate unsteady CFD of two-dimensional viscous flow [8] (the Reynolds number is sufficiently low for the flow to be laminar); Eqs. 2.3 and 2.9 are solved numerically [8]. The potential solution agrees rather well with viscous flow up to $\theta \simeq 20^o$.

How do we find the lift and drag force? The only force (per unit area) that acts on the cylinder surface is the pressure (in viscous flow there would also be a viscous stress, but it is usually much smaller). To find the lift force, F_L, we simply integrate the pressure over the surface. Usually the lift force is expressed as a lift coefficient, C_L, which is scaled with the dynamic pressure $\rho V_\infty^2/2$. The lift coefficient is obtained as

$$
\begin{aligned}
C_L = \frac{F_L}{\rho V_\infty^2/2} &= -\int_0^1 dx_3 \int_0^{2\pi} \frac{p_s}{\rho V_\infty^2/2} \sin\theta r_0 d\theta \\
&= -r_0 \int_0^1 dx_3 \int_0^{2\pi} (1 - 4\sin^2\theta)\sin\theta d\theta \\
&= -r_0 \left[-\cos\theta - 4\left(\frac{1}{12}\cos(3\theta) - \frac{3}{4}\cos\theta\right) \right]_0^{2\pi} = 0
\end{aligned}
$$
(4.74)

The $\sin\theta$ on the first line appears because we project the pressure force in the vertical direction (see Fig. 4.12) and minus sign is because pressure acts inwards, see Eq. 1.9 and Fig. 4.1. We assume in Eq. 4.74 that the length of the cylinder in the x_3 direction is one. The drag coefficient is computed as

$$
\begin{aligned}
C_D = \frac{F_D}{\rho V_\infty^2/2} &= -\int_0^1 dx_3 \int_0^{2\pi} (1 - 4\sin^2\theta)\cos\theta r_0 d\theta \\
&= -r_0 \int_0^1 dx_3 \int_0^{2\pi} \left[\sin\theta - \frac{4}{3}\sin^3\theta\right]_0^{2\pi} = 0
\end{aligned}
$$
(4.75)

The $\cos\theta$ on the first line appears because we project the pressure force in the horizontal direction (see Fig. 4.12). Equations 4.74 and 4.75 give $C_L = C_D = 0$; hence we find that inviscid flow around a cylinder creates neither lift nor drag. The reason is that the pressure is symmetric both with respect to $x_1 = 0$ and $x_2 = 0$. The lift force on the lower surface side cancels the force on the upper side. Same argument for the drag force: the pressure force on the upstream surface cancels that on the downstream surface.

4.4.7 Analytical solutions for flow around a cylinder with circulation

We will now introduce a second example of potential flow around cylinders, which is by far the most important one from engineering point of view. Here we will introduce the use of additional circulation which alters the locations of the stagnation points and creates lift. This approach is used in potential methods for predicting flow around airfoils in aeronautics (mainly helicopters) and windpower engineering.

We add the complex potential of a vortex line (see Eq. 4.61) to Eq. 4.67 so that

$$
f = \frac{V_\infty r_0^2}{z} + V_\infty z - i\frac{\Gamma}{2\pi}\ln z
$$
(4.76)
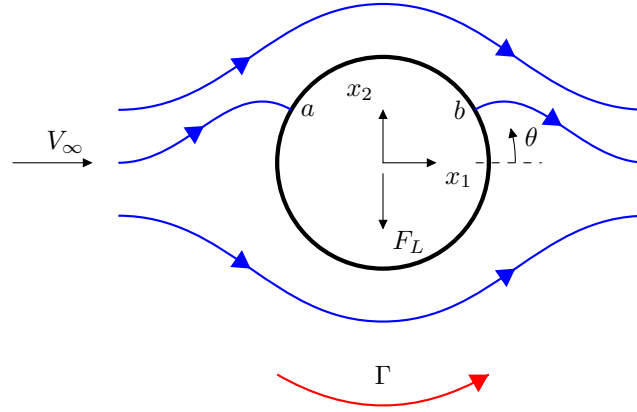
Figure 4.14: Flow around a cylinder of radius r_0 with additional circulation which give a (negative) lift force, see Eq. 4.85.
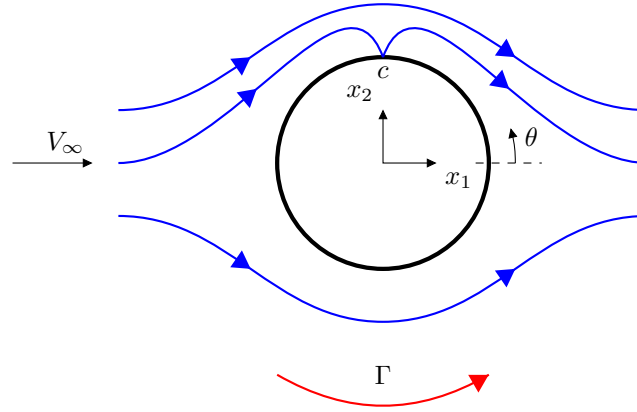
Figure 4.15: Flow around a cylinder of radius r_0 with maximal additional circulation.

On polar form it reads (see Eqs. 4.62 and 4.68)

$$f = V_\infty \left(\frac{r_0^2}{r}(\cos\theta - i\sin\theta) + r(\cos\theta + i\sin\theta) \right) - \frac{\Gamma}{2\pi}(i\ln r - \theta) \qquad (4.77)$$

The imaginary part gives the streamfunction

$$\Psi = V_\infty \left(r - \frac{r_0^2}{r} \right) \sin\theta - \frac{\Gamma}{2\pi}\ln r \qquad (4.78)$$

We get the velocity components as (see Eqs. 4.63 and 4.70)

$$v_r = \frac{1}{r}\frac{\partial\Psi}{\partial\theta} = V_\infty \left(1 - \frac{r_0^2}{r^2} \right)\cos\theta$$

$$v_\theta = -\frac{\partial\Psi}{\partial r} = -V_\infty \left(1 + \frac{r_0^2}{r^2} \right)\sin\theta + \frac{\Gamma}{2\pi r} \qquad (4.79)$$

The effect of the added vortex line is, as expected, to increase v_θ while leaving v_r unaffected. The larger the circulation, the larger v_θ.

The velocity at the surface, $r = r_0$, reads

$$v_{r,s} = 0$$
$$v_{\theta,s} = -2V_\infty \sin\theta + \frac{\Gamma}{2\pi r_0} \tag{4.80}$$

Now let's find the location of the stagnation points, i.e. where $v_{\theta,s} = 0$. Equation 4.80 gives

$$2V_\infty \sin\theta_{stag} = \frac{\Gamma}{2\pi r_0} \Rightarrow \theta_{stag} = \arcsin\left(\frac{\Gamma}{4\pi r_0 V_\infty}\right) \tag{4.81}$$

The two angles that satisfy this equation are located in the the first and second quadrants. The two positions are indicated with a and b in Fig. 4.14. For a limiting value of the circulation, Γ_{max}, the two locations s and b will merge at $\theta = \pi/2$, denoted with c in Fig. 4.15,

$$\Gamma_{max} = 4\pi V_\infty r_0. \tag{4.82}$$

This corresponds to the maximum value of the circulation for which there is a stagnation point on the cylinder surface. For circulation larger than Γ_{max}, the stagnation point will be located above the cylinder.

The pressure is obtained from Bernoulli equation as (see Eq. 4.73)

$$C_p = 1 - \frac{v_{\theta,s}^2}{V_\infty^2} = 1 - \left(-2\sin\theta + \frac{\Gamma}{2\pi r_0 V_\infty}\right)^2$$
$$= 1 - 4\sin^2\theta + \frac{4\Gamma\sin\theta}{2\pi r_0 V_\infty} - \left(\frac{\Gamma}{2\pi r_0 V_\infty}\right)^2 \tag{4.83}$$

We found in Section 4.4.6 that a cylinder without circulation gives neither drag nor lift, see Eqs. 4.74 and 4.75. What about the present case? Let's compute the lift. We found in Eq. 4.74 that the two first terms in Eq. 4.83 give no contribution to the lift. The last term cannot give any contribution to the lift because it is constant on the entire surface. Hence we only need to include the third term in Eq. 4.83 so that

$$C_L = \frac{F_L}{\rho V_\infty^2/2} = -\int_0^1 dx_3 \int_0^{2\pi} \frac{p_s}{\rho V_\infty^2/2} \sin\theta r_0 d\theta$$
$$= -r_0 \int_0^1 dx_3 \int_0^{2\pi} \frac{2\Gamma\sin\theta}{\pi r_0 V_\infty} \sin\theta d\theta \tag{4.84}$$
$$= -\left[\frac{\Gamma\theta}{\pi V_\infty} - \frac{\Gamma}{2\pi V_\infty}\sin(2\theta)\right]_0^{2\pi} = -\frac{2\Gamma}{V_\infty}$$

We find that the lift force on a unit length of the cylinder can be computed from the circulation as

$$F_L = -\rho V_\infty \Gamma \tag{4.85}$$

This relation is valid for any body and it is called the *Kutta-Joukowski* law who – independent of each other – formulated it. The reason to the sign of the lift force can easily be seen from Fig. 4.14. The stagnation points, where the pressure is largest, are located at the top of the cylinder and hence the pressure is higher on the top than on the bottom. The "lift" force is acting downwards, i.e. in the negative x_2 direction.
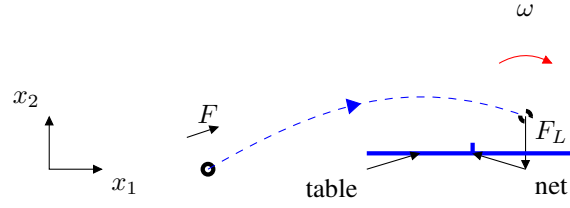
Figure 4.16: Table tennis. The loop uses the Magnus effect. Side view.
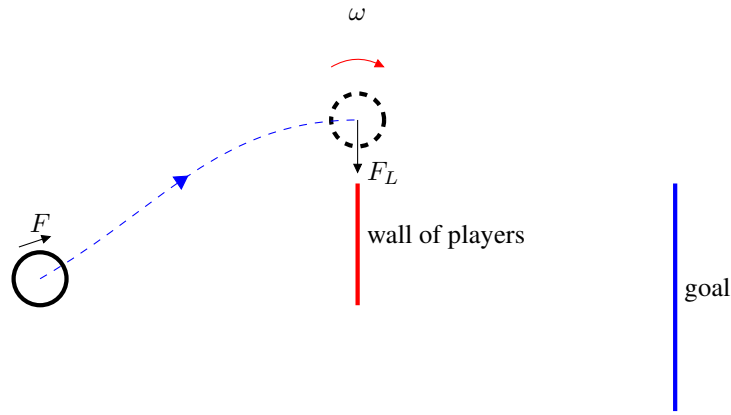
Figure 4.17: Football. A free-kick uses the Magnus effect. Top view
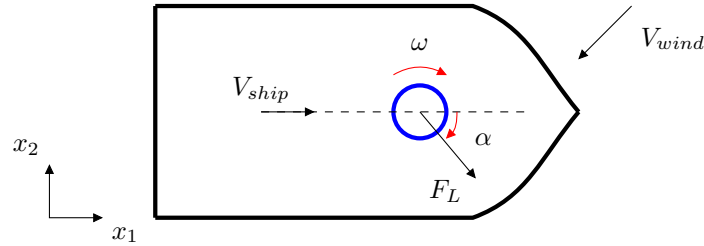
Figure 4.18: Flettner rotor (in blue) on a ship. The relative velocity between the ship and the wind is $V_{wind} + V_{ship}$. The ship moves with speed V_{ship}. Top view.

The drag is, however, still zero. In Eq. 4.75 we found that the first and the second terms in Eq. 4.83 gives no contribution to drag. Hence, we only need to consider the third terms. In the drag integral (see Eq. 4.75), this term in Eq. 4.83 gives rise to a term proportional to $\sin\theta\cos\theta$ whose contribution is zero. Hence, the additional circulation does not give rise to any drag.

4.4.7.1 *The Magnus effect*

Circulation around a cylinder is very similar to a rotating cylinder. Instead of adding a circulation, we let the cylinder rotate with speed ω. A rotating cylinder produces lift. This has interesting application in sports, for example football, table tennis and golf.

In table tennis, the ball must hit the table on the side of the opponent. One way to improve the chance that this will happen is to make a loop. This means that you hit the

ball slightly on the top. The ball experiences a force, F, when you hit it (see Fig. 4.16) and this force makes it rotate with rotation speed ω (clockwise direction). The rotation causes a lift, F_L, which acts downwards so that the ball drops down quickly and (hopefully) hits the table on the other side of the net. The lift force is downwards because the stagnation points are located on the upper surface. Recall that the relative velocity of the air is in the negative x_1 direction.

Another example where the Magnus effect is important is golf. Here the object is often vice versa. You want the ball to go as far as possible. Hence you hit it with a slice so that it spins with a positive ω (counter-clockwise). The result is a lift force in the positive x_2 direction which makes the ball go further.

A final sports example is football. Here the lift is used sideways. Imagine there is a free-kick rather close to the opponents' goal, see Fig. 4.17. The opponents erects a wall of players between the goal and the location of the free-kick. The player who makes the free-kick wants to make the ball go on the left side of the wall; after the wall of players, the ball should turn right towards the goal. The Magnus effect helps to achieve this. The player hits the ball with her/his left foot on the left side of the ball which creates a force F on the ball. This makes the ball rotate clockwise, see Fig. 4.17, and creates a lift force so that the ball after it has passed the wall turns to the right towards the goal. The reason that the ball turns to the right first after the wall (and not before) is that the forward momentum created by F (the player) is much larger than F_L.

If you are interested in football you may be pleased to learn that by use of fluid dynamics it is now scientifically proven that it was much harder to make a good freekick in 2010 worldcup than in 2014 [9]. Figure 7b in that paper is particularly interesting.

> As an experiment, two identical freekicks are made with the football used at the 2013 FIFA Confederations. The freekicks are made 25m from the goal. The initial velocity of the football is 30 m/s. The result of the two freekicks is that the two footballs reach the goal three meters from each other in the vertical direction. Why? Because the ball was rotated 45 degrees before the second freekick (see Figs. 2c,d) in [9].

Finally we give an engineering example of the use of the Magnus effect. The first Flettner rotors on ships were produced in 1924. It has recently gained new interest as the cost of fuel is rising. A Flettner rotor is a rotating cylinder (or many) on a ship, see Fig. 4.18. The diameter of this rotor can be a couple of meter and have a length (i.e. height) of $10 - 20$ meter. The ship is moving to the right with speed V_{ship}. The wind comes towards the ship from the left-front (relative wind at an angle of $\pi/4$). The Flettner rotor rotates in the clockwise direction. The Magnus effect creates a force in the orthogonal direction to the relative windspeed, i.e. at an angle of $-\pi/4$. Note that if the wind comes from the right instead of from the left, the rotor should rotate in the counter-clockwise direction. The additional propulsion force is $F_L \cos(\alpha)$. The Division of Fluid Dynamics recently took part in an EU project where we studied the flow around rotating cylinders in relation to Flettner rotors [10].

4.4.8 The flow around an airfoil

Flow around airfoils is a good example where potential methods are useful. These methods are still in use in wind engineering and for helicopters. At the Division of Fluid Dynamics we have an on-going PhD project where we use potential methods for computing the aerodynamic loads for windturbine rotorblades [11].
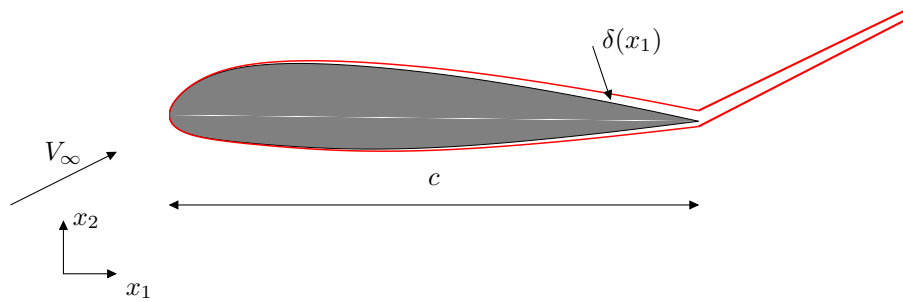
Figure 4.19: Airfoil. The boundary layers, $\delta(x_1)$, and the wake illustrated in red. $x_1 = 0$ and $x_1 = c$ at leading and trailing edge, respectively.
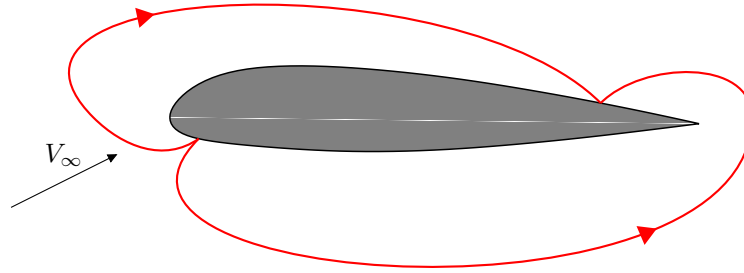
Figure 4.20: Airfoil. Streamlines from potential flow. Rear stagnation point at the upper surface (suction side).

The flow around airfoils is a good example where the flow can be treated as inviscid in large part of the flow. For low angles of attack (which is the case for, for example, an aircraft in cruise conditions) the boundary layers and the wake are thin. Outside these regions the flow is essentially inviscid.

Figure 4.19 (see also Fig. 16.1) shows a two-dimensional airfoil. The boundary layers and the wake are illustrated in red. The boundary layer is thinner on the pressure (lower) side than on the suction (upper) side. It grows slightly thicker towards the trailing edge (denoted by $\delta(x_1)$ in Fig. 4.19). When this flow is computed using potential methods, the location of the front stagnation point is reasonably well captured, see Fig. 4.20. However, the stagnation point near the trailing edge is located on the suction side which is clearly nonphysical. The flow on the pressure (lower) side cannot be expected to make a 180° turn at the trailing edge and then go in the negative x_1 direction towards the stagnation point located on the suction side.

The solution is to move the stagnation points in the same way as we did for the cylinder flow in Section 4.4.7. We want to move the rear stagnation point towards the trailing edge. This is achieved by adding a circulation in the clockwise direction, see Fig. 4.21. The magnitude of the circulation is determined by the requirement that
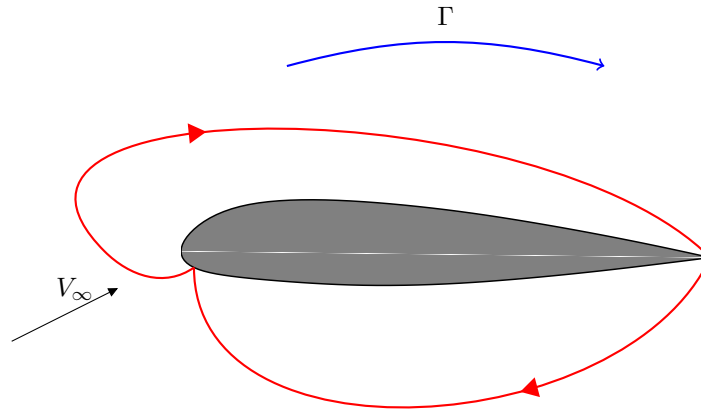
Figure 4.21: Airfoil. Streamlines from potential flow with added circulation. Rear stagnation point at the trailing edge.

the stagnation point should be located at the trailing edge. This is called the *Kutta condition*. The added circulation is negative (clockwise). In aeronautics, the sign of circulation is usually changed so that $\Gamma_{aeronautic} = -\Gamma$. The lift of a two-dimensional airfoil (or a two-dimensional section of a three-dimensional airfoil) is then computed as (see Eq. 4.85)

$$F_L = \rho V_\infty \Gamma_{aeronautic} \tag{4.86}$$

5 Turbulence

5.1 Introduction

ALMOST all fluid flow which we encounter in daily life is turbulent. Typical examples are flow around (as well as *in*) cars, aeroplanes and buildings. The boundary layers and the wakes around and after bluff bodies such as cars, aeroplanes and buildings are turbulent. Also the flow and combustion in engines, both in piston engines and gas turbines and combustors, are highly turbulent. Air movements in rooms are turbulent, at least along the walls where wall-jets are formed. Hence, when we compute fluid flow it will most likely be turbulent. In turbulent flow we usually divide the velocities in one time-averaged part $\bar{v}_i$, which is independent of time (when the mean flow is steady), and one fluctuating part v_i' so that $v_i = \bar{v}_i + v_i'$.

There is no definition on turbulent flow, but it has a number of characteristic features (see Pope [12] and Tennekes & Lumley [13]) such as:

I. Irregularity. Turbulent flow is irregular and chaotic (they may seem random, but they are governed by Navier-Stokes equation, Eq. 2.9). The flow consists of a spectrum of different scales (eddy sizes). We do not have any exact definition of an *turbulent eddy*, but we suppose that it exists in a certain region in space for a certain time and that it is subsequently destroyed (by the cascade process or by dissipation, see below). It has a characteristic velocity and length (called a velocity and length scale). The region covered by a large eddy may well enclose also smaller eddies. The largest eddies are of the order of the flow geometry (i.e. boundary layer thickness, jet width, etc). At the other end of the spectrum we have the smallest eddies which are dissipated by viscous forces (stresses) into thermal energy resulting in a temperature increase. Even though turbulence is chaotic it is deterministic and is described by the Navier-Stokes equations. **turbulent eddy**

II. Diffusivity. In turbulent flow the diffusivity increases. The turbulence increases the exchange of momentum in e.g. boundary layers, and reduces or delays thereby separation at bluff bodies such as cylinders, airfoils and cars. The increased diffusivity also increases the resistance (wall friction) and heat transfer in internal flows such as in channels and pipes.

III. Large Reynolds Numbers. Turbulent flow occurs at high Reynolds number. For example, the transition to turbulent flow in pipes occurs that $Re_D \simeq 2300$, and in boundary layers at $Re_x \simeq 500\,000$.

IV. Three-Dimensional. Turbulent flow is always three-dimensional and unsteady. However, when the equations are time averaged, we can treat the flow as two-dimensional (if the geometry is two-dimensional).

V. Dissipation. Turbulent flow is dissipative, which means that kinetic energy in the small (dissipative) eddies are transformed into thermal energy. The small eddies receive the kinetic energy from slightly larger eddies. The slightly larger eddies receive their energy from even larger eddies and so on. The largest eddies extract their energy from the mean flow. This process of transferring energy from the largest turbulent scales (eddies) to the smallest is called the *cascade process*, see Fig. Q.5. **cascade process**

VI. Continuum. Even though we have small turbulent scales in the flow they are much larger than the molecular scale and we can treat the flow as a continuum.

flow of kinetic energy
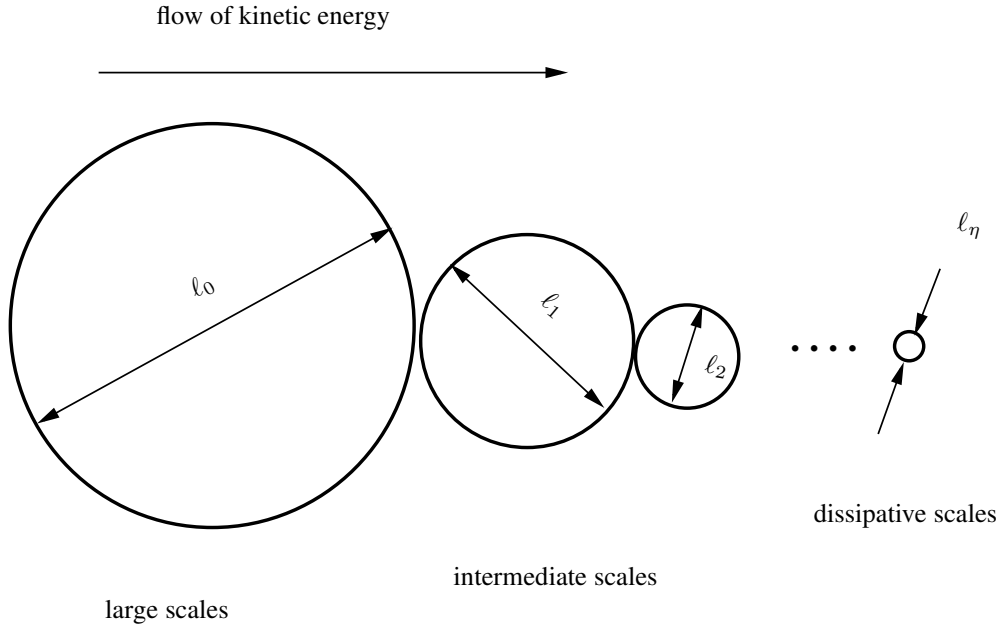
Figure 5.1: Cascade process with a spectrum of eddies. The energy-containing eddies are denoted by v_0; ℓ_1 and ℓ_2 denotes the size of the eddies in the inertial subrange such that $\ell_2 < \ell_1 < \ell_0$; ℓ_η is the size of the dissipative eddies.

5.2 Turbulent scales

The largest scales are of the order of the flow geometry (the boundary layer thickness, for example), with length scale ℓ_0 and velocity scale v_0. These scales extract kinetic energy from the mean flow which has a time scale comparable to the large scales, i.e.

$$\frac{\partial \bar{v}_1}{\partial x_2} \sim t_0^{-1} \sim v_0/\ell_0 \tag{5.1}$$

Part of the kinetic energy of the large scales is lost to slightly smaller scales with which the large scales interact. Through the *cascade process*, kinetic energy is in this way transferred from the largest scale to the smallest scales. At the smallest scales the frictional forces (viscous stresses) become large and the kinetic energy is transformed (dissipated) into thermal energy. The kinetic energy transferred per unit time from eddy-to-eddy (from an eddy to a slightly smaller eddy) is the same for each eddy size.

The dissipation is denoted by ε which is energy per unit time and unit mass ($\varepsilon = [m^2/s^3]$). The dissipation is proportional to the kinematic viscosity, ν, times the fluctuating velocity gradient up to the power of two (see Section 8.2). The friction forces exist of course at all scales, but they are largest at the smallest eddies. In reality a small fraction is dissipated at all scales. However it is assumed that most of the energy that goes into the large scales per unit time (say 90%) is finally dissipated at the smallest (dissipative) scales.

The smallest scales where dissipation occurs are called the Kolmogorov scales whose velocity scale is denoted by v_η, length scale by ℓ_η and time scale by τ_η. We assume that these scales are determined by viscosity, ν, and dissipation, ε. The argument is as follows.

viscosity: Since the kinetic energy is destroyed by viscous forces it is natural to assume that viscosity plays a part in determining these scales; the larger viscosity, the larger scales.

dissipation: The amount of energy per unit time that is to be dissipated is ε. The more energy that is to be transformed from kinetic energy to thermal energy, the larger the velocity gradients must be.

Having assumed that the dissipative scales are determined by viscosity and dissipation, we can express v_η, ℓ_η and τ_η in ν and ε using dimensional analysis. We write

$$
\begin{array}{ccc}
v_\eta & = & \nu^a \quad \varepsilon^b \\
[m/s] & = & [m^2/s] \quad [m^2/s^3]
\end{array}
\tag{5.2}
$$

where below each variable its dimensions are given. The dimensions of the left and the right side must be the same. We get two equations, one for meters $[m]$

$$
1 = 2a + 2b,
\tag{5.3}
$$

and one for seconds $[s]$

$$
-1 = -a - 3b,
\tag{5.4}
$$

which give $a = b = 1/4$. In the same way we obtain the expressions for ℓ_η and τ_η so that

$$
v_\eta = (\nu\varepsilon)^{1/4} \,, \; \ell_\eta = \left(\frac{\nu^3}{\varepsilon}\right)^{1/4} \,, \; \tau_\eta = \left(\frac{\nu}{\varepsilon}\right)^{1/2}
\tag{5.5}
$$

5.3 Energy spectrum

As mentioned above, the turbulence fluctuations are composed of a wide range of scales. We can think of them as eddies, see Fig. 5.1. It turns out that it is often convenient to use Fourier series to analyze turbulence. In general, any periodic function, g, with a period of $2L$ (i.e. $g(x) = g(x + 2L)$), can be expressed as a Fourier series, i.e.

$$
g(x) = \frac{1}{2}a_0 + \sum_{n=1}^{\infty}(a_n \cos(\kappa_n x) + b_n \sin(\kappa_n x))
\tag{5.6}
$$

where x is a spatial coordinate and

$$
\kappa_n = \frac{n\pi}{L} \quad \text{or} \quad \kappa = \frac{2\pi}{L}.
\tag{5.7}
$$

κ_n is called the wavenumber. The Fourier coefficients are given by

$$
a_n = \frac{1}{L}\int_{-L}^{L} g(x)\cos(\kappa_n x)dx
$$

$$
b_n = \frac{1}{L}\int_{-L}^{L} g(x)\sin(\kappa_n x)dx
$$

Parseval's formula states that

$$
\int_{-L}^{L} g^2(x)dx = \frac{L}{2}a_0^2 + L\sum_{n=1}^{\infty}(a_n^2 + b_n^2)
\tag{5.8}
$$

$$-\langle \bar{v}_i' \bar{v}_j' \rangle \frac{\partial \langle \bar{v}_i \rangle}{\partial x_j}$$
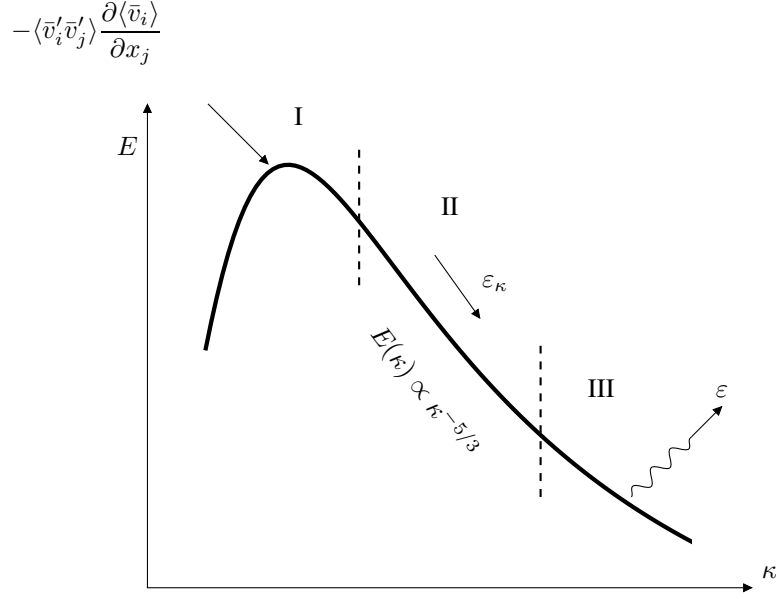
Figure 5.2: Spectrum for turbulent kinetic energy, k. I: Range for the large, energy containing eddies. II: the inertial subrange. III: Range for small, isotropic scales. For a discussion of ε_κ vs. ε, see Section 8.2.1. The wavenumber, κ, is proportional to the inverse of the length scale of a turbulent eddy, ℓ_κ, i.e. $\kappa \propto \ell_\kappa^{-1}$. For a discussion of ε_κ vs. ε, see Section 8.2.1.

For readers not familiar to Fourier series, a brief introduction is given in Appendix H. An example of a Fourier series and spectra are given in Appendix I. Let g be a fluctuating velocity component, say v_1'. The left side of Eq. 5.8 expresses $v_1'^2$ in physical space (vs. x) and the right side $v_1'^2$ in wavenumber space (vs. κ_n). The reader who is not familiar to the term "wavenumber", is probably more familiar to "frequency". In that case, express g in Eq. 5.6 as a series in *time* rather than in *space*. Then the left side of Eq. 5.8 expresses $v_1'^2$ as a function of time and the right side expresses $v_1'^2$ as a function of frequency.

The turbulent scales are distributed over a range of scales which extends from the largest scales which interact with the mean flow to the smallest scales where dissipation occurs, see Fig. 5.1. Let us think about how the kinetic energy of the eddies varies with eddy size. Intuitively we assume that large eddies have large fluctuating velocities which implies large kinetic energy, $v_i'v_i'/2$. It is convenient to study the kinetic energy of each eddy size in wavenumber space. In wavenumber space the energy of eddies can be expressed as

$$E(\kappa)d\kappa \tag{5.9}$$

where Eq. 5.9 expresses the contribution from the scales with wavenumber between κ and $\kappa + d\kappa$ to the turbulent kinetic energy k. The energy spectrum, $E(\kappa)$, corresponds to $g^2(\kappa)$ in Eq. 5.8. The dimension of wavenumber is one over length; thus we can think of wavenumber as proportional to the inverse of an eddy's diameter, i.e $\kappa \propto 1/d$. The total turbulent kinetic energy is obtained by integrating over the whole wavenumber

space, i.e.

$$k = \int_0^\infty E(\kappa)d\kappa = L \sum g^2(\kappa_n) \tag{5.10}$$

Think of this equation as a way to compute the kinetic energy by first sorting all eddies by size (i.e. wavenumber), then computing the kinetic energy of each eddy size (i.e. $E(\kappa)d\kappa$), and finally summing the kinetic energy of all eddy sizes (i.e. carrying out the integration). Note that the physical meaning of E is kinetic energy *per unit wavenumber* of eddies of size $\ell_\kappa \propto \kappa^{-1}$. Hence the dimension of E is v^2/κ, see Eq. 5.10; for a discussion on the dimension of E, see Appendix I.

The kinetic energy is the sum of the kinetic energy of the three fluctuating velocity components, i.e.

$$k = \frac{1}{2}\left(\overline{v_1'^2} + \overline{v_2'^2} + \overline{v_3'^2}\right) = \frac{1}{2}\overline{v_i'v_i'} \tag{5.11}$$

The spectrum of E is shown in Fig. 5.2. We find region I, II and III which are discussed below.

I. In this region we have the large eddies which carry most of the energy. These eddies interact with the mean flow and extract energy from the mean flow. This energy transfer takes places via the production term, P^k, in the transport equation for turbulent kinetic energy, see Eq. 8.14. Part of the energy extracted per unit time by the largest eddies is transferred (per unit time) to slightly smaller scales. The eddies' velocity and length scales are v_0 and ℓ_0, respectively.

III. Dissipation range. The eddies are small and isotropic and it is here that the dissipation occurs. The energy transfer from turbulent kinetic energy to thermal energy (increased temperature) is governed by ε in the transport equation for turbulent kinetic energy, see Eq. 8.14. The scales of the eddies are described by the Kolmogorov scales (see Eq. 5.5)

II. Inertial subrange. The existence of this region requires that the Reynolds number is high (fully turbulent flow). The eddies in this region represent the mid-region. The turbulence is also in this region isotropic. This region is a "transport region" (i.e. in wavenumber space) in the cascade process. The "transport" in wavenumber space is called *spectral transfer*. Energy per time unit, $P^k = \varepsilon$, is **spectral transfer** coming from the large eddies at the lower part of this range and is transferred per unit time to the dissipation range at the higher part. Note that the relation $P^k = \{\text{dissipation at small scales}\}$, see Fig. 5.2, is given by the assumption of the cascade process, i.e. that the energy transfer per unit time from eddy-size–to–eddy-size is the same for all eddy sizes.

The kinetic energy, $k_\kappa = v_{\kappa,i}'v_{\kappa,i}'/2$, of an eddy of size (lengthscale), $1/\kappa$, represents the kinetic energy of all eddies of this size. The kinetic energy of all eddies (of all size) is computed by Eq. 5.11. The eddies in this region are independent of both the large, energy-containing eddies and the eddies in the dissipation range. One can argue that the eddies in this region should be characterized by the spectral transfer of energy per unit time (ε) and the size of the eddies, $1/\kappa$. Dimensional analysis gives

$$\begin{array}{ccccc} E & = & \kappa^a & \varepsilon^b & \\ {[m^3/s^2]} & = & [1/m] & [m^2/s^3] & \end{array} \tag{5.12}$$

We get two equations, one for meters $[m]$

$$3 = -a + 2b,$$

and one for seconds $[s]$

$$-2 = -3b,$$

so that $b = 2/3$ and $a = -5/3$. Inserted in Eq. 5.12 we get

$$E(\kappa) = C_K \varepsilon^{\frac{2}{3}} \kappa^{-\frac{5}{3}} \tag{5.13}$$

where the Kolmogorov constant $C_K \simeq 1.5$. This is a very important law (Kolmogorov spectrum law or the $-5/3$ law) which states that, if the flow is fully turbulent (high Reynolds number), the energy spectra should exhibit a $-5/3$-decay in the inertial region (region II, Fig. 5.2).

Above we state that the eddies in Region II and III are *isotropic*. This means that – in average – the eddies have no preferred direction, i.e. the fluctuations in all directions are the same so that $\overline{v_1'^2} = \overline{v_2'^2} = \overline{v_3'^2}$. Note that is not true instantaneously, i.e. in general $v_1' \neq v_2' \neq v_3'$. Furthermore, isotropic turbulence implies that if a coordinate direction is switched (i.e. rotated 180°), nothing should change. For example if the x_1 coordinate direction is rotated 180° the $\overline{v_1' v_2'}$ should remain the same, i.e. $\overline{v_1' v_2'} = -\overline{v_1' v_2'}$. This is possible only if $\overline{v_1' v_2'} = 0$. Hence, all shear stresses are zero in isotropic turbulence. Using our knowledge in tensor notation, we know that an isotropic tensor can be written as const. $\cdot \delta_{ij}$. Hence, the Reynolds stress tensor for small scales can be written as $\overline{v_i' v_j'} = \text{const.}\delta_{ij}$ which, again, shows us that the shear stresses are zero in isotropic turbulence.

isotropic turbulence

As discussed on p. 71, the concept of the cascade process assumes that the energy extracted per unit time by the large turbulent eddies is transferred (per unit time) by non-linear interactions through the inertial range to the dissipative range where the kinetic energy is transformed (per unit time) to thermal energy (increased temperature). The spectral transfer rate of kinetic energy from eddies of size $1/\kappa$ to slightly smaller eddies can be estimated as follows. An eddy loses (part of) its kinetic energy during one revolution. The kinetic energy of the eddy is proportional to v_κ^2 and the time for one revolution is proportional to ℓ_κ/v_κ. Hence, the energy spectral transfer rate, ε_κ, for an eddy of length scale $1/\kappa$ can be estimated as (see Fig. 5.2)

$$\varepsilon_\kappa \sim \frac{v_\kappa^2}{t_\kappa} \sim \frac{v_\kappa^2}{\ell_\kappa/v_\kappa} \sim \frac{v_\kappa^3}{\ell_\kappa} \tag{5.14}$$

Kinetic energy is transferred per unit time to smaller and smaller eddies until the transfer takes place by dissipation (i.e. increased temperature) at the Kolmogorov scales. In the inertial subrange, the cascade process assumes that $\varepsilon_\kappa = \varepsilon$. Applying Eq. 5.14 for the large energy-containing eddies gives

$$\varepsilon_0 \sim \frac{v_0^2}{\ell_0/v_0} \sim \frac{v_0^3}{\ell_0} \sim \varepsilon_\kappa = \varepsilon \tag{5.15}$$

The dissipation at small scales (large wavenumbers) is determined by how much energy per unit time enters the cascade process at the large scales (small wavenumbers). We

generation	x_1	x_2	x_3
1st	1	0	0
2nd	0	1	1
3rd	2	1	1
4th	2	3	3
5th	6	5	5
6th	10	11	11
7th	22	21	21

Table 5.1: Number of eddies at each generation with their axis aligned in the x_1, x_2 or x_3 direction, see Fig. 5.3.

can now estimate the ratio between the large eddies (with v_0 and ℓ_0) to the Kolmogorov eddies (v_η and ℓ_η). Equations 5.5 and 5.15 give

$$\frac{v_0}{v_\eta} = (\nu\varepsilon)^{-1/4}v_0 = \left(\nu v_0^3/\ell_0\right)^{-1/4} v_0 = (v_0\ell_0/\nu)^{1/4} = Re^{1/4}$$

$$\frac{\ell_0}{\ell_\eta} = \left(\frac{\nu^3}{\varepsilon}\right)^{-1/4} \ell_0 = \left(\frac{\nu^3\ell_0}{v_0^3}\right)^{-1/4} \ell_0 = \left(\frac{\nu^3}{v_0^3\ell_0^3}\right)^{-1/4} = Re^{3/4} \qquad (5.16)$$

$$\frac{\tau_o}{\tau_\eta} = \left(\frac{\nu\ell_0}{v_0^3}\right)^{-1/2} \tau_0 = \left(\frac{v_0^3}{\nu\ell_0}\right)^{1/2} \frac{\ell_0}{v_0} = \left(\frac{v_0\ell_0}{\nu}\right)^{1/2} = Re^{1/2}$$

where $Re = v_0\ell_0/\nu$. We find that the ratio of the velocity, length and time scales of the energy-containing eddies to the Kolmogorov eddies increases with increasing Reynolds number. This means that the eddy range (wavenumber range) of the intermediate region (region II, the inertial region) increases with increasing Reynolds number. Hence, the larger the Reynolds number, the larger the wavenumber range of the intermediate range where the eddies are independent of both the large scales and the viscosity. or in other words: the larger the Reynolds number, the larger the difference between the largest and the smallest scales. This is the very reason why it is so expensive (in terms of computer power) to solve the Navier-Stokes equations. With a computational grid we must resolve all eddies. Hence, as the Reynolds number increases, the number of grid cells increases rapidly, see Eq. 28.1.

5.4 The cascade process created by vorticity

The interaction between vorticity and velocity gradients is an essential ingredient to create and maintain turbulence. Disturbances are amplified by interaction between the vorticity vector and the velocity gradients; the disturbances are turned into chaotic, three-dimensional fluctuations, i.e. into turbulence. Two idealized phenomena in this interaction process can be identified: vortex stretching and vortex tilting.

The equation for the instantaneous vorticity ($\omega_i = \bar{\omega}_i + \omega_i'$) reads (see Eq. 4.20)

$$\frac{\partial \omega_i}{\partial t} + v_j \frac{\partial \omega_i}{\partial x_j} = \omega_j \frac{\partial v_i}{\partial x_j} + \nu \frac{\partial^2 \omega_i}{\partial x_j \partial x_j}$$

$$\omega_i = \epsilon_{ijk} \frac{\partial v_k}{\partial x_j} \qquad (5.17)$$
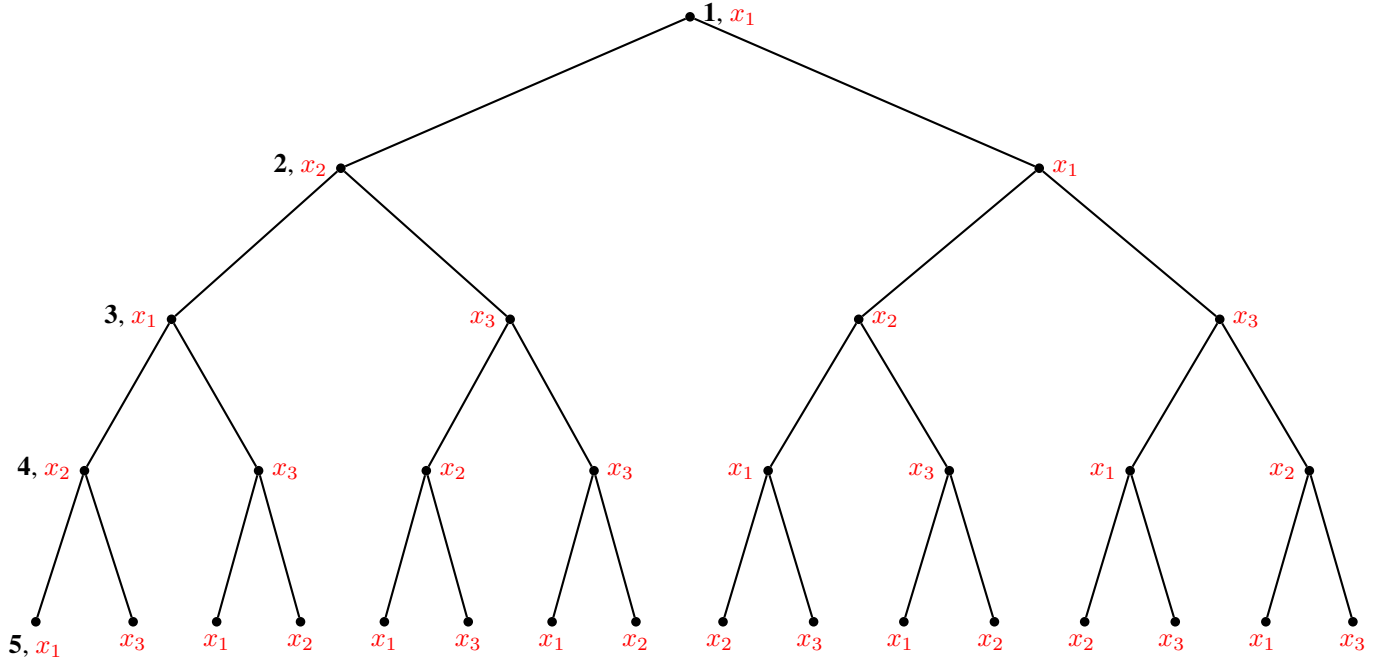
Figure 5.3: Family tree of turbulent eddies (see also Table 5.1). Five generations (indidcated in bold). Orientation of eddy is indicated in red. The large original eddy, with axis aligned in the x_1 direction, is 1st generation. Adapted from [14].

As we learnt in Section 4.2 this equation is not an ordinary convection-diffusion equation: it has an additional term on the right side which represents amplification and rotation/tilting of the vorticity lines (the first term on the right side). The $i = j$ components of this term represent (see Eq. 4.21) *vortex stretching*. A positive $\partial v_1'/\partial x_1$ will stretch the cylinder, see Fig. 4.2 and from the requirement that the volume must not change (incompressible continuity equation) we find that the radius of the cylinder will decrease. We may neglect the viscosity since viscous diffusion at high Reynolds number is much smaller than the turbulent one and since viscous dissipation occurs at small scales (see p. 71). Thus we can assume that there are no viscous stresses acting on the cylindrical fluid element surface which means that the angular momentum

Vortex stretching

$$r^2 \omega_1' = \text{const.} \qquad (5.18)$$

remains constant as the radius of the fluid element decreases. Note that also the circulation, Γ – which is the integral of the tangential velocity round the perimeter, see Eq. 1.23 – is constant. Equation 5.18 shows that the vorticity increases if the radius decreases (and vice versa). As was mentioned above, the continuity equation shows that stretching results in a decrease of the radius of a slender fluid element and an increase of the vorticity component (i.e. the tangential velocity component) aligned with the element. For example, an extension of a fluid element in one direction (x_1 direction) decreases the length scales in the x_2 direction and increases ω_1', see Fig. 5.4. At the same time, vortex tilting creates small-scale vorticity in the x_2 and x_3 direction, ω_2' and ω_3'. The increased ω_1' means that the velocity fluctuation in the x_2 direction is increased, see Fig. 5.5. The increased v_2' velocity component will stretch smaller fluid elements aligned in the x_2 direction, see Fig. 5.5. This will increase their vortic-
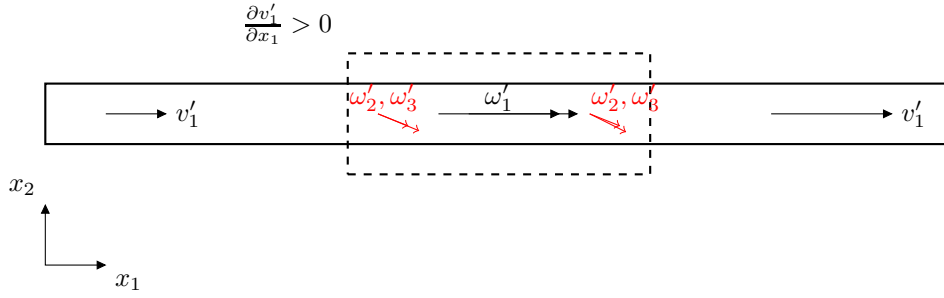
Figure 5.4: A fluid element is stretched by $\dfrac{\partial v_1'}{\partial x_1} > 0$. Its radius decreases (from dashed line to solid line).
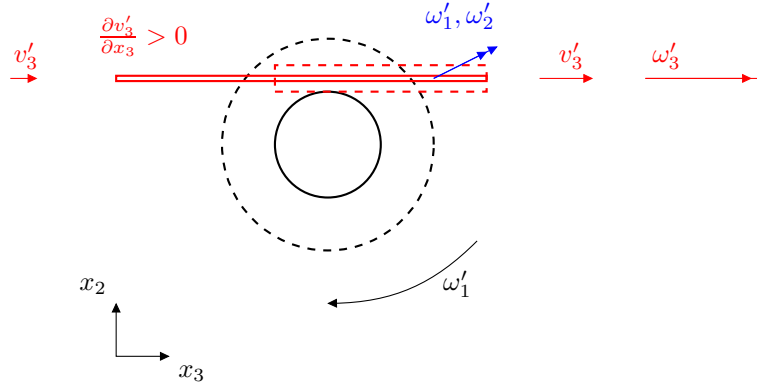
Figure 5.5: The rotation rate of the fluid element (black circles) in Fig. 5.4 increases and its radius decreases. This creates a positive $\dfrac{\partial v_3'}{\partial x_3} > 0$ which stretches the small red fluid element aligned in the x_3 direction and increases ω_3'. The radius of the red fluid element decreases.

ity ω_2' and decrease their radius. In the same way will the increased ω_1' also stretch a fluid element aligned in the x_3 direction and increase ω_3' and decrease its radius. At each stage, the length scale of the eddies – whose velocity scale are increased – decreases. Figure 5.3 illustrates how a large eddy whose axis is oriented in the x_1 axis in a few generations creates – through vortex stretching – smaller and smaller eddies with larger and larger velocity gradients. Here a generation is related to a wavenumber in the energy spectrum (Fig. 5.2); young generations correspond to high wavenumbers. The smaller the eddies, the less the original orientation of the large eddy is recalled. In other words, the small eddies "don't remember" the characteristics of their original ancestor. The small eddies have no preferred direction. They are *isotropic*. The creation of multiple eddies by vortex stretching from one original eddies is illustrated in Fig. 5.3 and Table 5.1. The large original eddy (1st generation) is aligned in the x_1 direction. It creates eddies in the x_2 and x_3 direction (2nd generation); the eddies in the x_2 direction create new eddies in the x_1 and x_3 (3rd generation) and so on. For each generation the eddies become more and more isotropic as they get smaller.

The $i \neq j$ components in the first term on the right side in Eq. 4.21 represent *vortex tilting*. Again, take a slender fluid element, now with its axis aligned with the x_2 axis, Fig. 4.3. The velocity gradient $\partial v_1/\partial x_2$ (or $\partial v_1'/\partial x_2$, which is equivalent) will tilt the fluid element so that it rotates in the clock-wise direction. As a result, the second term $\omega_2 \partial v_1/\partial x_2$ in line one in Eq. 4.21 gives a contribution to ω_1 (and ω_1'). This shows how vorticity in one direction is transferred to the other two directions through vortex tilting.

Vortex tilting

Vortex stretching and vortex tilting qualitatively explain how interaction between vorticity and velocity gradient create vorticity in all three coordinate directions from a disturbance which initially was well defined in one coordinate direction. Once this process has started it continues, because vorticity generated by vortex stretching and vortex tilting interacts with the velocity field and creates further vorticity and so on. The vorticity and velocity field becomes chaotic and three-dimensional: turbulence has been created. The turbulence is also maintained by these processes.

From the discussion above we can now understand why turbulence always must be three-dimensional (Item IV on p. 70). If the instantaneous flow is two-dimensional ($x_1 - x_2$ plane) we find that the vortex-stretching/tilting term on the right side of Eq. 5.17 vanishes because the vorticity vector and the velocity vector are orthogonal. The only non-zero component of vorticity vector is ω_3 because

$$\omega_1 = \frac{\partial v_3}{\partial x_2} - \frac{\partial v_2}{\partial x_3} \equiv 0$$

$$\omega_2 = \frac{\partial v_1}{\partial x_3} - \frac{\partial v_3}{\partial x_1} \equiv 0.$$

Since $v_3 = 0$, we get $\omega_j \partial v_i/\partial x_j = 0$.

6 Turbulent mean flow

6.1 Time averaged Navier-Stokes

WHEN the flow is turbulent it is preferable to decompose the instantaneous variables (for example the velocity components and the pressure) into a mean value and a fluctuating value, i.e.

$$
\begin{aligned}
v_i &= \bar{v}_i + v_i' \\
p &= \bar{p} + p'
\end{aligned}
\tag{6.1}
$$

where the bar, $\bar{\cdot}$, denotes the time averaged value defined as

$$
\bar{v} = \frac{1}{2T} \int_{-T}^{T} v\,dt.
\tag{6.2}
$$

where T is sufficiently large. When we time average Eq. 6.1 we get

$$
\bar{v}_i = \bar{\bar{v}}_i + \overline{v_i'} = \bar{v}_i + \overline{v_i'}
\tag{6.3}
$$

where we used the fact that $\bar{\bar{v}}_i = \bar{v}_i$, see Section 8.1.4. Hence, Eq. 6.3 gives

$$
\overline{v_i'} = 0, \quad \overline{p'} = 0
\tag{6.4}
$$

One reason why we decompose the variables is that when we measure flow quantities we are usually interested in their mean values rather than their time histories. Another reason is that when we want to solve the Navier-Stokes equation numerically it would require a very fine grid to resolve all turbulent scales and it would also require a fine resolution in time (turbulence is always unsteady).

The continuity equation and the Navier-Stokes equation for incompressible flow with constant viscosity read

$$
\frac{\partial v_i}{\partial x_i} = 0
\tag{6.5}
$$

$$
\rho \frac{\partial v_i}{\partial t} + \rho \frac{\partial v_i v_j}{\partial x_j} = -\frac{\partial p}{\partial x_i} + \mu \frac{\partial^2 v_i}{\partial x_j \partial x_j}
\tag{6.6}
$$

The gravitation term, $-\rho g_i$, has been omitted which means that the p is the *hydrodynamic* pressure (i.e. when $v_i \equiv 0$, then $p \equiv 0$, see p. 37). Inserting Eq. 6.1 into the continuity equation (6.5)

$$
\frac{\partial \overline{\bar{v}_i + v_i'}}{\partial x_i} = \frac{\partial \overline{\bar{v}}_i}{\partial x_i} + \frac{\partial \overline{v_i'}}{\partial x_i} = \frac{\partial \overline{\bar{v}}_i}{\partial x_i} = \frac{\partial \bar{v}_i}{\partial x_i}
\tag{6.7}
$$

where we used the fact that $\overline{v_i'} = 0$ (see Eq. 6.4 and $\bar{\bar{v}}_i = \bar{v}_i$, see section 8.1.4).

Next, we use the decomposition in Navier-Stokes equation (Eq. 6.6)

$$
\underbrace{\rho \frac{\partial \overline{(\bar{v}_i + v_i')}}{\partial t}}_{I} + \underbrace{\rho \frac{\partial \overline{(\bar{v}_i + v_i')(\bar{v}_j + v_j')}}{\partial x_j}}_{II} = -\underbrace{\frac{\partial (\overline{\bar{p} + p'})}{\partial x_i}}_{III} + \underbrace{\mu \frac{\partial^2 (\overline{\bar{v}_i + v_i'})}{\partial x_j \partial x_j}}_{IV}
\tag{6.8}
$$

Let us consider the equation term-by-term.

Term I:

$$\frac{\partial \overline{(\bar{v}_i + v'_i)}}{\partial t} = \frac{\partial \overline{\bar{v}_i}}{\partial t} + \frac{\partial \overline{v'_i}}{\partial t} = \frac{\partial \overline{\bar{v}_i}}{\partial t} = \frac{\partial \bar{v}_i}{\partial t}$$

We assume that the mean flow, $\bar{v}_i$, is steady, and hence the term is zero.

Term II:

$$\frac{\partial \overline{(\bar{v}_i + v'_i)(\bar{v}_j + v'_j)}}{\partial x_j} = \frac{\partial \overline{\bar{v}_i \bar{v}_j + \bar{v}_i v'_j + v'_i \bar{v}_j + v'_i v'_j}}{\partial x_j}$$

$$= \frac{\partial \overline{\bar{v}_i \bar{v}_j}}{\partial x_j} + \frac{\partial \overline{\bar{v}_i v'_j}}{\partial x_j} + \frac{\partial \overline{v'_i \bar{v}_j}}{\partial x_j} + \frac{\partial \overline{v'_i v'_j}}{\partial x_j}$$

- Section 8.1.4 shows that $\overline{\bar{v}_i \bar{v}_j} = \bar{v}_i \bar{v}_j$.
- Section 8.1.3 shows that $\overline{\bar{v}_i v'_j} = \bar{v}_i \overline{v'_j} = 0$ and $\overline{\bar{v}_j v'_i} = \bar{v}_j \overline{v'_i} = 0$

Hence, Term II reads

$$\frac{\partial \bar{v}_i \bar{v}_j}{\partial x_j} + \frac{\partial \overline{v'_i v'_j}}{\partial x_j}$$

Term III:

$$\frac{\partial \overline{(\bar{p} + p')}}{\partial x_i} = \frac{\partial \overline{\bar{p}}}{\partial x_i} + \frac{\partial \overline{p'}}{\partial x_i} = \frac{\partial \bar{p}}{\partial x_i}$$

Term IV:

$$\frac{\partial^2 \overline{(\bar{v}_i + v'_i)}}{\partial x_j \partial x_j} = \frac{\partial^2 \overline{\bar{v}_i}}{\partial x_j \partial x_j} + \frac{\partial^2 \overline{v'_i}}{\partial x_j \partial x_j} = \frac{\partial^2 \bar{v}_i}{\partial x_j \partial x_j}$$

Now we van finally write the *time averaged* continuity equation and Navier-Stokes equation

$$\frac{\partial \bar{v}_i}{\partial x_i} = 0 \tag{6.9}$$

$$\rho \frac{\partial \bar{v}_i \bar{v}_j}{\partial x_j} = -\frac{\partial \bar{p}}{\partial x_i} + \frac{\partial}{\partial x_j}\left(\mu \frac{\partial \bar{v}_i}{\partial x_j} - \rho \overline{v'_i v'_j}\right) \tag{6.10}$$

It is assumed that the mean flow is steady. This equation is the time-averaged Navier-Stokes equation and it is often called the *Reynolds Averaged Navies-Stokes* (RANS) equation. A new term $\rho \overline{v'_i v'_j}$ appears on the right side of Eq. 6.10 which is **RANS** called the *Reynolds stress tensor*. The tensor is symmetric (for example $\overline{v'_1 v'_2} = \overline{v'_2 v'_1}$). It represents correlations between fluctuating velocities. It is an additional stress term due to turbulence (fluctuating velocities) and it is unknown. We need a model for $\overline{v'_i v'_j}$ to close the equation system in Eq. 6.10. This is called the *closure problem*: the num- ber of unknowns (ten: three velocity components, pressure, six stresses) is larger than **closure** the number of equations (four: the continuity equation and three components of the **problem** Navier-Stokes equations).

The continuity equation applies both for the instantaneous velocity, v_i (Eq. 6.5), and for the time-averaged velocity, $\bar{v}_i$ (Eq. 6.9); hence it applies also for the fluctuating velocity, v'_i, i.e.

$$\frac{\partial v'_i}{\partial x_i} = 0 \tag{6.11}$$
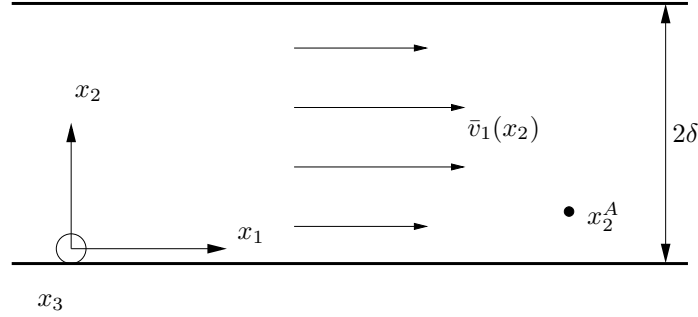
Figure 6.1: Flow between two infinite parallel plates. The width (i.e. length in the x_3 direction) of the plates, Z_{max}, is much larger that the separation between the plates, i.e. $Z_{max} \gg \delta$.

6.1.1 Boundary-layer approximation

For boundary-layer type of flow (i.e. boundary layers along a flat plate, channel flow, pipe flow, jet and wake flow, etc.) the following relations apply

$$\bar{v}_2 \ll \bar{v}_1, \ \frac{\partial \bar{v}_1}{\partial x_1} \ll \frac{\partial \bar{v}_1}{\partial x_2}, \tag{6.12}$$

Assume steady ($\partial/\partial t = 0$), two-dimensional ($\bar{v}_3 = \partial/\partial x_3 = 0$) boundary-layer flow. First we re-write the left side of Eq. 6.10 using the continuity equation

$$\rho \frac{\partial \bar{v}_i \bar{v}_j}{\partial x_j} = \rho \bar{v}_j \frac{\partial \bar{v}_i}{\partial x_j} + \underbrace{\rho \bar{v}_i \frac{\partial \bar{v}_j}{\partial x_j}}_{=0} = \rho \bar{v}_j \frac{\partial \bar{v}_i}{\partial x_j} \tag{6.13}$$

Using Eq. 6.13, Eq. 6.10 can be written

$$\rho \bar{v}_1 \frac{\partial \bar{v}_1}{\partial x_1} + \rho \bar{v}_2 \frac{\partial \bar{v}_1}{\partial x_2} = -\frac{\partial \bar{p}}{\partial x_1} + \frac{\partial}{\partial x_2} \underbrace{\left[\mu \frac{\partial \bar{v}_1}{\partial x_2} - \rho \overline{v'_1 v'_2} \right]}_{\tau_{12,tot}} \tag{6.14}$$

x_1 and x_2 denote the streamwise and wall-normal coordinate, respectively, see Fig. 6.1. Note that the two terms on the left side are of the same order, because they both include the product of one large ($\bar{v}_1$ or $\partial/\partial x_2$) and one small ($\bar{v}_2$ or $\partial/\partial x_1$) part.

In addition to the viscous shear stress, $\mu \partial \bar{v}_1/\partial x_2$, an additional *turbulent* one – a **shear** Reynolds shear stress – appears on the right side of Eq. 6.14. The total shear stress is **stress** thus

$$\tau_{12,tot} = \mu \frac{\partial \bar{v}_1}{\partial x_2} - \rho \overline{v'_1 v'_2} \tag{6.15}$$

6.2 Wall region in fully developed channel flow

The region near the wall is very important. Here the velocity gradient is largest as the velocity drops down to zero at the wall over a very short distance. One important quantity is the wall shear stress which is defined as

$$\tau_w = \mu \frac{\partial \bar{v}_1}{\partial x_2} \bigg|_w \tag{6.16}$$
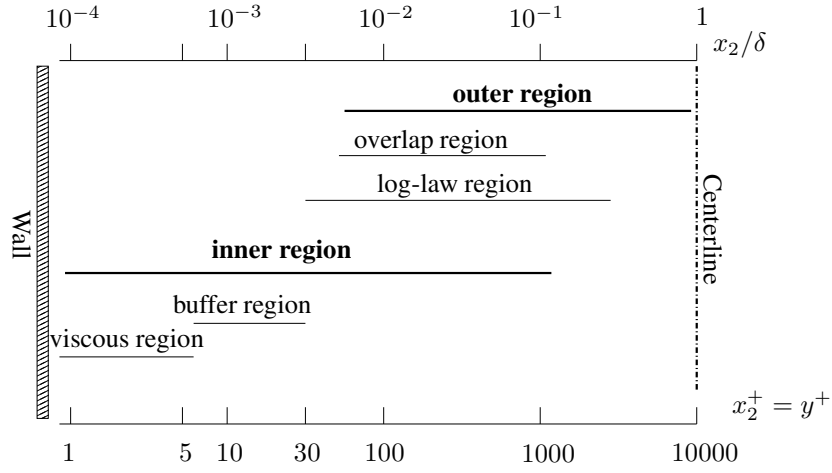
Figure 6.2: The wall region (adapted from Ch.7 in [12]) for $Re_\tau = 10\,000$. δ denotes half width of the channel, see Fig. 6.1 and $x_2^+ = x_2 u_\tau/\nu$ denotes the normalized wall distance.

From the wall shear stress, we can define a *wall friction velocity*, u_τ, as **wall friction velocity**

$$\tau_w = \rho u_\tau^2 \Rightarrow u_\tau = \left(\frac{\tau_w}{\rho}\right)^{1/2} \tag{6.17}$$

In order to take a closer look at the near-wall region, let us, again, consider fully developed channel flow between two infinite plates, see Fig. 6.1. In fully developed channel flow, the streamwise derivative of the streamwise velocity component is zero (this *is* the definition of fully developed flow), i.e. $\partial \bar{v}_1/\partial x_1 = 0$. The continuity equation gives now $\bar{v}_2 = 0$, see Eq. 3.18 at p. 37. The first term on the left side of Eq. 6.14 is zero because we have fully developed flow ($\partial \bar{v}_1/\partial x_1 = 0$) and the last term is zero because $\bar{v}_2 \equiv 0$. The streamwise momentum equation, Eq. 6.14, can now be written

$$0 = -\frac{\partial \bar{p}}{\partial x_1} + \frac{\partial}{\partial x_2}\left(\mu\frac{\partial \bar{v}_1}{\partial x_2} - \rho\overline{v_1'v_2'}\right) \tag{6.18}$$

We know that the first term is a function only of x_1 and the two terms in parenthesis are functions of x_2 only; hence they must be constant (see Eq. 3.24 and the text related to this equation), i.e.

$$-\frac{\partial \bar{p}}{\partial x_1} = \text{constant}$$

$$\frac{\partial}{\partial x_2}\left(\mu\frac{\partial \bar{v}_1}{\partial x_2} - \rho\overline{v_1'v_2'}\right) = \frac{\partial \tau_{12,tot}}{\partial x_2} = \text{constant} \tag{6.19}$$

where the total stress, $\tau_{12,tot}$, is given by Eq. 6.15. Integrating Eq. 6.18 from $x_2 = 0$ to x_2 gives

$$\tau_{12,tot}(x_2) - \tau_w = \frac{\partial \bar{p}}{\partial x_1}x_2 \Rightarrow \tau_{12,tot} = \tau_w + \frac{\partial \bar{p}}{\partial x_1}x_2 = \tau_w\left(1 - \frac{x_2}{\delta}\right) \tag{6.20}$$

At the last step we used the fact that the pressure gradient balances the wall shear stress, i.e. $-\partial \bar{p}/\partial x_1 = \tau_w/\delta$, see Eq. 3.30 (note that $h = 2\delta$) and Eq. 6.38.

The wall region can be divided into one outer and one inner region, see Fig. 6.2. The inner region includes the viscous region, $x_2^+ \lesssim 5$ (dominated by the viscous diffusion), and the logarithmic region, $x_2^+ \gtrsim 30$ (dominated by turbulent diffusion); the logarithmic region is sometimes called the *inertial region*, because the turbulent stresses stem from the inertial (i.e. the non-linear convection) term. The buffer region acts as a transition region between these two regions where viscous diffusion of streamwise momentum is gradually replaced by turbulent diffusion. In the inner region, the total shear stress is approximately constant and equal to the wall shear stress τ_w, see Fig. 6.3. Note that the total shear stress is constant only close to the wall (Fig. 6.3b); further away from the wall it decreases (in fully developed channel flow it decreases linearly with the distance from the wall, see Eq. 6.20 and Fig. 6.3a). The Reynolds shear stress vanishes at the wall because $v_1' = v_2' = 0$, and the viscous shear stress attains its wall-stress value $\tau_w = \rho u_\tau^2$. As we go away from the wall the viscous stress decreases and the turbulent one increases and at $x_2^+ \simeq 11$ they are approximately equal. In the logarithmic layer the viscous stress is negligible compared to the Reynolds stress.

At the wall, the velocity gradient is directly related to the wall shear stress, i.e. (see Eq. 6.16 and 6.17)

$$\left.\frac{\partial \bar{v}_1}{\partial x_2}\right|_w = \frac{\tau_w}{\mu} = \frac{\rho}{\mu}u_\tau^2 = \frac{1}{\nu}u_\tau^2 \tag{6.21}$$

Integration gives (recall that both ν and u_τ^2 are constant)

$$\bar{v}_1 = \frac{1}{\nu}u_\tau^2 x_2 + C_1$$

Since the velocity, $\bar{v}_1$, is zero at the wall, the integration constant $C_1 = 0$ so that

$$\frac{\bar{v}_1}{u_\tau} = \frac{u_\tau x_2}{\nu} \tag{6.22}$$

Equation 6.22 is expressed in *inner scaling* (or wall scaling) which means that $\bar{v}_1$ and x_2 are normalized with quantities related to the wall, i.e. the friction velocity stemming from the wall shear stress and the viscosity (here we regard viscosity as a quantity related to the wall, since the flow is dominated by viscosity). Often the plus-sign ('+') is used to denote inner scaling and equation Eq. 6.22 can then be written

$$\bar{v}_1^+ = x_2^+ \tag{6.23}$$

From the friction velocity and the viscosity we can define the *viscous length scale*, ℓ_ν, for the near-wall region as

$$x_2^+ = x_2/\ell_\nu \Rightarrow \ell_\nu = \frac{\nu}{u_\tau} \tag{6.24}$$

Further away from the wall at $30 \lesssim x_2^+ \lesssim 3000$ (or $0.003 \lesssim x_2/\delta \lesssim 0.3$), we encounter the *log-law region*, see Fig. 6.2. In this region the flow is assumed to be independent of viscosity. The Reynolds shear stress, $\rho \overline{v_1' v_2'}$, is in the region $x_2^+ \lesssim 200$ (i.e. $x_2/\delta \lesssim 0.1$) fairly constant and approximately equal to the wall shear stress, i.e.

$$\tau_w = \rho|\overline{v_1' v_2'}| \tag{6.25}$$

see Fig. 6.3b. Hence the friction velocity, u_τ, is a suitable velocity scale in the inner logarithmic region; it is used in the entire region.
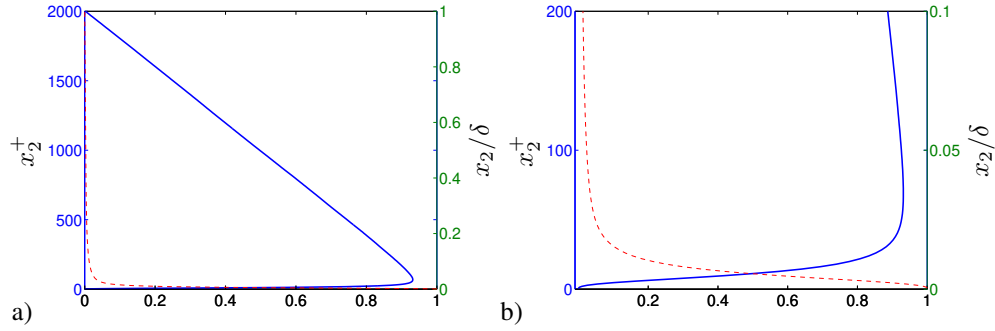
Figure 6.3: Reynolds shear stress. $Re_\tau = 2000$. a) lower half of the channel; b) zoom near the wall. DNS (Direct Numerical Simulation) data [15, 16]. ▬▬ : $-\rho\overline{v_1'v_2'}/\tau_w$; ▬ ▬ : $\mu(\partial\bar{v}_1/\partial x_2)/\tau_w$.
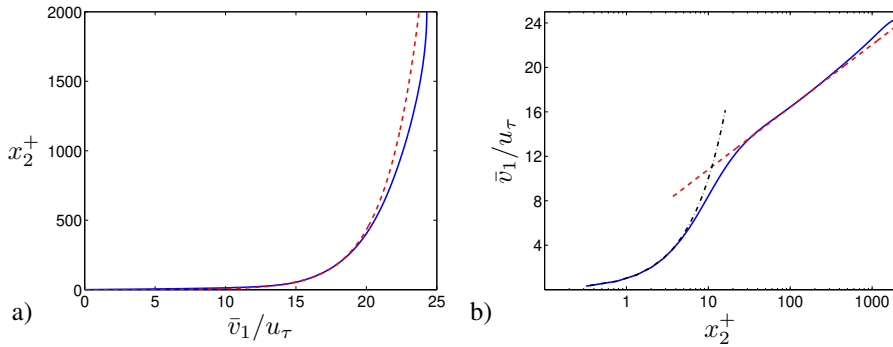
Figure 6.4: Velocity profiles in fully developed channel flow. $Re_\tau = 2000$. ▬▬ : DNS (Direct Numerical Simulation) data [15, 16]; ▬ ▬ : $\bar{v}_1/u_\tau = (\ln x_2^+)/0.41 + 5.2$; ▬ ▪ ▬ : $\bar{v}_1/u_\tau = x_2^+$.

What about the length scale? Near the wall, an eddy cannot be larger than the distance to the wall and it is the distance to the wall that sets an upper limit on the eddy-size. Hence it seems reasonable to take the wall distance as the characteristic length scale; a constant, κ, is added so that

$$\ell = \kappa x_2. \tag{6.26}$$

The velocity gradient can now be estimated as

$$\frac{\partial\bar{v}_1}{\partial x_2} = \frac{u_\tau}{\kappa x_2} \tag{6.27}$$

based on the velocity scale, u_τ, and the length scale κx_2. Another way of deriving the expression in Eq. 6.27 is to use the Boussinesq assumption (see Eq. 11.33) in which a turbulent Reynolds stress is assumed to be equal to the product between the turbulent viscosity and the velocity gradient as

$$-\overline{v_1'v_2'} = \nu_t\frac{\partial\bar{v}_1}{\partial x_2} \tag{6.28}$$

The turbulent viscosity, ν_t, represents the turbulence and has the same dimension as ν, i.e. $[m^2/s]$. Hence ν_t can be expressed as a product of a turbulent velocity scale and a
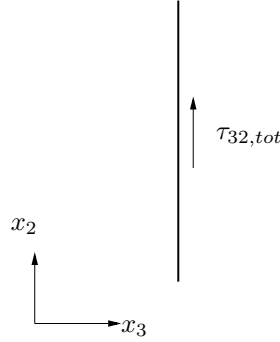
Figure 6.5: Symmetry plane of channel flow.

turbulent length scale, and in the log-law region that gives

$$\nu_t = u_\tau \kappa x_2 \tag{6.29}$$

so that Eq. 6.28 gives (inserting $-\overline{v_1' v_2'} = u_\tau^2$)

$$u_\tau^2 = \kappa u_\tau x_2 \frac{\partial \bar{v}_1}{\partial x_2} \Rightarrow \frac{\partial \bar{v}_1}{\partial x_2} = \frac{u_\tau}{\kappa x_2} \tag{6.30}$$

In non-dimensional form Eqs. 6.27 and 6.30 read

$$\frac{\partial \bar{v}_1^+}{\partial x_2^+} = \frac{1}{\kappa x_2^+} \tag{6.31}$$

Integration gives now

$$\begin{aligned} \bar{v}_1^+ &= \frac{1}{\kappa} \ln\left(x_2^+\right) + B \quad \text{or} \\ \frac{\bar{v}_1}{u_\tau} &= \frac{1}{\kappa} \ln\left(\frac{x_2 u_\tau}{\nu}\right) + B \end{aligned} \tag{6.32}$$

where B is an integration constant. Equation 6.32 is the logarithmic law due to von **log-law**
Kármán [17]. The constant, κ, is called the von Kármán constant. The constants in the
log-law are usually set to $\kappa = 0.41$ and $B = 5.2$.

As can be seen in Fig. 6.2 the log-law applies for $x_2^+ \lesssim 3000$ ($x_2/\delta \lesssim 0.3$).
Figure 6.4 – where the Reynolds number is lower than in Fig. 6.2 – shows that the log-
law fit the DNS (Direct Numerical Simulation) up to $x_2^+ \lesssim 500$ ($x_2/\delta \lesssim 0.25$). Hence,
the upper limit for the validity of the log-law is dependent on Reynolds number; the
larger the Reynolds number, the larger the upper limit.

In the outer region of the boundary layer, the relevant length scale is the boundary
layer thickness. The resulting velocity law is the *defect law*

$$\frac{\bar{v}_{1,c} - \bar{v}_1}{u_\tau} = F_D\left(\frac{x_2}{\delta}\right) \tag{6.33}$$

where c denotes centerline. The velocity in the log-region and the outer region (often
called the wake region) can be written as

$$\frac{\bar{v}_1}{u_\tau} = \frac{1}{\kappa} \ln(y^+) + B + \frac{2\Pi}{\kappa} \sin^2\left(\frac{\pi x_2}{2\delta}\right) \tag{6.34}$$

where $\kappa = 0.38$, $B = 4.1$ and $\Pi = 0.5$ are taken from boundary layer flow [18–20].
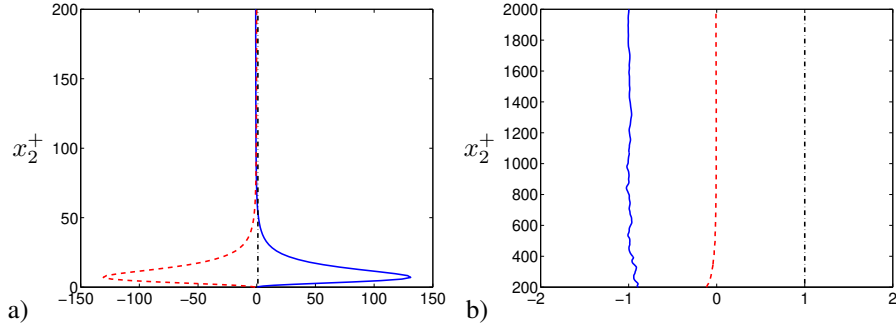
Figure 6.6: Fully developed channel flow. $Re_\tau = 2000$. Forces in the $\bar{v}_1$ equation, see Eq. 6.18. a) near the lower wall of the channel; b) lower half of the channel excluding the near-wall region. DNS (Direct Numerical Simulation) data [15, 16]. ———: $-\rho(\partial\overline{v_1'v_2'}/\partial x_2)/\tau_w$; – – –: $\mu(\partial^2\bar{v}_1/\partial x_2^2)/\tau_w$; – · – · : $-(\partial\bar{p}/\partial x_1)/\tau_w$.

6.3 Reynolds stresses in fully developed channel flow

The flow is two-dimensional ($\bar{v}_3 = 0$ and $\partial/\partial x_3 = 0$). Consider the $x_2 - x_3$ plane, see Fig. 6.5. Since nothing changes in the x_3 direction, the viscous shear stress

$$\tau_{32} = \mu\left(\frac{\partial\bar{v}_3}{\partial x_2} + \frac{\partial\bar{v}_2}{\partial x_3}\right) = 0 \tag{6.35}$$

because $\bar{v}_3 = \partial\bar{v}_2/\partial x_3 = 0$. The turbulent part shear stress, $\rho\overline{v_2'v_3'}$, can be expressed using the Boussinesq assumption (see Eq. 11.33)

$$-\rho\overline{v_2'v_3'} = \mu_t\left(\frac{\partial\bar{v}_3}{\partial x_2} + \frac{\partial\bar{v}_2}{\partial x_3}\right) = 0 \tag{6.36}$$

and it is also zero since $\bar{v}_3 = \partial\bar{v}_2/\partial x_3 = 0$. With the same argument, $\overline{v_1'v_3'} = 0$. However note that $\overline{v_3'^2} = \overline{v_3^2} \neq 0$. The reason is that although the *time-averaged* flow is two-dimensional (i.e. $\bar{v}_3 = 0$), the instantaneous turbulent flow is always three-dimensional and unsteady. Hence $v_3 \neq 0$ and $v_3' \neq 0$ so that $v_3'^2 \neq 0$. Consider, for example, the time series $v_3 = v_3' = (-0.25, 0.125, 0.125, -0.2, 0.2)$. This gives

$$\bar{v}_3 = (-0.25 + 0.125 + 0.125 - 0.2 + 0.2)/5 = 0$$

but

$$\overline{v_3'^2} = \overline{v_3^2} = \left[(-0.25)^2 + 0.125^2 + 0.125^2 + (-0.2)^2 + 0.2^2\right]/5 = 0.03475 \neq 0.$$

Figure 6.3 presents the Reynolds and the viscous shear stresses for fully developed flow. As can be seen, the viscous shear stress is negligible except very near the wall. It is equal to one near the wall and decreases rapidly for increasing wall distance. On the other hand, the Reynolds shear stress is zero at the wall (because the fluctuating velocities are zero at the wall) and increases for increasing wall distance. The intersection of the two shear stresses takes place at $x_2^+ \simeq 11$.

Looking at Eq. 6.18 we find that it is not really the shear stress that is interesting, but its gradient. The gradient of the shear stress, $-\partial(\rho\overline{v_1'v_2'})/\partial x_2$ and $\mu\partial^2\bar{v}_1/\partial x_2^2$ represent, together with the pressure gradient, $-\partial\bar{p}/\partial x_1$, the *forces* acting on the fluid.
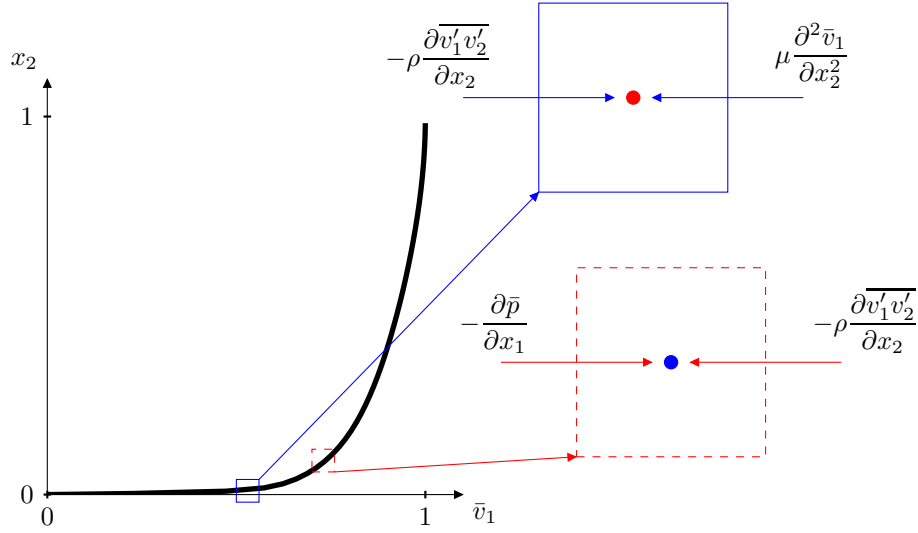
Figure 6.7: Forces in a boundary layer. The red (dashed line) and the blue (solid line) fluid particle are located at $x_2^+ \simeq 400$ and $x_2^+ \simeq 20$, respectively (see Fig. 6.6).

Figure 6.6 presents the forces. Start by looking at Fig. 6.6b which shows the forces in the region away from the wall, see the red fluid particle in Fig. 6.7. The pressure gradient is constant and equal to one: this is the force *driving* the flow. This agrees – fortunately – with our intuition. We can imagine that the fluid (air, for example) is driven by a fan. Another way to describe the behaviour of the pressure is to say that there is a pressure drop. The pressure must decrease in the streamwise direction so that the pressure gradient term, $-\partial \bar{p}/\partial x_1$, in Eq. 6.18 takes a positive value which pushes the flow in the x_1 direction. The force that balances the pressure gradient is the gradient of the Reynolds shear stress. This is the force *opposing* the movement of the fluid. This opposing force has its origin at the walls due to the viscous wall force (viscous shear stress multiplied by area).

Now let us have a look at the forces in the near-wall region, see Fig. 6.6a. Here the forces are two orders of magnitude larger than in Fig. 6.6b but they act over a very thin region ($x_2^+ \leq 40$ or $x_2/\delta < 0.02$). In this region the Reynolds shear stress gradient term is *driving* the flow and the opposing force is the viscous force, see the blue fluid particle in Fig. 6.7. We can of course make a force balance for a section of the channel, as we did for laminar flow, see Eq. 3.36 at p. 39 and Fig. 3.8 at p. 39 which reads

$$0 = \bar{p}_1 Z_{max} 2\delta - \bar{p}_2 Z_{max} 2\delta - 2\tau_w L Z_{max} \tag{6.37}$$

where L is the length of the section. We get

$$\frac{\Delta \bar{p}}{L} = -\frac{\partial \bar{p}}{\partial x_1} = \frac{\tau_w}{\delta} \tag{6.38}$$

As can be seen the pressure drop is directly related to the wall shear stress. In turbulent flow the velocity profile in the center region is much flatter than in laminar flow (cf. Fig. 6.4 and Fig. 3.7 at p. 38). This makes the velocity gradient near the wall (and the wall shear stress, τ_w) much larger in turbulent flow than in laminar flow: Eq. 6.38
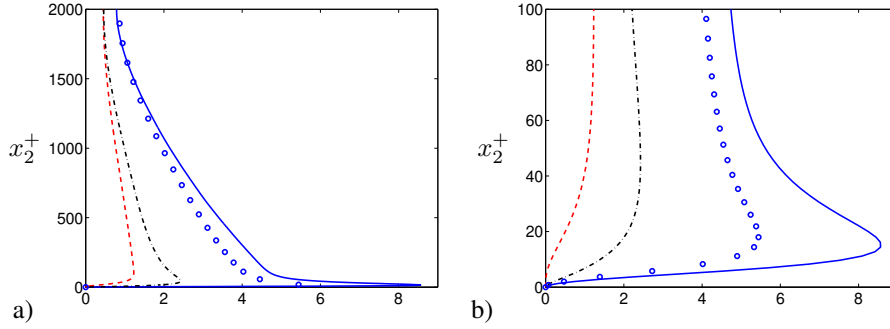
Figure 6.8: Normal Reynolds stresses and turbulent kinetic energy. $Re_\tau = 2000$. DNS (Direct Numerical Simulation) data [15, 16]. ——: $\rho \overline{v_1'^2}/\tau_w$; — —: $\rho \overline{v_2'^2}/\tau_w$; — ·—: $\rho \overline{v_3'^2}/\tau_w$; ○: k/u_τ^2.
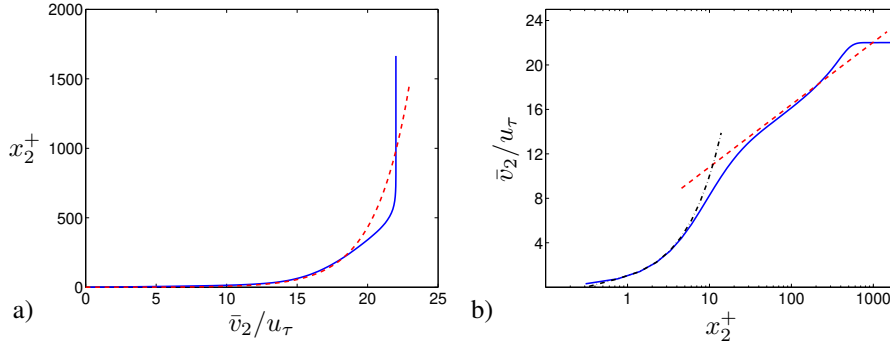
Figure 6.9: Velocity profiles in a boundary layer along a flat plate. ——: DNS (Direct Numerical Simulation) data [21]; — —: $\bar{v}_2/u_\tau = (\ln x_2^+)/0.41 + 5.2$; — ·—: $\bar{v}_2/u_\tau = x_2^+$.

shows why the pressure drop is larger in the former case compared to the latter; or — in other words – why a larger fan is required to push the flow in turbulent flow than in laminar flow.

Figure 6.8 presents the normal Reynolds stresses, $\rho \overline{v_1'^2}$, $\rho \overline{v_2'^2}$ and $\rho \overline{v_3'^2}$. As can be seen, the streamwise stress is largest and the wall-normal stress is smallest. The former is largest because the mean flow is in this direction; the latter is smallest because the turbulent fluctuations are dampened by the wall. The turbulent kinetic energy, $k = \overline{v_i' v_i'}/2$, is also included. Note that this is smaller than $\overline{v_1'^2}$.

6.4   Boundary layer

Up to now we have mainly discussed fully developed channel flow. What is the difference between that flow and a boundary layer flow? First, in a boundary layer flow the convective terms are not zero (or negligible), i.e. the left side of Eq. 6.14 is not zero. The flow in a boundary layer is continuously developing, i.e. its thickness, δ, increases continuously for increasing x_1. The flow in a boundary layer is described by Eq. 6.14. Second, in a boundary layer flow the wall shear stress is not determined by the pressure drop (indeed it is zero); the total shear stress is balanced by the convective terms. Third, the outer part of the boundary layer is highly intermittent, consisting of turbulent/non-turbulent motion.

However, the inner region of a boundary layer ($x_2/\delta < 0.1$) is principally the same

as for the fully developed channel flow, see Fig. 6.9: the linear and the log-law regions are very similar for the two flows. However, in boundary layer flow the log-law is valid only up to approximately $x_2/\delta \simeq 0.1$ (compared to approximately $x_2/\delta \simeq 0.3$ in channel flow)

(a) Point 1. $v_{rms} = 2.15$. (b) Point 2. $v_{rms} = 0.23$. (c) Point 3. $v_{rms} = 1.44$.
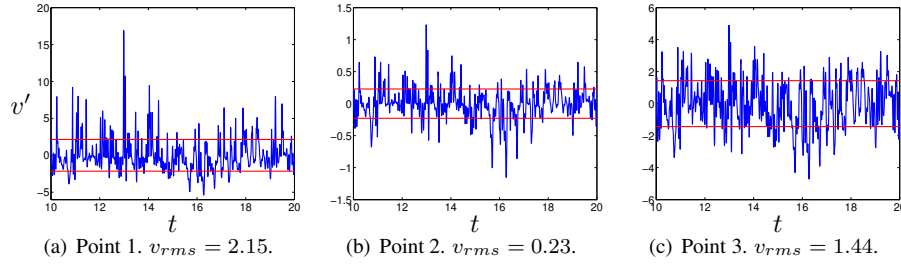
Figure 7.1: Time history of v'. Horizontal red lines show $\pm v_{rms}$.

7 Probability density functions

SOME statistical information is obtained by forming the mean and second moments, for example $\bar{v}$ and $\overline{v_2'^2}$, as was done in Section 6. The *root-mean-square* (RMS) can be defined from the second moment as

root-mean-square RMS

$$v_{rms} = \left(\overline{v'^2}\right)^{1/2} \tag{7.1}$$

The RMS is the same as the *standard deviation* which is equal to the square-root of the *variance*. In order to extract more information, probability density function is a useful statistical tool to analyze turbulence. From the velocity signals we can compute the probability densities (sometimes called *histograms*). With a probability density, f_v, of the v velocity, the mean velocity is computed as

standard deviation variance

$$\bar{v} = \int_{-\infty}^{\infty} v f_v(v) dv \tag{7.2}$$

Normalize the probability functions, so that

$$\int_{-\infty}^{\infty} f_v(v) dv = 1 \tag{7.3}$$

Here we integrate over v. The mean velocity can of course also be computed by integrating over time, as we do when we define a time average, (see Eq. 6.1 at p. 80), i.e.

$$\bar{v} = \frac{1}{2T} \int_{-T}^{T} v dt \tag{7.4}$$

where T is "sufficiently" large.

Consider the probability density functions of the fluctuations. The second moment corresponds to the variance of the fluctuations (or the square of the RMS, see Eq. 7.1), i.e.

$$\overline{v'^2} = \int_{-\infty}^{\infty} v'^2 f_{v'}(v') dv' \tag{7.5}$$

As in Eq. 7.4, $\overline{v'^2}$ is usually computed by integrating in time, i.e.

$$\overline{v'^2} = \frac{1}{2T} \int_{-T}^{T} v'^2(t) dt$$

(a) Point 1. $S = 1.51$ and $F = 7.68$.

(b) Point 2. $S = -0.27$ and $F = 5.81$.

(c) Point 3. $S = -0.09$ and $F = 2.77$.
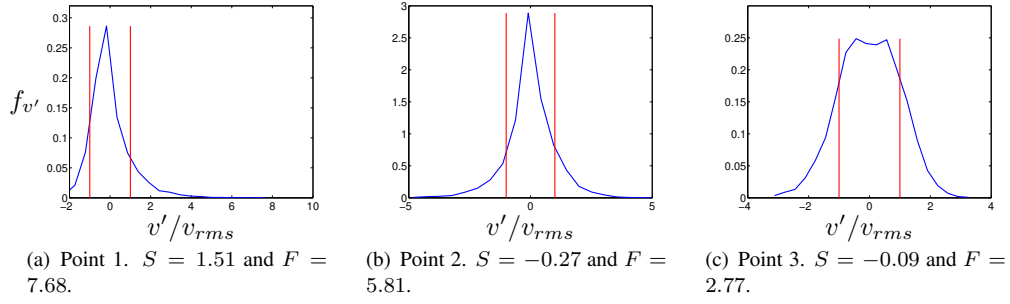
Figure 7.2: Probability density functions of time histories in Fig. 7.1. Vertical red lines show $\pm v_{rms}$. The skewness, S, and the flatness, F, are given for the three time histories.

A probability density function is symmetric if positive values are as frequent and large as the negative values. Figure 7.1 presents the time history of the v' history at three different points in a flow (note that $\overline{v'} = 0$). The red horizontal lines indicate the RMS value of v'. The resulting probability densities functions are shown in Fig. 7.2. The red vertical lines show plus and minus RMS of v'. Let us analyze the data at the three points.

Point 1. The time history of the velocity fluctuation (Fig. 7.1a) shows that there exists large positive values but no large negative values. The positive values are often larger than $+v_{rms}$ (the peak is actually close to $8v_{rms}$) but the negative values are seldom smaller than $-v_{rms}$. This indicates that the distribution of v' is skewed towards the positive side. This is confirmed in the PDF distribution, see Fig. 7.2a.

Point 2. The fluctuations at this point are much smaller and the positive values are as large the negative values; this means that the PDF should be symmetric which is confirmed in Fig. 7.2b. The extreme values of v' are approximately $\pm 1.5 v_{rms}$, see Figs. 7.1b and 7.2b.

Point 3. At this point the time history (Fig. 7.1c) shows that the fluctuations are clustered around zero and much values are within $\pm v_{rms}$. The time history shows that the positive and the negative values have the same magnitude. The PDF function in Fig. 7.2c confirms that there are many value around zero, that the extreme value are small and that positive and negative values are equally frequent (i.e. the PDF is symmetric).

In Fig. 7.2 we can judge whether the PDF is symmetric, but instead of "looking" at the probability density functions, we should use a definition of the degree of symmetry, which is the *skewness*. It is defined as   **skewness**

$$\overline{v'^3} = \int_{-\infty}^{\infty} v'^3 f_{v'}(v') dv'$$

and is commonly normalized by v_{rms}^3, so that the skewness, $S_{v'}$, of v' is defined as

$$S_{v'} = \frac{1}{v_{rms}^3} \int_{-\infty}^{\infty} v'^3 f_{v'}(v') dv' = \frac{1}{2 v_{rms}^3 T} \int_{-T}^{T} v'^3(t) dt$$

Note that f must be normalized (see Eq. 7.3).

There is yet another statistical quantity which sometimes is used for describing turbulent fluctuations, namely the *flatness*. The variance (the square of RMS) tells us how large the fluctuations are in average, but it does not tell us if the time history includes few very large fluctuations or if all are rather close to v_{rms}. The flatness gives this information, and it is defined computed from v'^4 and normalized by v_{rms}^4, i.e.

flatness

$$F = \frac{1}{v_{rms}^4} \int_{-\infty}^{\infty} v'^4 f_{v'}(v) dv$$

The fluctuations at Point 1 (see Fig. 7.1a) includes some samples which are very large and hence its flatness is large (see caption in Fig. 7.2a), whereas the fluctuation for Point 3 all mostly clustered within $\pm 2 v_{rms}$ giving a small flatness, see Fig. 7.1c and the caption in Fig. 7.2c. For a Gaussian distribution

$$f(v') = \frac{1}{v_{rms}} \exp\left(-\frac{(v' - v_{rms})^2}{2v_{rms}^2}\right)$$

for which $F = 3$.

8 Transport equations for turbulent kinetic energy

IN this section and Section 9 we will derive various transport equations. There are two tricks which often will be used. Both tricks simply use the product rule for derivative backwards.

Trick 1: Using the product rule we get

$$\frac{\partial A_i B_j}{\partial x_k} = A_i \frac{\partial B_j}{\partial x_k} + B_j \frac{\partial A_i}{\partial x_k} \tag{8.1}$$

This expression can be re-written as

$$A_i \frac{\partial B_j}{\partial x_k} = \frac{\partial A_i B_j}{\partial x_k} - B_j \frac{\partial A_i}{\partial x_k} \tag{8.2}$$

and then we call it the "product rule backwards".

Trick 2: Using the product rule we get

$$\frac{1}{2} \frac{\partial A_i A_i}{\partial x_j} = \frac{1}{2} \left(A_i \frac{\partial A_i}{\partial x_j} + A_i \frac{\partial A_i}{\partial x_j} \right) = A_i \frac{\partial A_i}{\partial x_j} \tag{8.3}$$

This trick is usually used backwards, i.e.

$$A_i \frac{\partial A_i}{\partial x_j} = \frac{1}{2} \frac{\partial A_i A_i}{\partial x_j} \tag{8.4}$$

8.1 Rules for time averaging

8.1.1 What is the difference between $\overline{v_1' v_2'}$ and $\overline{v_1'} \, \overline{v_2'}$?

Using Eq. 6.2 we get

$$\overline{v_1' v_2'} = \frac{1}{2T} \int_{-T}^{T} v_1' v_2' dt.$$

whereas

$$\overline{v_1'} \, \overline{v_2'} = \left(\frac{1}{2T} \int_{-T}^{T} v_1' dt \right) \left(\frac{1}{2T} \int_{-T}^{T} v_1' dt \right)$$

We take a numerical example. Let us the time series of v_1' and v_2' be

$$v_1' = [0.2, -0.3, 0.18, -0.08]$$
$$v_2' = [0.15, -0.25, 0.04, 0.06]$$

$$\overline{v_1'} = \frac{1}{N} \sum_{n=1}^{N} v_{1,n}' = (0.2 - 0.3 + 0.18 - 0.08)/4 = 0$$

$$\overline{v_2'} = \frac{1}{N} \sum_{n=1}^{N} v_{2,n}' = (0.15 - 0.25 + 0.04 + 0.06)/4 = 0$$

so that

$$\overline{v_1'} \, \overline{v_2'} = \left(\frac{1}{N} \sum_{n=1}^{N} v_{1,n}' \right) \left(\frac{1}{N} \sum_{n=1}^{N} v_{2,n}' \right) = 0 \cdot 0 = 0$$

However, the time average of their product is not zero, i.e.

$$\overline{v_1' v_2'} = \frac{1}{N} \sum_{n=1}^{N} v_{1,n}' v_{2,n}' = (0.2 \cdot 0.15 + 0.3 \cdot 0.25 + 0.18 \cdot 0.04 - 0.08 \cdot 0.06)/4 = 0.02685$$

8.1.2 What is the difference between $\overline{v_1'^2}$ and $\overline{v_1'}^2$?

Using Eq. 6.2 we get

$$\overline{v_1'^2} = \frac{1}{2T} \int_{-T}^{T} v'^2 dt.$$

whereas

$$\overline{v_1'}^2 = \left(\frac{1}{2T} \int_{-T}^{T} v' dt \right)^2.$$

The numerical example gives

$$\overline{v_1'^2} = \frac{1}{N} \sum_{n=1}^{N} v_{1,n}'^2 = (0.2^2 + 0.3^2 + 0.18^2 + 0.08^2)/4 = 0.0422$$

$$\overline{v_2'^2} = \frac{1}{N} \sum_{n=1}^{N} v_{2,n}'^2 = (0.15^2 + 0.25^2 + 0.04^2 + 0.06^2)/4 = 0.02255$$

but

$$\overline{v_1'}^2 = \left(\frac{1}{N} \sum_{n=1}^{N} v_{1,n}' \right)^2 = [(0.2 - 0.3 + 0.18 - 0.08)/4]^2 = 0$$

$$\overline{v_2'}^2 = \left(\frac{1}{N} \sum_{n=1}^{N} v_{2,n}' \right)^2 = [(0.15 - 0.25 + 0.04 + 0.06)/4]^2 = 0$$

8.1.3 Show that $\overline{\bar{v}_1 v_1'^2} = \bar{v}_1 \overline{v_1'^2}$

Using Eq. 6.2 we get

$$\overline{\bar{v}_1 v_1'^2} = \frac{1}{2T} \int_{-T}^{T} \bar{v}_1 v_1'^2 dt$$

and since $\bar{v}$ does not depend on t we can take it out of the integral as

$$\bar{v}_1 \frac{1}{2T} \int_{-T}^{T} v_1'^2 dt = \bar{v}_1 \overline{v_1'^2}$$

Now let us do it with numerical values. Assume that $\bar{v}_1 = 10$.

$$\overline{\bar{v}_1 v_1'^2} = \frac{1}{N} \sum_{n=1}^{N} \left(\frac{1}{N} \sum_{m=1}^{N} v_{1,m} \right) v_{1,n}'^2 =$$
$$= (10 \cdot 0.2^2 + 10 \cdot 0.3^2 + 10 \cdot 0.18^2 + 10 \cdot 0.08^2)/4 = 0.422$$

$$\bar{v}_1 \overline{v_1'^2} = \left(\frac{1}{N} \sum_{n=1}^{N} v_{1,n} \right) \left(\frac{1}{N} \sum_{n=1}^{N} v_{1,n}'^2 \right) =$$
$$= \left[10 \cdot (0.2^2 + 0.3^2 + 0.18^2 + 0.08^2)/4 \right] = 0.422$$

8.1.4   Show that $\bar{\bar{v}}_1 = \bar{v}_1$

Using Eq. 6.2 we get

$$\bar{\bar{v}}_1 = \frac{1}{2T} \int_{-T}^{T} \bar{v}_1 dt$$

and since $\bar{v}$ does not depend on t we can take it out of the integral as

$$\bar{v}_1 \frac{1}{2T} \int_{-T}^{T} dt = \bar{v}_1 \frac{1}{2T} 2T = \bar{v}_1$$

With numerical values we get

$$\bar{\bar{v}}_1 = \frac{1}{N} \sum_{n=1}^{N} = (10 + 10 + 10 + 10)/4 = 10 = \bar{v}_1$$

8.2   The Exact k Equation

The equation for turbulent kinetic energy, $k = \frac{1}{2}\overline{v'_i v'_i}$, is derived from the Navier-Stokes equation. Again, we assume incompressible flow (constant density) and constant viscosity (cf. Eq. 6.6). We subtract Eq. 6.10 from Eq. 6.6 and divide by density, multiply by v'_i and time average which gives

$$\overline{v'_i \frac{\partial}{\partial x_j} [v_i v_j - \bar{v}_i \bar{v}_j]} =$$

$$-\frac{1}{\rho}\overline{v'_i \frac{\partial}{\partial x_i} [p - \bar{p}]} + \nu \overline{v'_i \frac{\partial^2}{\partial x_j \partial x_j} [v_i - \bar{v}_i]} + \overline{\frac{\partial \overline{v'_i v'_j}}{\partial x_j} v'_i} \tag{8.5}$$

Using $v_j = \bar{v}_j + v'_j$, the left side can be rewritten as

$$\overline{v'_i \frac{\partial}{\partial x_j} \left[(\bar{v}_i + v'_i)(\bar{v}_j + v'_j) - \bar{v}_i \bar{v}_j \right]} = \overline{v'_i \frac{\partial}{\partial x_j} \left[\bar{v}_i v'_j + v'_i \bar{v}_j + v'_i v'_j \right]}. \tag{8.6}$$

Using the continuity equation $\partial v'_j/\partial x_j = 0$ (see Eq. 6.11), the first term is rewritten as

$$\overline{v'_i \frac{\partial}{\partial x_j} \left(\bar{v}_i v'_j \right)} = \overline{v'_i v'_j} \frac{\partial \bar{v}_i}{\partial x_j}. \tag{8.7}$$

For the second term in Eq. 8.6 we start using $\partial \bar{v}_j/\partial x_j = 0$

$$\overline{v'_i \frac{\partial}{\partial x_j} \left(v'_i \bar{v}_j \right)} = \overline{\bar{v}_j v'_i \frac{\partial v'_i}{\partial x_j}} \tag{8.8}$$

Next, we use **Trick 2**

$$\bar{v}_j \left(\overline{v'_i \frac{\partial v'_i}{\partial x_j}} \right) = \bar{v}_j \frac{\partial}{\partial x_j} \overline{\left(\frac{1}{2} v'_i v'_i \right)} = \bar{v}_j \frac{\partial}{\partial x_j} (k) = \frac{\partial}{\partial x_j} (\bar{v}_j k) \tag{8.9}$$

The third term in Eq. 8.6 can be written as (replace $\bar{v}_j$ by v'_j and use the same technique as in Eq. 8.9)

$$\frac{1}{2} \frac{\partial}{\partial x_j} \overline{\left(v'_j v'_i v'_i \right)}. \tag{8.10}$$

The first term on the right side of Eq. 8.5 is re-written using **Trick 1**

$$-\frac{1}{\rho}\overline{v'_i\frac{\partial p'}{\partial x_i}} = -\frac{1}{\rho}\frac{\partial \overline{p'v'_i}}{\partial x_i} + \frac{1}{\rho}\overline{p'\frac{\partial v'_i}{\partial x_i}} = -\frac{1}{\rho}\frac{\partial \overline{p'v'_i}}{\partial x_i} \tag{8.11}$$

where the continuity equation was used at the last step. The second term on the right side of Eq. 8.5 can be written

$$\nu\overline{v'_i\frac{\partial^2 v'_i}{\partial x_j\partial x_j}} = \nu\overline{v'_i\frac{\partial}{\partial x_j}\left(\frac{\partial v'_i}{\partial x_j}\right)} = \nu\overline{\frac{\partial}{\partial x_j}\left(v'_i\frac{\partial v'_i}{\partial x_j}\right)} - \nu\overline{\frac{\partial v'_i}{\partial x_j}\frac{\partial v'_i}{\partial x_j}} \tag{8.12}$$

applying **Trick 1** ($A = v'_i$ and $B = \partial v'_i/\partial x_j$). For the first term in Eq. 8.12 we use the same trick as in Eq. 8.9 so that

$$\nu\overline{\frac{\partial}{\partial x_j}\left(v'_i\frac{\partial v'_i}{\partial x_j}\right)} = \nu\overline{\frac{\partial}{\partial x_j}\left(\frac{1}{2}\left(v'_i\frac{\partial v'_i}{\partial x_j} + v'_i\frac{\partial v'_i}{\partial x_j}\right)\right)} =$$
$$\nu\overline{\frac{\partial}{\partial x_j}\left(\frac{1}{2}\left(\frac{\partial v'_i v'_i}{\partial x_j}\right)\right)} = \nu\frac{1}{2}\frac{\partial^2 \overline{v'_i v'_i}}{\partial x_j\partial x_j} = \nu\frac{\partial^2 k}{\partial x_j\partial x_j} \tag{8.13}$$

The last term on the right side of Eq. 8.5 is zero because it is time averaging of a fluctuation, i.e. $\overline{\bar{a}b'} = \bar{a}\bar{b}' = 0$. Now we can assemble the transport equation for the turbulent kinetic energy. Equations 8.7, 8.9, 8.11, 8.12 and 8.13 give

$$\underbrace{\frac{\partial \bar{v}_j k}{\partial x_j}}_{I} = \underbrace{-\overline{v'_i v'_j}\frac{\partial \bar{v}_i}{\partial x_j}}_{II} \underbrace{-\frac{\partial}{\partial x_j}\left[\frac{1}{\rho}\overline{v'_j p'} + \frac{1}{2}\overline{v'_j v'_i v'_i} - \nu\frac{\partial k}{\partial x_j}\right]}_{III} \underbrace{-\nu\overline{\frac{\partial v'_i}{\partial x_j}\frac{\partial v'_i}{\partial x_j}}}_{IV} \tag{8.14}$$

The terms in Eq. 8.14 have the following meaning.

I **Convection**.

II **Production**, P^k. The large turbulent scales extract energy from the mean flow. This term (including the minus sign) is almost always positive. It is largest for the energy-containing eddies, i.e. for small wavenumbers, see Fig. 5.2. This term originates from the convection term (the first term on the right side of Eq. 8.6). It can be noted that the production term is an acceleration term, $v'_j\partial\bar{v}_i/\partial x_j$, multiplied by a fluctuating velocity, v'_i, i.e. the product of an inertial force per unit mass (acceleration) and a fluctuating velocity. A force multiplied with a velocity corresponds to work per unit time. When the acceleration term and the fluctuating velocity are in opposite directions (i.e. when $P^k > 0$), the mean flow performs work on the fluctuating velocity field. When the production term is **negative**, it means that the fluctuations are doing work on the mean flow field. In this case, v'_j and the acceleration term, $v'_j\partial\bar{v}_i/\partial x_j$, have the same sign.

Using Eq. 1.11, the production terms reads

$$P^k = -\overline{v'_i v'_j}\frac{\partial \bar{v}_i}{\partial x_j} = -\overline{v'_i v'_j}(\bar{S}_{ij} + \bar{\Omega}_{ij}) = -\overline{v'_i v'_j}\bar{S}_{ij} \tag{8.15}$$

(the product of the symmetric tensor, $\overline{v'_i v'_j}$, and the anti-symmetric tensor, $\bar{\Omega}_{ij}$, is zero). Thus it is only the symmetric part of the velocity gradient ($\bar{S}_{ij}$, the part that *deforms* a fluid element) that creates turbulence. The production does not depend on $\bar{\Omega}_{ij}$, the part of the velocity gradient that rotates a fluid element. This is consistent with the fact that the stress tensor, σ_{ij}, depends only on S_{ij}, not on Ω_{ij}, see discussion below Eq. 2.5.
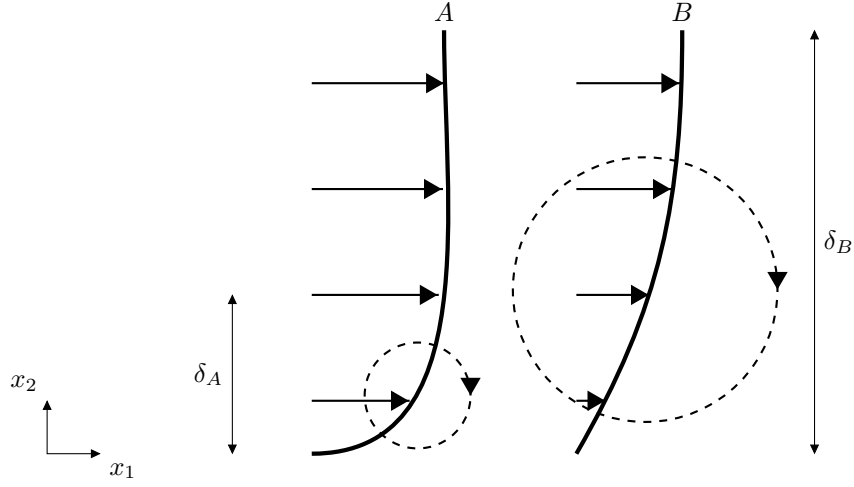
Figure 8.1: The size of the largest eddies (dashed lines) for different velocity profiles.

III The two first terms represent **turbulent diffusion** by pressure-velocity fluctuations, and velocity fluctuations, respectively. The last term is viscous diffusion. The velocity-fluctuation term originates from the convection term (the last term on the right side of Eq. 8.6).

IV **Dissipation**, ε. This term is responsible for transformation of kinetic energy at small scales to thermal energy. The term (excluding the minus sign) is always positive (it consists of velocity gradients squared). It is largest for large wavenumbers, see Fig. 5.2. The dissipation term stems from the viscous term (see Eq. 8.12) in the Navier-Stokes equation. It can be written as $\overline{v_i' \partial \tau_{ij}' / \partial x_j}$, see Eq. 4.1. The divergence of τ_{ij}' is a force vector (per unit mass), i.e. $T_i' = \partial \tau_{ij}' / \partial x_j$. The dissipation term can now be written $\overline{v_i' T_i'}$, which is a scalar product between two vectors. When the viscous stress vector is in the opposite direction to the fluctuating velocity, the term is negative (i.e. it is dissipative); this means that the viscose stress vector performs work and transforms kinetic energy into internal energy.

The transport equation for k can also be written in a simplified easy-to-read symbolic form as

$$C^k = P^k + D^k - \varepsilon \tag{8.16}$$

where C^k, P^k, D^k and ε correspond to terms I-IV in Eq. 8.14.

Above, it is stated that the production takes place at the large energy-containing eddies, i.e. we assume that the large eddies contribute much more to the production term more than the small eddies. There are two arguments for this:

1. The Reynolds stresses (which appear in P^k) are larger for large eddies than for small eddies.

2. The mean flow generates large eddies which will have same time scale as the mean velocity gradient, $\partial \bar{v}_i / \partial x_j$. In the fully turbulent region of a boundary layer, for example, both time scales are proportional to $\kappa x_2 / u_\tau$. The time scale of the velocity gradient is given by $\kappa x_2 / u_\tau$, see Eq. 6.27, and the time scale of
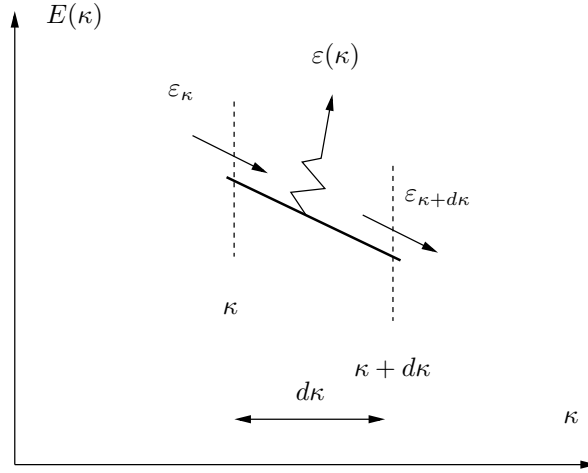
Figure 8.2: Zoom of the energy spectrum for a wavenumber located in Region II or III, see Fig. 5.2.

a large eddy is also given by $\ell_0/v_0 = \kappa x_2/u_\tau$. Figure 8.1 shows how different velocity profiles create different largest eddies. The largest eddies created by the velocity profile A are much smaller than those created by the velocity profile B, because the gradient of profile A acts over a much shorter length than the gradient of profile B.

In the cascade process (see Section 5.3) we assume that the viscous dissipation, ε, takes places at the smallest scales. How do we know that the majority of the dissipation takes place at the smallest scales? First, let us investigate how the time scale varies with eddy size. Consider the inertial subrange. let us denote the energy that is transferred in spectral space (i.e. from eddy-to-eddy) per unit time by ε_κ. How large is ε – that is generating heat – at wavenumber κ, which we here denote $\varepsilon(\kappa)$ (see Section 8.2.1 and Fig. 8.2)? Recall that the viscous dissipation, ε, is expressed as viscosity times the square of the velocity gradient, see Eq. 8.14. The velocity gradient for an eddy characterized by velocity v_κ and lengthscale ℓ_κ can be estimated as

$$\left(\frac{\partial v}{\partial x}\right)_\kappa \propto \frac{v_\kappa}{\ell_\kappa} \propto \left(v_\kappa^2\right)^{1/2} \kappa \tag{8.17}$$

since $\ell_\kappa \propto \kappa^{-1}$. We know that the energy spectrum (see Eqs. 5.10 and 5.13),

$$E(\kappa) \propto k_\kappa/\kappa \propto v_\kappa^2/\kappa \propto \kappa^{-5/3} \quad \Rightarrow \quad v_\kappa^2 \propto \kappa^{-2/3} \tag{8.18}$$

in the inertial region. Inserting Eq. 8.18 into Eq. 8.17 gives

$$\left(\frac{\partial v}{\partial x}\right)_\kappa \propto \left(\kappa^{-2/3}\right)^{1/2} \kappa \propto \kappa^{-1/3}\kappa \propto \kappa^{2/3} \tag{8.19}$$

Thus the viscous dissipation at wavenumber κ can be estimated as (see the last term in Eq. 8.14)

$$\varepsilon = \nu \overline{\frac{\partial v_i'}{\partial x_j}\frac{\partial v_i'}{\partial x_j}} \quad \Rightarrow \quad \varepsilon(\kappa) \propto \left(\frac{\partial v}{\partial x}\right)_\kappa^2 \propto \kappa^{4/3}, \tag{8.20}$$

i.e. $\varepsilon(\kappa)$ does indeed increase for increasing wavenumber.

The energy transferred from eddy-to-eddy per unit time in spectral space can also be used for estimating the velocity gradient of an eddy. The cascade process assumes that this energy transfer per unit time is the same for each eddy size, i.e. $\varepsilon_\kappa = \varepsilon = v_\kappa^3/\ell_\kappa = \ell_\kappa^2/\tau_\kappa^3 = \ell_0^2/\tau_0^3$, see Eq. 5.14. We find from $\ell_\kappa^2/\tau_\kappa^3 = \ell_0^2/\tau_0^3$ that for decreasing eddy size (decreasing ℓ_κ), the time scale, τ_κ, also decreases, i.e.

$$\tau_\kappa = \left(\frac{\ell_\kappa}{\ell_0}\right)^{2/3} \tau_0 \tag{8.21}$$

where τ_0 and ℓ_0 are constants (they are given by the flow we're looking at, for example a boundary layer which has the large scales, τ_0 and ℓ_0). Hence

$$\left(\frac{\partial v}{\partial x}\right)_\kappa \propto \frac{v_\kappa}{\ell_\kappa} \propto \tau_\kappa^{-1} \propto \ell_\kappa^{-2/3} \propto \kappa^{2/3}, \tag{8.22}$$

which is the same as Eq. 8.19.

8.2.1 Spectral transfer dissipation ε_κ vs. "true" viscous dissipation, ε

As a final note to the discussion in the previous section, it may be useful to look at the difference between the spectral transfer dissipation ε_κ, and the "true" viscous dissipation, ε; the former is the energy transferred from eddy-to-eddy per unit time, and the latter is the energy transformed per unit time to internal energy (i.e. increased temperature) for the entire spectrum (occurring mainly at the small, dissipative scales), see Fig. 5.2. Now consider Fig. 8.2 which shows a zoom of the energy spectrum. We assume that no mean flow energy production occurs between κ and $\kappa + d\kappa$, i.e. the region may be in the $-5/3$ region or in the dissipation region. Turbulent kinetic per unit time energy enters at wavenumber κ at a rate of ε_κ and leaves at wavenumber $\kappa + d\kappa$ a rate of $\varepsilon_{\kappa+d\kappa}$. If κ and $\kappa + d\kappa$ are located in the inertial region (i.e. the $-5/3$ region), then the usual assumption is that $\varepsilon_\kappa \simeq \varepsilon_{\kappa+d\kappa}$ and that there is no viscous dissipation to internal energy, i.e. $\varepsilon(\kappa) \simeq 0$. If there is viscous dissipation at wavenumber κ (which indeed is the case if zoomed region is located in the dissipative region), then $\varepsilon(\kappa)$ is simply obtained through an energy balance per unit time, i.e.

$$\varepsilon(\kappa) = \varepsilon_{\kappa+d\kappa} - \varepsilon_\kappa \tag{8.23}$$

8.3 The Exact k Equation: 2D Boundary Layers

In 2D boundary-layer flow, for which $\partial/\partial x_2 \gg \partial/\partial x_1$ and $\bar{v}_2 \ll \bar{v}_1$, the exact k equation reads

$$\frac{\partial \bar{v}_1 k}{\partial x_1} + \frac{\partial \bar{v}_2 k}{\partial x_2} = -\overline{v_1' v_2'}\frac{\partial \bar{v}_1}{\partial x_2}$$
$$- \frac{\partial}{\partial x_2}\left[\frac{1}{\rho}\overline{p' v_2'} + \frac{1}{2}\overline{v_2' v_i' v_i'} - \nu \frac{\partial k}{\partial x_2}\right] - \nu \overline{\frac{\partial v_i'}{\partial x_j}\frac{\partial v_i'}{\partial x_j}} \tag{8.24}$$

Note that the dissipation includes all derivatives. This is because the dissipation term is at its largest for small, isotropic scales for which all derivatives are of the same order and hence the usual boundary-layer approximation $\partial/\partial x_1 \ll \partial/\partial x_2$ does not apply for these scales.
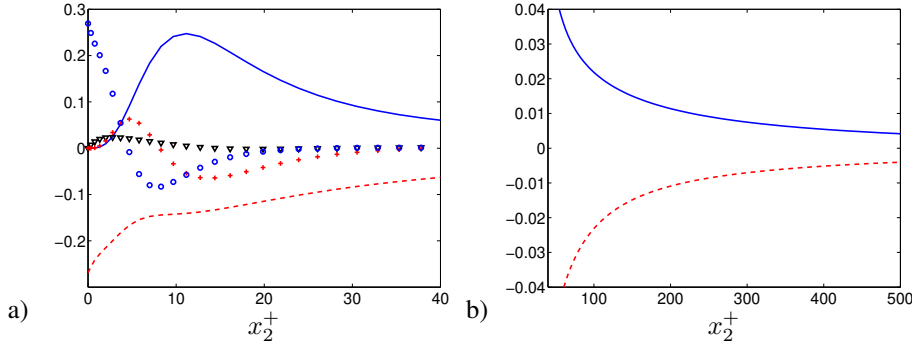
Figure 8.3: Channel flow at $Re_\tau = 2000$. Terms in the k equation scaled by u_τ^4/ν. $Re_\tau = 2000$. a) Zoom near the wall; b) Outer region. DNS (Direct Numerical Simulation) data [15, 16].
——— : P^k; — — : $-\varepsilon$; $\triangledown$: $-\partial\overline{v'p'}/\partial x_2$; $+$: $-\partial\overline{v_2'v_i'v_i'}/2/\partial x_2$; $\circ$: $\nu\partial^2 k/\partial x_2^2$.

(a) Velocity gradient

(b) Reynolds shear stress
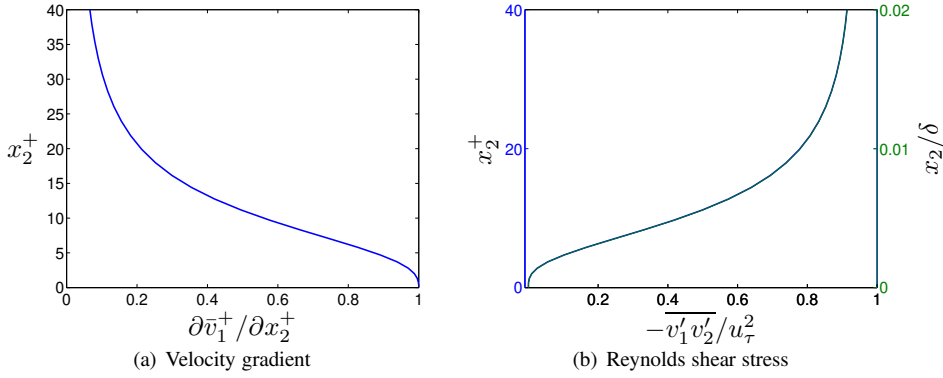
Figure 8.4: Channel flow at $Re_\tau = 2000$. DNS (Direct Numerical Simulation) data [15, 16].

Figure 8.3 presents the terms in Eq. 8.24 for fully developed channel flow. The left side is – since the flow is fully developed – zero. In the outer region (Fig. 8.3b) all terms are negligible except the production term and the dissipation term which balance each other. This is called *local equilibrium*, see p. 102. Closer to the wall (Fig. 8.3a) the other terms do also play a role. Note that the production and the dissipation terms close to the wall are two orders of magnitude larger than in the logarithmic region (Fig. 8.3b). At the wall the turbulent fluctuations are zero which means that the production term is zero. Since the region near the wall is dominated by viscosity the turbulent diffusion terms due to pressure and velocity are also small. The dissipation term and the viscous diffusion term attain their largest value at the wall and they much be equal to each other since all other terms are zero or negligible.

local equilibrium

The turbulence kinetic energy is produced by its main source term, the production term, $P^k = -\overline{v_1'v_2'}\partial\bar{v}_1/\partial x_2$. The velocity gradient is largest at the wall (see Fig. 8.4a) where the shear stress is zero (see Fig. 8.4b)); the former decreases and the magnitude of the latter increases with wall distance and their product takes its maximum at $x_2^+ \simeq 11$. Since P^k is largest here so is also k, see Fig. 6.8. k is transported in the x_2 direction by viscous and turbulent diffusion and it is destroyed (i.e. dissipated) by ε.

8.4 Spatial vs. spectral energy transfer

In Section 5.3 we discussed *spectral* transfer of turbulent kinetic energy from large to small eddies (which also applies to the transport of the Reynolds stresses). In Section 8.2 we derived the equation for *spatial* transport of turbulent kinetic energy. How are the spectral transfer and the spatial transport related? The reason that we in Section 5.3 only talked about spectral transfer was that we assumed homogeneous turbulence in which the spatial derivatives of the time-averaged turbulent quantities are zero, for example $\partial \overline{v_1'^2}/\partial x_i = 0$, $\partial k/\partial x_i = 0$ etc. (Note that the derivatives of the *instantaneous* turbulent fluctuations are non-zero even in homogeneous turbulence, i.e. $\partial v_1'/\partial x_i \neq 0$; the instantaneous flow field in turbulent flow is – as we mentioned at the beginning of this section, p. 70 – *always* three-dimensional and unsteady). In homogeneous turbulence the spatial transport terms (i.e. the convective term, term **I**, and the diffusion terms, term **III** in Eq. 8.14) are zero. Hence, in homogeneous turbulence there is no time-averaged spatial transport. However, there is *spectral transfer* of turbulent kinetic energy which takes place in wavenumber space, from large to small eddies. The production term (term **II** in Eq. 8.14) corresponds to the process in which large energy-containing eddies extract energy from the mean flow. The dissipation term (term **IV** in Eq. 8.14) corresponds to transformation of the turbulent kinetic energy at the small eddies to thermal energy. However, real flows are hardly ever homogeneous. Some flows may have one or two homogeneous directions. Consider, for example, fully developed channel turbulent flow. If the channel walls are very long and wide compared to the distance between the walls, 2δ, then the turbulence (and the flow) is homogeneous in the streamwise direction and the spanwise direction, i.e. $\partial \bar{v}_1/\partial x_1 = 0$, $\partial \overline{v_i'^2}/\partial x_1 = 0$, $\partial \overline{v_i'^2}/\partial x_3 = 0$ etc.

homogeneous turbulence

In non-homogeneous turbulence, the cascade process is not valid. Consider a large, turbulent eddy at a position x_2^A (see Fig. 6.1) in fully developed channel flow. The instantaneous turbulent kinetic energy, $k_\kappa = v_{\kappa,i}' v_{\kappa,i}'/2$, of this eddy may either be transferred in wavenumber space or transported in physical (spatial) space, or both. It may first be transported in physical space towards the center, and there lose its kinetic energy to smaller eddies. This should be kept in mind when thinking in terms of the cascade process. Large eddies which extract their energy from the mean flow may not give their energy to the slightly smaller eddies as assumed in Figs. 5.2 and 5.1, but k_κ may first be transported in physical space and then transferred in spectral space (i.e. to a smaller eddy).

In the inertial range (Region II), however, the cascade process is still a good approximation even in non-homogeneous turbulence. The reason is that the transfer of turbulent kinetic energy, k_κ, from eddy-to-eddy, occurs at a much faster rate than the spatial transport by convection and diffusion. In other words, the time scale of the cascade process is much smaller than that of convection and diffusion which have no time to transport k_κ in space before it is passed on to a smaller eddy by the cascade process. We say that the turbulence at these scales is in *local equilibrium*. The turbulence in the buffer layer and the logarithmic layer of a boundary layer (see Fig. 6.2) is in local equilibrium. In Townsend [22], this is (approximately) stated as:

local equilibrium

> the local rates of turbulent kinetic energy (i.e. production and dissipation) are so large that aspects of the turbulent motion concerned with these processes are independent of conditions elsewhere in the flow.

This statement simply means that production is equal to dissipation, i.e. $P^k = \varepsilon$, see Fig. 8.3.

In summary, care should be taken in non-homogeneous turbulence, regarding the validity of the cascade process for the large scales (Region I).

8.5 The overall effect of the transport terms

The overall effect (i.e. the net effect) of the production term is to increase k, i.e. if we integrate the production term over the entire domain, V, we get

$$\int_V P^k dV > 0 \tag{8.25}$$

Similarly, the net effect of the dissipation term is a negative contribution, i.e.

$$\int_V -\varepsilon dV < 0 \tag{8.26}$$

What about the overall effect of the *transport* terms, i.e. convection and diffusion? Integration of the convection term over the entire volume, V, gives, using Gauss divergence law,

$$\int_V \frac{\partial \bar{v}_j k}{\partial x_j} dV = \int_S \bar{v}_j k n_j dS \tag{8.27}$$

where S is the bounding surface of V. This shows that the net effect of the convection term occurs only at the boundaries. Inside the domain, the convection merely transports k with out adding or subtracting anything to the integral of k, $\int_V k dV$; the convection acts as a source term in part of the domain, but in the remaining part of the domain it acts as an equally large sink term. Similarly for the diffusion term, we get

$$
\begin{aligned}
&- \int_V \frac{\partial}{\partial x_j} \left(\frac{1}{2} \overline{v'_j v'_k v'_k} + \frac{1}{\rho} \overline{p' v'_j} - \nu \frac{\partial k}{\partial x_j} \right) V \\
&= - \int_S \left(\frac{1}{2} \overline{v'_j v'_k v'_k} + \frac{1}{\rho} \overline{p' v'_j} - \nu \frac{\partial k}{\partial x_j} \right) n_j dS
\end{aligned}
\tag{8.28}
$$

The only net contribution occurs at the boundaries. Hence, Eqs. 8.27 and 8.28 show that the transport terms only – as the word implies – *transports* k without giving any net effect except at the boundaries. Mathematically these terms are called *divergence terms*, i.e. they can both be written as the divergence of a vector A_j,

divergence terms

$$\frac{\partial A_j}{\partial x_j} \tag{8.29}$$

where A_j for the convection and the diffusion term reads

$$
A_j = \begin{cases} \bar{v}_j k & \text{convection term} \\ -\left(\frac{1}{2} \overline{v'_j v'_k v'_k} + \frac{1}{\rho} \overline{p' v'_j} - \nu \frac{\partial k}{\partial x_j} \right) & \text{diffusion term} \end{cases}
\tag{8.30}
$$

8.6 The transport equation for $\bar{v}_i \bar{v}_i / 2$

The equation for $K = \bar{v}_i \bar{v}_i / 2$ is derived in the same way as that for $\overline{v'_i v'_i}/2$. Multiply the time-averaged Navier-Stokes equations, Eq. 6.10, by $\bar{v}_i$ so that

$$\bar{v}_i \frac{\partial \bar{v}_i \bar{v}_j}{\partial x_j} = -\frac{1}{\rho} \bar{v}_i \frac{\partial \bar{p}}{\partial x_i} + \nu \bar{v}_i \frac{\partial^2 \bar{v}_i}{\partial x_j \partial x_j} - \bar{v}_i \frac{\partial \overline{v'_i v'_j}}{\partial x_j}. \tag{8.31}$$
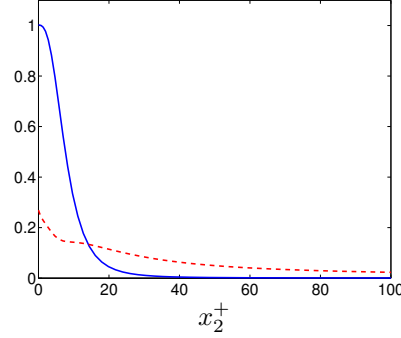
Figure 8.5: Channel flow at $Re_\tau = 2000$. Comparison of mean and fluctuating dissipation terms, see Eqs. 8.37 and 8.38. Both terms are normalized by u_τ^4/ν. DNS (Direct Numerical Simulation) data [15, 16]. ──── : $\nu(\partial\bar{v}_1/\partial x_2)^2$; ─ ─ : ε.

Using the continuity equation and **Trick 2** the term on the left side can be rewritten as

$$\bar{v}_i\frac{\partial\bar{v}_i\bar{v}_j}{\partial x_j} = \bar{v}_j\bar{v}_i\frac{\partial\bar{v}_i}{\partial x_j} = \bar{v}_j\frac{\frac{1}{2}\partial\bar{v}_i\bar{v}_i}{\partial x_j} = \frac{\partial\bar{v}_j K}{\partial x_j} \tag{8.32}$$

The viscous term in Eq. 8.31 is rewritten in the same way as the viscous term in Section 8.2, see Eqs. 8.12 and 8.13, i.e.

$$\nu\bar{v}_i\frac{\partial^2\bar{v}_i}{\partial x_j\partial x_j} = \nu\frac{\partial^2 K}{\partial x_j\partial x_j} - \nu\frac{\partial\bar{v}_i}{\partial x_j}\frac{\partial\bar{v}_i}{\partial x_j}. \tag{8.33}$$

Equations 8.32 and 8.33 inserted in Eq. 8.31 gives

$$\frac{\partial\bar{v}_j K}{\partial x_j} = \nu\frac{\partial^2 K}{\partial x_j\partial x_j} - \frac{\bar{v}_i}{\rho}\frac{\partial\bar{p}}{\partial x_i} - \nu\frac{\partial\bar{v}_i}{\partial x_j}\frac{\partial\bar{v}_i}{\partial x_j} - \bar{v}_i\frac{\partial\overline{v_i'v_j'}}{\partial x_j}. \tag{8.34}$$

The last term is rewritten using **Trick 1** as

$$-\bar{v}_i\frac{\partial\overline{v_i'v_j'}}{\partial x_j} = -\frac{\partial\bar{v}_i\overline{v_i'v_j'}}{\partial x_j} + \overline{v_i'v_j'}\frac{\partial\bar{v}_i}{\partial x_j}. \tag{8.35}$$

Note that the first term on the right side differs to the corresponding term in Eq. 8.14 by a factor of two since **Trick 2** cannot be used because $\bar{v}_i \neq v_i'$. Inserted in Eq. 8.34 gives (cf. Eq. 8.14)

$$\frac{\partial\bar{v}_j K}{\partial x_j} = \underbrace{\overline{v_i'v_j'}\frac{\partial\bar{v}_i}{\partial x_j}}_{-P^k,\ \text{sink}} \underbrace{-\frac{\bar{v}_i}{\rho}\frac{\partial\bar{p}}{\partial x_i}}_{\text{source}} - \frac{\partial}{\partial x_j}\left(\bar{v}_i\overline{v_i'v_j'} - \nu\frac{\partial K}{\partial x_j}\right) \underbrace{-\nu\frac{\partial\bar{v}_i}{\partial x_j}\frac{\partial\bar{v}_i}{\partial x_j}}_{\varepsilon_{mean},\ \text{sink}} \tag{8.36}$$

On the left side we have the usual convective term. On the right side we find:

- loss of energy to k due to the production term

- work performed by the pressure gradient; in channel flow, for example, this term gives a positive contribution to K (as expected) since $-\bar{v}_1\partial\bar{p}/\partial x_1 > 0$

- diffusion by velocity-stress interaction
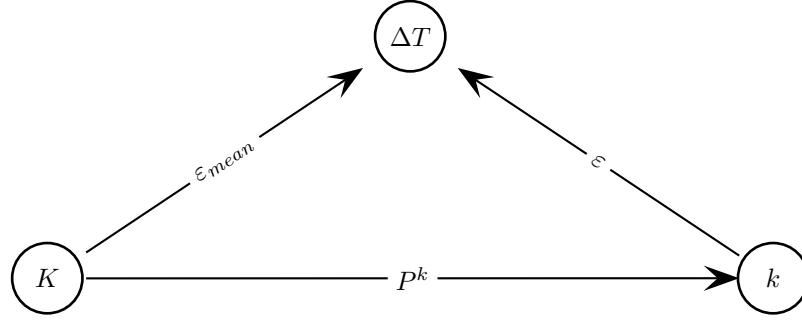
Figure 8.6: Transfer of energy between mean kinetic energy (K), turbulent kinetic energy (k) and internal energy (denoted as an increase in temperature, ΔT). $K = \frac{1}{2}\bar{v}_i\bar{v}_i$ and $k = \frac{1}{2}\overline{v'_i v'_i}$.

- viscous diffusion.

- viscous dissipation, ε_{mean}. This corresponds to the dissipation term in Eq. 2.23; if you replace v_i with $\bar{v}_i$ and use the continuity equation to get rid of the second velocity gradient in $\bar{S}_{ij}$ you find that the dissipation term in Eq. 2.23 (see Eq. 2.26), is identical to ε_{mean}.

Note that the first term in Eq. 8.36 is the same as the first term in Eq. 8.14 but with opposite sign: here we clearly can see that the main source term in the k equation (the production term) appears as a sink term in the K equation.

In the K equation the dissipation term and the negative production term (representing loss of kinetic energy to the k field) read

$$-\nu\frac{\partial \bar{v}_i}{\partial x_j}\frac{\partial \bar{v}_i}{\partial x_j} + \overline{v'_i v'_j}\frac{\partial \bar{v}_i}{\partial x_j}, \tag{8.37}$$

and in the k equation the production and the dissipation terms read

$$-\overline{v'_i v'_j}\frac{\partial \bar{v}_i}{\partial x_j} - \nu\overline{\frac{\partial v'_i}{\partial x_j}\frac{\partial v'_i}{\partial x_j}} \tag{8.38}$$

The gradient of the time-averaged velocity field, $\bar{v}_i$, is much smoother than the gradient of the fluctuating velocity field, v'_i. Hence, the dissipation by the turbulent fluctuations, ε, in the turbulent region (logarithmic region and further out from walls), is much larger than the dissipation by the mean flow (left side of Eq. 8.37). This is seen in Fig. 8.5 $(x_2^+ \gtrsim 15)$. The energy flow from the mean flow to internal energy is illustrated in Fig. 8.6. The major part of the energy flow goes from K to k and then to dissipation.

In the viscous-dominated wall region $(x_2^+ \lesssim 5)$, the mean dissipation, $\nu(\partial \bar{v}_1/\partial x_2)^2$, is much larger than ε, see Fig. 8.5. At the wall, the mean dissipation takes the value $\nu = 1/2000$ (normalized by u_τ^4/ν).

9 Transport equations for Reynolds stresses

I N this section we will derive the transport equation for the Reynolds stress tensor. This is an unknown quantity in the time-averaged Navier-Stokes equations, Eq. 6.10, which must be known before Eq. 6.10 can be solved. The most accurate way to find $\overline{v_i'v_j'}$ is, of course, to solve a transport equation for it. This is computationally expensive since we then need to solve six additional transport equations (recall that $\overline{v_i'v_j'}$ is symmetric, i.e. $\overline{v_1'v_2'} = \overline{v_2'v_1'}$ etc). Often, some simplifications are introduced, in which $\overline{v_i'v_j'}$ is *modeled* by expressing it as the product of a turbulent viscosity and velocity gradients. Two-equations models are commonly used in these simplified models; no transport equation for $\overline{v_i'v_j'}$ is solved.

In Section 8 we derived transport equations for kinetic turbulent energy, k, which is the trace of the Reynolds stress tensor $\overline{v_i'v_j'}$ divided by two, i.e. $k = \overline{v_i'v_i'}/2$. This means that k is equal to half the sum of the diagonal components of $\overline{v_i'v_j'}$, i.e. $k = 0.5(\overline{v_1'^2} + \overline{v_2'^2} + \overline{v_3'^2})$.

Now let us start to derive the transport equation for $\overline{v_i'v_j'}$. This approach is very similar to that we used when deriving the k equation in Section 8.2. Steady, incompressible flow with constant density and viscosity is assumed. Subtract Eq. 6.10 from Eq. 6.6 and divide by density, multiply by v_j' and time average and we obtain

$$
\overline{v_j'\frac{\partial}{\partial x_k}[v_iv_k - \bar{v}_i\bar{v}_k]} =
$$
$$
-\frac{1}{\rho}\overline{v_j'\frac{\partial}{\partial x_i}p'} + \nu\overline{v_j'\frac{\partial^2 v_i'}{\partial x_k \partial x_k}} + \overline{\frac{\partial \overline{v_i'v_k'}}{\partial x_k}v_j'}
\tag{9.1}
$$

Equation 6.10 is written with the index i as free index, i.e. $i = 1, 2$ or 3 so that the equation is an equation for v_1, v_2 or v_3. Now write Eq. 6.10 as an equation for v_j and multiply this equation by v_i'. We get

$$
\overline{v_i'\frac{\partial}{\partial x_k}[v_jv_k - \bar{v}_j\bar{v}_k]} =
$$
$$
-\frac{1}{\rho}\overline{v_i'\frac{\partial}{\partial x_j}p'} + \nu\overline{v_i'\frac{\partial^2 v_j'}{\partial x_k \partial x_k}} + \overline{\frac{\partial \overline{v_j'v_k'}}{\partial x_k}v_i'}
\tag{9.2}
$$

It may be noted that Eq. 9.2 is conveniently obtained from Eq. 9.1 by simply switching indices i and j. Adding Eqs. 9.1 and 9.2 together gives

$$
\overline{v_j'\frac{\partial}{\partial x_k}[v_iv_k - \bar{v}_i\bar{v}_k]} + \overline{v_i'\frac{\partial}{\partial x_k}[v_jv_k - \bar{v}_j\bar{v}_k]} =
$$
$$
-\frac{1}{\rho}\overline{v_i'\frac{\partial p'}{\partial x_j}} - \frac{1}{\rho}\overline{v_j'\frac{\partial p'}{\partial x_i}}
$$
$$
+\nu\overline{v_i'\frac{\partial^2 v_j'}{\partial x_k \partial x_k}} + \nu\overline{v_j'\frac{\partial^2 v_i'}{\partial x_k \partial x_k}}
$$
$$
+\overline{\frac{\partial \overline{v_j'v_k'}}{\partial x_k}v_i'} + \overline{\frac{\partial \overline{v_i'v_k'}}{\partial x_k}v_j'}
\tag{9.3}
$$

Note that each line in the equation is *symmetric*: if you switch indices i and j in any of the lines nothing changes. This is important: since the tensor $\overline{v_i'v_j'}$ is symmetric, all

terms in its transport equation must also be symmetric. Furthermore, you can check that the equation is correct according to the tensor notation rules. Indices i and j appear once in each term (not more, not less) and index k (the dummy index) appears exactly twice in each term (implying summation). Note that it is permitted to use any other index than k in some terms (but you must not use i and j). You could, for example, replace k with m in the first term and with q in the second term; however, usually we use the same dummy index in every term.

Using $v_i = \bar{v}_i + v'_i$, the first line can be rewritten as

$$\overline{v'_j \frac{\partial}{\partial x_k} \left[\bar{v}_i v'_k + v'_i \bar{v}_k + v'_i v'_k \right]} + \overline{v'_i \frac{\partial}{\partial x_k} \left[\bar{v}_j v'_k + v'_j \bar{v}_k + v'_j v'_k \right]} \qquad (9.4)$$

Using the continuity equation the first terms in the two groups are rewritten as

$$\overline{v'_j v'_k} \frac{\partial \bar{v}_i}{\partial x_k} + \overline{v'_i v'_k} \frac{\partial \bar{v}_j}{\partial x_k} \qquad (9.5)$$

We merge the second terms in the two groups in Eq. 9.4.

$$\overline{v'_j \frac{\partial v'_i \bar{v}_k}{\partial x_k}} + \overline{v'_i \frac{\partial v'_j \bar{v}_k}{\partial x_k}} = \bar{v}_k \overline{v'_j \frac{\partial v'_i}{\partial x_k}} + \bar{v}_k \overline{v'_i \frac{\partial v'_j}{\partial x_k}}$$

$$= \bar{v}_k \frac{\partial \overline{v'_i v'_j}}{\partial x_k} = \frac{\partial \overline{v'_i v'_j} \bar{v}_k}{\partial x_k} \qquad (9.6)$$

The continuity equation was used twice (to get the right side on the first line and to get the final expression) and the product rule was used backwards to get the second line. Re-writing also the third terms in the two groups in Eq. 9.4 in the same way, the second and the third terms in Eq. 9.4 can be written

$$\frac{\partial \overline{v'_i v'_j} \bar{v}_k}{\partial x_k} + \frac{\partial \overline{v'_i v'_j v'_k}}{\partial x_k} \qquad (9.7)$$

The second line in Eq. 9.3 is also re-written using **Trick 1**

$$-\frac{1}{\rho} \frac{\partial}{\partial x_j} \overline{v'_i p'} - \frac{1}{\rho} \frac{\partial}{\partial x_i} \overline{v'_j p'} + \frac{1}{\rho} \overline{p' \frac{\partial v'_i}{\partial x_j}} + \frac{1}{\rho} \overline{p' \frac{\partial v'_j}{\partial x_i}} \qquad (9.8)$$

It will later turn out that it is convenient to express all derivatives as $\partial/\partial x_k$. Therefore we re-write the derivative in the two first terms as

$$\frac{\partial}{\partial x_j} = \delta_{jk} \frac{\partial}{\partial x_k} \text{ and } \frac{\partial}{\partial x_i} = \delta_{ik} \frac{\partial}{\partial x_k} \qquad (9.9)$$

so that

$$-\delta_{jk} \frac{1}{\rho} \frac{\partial}{\partial x_k} \overline{v'_i p'} - \delta_{ik} \frac{1}{\rho} \frac{\partial}{\partial x_k} \overline{v'_j p'} + \frac{1}{\rho} \overline{p' \frac{\partial v'_i}{\partial x_j}} + \frac{1}{\rho} \overline{p' \frac{\partial v'_j}{\partial x_i}} \qquad (9.10)$$

The third line in Eq. 9.3 is also re-written using **Trick 1**

$$\nu \frac{\partial}{\partial x_k} \overline{\left(v'_i \frac{\partial v'_j}{\partial x_k} \right)} + \nu \frac{\partial}{\partial x_k} \overline{\left(v'_j \frac{\partial v'_i}{\partial x_k} \right)} - 2\nu \overline{\frac{\partial v'_i}{\partial x_k} \frac{\partial v'_j}{\partial x_k}}$$

The product rule is used backwards to merge the two first terms so that the third line in Eq. 9.3 reads

$$
\nu \frac{\partial}{\partial x_k} \overline{\left(v'_i \frac{\partial v'_j}{\partial x_k} + v'_j \frac{\partial v'_i}{\partial x_k} \right)} - 2\nu \overline{\frac{\partial v'_i}{\partial x_k} \frac{\partial v'_j}{\partial x_k}}
$$

$$
= \nu \frac{\partial}{\partial x_x} \left(\frac{\partial \overline{v'_i v'_j}}{\partial x_k} \right) - 2\nu \overline{\frac{\partial v'_i}{\partial x_k} \frac{\partial v'_j}{\partial x_k}} = \nu \frac{\partial^2 \overline{v'_i v'_j}}{\partial x_k \partial x_k} - 2\nu \overline{\frac{\partial v'_i}{\partial x_k} \frac{\partial v'_j}{\partial x_k}}
$$

$$(9.11)$$

The terms on the fourth line in Eq. 9.3 are zero because $\overline{\bar{a} b'} = \bar{a} \bar{b}' = 0$. We can now put everything together. Put the first term in Eq. 9.7 on the left side and the second term on the right side together with Eqs. 9.5, 9.10 and 9.11 so that

$$
\underbrace{\frac{\partial}{\partial x_k} (\bar{v}_k \overline{v'_i v'_j})}_{C_{ij}, \mathbf{I}} = \underbrace{-\overline{v'_j v'_k} \frac{\partial \bar{v}_i}{\partial x_k} - \overline{v'_i v'_k} \frac{\partial \bar{v}_j}{\partial x_k}}_{P_{ij}, \mathbf{II}}
$$

$$
\underbrace{- \frac{\partial}{\partial x_k} \left(\overline{v'_i v'_j v'_k} + \frac{1}{\rho} \delta_{jk} \overline{v'_i p'} + \frac{1}{\rho} \delta_{ik} \overline{v'_j p'} - \nu \frac{\partial \overline{v'_i v'_j}}{\partial x_k} \right)}_{D_{ij}, \mathbf{III}}
$$

$$(9.12)$$

$$
\underbrace{+ \frac{1}{\rho} \overline{p' \left(\frac{\partial v'_i}{\partial x_j} + \frac{\partial v'_j}{\partial x_i} \right)}}_{\Pi_{ij}, \mathbf{V}} - \underbrace{2\nu \overline{\frac{\partial v'_i}{\partial x_k} \frac{\partial v'_j}{\partial x_k}}}_{\varepsilon_{ij}, \mathbf{IV}}
$$

Note that the manipulation in Eq. 9.9 allows the diffusion (term III) to be written on a more compact form. After a derivation, it is always useful to check that the equation is correct according to the tensor notation rules.

- Every term – or group of terms – should include the free indices i and j (only once);

- Every term – or group of terms – should be symmetric in i and j;

- A dummy index (in this case index k) must appear exactly twice (=summation) in every term

Equation 9.12 can also be written in a simplified easy-to-read symbolic form as

$$
C_{ij} = P_{ij} + D_{ij} + \Pi_{ij} - \varepsilon_{ij} \tag{9.13}
$$

where Π_{ij} denotes the pressure-strain term

$$
\Pi_{ij} = \overline{\frac{p'}{\rho} \left(\frac{\partial v'_i}{\partial x_j} + \frac{\partial v'_j}{\partial x_i} \right)} \tag{9.14}
$$

Equation 9.12 is the (exact) transport equation of the Reynolds stress, $\overline{v'_i v'_j}$. It is called the *Reynolds stress equations*. It is an equation for a second-order tensor which consists of nine equations, but since it is symmetric we only need to consider six of them. Compare Eq. 9.12 with the equation for turbulent kinetic energy, Eq. 8.14. An alternative – and maybe easier – way to derive Eq. 8.14 is to first derive Eq. 9.12 and then take the trace (setting $i = j$) and divide by two. In both the k and the $\overline{v'_i v'_j}$ equations

Reynolds stress equations
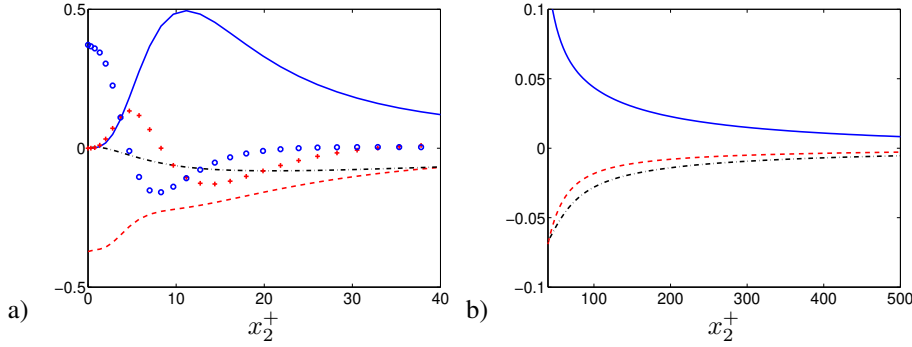
Figure 9.1: Channel flow at $Re_\tau = 2000$. Terms in the $\overline{v_1'^2}$ equation scaled by u_τ^4/ν. a) Zoom near the wall; b) Outer region. DNS (Direct Numerical Simulation) data [15, 16]. ——— : P_{11}; – – – : $-\varepsilon_{11}$; –·–·– : Π_{11}; + : $-\partial(\overline{v_2'v_1'^2})/\partial x_2$; ○ : $\nu\partial^2\overline{v_1'^2}/\partial x_2^2$.

there is a convection term (I), a production term (II), a diffusion term (III) and a dissipation term (IV). In the $\overline{v_i'v_j'}$ equation there is a fifth term (V), see Eq. 9.14, which is called the pressure strain term. The physical meaning of this term is to redistribute energy between the normal stress components (if we transform Eq. 9.12 to the principal coordinates of $\overline{v_i'v_j'}$ there are no shear stresses, only normal stresses). The average of the normal stresses is $\overline{v_{av}'^2} = \overline{v_i'v_i'}/3$. For a normal stress that is larger than $\overline{v_{av}'^2}$, the pressure-strain term is negative and vice-versa. It is often called the *Robin Hood* term because it – as Robin Hood – "takes from the rich and gives to the poor". Note that the trace of the pressure-strain term is zero, i.e.

pressure strain

Robin Hood

$$\Pi_{ii} = \frac{1}{\rho}\overline{p'\left(\frac{\partial v_i'}{\partial x_i} + \frac{\partial v_i'}{\partial x_i}\right)} = 0 \tag{9.15}$$

because of the continuity equation and this is the reason why this term does not appear in the k equation.

For 2D boundary layer flow, Eq. 9.12 reads

$$\frac{\partial}{\partial x_1}(\bar{v}_1\overline{v_i'v_j'}) + \frac{\partial}{\partial x_2}(\bar{v}_2\overline{v_i'v_j'}) = -\overline{v_j'v_2'}\frac{\partial \bar{v}_i}{\partial x_2} - \overline{v_i'v_2'}\frac{\partial \bar{v}_j}{\partial x_2}$$
$$-\frac{\partial}{\partial x_2}\left(\overline{v_i'v_j'v_2'} + \frac{1}{\rho}\delta_{j2}\overline{v_i'p'} + \frac{1}{\rho}\delta_{i2}\overline{v_j'p'} - \nu\frac{\partial\overline{v_i'v_j'}}{\partial x_2}\right) \tag{9.16}$$
$$+\frac{1}{\rho}\overline{p'\left(\frac{\partial v_i'}{\partial x_j} + \frac{\partial v_j'}{\partial x_i}\right)} - 2\nu\overline{\frac{\partial v_i'}{\partial x_k}\frac{\partial v_j'}{\partial x_k}}$$

Now let us look at this equation for fully developed channel flow for which

$$\bar{v}_2 = \bar{v}_3 = 0$$
$$\frac{\partial\overline{(\cdot)}}{\partial x_1} = \frac{\partial\overline{(\cdot)}}{\partial x_3} = 0 \tag{9.17}$$

Note that on the second line the streamwise (x_1) and the spanwise (x_3) derivatives operate on *time-averaged* quantities; those that operate on instantaneous quantities, such as in ε_{ij} and Π_{ij}, are not zero.
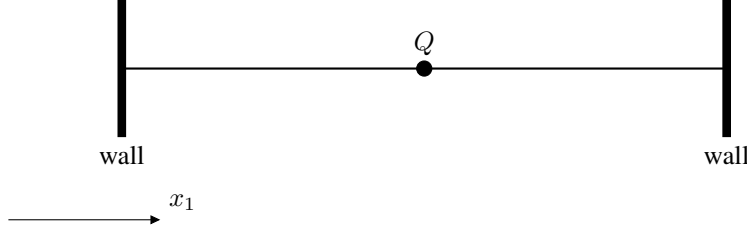
Figure 9.2: One-dimensional unsteady heat conduction. In the middle there is a heat source, Q.

9.1 Source terms

In order to analyze the Reynolds stress equation, Eq. 9.16, we will now look at the source terms. A positive source term in a transport equation, for example Φ, increases the value of Φ. A simple example is the one-dimensional unsteady heat conduction equation (Eq. 2.18 with $v_i \equiv 0$)

$$\frac{\partial T}{\partial t} = \alpha \frac{\partial^2 T}{\partial x_1^2} + Q \tag{9.18}$$

where Q is a heat source, see Fig. 9.2. If Q is positive, T will increase and vice-versa.

Now we will look at an important source term in the $\overline{v_i' v_j'}$ equation, namely the production term. The production term in Eq. 9.16 reads

$$P_{ij} = -\overline{v_j' v_2'} \frac{\partial \bar{v}_i}{\partial x_2} - \overline{v_i' v_2'} \frac{\partial \bar{v}_j}{\partial x_2} \tag{9.19}$$

In fully-developed channel flow, we get for the $\overline{v_1'^2}$ ($i = j = 1$), $\overline{v_2'^2}$ ($i = j = 2$), $\overline{v_3'^2}$ ($i = j = 3$) and $\overline{v_1' v_2'}$ ($i = 1, j = 2$) equations

$$P_{11} = -2\overline{v_1' v_2'} \frac{\partial \bar{v}_1}{\partial x_2} \tag{9.20a}$$

$$P_{22} = -2\overline{v_2' v_2'} \frac{\partial \bar{v}_2}{\partial x_2} = 0 \tag{9.20b}$$

$$P_{33} = -2\overline{v_3' v_2'} \frac{\partial \bar{v}_3}{\partial x_2} = 0 \tag{9.20c}$$

$$P_{12} = -\overline{v_2' v_2'} \frac{\partial \bar{v}_1}{\partial x_2} - \overline{v_1' v_2'} \frac{\partial \bar{v}_2}{\partial x_2} = -\overline{v_2'^2} \frac{\partial \bar{v}_1}{\partial x_2} \tag{9.20d}$$

using Eq. 9.17.

Figure 9.1 presents the terms in the $\overline{v_1'^2}$ equation (Eq. 9.16 with $i = j = 1$). As we saw for the k equation, the production term, P_{11}, reaches its maximum at $x_2 \simeq 11$ where also $\overline{v_1'^2}$ takes its maximum (Fig. 6.8). The pressure-strain term, Π_{11}, and the dissipation term act as sink terms. In the outer region (Fig. 9.1b) the production term balances the pressure-strain term and the dissipation term.

The terms in the wall-normal stress equation, $\overline{v_2'^2}$, are shown in Fig. 9.4. Here we find – as expected – that the pressure-strain term, Π_{22}, acts as the main source term. As mentioned previously, Π_{22} – the "Robin Hood" term – takes from the "rich" $\overline{v_1'^2}$ equation and gives to the "poor" $\overline{v_2'^2}$ equation energy because $\overline{v_1'^2}$ is large and $\overline{v_2'^2}$ is small.

Figure 9.4 presents the terms in the $\overline{v_3'^2}$ equation. As for the $\overline{v_2'^2}$ equation, the main source term is the pressure-strain term, but it may be noted that here it is positive near the wall; for the $\overline{v_2'^2}$ equation it goes negative near the wall since the pressure-strain term dampens $\overline{v_2'^2}$ near the wall. Another difference is that the pressure diffusion term, $2\partial\overline{v_3'p'}/\partial x_2$, is zero (as it is in the $\overline{v_1'^2}$ equation), whereas it near the wall gives an important contribution in the $\overline{v_2'^2}$ equation (it balances the negative pressure-strain term).

Figure 9.6 presents the terms in the $\overline{v_1'v_2'}$ equation. The production term – which should be a source term – is here negative. Indeed it should be. Recall that $\overline{v_1'v_2'}$ is here negative and hence its source must be negative; or, rather, the other way around: $\overline{v_1'v_2'}$ is negative because its production term, $P_{12} = -\overline{v_2'^2}\partial\overline{v}_1/\partial x_2$, is negative since $\partial\overline{v}_1/\partial x_2 > 0$. Note that in the upper half of the channel $\partial\overline{v}_1/\partial x_2 < 0$ and hence P_{12} and $\overline{v_1'v_2'}$ are positive. Furthermore, note that the dissipation, ε_{12}, is zero. This is because dissipation takes place at the smallest scales and they are isotropic. That implies there is no correlation between two fluctuating velocity components, e.g. $\overline{v_1'v_2'} = 0$ (in general, for $i \neq j$, the stresses $\overline{v_i'v_j'}$ in isotropic turbulence are zero). Hence, also their gradients are zero so that

$$\varepsilon_{12} = 2\nu\overline{\frac{\partial v_1'}{\partial x_k}\frac{\partial v_2'}{\partial x_k}} = 0 \qquad (9.21)$$

However, very close to the wall, $x_2^+ \leq 10$, $\varepsilon_{12} \neq 0$ because here the wall affects the dissipative scales making them non-isotropic; ε_{12} is positive since $\overline{v_1'v_2'} < 0$, see Fig. 9.6. When looking at the energy spectrum, neither the production term nor the dissipation of the mean kinetic energy enters the spectrum, see Fig. 9.3

The main sink term in the $\overline{v_1'v_2'}$ equation is the pressure-strain term, π_{12}, see Fig. 9.6. But since $\overline{v_1'v_2'} < 0$ in the lower half of the channel, it means that it is positive. In order to understand the sign of π_{12}, we can look at the pressure-strain term in the principal coordinate directions and transform it to the $x_1 - x_2$ coordinate system, see Eq. 11.52.

If you want to learn more how to derive transport equations of turbulent quantities, see [23] which can be downloaded here
http://www.tfd.chalmers.se/~lada/allpaper.html

9.2 Reynolds shear stress vs. the velocity gradient

In boundary-layer type of flow, the Reynolds shear stress and the velocity gradient $\partial\overline{v}_1/\partial x_2$ have nearly always opposite signs. For channel flow, for example, Eq. 9.20 shows that P_{12} is negative (and hence also $\overline{v_1'v_2'}$) in the lower half because $\partial\overline{v}_1/\partial x_2 > 0$ and it is positive in the upper half because $\partial\overline{v}_1/\partial x_2 < 0$. It can be summarized as:

- $P_{12} = -\overline{v_2'^2}\dfrac{\partial\overline{v}_1}{\partial x_2}$ is the source term in $\overline{v_1'v_2'}$ equation and it is large

    $\Rightarrow$ P_{12} and $\overline{v_1'v_2'}$ have the same sign. Compare Fig. 9.2 (temperature in ^oC and $T = 0$ at the boundaries): a negative source, Q, gives negative temperature and vice versa;

    $\Rightarrow$ $\overline{v_1'v_2'}$ and $\dfrac{\partial\overline{v}_1}{\partial x_2}$ have opposite sign;

    $\Rightarrow$ The production term in the k equation, $P^k = -\overline{v_1'v_2'}\dfrac{\partial\overline{v}_1}{\partial x_2} > 0$;

- P^k is always positive in fully-developed channel flow;

$$\nu \frac{\partial \bar{v}_i}{\partial x_j} \frac{\partial \bar{v}_i}{\partial x_j}$$

$$-\overline{v_i' v_j'} \frac{\partial \bar{v}_i}{\partial x_j}$$

$$\nu \overline{\frac{\partial v_i'}{\partial x_j} \frac{\partial v_i'}{\partial x_j}}$$

E

ε

κ
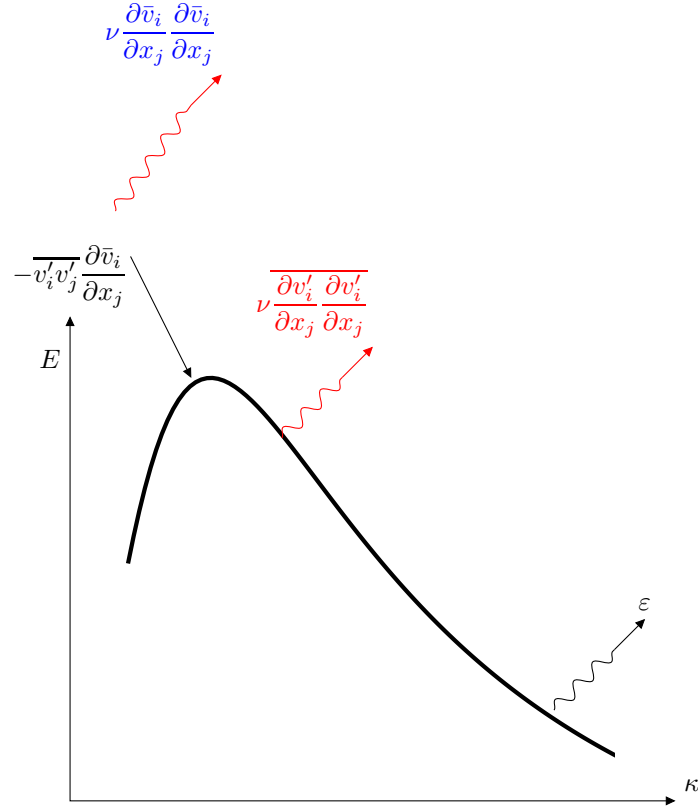
Figure 9.3: Energy spectrum. Transfer of kinetic energy. The cascade process assumes that the term in red are negligible (see also Fig. 8.2). The term in blue show the viscous dissipation of the mean flow.
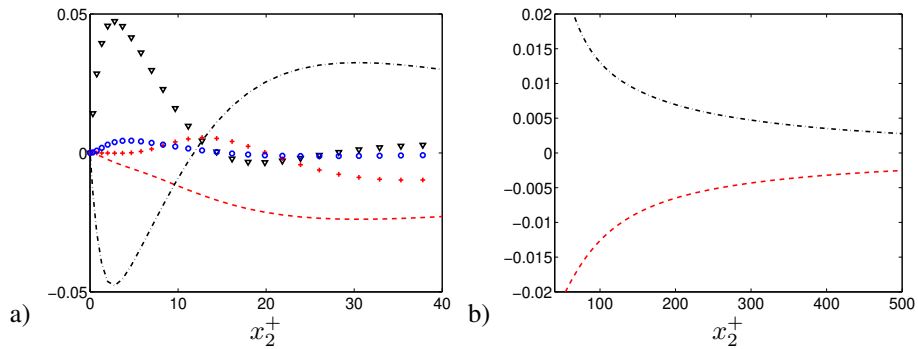
Figure 9.4: Channel flow at $Re_\tau = 2000$. Terms in the $\overline{v_2'^2}$ equation scaled by u_τ^4/ν. a) Zoom near the wall; b) Outer region. DNS (Direct Numerical Simulation) data [15, 16]. $-\!-$: $-\varepsilon_{22}$; $\triangledown$: $-2\partial \overline{v_2' p'}/\partial x_2$; $-\!\cdot\!-$: Π_{22}; $+$: $-\partial(\overline{v_2' v_2'^2})/\partial x_2$; $\circ$: $\nu\partial^2 \overline{v_2'^2}/\partial x_2^2$.
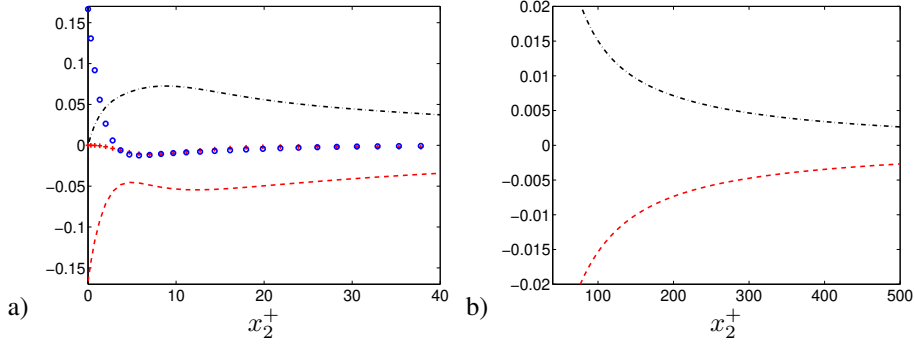
Figure 9.5: Channel flow at $Re_\tau = 2000$. Terms in the $\overline{v_3'^2}$ equation scaled by u_τ^4/ν. a) Zoom near the wall; b) Outer region. DNS (Direct Numerical Simulation) data [15, 16]. $- -$: $-\varepsilon_{33}$; $- \cdot -$: Π_{33}; $+$: $-\partial(\overline{v_2' v_3'^2})/\partial x_2$; $\circ$: $\nu \partial^2 \overline{v_3'^2}/\partial x_2^2$.
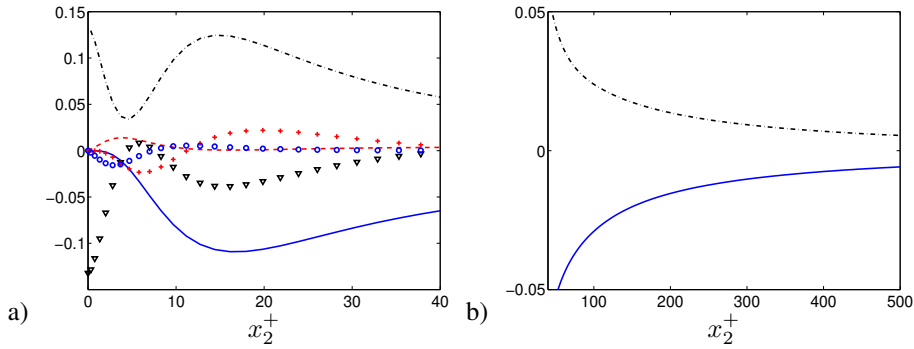
Figure 9.6: Channel flow at $Re_\tau = 2000$. Terms in the $\overline{v_1' v_2'}$ equation scaled by u_τ^4/ν. a) Zoom near the wall; b) Outer region. DNS (Direct Numerical Simulation) data [15, 16]. $\mathbf{—}$: P_{12}; $- -$: $-\varepsilon_{12}$; ∇: $-\partial \overline{v_1' p'}/\partial x_2$; $- \cdot -$: Π_{12}; $+$: $-\partial(\overline{v_1' v_2'^2})/\partial x_2$; $\circ$: $\nu \partial^2 \overline{v_1' v_2'}/\partial x_2^2$.
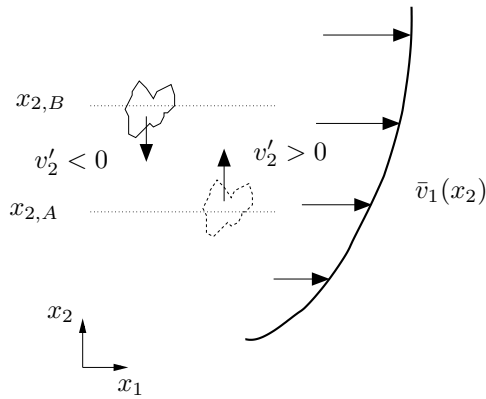
Figure 9.7: Sign of the Reynolds shear stress $-\rho \overline{v_1' v_2'}$ in a boundary layer.

- In general flows, P^k is <u>almost always</u> positive.

The fact that $\overline{v_1'v_2'}$ and $\partial \bar{v}_1/\partial x_2$ almost always have different signs can also be shown by physical argumentation. Consider the flow in a boundary layer, see Fig. 9.7. A fluid particle is moving downwards (particle drawn with solid line) from $x_{2,B}$ to $x_{2,A}$ with (the turbulent fluctuating) velocity v_2'. At its new location the v_1 velocity is in average smaller than at its old, i.e. $\bar{v}_1(x_{2,A}) < \bar{v}_1(x_{2,B})$. This means that when the particle at $x_{2,B}$ (which has streamwise velocity $v_1(x_{2,B})$) comes down to $x_{2,A}$ (where the streamwise velocity is $v_1(x_{2,A})$) it has an excess of streamwise velocity compared to its new environment at $x_{2,A}$. Thus the streamwise fluctuation is positive, i.e. $v_1' > 0$ and the correlation between v_1' and v_2' is in average negative ($\overline{v_1'v_2'} < 0$).

If we look at the other particle (dashed line in Fig. 9.7) we reach the same conclusion. The particle is moving upwards ($v_2' > 0$), and it is bringing a deficit in v_1 so that $v_1' < 0$. Thus, again, $v_1'v_2' < 0$. If we study this flow for a long time and average over time we get $\overline{v_1'v_2'} < 0$. If we change the sign of the velocity gradient so that $\partial \bar{v}_1/\partial x_2 < 0$ we will find that the sign of $\overline{v_1'v_2'}$ also changes.

In cases where the shear stress and the velocity gradient have the same sign (for example, in a wall jet) the reason is that the other terms (usually the transport terms) are more important than the production term.
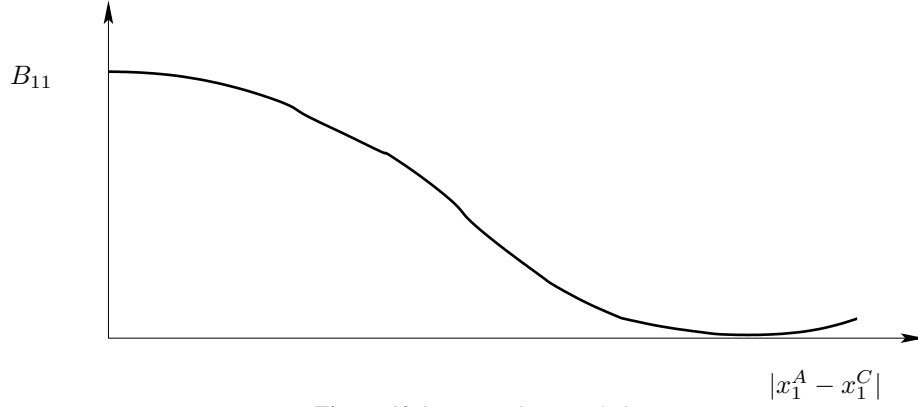
Figure 10.1: Two-point correlation.

10 Correlations

10.1 Two-point correlations

TWO-point correlations are useful when describing some characteristics of the turbulence. By "correlation", we mean *the tendency for two values or variables to change together, in either the same or opposite way*. Pick two points along the x_1 axis, say x_1^A and x_1^C, and sample the fluctuating velocity in, for example, the x_1 direction. We can then form the correlation of v_1' at these two points as

$$B_{11}(x_1^A, x_1^C) = \overline{v_1'(x_1^A)v_1'(x_1^C)} \tag{10.1}$$

Often, it is expressed as

$$B_{11}(x_1^A, \hat{x}_1) = \overline{v_1'(x_1^A)v_1'(x_1^A + \hat{x}_1)} \tag{10.2}$$

where $\hat{x}_1 = x_1^C - x_1^A$ is the separation distance between point A and C.

It is obvious that if we move point A and C closer to each other, B_{11} increases; when the two points are moved so close that they merge, then $B_{11} = \overline{v'^2}(x_1^A)$, see Fig. 10.1. If, on the other hand, we move point C further and further away from point A, then B_{11} will go to zero. It is convenient to normalize B_{11} so that it varies between -1 and $+1$. The normalized two-point correlation reads

$$B_{11}^{norm}(x_1^A, \hat{x}_1) = \frac{1}{v_{1,rms}(x_1^A)v_{1,rms}(x_1^A + \hat{x}_1)} \overline{v_1'(x_1^A)v_1'(x_1^A + \hat{x}_1)} \tag{10.3}$$

where subscript rms denotes root-mean-square, which for v_1', for example, is defined as

$$v_{1,rms} = \left(\overline{v_1'^2}\right)^{1/2} \tag{10.4}$$

RMS is the same as *standard deviation* (Python command `np.std` and Matlab/Octave command `std`) which is the square-root of the *variance* (Python command `np.var` and Matlab/Octave command `var`).

Consider a flow where the largest eddies have a length scale of L_{int}, see Fig. 10.2. We expect that the two point correlation, B_{11}, approaches zero for separation distance,
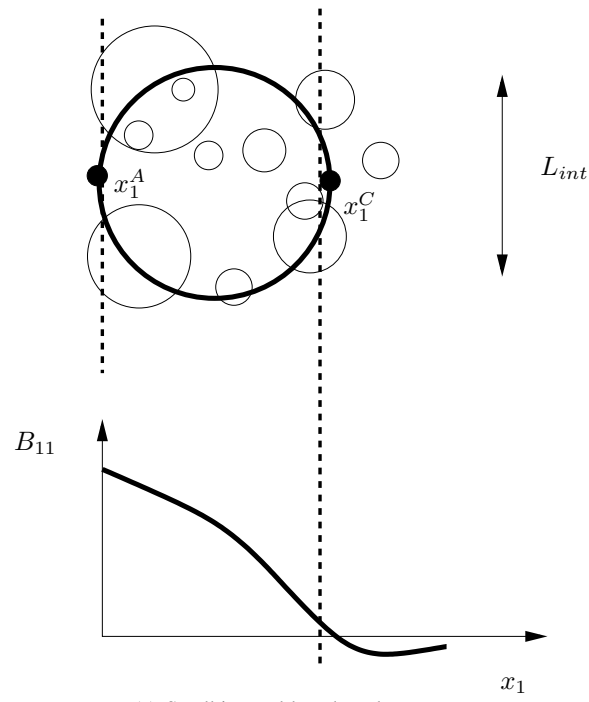
(a) Small integral length scale
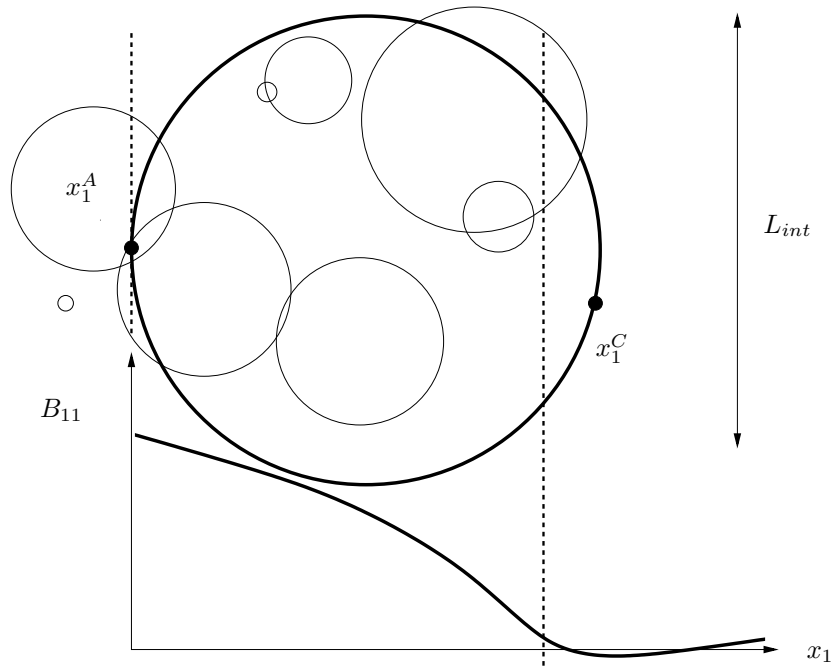
(b) Large integral length scale

Figure 10.2: Schematic relation between the two-point correlation, the largest eddies (thick lines) and the integral length scale, L_{int}.

$|x_1^A - x_1^C| > L_{int}$ because for separation distances larger than L_{int} there is no correlation between $v_1'(x_1^A)$ and $v_1'(x_1^C)$. Hence, flows with large eddies will have a two-point correlation function which decreases slowly with separation distance. For flows with small eddies, the two-point correlation, B_{11}, decreases rapidly with $\hat{x}_1$.

If the flow is homogeneous (see p.102) in the x_1 direction, the two-point correlation does not depend on the location of x_1^A, but it is only dependent on the separation of the two points, $\hat{x}_1$, i.e.

$$B_{11}^{norm}(\hat{x}_1) = \frac{1}{v_{1,rms}^2} \overline{v_1'(x_1)v_1'(x_1 + \hat{x}_1)} \qquad (10.5)$$

From the two-point correlation, B_{11}, an integral length scale, L_{int}, can be computed which is defined as the integral of B_{11} over the separation distance, i.e. **integral length scale**

$$L_{int}(x_1) = \int_0^\infty \frac{B_{11}(x_1, \hat{x}_1)}{v_{1,rms}^A v_{1,rms}^C} d\hat{x}_1 \qquad (10.6)$$

The integral length scale represents the length scale of the large energy-containing eddies. If the flow is homogeneous in the x_1 direction then L_{int} does not depend on x_1, and the integral length scale is then computed as

$$L_{int} = \int_0^\infty B_{11}^{norm}(\hat{x}_1) d\hat{x}_1 \qquad (10.7)$$

10.2 Auto correlation

Auto correlation is a "two-point correlation" in time, i.e. the correlation of a turbulent fluctuation with a separation in time. If we again choose the v_1' fluctuation, the auto correlation reads

$$B_{11}(t^A, \hat{t}) = \overline{v_1'(t^A)v_1'(t^A + \hat{t})} \qquad (10.8)$$

where $\hat{t} = t^C - t^A$, is the time separation distance between time A and C. If the mean flow is steady, the "time direction" is homogeneous and B_{11} is independent on t^A; in this case the auto-correlation depends only on time separation, $\hat{t}$, i.e.

$$B_{11}(\hat{t}) = \overline{v_1'(t)v_1'(t + \hat{t})} \qquad (10.9)$$

where the right side is time-averaged over t.

The normalized auto-correlation reads

$$B_{11}^{norm}(\hat{t}) = \frac{1}{v_{1,rms}^2} \overline{v_1'(t)v_1'(t + \hat{t})} \qquad (10.10)$$

In analogy to the integral length scale, L_{int}, the *integral time scale*, T_{int}, is defined as (assuming steady flow) **integral time scale**

$$T_{int} = \int_0^\infty B_{11}^{norm}(\hat{t}) d\hat{t} \qquad (10.11)$$

The integral time scale represents the time scale of the large energy-containing eddies. It is used an Assignment (see Section Q.3) for finding time samples that are *independent* (i.e. the time beween the samples is at least one integral timescale).
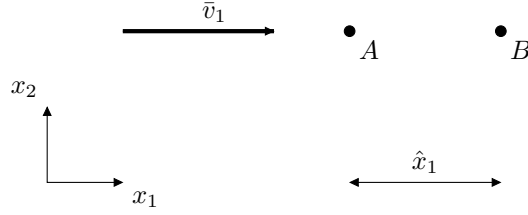
Figure 10.3: Two-point correlation and frozen turbulence.

10.3 Taylor's hypothesis of frozen turbulence

The autocorrelation, $B_{11}^{norm}(\hat{t})$, is much easier to measure than the two-point correlation, $B_{11}^{norm}(\hat{x}_1)$. Let us try to obtain the two-point correlation from the autocorrelation.

Consider the velocity fluctuation at point A (i.e. $v_1'^A(t)$) and B (i.e. $v_1'^B(t)$), see Fig. 10.3. Assume that the turbulent fluctuation at point A is transported by the mean velocity, $\bar{v}_1$, in a frozen state to point B. This is called Taylor's hypothesis of frozen turbulence. This asumption is better the smaller the turbulence intensity, $v_{1,rms}/\bar{v}_1$. It takes $\hat{x}_1/\bar{v}_1$ seconds for the fluid particle at point A to reach point B. Based on Taylor's hypothesis we can estimate v_1' at point A by measuring v_1' at point B $\hat{x}_1/\bar{v}_1$ seconds later. This gives

$$B_{11}^{norm}(\hat{x}_1) = \frac{1}{v_{1,rms}^2}\overline{v_1'^A(t)v_1'^B(t)} \simeq \frac{1}{v_{1,rms}^2}\overline{v_1'^B(t+\hat{x}_1/\bar{v}_1)v_1'^B(t)}$$

Based on Taylor's hypohesis, the integral length scale can in Fig. 10.3 be estimated from the integral time scale as

$$L_{int} = \bar{v}_1 T_{int} \tag{10.12}$$

MTF271 Turbulence Modeling

L. Davidson

Division of Fluid Dynamics
Department of Mechanics and Maritime Sciences
Chalmers University of Technology, Göteborg, Sweden
http://www.tfd.chalmers.se/~lada, lada@chalmers.se

This eBook can be downloaded at
http://www.tfd.chalmers.se/~lada/postscript_files/solids-and-fluids_turbulent-flow_turbulence-modelling.pdf

Recorded lectures are found at http://www.tfd.chalmers.se/~lada//comp_turb_model/recorded_lecture.html

Please find the MTF271 Lecture Notes

11 Reynolds stress models and two-equation models

11.1 Mean flow equations

11.1.1 Flow equations

For incompressible turbulent flow, all variables are divided into a mean part (time averaged) and fluctuating part. For the velocity vector this means that v_i is divided into a mean part $\bar{v}_i$ and a fluctuating part v_i' so that $v_i = \bar{v}_i + v_i'$. Time average and we get (see Eq. 6.9 at. p. 81):

$$\frac{\partial \bar{v}_i}{\partial x_i} = 0 \tag{11.1}$$

$$\frac{\partial \rho_0 \bar{v}_i}{\partial t} + \frac{\partial}{\partial x_j}\left(\rho_0 \bar{v}_i \bar{v}_j\right) = -\frac{\partial \bar{p}}{\partial x_i} + \mu \frac{\partial^2 \bar{v}_i}{\partial x_j \partial x_j} - \frac{\partial \tau_{ij}}{\partial x_j} - \beta \rho_0 (\bar{\theta} - \theta_0) g_i \tag{11.2}$$

(note that θ denotes temperature) where ρ_0 is a constant reference density, the volume force $f_i = -\beta(\bar{\theta} - \theta_0)g_i$ and the turbulent stress tensor (also called *Reynolds stress tensor*) is written as:

Reynolds stress tensor

$$\tau_{ij} = \rho_0 \overline{v_i' v_j'} \tag{11.3}$$

The pressure, $\bar{p}$, denotes the hydrodynamic pressure, see Eq. 3.22, which means that when the flow is still (i.e. $\bar{v}_i \equiv 0$), then the pressure is zero (i.e. $\bar{p} \equiv 0$). We have assumed that the temperature variations are small (typically smaller than 10 ^oC) so that the density variations can be neglected (using ρ_0) in all terms except the gravity term. This is called the *Boussinesq approximation*.

Boussinesq approximation

The body force f_i – which was omitted for convenience in Eq. 6.9 – has here been re-introduced. The body force in Eq. 11.2 is due to buoyancy, i.e. density differences. The basic form of the buoyancy force is $f_i = g_i$ where g_i denotes gravitational acceleration. Since the pressure, $\bar{p}$, is defined as the hydrodynamic pressure we have re-written the buoyancy source as

$$\rho_0 f_i \rightarrow (\rho - \rho_0) g_i \tag{11.4}$$

so that $\bar{p} \equiv 0$ when $\bar{v}_i \equiv 0$ (note that the true pressure decreases upwards as $\rho g \Delta h$ where Δh denotes change in height). If we let density depend on pressure and temperature, differentiation gives

$$d\rho = \left(\frac{\partial \rho}{\partial \theta}\right)_p d\theta + \left(\frac{\partial \rho}{\partial p}\right)_\theta dp \tag{11.5}$$

Our flow is incompressible, which means that the density does not depend on pressure, i.e. $\partial \rho / \partial p = 0$; it may, however, depend on temperature and mixture composition. Hence the last term in Eq. 11.5 is zero and we introduce the volumetric thermal expansion, β, so that

$$\beta = -\frac{1}{\rho_0}\left(\frac{\partial \rho}{\partial \theta}\right)_p \Rightarrow$$
$$d\rho = -\rho_0 \beta d\theta \Rightarrow \rho - \rho_0 = -\beta \rho_0 (\theta - \theta_0) \tag{11.6}$$

where β is a physical property which is tabulated in physical handbooks. For a perfect gas it is simply $\beta = \theta^{-1}$ (with θ in degrees Kelvin). Now we can re-write the buoyancy term as

$$(\rho - \rho_0) g_i = -\rho_0 \beta (\bar{\theta} - \theta_0) g_i \tag{11.7}$$

which is the last term in Eq. 11.2. Consider the case where x_3 is vertically upwards. Then $g_i = (0, 0, -g)$ and a large temperature in Eq. 11.7 results in a force vertically upwards, which agrees well with our intuition.

11.1.2 Temperature equation

The instantaneous temperature, θ, is also decomposed into a mean and a fluctuating component as $\theta = \bar{\theta} + \theta'$. The transport equation for θ reads (see Eq. 2.18 where temperature was denoted by T)

$$\frac{\partial \theta}{\partial t} + \frac{\partial v_i \theta}{\partial x_i} = \alpha \frac{\partial^2 \theta}{\partial x_i \partial x_i} \tag{11.8}$$

where $\alpha = k/(\rho c_p)$, see Eq. 2.18 on p. 28. Introducing $\theta = \bar{\theta} + \theta'$ we get

$$\frac{\partial \bar{\theta}}{\partial t} + \frac{\partial \bar{v}_i \bar{\theta}}{\partial x_i} = \alpha \frac{\partial^2 \bar{\theta}}{\partial x_i \partial x_i} - \frac{\partial \overline{v_i' \theta'}}{\partial x_i} \tag{11.9}$$

The last term on the right side is an additional term whose physical meaning is turbulent heat flux vector. This is similar to the Reynolds stress tensor on the right side of the time-averaged momentum equation, Eq. 11.2. The total heat flux vector – viscous plus turbulent – in Eq. 11.9 reads (cf. Eq. 2.14)

$$\frac{q_{i,tot}}{\rho c_p} = \frac{q_i}{\rho c_p} + \frac{q_{i,turb}}{\rho c_p} = \alpha \frac{\partial \bar{\theta}}{\partial x_i} - \overline{v_i' \theta'} \tag{11.10}$$

11.2 The exact $\overline{v_i' v_j'}$ equation

Now we want to solve the time-averaged continuity equation (Eq. 11.1) and the three momentum equations (Eq. 11.2). Unfortunately there are ten unknowns; the four usual ones ($\bar{v}_i$, $\bar{p}$) plus six turbulent stresses, $\overline{v_i' v_j'}$. We must *close* this equation system; it is called the *closure problem*. We must find some new equations for the turbulent stresses. We need a turbulence model.

closure problem

The most comprehensive turbulence model is to derive exact transport equations for the turbulent stresses. An exact equation for the Reynolds stresses can be derived from the Navies-Stokes equation. It is emphasized that this equation is exact; or, rather, as exact as the Navier-Stokes equations. The derivation follows the steps below.

- Set up the momentum equation for the instantaneous velocity $v_i = \bar{v}_i + v_i' \rightarrow$ Eq. (A)

- Time average $\rightarrow$ equation for $\bar{v}_i$, Eq. (B)

- Subtract Eq. (B) from Eq. (A) $\rightarrow$ equation for v_i', Eq. (C)

- Do the same procedure for $v_j \rightarrow$ equation for v_j', Eq. (D)

- Multiply Eq. (C) with v_j' and Eq. (D) with v_i', time average and add them together $\rightarrow$ equation for $\overline{v_i' v_j'}$

In Section 9 at p. 106 these steps are given in some detail. More details can also be found in [23] (set the SGS tensor to zero, i.e. $\tau_{ij}^a = 0$).

The final $\overline{v_i' v_j'}$-equation (Reynolds Stress equation) reads (see Eq. 9.12)

$$\underbrace{\frac{\partial \overline{v_i' v_j'}}{\partial t} + \bar{v}_k \frac{\partial \overline{v_i' v_j'}}{\partial x_k}}_{C_{ij}} = \underbrace{-\overline{v_i' v_k'}\frac{\partial \bar{v}_j}{\partial x_k} - \overline{v_j' v_k'}\frac{\partial \bar{v}_i}{\partial x_k}}_{P_{ij}} + \underbrace{\frac{\overline{p'}}{\rho}\left(\frac{\partial v_i'}{\partial x_j} + \frac{\partial v_j'}{\partial x_i}\right)}_{\Pi_{ij}}$$

$$\underbrace{-\frac{\partial}{\partial x_k}\left[\overline{v_i' v_j' v_k'} + \frac{\overline{p' v_j'}}{\rho}\delta_{ik} + \frac{\overline{p' v_i'}}{\rho}\delta_{jk}\right]}_{D_{ij,t}} + \underbrace{\nu\frac{\partial^2 \overline{v_i' v_j'}}{\partial x_k \partial x_k}}_{D_{ij,\nu}} \qquad (11.11)$$

$$\underbrace{-g_i \beta \overline{v_j' \theta'} - g_j \beta \overline{v_i' \theta'}}_{G_{ij}} - \underbrace{2\nu \overline{\frac{\partial v_i'}{\partial x_k}\frac{\partial v_j'}{\partial x_k}}}_{\varepsilon_{ij}}$$

where $D_{ij,t}$ and $D_{ij,\nu}$ denote turbulent and viscous diffusion, respectively. The total diffusion reads $D_{ij} = D_{ij,t} + D_{ij,\nu}$. This is analogous to the momentum equation where we have gradients of viscous and turbulent stresses which correspond to viscous and turbulent diffusion. Equation 11.11 can symbolically be written

$$C_{ij} = P_{ij} + \Pi_{ij} + D_{ij} + G_{ij} - \varepsilon_{ij}$$

where

C_{ij} Convection

P_{ij} Production

Π_{ij} Pressure-strain

D_{ij} Diffusion

G_{ij} Buoyancy production

ε_{ij} Dissipation

Which terms in Eq. 11.11 are known and which are unknown? First, let's think about which physical quantities we solve for.

$\bar{v}_i$ is obtained from the momentum equation, Eq. 11.2

$\overline{v_i' v_j'}$ is obtained from the modeled $\overline{v_i' v_j'}$ equation, Eq. 11.101

Hence the following terms in Eq. 11.11 are known (i.e. they do not need to be modeled)

- The left side

- The production term, P_{ij}

- The viscous part of the diffusion term, D_{ij}, i.e. D_{ij}^ν

- The buoyancy term, G_{ij} (provided that a transport equation is solved for $\overline{v_i' \theta'}$, Eq. 11.22; if not, $\overline{v_i' \theta'}$ is obtained from the Boussinesq assumption, Eq. 11.35)

11.3 The exact $\overline{v_i'\theta'}$ equation

If temperature variations occur we must solve for the mean temperature field, see Eq. 11.9. Then we need the unknown turbulent heat fluxes, $\overline{v_i'\theta'}$. To derive its transport equation, start with the equation for the fluctuating temperature. Subtract Eq. 11.9 from Eq. 11.8

$$\frac{\partial \theta'}{\partial t} + \frac{\partial}{\partial x_k}(v_k'\bar{\theta} + \bar{v}_k\theta' + v_k'\theta') = \alpha\frac{\partial^2\theta'}{\partial x_k \partial x_k} + \frac{\partial \overline{v_k'\theta'}}{\partial x_k} \tag{11.12}$$

To get the equation for the fluctuating velocity, v_i', subtract the equation for the mean velocity $\bar{v}_i$ (Eq. 11.2) from the equation for the instantaneous velocity, v_i (Eq. 6.6) so that

$$\frac{\partial v_i'}{\partial t} + \frac{\partial}{\partial x_k}(v_k'\bar{v}_i + \bar{v}_k v_i' + v_k'v_i') = -\frac{1}{\rho}\frac{\partial p'}{\partial x_i} + \nu\frac{\partial^2 v_i'}{\partial x_k \partial x_k} + \frac{\partial \overline{v_i'v_k'}}{\partial x_k} - g_i\beta\theta' \tag{11.13}$$

Multiply Eq. 11.12 with v_i' and multiply Eq. 11.13 with θ', add them together and time average

$$\frac{\partial \overline{v_i'\theta'}}{\partial t} + \overline{v_i'\frac{\partial}{\partial x_k}(v_k'\bar{\theta} + \bar{v}_k\theta' + v_k'\theta') + \theta'\frac{\partial}{\partial x_k}(\bar{v}_i v_k' + \bar{v}_k v_i' + v_i'v_k')}$$
$$= -\frac{\overline{\theta'}}{\rho}\frac{\partial p'}{\partial x_i} + \alpha\overline{v_i'\frac{\partial^2\theta'}{\partial x_k \partial x_k}} + \nu\overline{\theta'\frac{\partial^2 v_i'}{\partial x_k \partial x_k}} - g_i\beta\overline{\theta'\theta'} \tag{11.14}$$

The Reynolds stress term in Eq. 11.13 multiplied by θ' and time averaged is zero, i.e.

$$\overline{\frac{\partial \overline{v_i'v_j'}}{\partial x_k}\theta'} = \frac{\partial \overline{v_i'v_j'}}{\partial x_k}\overline{\theta'} = 0$$

If you have forgotten the rules for time-averaging, see Section 8.1.

The first term in the two parentheses on line 1 in Eq. 11.14 are combined into two production terms (using the continuity equation, $\partial v_k'/\partial x_k = 0$)

$$\overline{v_i'v_k'}\frac{\partial\bar{\theta}}{\partial x_k} + \overline{v_k'\theta'}\frac{\partial\bar{v}}{\partial x_k} \tag{11.15}$$

The second term in the two parenthesis on the first line of Eq. 11.14 are re-written using the continuity equation

$$\overline{v_i'\frac{\partial\bar{v}_k\theta'}{\partial x_k} + \theta'\frac{\partial\bar{v}_k v_i'}{\partial x_k}} = \bar{v}_k\left(\overline{v_i'\frac{\partial\theta'}{\partial x_k} + \theta'\frac{\partial v_i'}{\partial x_k}}\right) \tag{11.16}$$

Now the two terms can be merged (product rule backwards, Trick 1)

$$\bar{v}_k\left(\overline{v_i'\frac{\partial\theta'}{\partial x_k} + \theta'\frac{\partial v_i'}{\partial x_k}}\right) = \bar{v}_k\frac{\partial \overline{v_i'\theta'}}{\partial x_k} = \frac{\partial\bar{v}_k\overline{v_i'\theta'}}{\partial x_k} \tag{11.17}$$

where we used the continuity equation to obtain the right side. The last two terms on the first line in Eq. 11.14 are re-cast into turbulent diffusion terms using the same procedure as in Eqs. 11.16 and 11.17

$$\overline{v_i'\frac{\partial}{\partial x_k}(v_k'\theta') + \theta'\frac{\partial}{\partial x_k}(v_i'v_k')} = \frac{\partial \overline{v_i'v_k'\theta'}}{\partial x_k} \tag{11.18}$$

The viscous diffusion terms on the right side are re-written using the product rule backwards (Trick 1, see p. 94)

$$\overline{\alpha v_i' \frac{\partial^2 \theta'}{\partial x_k \partial x_k}} = \overline{\alpha v_i' \frac{\partial}{\partial x_k}\left(\frac{\partial \theta'}{\partial x_k}\right)} = \alpha \frac{\partial}{\partial x_k}\overline{\left(v_i' \frac{\partial \theta'}{\partial x_k}\right)} - \alpha \overline{\frac{\partial \theta'}{\partial x_k} \frac{\partial v_k'}{\partial x_k}}$$
$$\overline{\nu \theta' \frac{\partial^2 v_i'}{\partial x_k \partial x_k}} = \overline{\nu \theta' \frac{\partial}{\partial x_k}\left(\frac{\partial v_i'}{\partial x_k}\right)} = \nu \frac{\partial}{\partial x_k}\overline{\left(\theta' \frac{\partial v_i'}{\partial x_k}\right)} - \nu \overline{\frac{\partial \theta'}{\partial x_k} \frac{\partial v_k'}{\partial x_k}}$$
(11.19)

Inserting Eqs. 11.15, 11.17, 11.18 and 11.19 into Eq. 11.14 gives the transport equation for the heat flux vector $\overline{v_i'\theta'}$

$$\frac{\partial \overline{v_i'\theta'}}{\partial t} + \frac{\partial}{\partial x_k}\bar{v}_k \overline{v_i'\theta'} = \underbrace{-\overline{v_i'v_k'}\frac{\partial \bar{\theta}}{\partial x_k} - \overline{v_k'\theta'}\frac{\partial \bar{v}_i}{\partial x_k}}_{P_{i\theta}} \underbrace{-\frac{\overline{\theta'}}{\rho}\frac{\partial p'}{\partial x_i}}_{\Pi_{i\theta}} \underbrace{-\frac{\partial}{\partial x_k}\overline{v_k'v_i'\theta'}}_{D_{i\theta,t}}$$
$$\underbrace{+\alpha \frac{\partial}{\partial x_k}\overline{\left(v_i' \frac{\partial \theta'}{\partial x_k}\right)} + \nu \frac{\partial}{\partial x_k}\overline{\left(\theta' \frac{\partial v_i'}{\partial x_k}\right)}}_{D_{i\theta,\nu}} \underbrace{-(\nu + \alpha)\overline{\frac{\partial v_i'}{\partial x_k}\frac{\partial \theta'}{\partial x_k}}}_{\varepsilon_{i\theta}} \underbrace{-g_i\beta \overline{\theta'^2}}_{G_{i\theta}}$$
(11.20)

where $P_{i\theta}$, $\Pi_{i\theta}$ and $D_{i\theta,t}$ denote the production, scramble and turbulent diffusion term, respectively. The production term includes one term with the mean velocity gradient and one with the mean temperature gradient. On the last line, $D_{i\theta,\nu}$, $\varepsilon_{i\theta}$ and $G_{i\theta}$ denote viscous diffusion, dissipation and buoyancy term, respectively. The unknown terms – $\Pi_{i\theta}$, $D_{i\theta}$, $\varepsilon_{i\theta}$, $G_{i\theta}$ – have to be modeled as usual; this is out of the scope of the present course but the interested reader is referred to [24].

It can be noted that there is no usual viscous diffusion term in Eq. 11.20. The reason is that the viscous diffusion coefficients are different in the v_i equation and the θ equation (ν in the former case and α in the latter). However, if $\nu \simeq \alpha$ (which corresponds to a Prandtl number of unity, i.e. $Pr = \nu/\alpha \simeq 1$, see Eq. 2.19), the diffusion term in Eq. 11.20 assumes the familiar form

$$\alpha \frac{\partial}{\partial x_k}\overline{\left(v_i' \frac{\partial \theta'}{\partial x_k}\right)} + \nu \frac{\partial}{\partial x_k}\overline{\left(\theta' \frac{\partial v_i'}{\partial x_k}\right)}$$
$$= \alpha \frac{\partial^2 \overline{v_i'\theta'}}{\partial x_k \partial x_k} - \alpha \frac{\partial}{\partial x_k}\overline{\left(\theta' \frac{\partial v_i'}{\partial x_k}\right)} + \nu \frac{\partial^2 \overline{v_i'\theta'}}{\partial x_k \partial x_k} - \nu \frac{\partial}{\partial x_k}\overline{\left(v_i' \frac{\partial \theta'}{\partial x_k}\right)}$$
$$\simeq \left(\nu + \frac{\nu}{Pr}\right)\frac{\partial^2 \overline{v_i'\theta'}}{\partial x_k \partial x_k} - \nu \frac{\partial}{\partial x_k}\overline{\left(\theta' \frac{\partial v_i'}{\partial x_k}\right)} - \nu \frac{\partial}{\partial x_k}\overline{\left(v_i' \frac{\partial \theta'}{\partial x_k}\right)}$$
$$= \left(\nu + \frac{\nu}{Pr}\right)\frac{\partial^2 \overline{v_i'\theta'}}{\partial x_k \partial x_k} - D_{i\theta,\nu}$$
(11.21)

where $D_{i\theta,\nu}$ cancels the corresponding term in Eq. 11.20 if $\alpha = \nu$. Often the viscous diffusion is simplified in this way. Hence, if $\alpha \simeq \nu$ the transport equation for $\overline{v_i'\theta'}$ can be simplified as

$$\frac{\partial \overline{v_i'\theta'}}{\partial t} + \frac{\partial}{\partial x_k}\bar{v}_k \overline{v_i'\theta'} = \underbrace{-\overline{v_i'v_k'}\frac{\partial \bar{\theta}}{\partial x_k} - \overline{v_k'\theta'}\frac{\partial \bar{v}_i}{\partial x_k}}_{P_{i\theta}} \underbrace{-\frac{\overline{\theta'}}{\rho}\frac{\partial p'}{\partial x_i}}_{\Pi_{i\theta}} \underbrace{-\frac{\partial}{\partial x_k}\overline{v_k'v_i'\theta'}}_{D_{i\theta,t}}$$
$$\underbrace{+\left(\nu + \frac{\nu}{Pr}\right)\frac{\partial^2 \overline{v_i'\theta'}}{\partial x_k \partial x_k}}_{D_{i\theta,\nu}} \underbrace{-(\nu + \alpha)\overline{\frac{\partial v_i'}{\partial x_k}\frac{\partial \theta'}{\partial x_k}}}_{\varepsilon_{i\theta}} \underbrace{-g_i\beta \overline{\theta'^2}}_{G_{i\theta}}$$
(11.22)

The same question arises as for the $\overline{v_i'v_j'}$ equation: which terms need to be modeled in Eq. 11.22? The following quantities are known:

$\bar{v}_i$ is obtained from the momentum equation, Eq. 11.2

$\bar{\theta}$ is obtained from the temperature equation, Eq. 11.9

$\overline{v_i'v_j'}$ is obtained from the modeled $\overline{v_i'v_j'}$ equation, Eq. 11.101

$\overline{v_i'\theta'}$ is obtained from the modeled $\overline{v_i'\theta'}$ equation

Hence the following terms in Eq. 11.22 are known (i.e. they do not need to be modeled)

- The left side

- The production term, $P_{i\theta}$

- The viscous diffusion term, $D_{i\theta,\nu}$

- The buoyancy term, $G_{i\theta}$ (provided that a transport equation is solved for $\overline{\theta'^2}$; if not, $\overline{\theta'^2}$ is usually modeled via a relation to k)

11.4   The k equation

The turbulent kinetic energy is the sum of all normal Reynolds stresses, i.e.

$$k = \frac{1}{2}\left(\overline{v_1'^2} + \overline{v_2'^2} + \overline{v_3'^2}\right) \equiv \frac{1}{2}\overline{v_i'v_i'}$$

By taking the trace (setting indices $i = j$) of the equation for $\overline{v_i'v_j'}$ and dividing by two we get the equation for the turbulent kinetic energy:

$$\frac{\partial k}{\partial t} + \underbrace{\bar{v}_j \frac{\partial k}{\partial x_j}}_{C^k} = \underbrace{-\overline{v_i'v_j'}\frac{\partial \bar{v}_i}{\partial x_j}}_{P^k} \underbrace{-\nu\overline{\frac{\partial v_i'}{\partial x_j}\frac{\partial v_i'}{\partial x_j}}}_{\varepsilon}$$

$$(11.23)$$

$$\underbrace{-\frac{\partial}{\partial x_j}\left\{\overline{v_j'\left(\frac{p'}{\rho} + \frac{1}{2}v_i'v_i'\right)}\right\}}_{D_t^k} + \underbrace{\nu\frac{\partial^2 k}{\partial x_j \partial x_j}}_{D_\nu^k}\underbrace{-g_i\beta\overline{v_i'\theta'}}_{G^k}$$

where – as in the $\overline{v_i'v_j'}$ equation – D_t^k and D_ν^k denotes turbulent and viscous diffusion, respectively. The total diffusion reads $D^k = D_t^k + D_\nu^k$. Equation 11.23 can symbolically be written:

$$C^k = P^k + D^k + G^k - \varepsilon \qquad (11.24)$$

The known quantities in Eq. 11.23 are:

$\bar{v}_i$ is obtained from the momentum equation, Eq. 11.2

k is obtained from the modeled k equation, Eq. 11.97

Hence the following terms in Eq. 11.23 are known (i.e. they do not need to be modeled)

- The left side

- The viscous diffusion term, $D_{i,\nu}^k$

- The buoyancy term, G_{ij} (provided that a transport equation is solved for $\overline{v_i'\theta'}$, Eq. 11.22; if not, $\overline{v_i'\theta'}$ is obtained from the Boussinesq assumption, Eq. 11.35)

11.5 The ε equation

Two quantities are usually used in eddy-viscosity model to express the turbulent viscosity. In the $k - \varepsilon$ model, k and ε are used. The turbulent viscosity is estimated – using dimensional analysis – as the product of a turbulent velocity, $\mathcal{U}$, and length scale, $\mathcal{L}$,

$$\nu_t \propto \mathcal{U}\mathcal{L} \tag{11.25}$$

The velocity scale is taken as $k^{1/2}$ and the length scale as $k^{3/2}/\varepsilon$ which gives

$$\nu_t = C_\mu \frac{k^2}{\varepsilon}$$

where $C_\mu = 0.09$. An exact equation for the transport equation for the dissipation

$$\varepsilon = \nu \overline{\frac{\partial v_i'}{\partial x_j} \frac{\partial v_i'}{\partial x_j}}$$

can be derived (see, e.g., [25]), but it is very complicated and in the end many terms are found negligible. It is much easier to look at the k equation, Eq. 11.24, and to setup a similar equation for ε. The transport equation should include a convective term, C^ε, a diffusion term, D^ε, a production term, P^ε, a production term due to buoyancy, G^ε, and a destruction term, Ψ^ε, i.e.

$$C^\varepsilon = P^\varepsilon + D^\varepsilon + G^\varepsilon - \Psi^\varepsilon \tag{11.26}$$

The production and destruction terms, P^k and ε, in the k equation are used to formulate the corresponding terms in the ε equation. The terms in the k equation have the dimension $[m^2/s^3]$ (look at the unsteady term, $\partial k/\partial t$) whereas the terms in the ε equation have the dimension $[m^2/s^4]$ (cf. $\partial \varepsilon/\partial t$). Hence, we must multiply P^k and ε by a quantity which has the dimension $[1/s]$. One quantity with this dimension is the mean velocity gradient which might be relevant for the production term, but not for the destruction. A better choice should be $\varepsilon/k = [1/s]$. Hence, we get

$$P^\varepsilon + G^\varepsilon - \Psi^\varepsilon = \frac{\varepsilon}{k}\left(c_{\varepsilon 1}P^k + c_{\varepsilon 1}G^k - c_{\varepsilon 2}\varepsilon\right) \tag{11.27}$$

where we have added new unknown coefficients in front of each term. The turbulent diffusion term is expressed in the same way as that in the k equation (see Eq. 11.40) but with its own turbulent Prandtl number, σ_ε (see Eq. 11.37), i.e.

$$D^\varepsilon = \frac{\partial}{\partial x_j}\left[\left(\nu + \frac{\nu_t}{\sigma_\varepsilon}\right)\frac{\partial \varepsilon}{\partial x_j}\right] \tag{11.28}$$

The final form of the ε transport equation reads

$$\frac{\partial \varepsilon}{\partial t} + \bar{v}_j \frac{\partial \varepsilon}{\partial x_j} = \frac{\varepsilon}{k}(c_{\varepsilon 1}P^k + c_{\varepsilon 1}G^k - c_{\varepsilon 2}\varepsilon) + \frac{\partial}{\partial x_j}\left[\left(\nu + \frac{\nu_t}{\sigma_\varepsilon}\right)\frac{\partial \varepsilon}{\partial x_j}\right] \tag{11.29}$$

Note that this is a *modeled* equation since we have modeled the production, destruction and turbulent diffusion terms.

For details on how to derive the constants, see [26].

11.6 The Boussinesq assumption

In the Boussinesq assumption an eddy (i.e. a *turbulent*) viscosity is introduced to model the unknown Reynolds stresses in Eq. 11.2. Consider the diffusion terms in the incompressible momentum equation in the case of non-constant viscosity (see Eq. 2.6)

$$\frac{\partial}{\partial x_j}\left\{\nu\left(\frac{\partial \bar{v}_i}{\partial x_j}+\frac{\partial \bar{v}_j}{\partial x_i}\right)-\overline{v_i'v_j'}\right\} \tag{11.30}$$

Now we want to replace the Reynolds stress tensor, $\overline{v_i'v_j'}$, by a turbulent viscosity, ν_t, so that the diffusion terms can be written

$$\frac{\partial}{\partial x_j}\left\{(\nu+\nu_t)\left(\frac{\partial \bar{v}_i}{\partial x_j}+\frac{\partial \bar{v}_j}{\partial x_i}\right)\right\} \tag{11.31}$$

Note that ν_t is not constant. Identification of Eqs. 11.30 and 11.31 gives

$$-\overline{v_i'v_j'}=\nu_t\left(\frac{\partial \bar{v}_i}{\partial x_j}+\frac{\partial \bar{v}_j}{\partial x_i}\right) \tag{11.32}$$

This is identical to the assumption for the Newtonian, viscous stress for incompressible flow, see Eq. 2.4. Equation 11.32 is not valid upon contraction [3] (the right side will be zero due to continuity, but not the left side). Hence we add the trace of the left side to the right side so that

$$\overline{v_i'v_j'}=-\nu_t\left(\frac{\partial \bar{v}_i}{\partial x_j}+\frac{\partial \bar{v}_j}{\partial x_i}\right)+\frac{1}{3}\delta_{ij}\overline{v_k'v_k'}=-2\nu_t\bar{s}_{ij}+\frac{2}{3}\delta_{ij}k \tag{11.33}$$

Now the equation is valid also when it is contracted (i.e taking the trace); after contraction both left and right side are equal (as they must be) to $\overline{v_i'v_i'}=2k$. When Eq. 11.33 is included in Eq. 11.2 we replace six turbulent stresses with one new unknown (the turbulent viscosity, ν_t). This is of course a drastic simplification. With the Boussinesq assumption the momentum equation reads (see Eq. 11.2 and 11.33)

$$\frac{\partial \rho_0 \bar{v}_i}{\partial t}+\frac{\partial}{\partial x_j}\left(\rho_0 \bar{v}_i\bar{v}_j\right)$$
$$=-\frac{\partial \bar{p}_B}{\partial x_i}+\frac{\partial}{\partial x_j}\left[(\mu+\mu_t)\left(\frac{\partial \bar{v}_i}{\partial x_j}+\frac{\partial \bar{v}_j}{\partial x_i}\right)\right]-\beta\rho_0(\bar{\theta}-\theta_0)g_i \tag{11.34}$$

where the turbulent kinetic energy (last term in Eq. 11.33) has been incorporated in the pressure, i.e. $\bar{p}_B=\bar{p}+2k/3$. There is a fundamental difference between μ and μ_t: μ is different for each fluid (water, air, methane, ...) and depends mainly on temperature; μ_t depends on the flow, i.e. it is function of the location ($\mu_t=\mu_t(x_i)$).

If the mean temperature equation, Eq. 11.9, is solved for, we need an equation for the heat flux vector, $\overline{v_i'\theta'}$. One option is to solve its transport equation, Eq. 11.22. However, it is more common to used an eddy-viscosity model for the heat flux vector. The Boussinesq assumption reads

$$\overline{v_i'\theta'}=-\alpha_t\frac{\partial \bar{\theta}}{\partial x_i} \tag{11.35}$$

---

[3] contraction means that i is set to j

where α_t denotes the turbulent thermal diffusivity. Note that this is the same assumption as Fourier's law for a Newtonian flux, see Eq. 2.14. The turbulent thermal diffusivity, α_t, is usually obtained from the turbulent viscosity as

$$\alpha_t = \frac{\nu_t}{\sigma_\theta} \tag{11.36}$$

where σ_θ is the turbulent Prandtl number; it is an empirical constant which is usually set to $0.7 \leq \sigma_\theta \leq 0.9$. The physical meaning of the turbulent Prandtl number, σ_θ, is analogous to the physical meaning of the usual Prandtl number, see Eq. 2.19; it defines how efficient the turbulence transports (by diffusion) momentum compared to how efficient it transports thermal energy, i.e.

$$\sigma_\theta = \frac{\nu_t}{\alpha_t} \tag{11.37}$$

It is important to recognize that the viscosity (ν), the Prandtl number (Pr), the thermal diffusivity (α) are *physical* parameters which depend on the fluid (e.g. water or air) and its conditions (e.g. temperature). However, the turbulent viscosity (ν_t), the turbulent thermal diffusivity (α_t) and the turbulent Prandtl number (σ_θ) depend on the *flow* (e.g. mean flow gradients and turbulence).

11.7 Modeling assumptions

Now we will compare the modeling assumptions for the unknown terms in the $\overline{v_i'v_j'}$, $\overline{v_i'\theta'}$, k and ε equations and formulate modeling assumptions for the remaining terms in the Reynolds stress equation. This will give us the Reynolds Stress Model [RSM] (also called the Reynolds Stress Transport Model [RSTM]) where a (modeled) transport equation is solved for each stress. Later on, we will introduce a simplified algebraic model, which is called the Algebraic Stress Model [ASM] (this model is also called Algebraic Reynolds Stress Model, ARSM)

Summary of physical meaning:

P_{ij}, $P_{i\theta}$ and P^k are production terms of $\overline{v_i'v_j'}$, $\overline{v_i'\theta'}$ and k

G_{ij}, $G_{i\theta}$ and G^k are production terms of $\overline{v_i'v_j'}$, $\overline{v_i'\theta'}$ and k due to buoyancy

$D_{ij,t}$, $D_{i\theta,t}$, D_t^k are the turbulent diffusion terms of $\overline{v_i'v_j'}$, $\overline{v_i'\theta'}$ and k

$\Pi_{i\theta}$ is the pressure-scramble terms of $\overline{v_i'\theta'}$

Π_{ij} is the pressure-strain correlation term, which promotes isotropy of the turbulence

ε_{ij}, $\varepsilon_{i\theta}$ and ε are dissipation of $\overline{v_i'v_j'}$, $\overline{v_i'\theta'}$ and k, respectively. The dissipation takes place at the small-scale turbulence.

11.7.1 Production terms

In RSM and ASM the production terms are computed exactly

$$P_{ij} = -\overline{v_i'v_k'}\frac{\partial \bar{v}_j}{\partial x_k} - \overline{v_j'v_k'}\frac{\partial \bar{v}_i}{\partial x_k}, \quad P^k = \frac{1}{2}P_{ii} = -\overline{v_i'v_j'}\frac{\partial \bar{v}_i}{\partial x_j}$$

$$P_{i\theta} = -\overline{v_i'v_k'}\frac{\partial \bar{\theta}}{\partial x_k} - \overline{v_k'\theta'}\frac{\partial \bar{v}_i}{\partial x_k} \tag{11.38}$$

k is usually not solved for in RSM but a length-scale equation (i.e. ε or ω) is always part of an RSM and that equation includes P^k.

In the $k - \varepsilon$ model, the Reynolds stresses in the production term are computed using the Boussinesq assumption, which gives

$$
\begin{aligned}
-\overline{v_i'v_j'} &= \nu_t \left(\frac{\partial \bar{v}_i}{\partial x_j} + \frac{\partial \bar{v}_j}{\partial x_i} \right) - \frac{2}{3} \delta_{ij} k \\
P^k &= \left\{ \nu_t \left(\frac{\partial \bar{v}_i}{\partial x_j} + \frac{\partial \bar{v}_j}{\partial x_i} \right) - \frac{2}{3} \delta_{ij} k \right\} \frac{\partial \bar{v}_i}{\partial x_j} \\
&= \nu_t \left(\frac{\partial \bar{v}_i}{\partial x_j} + \frac{\partial \bar{v}_j}{\partial x_i} \right) \frac{\partial \bar{v}_i}{\partial x_j} = \nu_t 2\bar{s}_{ij}(\bar{s}_{ij} + \Omega_{ij}) = 2\nu_t \bar{s}_{ij}\bar{s}_{ij} \\
\bar{s}_{ij} &= \frac{1}{2} \left(\frac{\partial \bar{v}_i}{\partial x_j} + \frac{\partial \bar{v}_j}{\partial x_i} \right), \quad \Omega_{ij} = \frac{1}{2} \left(\frac{\partial \bar{v}_i}{\partial x_j} - \frac{\partial \bar{v}_j}{\partial x_i} \right), \quad \frac{\partial \bar{v}_i}{\partial x_j} = \bar{s}_{ij} + \Omega_{ij}
\end{aligned}
\tag{11.39}
$$

where on the third line we used the fact that $\bar{s}_{ij}\Omega_{ij} = 0$ because the product between a symmetric tensor ($\bar{s}_{ij}$) and an asymmetric tensor (Ω_{ij}) is zero. The incompressibility condition, $\partial \bar{v}_i / \partial x_i = 0$, was used to obtain the third line.

11.7.2 Diffusion terms

The diffusion terms in the k and ε-equations in the $k - \varepsilon$ model are modeled using the standard gradient hypothesis which reads

$$
\begin{aligned}
D^k &= \frac{\partial}{\partial x_j} \left[\left(\nu + \frac{\nu_t}{\sigma_k} \right) \frac{\partial k}{\partial x_j} \right] \\
D^\varepsilon &= \frac{\partial}{\partial x_j} \left[\left(\nu + \frac{\nu_t}{\sigma_\varepsilon} \right) \frac{\partial \varepsilon}{\partial x_j} \right]
\end{aligned}
\tag{11.40}
$$

The gradient hypothesis simply assumes that turbulent diffusion acts as to even out all inhomogeneities. In other words, it assumes that the turbulent diffusion term, D_t^k, transports k from regions where k is large to regions where k is small. The turbulent diffusion flux of k is expressed as

$$
d_{j,t}^k = \frac{1}{2} \overline{v_j'v_i'v_i'} = -\frac{\nu_t}{\sigma_k} \frac{\partial k}{\partial x_j}
\tag{11.41}
$$

Note that this is the same assumption as Fourier's law for a Newtonian flux, see Eq. 2.14. Only the triple correlations are included since the pressure diffusion usually is negligible (see Fig. 8.3 at p. 101). Taking the divergence of Eq. 11.41 (including the minus sign in Eq. 11.23) gives the turbulent diffusion term in Eq. 11.40.

Solving the equations for the Reynolds stresses, $\overline{v_i'v_j'}$, opens possibilities for a more advanced model of the turbulent diffusion terms. Equation 11.41 assumes that if the gradient is zero in x_j direction, then there is no diffusion flux in that direction. A more general gradient hypothesis can be formulated without this limitation, e.g.

$$
d_{j,t,G}^k \propto \overline{v_j'v_k'} \frac{\partial k}{\partial x_k}
\tag{11.42}
$$

which is called the general gradient diffusion hypothesis (GGDH). It was derived in [27] from the transport equation of the triple correlation $\overline{v_j'v_i'v_i'}$. In GGDH the turbulent

flux $d_{1,t,G}^k$, for example, is computed as

$$d_{1,t,G}^k \propto \overline{v_1' v_1'} \frac{\partial k}{\partial x_1} + \overline{v_1' v_2'} \frac{\partial k}{\partial x_2} + \overline{v_1' v_3'} \frac{\partial k}{\partial x_3} \qquad (11.43)$$

Hence, even if $\partial k / \partial x_1 = 0$ the diffusion flux $d_{1,t,G}^k$ may be non-zero. A quantity of dimension $[s]$ must be added to get the correct dimension, and as in Eq. 11.27 we take k/ε so that

$$d_{j,t,G}^k = c_k \frac{k}{\varepsilon} \overline{v_j' v_k'} \frac{\partial k}{\partial x_k} \qquad (11.44)$$

The diffusion term, D_t^k, in the k equation is obtained by taking the divergence of this equation

$$D_t^k = \frac{\partial d_{j,t,G}^k}{\partial x_j} = \frac{\partial}{\partial x_j} \left(c_k \frac{k}{\varepsilon} \overline{v_j' v_k'} \frac{\partial k}{\partial x_k} \right) \qquad (11.45)$$

This diffusion model may be used when the k equation is solved in an RSM or an ASM. The corresponding diffusion terms for the ε and $\overline{v_i' v_j'}$ equations read

$$
\begin{aligned}
D_t^\varepsilon &= \frac{\partial}{\partial x_j} \left(c_\varepsilon \, \overline{v_j' v_k'} \, \frac{k}{\varepsilon} \frac{\partial \varepsilon}{\partial x_k} \right) \\
D_{ij,t} &= \frac{\partial}{\partial x_k} \left(c_k \, \overline{v_k' v_m'} \, \frac{k}{\varepsilon} \frac{\partial \overline{v_i' v_j'}}{\partial x_m} \right)
\end{aligned}
\qquad (11.46)
$$

Equation 11.46 often causes numerical problems. A more stable alternative is to model the diffusion terms as in 11.40 which for $\overline{v_i' v_j'}$ reads

$$D_{ij,t} = \frac{\partial}{\partial x_m} \left(\frac{\nu_t}{\sigma_k} \frac{\partial \overline{v_i' v_j'}}{\partial x_m} \right) \qquad (11.47)$$

11.7.3   Dissipation term, ε_{ij}

The dissipation term ε_{ij} (see Eq. 11.11) is active for the small-scale turbulence. Because of the cascade process and vortex stretching (see Figs. 5.2 and 5.3) the small-scale turbulence is isotropic. This means that the velocity fluctuations of the small-scale turbulence have no preferred direction, see p. 75. This gives:

1. $\overline{v_1'^2} = \overline{v_2'^2} = \overline{v_3'^2}$.

2. All shear stresses are zero, i.e.

$$\overline{v_i' v_j'} = 0 \quad \text{if} \quad i \neq j$$

   because the fluctuations in two different coordinate directions are not correlated.

   What applies for the small-scale fluctuations (Items 1 and 2, above) must also apply for the gradients of the fluctuations, i.e.

$$
\begin{aligned}
\overline{\frac{\partial v_1'}{\partial x_k} \frac{\partial v_1'}{\partial x_k}} &= \overline{\frac{\partial v_2'}{\partial x_k} \frac{\partial v_2'}{\partial x_k}} = \overline{\frac{\partial v_3'}{\partial x_k} \frac{\partial v_3'}{\partial x_k}} \\
\overline{\frac{\partial v_i'}{\partial x_k} \frac{\partial v_j'}{\partial x_k}} &= 0 \quad \text{if} \quad i \neq j
\end{aligned}
\qquad (11.48)
$$
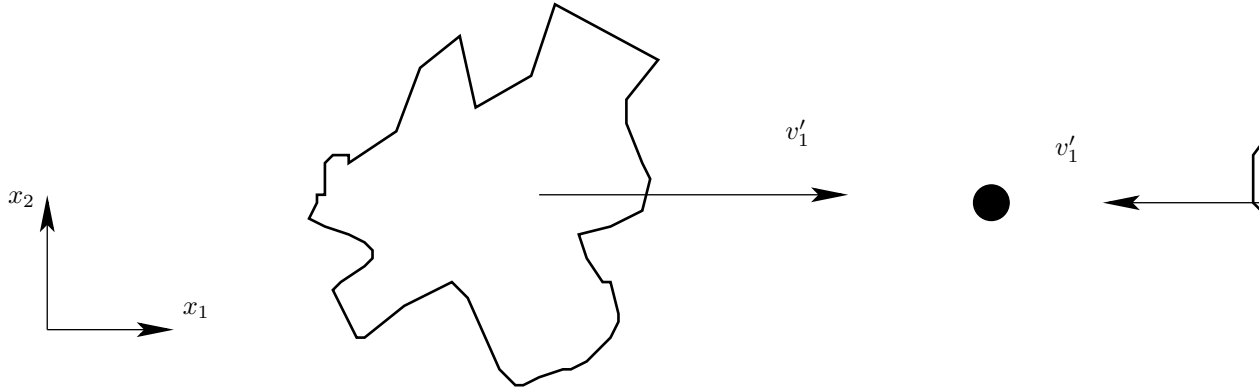
Figure 11.1: Physical illustration of the pressure-strain term.

The relations in Eq. 11.48 are conveniently expressed in tensor notation as

$$\varepsilon_{ij} = \frac{2}{3}\varepsilon\delta_{ij} \tag{11.49}$$

where the factor $2/3$ is included so that $\varepsilon = \frac{1}{2}\varepsilon_{ii}$ is satisfied, see Eqs. 11.11 and 11.23.

11.7.4 Slow pressure-strain term

The pressure-strain term, Π_{ij}, makes a large contribution to the $\overline{v'_i v'_j}$ equation. In Section 9 it was shown that for channel flow it is negative for the streamwise equation, $\overline{v'^2_1}$, and positive for the wall-normal, $\overline{v'^2_2}$, and spanwise, $\overline{v'^2_3}$, equations. Furthermore, it acts as a sink term for the shear stress equation. In summary, it was shown that the term acts as to make the turbulence more *isotropic*, i.e. decreasing the large normal stresses and the magnitude of the shear stress and increasing the small normal stresses. The pressure-strain term is often called the *Robin Hood* terms, because it "takes from the rich and gives to the poor".

The role of the pressure strain can be described in physical terms as follows. Assume that two fluid particles with fluctuating velocities v'_1 bounce into each other at O so that $\partial v'_1/\partial x_1 < 0$, see Fig. 11.1. As a result the fluctuating pressure p' increases at O so that

$$p'\frac{\partial v'_1}{\partial x_1} < 0$$

The fluid in the x_1 direction is performing work, moving fluid particles against the pressure gradient. The kinetic energy lost in the x_1 direction is transferred to the x_2 and x_3 directions and we assume that the collision makes fluid particles move in the other two directions, i.e.

$$\frac{\partial v'_2}{\partial x_2} > 0, \quad \frac{\partial v'_3}{\partial x_3} > 0 \tag{11.50}$$

Indeed, if $\partial v'_1/\partial x_1 < 0$, the continuity equation gives $\partial v'_2/\partial x_2 + \partial v'_3/\partial x_3 > 0$. However, in Eq. 11.50 we assume that not only their sum is positive but also that they both are positive. If this is to happen the kinetic energy in the x_1 direction must be

larger than that in the x_2 and x_3 direction, i.e. $\overline{v_1'^2} > \overline{v_2'^2}$ and $\overline{v_1'^2} > \overline{v_3'^2}$. If $\overline{v_3'^2} \simeq \overline{v_1'^2}$, the pressure strain re-distributes kinetic energy from both $\overline{v_1'^2}$ and $\overline{v_3'^2}$ to $\overline{v_2'^2}$.

Now let's assume that $\overline{v_1'^2} > \overline{v_2'^2}$ and $\overline{v_1'^2} > \overline{v_3'^2}$. The amount of kinetic energy transferred from the x_1 direction to the x_2 and x_3 directions, should be proportional to the difference of their energies, i.e.

$$\overline{p'\frac{\partial v_1'}{\partial x_1}} \propto -\frac{\rho}{2t}\left[\left(\overline{v_1'^2} - \overline{v_2'^2}\right) + \left(\overline{v_1'^2} - \overline{v_3'^2}\right)\right]$$

$$= -\frac{\rho}{t}\left[\overline{v_1'^2} - \frac{1}{2}\left(\overline{v_2'^2} + \overline{v_3'^2}\right)\right] = -\frac{\rho}{t}\left[\frac{3}{2}\overline{v_1'^2} - \frac{1}{2}\left(\overline{v_1'^2} + \overline{v_2'^2} + \overline{v_3'^2}\right)\right] = -\frac{\rho}{t}\left(\frac{3}{2}\overline{v_1'^2} - k\right) \tag{11.51}$$

where t denotes a turbulent timescale. The expression in Eq. 11.51 applies only to the normal stresses, i.e. the principal axis of $\overline{v_i'v_j'}$. Let us show that by transforming the fluctuations to a coordinate system which is rotated an angle $\alpha = \pi/4$ then $\overline{p'(\partial v_1'/\partial x_2 + \partial v_2'/\partial x_1)} \propto -\overline{v_1'v_2'}$ ($\alpha = \pi/4$ corresponds to the special case when the normal stresses are equal). We express Eq. 11.51 in principal coordinates, (x_{1*}, x_{2*}), and then transform the equation to (x_1, x_2) by rotating it angle $\alpha = \pi/4$, see Appendix Y.1. Replacing u_{12} in Eq. Y.6b by $\overline{v_1'v_2'}$ we get

$$\overline{v_1'v_2'} = 0.5\left(\overline{v_{1*}'^2} - \overline{v_{2*}'^2}\right) \tag{11.52}$$

since $\overline{v_{1*}'v_{2*}'} = \overline{v_{2*}'v_{1*}'}$. Now we have transformed the right side of Eq. 11.51 (the right side on the first line). Next step is to transform the left side, i.e. the velocity gradients. We use Eqs. Y.6b and Y.6c: replacing u_{12} and u_{21} by $\partial v_1'/\partial x_2$ and $\partial v_2'/\partial x_1$, respectively, and adding them gives

$$\frac{\partial v_2'}{\partial x_1} + \frac{\partial v_1'}{\partial x_2} = \frac{\partial v_{1*}'}{\partial x_{1*}} - \frac{\partial v_{2*}'}{\partial x_{2*}} \tag{11.53}$$

the pressure-strain term in Eqs. 11.11 and 11.51 can be written

$$\overline{p'\left(\frac{\partial v_2'}{\partial x_1} + \frac{\partial v_1'}{\partial x_2}\right)} = \overline{p'\left(\frac{\partial v_{1*}'}{\partial x_{1*}} - \frac{\partial v_{2*}'}{\partial x_{2*}}\right)} \tag{11.54}$$

Now we apply Eq. 11.51 in the x_{1*} and $-x_{2*}$ directions (looking at the right side of Eq. 11.54) so that

$$\overline{p'\left(\frac{\partial v_{1*}'}{\partial x_{1*}} - \frac{\partial v_{2*}'}{\partial x_{2*}}\right)} \propto -\frac{3\rho}{2t}\left(\overline{v_{1*}'^2} - \overline{v_{2*}'^2}\right) \tag{11.55}$$

Inserting Eqs. 11.52 and 11.54 into Eq. 11.55 gives finally

$$\overline{p'\left(\frac{\partial v_2'}{\partial x_1} + \frac{\partial v_1'}{\partial x_2}\right)} \propto -\frac{3}{t}\rho\overline{v_1'v_2'} \tag{11.56}$$

This shows that the pressure-strain term acts as a sink term in the shear stress equation. Thus, Eqs. 11.51 and 11.56 lead as to write

$$\Phi_{ij,1} \equiv \overline{p'\left(\frac{\partial v_i'}{\partial x_j} + \frac{\partial v_j'}{\partial x_i}\right)} = -c_1\rho\frac{\varepsilon}{k}\left(\overline{v_i'v_j'} - \frac{2}{3}\delta_{ij}k\right) \tag{11.57}$$
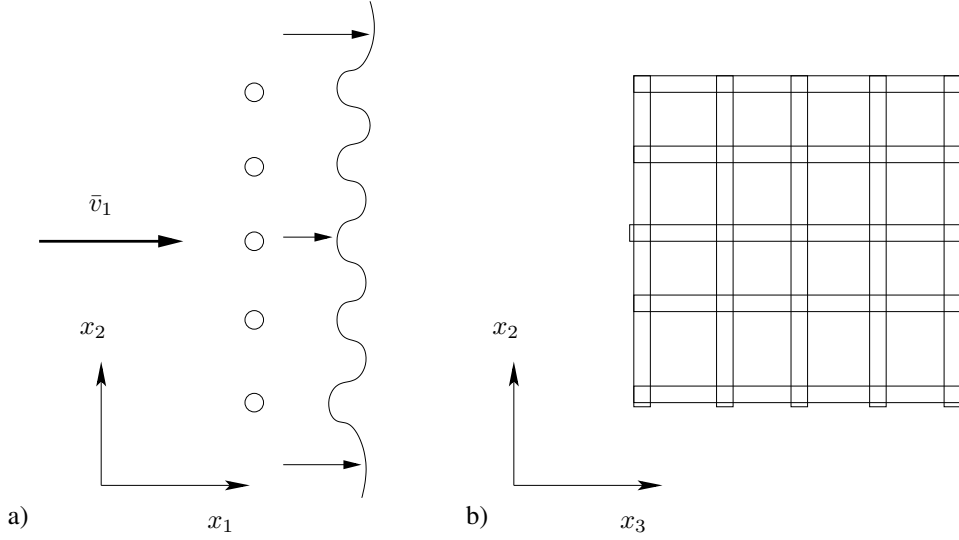
Figure 11.2: Decaying grid turbulence. The circles (a) and the thin rectangles (b) illustrates part of the grid which consists of a mesh of circular cylinders.

where Φ denotes the *modeled* pressure-strain term and subscript 1 means the slow part; the concept "slow" and "rapid" is discussed at p. 134. We have introduced the turbulent time scale $t = k/\varepsilon$ and a constant c_1. This pressure-strain model for the slow part was proposed by Rotta in 1951 [28].

Let us investigate how Eq. 11.57 behaves for decaying grid turbulence, see Fig. 11.2. Flow from left with velocity $\bar{v}_1$ passes through a grid. The grid creates velocity gradients behind the grid which generates turbulence. Further downstream the velocity gradients are smoothed out and the mean flow becomes constant. From this point and further downstream the flow represents homogeneous turbulence which is slowly approaching isotropic turbulence; furthermore the turbulence is slowly dying (i.e. decaying) due to dissipation. The exact $\overline{v_i' v_j'}$ equation for this flow reads (no production or diffusion because of homogeneity)

$$\bar{v}_1 \frac{d\overline{v_i' v_j'}}{dx_1} = \overline{\frac{p'}{\rho}\left(\frac{\partial v_i'}{\partial x_j} + \frac{\partial v_j'}{\partial x_i}\right)} - \varepsilon_{ij} \tag{11.58}$$

Rotta's pressure-strain model is supposed to reduce anisotropy. Thus it should be interesting to re-write Eq. 11.58 expressed in the normalized anisotropy Reynolds stress tensor which is defined as

$$a_{ij} = \frac{\overline{v_i' v_j'}}{k} - \frac{2}{3}\delta_{ij} \tag{11.59}$$

Note that when the turbulence is isotropic, then $a_{ij} = 0$. We introduce a_{ij} (Eq. 11.59), Rotta's model (Eq. 11.57) and the model for the dissipation tensor (11.49) into Eq. 11.58 so that

$$\bar{v}_1 \left(\frac{d(ka_{ij})}{dx_1} + \delta_{ij}\frac{2}{3}\frac{\partial k}{\partial x_1}\right) = -c_1\varepsilon a_{ij} - \frac{2}{3}\delta_{ij}\varepsilon \tag{11.60}$$

Analogously to Eq, 11.58, the k equation in decaying grid turbulence reads

$$\bar{v}_1 \frac{dk}{dx_1} = -\varepsilon \tag{11.61}$$

Inserting Eq. 11.61 in Eq. 11.60 and dividing by k we obtain

$$\bar{v}_1 \frac{da_{ij}}{dx_1} = -c_1 \frac{\varepsilon}{k} a_{ij} - \frac{2}{3} \delta_{ij} \frac{\varepsilon}{k} + \frac{\varepsilon}{k} a_{ij} + \frac{2}{3} \delta_{ij} \frac{\varepsilon}{k} = \frac{\varepsilon}{k} a_{ij}(1 - c_1) \qquad (11.62)$$

Provided that $c_1 > 1$ Rotta's model does indeed reduce non-isotropy as it should.

The model of the slow pressure-strain term in Eq. 11.57 can be extended by including terms which are non-linear in $\overline{v_i' v_j'}$. To make it general it is enough to include terms which are quadratic in $\overline{v_i' v_j'}$, since according to the Cayley-Hamilton theorem, a second-order tensor satisfies its own characteristic equation (see Section 1.20 in [29]); this means that terms that are cubic in $\overline{v_i' v_j'}$ (i.e. $\overline{v_i' v_j'}^3 = \overline{v_i' v_k'}\ \overline{v_k' v_m'}\ \overline{v_m' v_j'}$) can be expressed in terms that are linear and quadratic in $\overline{v_i' v_j'}$. The most general form of $\Phi_{ij,1}$ can be formulated as [30]

$$\Phi_{ij,1} = -c_1 \rho \left[\varepsilon a_{ij} + c_1' \left(a_{ik} a_{kj} - \frac{1}{3} \delta_{ij} a_{k\ell} a_{\ell k} \right) \right]$$

$$a_{ij} = \frac{\overline{v_i' v_j'}}{k} - \frac{2}{3} \delta_{ij} \qquad\qquad (11.63)$$

a_{ij} is an anisotropy tensor whose trace is zero. In isotropic flow all its components are zero. Note that the right side is trace-less (i.e. the trace is zero). This should be so since the exact form of Φ_{ij} is trace-less, i.e. $\Phi_{ii} = \overline{2p' \partial v_i' / \partial x_i} = 0$.

11.7.5 Rapid pressure-strain term

Above a model for the slow part of the pressure-strain term was developed using physical arguments. Here we will carry out a mathematical derivation of a model for the rapid part of the pressure-strain term.

The notation "rapid" comes from a classical problem in turbulence called the rapid distortion problem, where a very strong velocity gradient $\partial \bar{v}_i / \partial x_j$ is imposed so that initially the second term (the slow term) can be neglected, see Eq. 11.65. It is assumed that the effect of the mean gradients is much larger than the effect of the turbulence, i.e.

$$\left| \frac{\partial \bar{v}_i}{\partial x_j} \right| \bigg/ (\varepsilon/k) \to \infty \qquad\qquad (11.64)$$

Thus in this case it is the first term in Eq. 11.65 which gives the most "rapid" response in p'. The second "slow" term becomes important first at a later stage when turbulence has been generated.

Now we want to derive an exact equation for the pressure-strain term, Π_{ij}. Since it includes the fluctuating pressure, p', we start by deriving an exact equation for p' starting from Navier-Stokes equations.

1. Take the divergence of the incompressible Navier-Stokes equation assuming constant viscosity (see Eq. 6.6) i.e. $\dfrac{\partial}{\partial x_i} \left(v_j \dfrac{\partial v_i}{\partial x_j} \right) = \dots \Rightarrow$ Equation **A**.

2. Take the divergence of the incompressible time-averaged Navier-Stokes equation assuming constant viscosity (see Eq. 6.10) i.e. $\dfrac{\partial}{\partial x_i} \left(\bar{v}_j \dfrac{\partial \bar{v}_i}{\partial x_j} \right) = \dots \Rightarrow$ Equation **B**.
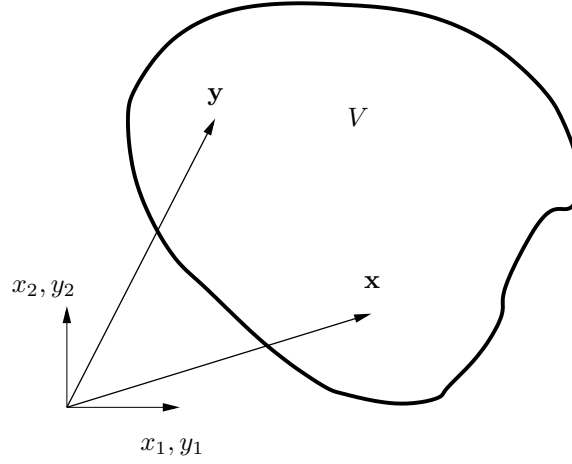
Figure 11.3: The exact solution to Eq. 11.66. The integral is carried out for all points, **y**, in volume V.

Subtraction of Equation **B** from Equation **A** gives a Poisson equation for the fluctuating pressure p'

$$\frac{1}{\rho}\frac{\partial^2 p'}{\partial x_j \partial x_j} = -\underbrace{2\frac{\partial \bar{v}_i}{\partial x_j}\frac{\partial v'_j}{\partial x_i}}_{\text{rapid term}} - \underbrace{\frac{\partial^2}{\partial x_i \partial x_j}\left(v'_i v'_j - \overline{v'_i v'_j}\right)}_{\text{slow term}} \qquad (11.65)$$

The factor two in the rapid term appears because when taking the divergence of the convective term there are two identical terms, see right-side of Eq. 8.6. For a Poisson equation

$$\frac{\partial^2 \varphi}{\partial x_j \partial x_j} = f \qquad (11.66)$$

there exists an exact analytical solution given by Green's formula, see Appendix Z (it is derived from Gauss divergence law)

$$\varphi(\mathbf{x}) = -\frac{1}{4\pi}\int_V \frac{f(\mathbf{y})dy_1 dy_2 dy_3}{|\mathbf{y}-\mathbf{x}|} \qquad (11.67)$$

where the integrals at the boundaries vanish because it is assumed that $f \to 0$ at the boundaries, see Fig. 11.3. Applying Eq. 11.67 on Eq. 11.65 gives

$$p'(\mathbf{x}) = \frac{\rho}{4\pi}$$

$$\int_V \left[\underbrace{2\frac{\partial \bar{v}_i(\mathbf{y})}{\partial y_j}\frac{\partial v'_j(\mathbf{y})}{\partial y_i}}_{\text{rapid term}} + \underbrace{\frac{\partial^2}{\partial y_i \partial y_j}\left(v'_i(\mathbf{y})v'_j(\mathbf{y}) - \overline{v'_i(\mathbf{y})v'_j(\mathbf{y})}\right)}_{\text{slow term}}\right]\frac{d\mathbf{y}^3}{|\mathbf{y}-\mathbf{x}|} \qquad (11.68)$$

where $d\mathbf{y}^3 = dy_1 dy_2 dy_3$. Now make two assumptions in Eq. 11.68:

i) the turbulence is homogeneous (i.e. the spatial derivative of all time-averaged fluctuating quantities is zero). This means that the last term in square brackets

is zero. This requirement is not as drastic as it may sound (although very few turbulent flows are homogeneous). This term is indeed very small compared to the second derivative of the instantaneous fluctuations, $v_i'(\mathbf{y})v_j'(\mathbf{y})$.

ii) the variation of $\partial \bar{v}_i/\partial x_j$ in space is small. The same argument can be used as above: the mean gradient $\partial \bar{v}_i/\partial x_j$ varies indeed much more slowly than the instantaneous velocity gradient, $\partial v_j'(\mathbf{y})/\partial y_i$

Assumption *i)* means that the last term in the integral in Eq. 11.68 is zero, i.e.

$$\frac{\partial^2 \overline{v_i'v_j'}}{\partial y_i \partial y_j} = 0$$

Assumption *ii)* means that the mean velocity gradient can be taken outside the integral. Now multiply Eq. 11.68 with $\partial v_i'/\partial x_j + \partial v_j'/\partial x_i$. Since this term is not a function of $\mathbf{y}$ it can be moved in under the integral. We obtain after time averaging

$$
\begin{aligned}
&\frac{1}{\rho}\overline{p'(\mathbf{x}) \left(\frac{\partial v_i'(\mathbf{x})}{\partial x_j} + \frac{\partial v_j'(\mathbf{x})}{\partial x_i} \right)} \\
&= \frac{\partial \bar{v}_k(\mathbf{x})}{\partial x_\ell} \underbrace{\frac{1}{2\pi} \int_V \overline{\left(\frac{\partial v_i'(\mathbf{x})}{\partial x_j} + \frac{\partial v_j'(\mathbf{x})}{\partial x_i} \right) \frac{\partial v_\ell'(\mathbf{y})}{\partial y_k}} \frac{d\mathbf{y}^3}{|\mathbf{y} - \mathbf{x}|}}_{M_{ijk\ell}} \\
&\quad + \underbrace{\frac{1}{4\pi} \int_V \overline{\left(\frac{\partial v_i'(\mathbf{x})}{\partial x_j} + \frac{\partial v_j'(\mathbf{x})}{\partial x_i} \right) \frac{\partial^2}{\partial y_k \partial y_\ell} (v_k'(\mathbf{y})v_\ell'(\mathbf{y}))} \frac{d\mathbf{y}^3}{|\mathbf{y} - \mathbf{x}|}}_{A_{ij}}
\end{aligned}
\tag{11.69}
$$

Note that the mean velocity gradient, $\partial \bar{v}/\partial x_\ell$, is taken at point $\mathbf{x}$ because it has been moved out of the integral. In order to understand this better, consider the integral

$$f(x) = \int_0^L \frac{g(\xi)d\xi}{|x - \xi|} \tag{11.70}$$

Note that x and ξ are coordinates along the same axis (think of them as two different points along the x axis). If the two points, x and ξ, are far from each other, then the denominator is large and the contribution to the integral is small. Hence, we only need to consider ξ points which are close to x. If we assume that $g(\xi)$ varies slowly with ξ, $g(\xi)$ can be moved out of the integral and since x is close to ξ, Eq. 11.70 can be written as

$$f(x) = g(x) \int_0^L \frac{d\xi}{|x - \xi|} \tag{11.71}$$

Going from Eq. 11.70 to Eq. 11.71 corresponds to moving the mean velocity gradient out of the integral. Equation 11.69 can be written on shorter form as

$$\overline{\frac{p'}{\rho} \left(\frac{\partial v_i'}{\partial x_j} + \frac{\partial v_j'}{\partial x_i} \right)} = A_{ij} + M_{ijk\ell} \frac{\partial \bar{v}_k}{\partial x_\ell} = \Phi_{ij,1} + \Phi_{ij,2} \tag{11.72}$$

where the first term represents the slow term, $\Phi_{ij,1}$ (see Eq. 11.57), and second term is the rapid term, $\Phi_{ij,2}$ (index 2 denotes the rapid part).

Now we will take a closer look at the rapid part (i.e. the second term) of $M_{ijk\ell}$. The second term of $M_{ijk\ell}$ in the integral in Eq. 11.69 can be rewritten as

$$
\begin{aligned}
\overline{\frac{\partial v'_j(\mathbf{x})}{\partial x_i} \frac{\partial v'_\ell(\mathbf{y})}{\partial y_k}} &= \frac{\partial}{\partial y_k}\left(\overline{v'_\ell(\mathbf{y})\frac{\partial v'_j(\mathbf{x})}{\partial x_i}}\right) - \overline{v'_\ell(\mathbf{y})\frac{\partial^2 v'_j(\mathbf{x})}{\partial y_k \partial x_i}} \\
&= \frac{\partial^2}{\partial y_k \partial x_i}\left(\overline{v'_\ell(\mathbf{y})v'_j(\mathbf{x})}\right) - \frac{\partial}{\partial y_k}\left(\overline{v'_j(\mathbf{x})\frac{\partial v'_\ell(\mathbf{y})}{\partial x_i}}\right) \quad (11.73)\\
&= \frac{\partial^2}{\partial y_k \partial x_i}\left(\overline{v'_\ell(\mathbf{y})v'_j(\mathbf{x})}\right)
\end{aligned}
$$

$\partial^2 v'_j(\mathbf{x})/\partial y_k \partial x_i$ on line 1 is zero because $v'_j(\mathbf{x})$ is not a function of $\mathbf{y}$. For the same reason the last term on line 2 is zero.

Note that the terms above as well as in Eq. 11.69 are two-point correlations, the two points being $\mathbf{x}$ and $\mathbf{y}$. Introduce the distance vector between the two points

$$
r_i = y_i - x_i \quad (11.74)
$$

Differentiating Eq. 11.74 gives

$$
\frac{\partial}{\partial r_i} = \frac{\partial}{\partial y_i} - \frac{\partial}{\partial x_i} \quad (11.75)
$$

Equation 11.74 is a coordinate transformation where we replace x_i and y_i with

    I. x_i and r_i, or

    II. y_i and r_i.

Assumption *i)* at p. 135 gives that $\partial/\partial x_i = 0$ (Item I) or $\partial/\partial y_i = 0$ (Item II). In other words, the two-point correlations are independent of where in space the two points are located; they are only dependent on the distance between the two points (i.e. r_i). Hence we can replace the spatial derivative by the distance derivative, i.e.

$$
\begin{aligned}
\frac{\partial}{\partial x_i} &= -\frac{\partial}{\partial r_i} \\
\frac{\partial}{\partial y_i} &= \frac{\partial}{\partial r_i}
\end{aligned} \quad (11.76)
$$

We can now write $M_{ijk\ell}$ in Eq. 11.69, using Eqs. 11.73 and 11.76, as

$$
\begin{aligned}
M_{ijk\ell} &= -\frac{1}{2\pi}\int_V \left[\frac{\partial^2}{\partial r_k \partial r_i}\left(\overline{v'_\ell v'_j}\right) + \frac{\partial^2}{\partial r_k \partial r_j}\left(\overline{v'_\ell v'_i}\right)\right]\frac{d\mathbf{r}^3}{|\mathbf{r}|} \\
&= a_{ijk\ell} + a_{jik\ell}
\end{aligned} \quad (11.77)
$$

It can be shown that $a_{ijk\ell}$ is symmetric with respect to index j and ℓ (recall that v'_ℓ and v'_j are not at the same point but separated by r_i), i.e.

$$
a_{ijk\ell} = a_{i\ell kj} \quad (11.78)
$$

see Appendix L on p. 438. Furthermore, Eq. 11.77 is independent of in which order the two derivatives are taken, so that $a_{ijk\ell}$ is symmetric with respect to i and k, i.e.

$$
a_{ijk\ell} = a_{kji\ell} \quad (11.79)
$$

Now let us formulate a general expression of $a_{ijk\ell}$ which is linear in $\overline{v_i'v_j'}$ and symmetric in (j, ℓ) and (i, k). We get

$$
\begin{aligned}
a_{ijk\ell} = {} & c_1\delta_{ik}\overline{v_j'v_\ell'} \\
& + c_2\delta_{j\ell}\overline{v_i'v_k'} \\
& + c_3(\delta_{ij}\overline{v_k'v_\ell'} + \delta_{kj}\overline{v_i'v_\ell'} + \delta_{i\ell}\overline{v_k'v_j'} + \delta_{k\ell}\overline{v_i'v_j'}) \\
& + c_4\delta_{j\ell}\delta_{ik}k \\
& + c_5(\delta_{ij}\delta_{k\ell} + \delta_{jk}\delta_{i\ell})k
\end{aligned}
\tag{11.80}
$$

Each line is symmetric in (j, ℓ) and (i, k). For example, on line 3, term 1 & term 3 and term 2 & term 4 are symmetric with respect to j and ℓ and term 1 & term 2 and term 3 & term 4 are symmetric with respect to i and k.

Consider Eq. 11.69. Here it is seen that if $i = j$ then $M_{ijk\ell} = 0$ due to the continuity equation; looking at Eq. 11.77 we get

$$
a_{iik\ell} = 0
\tag{11.81}
$$

Applying this condition to Eq. 11.80 gives

$$
\begin{aligned}
0 = {} & c_1\delta_{ik}\overline{v_i'v_\ell'} + c_2\delta_{i\ell}\overline{v_i'v_k'} + c_3(3\overline{v_k'v_\ell'} + \delta_{ki}\overline{v_i'v_\ell'} + \delta_{i\ell}\overline{v_k'v_i'} + \delta_{k\ell}\overline{v_i'v_i'}) \\
& + c_4\delta_{i\ell}\delta_{ik}k + c_5(3\delta_{k\ell} + \delta_{ik}\delta_{i\ell})k \\
= {} & c_1\overline{v_k'v_\ell'} + c_2\overline{v_\ell'v_k'} + c_3(3\overline{v_k'v_\ell'} + \overline{v_k'v_\ell'} + \overline{v_k'v_\ell'} + 2\delta_{k\ell}k) \\
& + c_4\delta_{k\ell}k + c_5(3\delta_{k\ell} + \delta_{k\ell})k \\
= {} & \overline{v_k'v_\ell'}(c_1 + c_2 + 5c_3) + k\delta_{k\ell}(c_4 + 2c_3 + 4c_5)
\end{aligned}
\tag{11.82}
$$

Green's third formula reads (see Appendix L on p. 438)

$$
a_{iji\ell} = 2\overline{v_j'v_\ell'}
\tag{11.83}
$$

Using Eq. 11.83 in Eq. 11.80 gives

$$
\begin{aligned}
2\overline{v_j'v_\ell'} = {} & 3c_1\overline{v_j'v_\ell'} + c_2\delta_{j\ell}\overline{v_i'v_i'} + c_3(\delta_{ij}\overline{v_i'v_\ell'} + \delta_{ij}\overline{v_i'v_\ell'} + \delta_{i\ell}\overline{v_i'v_j'} + \delta_{i\ell}\overline{v_i'v_j'}) \\
& + (3c_4\delta_{j\ell} + c_5(\delta_{ij}\delta_{i\ell} + \delta_{ji}\delta_{i\ell}))k \\
= {} & 3c_1\overline{v_j'v_\ell'} + 2c_2\delta_{j\ell}k + 4c_3\overline{v_j'v_\ell'} + (3c_4 + 2c_5)\delta_{j\ell})k \\
= {} & \overline{v_j'v_\ell'}(3c_1 + 4c_3) + \delta_{j\ell}k(2c_2 + 3c_4 + 2c_5)
\end{aligned}
\tag{11.84}
$$

Equations 11.82 and 11.84 give four equations

$$
\begin{aligned}
c_1 + c_2 + 5c_3 = 0, \quad & c_4 + 2c_3 + 4c_5 = 0 \\
3c_1 + 4c_3 - 2 = 0, \quad & 2c_2 + 3c_4 + 2c_5 = 0
\end{aligned}
\tag{11.85}
$$

for the five unknown constants. Let us express all constants in c_2 which gives

$$
c_1 = \frac{4c_2 + 10}{11}, \quad c_3 = -\frac{3c_2 + 2}{11}, \quad c_4 = -\frac{50c_2 + 4}{55}, \quad c_5 = \frac{20c_2 + 6}{55}
\tag{11.86}
$$

Inserting Eq. 11.86 into Eq. 11.80 and 11.72 gives

$$\phi_{ij,2} = M_{ijk\ell}\frac{\partial\bar{v}_k}{\partial x_\ell} = (a_{ijk\ell} + a_{jik\ell})\frac{\partial\bar{v}_k}{\partial x_\ell}$$

$$= c_1\left(\overline{v'_j v'_\ell}\frac{\partial\bar{v}_i}{\partial x_\ell} + \overline{v'_i v'_\ell}\frac{\partial\bar{v}_j}{\partial x_\ell}\right) + c_2\left(\overline{v'_i v'_k}\frac{\partial\bar{v}_k}{\partial x_j} + \overline{v'_j v'_k}\frac{\partial\bar{v}_k}{\partial x_i}\right)$$

$$+c_3\left(2\delta_{ij}\overline{v'_k v'_\ell}\frac{\partial\bar{v}_k}{\partial x_\ell} + \overline{v'_i v'_\ell}\frac{\partial\bar{v}_j}{\partial x_\ell} + \overline{v'_j v'_\ell}\frac{\partial\bar{v}_i}{\partial x_\ell} + \overline{v'_k v'_j}\frac{\partial\bar{v}_k}{\partial x_i} + \overline{v'_k v'_i}\frac{\partial\bar{v}_k}{\partial x_j}\right)$$

$$+c_4 k\left(\frac{\partial\bar{v}_i}{\partial x_j} + \frac{\partial\bar{v}_j}{\partial x_i}\right) + c_5 k\left(\frac{\partial\bar{v}_j}{\partial x_i} + \frac{\partial\bar{v}_i}{\partial x_j}\right)$$

$$(11.87)$$

We find that the c_1 term and the second and third part of the c_3 term can be merged. Furthermore, the c_2 term and the third and fourth part of the c_3 term can be merged as well as the c_4 and c_5 terms; using Eq. 11.85 we get

$$\phi_{ij,2} = -\frac{c_2+8}{11}P_{ij} - \frac{8c_2-2}{11}\mathcal{D}_{ij} + \frac{6c_2+4}{11}P^k + \frac{4-60c_2}{55}k\bar{s}_{ij}$$

$$\mathcal{D}_{ij} = -\overline{v'_i v'_k}\frac{\partial\bar{v}_k}{\partial x_j} - \overline{v'_j v'_k}\frac{\partial\bar{v}_k}{\partial x_i}$$

$$(11.88)$$

Finally we re-write this equation so that it is expressed in trace-less tensors

$$\Phi_{ij,2} = -\rho\frac{c_2+8}{11}\left(P_{ij} - \frac{2}{3}\delta_{ij}P^k\right)$$

$$-\rho\frac{8c_2-2}{11}\left(\mathcal{D}_{ij} - \frac{2}{3}\delta_{ij}P^k\right) - \frac{60c_2-4}{55}\rho k\bar{s}_{ij}$$

$$(11.89)$$

where $c_2 = 0.4$. Note that $\Phi_{ii} = 0$ as we required in Eq. 11.81. This pressure-strain model is called the LRR model and it was proposed in [31].

All three terms in Eq. 11.89 satisfy continuity and symmetry conditions. It might be possible to use a simpler pressure-strain model using one or any two terms. Since the first term is the most important one, a simpler model has been proposed [31, 32]

$$\Phi_{ij,2} = -c_2\rho\left(P_{ij} - \frac{2}{3}\delta_{ij}P^k\right)$$

$$(11.90)$$

It can be noted that there is a close similarity between the Rotta model and Eq. 11.90: both models represent "return-to-isotropy", the first expressed in $\overline{v'_i v'_j}$ and the second in P_{ij}. The model in Eq. 11.90 is commonly called the IP model (IP=Isotropization by Production) . Since two terms are omitted we should expect that the best value of γ should be different than $(c_2 + 8)/11$; a value of $\gamma = 0.6$ ($c_2 = -1.4$) was found to give good agreement with experimental data. Since Eq. 11.90 is a truncated form of Eq. 11.89 it does not satisfy all requirements that Eq. 11.89 do. Equation 11.90 does satisfy symmetry condition and continuity but it does not satisfy the integral condition in Eq. 11.83. Although Eq. 11.90 is a simpler, truncated version of Eq. 11.89, it is often found to give more accurate results [33]. Since the IP model is both simpler and seems to be more accurate than Eq. 11.89, it is one of the most popular models of the rapid pressure-strain term. The coefficients for the slow and rapid terms in the LRR and LRR-IP models are summarized in Table 11.1

	LRR model	**LRR-IP model**
c_1 (Eq. 11.57	1.5	1.5
c_2 (Eq. 11.89)	0.4	–
c_2 (Eq. 11.90)	–	0.6

Table 11.1: Constants in the LRR and LRR-IP pressure-strain models.
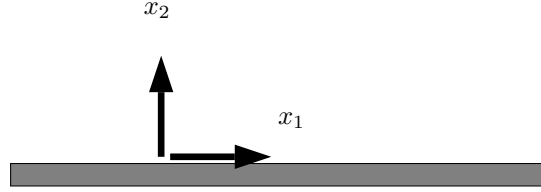
Figure 11.4: Modeling of wall correction in pressure-strain terms.

11.7.6 Wall model of the pressure-strain term

When we derived the rapid pressure-strain model using Green's function in Eq. 11.68 we neglected the influence of any boundaries. In wall-bounded domains it turns out that the effect of the walls must be taken into account. Both the rapid term in the LRR model and the IP model must be modified to include wall modeling.

The effect of the wall is to dampen turbulence. There are two main effects whose underlying physics are entirely different.

1. **Viscosity**. Close to the wall the viscous processes (viscous diffusion and dissipation) dominate over the turbulent ones (production and turbulent diffusion).

2. **Pressure**. When a fluid particle approaches a wall, the presence of the wall is felt by the fluid particle over a long distance. This is true for a fluid particle carried by the wind approaching a building as well as for a fluid particle carried by a fluctuating velocity approaching the wall in a turbulent boundary layer. In both cases it is the pressure that informs the fluid particle of the presence of the wall.

Since the pressure-strain term includes the fluctuating pressure, it is obviously the second of these two processes that we want to include in the wall model. Up to now we have introduced two terms for modeling the pressure-strain term, the slow and the fast term. It is suitable to include a slow and a fast **wall model term**, i.e.

$$\Phi_{ij} = \Phi_{ij,1} + \Phi_{ij,2} + \Phi_{ij,1w} + \Phi_{ij,2w} \tag{11.91}$$

where subscript w denotes wall modeling.

Consider a wall, see Fig. 11.4. The pressure fluctuations dampens the wall-normal fluctuations. Furthermore, the damping effect of the wall should decrease for increasing wall distance. We need to scale the wall-normal distance with a relevant quantity and the turbulent length scale, $k^{3/2}/\varepsilon$, seems to be a good candidate. For the wall-normal

fluctuations, the IP wall model reads [34]

$$\Phi_{22,1w} = -2c_{1w}\frac{\varepsilon}{k}\overline{v_2'^2}f$$

$$f = \min\left\{\frac{k^{\frac{3}{2}}}{2.55|n_{i,w}(x_i - x_{i,w})|\varepsilon}, 1.0\right\} \tag{11.92}$$

where $n_{i,w}(x_i - x_{i,w})$ denotes the distance to the wall. f may exceed one near the wall and that's why we put an upper limit on it. As explained above, this damping is inviscid (due to pressure) and affects the turbulent fluctuations well into the log-region. It has nothing to do with viscous damping. Away from the wall, in the fully turbulent region, the damping function goes to zero since the distance to the wall, $|n_{i,w}(x_i - x_{i,w})|$, increases faster than the turbulence length scale, $k^{3/2}/\varepsilon$. In the viscous region the wall model term, $\Phi_{22,1w}$, is not relevant and should be zero since it should account only for inviscid damping. Moreover, function f should not exceed one.

The IP wall model for the wall-parallel fluctuations reads

$$\Phi_{11,1w} = \Phi_{33,1w} = c_{1w}\frac{\varepsilon}{k}\overline{v_2'^2}f \tag{11.93}$$

The requirement that the sum of the pressure strain term should be zero. i.e. $\Phi_{ii,1w} = 0$, is now satisfied since $\Phi_{11,1w} + \Phi_{22,1w} + \Phi_{33,1w} = 0$.

The wall model for the shear stress is set as

$$\Phi_{12,1w} = -\frac{3}{2}c_{1w}\frac{\varepsilon}{k}\overline{v_1'v_2'}f \tag{11.94}$$

The factor $3/2$ is needed to ensure that $\Phi_{ii,1w} = 0$ is satisfied when the coordinate system is rotated. You can prove this by rotating the matrix $[\Phi_{11,1w}, \Phi_{12,1w}; \Phi_{21,1w}, \Phi_{22,1w}]$ and taking the trace of Φ in the principal coordinates system (i.e. taking the sum of the eigenvalues).

The general formula for a wall that is not aligned with a Cartesian coordinate axis reads [34]

$$\Phi_{ij,1w} = c_{1w}\frac{\varepsilon}{k}\left(\overline{v_k'v_m'}n_{k,w}n_{m,w}\delta_{ij} - \frac{3}{2}\overline{v_k'v_i'}n_{k,w}n_{j,w} - \frac{3}{2}\overline{v_k'v_j'}n_{i,w}n_{k,w}\right)f \tag{11.95}$$

An analogous wall model is used for the rapid part which reads

$$\Phi_{ij,2w} = c_{2w}\left(\Phi_{km,2}n_{k,w}n_{m,w}\delta_{ij} - \frac{3}{2}\Phi_{ki,2}n_{k,w}n_{j,w} - \frac{3}{2}\Phi_{kj,2}n_{i,w}n_{k,w}\right)f \tag{11.96}$$

11.8 The $k − ε$ model

The exact k equation is given by Eq. 11.23. By inserting the model assumptions for the turbulent diffusion (Eq. 11.40), the production (Eq. 11.39) and the buoyancy term (Eqs. 11.35 and 11.36) we get the *modeled* equation for k

$$\frac{\partial k}{\partial t} + \bar{v}_j\frac{\partial k}{\partial x_j} = \nu_t\left(\frac{\partial \bar{v}_i}{\partial x_j} + \frac{\partial \bar{v}_j}{\partial x_i}\right)\frac{\partial \bar{v}_i}{\partial x_j} + g_i\beta\frac{\nu_t}{\sigma_\theta}\frac{\partial \bar{\theta}}{\partial x_i}$$
$$-\varepsilon + \frac{\partial}{\partial x_j}\left[\left(\nu + \frac{\nu_t}{\sigma_k}\right)\frac{\partial k}{\partial x_j}\right] \tag{11.97}$$

In the same way, the modeled ε equation is obtained from Eq. 11.29

$$\frac{\partial \varepsilon}{\partial t} + \bar{v}_j \frac{\partial \varepsilon}{\partial x_j} = \frac{\varepsilon}{k} c_{\varepsilon 1} \nu_t \left(\frac{\partial \bar{v}_i}{\partial x_j} + \frac{\partial \bar{v}_j}{\partial x_i} \right) \frac{\partial \bar{v}_i}{\partial x_j}$$
$$+ c_{\varepsilon 1} g_i \frac{\varepsilon}{k} \frac{\nu_t}{\sigma_\theta} \frac{\partial \bar{\theta}}{\partial x_i} - c_{\varepsilon 2} \frac{\varepsilon^2}{k} + \frac{\partial}{\partial x_j} \left[\left(\nu + \frac{\nu_t}{\sigma_\varepsilon} \right) \frac{\partial \varepsilon}{\partial x_j} \right] \tag{11.98}$$

The turbulent viscosity is computed as

$$\nu_t = c_\mu \frac{k^2}{\varepsilon} \tag{11.99}$$

The standard values for the coefficients read

$$(c_\mu, c_{\varepsilon 1}, c_{\varepsilon 2}, \sigma_k, \sigma_\varepsilon) = (0.09, 1.44, 1.92, 1, 1.3) \tag{11.100}$$

For details on how to obtain these constants are obtained, see Section 11.14.2 and Section 3 in Introduction to turbulence models. In that report, details on wall-functions and low-Reynolds number models can be found in Sections 3 and 4, respectively.

11.9 The modeled $\overline{v_i' v_j'}$ equation with IP model

With the models for diffusion, pressure-strain and dissipation we get the <u>R</u>eynolds <u>S</u>tress <u>M</u>odel [RSM]

$$\frac{\partial \overline{v_i' v_j'}}{\partial t} + \quad \text{(unsteady term)}$$

$$\bar{v}_k \frac{\partial \overline{v_i' v_j'}}{\partial x_k} = \quad \text{(convection)}$$

$$-\overline{v_i' v_k'} \frac{\partial \bar{v}_j}{\partial x_k} - \overline{v_j' v_k'} \frac{\partial \bar{v}_i}{\partial x_k} \quad \text{(production)}$$

$$-c_1 \frac{\varepsilon}{k} \left(\overline{v_i' v_j'} - \frac{2}{3} \delta_{ij} k \right) \quad \text{(pressure strain, slow part)}$$

$$-c_2 \left(P_{ij} - \frac{2}{3} \delta_{ij} P^k \right) \quad \text{(pressure strain, rapid part, IP model))}$$

$$+c_{1w} \rho \frac{\varepsilon}{k} \left[\, \overline{v_k' v_m'} n_k n_m \delta_{ij} - \frac{3}{2} \overline{v_i' v_k'} n_k n_j \right.$$

$$\left. - \frac{3}{2} \overline{v_j' v_k'} n_k n_i \, \right] f \quad \text{(pressure strain, wall, slow part)}$$

$$+c_{2w} \left[\, \Phi_{km,2} n_k n_m \delta_{ij} - \frac{3}{2} \Phi_{ik,2} n_k n_j \right.$$

$$\left. - \frac{3}{2} \Phi_{jk,2} n_k n_i \, \right] f \quad \text{(pressure strain, wall, rapid part, IP model))}$$

$$+\nu \frac{\partial^2 \overline{v_i' v_j'}}{\partial x_k \partial x_k} \quad \text{(viscous diffusion)}$$

$$+\frac{\partial}{\partial x_m} \left[\frac{\nu_t}{\sigma_k} \frac{\partial \overline{v_i' v_j'}}{\partial x_m} \right] \quad \text{(turbulent diffusion)}$$

$$-g_i \beta \overline{v_j' \theta'} - g_j \beta \overline{v_i' \theta'} \quad \text{(buoyancy production)}$$

$$-\frac{2}{3} \varepsilon \delta_{ij} \quad \text{(dissipation)}$$

$$\tag{11.101}$$

11.10 Algebraic Reynolds Stress Model (ASM)

The <u>A</u>lgebraic Reynolds <u>S</u>tress <u>M</u>odel is a simplified Reynolds Stress Model. The RSM and $k - \varepsilon$ models are written in symbolic form (see p. 122 & 125) as:

$$\text{RSM} : C_{ij} - D_{ij} = P_{ij} + \Phi_{ij} - \varepsilon_{ij}$$
$$k - \varepsilon : \ C^k - D^k = P^k - \varepsilon \tag{11.102}$$

In ASM we assume that the transport (convective and diffusive) of $\overline{v'_i v'_j}$ is related to that of k, i.e.

$$C_{ij} - D_{ij} = \frac{\overline{v'_i v'_j}}{k} \left(C^k - D^k \right)$$

Inserting Eq. 11.102 into the equation above gives

$$P_{ij} + \Phi_{ij} - \varepsilon_{ij} = \frac{\overline{v'_i v'_j}}{k} \left(P^k - \varepsilon \right) \tag{11.103}$$

Thus the transport equation (PDE) for $\overline{v'_i v'_j}$ has been transformed into an *algebraic* equation based on the assumption in Eq. 11.102.

Now we want to re-write this equation as an equation for $\overline{v'_i v'_j}$. Insert the IP models for $\Phi_{ij,1}$ (Eq. 11.57) and $\Phi_{ij,2}$ (Eq. 11.90) and the isotropic model for ε_{ij} (Eq. 11.49) in Eq. 11.103 and multiply by k/ε so that

$$\frac{k}{\varepsilon} P_{ij} - c_1 \left(\overline{v'_i v'_j} - \frac{2}{3} \delta_{ij} k \right) - c_2 \frac{k}{\varepsilon} \left(P_{ij} - \frac{2}{3} \delta_{ij} P^k \right) - \frac{2}{3} \delta_{ij} k$$

$$+ \frac{k}{\varepsilon} \left(\Phi_{ij,1w} + \Phi_{ij,2w} \right) = \frac{\overline{v'_i v'_j}}{\varepsilon} \left(P^k - \varepsilon \right)$$

Collect all $\overline{v'_i v'_j}$ terms so that

$$\overline{v'_i v'_j} \left(\frac{P^k}{\varepsilon} - 1 + c_1 \right) =$$

$$\frac{k}{\varepsilon} \left[P_{ij} - c_2 \left(P_{ij} - \frac{2}{3} \delta_{ij} P^k \right) + \Phi_{ij,1w} + \Phi_{ij,2w} \right] + \frac{2}{3} \delta_{ij} k(-1 + c_1)$$

$$= \frac{k}{\varepsilon} \left[P_{ij} \boxed{-\delta_{ij} \frac{2}{3} P^k} - c_2 \left(P_{ij} - \frac{2}{3} \delta_{ij} P^k \right) + \Phi_{ij,1w} + \Phi_{ij,2w} \right] + \boxed{\frac{2}{3} \delta_{ij} k(P^k/\varepsilon} - 1 + c_1)$$

where $(2/3)\delta_{ij} P^k k/\varepsilon$ was added and subtracted at the last line (shown in boxes). Dividing both sides by $P^k/\varepsilon - 1 + c_1$ gives finally

$$\overline{v'_i v'_j} = \frac{2}{3} \delta_{ij} k + \frac{k}{\varepsilon} \frac{(1 - c_2) \left(P_{ij} - \frac{2}{3} \delta_{ij} P^k \right) + \Phi_{ij,1w} + \Phi_{ij,2w}}{c_1 + P^k/\varepsilon - 1} \tag{11.104}$$

In boundary layer flow Eq. 11.104 reads (without any wall terms, i.e. $\Phi_{ij,1w} = \Phi_{ij,2w} = 0$)

$$-\overline{v'_1 v'_2} = \frac{2}{3} (1 - c_2) \underbrace{\frac{c_1 - 1 + c_2 P^k/\varepsilon}{(c_1 - 1 + P^k/\varepsilon)}}_{c_\mu} \frac{k^2}{\varepsilon} \frac{\partial \overline{v}_1}{\partial y}$$

As can be seen, this model can be seen as an extension of an eddy-viscosity model where the c_μ constant is made a function of the ratio P^k/ε.

11.11   Explicit ASM (EASM or EARSM)

Equation 11.104 is an *implicit* equation for $\overline{v_i' v_j'}$, i.e. the Reynolds stresses appear both on the left and the right side of the equation. It would of course be advantageous to be able to get an *explicit* expression for the Reynolds stresses. Pope [35] managed to derive an explicit expression for ASM in two dimensions. He assumed that the Reynolds stress tensor can be expressed in the strain-rate tensor, $\bar{s}_{ij}$, and the vorticity tensor, Ω_{ij}. Furthermore, he showed that the coefficients, $G^{(n)}$, in that expression can be a function of not more than the following five invariants

$$
(k^2/\varepsilon^2)\bar{s}_{ij}\bar{s}_{ji}, \quad (k^2/\varepsilon^2)\bar{\Omega}_{ij}\bar{\Omega}_{ji}, \quad (k^3/\varepsilon^3)\bar{s}_{ij}\bar{s}_{jk}\bar{s}_{ki}
$$
$$
(k^3/\varepsilon^3)\bar{\Omega}_{ij}\bar{\Omega}_{jk}\bar{s}_{ki}, \quad (k^4/\varepsilon^4)\bar{\Omega}_{ij}\bar{\Omega}_{jk}\bar{s}_{km}\bar{s}_{mi}
\tag{11.105}
$$

There are five invariants because when $\bar{s}_{ij}$ and Ω_{ij} are transformed to principal coordinates, there are three eigenvalue for each of them. Furthermore, $\bar{s}_{ii} = 0$ which means there are only five independent invariants.

In two dimension the expression reads

$$
\overline{v_i' v_j'} = \frac{2}{3} k \delta_{ij} + G^{(1)} \frac{k^2}{\varepsilon} \bar{s}_{ij} + G^{(2)} \frac{k^3}{\varepsilon^2} (\bar{s}_{ik}\bar{\Omega}_{kj} - \bar{\Omega}_{ik}\bar{s}_{kj})
\tag{11.106}
$$

In general three-dimensional flow, the Reynolds stress tensor depends on 10 tensors, T_{ij}^n [35], i.e.

$$
\overline{v_i' v_j'} - \frac{2}{3} k \delta_{ij} = \sum_{n=1}^{10} G^{(n)} T_{ij}^n
$$

$$
T_{ij}^1 = \bar{s}_{ij}, \quad T_{ij}^2 = \bar{s}_{ik}\bar{\Omega}_{kj} - \bar{s}_{jk}\bar{\Omega}_{ki}, \quad T_{ij}^3 = \bar{s}_{ik}\bar{s}_{kj} - \frac{1}{3}\delta_{ij}\bar{s}_{ik}\bar{s}_{ki}
$$

$$
T_{ij}^4 = \bar{\Omega}_{ik}\bar{\Omega}_{kj} - \frac{1}{3}\delta_{ij}\bar{\Omega}_{ik}\bar{\Omega}_{ki}, \quad T_{ij}^5 = \bar{\Omega}_{ik}\bar{s}_{km}\bar{s}_{mj} - \bar{s}_{im}\bar{s}_{mk}\bar{\Omega}_{kj}
$$

$$
T_{ij}^6 = \bar{\Omega}_{im}\bar{\Omega}_{mk}\bar{s}_{kj} + \bar{s}_{ik}\bar{\Omega}_{km}\bar{\Omega}_{mj} - \frac{2}{3}\delta_{ij}\bar{\Omega}_{pm}\bar{\Omega}_{mk}\bar{s}_{kp}
$$

$$
T_{ij}^7 = \bar{\Omega}_{im}\bar{s}_{mk}\bar{\Omega}_{kn}\bar{\Omega}_{nj} - \bar{\Omega}_{im}\bar{\Omega}_{mk}\bar{s}_{kn}\bar{\Omega}_{nj}, \quad T_{ij}^8 = \bar{s}_{im}\bar{\Omega}_{mk}\bar{s}_{kn}\bar{s}_{nj} - \bar{s}_{im}\bar{s}_{mk}\bar{\Omega}_{kn}\bar{s}_{nj}
$$

$$
T_{ij}^9 = \bar{\Omega}_{im}\bar{\Omega}_{mk}\bar{s}_{kn}\bar{s}_{nj} - \bar{s}_{im}\bar{s}_{mk}\bar{\Omega}_{kn}\bar{\Omega}_{nj} - \frac{2}{3}\delta_{ij}\bar{\Omega}_{pm}\bar{\Omega}_{mk}\bar{s}_{kn}\bar{s}_{np}
$$

$$
T_{ij}^{10} = \bar{\Omega}_{im}\bar{s}_{mk}\bar{s}_{kn}\bar{\Omega}_{np}\bar{\Omega}_{pj} - \bar{\Omega}_{im}\bar{\Omega}_{mk}\bar{s}_{kn}\bar{s}_{np}\bar{\Omega}_{pj}
$$

$$
\tag{11.107}
$$

where T_{ij}^n may depend on the five invariants in Eq. 11.105. Equation 11.107 is a general form of a non-linear eddy-viscosity model. Any ASM may be written on the form of Eq. 11.107.

It may be noted that Eq. 11.107 includes only linear and quadratic terms of $\bar{s}_{ij}$ and $\bar{\Omega}_{ij}$. That is because of Cayley-Hamilton theorem which states that a second-order tensor satisfies its own characteristic equation (see Section 1.20 in [29]); hence cubic terms or higher can recursively be expressed in linear ($\bar{s}_{ij}$) and quadratic tensors ($\bar{s}_{ik}\bar{s}_{kj}$). Furthermore, note that all terms in Eq. 11.107 are symmetric and traceless as required by the left side, $\overline{v_i' v_j'} - 2\delta_{ij}k/3$.

11.12 Derivation of the Explicit Algebraic Reynolds Stress Model (EARSM)

The algebraic stress model (ASM) is given by Eq. 11.104. This equation is *implicit*, since the Reynolds stresses appear on the right side (in the production and the rapid pressure-strain terms). In this section we will derive an *explicit* algebraic Reynolds stress model (EARSM). The derivation presented here is based on [36]. Whereas the ASM employs the IP model (Eq. 11.90) for the rapid pressure-strain term, the EARSM is based on the LRR model (Eq. 11.89). Thus we start with Eq. 11.103 using the Rotta model for the slow part (Eq. 11.57) and the LRR model (Eq. 11.89) for the rapid part.

$$
\begin{aligned}
(a_{ij} + \tfrac{2}{3}\delta_{ij})(P^k - \varepsilon) = {} & P_{ij} - c_1\varepsilon a_{ij} - \frac{c_2 + 8}{11}\left(P_{ij} - \frac{2}{3}\delta_{ij}P^k\right) \\
& - \frac{8c_2 - 2}{11}\left(\mathcal{D}_{ij} - \frac{2}{3}\delta_{ij}P^k\right) - \frac{60c_2 - 4}{55}k\bar{s}_{ij} - \frac{2}{3}\delta_{ij}\varepsilon
\end{aligned}
$$
(11.108)

where the anisotropy tensor, a_{ij}, in Eq. 11.59 is used on the left side. The wall correction terms are neglected (as they usually are in the LRR model). Equation 11.108 is re-arranged as

$$
\begin{aligned}
a_{ij}(P^k + c_1\varepsilon - \varepsilon) = {} & P_{ij} - \frac{2}{3}\delta_{ij}P^k - \frac{c_2 + 8}{11}\left(P_{ij} - \frac{2}{3}\delta_{ij}P^k\right) \\
& - \frac{8c_2 - 2}{11}\left(\mathcal{D}_{ij} - \frac{2}{3}\delta_{ij}P^k\right) - \frac{60c_2 - 4}{55}k\bar{s}_{ij}
\end{aligned}
$$
(11.109)

Now we introduce the anisotropy tensor, a_{ij}, also on the right side. Start by expressing the production term, P_{ij} (see Eq. 11.11) in a_{ij}, $\bar{s}_{ij}$ and $\bar{\Omega}_{ij}$ (see Eq. 9.12)

$$
\begin{aligned}
P_{ij} &= -k(a_{ik} + \tfrac{2}{3}\delta_{ik})(\bar{s}_{jk} + \bar{\Omega}_{jk}) - k(a_{jk} + \tfrac{2}{3}\delta_{jk})(\bar{s}_{ik} + \bar{\Omega}_{ik}) \\
&= -\frac{4}{3}k\bar{s}_{ij} - ka_{ik}(\bar{s}_{jk} + \bar{\Omega}_{jk}) - ka_{jk}(\bar{s}_{ik} + \bar{\Omega}_{ik}) \\
&= -\frac{4}{3}k\bar{s}_{ij} - k(\bar{s}_{jk}a_{ik} + a_{jk}\bar{s}_{ki}) + k(a_{ik}\bar{\Omega}_{kj} - \bar{\Omega}_{ik}a_{kj})
\end{aligned}
$$
(11.110)

The production term, P^k, is equal to $0.5P_{ii}$, and Eq. 11.110 gives

$$
P^k = -k\bar{s}_{ik}a_{ik}
$$
(11.111)

so that we can express the P^k terms on the right side in Eq. 11.109 as

$$
\frac{2}{3}\delta_{ij}P^k\left(-1 + \frac{c_2 + 8}{11} + \frac{8c_2 - 2}{11}\right) = -\frac{2}{3}\delta_{ij}k\bar{s}_{ik}a_{ik}\frac{9c_2 - 5}{11}
$$
(11.112)

$\mathcal{D}_{ij}$ is the same thing as P_{ij} except that the indices on the velocity gradients (i.e. the tensors a and $\bar{\Omega}$ in Eq. 11.110 are switched), see Eq. 11.88. Hence we get (cf. Eq. 11.110)

$$
\mathcal{D}_{ij} = -\frac{4}{3}k\bar{s}_{ij} - k(\bar{s}_{jk}a_{ki} + a_{jk}\bar{s}_{ki}) - k(a_{ik}\bar{\Omega}_{kj} - \bar{\Omega}_{ik}a_{kj})
$$
(11.113)

Collect all terms including P_{ij}, $\bar{s}_{ij}$ and $\mathcal{D}_{ij}$ in Eq. 11.109

$$P_{ij}\left(1 - \frac{c_2 + 8}{11}\right) - \frac{8c_2 - 2}{11}\mathcal{D}_{ij} - \frac{60c_2 - 4}{55}k\bar{s}_{ij} - \frac{2}{3}\delta_{ij}k\bar{s}_{ik}a_{ik}\frac{9c_2 - 5}{11}$$

Inserting Eqs. 11.110 and 11.113 gives

$$k\left(1 - \frac{c_2 + 8}{11}\right)\left(-\frac{4}{3}\bar{s}_{ij} - (\bar{s}_{jk}a_{ik} + a_{jk}\bar{s}_{ki}) + (a_{ik}\bar{\Omega}_{kj} - \bar{\Omega}_{ik}a_{kj})\right)$$
$$-k\frac{8c_2 - 2}{11}\left(-\frac{4}{3}\bar{s}_{ij} - (\bar{s}_{jk}a_{ki} + a_{jk}\bar{s}_{ki}) - (a_{ik}\bar{\Omega}_{kj} - \bar{\Omega}_{ik}a_{kj})\right) \quad (11.114)$$
$$-\frac{2}{3}\delta_{ij}k\bar{s}_{ik}a_{ik}\frac{9c_2 - 5}{11} - \frac{60c_2 - 4}{55}k\bar{s}_{ij}$$

Gathering all terms including $\bar{s}_{ij}$ gives

$$-\frac{4}{3}k\bar{s}_{ij}\left(1 - \frac{c_2 + 8}{11} + \frac{8c_2 - 2}{11} - \frac{3}{4}\frac{60c_2 - 4}{55}\right) = -\frac{8}{15}k\bar{s}_{ij} \quad (11.115)$$

The terms including the product of the tensors a and s in Eq. 11.114 read

$$-k\left(1 - \frac{c_2 + 8}{11}\right)(\bar{s}_{jk}a_{ik} + a_{jk}\bar{s}_{ki}) + \frac{8c_2 - 2}{11}k(\bar{s}_{jk}a_{ki} + a_{jk}\bar{s}_{ki}) =$$
$$\frac{k}{11}(\bar{s}_{jk}a_{ki} + a_{jk}\bar{s}_{ki})(9c_2 - 5) \quad (11.116)$$

and the product of the tensors a and $\bar{\Omega}$ in Eq. 11.114 read

$$k\left(1 - \frac{c_2 + 8}{11}\right)(a_{ik}\bar{\Omega}_{kj} - \bar{\Omega}_{ik}a_{kj}) + k\frac{8c_2 - 2}{11}(a_{ik}\bar{\Omega}_{kj} - \bar{\Omega}_{ik}a_{kj}) =$$
$$\frac{k}{11}(a_{ik}\bar{\Omega}_{kj} - \bar{\Omega}_{ik}a_{kj})(1 + 7c_2) \quad (11.117)$$

Using Eqs. 11.115, 11.116, 11.117 and the underlined term in Eq. 11.114, Eq. 11.114 can now be written

$$-k\frac{8}{15}\bar{s}_{ij} + k\frac{1 + 7c_2}{11}(a_{ik}\bar{\Omega}_{kj} - \bar{\Omega}_{ik}a_{kj})$$
$$+k\frac{9c_2 - 5}{11}\left(\bar{s}_{jk}a_{ki} + a_{jk}\bar{s}_{ki} - \frac{2}{3}\delta_{ij}k\bar{s}_{ik}a_{ik}\right) \quad (11.118)$$

Equation 11.118 is the right side of Eq. 11.109. Insert Eq. 11.118 into Eq. 11.109 and divide by ε

$$a_{ij}\left(\frac{P^k}{\varepsilon} + c_1 - 1\right) = -\frac{k}{\varepsilon}\frac{8}{15}\bar{s}_{ij} + \frac{k}{\varepsilon}\frac{1 + 7c_2}{11}(a_{ik}\bar{\Omega}_{kj} - \bar{\Omega}_{ik}a_{kj})$$
$$+ \frac{k}{\varepsilon}\frac{9c_2 - 5}{11}\left(\bar{s}_{jk}a_{ki} + a_{jk}\bar{s}_{ki} - \frac{2}{3}\delta_{ij}k\bar{s}_{ik}a_{ik}\right) \quad (11.119)$$

The coefficient, c_2, in the LRR model is usually set to $c_2 = 0.4$, see Table 11.1. In [37–39], they noted that the relation in Eq. 11.119 is substantially simplified if $c_2 = 5/9$. This assumption is made in EARSM [36], which gives

$$a_{ij}\left(\frac{P^k}{\varepsilon} + c_1 - 1\right) = -\frac{8}{15}\hat{s}_{ij} + \frac{4}{9}(a_{ik}\hat{\Omega}_{kj} - \hat{\Omega}_{ik}a_{kj}) \quad (11.120)$$

where the strain-rate and vorticity tensors are made non-dimensional

$$\hat{s}_{ij} = \frac{k}{\varepsilon}\bar{s}_{ij}, \quad \hat{\Omega}_{ij} = \frac{k}{\varepsilon}\Omega_{ij} \tag{11.121}$$

Equation 11.120 can now be written as

$$Na_{ij} = -\frac{6}{5}\hat{s}_{ij} + (a_{ik}\hat{\Omega}_{kj} - \hat{\Omega}_{ik}a_{kj}) \tag{11.122}$$

$$N = \frac{9P^k}{4\varepsilon} + c_1', \quad c_1' = \frac{9}{4}(c_1 - 1) \tag{11.123}$$

The most general form of a_{ij} is given by Eq. 11.107. In two-dimensional flow, we will later show (see Section 11.12.1) that it is sufficient to include only the two first terms, i.e.

$$a_{ij} = \beta_1\hat{s}_{ij} + \beta_4(\hat{s}_{im}\hat{\Omega}_{mj} - \hat{\Omega}_{im}\hat{s}_{mj}) \tag{11.124}$$

where we now denote the coefficients by β_1 and β_4 as in [36]. In order to solve Eq. 11.122, insert Eq. 11.124 which gives

$$N(\beta_1\hat{s}_{ij} + \beta_4(\hat{s}_{ik}\hat{\Omega}_{kj} - \hat{\Omega}_{ik}\hat{s}_{kj})) = -\frac{6}{5}\hat{s}_{ij} + (\beta_1\hat{s}_{ik} + \beta_4(\hat{s}_{im}\hat{\Omega}_{mk} - \hat{\Omega}_{im}\hat{s}_{mk}))\hat{\Omega}_{kj}$$

$$-\hat{\Omega}_{ik}\left(\beta_1\hat{s}_{kj} + \beta_4(\hat{s}_{km}\hat{\Omega}_{mj} - \hat{\Omega}_{km}\hat{s}_{mj})\right)$$

$$= -\frac{6}{5}\hat{s}_{ij} + \beta_1(\hat{s}_{ik}\hat{\Omega}_{kj} - \hat{\Omega}_{ik}\hat{s}_{kj}) + \beta_4(\hat{s}_{im}\hat{\Omega}_{mk}\hat{\Omega}_{kj} - 2\hat{\Omega}_{im}\hat{s}_{mk}\hat{\Omega}_{kj} + \hat{\Omega}_{ik}\hat{\Omega}_{km}\hat{s}_{mj})$$

$$\tag{11.125}$$

The last tern including β_4 can be considerably simplified. Recall that $\hat{\Omega}_{11} = \hat{\Omega}_{22} = 0$ and $\hat{\Omega}_{12} = -\hat{\Omega}_{21}$, see Eq. 1.11. We get for the 11 component of Eq. 11.125

$$\hat{s}_{1m}\hat{\Omega}_{mk}\hat{\Omega}_{k1} - 2\hat{\Omega}_{1m}\hat{s}_{mk}\hat{\Omega}_{k1} + \hat{\Omega}_{1k}\hat{\Omega}_{km}\hat{s}_{m1}$$

$$= \hat{s}_{11}\hat{\Omega}_{12}\hat{\Omega}_{21} - 2\hat{\Omega}_{12}\hat{s}_{22}\hat{\Omega}_{21} + \hat{\Omega}_{12}\hat{\Omega}_{21}\hat{s}_{11} = 4\hat{s}_{11}\hat{\Omega}_{12}\hat{\Omega}_{21} \tag{11.126}$$

since $\hat{s}_{11} = -\hat{s}_{22}$ ($\hat{s}_{ii} = 0$ due to continuity). In the same way we get $4\hat{s}_{22}\hat{\Omega}_{12}\hat{\Omega}_{21}$ for the 22 component. The 12 component (and the 21 component) read

$$\hat{s}_{1m}\hat{\Omega}_{mk}\hat{\Omega}_{k2} - 2\hat{\Omega}_{1m}\hat{s}_{mk}\hat{\Omega}_{k2} + \hat{\Omega}_{1k}\hat{\Omega}_{km}\hat{s}_{m2}$$

$$= \hat{s}_{12}\hat{\Omega}_{21}\hat{\Omega}_{12} - 2\hat{\Omega}_{12}\hat{s}_{21}\hat{\Omega}_{12} + \hat{\Omega}_{12}\hat{\Omega}_{21}\hat{s}_{12} \tag{11.127}$$

$$= \hat{s}_{12}\hat{\Omega}_{21}\hat{\Omega}_{12} + 2\hat{\Omega}_{12}\hat{s}_{21}\hat{\Omega}_{21} + \hat{\Omega}_{12}\hat{\Omega}_{21}\hat{s}_{12} = 4\hat{\Omega}_{12}\hat{\Omega}_{21}\hat{s}_{12}$$

We find that the last term including β_4 in Eq. 11.125 can be written as $2II_\Omega\hat{s}_{ij}$ where $II_\Omega = \hat{\Omega}_{km}\hat{\Omega}_{mk} = \hat{\Omega}_{12}\hat{\Omega}_{21} + \hat{\Omega}_{21}\hat{\Omega}_{12} = 2\hat{\Omega}_{12}\hat{\Omega}_{21}$. Equation 11.125 can now be re-written as

$$N(\beta_1\hat{s}_{ij} + \beta_4(\hat{s}_{ik}\hat{\Omega}_{kj} - \hat{\Omega}_{ik}\hat{s}_{kj})) = -\frac{6}{5}\hat{s}_{ij} + \beta_1(\hat{s}_{ik}\hat{\Omega}_{kj} - \hat{\Omega}_{ik}\hat{s}_{kj}) + 2\beta_4 II_\Omega\hat{s}_{ij} \tag{11.128}$$

Separating $\hat{s}_{ij}$ and $(\hat{s}_{ik}\hat{\Omega}_{kj} - \hat{\Omega}_{ik}\hat{s}_{kj})$ we get two equations for β_1 and β_4

$$N\beta_1 = -\frac{6}{5} + 2\beta_4 II_\Omega$$

$$N\beta_4 = \beta_1 \tag{11.129}$$

so that

$$\beta_4 = -\frac{6}{5}\frac{1}{N^2 - 2II_\Omega}$$
$$\beta_1 = -\frac{6}{5}\frac{N}{N^2 - 2II_\Omega}$$

(11.130)

In order to get the final equation for N, multiply Eq. 11.124 by $\hat{s}_{jk}$ and then take the trace (which is equal to the production $P^k/\varepsilon = a_{ij}\hat{s}_{ji}$, see Eq. 11.111), i.e.

$$\frac{P^k}{\varepsilon} \equiv -a_{ij}\hat{s}_{ji} = -\beta_1 II_S + \beta_4(\hat{s}_{im}\hat{\Omega}_{mj} - \hat{\Omega}_{im}\hat{s}_{mj})\hat{s}_{ji}$$

(11.131)

where $II_S = \hat{s}_{ij}\hat{s}_{ji}$. The β_4 term reads

$$\begin{aligned}
&(\hat{s}_{12}\hat{\Omega}_{21} - \hat{\Omega}_{12}\hat{s}_{21})\hat{s}_{11} \\
&+(\hat{s}_{11}\hat{\Omega}_{12} - \hat{\Omega}_{12}\hat{s}_{22})\hat{s}_{21} \\
&+(\hat{s}_{22}\hat{\Omega}_{21} - \hat{\Omega}_{21}\hat{s}_{11})\hat{s}_{12} \\
&+(\hat{s}_{21}\hat{\Omega}_{12} - \hat{\Omega}_{21}\hat{s}_{12})\hat{s}_{22} = 0
\end{aligned}$$

(11.132)

since line 2 and 3 are zero and line 1 and 4 cancel each other ($\hat{\Omega}_{12} = -\hat{\Omega}_{21}$, $\hat{s}_{12} = \hat{s}_{21}$ and $\hat{s}_{11} = -\hat{s}_{22}$). β_1 is now obtained from Eq. 11.131 as

$$\beta_1 = -\frac{P^k}{II_S\varepsilon}$$

(11.133)

Inserting β_1 in Eq. 11.130 gives

$$\frac{P^k}{\varepsilon} = \frac{6}{5}\frac{N}{N^2 - 2II_\Omega}II_S$$

(11.134)

Equations 11.123 and 11.134 gives finally an equation for N

$$N = \frac{9}{4}\frac{6}{5}\frac{N}{N^2 - 2II_\Omega}II_S + c_1'$$

(11.135)

which is re-written as

$$N(N^2 - 2II_\Omega) - \frac{27}{10}II_S N - c_1'(N^2 - 2II_\Omega) = 0$$

so that

$$N^3 - c_1'N^2 - \left(\frac{27}{10}II_S + 2II_\Omega\right)N + 2c_1'II_\Omega = 0.$$

The analytical solution for the positive root reads [36]

$$N = \frac{c_1'}{3} + \left(P_1 + \sqrt{P_2}\right)^{1/3} + \text{sign}\left(P_1 - \sqrt{P_2}\right)\left|P_1 - \sqrt{P_2}\right|^{1/3}, P_2 \geq 0$$
$$N = \frac{c_1'}{3} + 2\left(P_1^2 - P_2\right)^{1/6}\cos\left[\frac{1}{3}\arccos\left(\frac{P_1}{\sqrt{P_1^2 - P_2}}\right)\right], P_2 < 0$$

(11.136)

where $0 \leq \xi \leq \pi$ in $\arccos(\xi)$ and

$$P_1 = \left(\frac{1}{27}c_1'^2 + \frac{9}{20}II_S - \frac{2}{3}II_\Omega \right) c_1'$$

$$P_2 = P_1^2 - \left(\frac{1}{9}c_1'^2 + \frac{9}{10}II_S + \frac{2}{3}II_\Omega \right)^3 \tag{11.137}$$

Equation 11.137 is valid for two-dimensional flow. For three-dimensional flow, Eq. 11.124 includes more (six) of the terms in 11.107. This derivation is given in [36]. It results in a 6th -order equation for N which must be solved numerically.

In the original LRR model, $c_1 = 1.5$ and $c_2 = 0.4$ (see Table 11.1). In the EARSM, $c_1 = 1.8$ and $c_2 = 5/9$; recall that this choice of c_2 simplifies the rapid pressure-strain model (cf. Eqs. 11.119 and 11.120).

11.12.1   The linear assumption of a_{ij}

In Eq. 11.124 we made an assumption for the relation of a_{ij} expressed in $\hat{s}_{ij}$ and $\hat{\Omega}_{ij}$. The argument is as follows [40]. We start from the assumption (cf. Eq. 11.122)

$$a_{ij} = \hat{s}_{ij} + (a_{im}\hat{\Omega}_{mj} - \hat{\Omega}_{im}a_{mj}) \tag{11.138}$$

Since $\hat{s}_{ij}$ and $\hat{\Omega}_{ij}$ are independent, a_{ij} must include one $\hat{s}_{ij}$ term, $a_{ij}^0 = \hat{s}_{ij}$. Insert this on the right side of Eq. 11.138

$$a_{ij} = \hat{s}_{ij} + (\hat{s}_{im}\hat{\Omega}_{mj} - \hat{\Omega}_{im}\hat{s}_{mj}) \tag{11.139}$$

which gives the term $a_{ij}^1 = \hat{s}_{im}\hat{\Omega}_{mj} - \hat{\Omega}_{im}\hat{s}_{mj}$. We continue to iterate. Inserting a_{ij}^1 on the right side of Eq. 11.138 gives $(a_{im}^1 = \hat{s}_{ik}\hat{\Omega}_{km} - \hat{\Omega}_{ik}\hat{s}_{km})$

$$a_{ij} = \hat{s}_{ij} + (\hat{s}_{ik}\hat{\Omega}_{km} - \hat{\Omega}_{ik}\hat{s}_{km})\hat{\Omega}_{mj} - \hat{\Omega}_{im}(\hat{s}_{mk}\hat{\Omega}_{kj} - \hat{\Omega}_{mk}\hat{s}_{kj}) = \hat{s}_{ij} - 2II_\Omega\hat{s}_{ij} \tag{11.140}$$

see Eqs. 11.125–11.128. We get

$$a_{ij}^2 \propto \hat{s}_{ij} = a_{ij}^0 \tag{11.141}$$

which shows that it is sufficient to include a_{ij}^0 and a_{ij}^1 and hence Eq. 11.124 is complete.

In 3D, we do not get the relation in Eq. 11.141 but another two iterations are required which gives five independent a_{ij}^r (i.e. $r = 4$).

11.13   Boundary layer flow

In order to better understand the Reynolds stress equation, Eq. 11.101, it is useful to look at its source terms which to a large degree govern the magnitude of $\overline{v_i'v_j'}$. A large source term in the equation for the $\overline{v_1'^2}$ equation, for example, will increase $\overline{v_1'^2}$ and vice versa, see Section 9.1. Let us study boundary layer flow (Fig. 11.5) where $\bar{v}_2 \simeq 0$, $\partial\bar{v}_1/\partial x_2 \gg \partial\bar{v}_1/\partial x_1$. The production P_{ij} has the form:

$$P_{ij} = -\overline{v_i'v_k'}\frac{\partial\bar{v}_j}{\partial x_k} - \overline{v_j'v_k'}\frac{\partial\bar{v}_i}{\partial x_k}$$
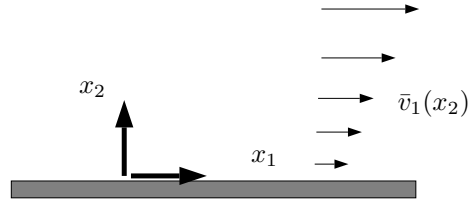
Figure 11.5: Boundary layer flow.

In this special case we get:

$$P_{11} = -2\overline{v_1' v_2'} \frac{\partial \bar{v}_1}{\partial x_2}$$

$$P_{12} = -\overline{v_2'^2} \frac{\partial \bar{v}_1}{\partial x_2}$$

$$P_{22} = 0$$

Is $\overline{v_2'^2}$ zero because its production term P_{22} is zero? No! The sympathetic term Φ_{ij}, which takes from the rich (i.e. $\overline{v_1'^2}$) and gives to the poor (i.e. $\overline{v_2'^2}$), saves the unfair situation! The IP model for $\Phi_{ij,1}$ and $\Phi_{ij,2}$ (Eq. 11.57) and $\Phi_{ij,2}$ (Eq. 11.90) gives

$$\Phi_{22,1} = c_1 \frac{\varepsilon}{k} \left(\frac{2}{3} k - \overline{v_2'^2} \right) > 0$$
$$\Phi_{22,2} = c_2 \frac{1}{3} P_{11} = -c_2 \frac{2}{3} \overline{v_1' v_2'} \frac{\partial \bar{v}_1}{\partial x_2} > 0$$

Note also that the dissipation term for the $\overline{v_1' v_2'}$ is zero, but it takes the value $\frac{2}{3}\varepsilon$ for the $\overline{v_1'^2}$ and $\overline{v_2'^2}$ equations (see p. 131). Since the modeled $\overline{v_1' v_2'}$ does not have any dissipation term, the question arises: what is the main sink term in the $\overline{v_1' v_2'}$ equation? The answer is, again, the pressure strain term $\Phi_{12,1}$ and $\Phi_{12,2}$.

11.14 Wall boundary conditions

There are two options for treating the wall boundary conditions.

- Use a coarse mesh near the walls and assume that the logarithmic law applies. This is called *wall functions*

- Use a fine mesh near the walls and modify the turbulence models to account for the viscous effects. This is called *Low-Reynolds number models*

11.14.1 Wall Functions

The natural way to treat wall boundaries is to make the grid sufficiently fine so that the sharp gradients prevailing there are resolved. Often, when computing complex three-dimensional flow, that requires too much computer resources. An alternative is to
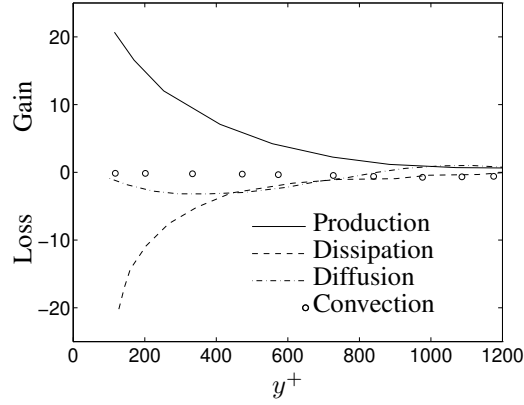
Figure 11.6: Boundary along a flat plate. Energy balance in k equation [41]. $Re_\delta \simeq 4400$, $u_*/U_0 \simeq 0.043$.
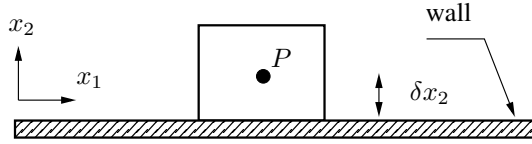
Figure 11.7: Wall-adjacent cell. Cell-centered finite volume grid.
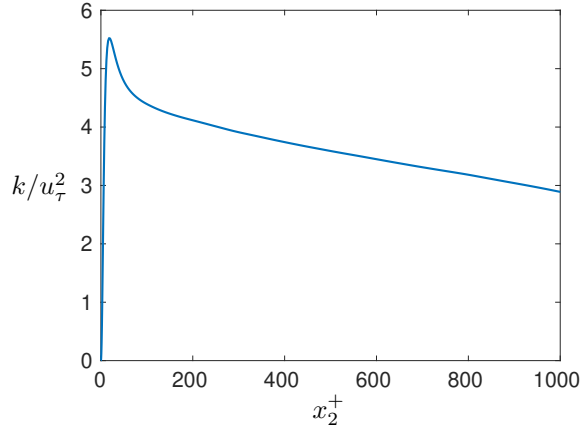
Figure 11.8: Turbulent kinetic energy in a boundary layer predicted by Large Eddy Simulations at $Re_\theta = 8\,200$ [42].

assume that the flow near the wall behaves like a turbulent boundary layer (see Fig. 6.2) and prescribe boundary conditions employing wall functions. The assumption that the flow near the wall has the characteristics of a that in a boundary layer if often not true at all. However, given a maximum number of nodes that we can afford to use in a computation, it is often preferable to use wall functions which allows us to use fine grid in other regions where the gradients of the flow variables are large.

The log-law we use can be written as

$$\frac{\bar{v}_1}{u_\tau} = \frac{1}{\kappa} \ln\left(\frac{E u_\tau x_2}{\nu}\right)$$ (11.142)
$$E = 9.0$$

Comparing this with the standard form of the log-law (see Eq. 6.32)

$$\frac{\bar{v}_1}{u_\tau} = \frac{1}{\kappa} \ln\left(\frac{u_\tau x_2}{\nu}\right) + B.$$ (11.143)

We find that

$$B = \frac{1}{\kappa} \ln E.$$

We compute the friction velocity from Equation 11.142 as

$$u_\tau = \frac{\kappa \bar{v}_{1,P}}{\ln(E u_\tau \delta x_2/\nu)}$$ (11.144)

where $\bar{v}_{1,P}$ is the velocity in the wall-adjacent cell and δx_2 is the distance from the cell center, P, to the wall, see Fig. 11.7. Equation 11.144 is solved by iterating (the newest value of u_τ is inserted at the right-hand side at every iteration). The equation converges very quickly. The wall shear stress, $\tau_w = \rho u_\tau^2$ (see Eq. 6.16) is then used as a force wall boundary condition for the $\bar{v}_1$ equation.

In a turbulent boundary layer the production term and the dissipation term in the log-law region ($30 < x_2^+ < 400$) are much larger than the other terms, see Figs. 8.3 and 11.6. Hence, we can approximate the modelled k equation (see Eq. 11.97) as

$$0 = P^k - \rho\varepsilon = \mu_t \left(\frac{\partial \bar{v}_1}{\partial x_2}\right)^2 - \rho\varepsilon.$$ (11.145)

where we have assumed that the buoyancy term is zero. In the log-law region the shear stress $-\rho\overline{v_1' v_2'}$ is equal to the wall shear stress τ_w, see Eq. 6.25 and Fig. 6.3. The Boussinesq assumption for the shear stress reads (see Eqs. 6.28 and 11.33)

$$\tau_w = -\rho\overline{v_1' v_2'} = \mu_t \frac{\partial \bar{v}_1}{\partial x_2}$$ (11.146)

Inserting Eq. 11.146 into Eq. 11.145 gives

$$0 = \frac{\overline{v_1' v_2'}^2}{\nu_t} - \varepsilon = \frac{u_\tau^4}{\nu_t} - \varepsilon$$ (11.147)

which with Eq. 11.99 gives

$$C_\mu = \left(\frac{u_\tau^2}{k}\right)^2$$ (11.148)

From experiments and DNS we have that in the log-law region of a boundary layer $u_\tau^2/k \simeq 0.3$ so that $C_\mu = 0.09$, see Figs. 6.8 and 11.8 (it may be noted that the **C_μ constant** DNS/LES data give a slightly larger values of k/u_τ^2 than $1/0.3$).

When we are using wall functions k and ε are not solved at the nodes adjacent to the walls. Instead they are fixed according to the theory presented above. The turbulent **b.c. for k**

kinetic energy is set from Eq. 11.148, i.e.

$$k_P = C_\mu^{-1/2} u_\tau^2 \qquad (11.149)$$

where the friction velocity u_τ is obtained, iteratively, from the log-law (Eq. 11.142). Index P denotes the first interior node (adjacent to the wall).

The dissipation ε is obtained from Eq. 11.145. The dissipation can thus be written as **b.c. for ε**

$$\varepsilon_P = P^k = \frac{u_\tau^3}{\kappa \delta x_2} \qquad (11.150)$$

where the velocity gradient in the production term $P^k = -\overline{v_1' v_2'} \partial \bar{v}_1 / \partial x_2 \simeq u_\tau^2 \partial \bar{v}_1 / \partial x_2$ is computed from the log-law (see Eqs. 6.27 and 11.142), i.e.

$$\frac{\partial \bar{v}_1}{\partial x_2} = \frac{u_\tau}{\kappa \delta x_2}. \qquad (11.151)$$

For the velocity component parallel to the wall the wall shear stress is used as a **b.c. for veloc-** force boundary condition (cf. prescribing heat flux in the temperature equation). When **ity** the wall is not parallel to any velocity component, it is more convenient to prescribe the turbulent viscosity [26].

The log-law is valid for $30 < x_2^+ < 400$. If x_2^+ for some wall-adjacent cells is small, the friction velocity, u_τ, is obtained from the linear law (see Eq. 6.22), i.e.

$$u_\tau = \left(\nu \frac{\bar{v}_{1,P}}{\delta x_2} \right)^{1/2} \qquad (11.152)$$

The point at which we switch from the log-law to the linear law is taken at $x_2^+ = 11$ which is the intersection point of the two laws. For $x_2^+ < 11$, $\bar{v}_1$ is set to zero at the wall and k and ε are set from Eqs. 11.149 and 11.150 taking u_τ from Eq. 11.152. For $11 < x_2^+ < 30$, a combination of the linear law and the log-law is sometimes used. In many commercial codes they interpolate between the linear law and the log-law for the velocity, k and ε. In STAR-CCM+ this is called *All y+ Wall Treatment*.

11.14.2 Low-Re Number Turbulence Models

In the previous section we discussed wall functions which are used in order to reduce the number of cells. However, we must be aware that this is an approximation which, if the flow near the boundary is important, can be rather crude. In many internal flows – where all boundaries are either walls, symmetry planes, inlet or outlets – the boundary layer may not be that important, as the flow field is often pressure-determined. For external flows (for example flow around cars, ships, aeroplanes etc.), however, the flow conditions in the boundaries are almost invariably important. When we are predicting heat transfer it is in general no good idea to use wall functions, because the heat transfer at the walls are very important for the temperature field in the whole domain.

When we chose not to use wall functions we thus insert sufficiently many grid lines near solid boundaries so that the boundary layer can be adequately resolved. However, when the wall is approached the viscous effects become more important and for $x_2^+ < 5$ the flow is viscous dominating, i.e. the viscous diffusion is much larger that the turbulent one (see Fig. 11.9). Thus, the turbulence models presented so far may not be correct since fully turbulent conditions have been assumed; this type of models are often referred to as high-Re number models. In this section we will discuss modifications of high-Re number models so that they can be used all the way down to the
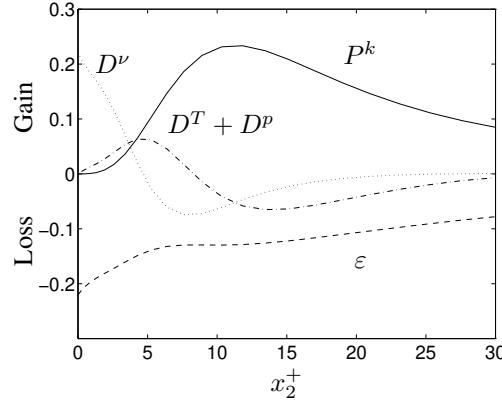
Figure 11.9: Flow in fully developed channel flow. Direct numerical simulations [43]. $Re = \bar{v}_{1,C}\delta/\nu = 7890$ (subscript C denotes the center of the channel). $u_\tau/\bar{v}_{1,C} = 0.050$. Energy balance in k equation. Production P^k, dissipation ε, turbulent diffusion (by velocity triple correlations and pressure) $D^T + D^p$, and viscous diffusion D^ν. All terms have been scaled with u_τ^4/ν.

wall. These modified models are called *low Reynolds number models*. Note that "high Reynolds number" and "low Reynolds number" do *not* refer to the global Reynolds number (for example Re_L, Re_x, Re_x etc.) but here we are talking about the local turbulent Reynolds number $Re_\ell = \mathcal{U}\ell/\nu$ formed by a turbulent fluctuation and turbulent length scale, see Eq. 5.16. This Reynolds number varies throughout the computational domain and is proportional to the ratio of the turbulent and physical viscosity ν_t/ν, i.e. $Re_\ell \propto \nu_t/\nu$. This ratio is of the order of 100 or larger in fully turbulent flow and it goes to zero when a wall is approached.

We start by studying how various quantities behave close to the wall when $x_2 \to 0$. Taylor expansion of the fluctuating velocities v_i' (also valid for the mean velocities $\bar{v}_i$) gives

$$
\begin{aligned}
v_1' &= a_0 + a_1 x_2 + a_2 x_2^2 + \ldots \\
v_2' &= b_0 + b_1 x_2 + b_2 x_2^2 + \ldots \\
v_3' &= c_0 + c_1 x_2 + c_2 x_2^2 + \ldots
\end{aligned}
\tag{11.153}
$$

where $a_0 \ldots c_2$ are functions of space and time. At the wall we have no-slip conditions, i.e. $v_1' = v_2' = v_3' = 0$ which gives $a_0 = b_0 = c_0$. Furthermore, at the wall $\partial v_1'/\partial x_1 = \partial v_3'/\partial x_3 = 0$ so that the continuity equation gives $\partial v_2'/\partial x_2 = 0$. This means that $b_1 = 0$. Equation 11.153 can now be written

$$
\begin{aligned}
v_1' &= a_1 x_2 \;+\; a_2 x_2^2 + \ldots \\
v_2' &= b_2 x_2^2 + \ldots \\
v_3' &= c_1 x_2 \;+\; c_2 x_2^2 + \ldots
\end{aligned}
\tag{11.154}
$$
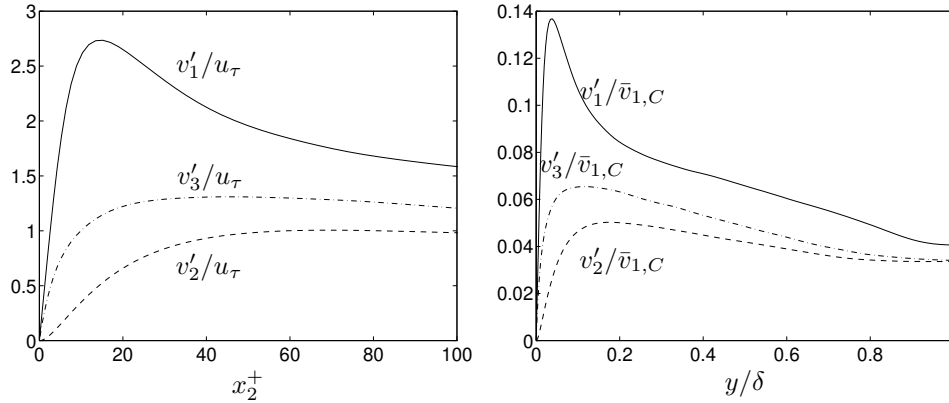
Figure 11.10: Flow between two parallel plates. Direct numerical simulations [43]. $Re = \bar{v}_{1C}\delta/\nu = 7890$. $u_\tau/\bar{v}_{1C} = 0.050$. Fluctuating velocity components $v_i' = \sqrt{\overline{v_1'^2}_i}$.

From Eq. 11.154 we immediately get

$$
\begin{array}{lll}
\overline{v_1'^2} & = \overline{a_1^2}x_2^2 + \ldots & = \mathcal{O}(x_2^2) \\
\overline{v_2'^2} & = \overline{b_2^2}x_2^4 + \ldots & = \mathcal{O}(x_2^4) \\
\overline{v_3'^2} & = \overline{c_1^2}x_2^2 + \ldots & = \mathcal{O}(x_2^2) \\
\overline{v_1'v_2'} & = \overline{a_1 b_2}x_2^3 + \ldots & = \mathcal{O}(x_2^3) \\
k & = \overline{(a_1^2 + c_1^2)}x_2^2 + \ldots & = \mathcal{O}(x_2^2) \\
\partial\bar{v}_1/\partial x_2 & = \overline{a_1} + \ldots & = \mathcal{O}(x_2^0) \\
\partial v_1'/\partial x_2 & = a_1 + \ldots & = \mathcal{O}(x_2^0) \\
\partial v_2'/\partial x_2 & = 2b_2 x_2 + \ldots & = \mathcal{O}(x_2^1) \\
\partial v_3'/\partial x_2 & = a_1 + \ldots & = \mathcal{O}(x_2^0)
\end{array}
\tag{11.155}
$$

In Fig. 11.10 DNS data of velocity fluctuations for the fully developed flow in a channel are presented.

11.14.3 Low-Re $k - \varepsilon$ Models

There exist a number of Low-Re number $k - \varepsilon$ models [44–48]. When deriving low-Re models it is common to study the behavior of the terms when $x_2 \to 0$ in the exact equations and require that the corresponding terms in the modelled equations behave in the same way. Let us study the exact k equation near the wall (see Eq. 8.24).

$$
\rho\bar{v}_1\frac{\partial k}{\partial x_1} + \rho\bar{v}_2\frac{\partial k}{\partial x_2} = \underbrace{-\rho\overline{v_1'v_2'}\frac{\partial\bar{v}_1}{\partial x_2}}_{\mathcal{O}(x_2^3)} - \frac{\partial\overline{p'v_2'}}{\partial x_2} \underbrace{-\frac{\partial}{\partial x_2}\left(\frac{1}{2}\rho\overline{v_2'v_i'v_i'}\right)}_{\mathcal{O}(x_2^3)}
$$
$$
+ \mu\frac{\partial^2 k}{\partial x_2^2} \underbrace{- \mu\overline{\frac{\partial v_i'}{\partial x_j}\frac{\partial v_i'}{\partial x_j}}}_{\mathcal{O}(x_2^0)}
\tag{11.156}
$$

The dissipation term includes all velocity gradients but most of them go to zero close to the wall, see Eq. 11.155. The only velocity gradients that do not go to zero are $\partial v_1'/\partial x_2$ and $\partial v_3'/\partial x_2$ and hence $\varepsilon \propto \mathcal{O}(x_2^0)$. The pressure diffusion $\partial\overline{p'v_2'}/\partial x_2$ term
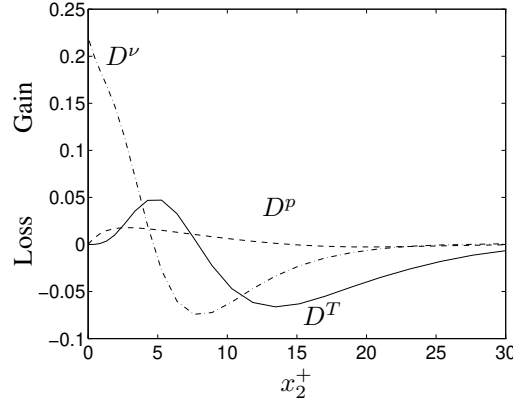
Figure 11.11: Flow between two parallel plates. Direct numerical simulations [43]. $Re = \bar{v}_{1,C}\delta/\nu = 7890$. $u_\tau/\bar{v}_{1,C} = 0.050$. Energy balance in k equation. Turbulent diffusion by velocity triple correlations D^T, Turbulent diffusion by pressure D^p, and viscous diffusion D^ν. All terms have been scaled with u_τ^4/ν.

is usually neglected, partly because it is not measurable, and partly because close to the wall it is not important, see Fig. 11.11 (see also [49]). The modelled equation reads (see Eq. 11.97)

$$\rho\bar{v}_1\frac{\partial k}{\partial x_1} + \rho\bar{v}_2\frac{\partial k}{\partial x_2} = \underbrace{\mu_t\left(\frac{\partial\bar{v}_1}{\partial x_2}\right)^2}_{\mathcal{O}(x_2^4)} + \underbrace{\frac{\partial}{\partial x_2}\left(\frac{\mu_t}{\sigma_k}\frac{\partial k}{\partial x_2}\right)}_{\mathcal{O}(x_2^4)}$$
$$+ \mu\frac{\partial^2 k}{\partial x_2^2} - \underbrace{\rho\varepsilon}_{\mathcal{O}(x_2^0)}$$

(11.157)

When arriving at that the production term is $\mathcal{O}(x_2^4)$ we have used

$$\nu_t = C_\mu\frac{k^2}{\varepsilon} = \frac{\mathcal{O}(x_2^4)}{\mathcal{O}(x_2^0)} = \mathcal{O}(x_2^4)$$

(11.158)

Comparing Eqs. 11.156 and 11.157 we find that the dissipation term in the modelled equation behaves in the same way as in the exact equation when $x_2 \to 0$. However, both the modelled production and the diffusion term are of $\mathcal{O}(x_2^4)$ whereas the exact terms are of $\mathcal{O}(x_2^3)$. This inconsistency of the modelled terms can be removed by replacing the C_μ constant by $C_\mu f_\mu$ where f_μ is a damping function f_μ so that

$$f_\mu = \mathcal{O}(x_2^{-1})$$

(11.159)

when $x_2 \to 0$ and $f_\mu \to 1$ when $x_2^+ \geq 50$. Now we get $\nu_t = \mathcal{O}(x_2^3)$. Please note that the term "damping term" in this case is not correct since f_μ actually is increasing μ_t when $x_2 \to 0$ rather than damping it. However, it is common to call all low-Re number functions for "damping functions".

Instead of introducing a damping function f_μ, we can choose to solve for a modified dissipation which is denoted $\tilde{\varepsilon}$, see Refs. [26, 50]

It is possible to compare the exact and the modeled ε equation when deriving damping functions for the ε equation [51]. An alternative way is to study the modelled

ε equation near the wall and keep only the terms which do not tend to zero. From Eq. 11.29 we get (note that $\partial \varepsilon / \partial x_2 = \mathcal{O}(x_2^0)$, $\partial \varepsilon / \partial x_1 = \mathcal{O}(x_2^0)$)

$$
\underbrace{\rho \bar{v}_1 \frac{\partial \varepsilon}{\partial x_1}}_{\mathcal{O}(x_2^1)} + \underbrace{\rho \bar{v}_2 \frac{\partial \varepsilon}{\partial x_2}}_{\mathcal{O}(x_2^2)} = \underbrace{C_{\varepsilon 1} \frac{\varepsilon}{k} P^k}_{\mathcal{O}(x_2^1)} + \underbrace{\frac{\partial}{\partial x_2} \left(\frac{\mu_t}{\sigma_\varepsilon} \frac{\partial \varepsilon}{\partial x_2} \right)}_{\mathcal{O}(x_2^2)}
$$
$$
+ \underbrace{\mu \frac{\partial^2 \varepsilon}{\partial x_2^2}}_{\mathcal{O}(x_2^0)} - \underbrace{C_{\varepsilon 2} \rho \frac{\varepsilon^2}{k}}_{\mathcal{O}(x_2^{-2})} \tag{11.160}
$$

The left-side has been written on non-conservative form (see Section 2.4) which makes it easier to see that the term goes to zero at the wall. Furthermore, it has been assumed that the turbulent viscosity has been suitable modified so that $\nu_t = \mathcal{O}(x_2^3)$. We find that the only terms which do not vanish at the wall are the viscous diffusion term and the dissipation term so that close to the wall the dissipation equation reads

$$
0 = \mu \frac{\partial^2 \varepsilon}{\partial x_2^2} - C_{\varepsilon 2} \rho \frac{\varepsilon^2}{k}. \tag{11.161}
$$

This equation needs to be modified since the diffusion term cannot balance the destruction term when $x_2 \to 0$. We multiply the destruction term by $f_2 \propto \mathcal{O}(x_2^2)$ For more details, see [26].

11.14.4 Wall boundary Condition for k

The wall boundary condition of k is simple. Since the first cell is in the viscous sublayer ($x_2^+ \simeq 1$) and the turbulent fluctuations are zero at the wall we set

$$
k = 0 \tag{11.162}
$$

11.14.5 Different ways of prescribing ε at or near the wall

When setting wall boundary condition for ε we look at the k equation. The largest term in the k equation (see Eq. 11.156) close to the wall, are the dissipation term and the viscous diffusion term which both are of $\mathcal{O}(x_2^0)$ so that

$$
0 = \mu \frac{\partial^2 k}{\partial x_2^2} - \rho \varepsilon. \tag{11.163}
$$

From this equation we get immediately a boundary condition for ε as

$$
\varepsilon_{wall} = \nu \frac{\partial^2 k}{\partial x_2^2}. \tag{11.164}
$$

From Eq. 11.163 we can derive alternative boundary conditions. The exact form of the dissipation term close to the wall reads (see Eq. 8.24)

$$
\varepsilon = \nu \overline{\left\{ \left(\frac{\partial v_1'}{\partial x_2} \right)^2 + \left(\frac{\partial v_3'}{\partial x_2} \right)^2 \right\}} \tag{11.165}
$$

where $\partial/\partial x_2 \gg \partial/\partial x_1 \simeq \partial/\partial x_3$ and $\partial v_1'/\partial x_2 \simeq \partial v_3'/\partial x_2 \gg \partial v_2'/\partial x_2$ have been assumed. Using Taylor expansion gives (see Eq. 11.154)

$$\varepsilon = \nu \left(\overline{a_1^2} + \overline{c_1^2} \right) + \ldots \tag{11.166}$$

In the same way we get an expression for the turbulent kinetic energy (see Eq. 11.154)

$$k = \frac{1}{2} \left(\overline{a_1^2} + \overline{c_1^2} \right) x_2^2 + \ldots \tag{11.167}$$

so that

$$\left(\frac{\partial \sqrt{k}}{\partial x_2} \right)^2 = \frac{1}{2} \left(\overline{a_1^2} + \overline{c_1^2} \right) + \ldots \tag{11.168}$$

Comparing Eqs. 11.166 and 11.168 we find

$$\varepsilon_{wall} = 2\nu \left(\frac{\partial \sqrt{k}}{\partial x_2} \right)^2 . \tag{11.169}$$

In many $k - \varepsilon$ models the following form is used

$$\varepsilon_P = 2\nu \frac{k}{x_2^2} \tag{11.170}$$

where subscript P denotes wall-adjacent cells, see Fig. 11.7. This is not really a boundary condition; instead we prescribe ε at the wall-adjacent cells. This is obtained by assuming $a_1 = c_1$ in Eqs. 11.166 and 11.167 so that

$$\begin{aligned} \varepsilon &= 2\nu \overline{a_1^2} \\ k &= \overline{a_1^2} x_2^2 \end{aligned} \tag{11.171}$$

which gives Eq. 11.170.
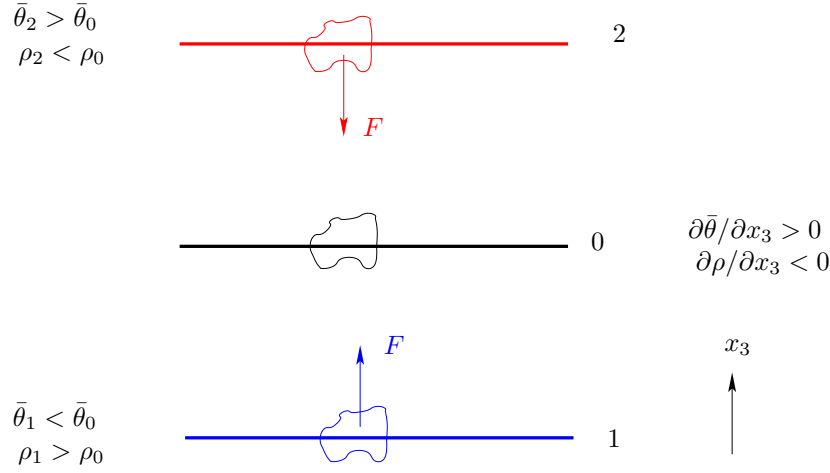
Figure 12.1: Stable stratification due to positive temperature gradient $\partial\bar{\theta}/\partial x_3 > 0$.

12 Reynolds stress models vs. eddy-viscosity models

In this section we present three fundamental physical processes which Reynolds stress models are able to handle whereas eddy-viscosity models fail. The reason for the superiority of the former model is in all cases that the production term is treated exactly, whereas in eddy-viscosity models it is modeled.

12.1 Stable and unstable stratification

In flows where buoyancy is dominating, the temperature has a large effect on the turbulence through the buoyancy term G_{ij}, see Eq. 11.11. If the temperature increases upwards (i.e. $\partial\bar{\theta}/\partial x_3 > 0$), then the flow is **stably stratified**. This is illustrated in Fig. 12.1. Consider $\partial\bar{\theta}/\partial x_3 > 0$. This means that the density decreases with increasing vertical height, i.e. $\partial\rho/\partial x_3 < 0$. If a fluid particle is displaced from its equilibrium level 0 up to level 2, see Fig. 12.1, it is heavier then the surrounding at this new level ($\rho_0 > \rho_2$). Hence, the buoyancy forces the particle back to its original position 0. In this way the vertical turbulent fluctuations are dampened. Similarly if a particle originating at level 0, is moved down to level 1. Here it is lighter than its new environment, and buoyancy takes it back to its original level 0.

For the case of **unstable stratification**, the situation is reversed. Cold fluid is located on top of hot fluid, i.e. $\partial\bar{\theta}/\partial x_3 < 0$ and $\partial\rho/\partial x_3 > 0$. In Fig. 12.1 we would then have $\rho_2 > \rho_0$. If a fluid particle at level 0 is displaced upwards to level 2, it is at this location lighter than its new environment; hence it continues to move upwards. If it is moved down to level 1 it is heavier than its new environments and it will then continue downwards. Hence, turbulent fluctuations are enhanced. This flow situation is called **unstable stratification**.

Now we will investigate how the Reynolds stress model behaves in stable conditions, i.e. when $\partial\bar{\theta}/\partial x_3 > 0$. The production term due to buoyancy reads (see Eq. 11.11)

$$G_{33} = 2g\beta\overline{v'_3\theta'} \tag{12.1}$$

since $g_i = (0, 0, -g)$. From the equation for the turbulent heat flux, $\overline{v'_3\theta'}$ (i.e. Eq. 11.22

with $i = 3$), we find the production term for $\overline{v'_3 \theta'}$

$$P_{3\theta} = -\overline{v'_3 v'_k} \frac{\partial \bar{\theta}}{\partial x_k} - \overline{v'_k \theta'} \frac{\partial \bar{v}_3}{\partial x_k} \tag{12.2}$$

In the case illustrated in Fig. 12.1, the production term due to temperature gradient reads $P_{3\theta} = -\overline{v'^2_3} \partial \bar{\theta}/\partial x_3 < 0$ (recall that we assume that buoyancy dominates so that the first term in Eq. 12.2 is much larger than the second one). Since the main source term in the $\overline{v'_3 \theta'}$ equation, $P_{3\theta}$, is negative, it makes $\overline{v'_3 \theta'} < 0$ so that $G_{33} < 0$ (see Eq. 12.1). Thus, for the case illustrated in Fig. 12.1, we find that the production term, G_{33}, due to buoyancy yields a damping of the vertical fluctuations as it should. Note that the horizontal turbulent fluctuations are not affected by the buoyancy term, G_{ij}, since $G_{11} = G_{22} = 0$ because the gravity is in the x_3 direction (i.e. $g_1 = g_2 = 0$).

If the situation in Fig. 12.1 is reversed so that $\partial \bar{\theta}/\partial x_3 < 0$ the vertical fluctuations are instead augmented. This is called **unstably stratified** conditions.

When eddy-viscosity models are used, transport equations are usually not solved for $\overline{v'_i \theta'}$. Instead the heat flux tensor is modeled with an eddy-viscosity assumption using the Boussinesq assumption, see Eq. 11.35. The buoyancy term, G^k, in the k equation reads, see Eq. 11.11 (take the trace of G_{ij} and divide by two)

$$G^k = 0.5 G_{ii} = -g_i \beta \overline{v'_i \theta'} \tag{12.3}$$

For $g_i = (0, 0, -g)$, it reads $G^k = g\beta \overline{v'_3 \theta'}$ which with Eq. 11.35 gives

$$G^k = -g\beta \frac{\nu_t}{\sigma_\theta} \frac{\partial \bar{\theta}}{\partial x_3} \tag{12.4}$$

Hence it is seen that in stably stratified conditions, $G^k < 0$ as required. The difference between an eddy-viscosity model and a Reynolds stress model, is that the former reduces k whereas the latter reduces only the vertical fluctuations.

12.2   Curvature effects

When the streamlines in boundary layer flow have a convex curvature, the turbulence is stabilized. This dampens the turbulence [52, 53], especially the shear stress and the Reynolds stress normal to the wall. Concave curvature destabilizes the turbulence. The ratio of boundary layer thickness δ to curvature radius R is a common parameter for quantifying the curvature effects on the turbulence. The work reviewed by Bradshaw [52] demonstrates that even such small amounts of convex curvature as $\delta/R = 0.01$ can have a significant effect on the turbulence. In [54] they carried out an experimental investigation on a configuration simulating the flow near a trailing edge of an airfoil, where they measured $\delta/R \simeq 0.03$. They reported a 50 percent decrease of $\rho \overline{v'^2_2}$ (Reynolds stress in the normal direction to the wall) owing to curvature. The reduction of $\rho \overline{v'^2_1}$ and $-\rho \overline{v'_1 v'_2}$ was also substantial. In addition they reported significant damping of the turbulence in the shear layer in the outer part of the separation region.

An illustrative model case is curved boundary layer flow, see Fig. 12.2. A polar coordinate system $r - \theta$ with $\hat{\theta}$ locally aligned with the streamline is introduced. As $v_\theta = v_\theta(r)$ (with $\partial v_\theta/\partial r > 0$ and $v_r = 0$), the radial inviscid momentum equation (i.e. the terms including viscosity are omitted) degenerates to

$$\frac{\rho v_\theta^2}{r} - \frac{\partial p}{\partial r} = 0 \tag{12.5}$$
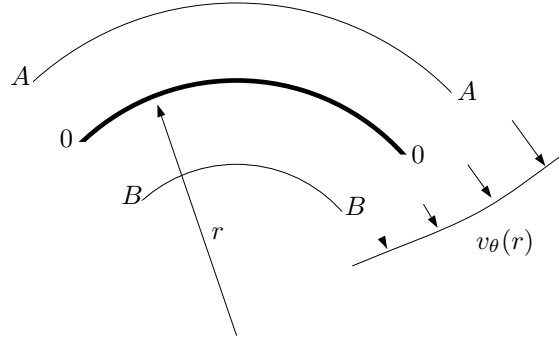
Figure 12.2: Flow in a polar coordinate system illustrating streamline curvature. The streamline is aligned with the θ axis.
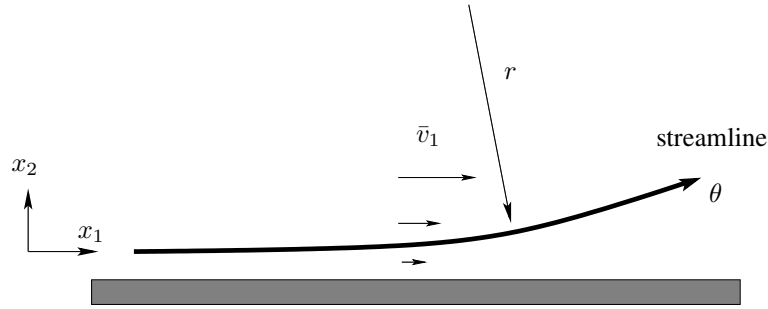
Figure 12.3: Streamline curvature occurring when the flow approaches, for example, a separation region or an obstacle.

Here the variables are instantaneous or laminar. The centrifugal force exerts a force in the normal direction (outward) on a fluid following the streamline, which is balanced by the pressure gradient. Since we have assumed that $\partial v_\theta / \partial r > 0$, Eq. 12.5 shows that the pressure gradient increases with r. If the fluid by some disturbance (e.g. turbulent fluctuation) is displaced outwards to level A, it encounters a pressure gradient larger than that to which it was accustomed at $r = r_0$, since $(v_\theta)_A > (v_\theta)_0$, which from Eq. 12.5 gives $(\partial p/\partial r)_A > (\partial p/\partial r)_0$. Hence the fluid is forced back to $r = r_0$. Similarly, if the fluid is displaced inwards to level B, the pressure gradient is smaller here than at $r = r_0$ and cannot keep the fluid at level B. Instead the centrifugal force drives it back to its original level.

It is clear from the model problem above that convex curvature, when $\partial v_\theta / \partial r > 0$, has a stabilizing effect on (turbulent) fluctuations, at least in the radial direction. It is discussed below how the Reynolds stress model responds to streamline curvature.

Assume that there is a flat-plate boundary layer flow, see Fig. 12.3. The ratio of the normal stresses $\rho \overline{v_1'^2}$ to $\rho \overline{v_2'^2}$ is typically 5 (or more). At one x_1 station, the flow is deflected upwards. How will this affect turbulence? Let us study the effect of concave streamline curvature. The production terms P_{ij} owing to rotational strains (i.e.

	$\partial \mathbf{V}_\theta / \partial \mathbf{r} > \mathbf{0}$	$\partial \mathbf{V}_\theta / \partial \mathbf{r} < \mathbf{0}$
convex curvature	stabilizing	destabilizing
concave curvature	destabilizing	stabilizing

Table 12.1: Effect of streamline curvature on turbulence.
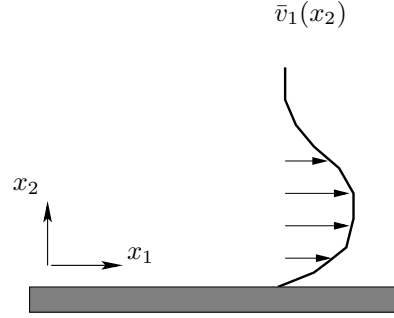
$$\bar{v}_1(x_2)$$

Figure 12.4: The velocity profile for a wall jet.

$\partial \bar{v}_1 / \partial x_2,\ \partial \bar{v}_2 / \partial x_1)$ can be written as (see Eq. 11.11):

$$\text{RSM, } \overline{v_1'^2} - \text{eq.} : \quad P_{11} = -2\overline{v_1'v_2'}\frac{\partial \bar{v}_1}{\partial x_2} \tag{12.6a}$$

$$\text{RSM, } \overline{v_1'v_2'} - \text{eq.} : \quad P_{12} = \boxed{-\overline{v_1'^2}\frac{\partial \bar{v}_2}{\partial x_1}} - \overline{v_2'^2}\frac{\partial \bar{v}_1}{\partial x_2} \tag{12.6b}$$

$$\text{RSM, } \overline{v_2'^2} - \text{eq.} : \quad P_{22} = \boxed{-2\overline{v_1'v_2'}\frac{\partial \bar{v}_2}{\partial x_1}} \tag{12.6c}$$

$$k - \varepsilon \quad P^k = \nu_t \left(\frac{\partial \bar{v}_1}{\partial x_2} + \boxed{\frac{\partial \bar{v}_2}{\partial x_1}} \right)^2 \tag{12.6d}$$

The terms in boxes appear because of the streamline curvature.

As long as the streamlines are parallel to the wall, all production is a result of $\partial \bar{v}_1 / \partial x_2$. However as soon as the streamlines are deflected, there are more terms resulting from $\partial \bar{v}_2 / \partial x_1$. Even if $\partial \bar{v}_2 / \partial x_1$ is much smaller than $\partial \bar{v}_1 / \partial x_2$ it will still contribute non-negligibly to P_{12} as $\rho \overline{v_1'^2}$ is much larger than $\rho \overline{v_2'^2}$. Thus the magnitude of P_{12} will increase (P_{12} is negative) as $\partial \bar{v}_2 / \partial x_1 > 0$. An increase in the magnitude of P_{12} will increase $-\overline{v_1'v_2'}$, which in turn will increase P_{11} and P_{22}. This means that $\rho \overline{v_1'^2}$ and $\rho \overline{v_2'^2}$ will be larger and the magnitude of P_{12} will be further increased, and so on. It is seen that there is a positive feedback, which continuously increases the Reynolds stresses. The turbulence is *destabilized* owing to concave curvature of the streamlines. Note that eddy-viscosity models such as $k - \varepsilon$ and $k - \omega$ models cannot account for streamline curvature since the two rotational strains, $\partial \bar{v}_1 / \partial x_2$ and $\partial \bar{v}_2 / \partial x_1$, in the production term are multiplied by the same coefficient (the turbulent viscosity).

Above, we have assumed concave curvature and positive velocity gradient. There are two other options.

1. If the flow (concave curvature) is a wall jet flow where $\partial \bar{v}_1 / \partial x_2 < 0$ in the
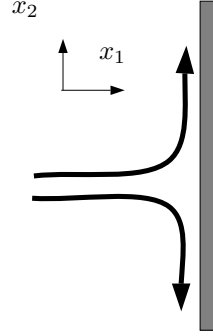
Figure 12.5: The flow pattern for stagnation flow.

outer part (see Fig. 12.4) the situation will be reversed: the turbulence will be *stabilized*.

2. If the streamline (and the wall) is deflected downwards, the situation will be as follows: the turbulence is stabilizing when $\partial \bar{v}_1 / \partial x_2 > 0$, and destabilizing for $\partial \bar{v}_1 / \partial x_2 < 0$.

The stabilizing or destabilizing effect of streamline curvature depends on the type of curvature (convex or concave), and whether there is an increase or decrease in tangential momentum with radial distance from its origin (i.e. the sign of $\partial V_\theta / \partial r$). For convenience, these cases are summarized in Table 12.1. It should be noted that concave or convex depends on from which point the streamline is viewed. The streamline in Fig. 12.3, for example, is concave when viewed from the wall but convex when viewed from the origin of the circle with radius r.

12.3 Stagnation flow

The $k - \varepsilon$ model does in this type of flow not model the normal stresses properly, whereas ASM/RSM do. The production term in the k equations for RSM/ASM and $k - \varepsilon$ model in stagnation flow (see Fig. 12.5) due to $\partial \bar{v}_1 / \partial x_1$ and $\partial \bar{v}_2 / \partial x_2$ (which are the dominant strains) is:

$$RSM/ASM : 0.5\left(P_{11} + P_{22}\right) = -\overline{v_1'^2}\frac{\partial \bar{v}_1}{\partial x_1} - \overline{v_2'^2}\frac{\partial \bar{v}_2}{\partial x_2} = -\frac{\partial \bar{v}_1}{\partial x_1}(\overline{v_1'^2} - \overline{v_2'^2}) \quad (12.7)$$

$$k - \varepsilon : P^k = 2\nu_t\left\{\left(\frac{\partial \bar{v}_1}{\partial x_1}\right)^2 + \left(\frac{\partial \bar{v}_2}{\partial x_2}\right)^2\right\} \quad (12.8)$$

where continuity $\partial \bar{v}_1 / \partial x_1 = -\partial \bar{v}_2 / \partial x_2$ has been employed. In RSM, the two terms are added with sign. In the $k - \varepsilon$ model, however, the production will be large because the difference in sign of the two terms is not taken into account because it includes the square of the velocity gradients.

12.4 RSM/ASM versus $k - \varepsilon$ models

- Advantages with $k - \varepsilon$ models (or eddy viscosity models):

    i) simple due to the use of an isotropic eddy (turbulent) viscosity

    ii) stable via stability-promoting second-order gradients in the mean-flow equations

    iii) work reasonably well for a large number of engineering flows

- Disadvantages:

    i) isotropic, and thus not good in predicting normal stresses $(\overline{v_1'^2}, \overline{v_2'^2}, \overline{v_3'^2})$

    ii) as a consequence of *i)* it is unable to account for curvature effects

    iii) as a consequence of *i)* it is unable to account for irrotational strains (stagnation flow)

    iv) in boundary layers approaching separation, the production due to normal stresses is of the same magnitude as that due to shear stresses [55].

- Advantages with ASM/RSM:

    i) the production terms do not need to be modeled

    ii) thanks to *i)* it can selectively augment or damp the stresses due to curvature effects (RSM is better than ASM because the convective terms are accounted for) and it is more accurate for boundary layers approaching separation, buoyancy etc.

- Disadvantages with RSM:

    i) RSM is complex and difficult to implement, especially implicit ASM

    ii) numerically unstable because small stabilizing second-order derivatives in the momentum equations (only <u>viscous</u> diffusion)

    iii) CPU time consuming

13 Realizability

There are a number of realizability constraints. The usual two ones are that all normal stresses should stay positive and that the correlation coefficient for the shear stress should not exceed one, i.e.

$$\overline{v_i'^2} \geq 0 \text{ for all } i$$

$$\frac{|\overline{v_i'v_j'}|}{\left(\overline{v_i'^2}\ \overline{v_j'^2}\right)^{1/2}} \leq 1 \text{ no summation over } i \text{ and } j, \ i \neq j \tag{13.1}$$

These criteria are seldom used in RSMs. However, satisfying the first criteria is actually of importance for eddy-viscosity models in stagnation flow [56]. Assume that the flow is in the x_1 direction and that it approaches the wall (see Fig. 12.5). The Boussinesq assumption for the normal stress $\overline{v_1'^2}$ reads (cf. Eq. 12.7)

$$\overline{v_1'^2} = \frac{2}{3}k - 2\nu_t \frac{\partial \bar{v}_1}{\partial x_1} = \frac{2}{3}k - 2\nu_t \bar{s}_{11} \tag{13.2}$$

It is seen that if $\bar{s}_{11}$ gets too large then $\overline{v_1'^2} < 0$ which is nonphysical, i.e. non-realizable.

Let's now briefly repeat the concept "invariants". This means something that is independent of the coordinate system. Here we mean independent of rotation of the coordinate system. If a tensor is symmetric, then we know that it has real eigenvalues which means that we can rotate the coordinate system so that the off-diagonal components vanish (see, e.g., [29]). This corresponds to the principal coordinate directions. For the strain tensor it means that the off-diagonal components of $\bar{s}_{ij}$ vanish and this is the coordinate system where the diagonal components become largest (e.g. $\bar{s}_{11}$ in Eq. 13.2). This is thus the coordinate system in which the danger of negative $\overline{v_1'^2}$ from Eq. 13.2 is largest. The equation for finding the eigenvalues of a tensor C_{ij} is (see e.g. [29] or [57])

$$|C_{ij} - \delta_{ij}\lambda| = 0 \tag{13.3}$$

which gives, in 2D,

$$\begin{vmatrix} C_{11} - \lambda & C_{12} \\ C_{21} & C_{22} - \lambda \end{vmatrix} = 0 \tag{13.4}$$

The resulting equation is

$$\lambda^2 - I_1^{2D}\lambda + I_2^{2D} = 0$$
$$I_1^{2D} = C_{ii} \tag{13.5}$$
$$I_2^{2D} = \frac{1}{2}(C_{ii}C_{jj} - C_{ij}C_{ij}) = \det(C_{ij})$$

Since Eq. 13.5 is the same irrespectively of the orientation of the original coordinate system, it follows that its coefficients I_1^{2D} and I_2^{2D} are invariants.

In 3D, Eq. 13.3 gives

$$\begin{vmatrix} C_{11} - \lambda & C_{12} & C_{13} \\ C_{21} & C_{22} - \lambda & C_{23} \\ C_{31} & C_{32} & C_{33} - \lambda \end{vmatrix} = 0 \tag{13.6}$$

which gives

$$\lambda^3 - I_1^{3D}\lambda^2 + I_2^{3D}\lambda - I_3^{3D} = 0$$
$$I_1^{3D} = C_{ii}$$
$$I_2^{3D} = \frac{1}{2}(C_{ii}C_{jj} - C_{ij}C_{ij}) \tag{13.7}$$
$$I_3^{3D} = \frac{1}{6}\left(2C_{ij}C_{jk}C_{ki} - 3C_{ij}C_{ji}C_{kk} + C_{ii}C_{jj}C_{kk}\right) = \det(C_{ij})$$

The invariants are I_1^{3D}, I_2^{3D} and I_2^{3D}.

Let's go back to Eq. 13.2 and assume incompressible 2D flow. The first invariant reads (cf. Eq. 13.5)

$$I_1^{2D} = \bar{s}_{ii} = \bar{s}_{11} + \bar{s}_{22} = \lambda_1 + \lambda_2 = 0 \tag{13.8}$$

It is zero due to the continuity equation. The second invariant of $\bar{s}_{ij}$ reads

$$I_2^{2D} = -\bar{s}_{ij}\bar{s}_{ij}/2, \tag{13.9}$$

(see Eq. 13.5) which is independent of the orientation of the coordinate system (hence the name "invariant"). The solution to Eq. 13.5, using Eq. 13.8, is

$$\lambda_{1,2} = \pm\left(-I_2^{2D}\right)^{1/2} = \pm\left(\frac{\bar{s}_{ij}\bar{s}_{ij}}{2}\right)^{1/2} \tag{13.10}$$

The eigenvalues of $\bar{s}_{ij}$ correspond to the strains in the principal axis. As discussed above, we apply Eq. 13.2 in the principal coordinate directions of $\bar{s}_{ij}$. Hence, $\bar{s}_{11}$ in Eq. 13.2 is replaced by the largest eigenvalue so that

$$\overline{v_1'^2} = \frac{2}{3}k - 2\nu_t\lambda_1 \tag{13.11}$$

The requirement $\overline{v_1'^2} \geq 0$ gives now together with Eq. 13.11

$$\nu_t \leq \frac{k}{3|\lambda_1|} = \frac{k}{3}\left(\frac{2}{\bar{s}_{ij}\bar{s}_{ij}}\right)^{1/2} \tag{13.12}$$

In 3D, Eq. 13.7 instead of Eq. 13.5 is used, and Eq. 13.10 is replaced by [56]

$$|\lambda_k| = \left(\frac{2\bar{s}_{ij}\bar{s}_{ij}}{3}\right)^{1/2} \tag{13.13}$$

This is a simple modification of an eddy-viscosity model, and it ensures that the normal stresses stay positive.

13.1 Two-component limit

Another realizability constraint is to require that when $\overline{v_i'^2}$ approaches zero near walls, it should do so smoothly. One way to ensure this is to require that the derivative of $\overline{v_i'^2}$ should go to zero when $\overline{v_i'^2}$ goes to zero, i.e.

$$\overline{v_i'^2} \to 0 \ \Rightarrow \ \frac{d\overline{v_i'^2}}{dt} \to 0 \tag{13.14}$$

where d/dt denotes the material derivative (think of Eq. 13.14 in Lagrangian coordinates, i.e. we follow a fluid particle as it approaches the wall). Equation 13.14 requires that when $\overline{v_i'^2}$ approaches zero, the left side (and thus also the right side) of the transport equation of $\overline{v_i'^2}$ should also do so. Since we are here concerned about the pressure-strain term, we'll take a look at how it behaves near walls when $\overline{v_i'^2} \to 0$. This is of some relevance in near-wall turbulence where the wall-normal stress goes to zero faster than the wall-parallel ones: this state of turbulence is called the two-component limit [58]. The wall-normal component goes to zero as $\overline{v_2'^2} = \mathcal{O}(x_2^4)$ whereas $\overline{v_1'^2}$ and $\overline{v_3'^2}$ go to zero as $\mathcal{O}(x_2^2)$, see Section 4 in Introduction to turbulence models. Neither the form of $\Phi_{ij,2}$ in Eq. 11.90 nor Eq. 11.89 satisfy the requirement that $\Phi_{22,2} = 0$ when $\overline{v_2'^2} = 0$ [30]. In Eq. 11.90, for example,

$$\Phi_{22,2} \to c_2 \frac{2}{3} \delta_{ij} P^k \neq 0 \tag{13.15}$$

even if $\overline{v_2'^2} = 0$. Very complex forms of $\Phi_{ij,2}$ have been proposed [59] [CL96] which include terms cubic in $\overline{v_i' v_j'}$. The CL96 model does satisfy the two-component limit. Another advantage of the CL96 model is that it does not need any wall distances, which is valuable in complex geometries.

The models of the slow pressure-strain in Eq. 11.57 (linear model) and Eq. 11.63 (non-linear model) do also not satisfy the two-component limit. The Rotta model (Eq. 11.57), for example, gives

$$\Phi_{22,1} \to c_1 \rho \frac{2\varepsilon}{3} \neq 0 \tag{13.16}$$

when $\overline{v_2'^2} \to 0$. The only way to ensure that $\Phi_{22,1} \to 0$ is to make $c_1 \to 0$ when the wall is approached. A convenient parameter proposed in [58] is A which is an expression of A_2 and A_3 (the second and third invariant of a_{ij}, respectively), i.e.

$$A_2 = a_{ij} a_{ji}, \ A_3 = a_{ij} a_{jk} a_{ki}, \ A = 1 - \frac{9}{8}(A_2 - A_3) \tag{13.17}$$

The parameter $A = 0$ in the two-component limit and $A = 1$ in isotropic turbulence. Thus A is a suitable parameter to use when damping the constant c_1 as the wall is approached.

14   Non-linear Eddy-viscosity Models

In traditional eddy-viscosity models the turbulent stress $\overline{v_i'v_j'}$ is formulated from the Boussinesq assumption, i.e.

$$
\begin{aligned}
a_{ij} &= -2\nu_t \frac{\bar{s}_{ij}}{k} \\
\bar{s}_{ij} &= \frac{1}{2}\left(\frac{\partial \bar{v}_i}{\partial x_j} + \frac{\partial \bar{v}_j}{\partial x_i}\right)
\end{aligned}
\tag{14.1}
$$

where the anisotropy tensor is defined as (see Eq. 11.59)

$$
a_{ij} \equiv \frac{\overline{v_i'v_j'}}{k} - \frac{2}{3}\delta_{ij}
\tag{14.2}
$$

The relation between the stress $\overline{v_i'v_j'}$ and the velocity gradient in Eq. 14.1 is, as can be seen, linear. One way to make eddy-viscosity models more general is to include non-linear terms of the strain-rate (i.e. the velocity gradient) [35]. A subset of the most general form (given by 11.107) reads [60]

$$
\begin{aligned}
a_{ij} =& \boxed{-2c_\mu\tau\bar{s}_{ij}} \\
&+ c_1\tau^2\left(\bar{s}_{ik}\bar{s}_{kj} - \frac{1}{3}\bar{s}_{\ell k}\bar{s}_{\ell k}\delta_{ij}\right) + c_2\tau^2\left(\bar{\Omega}_{ik}\bar{s}_{kj} - \bar{s}_{ik}\bar{\Omega}_{kj}\right) \\
&+ c_3\tau^2\left(\bar{\Omega}_{ik}\bar{\Omega}_{jk} - \frac{1}{3}\bar{\Omega}_{\ell k}\bar{\Omega}_{\ell k}\delta_{ij}\right) + c_4\tau^3\left(\bar{s}_{ik}\bar{s}_{k\ell}\bar{\Omega}_{\ell j} - \bar{\Omega}_{i\ell}\bar{s}_{\ell k}\bar{s}_{kj}\right) \\
&+ c_5\tau^3\left(\bar{\Omega}_{i\ell}\bar{\Omega}_{\ell m}\bar{s}_{mj} + \bar{s}_{i\ell}\bar{\Omega}_{\ell m}\bar{\Omega}_{mj} - \frac{2}{3}\bar{\Omega}_{mn}\bar{\Omega}_{n\ell}\bar{s}_{\ell m}\delta_{ij}\right) \\
&+ c_6\tau^3\bar{s}_{k\ell}\bar{s}_{k\ell}\bar{s}_{ij} + c_7\tau^3\bar{\Omega}_{k\ell}\bar{\Omega}_{k\ell}\bar{s}_{ij} \\
\bar{\Omega}_{ij} =& \frac{1}{2}\left(\frac{\partial \bar{v}_i}{\partial x_j} - \frac{\partial \bar{v}_j}{\partial x_i}\right)
\end{aligned}
\tag{14.3}
$$

where τ is a turbulent time scale; for a non-linear $k-\varepsilon$ model $\tau = k/\varepsilon$, and for a non-linear $k-\omega$ model $\tau = 1/\omega$. The tensor groups correspond to a subset of Eq. 11.107:

Line 1: T_{ij}^1,

Line 2: T_{ij}^3 and T_{ij}^2

Line 3: T_{ij}^4 and T_{ij}^5

Line 4: T_{ij}^6

Line 5: T_{ij}^1 multiplied by the invariants $\bar{s}_{k\ell}\bar{s}_{k\ell}$ and $\bar{\Omega}_{k\ell}\bar{\Omega}_{k\ell}$

The expression in Eq. 14.3 is cubic in $\partial \bar{v}_i/\partial x_j$. However, note that it is only quadratic in $\bar{s}_{ij}$ and $\bar{\Omega}_{ij}$. This is due to Cayley-Hamilton theorem which states that a tensor is only linearly independent up to quadratic terms, see p. 134; this means that, for example, $\bar{s}_{ij}^3 = \bar{s}_{ik}\bar{s}_{k\ell}\bar{s}_{\ell j}$ can be expressed as a linear combination of $\bar{s}_{ij}^2 = \bar{s}_{ik}\bar{s}_{kj}$ and $\bar{s}_{ij}$.

a_{ij} is symmetric and its trace is zero; it is easily verified that the right side of Eq. 14.3 also has these properties (see Exam 2017-05-30, Answers, Question T3a).

Examples of non-linear models (sometimes also called *explicit* algebraic Reynolds stress models, EARSM) in the literature are the models presented in [36,60–62]. EARSMs are very popular — especially the model in [36] — in the aeronautical community where explicit time-marching solvers are used. They are computationally cheap, more accurate than linear eddy-viscosity models and they do not give rise to any numerical instabilities as in implicit solvers (like SIMPLE). In implicit solvers a large turbulent viscosity in the diffusion term of the momentum equations is needed to stabilize the solution procedure.

Let's take a closer look on Eq. 14.3 in fully developed channel flow ($\bar{v}_2 = \bar{v}_3 = \partial/\partial x_1 = \partial/\partial x_3 \equiv 0$); we obtain

$$
\begin{aligned}
a_{11} &= \frac{1}{12}\tau^2 \left(\frac{\partial \bar{v}_1}{\partial x_2}\right)^2 (c_1 + 6c_2 + c_3) \\
a_{22} &= \frac{1}{12}\tau^2 \left(\frac{\partial \bar{v}_1}{\partial x_2}\right)^2 (c_1 - 6c_2 + c_3) \\
a_{33} &= -\frac{1}{6}\tau^2 \left(\frac{\partial \bar{v}_1}{\partial x_2}\right)^2 (c_1 + c_3) \\
a_{12} &= -c_\mu \tau \frac{\partial \bar{v}_1}{\partial x_2} + \frac{1}{4}\tau^3 \left(\frac{\partial \bar{v}_1}{\partial x_2}\right)^3 (-c_5 + c_6 + c_7)
\end{aligned}
\tag{14.4}
$$

Using values on the constants as in [60], i.e $c_1 = -0.05$, $c_2 = 0.11$, $c_3 = 0.21$, $c_4 = -0.8$ $c_5 = 0$, $c_6 = -0.5$ and $c_7 = 0.5$ we get

$$
\begin{aligned}
a_{11} &= \frac{0.82}{12}\tau^2 \left(\frac{\partial \bar{v}_1}{\partial x_2}\right)^2 &\Rightarrow \overline{v_1'^2} &= \frac{2}{3}k + \frac{0.82}{12}k\tau^2 \left(\frac{\partial \bar{v}_1}{\partial x_2}\right)^2 \\
a_{22} &= \frac{-0.5}{12}\tau^2 \left(\frac{\partial \bar{v}_1}{\partial x_2}\right)^2 &\Rightarrow \overline{v_2'^2} &= \frac{2}{3}k - \frac{0.5}{12}k\tau^2 \left(\frac{\partial \bar{v}_1}{\partial x_2}\right)^2 \\
a_{33} &= \frac{-0.16}{12}\tau^2 \left(\frac{\partial \bar{v}_1}{\partial x_2}\right)^2 &\Rightarrow \overline{v_3'^2} &= \frac{2}{3}k - \frac{0.16}{12}k\tau^2 \left(\frac{\partial \bar{v}_1}{\partial x_2}\right)^2 \\
a_{12} &= -c_\mu \frac{k}{\varepsilon}\frac{\partial \bar{v}_1}{\partial x_2}
\end{aligned}
\tag{14.5}
$$

We find that indeed the non-linear model gives anisotropic normal Reynolds stresses.

In Eqs. 14.4 and 14.5 we have assumed that the only strain is $\partial \bar{v}_1/\partial x_2$. When we discussed streamline curvature effects at p. 163 we found that it is important to investigate the effect of secondary strains such as $\partial \bar{v}_2/\partial x_1$. Let's write down Eq. 14.3 for the strain $\partial \bar{v}_2/\partial x_1$

$$
\begin{aligned}
a_{11} &= \frac{1}{12}\tau^2 \left(\frac{\partial \bar{v}_2}{\partial x_1}\right)^2 (c_1 - 6c_2 + c_3) \\
a_{22} &= \frac{1}{12}\tau^2 \left(\frac{\partial \bar{v}_2}{\partial x_1}\right)^2 (c_1 + 6c_2 + c_3) \\
a_{33} &= -\frac{1}{6}\tau^2 \left(\frac{\partial \bar{v}_2}{\partial x_1}\right)^2 (c_1 + c_3) \\
a_{12} &= -\frac{1}{4}\tau^3 \left(\frac{\partial \bar{v}_2}{\partial x_1}\right)^3 (c_5 + c_6 + c_7)
\end{aligned}
\tag{14.6}
$$

Inserting the constants from [60] (see above) we obtain

$$
\begin{aligned}
a_{11} &= -\frac{0.5}{12}\tau^2\left(\frac{\partial \bar{v}_2}{\partial x_1}\right)^2 \\
a_{22} &= \frac{0.82}{12}\tau^2\left(\frac{\partial \bar{v}_2}{\partial x_1}\right)^2 \\
a_{33} &= -\frac{0.16}{12}\tau^2\left(\frac{\partial \bar{v}_2}{\partial x_1}\right)^2 , \ a_{12} = 0
\end{aligned}
\tag{14.7}
$$

As can be seen the coefficient for a_{22} is larger than that in Eq. 14.5, and hence the model is slightly more sensitive to the secondary strain, $\partial \bar{v}_2/\partial x_1$, than to the primary one, $\partial \bar{v}_1/\partial x_2$. Thus, the non-linear models are able to account for streamline curvature, but due to the choice of constants $c_5 + c_6 + c_7 = 0$ this effect is weak.

15 The V2F Model

In the V2F model of [56, 63, 64] two additional equations, apart from the k and ε-equations, are solved: the wall-normal stress $\overline{v_2'^2}$ and a function f. This is a model which aims at improving modeling of wall effects on the turbulence.

Walls affect the fluctuations in the wall-normal direction, $\overline{v_2'^2}$, in two ways. The wall damping of $\overline{v_2'^2}$ is felt by the turbulence fairly far from the wall ($x_2^+ \lesssim 200$) through the pressure field (i.e. the pressure-strain term) whereas the viscous damping takes place within the viscous and buffer layer ($x_2^+ \lesssim 10$). In usual eddy-viscosity models both these effects are accounted for through damping functions. The damping of $\overline{v_2'^2}$ is in the RSM accounted for through the modeled pressure-strain terms $\Phi_{22,1w}$ and $\Phi_{22,2w}$ (see Eqs. 11.95 and Eq. 11.96). They go to zero far away from the wall ($x_2^+ \gtrsim 400$).

In the V2F model the problem of accounting for the wall damping of $\overline{v_2'^2}$ is simply resolved by solving its transport equation. The $\overline{v_2'^2}$ equation in boundary-layer form reads (see Eq. 9.16 at p. 109)

$$\frac{\partial \rho \bar{v}_1 \overline{v_2'^2}}{\partial x_1} + \frac{\partial \rho \bar{v}_2 \overline{v_2'^2}}{\partial x_2} = \frac{\partial}{\partial x_2}\left[(\mu + \mu_t)\frac{\partial \overline{v_2'^2}}{\partial x_2}\right] - 2\overline{v_2'\frac{\partial p'}{\partial x_2}} - \rho \varepsilon_{22} \qquad (15.1)$$

in which the diffusion term has been modeled with an eddy-viscosity assumption, see Eq. 11.47 at p. 130. Note that the production term $P_{22} = 0$ because in boundary-layer approximation $\bar{v}_2 \ll \bar{v}_1$ and $\partial/\partial x_1 \ll \partial/\partial x_2$. The model for the dissipation term, ε_{22}, is taken as

$$\varepsilon_{22}^{model} = \frac{\overline{v_2'^2}}{k}\varepsilon$$

This is a more elaborate model than in RSM (see Eq. 11.49). Add and subtract ε_{22}^{model} on the right side of Eq. 15.1 yields

$$\begin{aligned}
\frac{\partial \rho \bar{v}_1 \overline{v_2'^2}}{\partial x_1} + \frac{\partial \rho \bar{v}_2 \overline{v_2'^2}}{\partial x_2} = \\
\frac{\partial}{\partial x_2}\left[(\mu + \mu_t)\frac{\partial \overline{v_2'^2}}{\partial x_2}\right] - 2\overline{v_2'\frac{\partial p'}{\partial x_2}} - \rho \varepsilon_{22} + \rho \frac{\overline{v_2'^2}}{k}\varepsilon - \rho \frac{\overline{v_2'^2}}{k}\varepsilon
\end{aligned} \qquad (15.2)$$

In the V2F model $\mathcal{P}$ is now defined as

$$\mathcal{P} = -\frac{2}{\rho}\overline{v_2'\frac{\partial p'}{\partial x_2}} - \varepsilon_{22} + \frac{\overline{v_2'^2}}{k}\varepsilon \qquad (15.3)$$

so that Eq. 15.2 can be written as

$$\frac{\partial \rho \bar{v}_1 \overline{v_2'^2}}{\partial x_1} + \frac{\partial \rho \bar{v}_2 \overline{v_2'^2}}{\partial x_2} = \frac{\partial}{\partial x_2}\left[(\mu + \mu_t)\frac{\partial \overline{v_2'^2}}{\partial x_2}\right] + \rho \mathcal{P} - \rho \frac{\overline{v_2'^2}}{k}\varepsilon \qquad (15.4)$$

$\mathcal{P}$ is the source term in the $\overline{v_2'^2}$-equation above, and it includes the velocity-pressure gradient term and the difference between the exact and the modeled dissipation. Note that this term is commonly split into a diffusion term and the pressure-strain term as

$$\overline{v_2'\frac{\partial p'}{\partial x_2}} = \frac{\partial \overline{v_2' p'}}{\partial x_2} - \overline{p'\frac{\partial v_2'}{\partial x_2}}$$

Physically, the main agent for generating wall-normal stress is indeed the pressure-strain term via re-distribution, see example in Section 11.13.

A new variable $f = \mathcal{P}/k$ is defined and a relaxation equation is formulated for f as

$$L^2 \frac{\partial^2 f}{\partial x_2^2} - f = -\frac{\Phi_{22}}{\rho k} - \frac{1}{T}\left(\frac{\overline{v_2'^2}}{k} - \frac{2}{3}\right)$$

$$T = \max\left\{\frac{k}{\varepsilon}, C_T\left(\frac{\nu}{\varepsilon}\right)^{1/2}\right\}$$

$$\frac{\Phi_{22}}{\rho k} = \frac{C_1}{T}\left(\frac{2}{3} - \frac{\overline{v_2'^2}}{k}\right) + C_2 \frac{\nu_t}{k}\left(\frac{\partial \bar{v}_1}{\partial x_2}\right)^2 \tag{15.5}$$

$$L = C_L \max\left\{\frac{k^{3/2}}{\varepsilon}, C_\eta\left(\frac{\nu^3}{\varepsilon}\right)^{1/4}\right\}$$

where Φ_{22} is the IP model of the pressure-strain term, see Eqs. 11.57 and 11.90, the first term being the slow term, and the second the rapid term. The constants are given the following values: $c_\mu = 0.23$, $C_T = 6$, $c_{\varepsilon 1} = 1.44$, $c_{\varepsilon 2} = 1.9$, $\sigma_k = 0.9$, $\sigma_\varepsilon = 1.3$, $C_1 = 1.3$, $C_2 = 0.3$, $C_L = 0.2$, $C_\eta = 90$.

The boundary condition for f is obtained from the $\overline{v_2'^2}$ equation. Near the wall, the $\overline{v_2'^2}$ equation reads

$$0 = \nu \frac{\partial^2 \overline{v_2'^2}}{\partial x_2^2} + fk - \frac{\overline{v_2'^2}}{k}\varepsilon \tag{15.6}$$

The first and the last term behave as $\mathcal{O}(x_2^2)$ as $x_2 \to 0$ because Taylor analysis gives $\overline{v_2'^2} = \mathcal{O}(x_2^4)$, $\varepsilon = \mathcal{O}(x_2^0)$ and $k = \mathcal{O}(x_2^2)$, see Section 11.14.2. Furthermore, $\varepsilon = 2\nu k/x_2^2$ (see Eq. 11.170); using this expression to replace k in Eq. 15.6 gives

$$0 = \frac{\partial^2 \overline{v_2'^2}}{\partial x_2^2} + \frac{f\varepsilon x_2^2}{2\nu^2} - \frac{2\overline{v_2'^2}}{x_2^2} \tag{15.7}$$

Assuming that f and ε are constant very close to the wall, this equation turns into an ordinary second-order differential equation with the solution

$$\overline{v_2'^2} = Ax_2^2 + \frac{B}{x_2} - \varepsilon f \frac{x_2^4}{20\nu^2}$$

Since $\overline{v_2'^2} = \mathcal{O}(x_2^4)$ as $x_2 \to 0$, both constants must be zero, i.e. $A = B = 0$, so we get

$$f = -\frac{20\nu^2}{\varepsilon}\frac{\overline{v_2'^2}}{x_2^4} \tag{15.8}$$

For more details, see [65].

Above we have derived the $\overline{v_2'^2}$ equation in boundary layer form assuming that x_2 is the wall-normal coordinate. In general, three-dimensional flow it reads

$$\frac{\partial \rho \bar{v}_j v^2}{\partial x_j} = \frac{\partial}{\partial x_j}\left[(\mu + \mu_t)\frac{\partial v^2}{\partial x_j}\right] + \rho fk - \rho \frac{v^2}{k}\varepsilon$$

$$L^2 \frac{\partial^2 f}{\partial x_j \partial x_j} - f = -\frac{\Phi_{22}}{\rho k} - \frac{1}{T}\left(\frac{v^2}{k} - \frac{2}{3}\right) \tag{15.9}$$

$$\frac{\Phi_{22}}{\rho k} = \frac{C_1}{T}\left(\frac{2}{3} - \frac{v^2}{k}\right) + C_2\frac{P^k}{k}$$
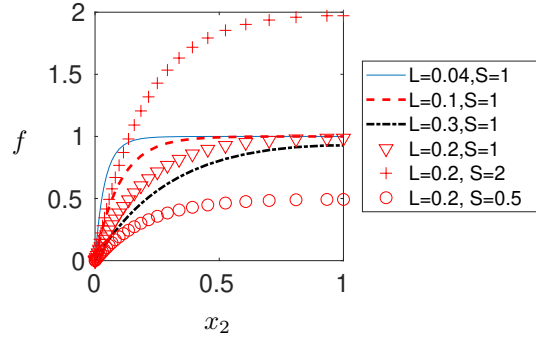
Figure 15.1: Illustration of Eq. 15.12

In the V2F model a transport equation for the normal stress normal to walls is solved for. If the wall lies in the $x_1 - x_3$ plane, then $v^2 = \overline{v_2'^2}$. However, if a wall lies in the $x_2 - x_3$ plane, for example, this means that the transport equation for $\overline{v_2'^2}$ is turned into an equation for $\overline{v_1'^2}$, i.e. $v^2 = \overline{v_1'^2}$. This is done automatically since in the general formulation in Eq. 15.9, $\partial\bar{v}_1/\partial x_2$ in the expression for Φ_{22} is replaced by P^k. If the wall lies in the $x_2 - x_3$ plane the largest velocity gradient will be $\partial\bar{v}_2/\partial x_1$ or $\partial\bar{v}_3/\partial x_1$.

Why does the right side of Eq. 15.5 has the form it has? Far from the wall, the source term in the $\overline{v_2'^2}$-equation simplifies to Φ_{22} plus isotropic dissipation (see Eq. 15.1). This is what happens, because far from the wall when $\partial^2 f/\partial x_2^2 \simeq 0$, so that Eq. 15.5 can be written ($T = k/\varepsilon$)

$$kf \equiv \mathcal{P} \rightarrow \Phi_{22} + \varepsilon(\overline{v_2'^2}/k - 2/3) \tag{15.10}$$

When this expression is inserted in Eq. 15.4 we get

$$\frac{\partial\rho\bar{v}_1\overline{v_2'^2}}{\partial x_1} + \frac{\partial\rho\bar{v}_2\overline{v_2'^2}}{\partial x_2} = \frac{\partial}{\partial x_2}\left[(\mu + \mu_t)\frac{\partial\overline{v_2'^2}}{\partial x_2}\right] + \rho\Phi_{22} - \frac{2}{3}\rho\varepsilon \tag{15.11}$$

which is the usual form of the modeled $\overline{v_2'^2}$-equation with isotropic dissipation. Near the wall, the diffusion term $\partial^2 f/\partial x_2^2$ makes f go from the value of its source term to its (negative) wall value (see Eq. 15.8) over the lengthscale L. This is how the influence of the source term $\mathcal{P}$ in Eq. 15.4 is reduced as the wall is approached. The behavior of the equation for f (Eq. 15.5) is illustrated in Fig. 15.1 where the equation

$$L^2\frac{\partial^2 f}{\partial x_2^2} - f + S = 0 \tag{15.12}$$

has been solved with $f = 0$ at the wall and with different L and S.

As can be seen, f is, as required, reduced as the wall is approached. Furthermore, f approaches the value of the source term as $x_2 > L$. The influence of the lengthscale L is nicely illustrated: the larger L, the further away from the wall does f go to its far-field value.

In the V2F model the turbulent viscosity is computed from

$$\nu_t = C_\mu\overline{v_2'^2}T \tag{15.13}$$

The k and ε-equations are also solved (without damping functions). For convenience, the boundary conditions are given again

$$
\begin{aligned}
k &= 0, \ \overline{v_2'^2} = 0 \\
\varepsilon &= 2\nu k/x_2^2 \\
f &= -\frac{20\nu^2 \overline{v_2'^2}}{\varepsilon x_2^4}
\end{aligned}
\tag{15.14}
$$

The boundary condition for f makes the equation system numerically unstable. One way to get around that problem is to solve both the k, ε and $\overline{v_2'^2}$, f equations coupled [65]. An alternative is to use the $\zeta - f$ model [66] which is more stable. In this model they solve for the ratio $\overline{v_2'^2}/k$ instead of for $\overline{v_2'^2}$ which gives a simpler wall boundary condition for f, namely $f = 0$.

15.1 Modified V2F model

In [67] they proposed a modification of the V2F model allowing the simple explicit boundary condition $f = 0$ at walls. They introduced a new variable

$$
f^* = f - 5\varepsilon v^2/k^2
$$

and they neglected the term

$$
-5L^2 \frac{\partial^2}{\partial x_j \partial x_j} \left(\frac{\varepsilon v^2}{k^2} \right)
$$

The resulting $\overline{v_2'^2}$ and f^*-equation read [67]

$$
\frac{\partial \bar{v}_j v^2}{\partial x_j} = \frac{\partial}{\partial x_j} \left[(\nu + \nu_t) \frac{\partial v^2}{\partial x_j} \right] + kf^* - 6\frac{v^2}{k}\varepsilon
\tag{15.15}
$$

$$
\begin{aligned}
-L^2 \frac{\partial^2 f^*}{\partial x_j \partial x_j} + f^* &= -\frac{1}{T} \left[(C_1 - 6)\frac{v^2}{k} - \frac{2}{3}(C_1 - 1) \right] + C_2 \frac{P^k}{k} \\
P^k &= \nu_t \left(\frac{\partial \bar{v}_i}{\partial x_j} + \frac{\partial \bar{v}_j}{\partial x_i} \right) \frac{\partial \bar{v}_i}{\partial x_j} \\
T &= \max \left\{ \frac{k}{\varepsilon}, 6 \left(\frac{\nu}{\varepsilon} \right)^{1/2} \right\} \\
L &= C_L \max \left\{ \frac{k^{3/2}}{\varepsilon}, C_\eta \left(\frac{\nu^3}{\varepsilon} \right)^{1/4} \right\}
\end{aligned}
\tag{15.16}
$$

Boundary conditions at the walls are

$$
\begin{aligned}
k &= 0, \ v^2 = 0 \\
\varepsilon &= 2\nu k/x_2^2 \\
f^* &= 0
\end{aligned}
$$

This modified model is numerically much more stable. Note that the modified model is identical to the original model far from the wall.

15.2   Realizable V2F model

The realizable condition for stagnation flow (see p. 165) is used also for the V2F model, and they read [67]

$$
\begin{aligned}
T &= \min\left[\frac{k}{\varepsilon}, \frac{0.6k}{\sqrt{6}C_\mu v^2 \left(\bar{s}_{ij}\bar{s}_{ij}\right)^{1/2}}\right] \\
L &= \min\left[\frac{k^{3/2}}{\varepsilon}, \frac{k^{3/2}}{\sqrt{6}C_\mu v^2 \left(2\bar{s}_{ij}\bar{s}_{ij}\right)^{1/2}}\right]
\end{aligned}
\tag{15.17}
$$

These realizable conditions have been further investigated by Sveningsson [65,68–71], and it was found that the limitation on T is indeed important, whereas that for L is not. Furthermore, it was found that it is important to impose the limitation on T in a consistent manner. For instance, if the limit is used in the f equation, it must for consistency also be used for ε/k in Eq. 15.15.

15.3   To ensure that $v^2 \leq 2k/3$

In the V2F model, v^2 denotes the generic wall-normal stress. Thus it should be the smallest one. This is not ensured in the V2F models presented above. Below the simple modification proposed by [72] is presented.

The source term kf in the v^2-equation (Eq. 15.15) includes the modeled velocity-pressure gradient term which is dampened near walls as f goes to zero. Since v^2 represents the wall-normal normal stress, it should be the smallest normal stress, i.e. $\overline{v_2'^2} \leq \overline{v_1'^2}$ and $\overline{v_2'^2} \leq \overline{v_3'^2}$, and thus $\overline{v_2'^2}$ should be smaller than or equal to $\frac{2}{3}k$. In the homogeneous region far away from the wall, the Laplace term is assumed to be negligible i.e. $\partial^2 f/\partial x_j \partial x_j \to 0$. Then Eq. 15.16 reduces to $f = $ right side.

It turns out that in the region far away from the wall, the Laplace term is not negligible, and as a consequence v^2 gets too large so that $v^2 > \frac{2}{3}k$. A simple modification is to use the right side of Eq. 15.16 as an upper bound on the source term kf in the v^2-equation, i.e.

$$
v^2_{source} = \min\left\{kf, -\frac{\varepsilon}{k}\left[(C_1 - 6)v^2 - \frac{2k}{3}(C_1 - 1)\right] + C_2 P^k\right\}
\tag{15.18}
$$

This modification ensures that $v^2 \leq 2k/3$. For more details, see [72].
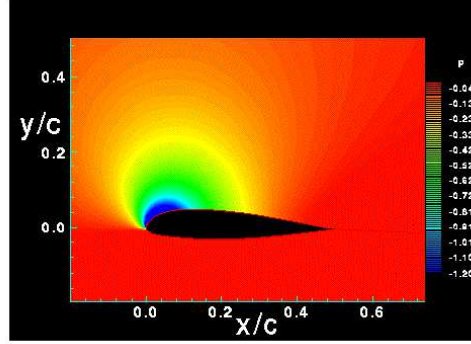
Figure 16.1: Flow around an airfoil. Pressure contours. Red: high pressure; blue: low pressure

16   The SST Model

The SST (<u>S</u>hear <u>S</u>tress <u>T</u>ransport) model of [73] is an eddy-viscosity model which includes two main novelties:

1. It is combination of a $k - \omega$ model (in the inner boundary layer) and $k - \varepsilon$ model (in the outer region of the boundary layer as well as outside of it);

2. A limitation of the shear stress in adverse pressure gradient regions.

   The $k - \varepsilon$ model has two main weaknesses: it over-predicts the shear stress in adverse pressure gradient flows because of too large length scale (due to too low dissipation) and it requires near-wall modification (i.e. low-Re number damping functions/terms). Various $k - \omega$ models are presented in Section 4 Introduction to turbulence

   One example of adverse pressure gradient is the flow along the surface of an airfoil, see Fig. 16.1. Consider the upper surface (suction side). Starting from the leading edge, the pressure decreases because the velocity increases. At the crest (at $x/c \simeq 0.15$) the pressure reaches its minimum and increases further downstream as the velocity decreases. This region is called the *adverse pressure gradient* (APG) region.

   The $k - \omega$ model is better than the $k - \varepsilon$ model at predicting adverse pressure gradient flow and the standard $k - \omega$ model of [74] (see also [26]) does not use any damping functions. However, the disadvantage of the standard $k - \omega$ model is that it is dependent on the free-stream value of ω [75, 76].

   In order to improve both the $k - \varepsilon$ and the $k - \omega$ model, it was suggested in [73] to combine the two models. Before doing this, it is convenient to transform the $k - \varepsilon$ model into a $k - \omega$ model using the relation $\omega = \varepsilon/(\beta^* k)$, where $\beta^* = c_\mu$. The left-hand side of the ω equation will consist of the convection term, $d\omega/dt$, which denotes the material derivative, assuming steady flow, see Eq. 2.27. Let us express the left-hand side of the ω equation as a combination of the left-hand sides of the ε and the k equations by using the chain rule, i.e.

$$\frac{d\omega}{dt} = \frac{d}{dt}\left(\frac{\varepsilon}{\beta^* k}\right) = \frac{1}{\beta^* k}\frac{d\varepsilon}{dt} + \frac{\varepsilon}{\beta^*}\frac{d(1/k)}{dt}$$
$$= \frac{1}{\beta^* k}\frac{d\varepsilon}{dt} - \frac{\varepsilon}{\beta^* k^2}\frac{dk}{dt} = \frac{1}{\beta^* k}\frac{d\varepsilon}{dt} - \frac{\omega}{k}\frac{dk}{dt}$$

$$(16.1)$$

Now we have transformed the left side of the ω equation. The right side should be transformed in the same manner. For example, the production of the ω equation will consist of two terms, one term from the ε equation

$$\frac{1}{\beta^* k} P_\varepsilon \quad \text{(the first term at the right side in Eq. 16.1)} \tag{16.2}$$

and one from the k equation

$$-\frac{\omega}{k} P^k \quad \text{(the second term at the right side in Eq. 16.1)} \tag{16.3}$$

In the same way we transform the entire right side inserting the modeled equations for k and ε so that

$$\frac{D\omega}{Dt} = \underbrace{\left[\frac{1}{\beta^* k} P_\varepsilon - \frac{\omega}{k} P^k\right]}_{\text{Production, } P_\omega} - \underbrace{\left[\frac{1}{\beta^* k} \Psi_\varepsilon - \frac{\omega}{k} \Psi_k\right]}_{\text{Destruction, } \Psi_\omega} +$$

$$\underbrace{\left[\frac{1}{\beta^* k} D_\varepsilon^T - \frac{\omega}{k} D_k^T\right]}_{\text{Turbulent diffusion, } D_\omega^T} + \underbrace{\left[\frac{\nu}{\beta^* k} \frac{\partial^2 \varepsilon}{\partial x_j^2} - \frac{\nu\omega}{k} \frac{\partial^2 k}{\partial x_j^2}\right]}_{\text{Viscous diffusion, } D_\omega^\nu} \tag{16.4}$$

- Production term

$$P_\omega = \frac{1}{\beta^* k} P_\varepsilon - \frac{\omega}{k} P^k = C_{\varepsilon 1} \frac{\varepsilon}{\beta^* k^2} P^k - \frac{\omega}{k} P^k$$

$$= (C_{\varepsilon 1} - 1) \frac{\omega}{k} P^k \tag{16.5}$$

- Destruction term

$$\Psi_\omega = \frac{1}{\beta^* k} \Psi_\varepsilon - \frac{\omega}{k} \Psi_k = \frac{1}{\beta^* k} C_{\varepsilon 2} \frac{\varepsilon^2}{k} - \frac{\omega}{k} \varepsilon$$

$$= (C_{\varepsilon 2} - 1) \beta^* \omega^2 \tag{16.6}$$

- Viscous diffusion term

$$\begin{aligned}
D_\omega^\nu &= \frac{\nu}{\beta^* k} \frac{\partial^2 \varepsilon}{\partial x_j^2} - \frac{\nu\omega}{k} \frac{\partial^2 k}{\partial x_j^2} = \frac{\nu}{k} \frac{\partial^2 \omega k}{\partial x_j^2} - \frac{\nu\omega}{k} \frac{\partial^2 k}{\partial x_j^2} \\
&= \frac{\nu}{k} \left[\frac{\partial}{\partial x_j} \left(\omega \frac{\partial k}{\partial x_j} + k \frac{\partial \omega}{\partial x_j}\right)\right] - \nu \frac{\omega}{k} \frac{\partial^2 k}{\partial x_j^2} \\
&= \frac{\nu}{k} \left[\frac{\partial \omega}{\partial x_j} \frac{\partial k}{\partial x_j} + \omega \frac{\partial^2 k}{\partial x_j^2} + \frac{\partial k}{\partial x_j} \frac{\partial \omega}{\partial x_j} + k \frac{\partial^2 \omega}{\partial x_j^2}\right] - \nu \frac{\omega}{k} \frac{\partial^2 k}{\partial x_j^2} \\
&= \frac{2\nu}{k} \frac{\partial \omega}{\partial x_j} \frac{\partial k}{\partial x_j} + \frac{\partial}{\partial x_j} \left(\nu \frac{\partial \omega}{\partial x_j}\right)
\end{aligned} \tag{16.7}$$

The turbulent diffusion term is obtained as (the derivation is found in [77] which can be downloaded from http://www.tfd.chalmers.se/~lada)

$$D_\omega^T = \frac{2\nu_t}{\sigma_\varepsilon k} \frac{\partial k}{\partial x_j} \frac{\partial \omega}{\partial x_j} + \frac{\omega}{k} \left(\frac{\nu_t}{\sigma_\varepsilon} - \frac{\nu_t}{\sigma_k}\right) \frac{\partial^2 k}{\partial x_j^2} +$$

$$+ \frac{\omega}{k} \left(\frac{1}{\sigma_\varepsilon} - \frac{1}{\sigma_k}\right) \frac{\partial \nu_t}{\partial x_j} \frac{\partial k}{\partial x_j} + \frac{\partial}{\partial x_j} \left(\frac{\nu_t}{\sigma_\varepsilon} \frac{\partial \omega}{\partial x_j}\right) \tag{16.8}$$

In the standard $k - \varepsilon$ model we have $\sigma_k = 1$ and $\sigma_\varepsilon = 1.3$. If we assume that $\sigma_k = \sigma_\varepsilon$ in the second and third term of the right-hand side, we can considerably simplify the turbulence diffusion so that

$$D_\omega^T = \frac{2\nu_t}{\sigma_\varepsilon k} \frac{\partial k}{\partial x_j} \frac{\partial \omega}{\partial x_j} + \frac{\partial}{\partial x_j} \left(\frac{\nu_t}{\sigma_\varepsilon} \frac{\partial \omega}{\partial x_j} \right) \tag{16.9}$$

We can now finally write the ε equation formulated as an equation for ω

$$\frac{\partial}{\partial x_j}(\bar{v}_j \omega) = \frac{\partial}{\partial x_j} \left[\left(\nu + \frac{\nu_t}{\sigma_\varepsilon} \right) \frac{\partial \omega}{\partial x_j} \right] + \alpha \frac{\omega}{k} P^k - \beta \omega^2$$
$$+ \frac{2}{k} \left(\nu + \frac{\nu_t}{\sigma_\varepsilon} \right) \frac{\partial k}{\partial x_i} \frac{\partial \omega}{\partial x_i} \tag{16.10}$$
$$\alpha = C_{\varepsilon 1} - 1 = 0.44, \beta = (C_{\varepsilon 2} - 1)\beta^* = 0.0828$$

Since the $k - \varepsilon$ model will be used for the outer part of the boundary layer, the viscous part of the cross-diffusion term (second line) is usually neglected (the viscous terms are negligible in the outer region). The turbulent viscosity is computed as (using dimensional analysis)

$$\nu_t = \frac{k}{\omega} \tag{16.11}$$

In the SST model the coefficients are smoothly switched from $k - \omega$ values in the inner region of the boundary layer to $k - \varepsilon$ values in the outer region. Functions of the form

$$F_1 = \tanh(\xi^4), \quad \xi = \min \left[\max \left\{ \frac{\sqrt{k}}{\beta^* \omega y}, \frac{500\nu}{y^2 \omega} \right\}, \frac{4\sigma_{\omega 2} k}{CD_\omega y^2} \right] \tag{16.12}$$

are used. $F_1 = 1$ in the near-wall region and $F_1 = 0$ in the outer region. The β-coefficient, for example, is computed as

$$\beta_{SST} = F_1 \beta_{k-\omega} + (1 - F_1)\beta_{k-\varepsilon} \tag{16.13}$$

where $\beta_{k-\omega} = 0.075$ and $\beta_{k-\varepsilon} = 0.0828$. Since the standard $k - \omega$ model does not include any cross-diffusion term, the last term in the ω equation (second line in Eq. 16.10) should only be active in the $k - \varepsilon$ region; hence it is multiplied by $(1 - F_1)$.

At p. 176 it was mentioned that the $k - \omega$ model is better than the $k - \varepsilon$ model in predicting adverse pressure-gradient flows because it predicts a smaller shear stress. Still, the predicted shear stress is too large. This brings us to the second modification (see p. 176). When introducing this second modification, the author in [73] noted that a model (the Johnson - King model [JK]) which is based on a transport equation of the main shear stress $\overline{v_1' v_2'}$, predicts adverse pressure gradient flows much better than the $k - \omega$ model. In the JK model, the $\overline{v_1' v_2'}$ transport equation is built on Bradshaw's assumption [78]

$$- \overline{v_1' v_2'} = a_1 k \tag{16.14}$$

where $a_1 = c_\mu^{1/2} = \beta^{*1/2}$. In boundary layer flow, the Boussinesq assumption can be written as

$$- \overline{v_1' v_2'} = \underbrace{\frac{k}{\omega}}_{\nu_t, k-\omega} \frac{\partial \bar{v}_1}{\partial x_2} = \underbrace{\frac{c_\mu k^2}{\varepsilon}}_{\nu_t, k-\varepsilon} \frac{\partial \bar{v}_1}{\partial x_2} = c_\mu^{1/2} k \left[\frac{c_\mu k^2}{\varepsilon^2} \left(\frac{\partial \bar{v}_1}{\partial x_2} \right)^2 \right]^{1/2} = c_\mu^{1/2} k \left(\frac{P^k}{\varepsilon} \right)^{1/2} \tag{16.15}$$

It is found from experiments that in boundary layers of adverse pressure gradient flows, the production is much larger than the dissipation ($P^k \gg \varepsilon$) and that $-\overline{v_1' v_2'} \simeq c_\mu^{1/2} k$. When the Boussinesq assumption is used in the $k - \omega$ model for adverse pressure gradient flows, $P^k \gg \varepsilon$, and hence (see Eq. 16.15)

$$-\frac{\overline{v_1' v_2'}}{c_\mu^{1/2} k} \gg 1 \qquad (16.16)$$

which explains why the Boussinesq assumption over-predicts the shear stress and works poorly in this type of flow (recall that according to experiments $-\overline{v_1' v_2'} \simeq c_\mu^{1/2} k$). To reduce $|\overline{v_1' v_2'}|$ in Eq. 16.15 in adverse pressure gradient flow, [73] proposed to re-define the turbulent eddy viscosity including the expression in Eq. 16.14. We have two expressions for the turbulent viscosity (expressing a Johnson-King-turbulent viscosity with the Boussinesq assumption)

$$\nu_t = \frac{-\overline{v_1' v_2'}}{\bar{\Omega}} = \frac{c_\mu^{1/2} k}{\bar{\Omega}} \quad \text{Johnson-King} \qquad (16.17a)$$

$$\nu_t = \frac{k}{\omega} = \frac{c_\mu^{1/2} k}{c_\mu^{1/2} \omega} \quad k - \omega \text{ model} \qquad (16.17b)$$

where $\bar{\Omega}$ is the absolute vorticity (in boundary layer flow $\bar{\Omega} = \partial \bar{v}_1 / \partial x_2$); in (a) the Boussinesq assumption together with Eq. 16.14 were used and (b) is taken from the $k - \omega$ model. We want (a) to apply only in the boundary layer and hence we multiply it with a function F_2

$$F_2 = \tanh(\xi^2), \quad \xi = \max\left\{ \frac{2\sqrt{k}}{\beta^* \omega y}, \frac{500\nu}{y^2 \omega} \right\}, \qquad (16.18)$$

Then we take the minimum of (a) and (b) so that

$$\nu_t = \frac{c_\mu^{1/2} k}{\max(c_\mu^{1/2} \omega, F_2 \bar{\Omega})} \qquad (16.19)$$

When the production is large (i.e. when $\bar{\Omega}$ is large), Eq. 16.19 reduces ν_t according to the Johnson - King model, i.e. Eq. 16.17a. It is important to ensure that this limitation is not active in usual boundary layer flows where $P^k \simeq \varepsilon$. It can be seen that ν_t is reduced only in regions where $P^k > \varepsilon$, because if $P^k < \varepsilon$ then $\bar{\Omega} < c_\mu^{1/2} \omega$ since

$$\bar{\Omega}^2 = \frac{1}{\nu_t} \nu_t \bar{\Omega}^2 = \frac{\omega}{k} P^k < \frac{\omega}{k} \varepsilon = c_\mu \omega^2 \qquad (16.20)$$

Hence, in regions where $P^k < \varepsilon$, Eq. 16.19 returns to $\nu_t = k/\omega$ as it should.

To summarize the SST modification:

- the second part, $c_\mu^{1/2} k / \Omega$ in Eq. 16.19 (which mimics the Johnson-King model), is active in APG flow

- the first part, k/ω in Eq. 16.19 (which corresponds to the usual Boussinesq model), should be active in the remaining part of the flow. Equation 16.20 shows that (it is likely that) the second part is active only in APG regions and not elsewhere.

Today, the SST model has been slightly further developed. Two modifications have been introduced [79]. The first modification is that the absolute vorticity $\bar{\Omega}$ in Eq. 16.19 has been replaced by $|\bar{s}| = (2\bar{s}_{ij}\bar{s}_{ij})^{1/2}$ which comes from the production term using the Boussinesq assumption (see Eq. 11.39), i.e.

$$
\begin{aligned}
|\bar{s}|^2 &= \left(\frac{\partial \bar{v}_i}{\partial x_j} + \frac{\partial \bar{v}_j}{\partial x_i}\right)\frac{\partial \bar{v}_i}{\partial x_j} = 2\bar{s}_{ij}(\bar{s}_{ij} + \bar{\Omega}_{ij}) = 2\bar{s}_{ij}\bar{s}_{ij} \\
\bar{\Omega}_{ij} &= \frac{1}{2}\left(\frac{\partial \bar{v}_i}{\partial x_j} - \frac{\partial \bar{v}_j}{\partial x_i}\right)
\end{aligned}
\tag{16.21}
$$

where $\bar{s}_{ij}\bar{\Omega}_{ij} = 0$ because $\bar{s}_{ij}$ is symmetric and $\bar{\Omega}_{ij}$ is anti-symmetric. Equation 16.19 with $|\bar{s}|$ limits ν_t in stagnation regions similar to Eq. 13.12. The second modification in the SST model is that the production term in the new SST model is limited by 10ε, i.e.

$$
P_{k,new} = \min\left(P^k, 10\varepsilon\right)
\tag{16.22}
$$

The final form of the SST model is given in Eq. 20.5 at p. 213.

17 Overview of RANS models

This section presents a short overview of the presented RANS models. First the models can be classified as models based on eddy viscosity (i.e. turbulent viscosity) or models in which equations are solved (algebraic or differential) to obtain the Reynolds stress tensor, $\overline{v'_i v'_j}$. Eddy-viscosity models, which are based on the Boussinesq assumption, see Eq. 11.33, are

Eddy-viscosity models

- standard $k - \varepsilon$ (see Section 11.8) and $k - \omega$ models

- combination of $k - \varepsilon$ and $k - \omega$ models such as the SST model, see Section 16.

There are more elaborate eddy-viscosity models such as

non-linear models

- non-linear models, see Section 14

Models *not* based on the eddy-viscosity are the Reynolds stress models such as

- the Reynolds stress transport model (RSM or RSTM), in which *transport* equations are solved for $\overline{v'_i v'_j}$, see Eq. 11.101.

RSM

- the Algebraic Reynolds stress model, ASM, in which *algebraic* equations are solved for $\overline{v'_i v'_j}$, see Eq. 11.104.

ASM

explicit ASM

- explicit Algebraic Reynolds stress models, in which *explicit* algebraic equations are solved for $\overline{v'_i v'_j}$, see Section 11.11.

Finally, there is a class of models which are somewhere in between two-equation eddy-viscosity models and Reynolds stress models, and that is

V2F

- V2F models, see Section 15

The V2F model is an eddy-viscosity model and the model is based on four transport equations.
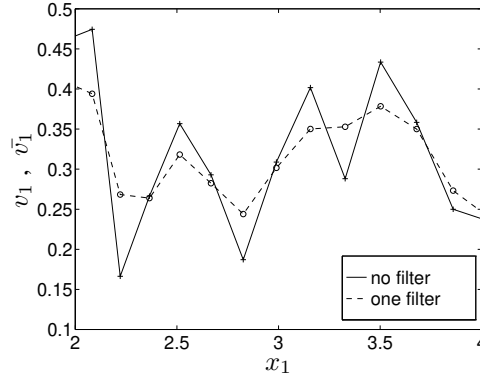
Figure 18.1: Filtering the velocity.

18 Large Eddy Simulations

18.1 Time averaging and filtering

IN CFD we time average our equations to get the equations in steady form. This is called Reynolds time averaging:

$$\langle \Phi \rangle = \frac{1}{2T} \int_{-T}^{T} \Phi(t) dt, \ \Phi = \langle \Phi \rangle + \Phi' \tag{18.1}$$

(note that we use the notation $\langle . \rangle$ for time averaging). In LES we filter (volume average) the equations. In 1D we get (see Fig. 18.1)

$$\bar{\Phi}(x,t) = \frac{1}{\Delta x} \int_{x-0.5\Delta x}^{x+0.5\Delta x} \Phi(\xi,t) d\xi$$
$$\Phi = \bar{\Phi} + \Phi''$$

Since in LES we do not average in time, the filtered variables are functions of space and time. The equations for the filtered variables have the same form as Navier-Stokes, i.e.

$$\frac{\partial \bar{v}_i}{\partial t} + \frac{\partial}{\partial x_j} (\bar{v}_i \bar{v}_j) = -\frac{1}{\rho} \frac{\partial \bar{p}}{\partial x_i} + \nu \frac{\partial^2 \bar{v}_i}{\partial x_j \partial x_j} - \frac{\partial \tau_{ij}}{\partial x_j}$$
$$\frac{\partial \bar{v}_i}{\partial x_i} = 0 \tag{18.2}$$

where the subgrid stresses are given by

$$\tau_{ij} = \overline{v_i v_j} - \bar{v}_i \bar{v}_j \tag{18.3}$$

It should be noted that it is formally incorrect to denote τ_{ij} as a stress since the density is omitted (see, e.g., the text below Eq. 6.10 and Eq. 11.3). Contrary to Reynolds time averaging where $\langle v_i' \rangle = 0$, we have here

$$\overline{v_i''} \neq 0$$

$$\overline{\bar{v}_i} \neq \bar{v}_i$$

This is true for box filters. Note that for the spectral cut-off filter $\bar{v}_i = \bar{\bar{v}}_i$, see p. 185. However, in finite volume methods, box filters are always used. In this course we use box filters, if not otherwise stated.

Let's look at the filtering of Eq. 18.2 in more detail. The pressure gradient term, for example, reads

$$\overline{\frac{\partial p}{\partial x_i}} = \frac{1}{V} \int_V \frac{\partial p}{\partial x_i} dV \tag{18.4}$$

Now we want to move the derivative out of the integral. When is that allowed? The answer is "if the integration region is not a function of x_i", i.e. if V is constant. In finite volume methods, the filtering volume, V, is (almost always) identical to the control volume. In general, the size of the control volume varies in space. Fortunately, it can be shown that if V is a function of x_i, the error we do when moving the derivative out of the integral is proportional to $(\Delta x)^2$ [80], i.e. it is an error of second order. Since this is the order of accuracy of our finite volume method anyway, we can accept this error. Now let's move the derivative out of the integral, i.e.

$$\overline{\frac{\partial p}{\partial x_i}} = \frac{\partial}{\partial x_i} \left(\frac{1}{V} \int_V p dV \right) + \mathcal{O}\left((\Delta x)^2\right) = \frac{\partial \bar{p}}{\partial x_i} + \mathcal{O}\left((\Delta x)^2\right) \tag{18.5}$$

All linear terms are treated in the same way.

Now we take a look at the non-linear term in Eq. 18.2, i.e. the convective term. First we filter the term and move the derivative out of the integral, i.e.

$$\overline{\frac{\partial v_i v_j}{\partial x_j}} = \frac{\partial}{\partial x_j} \left(\frac{1}{V} \int_V v_i v_j dV \right) + \mathcal{O}\left((\Delta x)^2\right) = \frac{\partial}{\partial x_j}(\overline{v_i v_j}) + \mathcal{O}\left((\Delta x)^2\right)$$

There is still a problem with the formulation of this term: it includes an integral of a product, i.e. $\overline{v_i v_j}$; we want it to appear like a product of integrals, i.e. $\bar{v}_i \bar{v}_j$. To achieve this we simple add the term we want ($\bar{v}_i \bar{v}_j$) and subtract the one we don't want ($\overline{v_i v_j}$) on both the right and left side. This is how we end up with the convective term and the SGS term in Eq. 18.2.

The filtering in Eq. 18.2 is usually achieved through the finite-volume discretization. This means that no additional filtering is done. This is called *implicit* filtering. Hence, the discretized momentum equations in RANS and LES (Eqs. 6.6 and 18.2) are identical. The only difference is the magnitude of the modeled Reynolds stresses, which are much larger in RANS than in LES.

18.2   Differences between time-averaging (RANS) and space filtering (LES)

In **RANS**, if a variable is time averaged twice ($\langle\langle v \rangle\rangle$), it is the same as time averaging once ($\langle v \rangle$). This is because $\langle v \rangle$ is not dependent on time. From Eq. 18.1 we get

$$\langle\langle v \rangle\rangle = \frac{1}{2T} \int_{-T}^{T} \langle v \rangle dt = \frac{1}{2T} \langle v \rangle 2T = \langle v \rangle$$

This is obvious if the flow is steady, i.e. $\partial \langle v \rangle / \partial t = 0$. If the flow is unsteady, we must assume a separation in time scales so that the variation of $\langle v \rangle$ during the time interval T is negligible, i.e. $\partial/\partial t \ll 1/T$. In practice this requirement is rarely satisfied.

In **LES**, $\bar{\bar{v}} \neq \bar{v}$ (and since $v = \bar{v} + v''$ we get $\overline{v''} \neq 0$).
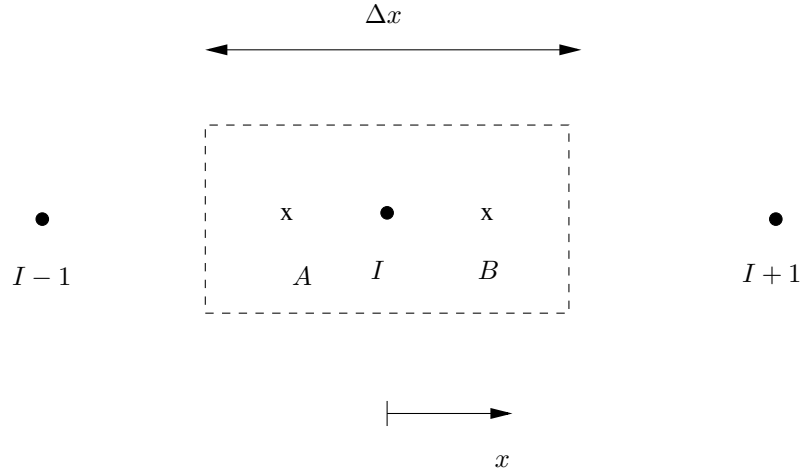
Figure 18.2: Box filter illustrated for a control volume.

Let's filter $\bar{v}_I$ once more (filter size Δx, see Fig. 18.2. For simplicity we do it in 1D. (Note that subscript I denotes node number.)

$$
\begin{aligned}
\bar{\bar{v}}_I &= \frac{1}{\Delta x} \int_{-\Delta x/2}^{\Delta x/2} \bar{v}(\xi) d\xi = \frac{1}{\Delta x} \left(\int_{-\Delta x/2}^{0} \bar{v}(\xi) d\xi + \int_{0}^{\Delta x/2} \bar{v}(\xi) d\xi \right) = \\
&= \frac{1}{\Delta x} \left(\frac{\Delta x}{2} \bar{v}_A + \frac{\Delta x}{2} \bar{v}_B \right).
\end{aligned}
\tag{18.6}
$$

The trapezoidal rule, which is second-order accurate, was used to estimate the integrals. $\bar{v}$ at locations A and B (see Fig. 18.2) is estimated by linear interpolation, which gives

$$
\begin{aligned}
\bar{\bar{v}}_I &= \frac{1}{2} \left[\left(\frac{1}{4} \bar{v}_{I-1} + \frac{3}{4} \bar{v}_I \right) + \left(\frac{3}{4} \bar{v}_I + \frac{1}{4} \bar{v}_{I+1} \right) \right] \\
&= \frac{1}{8} \left(\bar{v}_{I-1} + 6\bar{v}_I + \bar{v}_{I+1} \right) \neq \bar{v}_I
\end{aligned}
\tag{18.7}
$$

18.3 Resolved & SGS scales

The basic idea in LES is to resolve (large) grid scales (GS), and to model (small) subgrid-scales (SGS). Even if LES is always made unsteady, we are usually interested in the time-averaged results. This means that we time-average all quantities for post-processing, e.g. $\langle \bar{v}_i \rangle$ where the brackets denote time-averaging. From the LES equations, Eq. 18.2, we get the resolved (GS) velocities, $\bar{v}_i$. Then we can compute the resolved fluctuations as $\bar{v}_i' = \bar{v}_i - \langle \bar{v}_i \rangle$.

The limit (cut-off) between GS and SGS is supposed to take place in the inertial subrange (II), see Fig. 18.3.

    I: large, energy-containing scales
    II: inertial subrange (Kolmogorov $-5/3$-range)
    III: dissipation subrange
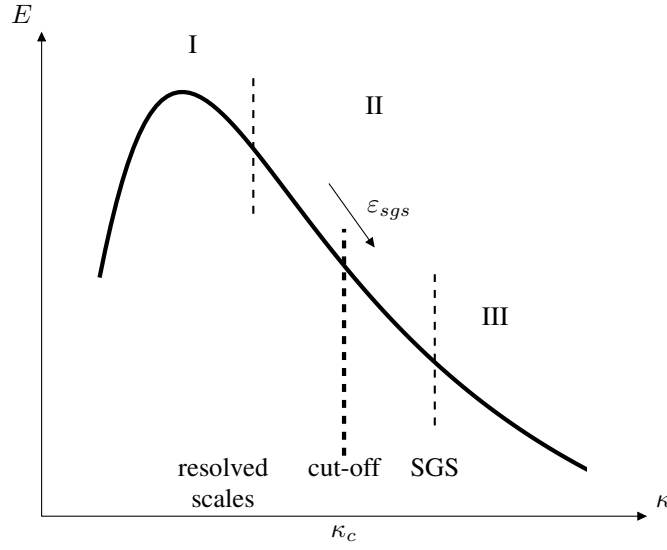
Figure 18.3: Spectrum of velocity.

18.4   The box-filter and the cut-off filter

The box filtering is formally defined as (1D)

$$\bar{v}(x) = \int_{-\infty}^{\infty} G_B(r)v(x-r)dr$$

$$G_B(r) = \begin{cases} 1/\Delta, \text{if } r \leq \Delta/2 \\ 0, \text{if } r > \Delta/2 \end{cases} \tag{18.8}$$

$$\int_{-\infty}^{\infty} G_B(r)dr = 1$$

However, it is often convenient to study the filtering process in the spectral space. The filter in spectral space is particular simple: we simply set the contribution from wavenumbers larger than cut-off to zero. Hence the cut-off filter filters out all scales with wavenumber larger than the cut-off wavenumber $\kappa_c = \pi/\Delta$. It is defined as

$$\hat{G}_C(\kappa) = \begin{cases} 1 & \text{if } \kappa \leq \kappa_c \\ 0 & \text{otherwise} \end{cases} \tag{18.9}$$

We now look at what happens when we filter twice in spectral space. It appears that the calculations for this gets much easier if we first introduce the Fourier transform. The Fourier transform is defined as (cf. Eq. H.28)

$$\hat{v}(\kappa) = \int_0^{\infty} v(r) \exp(-2\pi\iota\kappa r)dr \tag{18.10}$$

and its inverse

$$v(r) = \int_0^{\infty} \hat{v}(\kappa) \exp(2\pi\iota\kappa r)d\kappa \tag{18.11}$$

where κ denotes the wavenumber and $\imath = \sqrt{-1}$. A slightly different definition has been chosen here compared to Eq. H.28. It is chosen since no factor 2π appears in front of the integral in Eq. 18.11 (the Fourier par is *symmetric*); as a consequence it is also absent in Eq. 18.12.

Note that it is physically meaningful to use Fourier transforms only in a homogeneous coordinate direction; in non-homogeneous directions the Fourier coefficients – which are not a function of space – have no meaning. Using the convolution theorem (saying that the integrated product of two functions is equal to the product of their Fourier transforms), we can filter $\hat{v}$ using Eqs. 18.10 and 18.8

$$
\begin{aligned}
\overline{\widehat{v}}(\kappa) = \widehat{\overline{v}}(\kappa) &= \int_0^\infty \overline{v}(\eta)\exp(-2\pi\imath\kappa\eta)d\eta \\
&= \int_0^\infty \int_0^\infty \exp(-2\pi\imath\kappa\eta)G(\alpha)v(\eta-\alpha)d\alpha d\eta \\
&= \int_0^\infty \int_0^\infty \exp(-2\pi\imath\kappa\alpha)\exp(-2\pi\imath\kappa(\eta-\alpha))G(\alpha)v(\eta-\alpha)d\alpha d\eta \\
&= \int_0^\infty \int_0^\infty \exp(-2\pi\imath\kappa\alpha)\exp(-2\pi\imath\kappa\xi)G(\alpha)v(\xi)d\xi d\alpha = \hat{G}(\kappa)\hat{v}(\kappa)
\end{aligned}
\tag{18.12}
$$

(in the last line we used $\xi = \eta - \alpha$). If we use the cut-off filter and filter twice we get

$$
\overline{\overline{\hat{v}}} = \hat{G}_C \hat{G}_C \hat{v} = \hat{G}_C \hat{v}
\tag{18.13}
$$

since $\hat{G}_C^2 = \hat{G}_C$, see Eq 18.9. Since $\overline{\overline{\hat{v}}} = \overline{\hat{v}}$ for the Fourier transform $\hat{v}$, we know that – when using the cuf-off filter – $\overline{\overline{v}} = \overline{v}$. Thus, contrary to the box-filter (see Eq. 18.7), nothing happens when we filter twice in spectral space. The box filter is sharp in physical space but not in wavenumber space; for the cut-off filter it is vice versa.

In finite volume methods box filtering is always used. Furthermore *implicit* filtering is employed. This means that the filtering is the same as the discretization (=integration over the control volume is equal to the filter volume, see Eq. 18.17).

18.5 Highest resolved wavenumbers

Any function can be expressed as a Fourier series such as Eq. 18.11 (see Section 5.3, Eq. H.28 and Section I) provided that the coordinate direction is homogeneous. Let's choose the fluctuating velocity in the x_1 direction, i.e. v_1', and let it be a function of x_1. We require it to be homogeneous, i.e. its RMS, $v_{1,rms}$, does not vary with x_1. Now we ask the question: on a given grid, what is the highest wavenumber that is resolved? Or, in other words, what is the cut-off wavenumber?

Consider Fig. 18.4 (cf. Section I). We assume that v_2' is periodic which makes it convenient to use Fourier transform. We construct v_2' as a sum of four Fourier components

$$
v_2'(x_2) = b_1 \cos\left(\frac{2\pi}{L/1}x_2\right) + b_2 \cos\left(\frac{2\pi}{L/2}x_2\right) + b_3 \cos\left(\frac{2\pi}{L/3}x_2\right) + b_4 \cos\left(\frac{2\pi}{L/4}x_2\right)
$$

The thick line in Fig. 18.4 shows how v_2' varies with x_2. The blue circles show the Fourier component with the highest wave number, $m = 4$. How many grid point does it take to resolve this Fourier component?

Figure 18.5 shows an example how to resolve the highest Fourier component on two different grids. The wave shown in Fig. 18.5a reads

$$
v_1' = 0.25\left[1 + 0.8\sin(\kappa_1 x_1)\right]
\tag{18.14}
$$
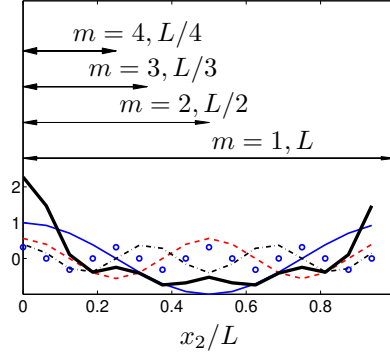
Figure 18.4: v_2' vs. x_2/L. ▬ : term 1 ($m = 1$); ▬ ▬ : term 2 ($m = 2$); ▬ · ▬ : term 3 ($m = 3$); ○: term 4 ($m = 4$); ▬ : v_2'. Python/Matlab/Octave code is given in Section I.3.
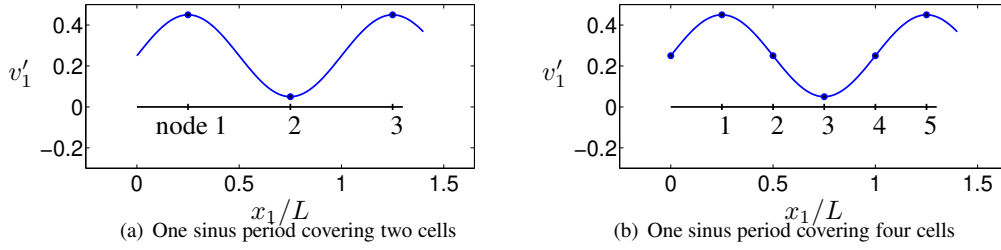
Figure 18.5: Physical and wavenumber space. Sinus curves with different wavenumbers illustrated in physical space.

and it covers two cells ($\Delta x_1/L = 0.5$). If we define this as the cut-off wavenumber we get $\kappa_{1,c}L = \kappa_{1,c}2\Delta x_1 = 2\pi$ (i.e. $\sin(\kappa_{1,c}2\Delta x_1) = \sin(2\pi)$; recall that 2π is one period) so that

$$\kappa_{1,c} = 2\pi/(2\Delta x_1) = \pi/\Delta x_1 \qquad (18.15)$$

It is of course questionable if v_1' in Fig. 18.5a really is resolved since the sinus wave covers only two cells. However this is the usual definition of the cut-off wavenumber.

If we require that the highest resolved wavenumber should be covered by four cells ($\Delta x_1/L = 0.25$), as in Fig. 18.5b, then the cut-off wavenumber is given by $\kappa_{1,c} = 2\pi/(4\Delta x_1) = \pi/(2\Delta x_1)$.

18.6 Subgrid model

We need a subgrid model to model the turbulent scales which cannot be resolved by the grid and the discretization scheme.

The simplest model is the Smagorinsky model [81]:

$$\tau_{ij} - \frac{1}{3}\delta_{ij}\tau_{kk} = -\nu_{sgs}\left(\frac{\partial \bar{v}_i}{\partial x_j} + \frac{\partial \bar{v}_j}{\partial x_i}\right) = -2\nu_{sgs}\bar{s}_{ij}$$
$$\nu_{sgs} = (C_S\Delta)^2\sqrt{2\bar{s}_{ij}\bar{s}_{ij}} \equiv (C_S\Delta)^2\,|\bar{s}| \qquad (18.16)$$

and the filter-width is taken as the local grid size

$$\Delta = (\Delta V_{IJK})^{1/3} \qquad (18.17)$$

The scalar $|\bar{s}|$ is the norm (i.e. the "length") of $\partial \bar{v}_i / \partial x_j + \partial \bar{v}_j / \partial x_i$ in the Boussinesq assumption, see Eq. 16.21. The Smagorinsky model is derived as follows. The turbulent viscosity may – as in RANS – be obtained through dimensional analysis as (see Eq. 11.25)

$$\nu_{sgs} = \mathcal{U}\mathcal{L}. \tag{18.18}$$

The turbulent velocity scale, $\mathcal{U}$, is obtained as the first term in Taylor expansion, $\mathcal{L}\partial \bar{v}/\partial x$, and the length scale , $\mathcal{L}$, is taken as $C_S\Delta$ which gives

$$\nu_{sgs} = (C_S\Delta)^2 |\bar{s}| \tag{18.19}$$

where the one-dimensional velocity gradient, $\partial \bar{v}/\partial x$ was replaced by the general three-dimensional gradient, $|\bar{s}|$. Near the wall, the SGS viscosity becomes quite large since the velocity gradient is very large at the wall. However, because the SGS turbulent fluctuations near a wall go to zero, so must the SGS viscosity. A damping function f_μ is added to ensure this

$$f_\mu = 1 - \exp(-x_2^+/26) \tag{18.20}$$

A more convenient way to dampen the SGS viscosity near the wall is simply to use the RANS length scale as an upper limit, i.e.

$$\Delta = \min\left\{(\Delta V_{IJK})^{1/3}, \kappa n\right\} \tag{18.21}$$

where n is the distance to the nearest wall.

Disadvantage of Smagorinsky model: the "constant" C_S is not constant, but it is flow-dependent. It is found to vary in the range from $C_S = 0.065$ [82] to $C_S = 0.25$ [83].

18.7 Smagorinsky model vs. mixing-length model

The eddy viscosity according to the mixing length theory reads in boundary-layer flow [84, 85]

$$\nu_t = \ell^2 \left|\frac{\partial \bar{v}_1}{\partial x_2}\right|.$$

Generalized to three dimensions, we have

$$\nu_t = \ell^2 \left[\left(\frac{\partial \bar{v}_i}{\partial x_j} + \frac{\partial \bar{v}_j}{\partial x_i}\right)\frac{\partial \bar{v}_i}{\partial x_j}\right]^{1/2} = \ell^2 \left(2\bar{s}_{ij}\bar{s}_{ij}\right)^{1/2} \equiv \ell^2 |\bar{s}|.$$

In the Smagorinsky model the SGS turbulent length scale corresponds to $\ell = C_S\Delta$ so that

$$\nu_{sgs} = (C_S\Delta)^2 |\bar{s}|$$

which is the same as Eq. 18.16

18.8 Energy path

The path of kinetic energy is illustrated in Fig. 18.6. At cut-off, SGS kinetic energy is dissipated

$$\varepsilon_{sgs} = -\tau_{ij}\bar{s}_{ij} = 2\nu_{sgs}\bar{s}_{ij}\bar{s}_{ij} \tag{18.22}$$

from the resolved turbulence. This energy is transferred to the SGS scales and act as production term ($P_{k_{sgs}}$) in the k_{sgs} equation. The SGS kinetic energy is then transferred to higher wave-numbers via the cascade effect and the kinetic energy is finally

$$-\langle \bar{v}'_i \bar{v}'_j \rangle \frac{\partial \langle \bar{v}_i \rangle}{\partial x_j}$$

inertial subrange, $E \propto \kappa^{-5/3}$

$\varepsilon_{sgs} = P^k_{sgs}$

E

ε

κ

κ_c
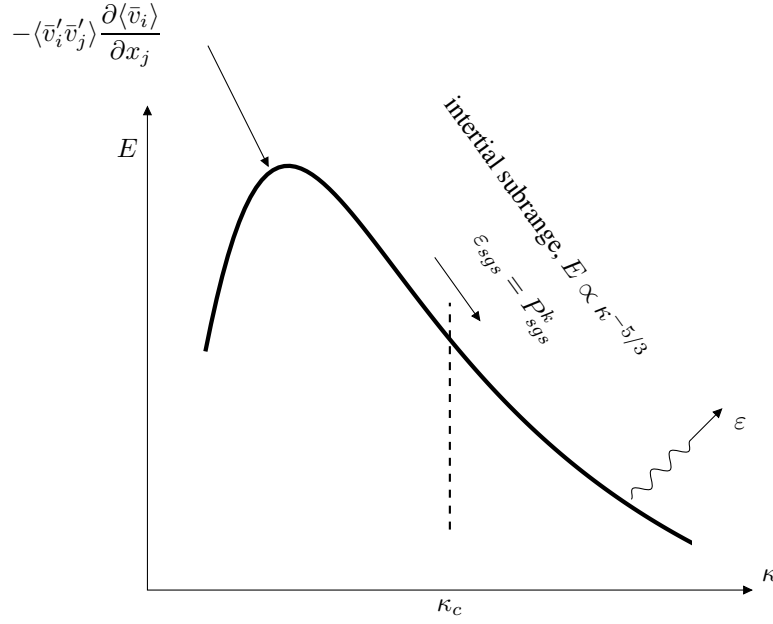
Figure 18.6: Energy spectrum.

dissipated (ε=physical dissipation) in the dissipation range. It should be mentioned that this process is an idealized one. We assume that ALL dissipation takes place in the dissipation range. This is a good approximation, but in reality dissipation (i.e. transfer of energy from kinetic energy to internal energy which corresponds to an increase in temperature) takes place at all wave numbers, and the dissipation increases for increasing wave number, see Eq. 8.20.

18.9 SGS kinetic energy

The SGS kinetic energy k_{sgs} can be estimated from the Kolmogorov $-5/3$ law. The total turbulent kinetic energy is obtained from the energy spectrum as

$$k = \int_0^\infty E(\kappa) d\kappa$$

Changing the lower integration limit to wavenumbers larger than cut-off (i.e. κ_c) gives the SGS kinetic energy

$$k_{sgs} = \int_{\kappa_c}^\infty E(\kappa) d\kappa \tag{18.23}$$

The Kolmogorov $-5/3$ law now gives

$$k_{sgs} = \int_{\kappa_c}^\infty C_K \kappa^{-5/3} \varepsilon^{2/3} d\kappa$$

where $C_K = 1.5$ (Note that for these high wavenumbers, the Kolmogorov spectrum ought to be replaced by the Kolmogorov-Pau spectrum in which an exponential decaying function is added for high wavenumbers [84, Chapter 3]). Carrying out the
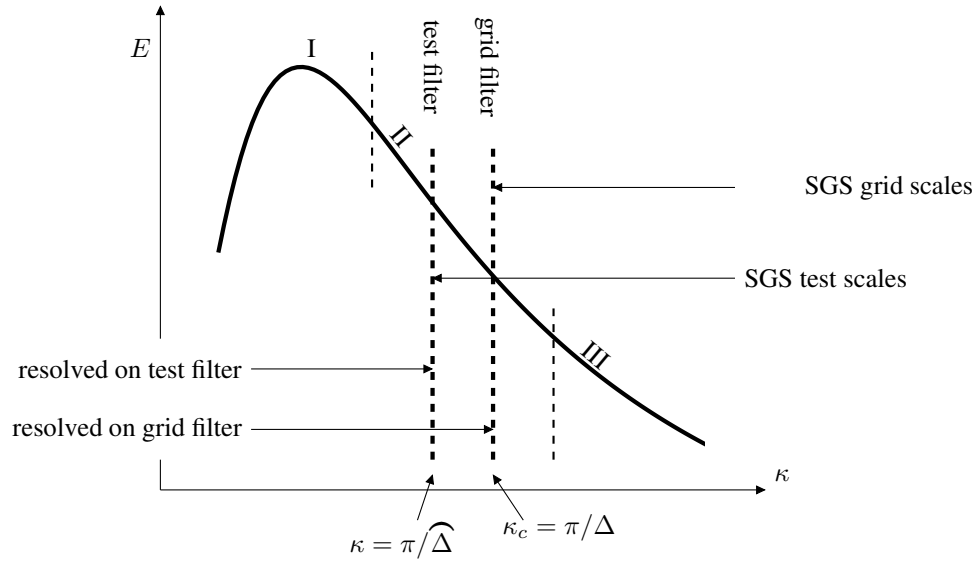
Figure 18.7: Energy spectrum with grid and test filter.

integration and replacing κ_c with π/Δ we get

$$k_{sgs} = \frac{3}{2}C_K\left(\frac{\Delta\varepsilon}{\pi}\right)^{2/3}$$ (18.24)

In the same way as k_{sgs} can be computed from Eq. 18.23, the resolved turbulent kinetic energy, k_{res}, is obtained from

$$k_{res} = \int_0^{\kappa_c} E(\kappa)d\kappa$$

18.10   LES vs. RANS

LES can handle many flows which RANS (Reynolds Averaged Navier Stokes) cannot; the reason is that in LES large, turbulent scales are resolved. Examples are:

- o Flows with large separation

- o Bluff-body flows (e.g. flow around a car); the wake often includes large, un-steady, turbulent structures

- o Transition

- In RANS all turbulent scales are modeled $\Rightarrow$ <u>inaccurate</u>

- In LES only small, isotropic turbulent scales are modeled $\Rightarrow$ <u>accurate</u>

- LES is *very* much more expensive than RANS.

18.11 The dynamic model

In this model of [86] the constant C is not arbitrarily chosen (or optimized), but it is computed.

If we apply two filters to Navier-Stokes [grid filter and a second, coarser filter (test filter, denoted by $\frown$)] where $\widehat{\Delta} = 2\Delta$ we get

$$\frac{\partial \widehat{\bar{v}}_i}{\partial t} + \frac{\partial}{\partial x_j}\left(\widehat{\bar{v}}_i\widehat{\bar{v}}_j\right) = -\frac{1}{\rho}\frac{\partial \widehat{\bar{p}}}{\partial x_i} + \nu\frac{\partial^2 \widehat{\bar{v}}_i}{\partial x_j \partial x_j} - \frac{\partial T_{ij}}{\partial x_j} \tag{18.25}$$

where the subgrid stresses on the test level now are given by

$$T_{ij} = \widehat{\overline{v_i v_j}} - \widehat{\bar{v}}_i\widehat{\bar{v}}_j \tag{18.26}$$

$$\frac{\partial \widehat{\bar{v}}_i}{\partial t} + \frac{\partial}{\partial x_j}\left(\widehat{\bar{v}}_i\widehat{\bar{v}}_j\right) = -\frac{1}{\rho}\frac{\partial \widehat{\bar{p}}}{\partial x_i} + \nu\frac{\partial^2 \widehat{\bar{v}}_i}{\partial x_j \partial x_j} - \frac{\partial \widehat{\tau}_{ij}}{\partial x_j}$$
$$- \frac{\partial}{\partial x_j}\left(\widehat{\overline{v_i v_j}} - \widehat{\bar{v}}_i\widehat{\bar{v}}_j\right) \tag{18.27}$$

Identification of Eqs. 18.25 and 18.27 gives

$$\widehat{\overline{v_i v_j}} - \widehat{\bar{v}}_i\widehat{\bar{v}}_j + \widehat{\tau}_{ij} = T_{ij} \tag{18.28}$$

The *dynamic* Leonard stresses are now defined as

$$\mathcal{L}_{ij} \equiv \widehat{\overline{v_i v_j}} - \widehat{\bar{v}}_i\widehat{\bar{v}}_j = T_{ij} - \widehat{\tau}_{ij} \tag{18.29}$$

The trace of this relation reads

$$\mathcal{L}_{ii} \equiv T_{ii} - \widehat{\tau}_{ii}$$

With this expression we can re-formulate Eq. 18.29 as

$$\mathcal{L}_{ij} - \frac{1}{3}\delta_{ij}\mathcal{L}_{kk} = T_{ij} - \frac{1}{3}\delta_{ij}T_{kk} - \left(\widehat{\tau}_{ij} - \frac{1}{3}\delta_{ij}\widehat{\tau}_{kk}\right) \tag{18.30}$$

In the energy spectrum, the test filter is located at lower wave number than the grid filter, see Fig. 18.7.

18.12 The test filter

The test filter is twice the size of the grid filter, i.e. $\widehat{\Delta} = 2\Delta$.

The test-filtered variables are computed by integration over the test filter. For example, the 1D example in Fig. 18.8 $\widehat{\bar{v}}$ is computed as ($\widehat{\Delta x} = 2\Delta x$)

$$\begin{aligned}
\widehat{\bar{v}}_P &= \frac{1}{2\Delta x}\int_W^E \bar{v}dx = \frac{1}{2\Delta x}\left(\int_W^P \bar{v}dx + \int_P^E \bar{v}dx\right) \\
&= \frac{1}{2\Delta x}\left(\bar{v}_w\Delta x + \bar{v}_e\Delta x\right) = \frac{1}{2}\left(\frac{\bar{v}_W + \bar{v}_P}{2} + \frac{\bar{v}_P + \bar{v}_E}{2}\right) \\
&= \frac{1}{4}\left(\bar{v}_W + 2\bar{v}_P + \bar{v}_E\right)
\end{aligned} \tag{18.31}$$
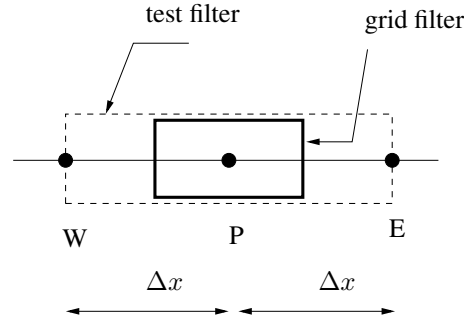
Figure 18.8: Control volume for grid and test filter.
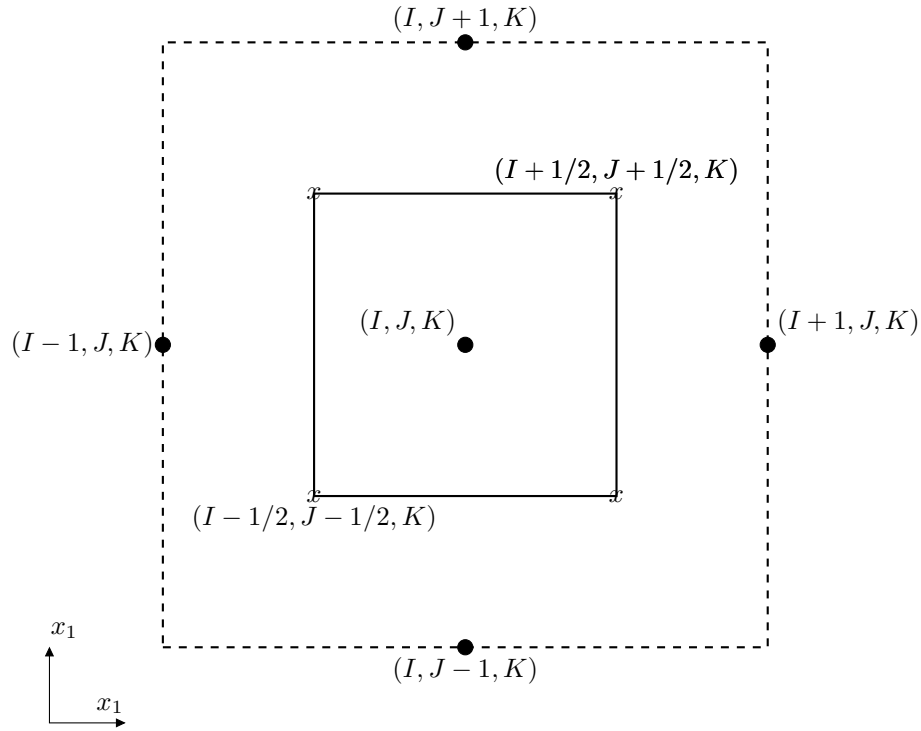
Figure 18.9: A 2D test filter control volume.

18.12.1 2D filtering

In 2D, we do as in 1D: first compute the value at the center of the four squares (or rectangles) surrounding the node (I, J, K), marked by x, see Fig. 18.9. For the lower-left square, for example, we get

$$\bar{v}^f_{I-1/2,J-1/2,K} = \frac{1}{4}(\bar{v}_{I-1,J-1,K} + \bar{v}_{I-1,J,K} + \bar{v}_{I,J-1,K} + \bar{v}_{I,J,K}) \qquad (18.32)$$

Next, the test filtered variable is computed as

$$\widehat{\bar{v}}_{I,J,K} = \frac{1}{4}(\bar{v}^f_{I-1/2,J-1/2,K} + \bar{v}^f_{I-1/2,J+1/2,K} + \bar{v}^f_{I+1/2,J-1/2,K} + \bar{v}^f_{I+1/2,J+1/2,K})$$
(18.33)

18.12.2 3D filtering

In 3D we have eight cubes. Filtering at the test level is carried out in the same way by integrating over the test cell assuming linear variation of the variables [87]. For the bottom-lower-left cube, for example, we get

$$\bar{v}^f_{I-1/2,J-1/2,K-1/2} = \frac{1}{8}(\bar{v}_{I-1,J-1,K} + \bar{v}_{I-1,J,K} + \bar{v}_{I,J-1,K} + \bar{v}_{I,J,K}$$
$$+ \bar{v}_{I-1,J-1,K-1} + \bar{v}_{I-1,J,K-1} + \bar{v}_{I,J-1,K-1} + \bar{v}_{I,J,K-1})$$
(18.34)

Next, the test filtered variable is computed as

$$\widehat{\bar{v}}_{I,J,K} = \frac{1}{8}(\bar{v}^f_{I-1/2,J-1/2,K-1/2} + \bar{v}^f_{I+1/2,J-1/2,K-1/2}$$
$$+ \bar{v}^f_{I-1/2,J+1/2,K-1/2} + \bar{v}^f_{I+1/2,J+1/2,K-1/2}$$
$$+ \bar{v}^f_{I-1/2,J-1/2,K+1/2} + \bar{v}^f_{I+1/2,J-1/2,K+1/2}$$
$$+ \bar{v}^f_{I-1/2,J+1/2,K+1/2} + \bar{v}^f_{I+1/2,J+1/2,K+1/2})$$
(18.35)

18.13 Stresses on grid, test and intermediate level

The stresses on the grid level, test level and intermediate level (dynamic Leonard stresses) have the form

$$\tau_{ij} = \overline{v_i v_j} - \bar{v}_i \bar{v}_j \quad \textbf{stresses with } \ell < \Delta$$

$$T_{ij} = \widehat{\overline{v_i v_j}} - \widehat{\bar{v}}_i \widehat{\bar{v}}_j \quad \textbf{stresses with } \ell < \widehat{\Delta}$$

$$\mathcal{L}_{ij} = T_{ij} - \widehat{\tau}_{ij} \quad \textbf{stresses with } \Delta < \ell < \widehat{\Delta}$$

Thus the dynamic Leonard stresses represent the stresses with lengthscale, ℓ, in the range between Δ and $\widehat{\Delta}$.

Assume now that the same functional form for the subgrid stresses that is used at the grid level (τ_{ij}) also can be used at the test filter level (T_{ij}). If we use the Smagorinsky model we get

$$\tau_{ij} - \frac{1}{3}\delta_{ij}\tau_{kk} = -2C\Delta^2|\bar{s}|\bar{s}_{ij}$$
(18.36)

$$T_{ij} - \frac{1}{3}\delta_{ij}T_{kk} = -2C\widehat{\Delta}^2|\widehat{\bar{s}}|\widehat{\bar{s}}_{ij}$$
(18.37)

where

$$\widehat{\bar{s}}_{ij} = \frac{1}{2}\left(\frac{\partial \widehat{\bar{v}}_i}{\partial x_j} + \frac{\partial \widehat{\bar{v}}_j}{\partial x_i}\right), \ |\widehat{\bar{s}}| = \left(2\widehat{\bar{s}}_{ij}\widehat{\bar{s}}_{ij}\right)^{1/2}$$

Note that C in Eq. 18.36 is not squared (cf. the Smagorinsky model, Eq. 18.16 at p.187). Hence, C should be compared with C_S^2. Applying the test filter to Eq. 18.36

(assuming that C varies slowly), substituting this equation and Eq. 18.37 into Eq. 18.30 gives

$$\mathcal{L}_{ij} - \frac{1}{3}\delta_{ij}\mathcal{L}_{kk} = -2C\left(\widehat{\Delta}^2\,|\widehat{\bar{s}}\,|\widehat{\bar{s}}_{ij} - \widehat{\Delta^2|\bar{s}|\bar{s}_{ij}}\right) \tag{18.38}$$

where we used the relation

$$\frac{1}{3}\delta_{ij}\mathcal{L}_{kk} = \frac{1}{3}\delta_{ij}T_{kk} - \frac{1}{3}\delta_{ij}\widehat{\tau}_{kk}$$

obtained from Eq. 18.29. In Eq. 18.38 we have made the assumption $\widehat{C\Delta^2|\bar{s}|\bar{s}_{ij}} \simeq C\widehat{\Delta^2|\bar{s}|\bar{s}_{ij}}$.

Note that the "constant" C in Eq. 18.38 really is a function of both space and time, i.e. $C = C(x_i, t)$.

Equation 18.38 is a tensor equation, and we have five ($\bar{s}_{ij}$ is symmetric and traceless) equations for C. Lilly [88] suggested to satisfy Eq. 18.38 in a least-square sense. Let us define the error as the difference between the left-hand side and the right-hand side of Eq. 18.38 raised to the power of two, i.e.

$$Q = \left(\mathcal{L}_{ij} - \frac{1}{3}\delta_{ij}\mathcal{L}_{kk} + 2CM_{ij}\right)^2 \tag{18.39a}$$

$$M_{ij} = \left(\widehat{\Delta}^2\,|\widehat{\bar{s}}\,|\widehat{\bar{s}}_{ij} - \Delta^2\widehat{|\bar{s}|\bar{s}_{ij}}\right) \tag{18.39b}$$

The error, Q, has a minimum (or maximum) when $\partial Q/\partial C = 0$. Carrying out the derivation of 18.39a gives

$$\frac{\partial Q}{\partial C} = 4M_{ij}\left(\mathcal{L}_{ij} + 2CM_{ij}\right) = 0 \tag{18.40}$$

Note that $\frac{1}{3}\delta_{ij}\mathcal{L}_{kk}M_{ij} = \frac{1}{3}\mathcal{L}_{kk}M_{ii} = 0$ since $\widehat{\bar{s}}_{ii} = \bar{s}_{ii} = 0$ thanks to continuity. Since $\partial^2 Q/\partial C^2 = 8M_{ij}M_{ij} > 0$ we find that Eq. 18.40 represents indeed a minimum. Equation 18.40 finally gives

$$C = -\frac{\mathcal{L}_{ij}M_{ij}}{2M_{ij}M_{ij}} \tag{18.41}$$

It turns out that the dynamic coefficient C fluctuates wildly both in space and time. This causes numerical problems, and it has been found necessary to average C in homogeneous direction(s). Furthermore, C must be clipped to ensure that the total viscosity stays positive ($\nu + \nu_{sgs} \geq 0$).

In real 3D flows, there is no homogeneous direction. Usually local averaging and clipping (i.e. requiring that C stays within pre-defined limits) of the dynamic coefficient is used.

Use of one-equation models solve these numerical problems (see p. 202).

18.14 Numerical dissipation

The main function of an SGS model is to dissipate (i.e. to dampen) resolved turbulent fluctuations. The SGS model is – hopefully – designed to give a proper amount of dissipation. This is the reason why in LES we should use a central differencing scheme,
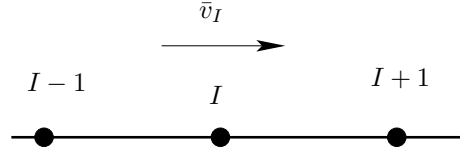
Figure 18.10: Numerical dissipation.

because this class of schemes does not give any *numerical* dissipation. All upwind schemes give numerical dissipation in addition to the modeled SGS dissipation. Indeed, there are LES-methods in which upwind schemes are used to create dissipation and where no SGS model is used at all (e.g. MILES [89]). However, in this course we focus on ensuring proper dissipation through an SGS model rather than via upwind differencing. It can be shown using Neumann stability analysis that all upwind schemes are dissipative (see *Further reading* at
`http://www.tfd.chalmers.se/~lada/comp_turb_model/`). Below it is shown that first-order upwind schemes are dissipative.

The first-derivative in the convective term is estimated by first-order upwind differencing as (finite difference, see Fig. 18.10)

$$\bar{v}\left(\frac{\partial \bar{v}}{\partial x}\right)_{exact} = \bar{v}_I\left(\frac{\bar{v}_I - \bar{v}_{I-1}}{\Delta x} + \mathcal{O}\left(\Delta x\right)\right) \tag{18.42}$$

where we have assumed $\bar{v}_I > 0$. Taylor expansion gives

$$\bar{v}_{I-1} = \bar{v}_I - \Delta x\frac{\partial \bar{v}}{\partial x} + \frac{1}{2}(\Delta x)^2\frac{\partial^2 \bar{v}}{\partial x^2} + \mathcal{O}\left((\Delta x)^3\right)$$

so that

$$\frac{\bar{v}_I - \bar{v}_{I-1}}{\Delta x} = \frac{\partial \bar{v}}{\partial x} - \frac{1}{2}\Delta x\frac{\partial^2 \bar{v}}{\partial x^2} + \mathcal{O}\left((\Delta x)^2\right)$$

Insert this into Eq. 18.42

$$\bar{v}\left(\frac{\partial \bar{v}}{\partial x}\right)_{exact} = \bar{v}\frac{\partial \bar{v}}{\partial x} - \underbrace{\frac{1}{2}\Delta x\bar{v}\frac{\partial^2 \bar{v}}{\partial x^2}}_{\mathcal{O}(\Delta x)} + \bar{v}\mathcal{O}\left((\Delta x)^2\right) \tag{18.43}$$

where the second term on the right side corresponds to the error term in Eq. 18.42. When this expression is inserted into the LES momentum equations, the second term on the right-hand side will act as an additional (numerical) diffusion term. The total diffusion term will have the form

$$\text{diffusion term} = \frac{\partial}{\partial x}\left\{(\nu + \nu_{sgs} + \nu_{num})\frac{\partial \bar{v}}{\partial x}\right\} \tag{18.44}$$

where the additional numerical viscosity, $\nu_{num} = 0.5|\bar{v}|\Delta x$, see Eq. 18.43. This means that the total dissipation due to SGS viscosity and numerical viscosity is (cf. Eq. 18.22)

$$\varepsilon_{sgs+num} = 2(\nu_{sgs} + \nu_{num})\bar{s}_{ij}\bar{s}_{ij}$$

For more details on derivation of equations transport equations of turbulent kinetic energies, see [23].

18.15 Scale-similarity Models

In the models presented in the previous sections (the Smagorinsky and the dynamic models) the total SGS stress $\tau_{ij} = \overline{v_i v_j} - \bar{v}_i \bar{v}_j$ was modeled with an eddy-viscosity hypothesis. In scale-similarity models the total stress is split up as

$$
\begin{aligned}
\tau_{ij} = \overline{v_i v_j} - \bar{v}_i \bar{v}_j &= \overline{(\bar{v}_i + v_i'')(\bar{v}_j + v_j'')} - \bar{v}_i \bar{v}_j \\
&= \overline{\bar{v}_i \bar{v}_j} + \overline{\bar{v}_i v_j''} + \overline{\bar{v}_j v_i''} + \overline{v_i'' v_j''} - \bar{v}_i \bar{v}_j \\
&= (\overline{\bar{v}_i \bar{v}_j} - \bar{v}_i \bar{v}_j) + \left[\overline{\bar{v}_i v_j''} + \overline{\bar{v}_j v_i''} \right] + \overline{v_i'' v_j''}
\end{aligned}
$$

where the term in brackets is denoted the Leonard stresses, the term in square brackets is denoted cross terms, and the last term is denoted the Reynolds SGS stress. Thus

$$
\begin{aligned}
\tau_{ij} &= L_{ij} + C_{ij} + R_{ij} \\
L_{ij} &= \overline{\bar{v}_i \bar{v}_j} - \bar{v}_i \bar{v}_j \\
C_{ij} &= \overline{\bar{v}_i v_j''} + \overline{\bar{v}_j v_i''} \\
R_{ij} &= \overline{v_i'' v_j''}.
\end{aligned}
\tag{18.45}
$$

Note that the Leonard stresses, L_{ij}, are *computable*, i.e. they are exact and don't need to be modeled.

In scale-similarity models the main idea is that the turbulent scales just above cut-off wavenumber, κ_c, (scales smaller than Δ) are similar to the ones just below κ_c (scales larger than Δ); hence the word "scale-similar". Looking at Eq. 18.45 it seems natural to assume that the cross term is responsible for the interaction between resolved scales ($\bar{v}_i$) and modeled scales (v_i''), since C_{ij} includes both scales.

18.16 The Bardina Model

In the Bardina model the Leonard stresses L_{ij} are computed explicitly, and the sum of the cross term C_{ij} and the Reynolds term is modeled as [90, 91]

$$
C_{ij}^M = c_r (\bar{v}_i \bar{v}_j - \overline{\bar{v}}_i \overline{\bar{v}}_j)
\tag{18.46}
$$

and $R_{ij}^M = 0$ (superscript M denotes <u>M</u>odeled). It was found that this model was not sufficiently dissipative, and thus a Smagorinsky model was added

$$
\begin{aligned}
C_{ij}^M &= c_r (\bar{v}_i \bar{v}_j - \overline{\bar{v}}_i \overline{\bar{v}}_j) \\
R_{ij}^M &= -2C_S^2 \Delta^2 |\bar{s}| \bar{s}_{ij}
\end{aligned}
\tag{18.47}
$$

18.17 Redefined terms in the Bardina Model

In [91] it was found that the Leonard term L_{ij} and the cross term C_{ij} are not Galilean invariant by themselves, but only the sum $L_{ij} + C_{ij}$ is (see Appendix M). As a consequence, if the cross term is neglected, the Leonard stresses must not be computed explicitly, because then the modeled momentum equations do not satisfy Galilean invariance.
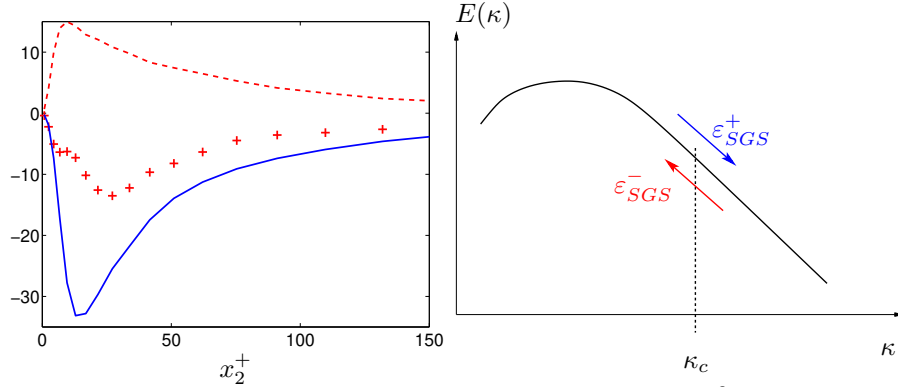
Figure 18.11: Dissipation terms and production term from DNS data. 96^3 mesh data filtered onto a 48^3 mesh. $Re_\tau = 500$. ━━ : $-\varepsilon_{SGS}^+$; ━ ━ : $-\varepsilon_{SGS}^-$; +: $-\varepsilon_{SGS}$.

The stresses in the Bardina model can be redefined to make them Galilean invariant for any value c_r A modified Leonard stress tensor L_{ij}^m is defined as [92]

$$
\begin{aligned}
\tau_{ij}^m &= \tau_{ij} = C_{ij}^m + L_{ij}^m + R_{ij}^m \\
L_{ij}^m &= c_r \left(\overline{\overline{v}_i \overline{v}_j} - \overline{\overline{v}}_i \overline{\overline{v}}_j \right) \\
C_{ij}^m &= 0 \\
R_{ij}^m &= R_{ij} = \overline{v_i'' v_j''}
\end{aligned}
\tag{18.48}
$$

Note that the modified Leonard stresses is the same as the "unmodified" one plus the modeled cross term C_{ij} in the Bardina model with $c_r = 1$ (right-hand side of Eq. 18.46), i.e.

$$
L_{ij}^m = L_{ij} + C_{ij}^M
$$

In order to make the model sufficiently dissipative a Smagorinsky model is added, and the total SGS stress τ_{ij} is modeled as

$$
\tau_{ij} = \overline{\overline{v}_i \overline{v}_j} - \overline{\overline{v}}_i \overline{\overline{v}}_j - 2(C_S \Delta)^2 |\bar{s}| \bar{s}_{ij}
\tag{18.49}
$$

Below we verify that the modified Leonard stress is Galilean invariant.

$$
\begin{aligned}
\frac{1}{c_r} L_{ij}^{m*} &= \overline{\overline{v}_i^* \overline{v}_j^*} - \overline{\overline{v}}_i^* \overline{\overline{v}}_j^* = \overline{(\overline{v}_i + V_i)(\overline{v}_j + V_j)} - \overline{(\overline{v}_i + V_i)} \; \overline{(\overline{v}_j + V_j)} \\
&= \overline{\overline{v}_i \overline{v}_j} + \overline{\overline{v}}_i V_j + \overline{\overline{v}}_j V_i - \overline{\overline{v}}_i \overline{\overline{v}}_j - \overline{\overline{v}}_i V_j - V_i \overline{\overline{v}}_j \\
&= \overline{\overline{v}_i \overline{v}_j} - \overline{\overline{v}}_i \overline{\overline{v}}_j = \frac{1}{c_r} L_{ij}^m
\end{aligned}
\tag{18.50}
$$

18.18 A dissipative scale-similarity model.

Above it was mentioned that when the first scale-similarity model was proposed it was found that it is not sufficiently dissipative [90]. An eddy-viscosity model has to be added to make the model sufficiently dissipative; these models are called *mixed* models. Ref. [93] presents and evaluates a dissipative scale-similarity model.

The filtered Navier-Stokes read

$$
\frac{d\bar{v}_i}{dt} + \frac{1}{\rho} \frac{\partial \bar{p}}{\partial x_i} = \nu \frac{\partial^2 \bar{v}_i}{\partial x_k \partial x_k} - \frac{\partial \tau_{ik}}{\partial x_k}
\tag{18.51}
$$

where d/dt and τ_{ik} denote the material derivative and the SGS stress tensor, respectively. The SGS stress tensor is given by

$$\tau_{ik} = \overline{v_i v_k} - \bar{v}_i \bar{v}_k. \tag{18.52}$$

When it is modeled with the standard scale-similarity model, it is not sufficiently dissipative. Let us take a closer look at the equation for the resolved, turbulent kinetic energy, $k = \langle v_i' v_i' \rangle / 2$, which reads

$$
\begin{aligned}
\frac{dk}{dt} + \langle \bar{v}_k' \bar{v}_i' \rangle \frac{\partial \langle \bar{v}_i \rangle}{\partial x_k} &+ \frac{\partial \langle \bar{p}' \bar{v}_i' \rangle}{\partial x_i} + \frac{1}{2} \frac{\partial \langle \bar{v}_k' \bar{v}_i' \bar{v}_i' \rangle}{\partial x_k} = \nu \left\langle \frac{\partial^2 \bar{v}_i'}{\partial x_k \partial x_k} \bar{v}_i' \right\rangle - \\
\left\langle \left(\frac{\partial \tau_{ik}}{\partial x_k} - \left\langle \frac{\partial \tau_{ik}}{\partial x_k} \right\rangle \right) \bar{v}_i' \right\rangle &= \nu \left\langle \frac{\partial^2 \bar{v}_i'}{\partial x_k \partial x_k} \bar{v}_i' \right\rangle - \left\langle \frac{\partial \tau_{ik}}{\partial x_k} \bar{v}_i' \right\rangle = \\
\nu \frac{\partial^2 k}{\partial x_k \partial x_k} &- \nu \underbrace{\left\langle \frac{\partial \bar{v}_i'}{\partial x_k} \frac{\partial \bar{v}_i'}{\partial x_k} \right\rangle}_{\varepsilon} - \underbrace{\left\langle \frac{\partial \tau_{ik}}{\partial x_k} \bar{v}_i' \right\rangle}_{\varepsilon_{SGS}}
\end{aligned} \tag{18.53}
$$

The first term on the last line is the viscous diffusion term and the second term, ε, is the viscous dissipation term which is always positive. The last term, ε_{SGS}, is a source term arising from the SGS stress tensor, which can be positive or negative. When it is positive, forward scattering takes place (i.e. it acts as a dissipation term); when it is negative, back scattering occurs.

Figure 18.11 presents SGS dissipation, ε_{SGS} in Eq. 18.53, computed from filtered DNS data. The forward scatter, ε_{SGS}^+, and back scatter, ε_{SGS}^-, SGS dissipation are defined as the sum of all instants when ε_{SGS} is positive and negative, respectively. As can be seen, the scale-similarity model is slightly dissipative (i.e. $\varepsilon_{SGS} > 0$), but the forward and back scatter dissipation are both much larger than ε_{SGS}.

One way to make the SGS stress tensor strictly dissipative is to set the back scatter to zero, i.e. $\max(\varepsilon_{SGS}, 0)$. This could be achieved by setting $\partial \tau_{ik} / \partial x_k = 0$ when its sign is different from that of $\bar{v}_i'$ (see the last term in Eq. 18.53). This would work if we were solving for k. Usually we do not, and the equations that we do solve (the filtered Navier-Stokes equations) are not directly affected by the dissipation term, ε_{SGS}.

Instead we have to modify the SGS stress tensor as it appears in the filtered Navier-Stokes equations, Eq. 18.51. The second derivative on the right side is usually called a *diffusion* term because it acts like a diffusion transport term. When analyzing the stability properties of discretized equations to an imposed disturbance, $\bar{v}'$, using Neumann analysis (see, for example, Chapter 8 in [94]), this term is referred to as a *dissipation* term. In stability analysis the concern is to dampen numerical oscillations; in connection with SGS models, the aim is to dampen turbulent resolved fluctuations. It is shown in Neumann analysis that the diffusion term in the Navier-Stokes equations is dissipative, i.e. it dampens numerical oscillations. However, since it is the resolved *turbulent fluctuations*, i.e. k in Eq. 18.53, that we want to dissipate, we must consider the filtered Navier-Stokes equations for the fluctuating velocity, $\bar{v}_i'$. The viscous diffusion term in the momentum equations appears in the first term on the right side (first line) in Eq. 18.53. To ensure that $\varepsilon_{SGS} > 0$, we set $-\partial \tau_{ik} / \partial x_k$ to zero when its sign is different from that of the viscous diffusion term (cf. the two last terms on the second line in Eq. 18.53). This is achieved by defining a sign function; for details, see [93].

18.19 Forcing

An alternative way to modify the scale-similarity model is to omit the *forward* scatter, i.e. to include instants when the subgrid stresses act as *counter-gradient* diffusion. In hybrid LES-RANS, the stresses can then be used as forcing at the interface between URANS and LES. This new approach is the focus of [95].

18.20 Numerical method

A numerical method based on an implicit, finite volume method with collocated grid arrangement, central differencing in space, and Crank-Nicolson ($\alpha = 0.5$) in time is briefly described below. The discretized momentum equations read

$$\bar{v}_i^{n+1/2} = \bar{v}_i^n + \Delta t H \left(\bar{v}^n, \bar{v}_i^{n+1/2} \right)$$
$$-\alpha \Delta t \frac{\partial \bar{p}^{n+1/2}}{\partial x_i} - (1-\alpha) \Delta t \frac{\partial \bar{p}^n}{\partial x_i} \tag{18.54}$$

where H includes convective, viscous and SGS terms. In SIMPLE notation this equation reads

$$a_P \bar{v}_i^{n+1/2} = \sum_{nb} a_{nb} \bar{v}^{n+1/2} + S_U - \alpha \Delta t \frac{\partial \bar{p}^{n+1/2}}{\partial x_i} \Delta V$$

where S_U includes all source terms except the implicit pressure. The face velocities $\bar{v}_{f,i}^{n+1/2} = 0.5(\bar{v}_{i,j}^{n+1/2} + \bar{v}_{i,j-1}^{n+1/2})$ (note that j denotes node number and i is a tensor index) do not satisfy continuity. Create an intermediate velocity field by subtracting the implicit pressure gradient from Eq. 18.54, i.e.

$$\bar{v}_i^* = \bar{v}_i^n + \Delta t H \left(\bar{v}^n, \bar{v}_i^{n+1/2} \right) - (1-\alpha) \Delta t \frac{\partial \bar{p}^n}{\partial x_i} \tag{18.55a}$$

$$\Rightarrow \bar{v}_i^* = \bar{v}_i^{n+1/2} + \alpha \Delta t \frac{\partial \bar{p}^{n+1/2}}{\partial x_i} \tag{18.55b}$$

Take the divergence of Eq. 18.55b and require that $\partial \bar{v}_{f,i}^{n+1/2}/\partial x_i = 0$ so that

$$\frac{\partial^2 \bar{p}^{n+1}}{\partial x_i \partial x_i} = \frac{1}{\Delta t \alpha} \frac{\partial \bar{v}_{f,i}^*}{\partial x_i} \tag{18.56}$$

The Poisson equation for $\bar{p}^{n+1}$ is solved with an efficient multigrid method [96]. In the 3D MG we use a plane-by-plane 2D MG. The face velocities are corrected as

$$\bar{v}_{f,i}^{n+1} = \bar{v}_{f,i}^* - \alpha \Delta t \frac{\partial \bar{p}^{n+1}}{\partial x_i} \tag{18.57}$$

A few iterations (typically two) solving the momentum equations and the Poisson pressure equation are required each time step to obtain convergence. More details can be found [97].

1. Solve the discretized filtered Navier-Stokes equation, Eq. 18.55a, for $\bar{v}_1$, $\bar{v}_2$ and $\bar{v}_3$.

2. Create an intermediate velocity field $\bar{v}_i^*$ from Eq. 18.55b.

	RANS	LES
Domain	2D or 3D	always 3D
Time domain	steady or unsteady	always unsteady
Space discretization	2nd order upwind	central differencing
Time discretization	1st order	2nd order (e.g. C-N)
Turbulence model	at least two equations	zero- or one-equation

Table 18.1: Differences between a finite volume RANS and LES code.
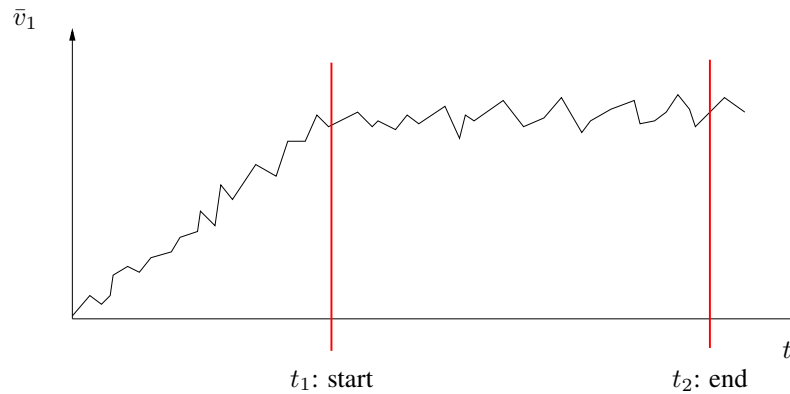
Figure 18.12: Time averaging in LES.

3. Use linear interpolation to obtain the intermediate velocity field, $\bar{v}_{f,i}$, at the face

4. The Poisson equation (Eq. 18.56) is solved with an efficient multigrid method [96].

5. Compute the face velocities (which satisfy continuity) from the pressure and the intermediate face velocity from Eq. 18.57

6. Step 1 to 4 is performed till convergence (normally two or three iterations) is reached.

7. The turbulent viscosity is computed.

8. Next time step.

Since the Poisson solver in [96] is a nested MG solver, it is difficult to parallelize with MPI (Message Passing Interface) on large Linux clusters. Hence, when we do large simulations ($> 20M$ cells) we use a traditional SIMPLE method.

18.20.1 RANS vs. LES

Above a numerical procedure suitable for LES was described. However, in general, any numerical procedure for RANS can also be used for LES; for example pressure-correction methods such as SIMPLE [98, 99] are often used for LES. What are the specific requirements to carry out LES with a finite volume code? If you have a RANS finite volume code, it is very simple to transform that into an LES code. An LES code is actually simpler than a RANS code. Both the discretization scheme and and the turbulence model are simpler in LES than in RANS, see Table 18.1.

It is important to use a non-dissipative discretization scheme which does not introduce any additional numerical dissipation, see Section 18.14; hence a second-order (or higher) central differencing scheme should be employed.

The time discretization should also be non-dissipative. The Crank-Nicolson scheme is suitable.

As mentioned above, turbulence models in LES are simple. There are two reasons: first, only the small-scale turbulence is modeled and, second, no equation for the turbulent length scale is required since the turbulent length scale can be taken as the filter width, Δ.

In LES we are doing unsteady simulations. The question then arises, when can we start to time average and for how long? This is exactly the same question we must ask ourselves whenever doing an experiment in, for example, a windtunnel. We start the windtunnel: when has the flow (and the turbulence) reached fully developed conditions so that we can start to measure the flow? Next question: for how long should we carry out the measurements?

Both in LES and the windtunnel, the recorded time history of the $\bar{v}_1$ velocity at a point may look like in Fig. 18.12. Time averaging can start at time t_1 when the flow seems to have reached fully developed conditions. It is difficult to judge for how long one should carry out time averaging. Usually it is a good idea to form a characteristic time scale from a velocity, V (free-stream or bulk velocity), and a length scale, L (width of a wake or a body, length of a recirculation region), and use this to estimate the required averaging time; 100 time units, i.e. $100L/V$, may be a suitable averaging time for the flow around a bluff body; a value of 10 may be sufficient if L is the length of a recirculation region. The theoretical statistical error varies with number of independent samples, N, as $N^{-1/2}$, see Eq. Q.2 on p. 461.

18.21 One-equation k_{sgs} model

A one-equation model can be used to model the SGS turbulent kinetic energy. The equation can be written on the same form as the RANS k-equation, i.e.

$$\frac{\partial k_{sgs}}{\partial t} + \frac{\partial}{\partial x_j}(\bar{v}_j k_{sgs}) = \frac{\partial}{\partial x_j}\left[(\nu + \nu_{sgs})\frac{\partial k_{sgs}}{\partial x_j}\right] + P_{k_{sgs}} - \varepsilon$$

$$\nu_{sgs} = c_k \Delta k_{sgs}^{1/2}, \quad P_{k_{sgs}} = 2\nu_{sgs}\bar{s}_{ij}\bar{s}_{ij}, \quad \varepsilon = C_\varepsilon \frac{k_{sgs}^{3/2}}{\Delta} \tag{18.58}$$

Note that the production term, $P_{k_{sgs}}$, is equivalent to the SGS dissipation in the equation for the resolved turbulent kinetic energy (look at the flow of kinetic energy discussed at the end of [100]).

18.22 Smagorinsky model derived from the k_{sgs} equation

We can use the one-equation model to derive the Smagorinsky model, Eq. 18.16. The length scale in the Smagorinsky model is the filter width, $\Delta \propto \kappa_{II}^{-1}$, see Fig. 18.13. The cut-off takes place in the inertial subrange where diffusion and convection in the k_{sgs} equation are negligible (their time scales are too large so they have no time to adapt to rapid changes in the velocity gradients, $\bar{s}_{ij}$). Hence, production and dissipation in Eq. 18.58 are in balance so that

$$P_{k_{sgs}} = 2\nu_{sgs}\bar{s}_{ij}\bar{s}_{ij} = \varepsilon \tag{18.59}$$
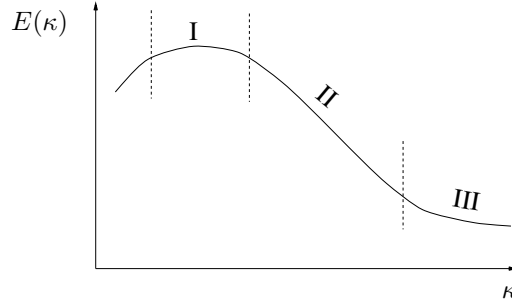
Figure 18.13: Spectrum for k. I: Range for the large, energy containing eddies; II: the inertial subrange for isotropic scales, independent of the large scales (ℓ) and the dissipative scales (ν); III: Range for small, isotropic, dissipative scales.

Let us replace ε by SGS viscosity and Δ. We can write the SGS viscosity as

$$\nu_{sgs} = \varepsilon^a (C_S \Delta)^b \tag{18.60}$$

Dimensional analysis yields $a = 1/3, b = 4/3$ so that

$$\nu_{sgs} = (C_S \Delta)^{4/3} \varepsilon^{1/3}. \tag{18.61}$$

Eq. 18.59 substituted into Eq. 18.61 gives

$$\begin{aligned} \nu_{sgs}^3 &= (C_S \Delta)^4 \varepsilon = (C_S \Delta)^4 \nu_{sgs} (2\bar{s}_{ij}\bar{s}_{ij}) \\ \Rightarrow \nu_{sgs} &= (C_S \Delta)^2 |\bar{s}| \\ |\bar{s}| &= (2\bar{s}_{ij}\bar{s}_{ij})^{1/2} \end{aligned} \tag{18.62}$$

which is the Smagorinsky model.

18.23 A dynamic one-equation model

One of the drawbacks of the dynamic model of [86] (see p. 191) is the numerical instability associated with the negative values and large variation of the C coefficient. Usually this problem is fixed by averaging the coefficient in some homogeneous flow direction. In real applications ad-hoc local smoothing and clipping is used. Below a dynamic one-equation model is presented. The main object when developing this model was that it should be applicable to real industrial flows. Furthermore, being a dynamic model, it has the great advantage that the coefficients are *computed* rather than being prescribed.

The equation for the subgrid kinetic energy reads [101, 102] (see also [103, 104])

$$\begin{aligned} \frac{\partial k_{sgs}}{\partial t} + \frac{\partial}{\partial x_j}(\bar{v}_j k_{sgs}) &= P_{k_{sgs}} + \frac{\partial}{\partial x_j}\left(\nu_{eff}\frac{\partial k_{sgs}}{\partial x_j}\right) - C_* \frac{k_{sgs}^{3/2}}{\Delta} \\ P_{k_{sgs}} &= -\tau_{ij}^a \bar{v}_{i,j}, \ \tau_{ij}^a = -2C\Delta k_{sgs}^{\frac{1}{2}}\bar{s}_{ij} \end{aligned} \tag{18.63}$$

with $\nu_{eff} = \nu + 2C_{hom}\Delta k_{sgs}^{\frac{1}{2}}$. The C in the production term $P_{k_{sgs}}$ is computed dynamically (cf. Eq. 18.41). To ensure numerical stability, a *constant* value (in space) of C (C_{hom}) is used in the diffusion term in Eq. 18.63 and in the momentum equations.

C_{hom} is computed by requiring that C_{hom} should yield the same total production of k_{sgs} as C, i.e.

$$\langle 2C\Delta k_{sgs}^{\frac{1}{2}}\bar{s}_{ij}\bar{s}_{ij}\rangle_{xyz} = 2C_{hom}\langle\Delta k_{sgs}^{\frac{1}{2}}\bar{s}_{ij}\bar{s}_{ij}\rangle_{xyz}$$

The dissipation term $\varepsilon_{k_{sgs}}$ is estimated as:

$$\varepsilon_{k_{sgs}} \equiv \nu\mathcal{T}_f(v_{i,j},v_{i,j}) = C_*\frac{k_{sgs}^{3/2}}{\Delta}. \tag{18.64}$$

Now we want to find a dynamic equation for C_*. The equations for k_{sgs} and K read in symbolic form

$$T(k_{sgs}) \equiv C_{k_{sgs}} - D_{k_{sgs}} = P_{k_{sgs}} - C_*\frac{k_{sgs}^{3/2}}{\Delta}$$
$$T(K) \equiv C_K - D_K = P^K - C_*\frac{K^{3/2}}{\widehat{\Delta}} \tag{18.65}$$

Since the turbulence on both the grid level and the test level should be in local equilibrium (in the inertial $-5/3$ region), the left-hand side of the two equations in Eq. 18.65 should be close to zero. An even better approximation should be to assume $T(k_{sgs}) = T(K)$, i.e.

$$\widehat{P}_{k_{sgs}} - \frac{1}{\Delta}\widehat{C_*k_{sgs}}^{3/2} = P^K - C_*\frac{K^{3/2}}{\widehat{\Delta}},$$

so that

$$C_*^{n+1} = \left(P^K - \widehat{P}_{k_{sgs}} + \frac{1}{\Delta}\widehat{C_*^n k_{sgs}^{3/2}}\right)\frac{\widehat{\Delta}}{K^{\frac{3}{2}}}. \tag{18.66}$$

The idea is to put the local dynamic coefficients in the source terms, i.e. in the production and the dissipation terms of the k_{sgs} equation (Eq. 18.63). In this way the dynamic coefficients C and C_* don't need to be clipped or averaged in any way. This is a big advantage compared to the standard dynamic model of Germano (see discussion on p. 194).

18.24   A Mixed Model Based on a One-Eq. Model

Recently a new dynamic scale-similarity model was presented by [105]. In this model a dynamic one-equation SGS model is solved, and the scale-similarity part is estimated in a similar way as in Eq. 18.49.

18.25   Applied LES

At the Department we used LES for applied flows such as flow around a cube [106, 107], the flow and heat transfer in a square rotating duct [108, 109], the flow around a simplified bus [107, 110], a simplified car [111–113] and the flow around an airfoil [114, 115], detailed SUV [116], trains and buses subjected to sidewinds and wind gusts [117–119]. We have also done some work on buoyancy-affected flows [120–126].
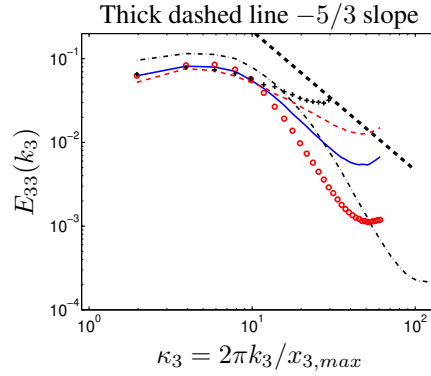
Figure 18.14: Energy spectra in fully developed channel flow [128]. δ denotes half channel width. Number of cells expressed as $(\delta/\Delta x_1, \delta/\Delta x_3)$. ——— : $(10, 20)$; — — : $(20, 20)$; — · — : $(10, 40)$; ○: $(5, 20)$; +: $(10, 10)$.

18.26 Resolution requirements

The near-wall grid spacing should be about one wall unit in the wall-normal direction. This is similar to the requirement in RANS (Reynolds-Averaged Navier-Stokes) using low-Re number models. The resolution requirements in wall-parallel planes for a well-resolved LES in the near-wall region expressed in wall units are approximately

$$x_1^+ \lesssim 100 \text{ (streamwise) and } x_3^+ \lesssim 30 \text{(spanwise)} \tag{18.67}$$

and, of course, $x_2^+ < 1$. This enables resolution of the near-wall turbulent structures in the viscous sub-layer and the buffer layer consisting of high-speed in-rushes and low-speed ejections [127], often called the streak process. At low to medium Reynolds numbers the streak process is responsible for the major part of the turbulence production. These structures must be resolved in an LES in order to achieve accurate results. Then the spectra of the resolved turbulence will exhibit $-5/3$ range, see figure on p. 73.

In applied LES, this kind of resolution can hardly ever be afforded. In outer scaling (i.e. comparing the resolution to the boundary layer thickness, δ), we can afford

$$\delta/\Delta x_1 = 10 - 20 \text{ and} \delta/\Delta x_3 = 29 - 40 \tag{18.68}$$

and, of course, $x_2^+ < 1$. This resolution requirement is relevant in the log-region. You can investigate if this requirement is satisfied for the flow over a hump in an Assignment in Section T.7.

The spectra in the log region will look something like that shown in Fig. 18.14 [128]. Energy spectra are actually not very reliable to judge if a LES simulation is well resolved or not. In [128, 129] different ways to estimate the resolution of an LES were investigated. The suggestion in these works is to use the ratio of integral lengthscale to cell size (if the ratio is larger than, say, 16, the resolution is sufficient). The integral lengthscale is computed from two-point correlations is the best way to estimate if an LES is sufficiently resolved or not. Two-point correlations to estimate resolution are evaluated in an Assignment, see Section T.7.2.

Even if the turbulence in boundary layer seldom can be resolved, the flow in recirculation regions and shear layer can. In [130] the flow ($Re \simeq 10^6$) over a bump was computed. The geometry is shown in Fig. 18.15. The turbulence in the boundary layer on the bump was very poorly resolved: $\Delta x_1/\delta_{in} = 0.33$, $\Delta x_3/\delta_{in} = 0.44$,
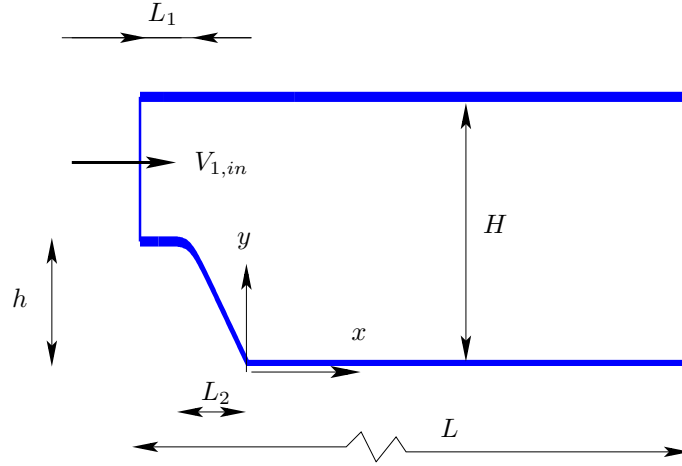
Figure 18.15: Onera bump. Computational domain (not to scale).
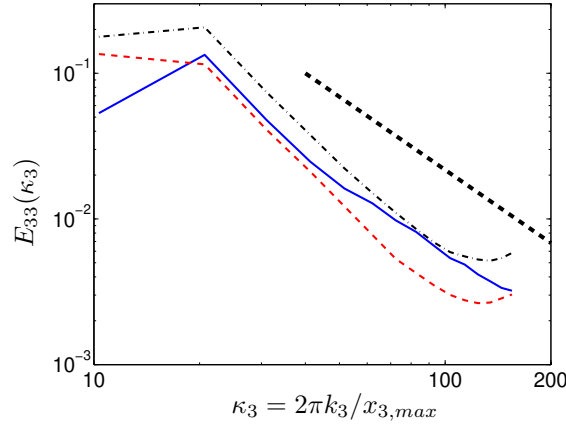
Figure 18.16: Energy spectra $E_{33}(\kappa_3)$ in the recirculation region and the shear layer downstream the bump ($x_1/H = 1.2$). Thick dashed line shows $-5/3$ slope. ——— : $x_2/H = 0.0035$ (near the wall); $\mathbf{-\ -}$: $x_2/H = 0.13$; $\mathbf{-\ \cdot\ -}$: $x_2/H = 0.34$ (in the shear layer).

$\Delta x_1^+ = 1300$ and $\Delta x_3^+ = 1800$. Nevertheless, the turbulence in the recirculation region and in the shear layer downstream the bump turned out to be well resolved, see Fig. 18.16.

For wall-bounded flows at high Reynolds numbers of engineering interest, the computational resource requirement of accurate LES is prohibitively large. Indeed, the requirement of near-wall grid resolution is the main reason why LES is too expensive for engineering flows, which was one of the lessons learned in the LESFOIL project [131, 132].

19 URANS: Unsteady RANS

To perform an accurate LES, a very fine mesh must be used. This causes problems, for example, near walls. LES is very good for wake flow, where the flow is governed by large, turbulent structures, which can be captured by a fairly coarse mesh. However, if attached boundary layers are important, LES will probably give poor predictions in these regions, unless fine grids are used.

An alternative to LES for industrial flows can be **unsteady** RANS (Reynolds-Averaged Navier-Stokes), often denoted **URANS** (Unsteady RANS). In URANS the usual Reynolds decomposition is employed, i.e.

$$\bar{v}(t) = \frac{1}{2T} \int_{t-T}^{t+T} v(t) dt, \; v = \bar{v} + v'' \tag{19.1}$$

The URANS equations are the usual RANS equations, but with the transient (unsteady) term retained; on incompressible form they read

$$\frac{\partial \bar{v}_i}{\partial t} + \frac{\partial}{\partial x_j}(\bar{v}_i \bar{v}_j) = -\frac{1}{\rho}\frac{\partial \bar{p}}{\partial x_i} + \nu \frac{\partial^2 \bar{v}_i}{\partial x_j \partial x_j} - \frac{\partial \overline{v_i'' v_j''}}{\partial x_j}$$
$$\frac{\partial \bar{v}_i}{\partial x_i} = 0 \tag{19.2}$$

Note that the dependent variables are now not only function of the space coordinates, but also function of time, i.e. $\bar{v}_i = \bar{v}_i(x_1, x_2, x_3, t)$, $\bar{p} = \bar{p}(x_1, x_2, x_3, t)$ and $\overline{v_i'' v_j''} = \overline{v_i'' v_j''}(x_1, x_2, x_3, t)$.

Even if the results from URANS are unsteady, one is often interested only in the time-averaged flow. We denote here the time-averaged velocity as $\langle \bar{v} \rangle$, which means that we can decompose the results from an URANS as a time-averaged part, $\langle \bar{v} \rangle$, a resolved fluctuation, $\bar{v}'$, and the modeled, turbulent fluctuation, v'', i.e.

$$v = \bar{v} + v'' = \langle \bar{v} \rangle + \bar{v}' + v'' \tag{19.3}$$

see Fig. 19.1. The modeled turbulent fluctuation, v'', is not shown in the figure; when this is added to $\langle \bar{v} \rangle + \bar{v}'$ we obtain v.

What type of turbulence model should be used in URANS? That depends on type of flow. If the flow has strong vortex shedding, the standard high-Re number $k - \varepsilon$
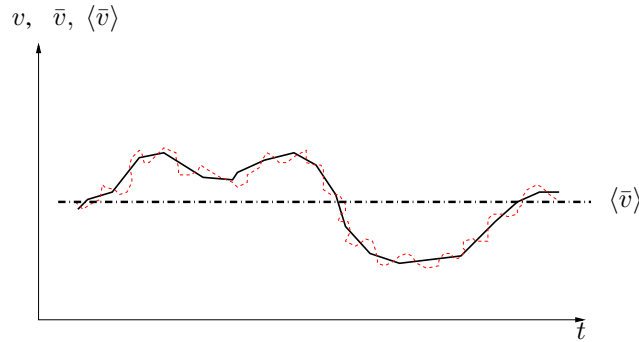
Figure 19.1: Decomposition of velocities in URANS. ▬▬ : $\bar{v}$; ▬ ▬ : v; ▬ · ▬ $\langle \bar{v} \rangle$.

model can be used, i.e.

$$\frac{\partial \rho k}{\partial t} + \frac{\partial \rho \bar{v}_j k}{\partial x_j} = \frac{\partial}{\partial x_j} \left[\left(\mu + \frac{\mu_t}{\sigma_k} \right) \frac{\partial k}{\partial x_j} \right] + P^k - \rho \varepsilon \tag{19.4}$$

$$\frac{\partial \rho \varepsilon}{\partial t} + \frac{\partial \rho \bar{v}_j \varepsilon}{\partial x_j} = \frac{\partial}{\partial x_j} \left[\left(\mu + \frac{\mu_t}{\sigma_\varepsilon} \right) \frac{\partial \varepsilon}{\partial x_j} \right] + \frac{\varepsilon}{k} \left(c_{1\varepsilon} P^k - c_{\varepsilon 2} \rho \varepsilon \right) \tag{19.5}$$

$$\mu_t = c_\mu \rho \frac{k^2}{\varepsilon} \tag{19.6}$$

With an eddy-viscosity, the URANS equations read

$$\frac{\partial \rho \bar{v}_i}{\partial t} + \frac{\partial \rho \bar{v}_i \bar{v}_k}{\partial x_k} = -\frac{\partial \bar{p}}{\partial x_i} + \frac{\partial}{\partial x_k} \left[(\mu + \mu_t) \frac{\partial \bar{v}_i}{\partial x_k} \right] \tag{19.7}$$

Usually the standard $k - \varepsilon$ model is not a good URANS model because it gives too much modeled dissipation (i.e. too large turbulent viscosity), which dampens the resolved fluctuations too much. The V2F and non-linear eddy-viscosity models are better.

So we are doing unsteady simulations, but still we time average the equations. How is this possible? The theoretical answer is that the time, T, in Eq. 19.1 should be much smaller than the resolved time scale, i.e. the modeled turbulent fluctuations, v'', should have a much smaller time scale than the resolved ones, $\bar{v}'$. This is called *scale separation*. In practice this requirement is often not satisfied [97]. On the other hand, how do the momentum equation, Eq. 19.7, know how they were time averaged? Or if they were volume filtered? The answer is that they don't. The URANS momentum equation and the LES momentum equation are exactly the same, except that we denote the turbulent viscosity in the former case by ν_t and in the latter case by ν_{sgs}. In URANS, much more of the turbulence is modeled than in LES, and, hence, the turbulent viscosity, ν_t, is much larger than the SGS viscosity, ν_{sgs}.

The common definition of URANS is that the turbulent length scale is not determined by the grid, whereas in LES it is. In URANS we do usually not care about scale separation. What we care about is that the turbulence model and the discretization scheme should not be too dissipative, i.e. they should not kill the resolved fluctuations, $\bar{v}'$.

The standard $k - \varepsilon$ model (Eq. 19.4 and 19.5) was used in [133] for two-dimensional URANS simulations computing the flow around a triangular flame-holder in a channel, see Fig. 19.2. This flow has a very regular vortex shedding. and the flow actually has a scale separation. In Fig. 19.3 the $\bar{v}_2$ velocity in a point above the flame-holder is shown and it can be seen that the velocity varies with time in a sinusoidal manner.

When we're doing URANS, the question arises how the results should be time averaged, i.e. when should we start to average and for how long. This issue is the same when doing LES, and this was discussed in connection to Fig. 18.12.

19.1 Turbulence Modeling

In URANS, part of the turbulence is modeled (v'') and part of the turbulence is resolved ($\bar{v}'$). If we want to compare computed turbulence with experimental turbulence, we must add these two parts together. Profiles downstream the flameholder are shown in Fig. 19.4. It can be seen that here the resolved and the modeled turbulence are of the same magnitude.
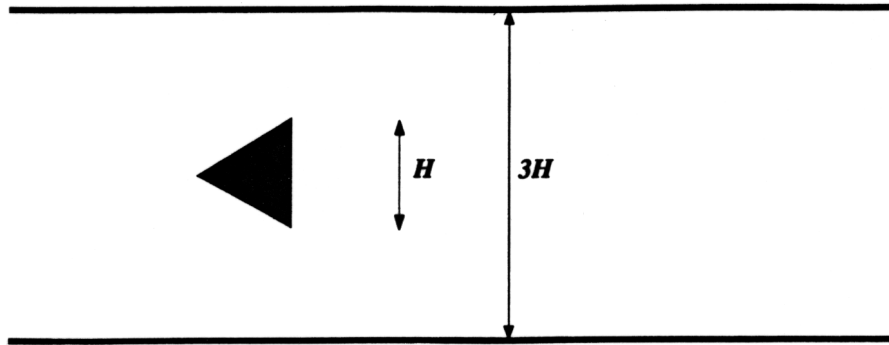
Figure 19.2: Configuration of the flow past a triangular flameholder. Flow from left to right
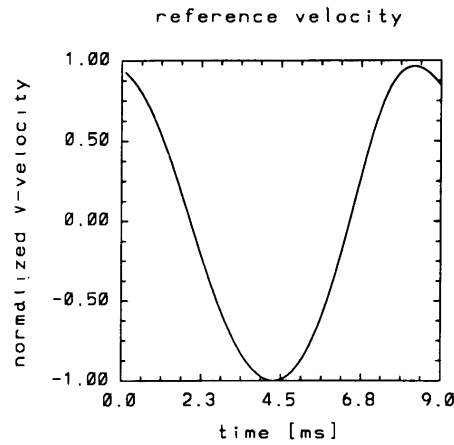
Figure 19.3: 2D URANS $k - \varepsilon$ simulations [133]. One cycle of the $\bar{v}_2$ velocity in a cell near the upper-right corner of the flameholder.

If the turbulence model in URANS generates "too much" eddy viscosity, the flow may not become unsteady at all, because the unsteadiness is dampened out; the reason for this is that the turbulence model is too dissipative. It was found in [134, 135] when using URANS for the flow around a surface-mounted cube and around a car, that the standard $k - \varepsilon$ model was too dissipative. Non-linear models like that of [136] was found to be less dissipative, and was successfully applied in URANS-simulations for these two flows.

19.2 Discretization

In LES it is well-known that non-dissipative discretization schemes should be used. The reason is that we don't want to dampen out resolved, turbulent fluctuations. This is to some extent true also for URANS. In the predictions on the flame-holder presented above, the hybrid discretization scheme for the convective terms was used together
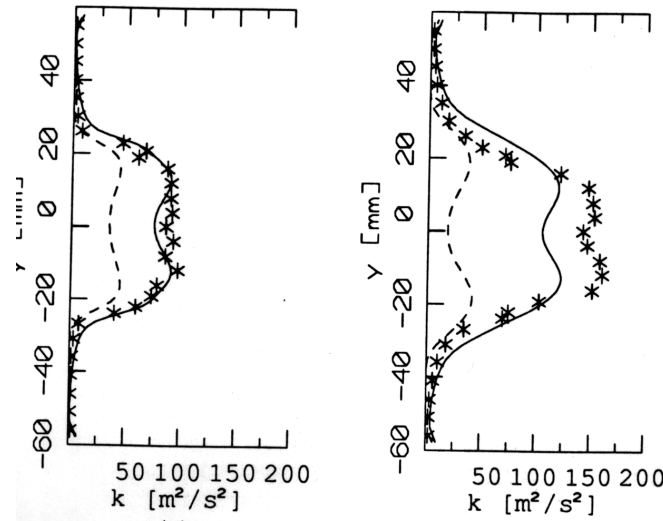
Figure 19.4: 2D URANS $k - \varepsilon$ simulations compared with experiment [133]. Solid lines: total turbulent kinetic energy; dashed lines: resolved turbulent kinetic energy: $*$: experimental data. Left figure: $x = 0.43H$; right figure: $x = 1.1H$ ($x = 0$ at the downstream vertical plane of the flame-holder).

with fully implicit first-order discretization in time; this gives first-order accuracy in both space and time. The turbulence model that was used was the standard $k - \varepsilon$ model. Thus, both the discretization and the turbulence model have high dissipation. The reason why the unsteadiness in these computations was not dampened out is that the vortex shedding in this flow is very strong.

In general, a discretization scheme which has little numerical dissipation should be used. How dissipative a scheme needs to be in order to be stable is flow dependent; for some simple flows, it may work with no dissipation at all (i.e. central differencing), whereas for industrially complex flows maybe a bounded second-order scheme must be used. For time discretization, the second-order accurate Crank-Nicolson works in most cases.

In [134] LES and URANS simulations were carried out of the flow around a surface-mounted cube (Fig. 19.5) with a coarse mesh using wall-functions. Two different discretization schemes were used: the central scheme and the Mars scheme (a blend between central differencing and a bounded upwind scheme of second-order accuracy). In Fig. 19.6 the time-averaged velocity profile upstream of the cube ($x_1 = -0.6H$) using URANS and LES with central differencing are shown together with URANS and the Mars scheme. It is seen that with LES and central differencing nonphysical oscillations are present (this was also found in [106]). However, LES with the Mars scheme (in which some numerical dissipation is present) and URANS with the central scheme (where the modeling dissipation is larger than in LES) no such nonphysical oscillations are present. The main reason to the nonphysical oscillations is that the predicted flow in this region does not have any resolved fluctuations. If turbulent unsteady inlet fluctuations are used, the nonphysical oscillations do usually not appear, even if a central differencing scheme is used. In this case the turbulent, resolved fluctuations dominate over any numerical oscillations.
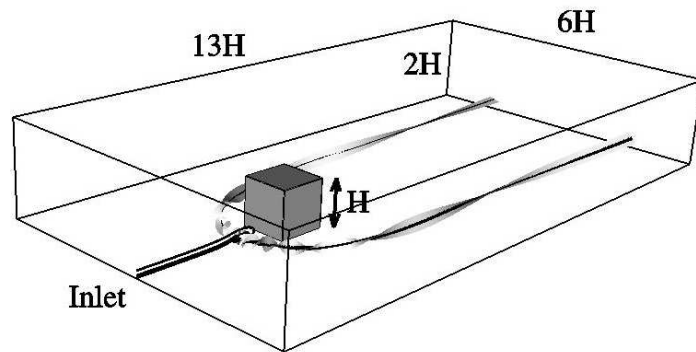
Figure 19.5: URANS simulations of the flow around a surface-mounted cube.
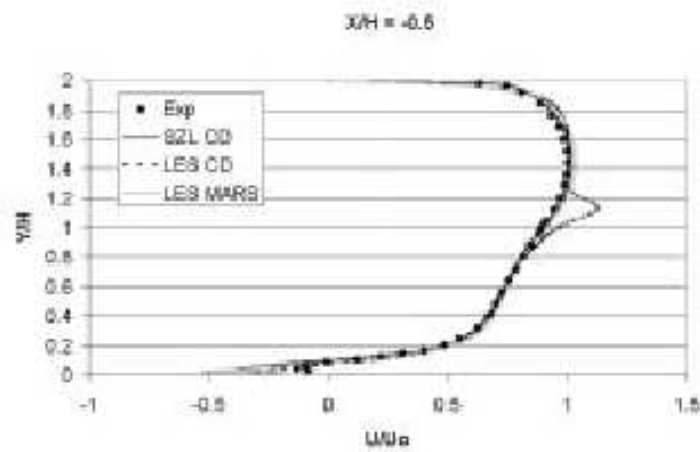
Figure 19.6: URANS simulations of the flow around a surface-mounted cube. Velocity profiles upstream the cube [134].

20 DES: Detached-Eddy-Simulations

D ES (Detached Eddy Simulation) is a mix of LES and URANS. The aim is to treat the boundary layer with RANS and capture the outer detached eddies with LES. Since the flow in the boundary layer will be strongly influenced by the unsteady LES in the outer region, the flow in the boundary layer will also be unsteady. Hence the boundary layer is treated with unsteady RANS (URANS). The DES was originally developed for wings at very high angles of attack.

The RANS model that was originally used was the one-equation model proposed in [137]. It can be written [131, 137, Sect. 4.6]

$$\frac{\partial \rho \tilde{\nu}_t}{\partial t} + \frac{\partial \rho \bar{v}_j \tilde{\nu}_t}{\partial x_j} = \frac{\partial}{\partial x_j} \left(\frac{\mu + \mu_t}{\sigma_{\tilde{\nu}_t}} \frac{\partial \tilde{\nu}_t}{\partial x_j} \right) + \frac{C_{b2} \rho}{\sigma_{\tilde{\nu}_t}} \frac{\partial \tilde{\nu}_t}{\partial x_j} \frac{\partial \tilde{\nu}_t}{\partial x_j} + P - \Psi \tag{20.1}$$
$$\nu_t = \tilde{\nu}_t f_1$$

The production term P and the destruction term Ψ have the form

$$P = C_{b1} \rho \left(\bar{s} + \frac{\tilde{\nu}_t}{\kappa^2 d^2} f_2 \right) \tilde{\nu}_t$$
$$\bar{s} = (2 \bar{s}_{ij} \bar{s}_{ij})^{1/2}, \quad \Psi = C_{w1} \rho f_w \left(\frac{\tilde{\nu}_t}{d} \right)^2 \tag{20.2}$$

d in the RANS SA model is equal to the distance to the nearest wall.

In DES [138], d is taken as the minimum of the RANS turbulent length scale d and the cell length $\Delta = \max(\Delta x_\xi, \Delta x_\eta, \Delta x_\zeta)$, i.e.

$$\tilde{d} = \min(d, C_{des} \Delta). \tag{20.3}$$

Δx_ξ, Δx_η and Δx_ζ denote the cell length in the three grid directions ξ, η and ζ. The constant C_{des} is usually set to 0.65.

In the boundary layer $d < C_{des} \Delta$ and thus the model operates in RANS mode. Outside the turbulent boundary layer $d > C_{des} \Delta$ so that the model operates in LES mode. The modeled length scale is reduced and the consequence is that the destruction term Ψ increases, which gives a reduction in the turbulent viscosity $\tilde{\nu}_t$. A reduced $\tilde{\nu}_t$ gives a smaller production term P so that the turbulent viscosity is further reduced.

At first sight it may seem that as the model switches from RANS mode to LES mode thus reducing d, this would give rise to an increased production term P through the second term (see Eq. 20.2). However, this second term is a viscous term and is active only close to the wall. This term is sometimes neglected [139].

20.1 DES based on two-equation models

The model described above is a one-equation model. In RANS mode it takes its length scale from the wall distance, which in many situations is not a relevant turbulent length scale. Recently, DES models based on two-equation models were proposed [140–142]. In these models the turbulent length scale is either obtained from the two turbulent quantities (e.g. $k^{3/2}/\varepsilon$ or $k^{1/2}/\omega$) or the filter width Δ. A model based on the $k - \varepsilon$

model can read

$$\frac{\partial k}{\partial t} + \frac{\partial}{\partial x_j}(\bar{v}_j k) = \frac{\partial}{\partial x_j}\left[\left(\nu + \frac{\nu_t}{\sigma_k}\right)\frac{\partial k}{\partial x_j}\right] + P^k - \varepsilon_T$$

$$\frac{\partial \varepsilon}{\partial t} + \frac{\partial}{\partial x_j}(\bar{v}_j \varepsilon) = \frac{\partial}{\partial x_j}\left[\left(\nu + \frac{\nu_t}{\sigma_\varepsilon}\right)\frac{\partial \varepsilon}{\partial x_j}\right] + \frac{\varepsilon}{k}(C_1 P^k - C_2 \varepsilon)$$

$$P^k = 2\nu_t \bar{s}_{ij}\bar{s}_{ij}, \quad \nu_t = k^{1/2}\ell_t$$

The turbulent length scale, ℓ_t, and the turbulent dissipation, ε_T, are computed as [142, 143]

$$\ell_t = \min\left(C_\mu \frac{k^{3/2}}{\varepsilon}, C_{DES}\Delta\right)$$

$$\varepsilon_T = \max\left(\varepsilon, C_\varepsilon \frac{k^{3/2}}{\Delta}\right)$$

(20.4)

In other models [79, 140] only the dissipation term, ε_T is modified. When the grid is sufficiently fine, the length scale is taken as Δ. The result is that the dissipation in the k equation increases so that k decreases which gives a reduced ν_t. In regions where the turbulent length scales are taken from Δ (LES mode) the ε-equation is still solved, but ε is not used. However, ε is needed as soon as the model switches to RANS model again. A third alternative is to modify only the turbulent length scale appearing in the turbulent viscosity [143].

A rather new approach is to reduce the destruction term in the ε equation as in PANS [144, 145] (Partially Averaged Navier-Stokes, see Section 23) and PITM [146] (Partially Integrated Transport Modeling, see Section 24). In these models ε increases because of its reduced destruction term which decreases both k and ν_t. A low-Reynolds number PANS was recently proposed [145] in which the near-wall modifications were taken from the AKN model [47]. In [147] different ways of treating the interface between the URANS and LES regions were evaluated.

In the RANS mode the major part of the turbulence is modeled. When the model switches to LES mode, the turbulence is supposed to be represented by resolved turbulence. This poses a major problem with this type of models. If the switch occurs at location x_1, say, it will take some distance L before the momentum equations start to resolve any turbulence. This is exactly what happens at an inlet in an LES simulation if no real turbulence is given as inlet boundary conditions. One way to get around this is to impose turbulence fluctuations as forcing conditions [100, 148–151] at the location where the model switches from RANS mode to LES mode. The forcing is added in the form of a source term (per unit volume) in the momentum equations.

20.2 DES based on the $k - \omega$ SST model

The standard $k - \omega$ model SST reads [73, 79]

$$\frac{\partial k}{\partial t} + \frac{\partial}{\partial x_j}(\bar{v}_j k) = \frac{\partial}{\partial x_j}\left[\left(\nu + \frac{\nu_t}{\sigma_k}\right)\frac{\partial k}{\partial x_j}\right] + P^k - \beta^* k\omega$$

$$\frac{\partial \omega}{\partial t} + \frac{\partial}{\partial x_j}(\bar{v}_j \omega) = \frac{\partial}{\partial x_j}\left[\left(\nu + \frac{\nu_t}{\sigma_\omega}\right)\frac{\partial \omega}{\partial x_j}\right] + \alpha\frac{P^k}{\nu_t} - \beta\omega^2$$

$$+ 2(1 - F_1)\sigma_{\omega 2}\frac{1}{\omega}\frac{\partial k}{\partial x_i}\frac{\partial \omega}{\partial x_i}$$

$$F_1 = \tanh(\xi^4), \quad \xi = \min\left[\max\left\{\frac{\sqrt{k}}{\beta^* \omega d}, \frac{500\nu}{d^2\omega}\right\}\frac{4\sigma_{\omega_{k-\varepsilon}}k}{CD_\omega d^2}\right] \quad (20.5)$$

$$CD_\omega = \max\left\{2\sigma_{\omega_{k-\varepsilon}}\frac{1}{\omega}\frac{\partial k}{\partial x_i}\frac{\partial \omega}{\partial x_i}, 10^{-10}\right\}$$

$$\nu_t = \frac{a_1 k}{\max(a_1\omega, |\bar{s}|F_2)}$$

$$F_2 = \tanh(\eta^2), \quad \eta = \max\left\{\frac{2k^{1/2}}{\beta^* \omega d}, \frac{500\nu}{d^2\omega}\right\}$$

where d is the distance to the closest wall node. The SST model behaves as a $k - \omega$ model near the wall where $F_1 = 1$ and a $k - \varepsilon$ model far from walls ($F_1 = 0$). All coefficients are blended between the $k - \omega$ and the $k - \varepsilon$ model using the function F_1, for α, for example,

$$\alpha = F_1\alpha_{k-\omega} + (1 - F_1)\alpha_{k-\varepsilon} \quad (20.6)$$

The constants take the following values:

$$\beta^* = 0.09, \quad a_1 = 0.3$$

$$\alpha_{k-\omega} = 5/9, \quad \beta_{k-\omega} = 3/40, \quad \sigma_{k,k-\omega} = 0.85, \quad \sigma_{\omega,k-\omega} = 0.5 \quad (20.7)$$

$$\alpha_{k-\varepsilon} = 0.44, \quad \beta_{k-\varepsilon} = 0.0828, \quad \sigma_{k,k-\varepsilon} = 1, \quad \sigma_{\omega,k-\varepsilon} = 0.856.$$

In DES the dissipation term in the k equation is modified as [79]

$$\beta^* k\omega \to \beta^* k\omega F_{DES}, \quad F_{DES} = \max\left\{\frac{L_t}{C_{DES}\Delta}, 1\right\} = \max\left\{\frac{k^{1/2}}{C_{DES}\beta^*\Delta\omega}, 1\right\}$$

$$\Delta = \max\left\{\Delta x_1, \Delta x_2, \Delta x_3\right\}, \quad L_t = \frac{k^{1/2}}{\beta^*\omega}$$

$$(20.8)$$

where $C_{DES} = 0.61$.

Again, the DES modification is meant to switch the turbulent length scale from a RANS length scale ($\propto k^{1/2}/\omega$) to a LES length scale ($\propto \Delta$) when the grid is sufficiently fine. When F_{DES} is larger than one, the dissipation term in the k equation increases which in turn decreases k and thereby also the turbulent viscosity. With a smaller turbulent viscosity in the momentum equations, the modeled dissipation (i.e the damping) is reduced and the flow is induced to go unsteady. The result is, hopefully, that a large part of the turbulence is resolved rather than being modeled.

Equation 20.8 shows that it is the grid that determines the location where the model switches between RANS and LES. Hence it is crucial to generate an appropriate grid. The larger the maximum cell size (usually Δx or Δz) is made, the further out from the wall does the switch take place.
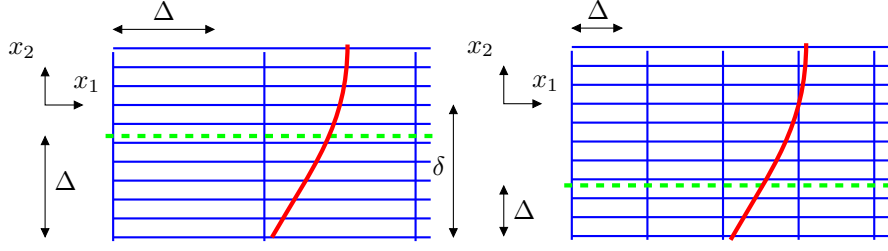
Figure 20.1: Grid (in blue) and a velocity profile (in red). RANS-LES interface is shown by the dashed-green line.

20.3   DDES

In some flows it may occur that the F_{DES} term switches to LES in the boundary layer because Δx or Δz (Δx_1 or Δx_3) are too small (smaller than the boundary layer thickness, δ). This means that the flow in the boundary layer is treated in LES mode with too a coarse mesh. This results in a poorly resolved LES and hence inaccurate predictions. Two grids are shown in Fig. 20.1. The grid on the left is a good DES mesh. Here $\Delta = C_{DES}\Delta x_1$ (assuming $\Delta x_3 < \Delta x_1$) is proportional to the boundary layer thickness, δ. The grid on the right is refined in the x_1 direction. The result is that $\Delta < \delta$ and hence the outer part of the boundary layer is in LES mode. If the resolution in the spanwise and streamwise direction does not satisfy the requirements for LES resolution (see Eq. 18.68), the predictions will be inaccurate due to a poorly resolved LES region.

Different proposals have been made [152, 153] to *protect* the boundary layer from the LES mode

$$F_{DDES} = \max\left\{\frac{L_t}{C_{DES}\Delta}(1 - F_S), 1\right\} \tag{20.9}$$

where F_S is taken as F_1 or F_2 (see Eqs. 16.12 and 16.18) of the SST model. In [79] $F = F_2$. This is called DDES (Delayed DES).

21 Hybrid LES-RANS

W HEN simulating bluff body flows, LES (Large Eddy Simulation) is the ideal method. Bluff body flows are dominated by large turbulent scales that can be resolved by LES without too fine a resolution and accurate results can thus be obtained at an affordable cost. On the other hand, it is a challenging task to make accurate predictions of wall-bounded flows with LES. The near-wall grid spacing should be about one wall unit in the wall-normal direction. This is similar to the requirement in RANS using low-Re number models. The resolution requirements in wall-parallel planes for a well-resolved LES in the near-wall region expressed in wall units are approximately 100 (streamwise) and 30 (spanwise). This enables resolution of the near-wall turbulent structures in the viscous sub-layer and the buffer layer consisting of high-speed in-rushes and low-speed ejections [127], often called the streak process.

An event of a high-speed in-rush is illustrated in Fig. 21.1. In the lower part of the figure the spanwise vortex line is shown. Initially it is a straight line, but due to a disturbance – e.g. a turbulent fluctuation – the mid-part of the vortex line is somewhat lifted up away from the wall. The mid-part of the vortex line experiences now a higher $\bar{v}_1$ velocity (denoted by U in the figure) than the remaining part of the vortex line. As a result the mid-part is lifted up even more and a tip of a hairpin vortex is formed. The vorticity of the legs of the hairpin lift each other through self-induction which helps lifting the tip even more. In the $x_1 - x_2$ plane (upper part of Fig. 21.1) the instantaneous and mean velocity profiles (denoted by U and $\bar{U}$ in the figure, respectively) are shown as the hairpin vortex is created. It can be seen that an inflection point is created in the instantaneous velocity profile, U, and the momentum deficit in the inner layer increases for increasing x_1. Eventually the momentum deficit becomes too large and the high-speed fluid rushes in compensating for the momentum deficit. The in-rush event is also called a *sweep*. There are also events which occurs in the other direction, i.e. low-speed fluid is ejected away from the wall. These events are called *bursts* or *ejections*. The spanwise separation between sweeps and bursts is very small (approximately 100 viscous units, see Fig. 21.1). This is the main reason why the grid must be very fine in the spanwise direction. The streamwise distance between the events is related to the boundary layer thickness (4δ, see Fig. 21.1). The process by which the events are formed is similar to the later stage in the transition process from laminar to turbulent flow. Figure 21.2 presents the instantaneous field of the streamwise velocity fluctuation, v_1' in the viscous wall region. As can be seen, the turbulent structures very elongated in the streamwise direction.

At low to medium Reynolds numbers the streak process is responsible for the major part of the turbulence production. These structures must be resolved in an LES in order to achieve accurate results. Thus, for wall-bounded flows at high Reynolds numbers of engineering interest, the computational resource requirement of accurate LES is prohibitively large. Indeed, the requirement of near-wall grid resolution is the main reason why LES is too expensive for engineering flows, which was one of the lessons learned in the LESFOIL project [131, 132].

The object of hybrid LES-RANS (and of DES) is to eliminate the requirement of high near-wall resolution in wall-parallel planes. In the near-wall region (the URANS region), a low-Re number RANS turbulence model (usually an eddy-viscosity model) is used. In the outer region (the LES region), the usual LES is used, see Fig. 21.3. The idea is that the effect of the near-wall turbulent structures should be modeled by the RANS turbulence model rather than being resolved. In the LES region, coarser
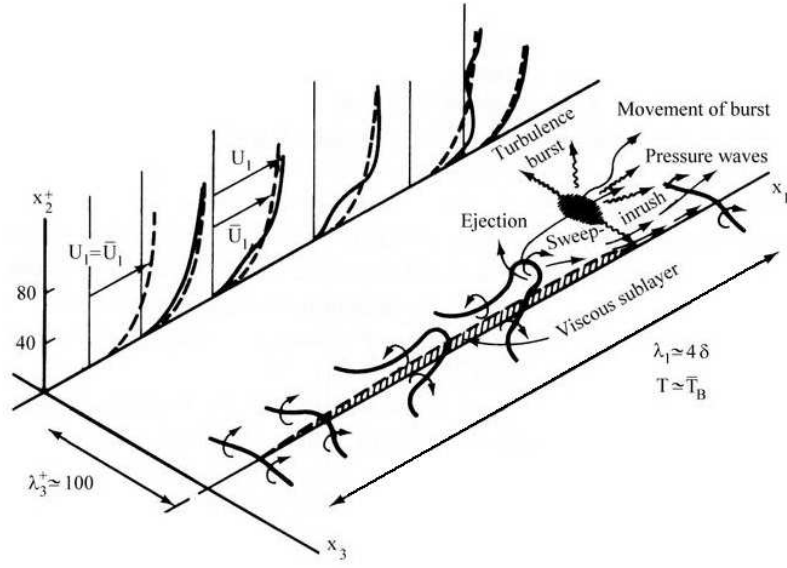
Figure 21.1: Illustration of near-wall turbulence (taken from [84]).
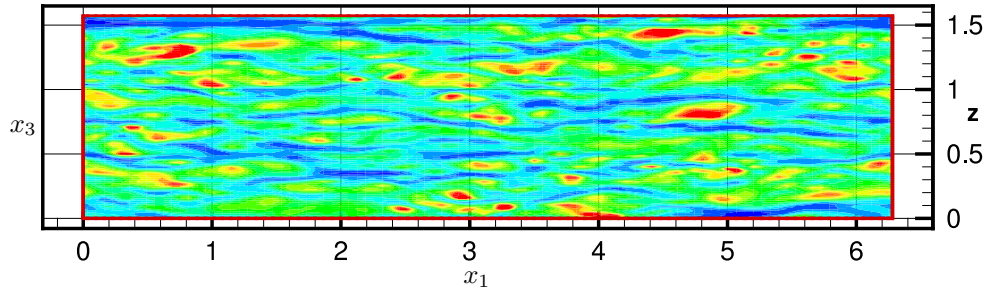
Figure 21.2: Fluctuating streamwise velocity in a wall-parallel plane at $x_2^+ = 5$. DNS of channel flow [100].
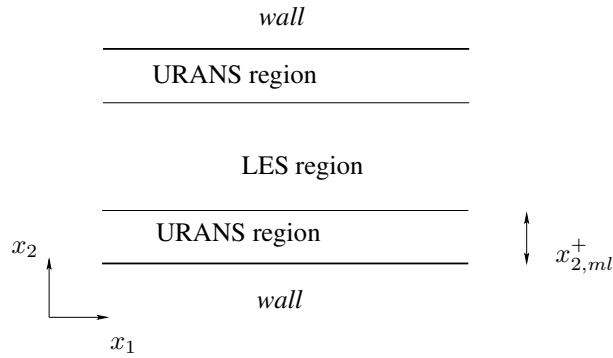
Figure 21.3: The LES and URANS region.

grid spacing in wall-parallel planes can be used. The grid resolution in this region is

	URANS region	LES region
ℓ	$\kappa c_\mu^{-3/4} n [1 - \exp(-0.2 k^{1/2} n/\nu)]$	$\ell = \Delta$
ν_T	$\kappa c_\mu^{1/4} k^{1/2} n [1 - \exp(-0.014 k^{1/2} n/\nu)]$	$0.07 k^{1/2} \ell$
C_ε	1.0	1.05

Table 21.1: Turbulent viscosity and turbulent length scales in the URANS and LES regions. n and κ denote the distance to the nearest wall and von Kármán constant ($= 0.41$), respectively. $\Delta = (\delta V)^{1/3}$

.

presumably dictated by the requirement of resolving the largest turbulent scales in the flow (which are related to the outer length scales, e.g. the boundary layer thickness) rather than the near-wall turbulent processes. The unsteady momentum equations are solved throughout the computational domain. The turbulent RANS viscosity is used in the URANS region, and the turbulent SGS viscosity is used in the LES region.

Hybrid LES-RANS is similar to DES (Detached Eddy Simulations) [138, 153, 154]. The main difference is that the original DES aims at covering the whole attached boundary layer with URANS, whereas hybrid LES-RANS aims at covering only the inner part of the boundary layer with URANS. In later work DES has been used as a wall model [149, 155] – called wall-modelled LES – and, in this form, DES is similar hybrid LES-RANS.

21.1 Momentum equations in hybrid LES-RANS

The incompressible Navier-Stokes equations with an added turbulent/SGS viscosity read

$$\frac{\partial \bar{v}_i}{\partial t} + \frac{\partial}{\partial x_j}(\bar{v}_i \bar{v}_j) = -\frac{1}{\rho}\frac{\partial \bar{p}}{\partial x_i} + \frac{\partial}{\partial x_j}\left[(\nu + \nu_T)\frac{\partial \bar{v}_i}{\partial x_j}\right] \qquad (21.1)$$

where $\nu_T = \nu_t$ (ν_t denotes the turbulent RANS viscosity) for $x_2 \leq x_{2,ml}$ (the URANS region, see Fig. 21.3) and, for $x_2 > x_{2,ml}$ (the LES region), $\nu_T = \nu_{sgs}$.

21.2 The one-equation hybrid LES-RANS model

When a one-equation model is employed in both the URANS region and the LES region, it reads

$$\frac{\partial k_T}{\partial t} + \frac{\partial}{\partial x_j}(\bar{v}_j k_T) = \frac{\partial}{\partial x_j}\left[(\nu + \nu_T)\frac{\partial k_T}{\partial x_j}\right] + P_{k_T} - C_\varepsilon \frac{k_T^{3/2}}{\ell} \qquad (21.2)$$

$$P_{k_T} = -\tau_{ij}\bar{s}_{ij}, \quad \tau_{ij} = -2\nu_T \bar{s}_{ij}$$

In the inner region ($x_2 \leq x_{2,ml}$) k_T corresponds to the RANS turbulent kinetic energy, k; in the outer region ($x_2 > x_{2,ml}$) it corresponds to the subgrid-scale kinetic turbulent energy (k_{sgs}). No special treatment is used in the equations at the matching plane except that the form of the turbulent viscosity and the turbulent length scale are different in the two regions, see Table 21.1. At the walls, $k_T = 0$.

When prescribing the location of the RANS-LES interface, the velocity profile may show unphysical behaviour near the interface because of the rapid variation of the turbulence viscosity. Much work on forcing have been presented in order to alleviate this problem [100, 128, 149, 150].

22 The SAS model

22.1 Resolved motions in unsteady

WHEN doing URANS or DES, the momentum equations are triggered through instabilities to go unsteady in regions where the grid is fine enough. In URANS or in DES operating in RANS mode, high turbulent viscosity often dampens out these instabilities. In many cases this is an undesired feature, because if the flow wants to go unsteady, it is usually a bad idea to force the equations to stay steady. One reason is that there may not be any steady solution. Hence, the equations will not converge. Another reason is that if the numerical solution wants to go unsteady, the large turbulent scales — i.e. part of the turbulent spectrum — will be resolved instead of being modeled. This leads to a more accurate prediction of the flow.

One way to improve a RANS model's ability to resolve large-scale motions is to use the SAS (Scale- Adaptive Simulation) model

22.2 The von Kármán length scale

The von Kármán length scale

$$L_{vK,1D} = \kappa \left| \frac{\partial \langle \bar{v}_1 \rangle / \partial x_2}{\partial^2 \langle \bar{v}_1 \rangle / \partial x_2^2} \right| \tag{22.1}$$

which includes the second velocity gradient is a suitable length scale for detecting unsteadiness. The von Kármán length scale is smaller for an instantaneous velocity profile than for a time averaged velocity, see Fig. 22.1. This is interesting because, as noted in [156], the von Kármán length scale decreases when the momentum equations resolve (part of) the turbulence spectrum.

The first and second derivatives in Eq. 22.1 are given in boundary layer form. We want to extend this expression to a general one, applicable in three dimensions. In the same way as in, for example, the Smagorinsky model, we take the first derivative as $|\bar{s}| = (2\bar{s}_{ij}\bar{s}_{ij})^{1/2}$. The second derivative can be generalized in a number of ways. In the SAS model it is taken as

$$U'' = \left(\frac{\partial^2 \bar{v}_i}{\partial x_j \partial x_j} \frac{\partial^2 \bar{v}_i}{\partial x_k \partial x_k} \right)^{0.5} \tag{22.2}$$

Note than in a CFD code, Eqs. 22.3 and 22.2 are always used, but when the flow is steady it is equal to the time-averaged version, i.e. Eqs. T.8 and T.9.

There are other options how to compute this second derivative, see Eq. S.3 at p. 482. Hence, the general three-dimensional expression for the von Kármán length scale reads

$$L_{vK,3D} = \kappa \frac{|\bar{s}|}{|U''|} \tag{22.3}$$

In [157] they derived a one-equation ν_t turbulence model where the von Kármán length scale was used. The model was called the SAS model. Later, based on the $k - k^{1/2}L$ model of Rotta [158], Menter & Egorov [156] derived a new $k - kL$ model using the von Kármán length scale. Finally, in [159] they modified the $k - \omega$-SST model to include the SAS features; they called this model the SST-SAS model. This model is described in more detail below.
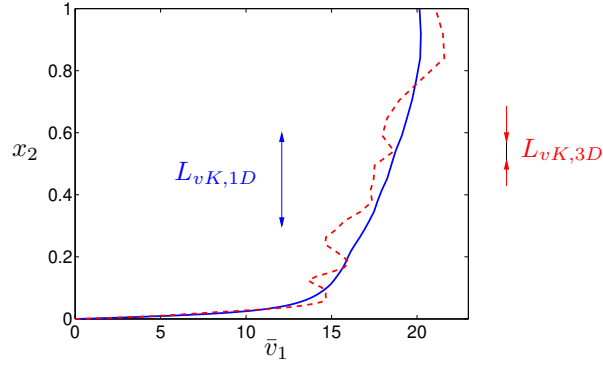
Figure 22.1: Velocity profiles from a DNS of channel flow. Solid line: time-averaged velocity with length scale $L_{x,1D}$, Eq. 22.1 ; dashed line: instantaneous velocity with length scale $L_{vK,3D}$, Eq. 22.3.

The SST-SAS model

The $k - \omega$ SST model is given in Eq. 20.5 at p. 213 (see also the section starting at p. 176) Now, Menter & Egorov [159] introduced a SAS-term in the ω equation. The object of this term is to decrease the turbulent viscosity when unsteadiness is detected, i.e. when the von Kármán length scale becomes small. The production term in the ω equation in the $k-\omega$-SST model reads $P_\omega = \alpha P^k/\nu_t \propto |\bar{s}|^2$. To decrease the turbulent viscosity we should increase ω. Thus it seems reasonable to add a new production term proportional to $P_\omega L_t/L_{vK,3D}$ where L_t denotes a RANS length scale. The additional term reads

$$\tilde{\zeta}_2 \kappa |\bar{s}|^2 \frac{L_t}{L_{vK,3D}}, \quad L_t = \frac{k^{1/2}}{\omega c_\mu^{1/4}} \tag{22.4}$$

When unsteadiness occurs — i.e. when the momentum equations attempt to resolve part of the turbulence spectrum — this term reacts as follows:

- Local unsteadiness will create velocity gradients which decrease von Kármán length scale, $L_{vK,3D}$ (see Fig. 22.1)

- As a consequence the additional source, Eq. 22.4, in the ω equation increases

- This gives an increase in ω and hence a decrease in ν_t

- The decreased turbulent viscosity will allow the unsteadiness to stay alive and, perhaps, grow.

The last item in the list above is the main object of the SAS model. The reaction to local unsteadiness in a eddy-viscosity model without the SAS feature is as follows: the increased local velocity gradients will create additional production of turbulent kinetic energy and give an increased turbulent viscosity which will dampen/kill the local unsteadiness. As mentioned in the introduction to this chapter, this is an undesirable feature.

When incorporating the additional production term (Eq. 22.4) in the $k - \omega$-SST

model, the last term in the ω equation is replaced by (for further details, see [159])

$$P_{SAS} = F_{SAS} \max\left(T_1 - T_2, 0\right)$$

$$T_1 = \tilde{\zeta}_2 \kappa S^2 \frac{L}{L_{vK,3D}}$$

$$T_2 = \frac{2k}{\sigma_\Phi} \max\left(\frac{1}{\omega^2} \frac{\partial \omega}{\partial x_j} \frac{\partial \omega}{\partial x_j}, \frac{1}{k^2} \frac{\partial k}{\partial x_j} \frac{\partial k}{\partial x_j}\right) \qquad (22.5)$$

$$L = \frac{k^{1/2}}{\omega c_\mu^{1/4}}$$

Note that the term T_1 is the "real" additional SAS term; T_2 is included to make sure that the model in steady flow works as a $k - \omega$ SST model.

22.3 The second derivative of the velocity

To compute U'' in Eq. 22.2, we need to compute the second velocity gradients. In finite volume methods there are two main options for computing second derivatives.

Option I: compute the first derivatives at the faces

$$\left(\frac{\partial v}{\partial x_2}\right)_{j+1/2} = \frac{v_{j+1} - v_j}{\Delta x_2}, \qquad \left(\frac{\partial v}{\partial x_2}\right)_{j-1/2} = \frac{v_j - v_{j-1}}{\Delta x_2}$$

and then

$$\Rightarrow \left(\frac{\partial^2 v}{\partial x_2^2}\right)_j = \frac{v_{j+1} - 2v_j + v_{j-1}}{(\Delta x_2)^2} + \frac{(\Delta x_2)^2}{12} \frac{\partial^4 v}{\partial x_2^4}$$

Option II: compute the first derivatives at the center

$$\left(\frac{\partial v}{\partial x_2}\right)_{j+1} = \frac{v_{j+2} - v_j}{2\Delta x_2}, \qquad \left(\frac{\partial v}{\partial x_2}\right)_{j-1} = \frac{v_j - v_{j-2}}{2\Delta x_2}$$

and then

$$\Rightarrow \left(\frac{\partial^2 v}{\partial x_2^2}\right)_j = \frac{v_{j+2} - 2v_j + v_{j-2}}{4(\Delta x_2)^2} + \frac{(\Delta x_2)^2}{3} \frac{\partial^4 v}{\partial x_2^4}$$

In [160], Option I was used unless otherwise stated.

22.4 Evaluation of the von Kármán length scale in channel flow

In Fig. 22.2 the turbulent length scale, $\langle L_{vK,3D}\rangle$, is evaluated using DNS data of fully developed channel flow. When using DNS data only viscous dissipation of resolved turbulence affects the equations. This implies that the smallest scales that can be resolved are related to the grid scale. The von Kármán length scale based on instantaneous velocities, $\langle L_{vK,3D}\rangle$, is presented in Fig. 22.2. For $x_2 > 0.2$, its magnitude is close to Δx_2 which confirms that the von Kármán length scale is related to the smallest resolvable scales. Closer to the wall, $\langle L_{vK,3D}\rangle$ increases slightly whereas Δx_2 continues to decrease.

The von Kármán length scale, $L_{vK,1D}$, based on the averaged velocity profile $\langle \bar{v}_1\rangle = \langle \bar{v}_1\rangle(x_2)$ is also included in Fig. 22.2, and as can be seen it is much larger than $\langle L_{vK,3D}\rangle$. Near the wall $L_{vK,1D}$ increases because the time-average second derivative, $\partial^2 \langle \bar{v}_1\rangle / \partial x_2^2$, goes to zero as the wall is approached. No such behavior is seen for the three-dimensional formulation, $\langle L_{vK,3D}\rangle$.
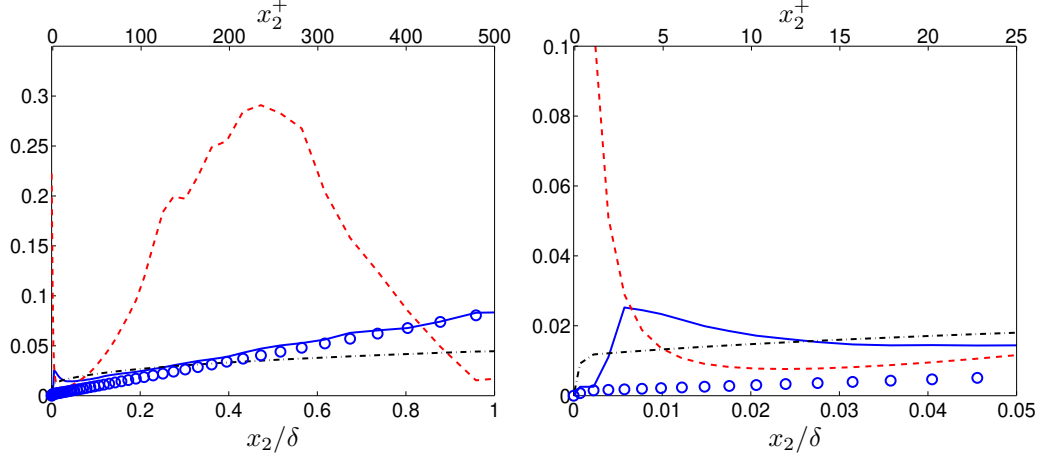
Figure 22.2: Turbulent length scales in fully developed channel flow. Left: global view; right: zoom. DNS. 96^3 mesh. $Re_\tau = 500$. $\Delta x_1/\delta = 0.065$, $\Delta x_3/\delta = 0.016$, x_2-stretching of 9%. ——— : $\langle L_{vK,3D}\rangle$; — — : $L_{vK,1D}$; — · — : $(\Delta x_1 \Delta x_2 \Delta x_3)^{1/3}$; ∘ : Δx_2.
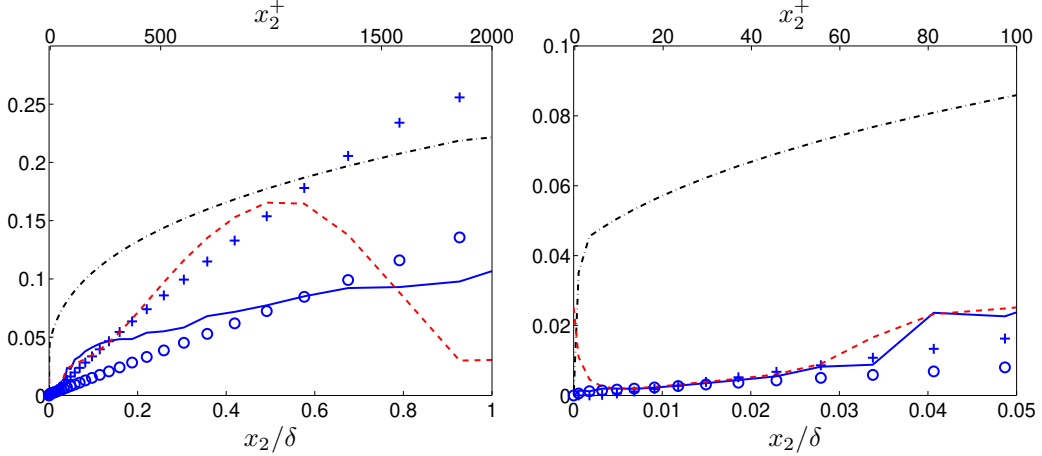
Figure 22.3: Turbulent length scales in fully developed channel flow. Hybrid LES-RANS. Left: global view; right: zoom. $32 \times 64 \times 32$ mesh. $Re_\tau = 2000$. $\Delta x_1/\delta = 0.39$, $\Delta x_3/\delta = 0.19$, x_2-stretching of 17%. ——— : $\langle L_{vK,3D}\rangle$; — — : $L_{vK,1D}$; — · — : $(\Delta x_1 \Delta x_2 \Delta x_3)^{1/3}$; ∘ : Δx_2; + : $\ell_{k-\omega} = k^{0.5}/(c_\mu^{1/4}\omega)$.

In Fig. 22.3, data from hybrid LES-RANS are used (taken from [100]). When using hybrid LES-RANS, part of the turbulence is resolved and part of the turbulence is modeled. The resolved turbulence is dissipated by a modeled dissipation, $-2\langle\nu_T \bar{s}_{ij}\bar{s}_{ij}\rangle$ (ν_T denotes SGS or RANS turbulent viscosity), and $\nu_T \gg \nu$. As a result, the length scale of the smallest resolved turbulence is larger in hybrid LES-RANS than in DNS. Close to the wall in the URANS region ($x_2 < 0.031\delta$), the resolved turbulence is dampened by the high turbulent viscosity, and as a results $\langle L_{vK,3D}\rangle$ follows closely $L_{vK,1D}$.

The RANS turbulent length scale, $\ell_{k-\omega}$, from a 1D RANS simulation at $Re_\tau = 2000$ with the $k - \omega$ SST model is also included in Fig. 22.3. In the inner region ($x_2 < 0.5\delta$), its behavior is close to that of the von Kármán length scale, $L_{vK,1D}$. In the center region the RANS turbulent length scale continues to increase which is physically correct. However, the von Kármán length scale, $L_{vK,1D}$, goes to zero because the

velocity derivative goes to zero.

Two filter scales are included in Figs. 22.2 and 22.3. In the DNS-simulations, $\Delta x_2 < (\Delta x_1 \Delta x_2 \Delta x_3)^{1/3}$ near the wall, whereas far from the wall $\Delta x_2 > (\Delta x_1 \Delta x_2 \Delta x_3)^{1/3}$ because of the stretching in the x_2 direction and because of small Δx_1 and Δx_3. In the hybrid simulations, it can be noted that the three-dimensional filter width is more that twice as large as the three-dimensional formulation of the von Kármán length scale, i.e. $(\Delta x_1 \Delta x_3 \Delta x_3)^{1/3} > 2\langle L_{vK,3D} \rangle$.

In [160], the SST-SAS model has been evaluated in channel flow, flow in an asymmetric diffusor and flow over an axi-symmetric hill.

23   The PANS Model

THE PANS method uses the so-called "partial averaging" concept, which corresponds to a filtering operation for a portion of the fluctuating scales [161].

To close the system of the partially-averaged Navier-Stokes equations, as in RANS (see Eq. 11.2) and LES (see Eq. 18.2), a model is needed for τ_{ij}. In [161] they proposed using the conventional eddy viscosity concept so that $\tau_{ij} = -2\nu_t \bar{s}_{ij}$, where $\bar{s}_{ij}$ is the strain-rate tensor of the computed flow and ν_t is the PANS eddy viscosity.

In order to formulate the PANS eddy viscosity, they defined in [161] another two quantities, the partially-averaged turbulent kinetic energy, k and its dissipation rate ε, so that $\nu_t = C_\mu k^2/\varepsilon$. In the derivation of the transport equations for k and ε, two parameters, f_k and f_ε, have been introduced, relating the unresolved to the resolved fluctuating scales. Parameter f_k defines the ratio of unresolved (partially-averaged) turbulent kinetic energy (k) to the total kinetic energy (k_{tot}), and f_ε is the ratio between the unresolved (ε) and the total (ε_{tot}) dissipation rates. These give

$$k_{tot} = \frac{k}{f_k} \text{ and } \varepsilon_{tot} = \frac{\varepsilon}{f_\varepsilon} \tag{23.1}$$

The extent of the resolved part is now determined by f_k and f_ε. Usually $f_\varepsilon = 1$; $f_\varepsilon < 1$ implies that dissipative scales are resolved. In [161, 162] they employed the standard $k - \varepsilon$ model as the base model.

The k_{tot} equation is derived by multiplying the RANS k_{tot} equation (Eq. 11.97) in the $k - \varepsilon$ model by f_k, i.e. (for simplicity we omit the buoyancy term)

$$f_k \left\{ \frac{\partial k_{tot}}{\partial t} + \bar{V}_j \frac{\partial k_{tot}}{\partial x_j} \right\} = f_k \left\{ P^{k,tot} - \varepsilon_{tot} + \frac{\partial}{\partial x_j} \left[\left(\nu + \frac{\nu_{t,tot}}{\sigma_k} \right) \frac{\partial k_{tot}}{\partial x_j} \right] \right\} \tag{23.2}$$

where V_i denotes the RANS velocity. Note than the *tot* index is here equivalent to $RANS$. The left side can be re-written

$$f_k \left\{ \frac{\partial k_{tot}}{\partial t} + \bar{V}_j \frac{\partial k_{tot}}{\partial x_j} \right\} = \frac{\partial k}{\partial t} + \bar{V}_j \frac{\partial k}{\partial x_j} = \frac{\partial k}{\partial t} + \bar{v}_j \frac{\partial k}{\partial x_j} + (\bar{V}_j - \bar{v}_j) \frac{\partial k}{\partial x_j} \tag{23.3}$$

Note that we have assumed that f_k is constant (non-constant f_k is accounted for in Section 23.1.1). The convective term must be expressed in $\bar{v}_j$ (the PANS averaged velocity) rather than in $\bar{V}_j$ (the RANS averaged velocity), because it is $\bar{v}_j$ that transports k because $\bar{v}_j$ represents the PANS resolved part of v_j. Anyway, the last term on the right side in Eq. 23.3 is usually neglected.

The diffusion term is re-written using Eq. 23.1

$$f_k \left\{ \frac{\partial}{\partial x_j} \left[\left(\nu + \frac{\nu_{t,tot}}{\sigma_k} \right) \frac{\partial k_{tot}}{\partial x_j} \right] \right\} = \frac{\partial}{\partial x_j} \left[\left(\nu + \frac{\nu_{t,tot}}{\sigma_k} \right) \frac{\partial k}{\partial x_j} \right]$$
$$= \frac{\partial}{\partial x_j} \left[\left(\nu + \frac{\nu_t}{\sigma_{ku}} \right) \frac{\partial k}{\partial x_j} \right] \tag{23.4}$$

where

$$\sigma_{ku} = \sigma_k \frac{f_k^2}{f_\varepsilon} \tag{23.5}$$

and

$$\nu_t = c_\mu \frac{k^2}{\varepsilon} \tag{23.6}$$

The source terms in Eq. 23.2 are replaced by P^k and ε, i.e.

$$f_k \left(P^{k,tot} - \varepsilon_{tot} \right) = P^k - \varepsilon \tag{23.7}$$

This relation implies

$$P^{k,tot} = \frac{1}{f_k}(P^k - \varepsilon) + \frac{\varepsilon}{f_\varepsilon} \tag{23.8}$$

Using Eqs. 23.3, 23.4 and 23.7 the final transport equation for k can now be written as

$$\frac{\partial k}{\partial t} + \frac{\partial(k\bar{v}_j)}{\partial x_j} = \frac{\partial}{\partial x_j}\left[\left(\nu + \frac{\nu_t}{\sigma_{ku}}\right)\frac{\partial k}{\partial x_j}\right] + P^k - \varepsilon \tag{23.9}$$

where the production term, P^k, is expressed in terms of the PANS eddy viscosity, ν_t, and the strain rate of PANS-resolved flow field, i.e.

$$P^k = \nu_t \left(\frac{\partial \bar{v}_i}{\partial x_j} + \frac{\partial \bar{v}_j}{\partial x_i}\right)\frac{\partial \bar{v}_i}{\partial x_j} \tag{23.10}$$

The ε equation is derived by multiplying the RANS ε_{tot} equation by f_ε, i.e.

$$
\begin{aligned}
f_\varepsilon\left[\frac{\partial \varepsilon_{tot}}{\partial t} + \frac{\partial(\varepsilon_{tot}\bar{V}_j)}{\partial x_j}\right] &= \frac{\partial \varepsilon}{\partial t} + \frac{\partial(\varepsilon\bar{v}_j)}{\partial x_j} = \\
&= f_\varepsilon\left\{\frac{\partial}{\partial x_j}\left[\left(\nu + \frac{\nu_{t,tot}}{\sigma_\varepsilon}\right)\frac{\partial \varepsilon_{tot}}{\partial x_j}\right] + C_{\varepsilon 1}P^{k,tot}\frac{\varepsilon_{tot}}{k_{tot}} - C_{\varepsilon 2}\frac{\varepsilon_{tot}^2}{k_{tot}}\right\}
\end{aligned}
\tag{23.11}
$$

where f_ε is assumed to be constant. As in the k equation, the additional term $(\bar{V}_j - \bar{v}_j)\partial\varepsilon/\partial x_j$ is neglected. The diffusion term is re-written using Eq. 23.1

$$
\begin{aligned}
f_\varepsilon\left\{\frac{\partial}{\partial x_j}\left[\left(\nu + \frac{\nu_{t,tot}}{\sigma_\varepsilon}\right)\frac{\partial \varepsilon_{tot}}{\partial x_j}\right]\right\} &= \frac{\partial}{\partial x_j}\left[\left(\nu + \frac{\nu_{t,tot}}{\sigma_\varepsilon}\right)\frac{\partial \varepsilon}{\partial x_j}\right] \\
&= \frac{\partial}{\partial x_j}\left[\left(\nu + \frac{\nu_t}{\sigma_{\varepsilon u}}\right)\frac{\partial \varepsilon}{\partial x_j}\right]
\end{aligned}
\tag{23.12}
$$

where

$$\sigma_{\varepsilon u} = \sigma_\varepsilon \frac{f_k^2}{f_\varepsilon} \tag{23.13}$$

In the same way, the production and destruction terms are re-formulated as (using Eqs. 23.1 and 23.8)

$$
\begin{aligned}
f_\varepsilon\left\{C_{\varepsilon 1}P^{k,tot}\frac{\varepsilon_{tot}}{k_{tot}} - C_{\varepsilon 2}\frac{\varepsilon_{tot}^2}{k_{tot}}\right\} &= C_{\varepsilon 1}\frac{\varepsilon f_k}{k}\left(\frac{1}{f_k}(P^k - \varepsilon) + \frac{\varepsilon}{f_\varepsilon}\right) - C_{\varepsilon 2}\frac{\varepsilon^2 f_k}{f_\varepsilon k} \\
&= C_{\varepsilon 1}\frac{\varepsilon}{k}P^k - C_{\varepsilon 1}\frac{\varepsilon^2}{k} + C_{\varepsilon 1}\frac{\varepsilon^2 f_k}{k f_\varepsilon} - C_{\varepsilon 2}\frac{\varepsilon^2 f_k}{f_\varepsilon k} \\
&= C_{\varepsilon 1}\frac{\varepsilon}{k}P^k - C_{\varepsilon 2}^*\frac{\varepsilon^2}{k}
\end{aligned}
\tag{23.14}
$$

where

$$C_{\varepsilon 2}^* = C_{\varepsilon 1} + \frac{f_k}{f_\varepsilon}(C_{\varepsilon 2} - C_{\varepsilon 1}) \tag{23.15}$$

The ε equation in the PANS model now takes the following form

$$\frac{\partial \varepsilon}{\partial t} + \frac{\partial(\varepsilon\bar{v}_j)}{\partial x_j} = \frac{\partial}{\partial x_j}\left[\left(\nu + \frac{\nu_t}{\sigma_{\varepsilon u}}\right)\frac{\partial \varepsilon}{\partial x_j}\right] + C_{\varepsilon 1}P^k\frac{\varepsilon}{k} - C_{\varepsilon 2}^*\frac{\varepsilon^2}{k} \tag{23.16}$$

The PANS equation for k, Eq. 23.9, was derived by multiplying the RANS equation for k_{tot} by f_k which was assumed to be constant in space and in time. By referring to Eqs. 23.4, 23.6 and 23.5, the turbulent diffusion term was obtained as

$$f_k \frac{\partial}{\partial x_j} \left(\frac{\nu_{t,tot}}{\sigma_k} \frac{\partial k_{tot}}{\partial x_j} \right) = \frac{\partial}{\partial x_j} \left(\frac{\nu_{t,tot}}{\sigma_k} \frac{\partial k}{\partial x_j} \right) \qquad (23.17a)$$

$$= \frac{\partial}{\partial x_j} \left(\frac{\nu_t}{\sigma_{ku}} \frac{\partial k}{\partial x_j} \right) \qquad (23.17b)$$

The expression on the right-hand side of Eq. 23.17(a) suggests that the turbulent transport for the PANS-modeled turbulent kinetic energy, k, is actually formulated in terms of the RANS turbulent viscosity from the base model. This is different from the turbulent diffusion in subgrid scale (SGS) modeling of LES with a one-equation k_{sgs} model, which reads

$$\frac{\partial}{\partial x_j} \left(\frac{\nu_{sgs}}{\sigma_k} \frac{\partial k_{sgs}}{\partial x_j} \right) \qquad (23.18)$$

In Eq. 23.18 the *SGS* turbulent viscosity is invoked for the transport of k_{sgs}, whereas on the right-hand side of Eq. 23.17(a) the *total* (i.e. the RANS) turbulent viscosity has been used for k. Equation 23.17(a) suggests that, when used as an SGS model, the modeled turbulent diffusion in the PANS formulation is a factor of $\sigma_k/\sigma_{ku} = f_\varepsilon/f_k^2$ larger than in Eq. 23.18, see Eqs. 23.9 and 23.17(b). With $f_\varepsilon = 1$ and $f_k = 0.4$, for example, this factor is larger than six. The modification of the diffusion coefficient, σ_{ku}, is a unique property of the PANS model. In other models, such as DES [163], X-LES [142] and PITM [146], the sink term in the k, ε or ω equation is modified, but not the diffusion term. The only difference between PANS and PITM is that in the former model the diffusion coefficients in the k and ε are modified.

A Low Reynolds number PANS model was presented in [145, 164] which reads

$$\frac{\partial k}{\partial t} + \frac{\partial (k\bar{v}_j)}{\partial x_j} = \frac{\partial}{\partial x_j} \left[\left(\nu + \frac{\nu_t}{\sigma_{ku}} \right) \frac{\partial k}{\partial x_j} \right] + (P^k - \varepsilon)$$

$$\frac{\partial \varepsilon}{\partial t} + \frac{\partial (\varepsilon\bar{v}_j)}{\partial x_j} = \frac{\partial}{\partial x_j} \left[\left(\nu + \frac{\nu_t}{\sigma_{\varepsilon u}} \right) \frac{\partial \varepsilon}{\partial x_j} \right] + C_{\varepsilon 1} P^k \frac{\varepsilon}{k} - C_{\varepsilon 2}^* \frac{\varepsilon^2}{k}$$

$$\nu_t = C_\mu f_\mu \frac{k^2}{\varepsilon}, C_{\varepsilon 2}^* = C_{\varepsilon 1} + \boxed{\frac{f_k}{f_\varepsilon}} (C_{\varepsilon 2} f_2 - C_{\varepsilon 1})$$

$$\sigma_{ku} \equiv \sigma_k \boxed{\frac{f_k^2}{f_\varepsilon}}, \sigma_{\varepsilon u} \equiv \sigma_\varepsilon \boxed{\frac{f_k^2}{f_\varepsilon}} \qquad (23.19)$$

$$f_2 = \left[1 - \exp\left(-\frac{y^*}{3.1} \right) \right]^2 \left\{ 1 - 0.3\exp\left[-\left(\frac{R_t}{6.5} \right)^2 \right] \right\}$$

$$f_\mu = \left[1 - \exp\left(-\frac{y^*}{14} \right) \right]^2 \left\{ 1 + \frac{5}{R_t^{3/4}}\exp\left[-\left(\frac{R_t}{200} \right)^2 \right] \right\}$$

$$R_t = \frac{k^2}{\nu\varepsilon}, \quad y^* = \frac{U_\varepsilon y}{\nu}, \quad U_\varepsilon = (\varepsilon\nu)^{1/4}$$

The modifications introduced by the PANS modeling as compared to its parent RANS model are highlighted by boxes. The model constants take the same values as in the LRN model [47], i.e.

$$C_{\varepsilon 1} = 1.5, C_{\varepsilon 2} = 1.9, \sigma_k = 1.4, \sigma_\varepsilon = 1.4, C_\mu = 0.09 \qquad (23.20)$$

23.1 PANS as a hybrid LES-RANS model

A new approach to use the partially averaged Navier-Stokes (PANS) model as a hybrid RANS-LES model was presented by Davidson [165]. It was evaluated in fully developed channel flow and embedded LES in a hump flow. For the channel flow, the two RANS-LES interfaces are parallel to the walls. In the URANS region, f_k is set to one. In the LES region, f_k is set to a constant value (the baseline value is $f_k = 0.4$) or it is computed. It is found that the new model gives good results for channel flow for a large span of Reynolds numbers ($4\,000 \leq Re_\tau \leq 32\,000$). In the channel flow simulations, three different grids are used in the wall-parallel planes, 32^2, 64^2 and 128^2, and the model yields virtually grid-independent flow fields and turbulent viscosities. Embedded LES is used for the hump flow which is well predicted. The RANS-LES interface is normal to the flow from the inlet. RANS is used upstream of the interface. Downstream this interface, RANS is used near the wall and LES is used away from the wall.

23.1.1 The interface conditions at the RANS-LES interface

The interface plane separates the URANS region near the wall and the LES region in the outer region. In the former region, the turbulent viscosity, ν_t, should be a RANS viscosity and in the latter region it should be an SGS viscosity. Hence ν_t must decrease rapidly when going from the URANS region to the LES region. This is achieved by
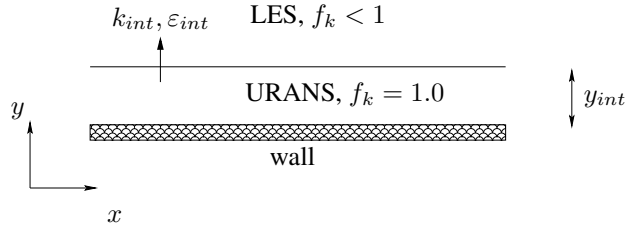
Figure 23.1: The URANS and the LES regions.
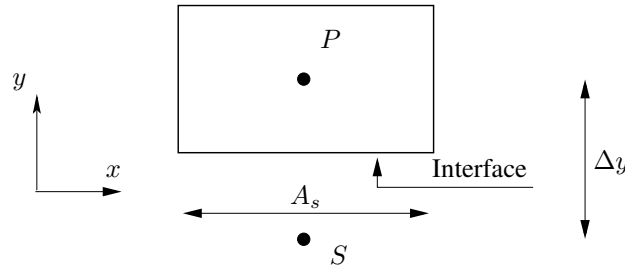
Figure 23.2: Control volume, P, in the LES region adjacent to the interface.

setting the usual convection and diffusion fluxes of k [4] at the interface to zero. New fluxes are introduced in which the interface condition is set to $k_{int} = f_k k_{RANS}$, where k_{RANS} is the k value in the cell located in the URANS region adjacent to the interface. Unless otherwise stated, no modification is made for the convection and diffusion of ε across the interface. The implementation is presented in some detail below. We write the discretized equation in the y direction (see Figs. 23.1 and 23.2) as [99]

$$a_P k_P = a_N k_N + a_S k_S + S_U, \quad a_P = a_S + a_N - S_P$$

where a_S and a_N are related to the convection and diffusion through the south and north face, respectively, and S_U and $S_P k_P$ include the production and the dissipation term, respectively. For a cell in the LES region adjacent to the interface (cell P), a_S is set to zero, setting the usual convection and diffusion fluxes to zero. New fluxes, including f_k, are incorporated in additional source terms as

$$
\begin{aligned}
S_U &= (C_s + D_s) f_k k_S, \quad S_P = -(C_s + D_s) \\
C_s &= \max\left(\bar{v}_s A_s, 0\right), \quad D_s = \frac{\mu_{tot} A_s}{\Delta y}
\end{aligned}
\tag{23.21}
$$

where C_s and D_s denote convection (first-order upwind) and diffusion, respectively, through the south face, and A_s is the south area of the cell. As can be seen, the k_S is multiplied by f_k and hence the new convective flux is a factor f_k smaller than the original one. Also the diffusion flux is smaller; it is $D_s(f_k k_S - k_P)$ compared with the original flux $D_s(k_S - k_P)$.

The interface is defined along gridlines. The approach presented above is also applicable when the location is automatically computed where the extent of the RANS region varies along the wall. The convective and diffusive fluxes are modified in exactly the same way.

The method of adding a new flux in the k equation is similar to the method proposed in [166]. In that work they take into account the spatial variation of f_k. A decrease of f_k in space – as occurs at the interface in Fig. 23.1 – means that the turbulent kinetic energy should be transferred from modeled to resolved. This is done by introducing a sink term in the k equation which decreases the turbulent viscosity. [166] also add a turbulent diffusion term in the momentum equation which appears as a source term in the equation for turbulent resolved kinetic energy. No source term is used in the momentum equations in this method. A further difference is that this method modifies the equations only in the LES region (in which k is reduced), not in the RANS region. The reason is that this effect is believed to be the most critical; it is important that the resolved turbulence on the LES side of the interface is activated as soon as possible (i.e. as close as possible to the interface). The total turbulent kinetic energy across the interface is not conserved, but as shown below, the total turbulent kinetic energy that is lost across the interface is not large. For more details and results, see Davidson [165].

23.2 Zonal PANS: different treatments of the RANS-LES interface

In [166], a method was proposed to include the effect of the gradient of f_k in PANS. This approach was used at RANS-LES interfaces by Davidson [147]. Four different interface models are evaluated in fully developed channel flow and embedded LES of

---

[4]from here on, the modelled turbulent kinetic energy and its viscous dissipation, LES or RANS mode, are denoted by k and ε

channel flow; in both cases, PANS is used as a zonal model with $f_k = 1$ in the URANS region and $f_k = 0.4$ in the LES region. In fully developed channel flow, the RANS-LES interface is parallel to the wall (horizontal) and in embedded LES it is parallel to the inlet (vertical).

The importance of the location of the horizontal interface in fully developed channel flow is also investigated. It is found that the location – and the choice of the treatment at the interface – may be critical at low Reynolds number or if the interface is placed too close to the wall. The reason is that the modeled turbulent shear stress at the interface is large and hence the relative strength of the resolved turbulence is small. In RANS, the turbulent viscosity – and consequently also the modeled Reynolds shear stress – is only weakly dependent on Reynolds number. It is found that that also applies in the URANS region.

23.2.1 The Interface Condition

The commutation error in PANS was recently addressed in [166]. In PANS, the equation for the modeled turbulent kinetic energy, k, is derived by multiplying the k_{tot} equation ($k_{tot} = k_{res} + k$) by f_k where k_{res} denotes the resolved turbulent kinetic energy. The convective term in the k equation with constant f_k is then obtained as (see Eq. 23.3)

$$f_k \frac{dk_{tot}}{dt} = \frac{d(f_k k_{tot})}{dt} = \frac{dk}{dt} \tag{23.22}$$

where

$$f_k = \frac{k}{k_{tot}}. \tag{23.23}$$

Now, if f_k varies in space, we get instead

$$f_k \frac{dk_{tot}}{dt} = \frac{d(f_k k_{tot})}{dt} - k_{tot} \frac{df_k}{dt} = \frac{dk}{dt} - k_{tot} \frac{df_k}{dt} \tag{23.24}$$

Since f_k here is constant in time, $df_k/dt = \bar{v}_i \partial f_k/\partial x_i$. The second term on the right side of Eq. 23.24 is the commutation term; it represents (excluding the minus sign) energy transfer from resolved to modeled turbulence. It can be written (on the right side of the k equation)

$$k_{tot} \frac{df_k}{dt} = (k + k_{res}) \frac{df_k}{dt} = k \frac{df_k}{dt} + \frac{\langle \bar{v}_i' \bar{v}_i' \rangle}{2} \frac{df_k}{dt} \tag{23.25}$$

The commutation term in the k_{res} equation is the same but with opposite sign, i.e.

$$-k \frac{df_k}{dt} - \frac{\langle \bar{v}_i' \bar{v}_i' \rangle}{2} \frac{df_k}{dt} \tag{23.26}$$

The question is now which term should be added to the momentum equations to get the commutation term in the k_{res} equation. We start by the second term in Eq. 23.26. This term can be represented by the source term

$$S_i^1 = -\frac{1}{2} \bar{v}_i' \frac{df_k}{dt} \tag{23.27}$$

in the momentum equation. To show that this term corresponds to the commutation term in Eq. 23.26, consider the momentum equation for the fluctuating velocity, $\bar{v}_i'$.

LES, $f_k = 0.4$

URANS, $f_k = 1$

y

y_{int}

wall

x
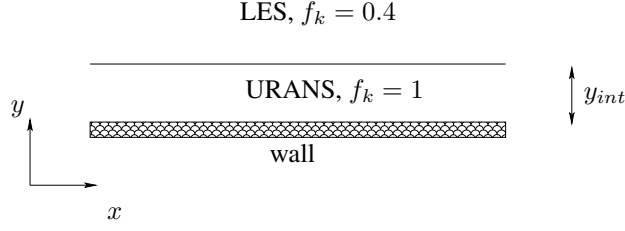
Figure 23.3: The URANS and the LES regions near a wall.

x_I x_{tr}

$\bar{v}', \bar{v}', \bar{w}'$

$0.4 < f_k < 1$

RANS
$f_k = 1$

LES
$f_k = 0.4$

y

2δ

x

L
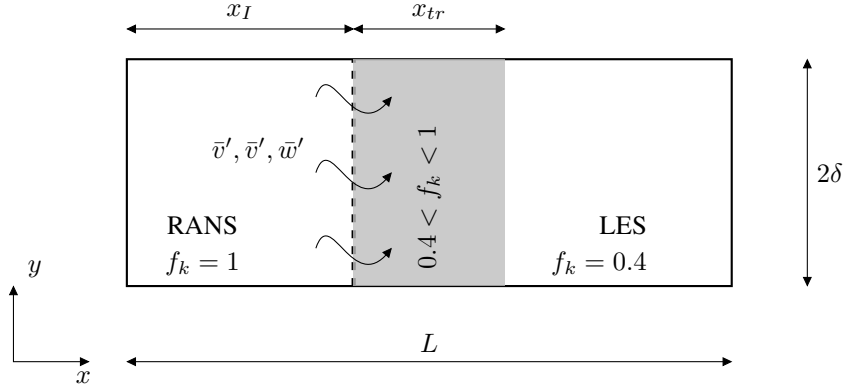
Figure 23.4: Embedded LES. Vertical thick line shows the interface at $x_I = 0.95$. f_k varies linearly in the gray area (width x_{tr}) from 1 to 0.4. $\delta = 1$.

Multiplying S_i^1 by $\bar{v}_i' = \bar{v}_i - \langle \bar{v}_i \rangle$ and time-averaging gives the source term in the k_{res} equation as

$$-\left\langle (\bar{v}_i - \langle \bar{v}_i \rangle) \frac{1}{2} \bar{v}_i' \frac{df_k}{dt} \right\rangle = -\left\langle \frac{1}{2} \bar{v}_i' \bar{v}_i' \frac{df_k}{dt} \right\rangle = -\frac{1}{2} \langle \bar{v}_i' \bar{v}_i' \rangle \frac{df_k}{dt} \qquad (23.28)$$

Equation 23.28 is equal to the time average of the second term in Eq. 23.26 as it should.

A term corresponding to the first term in Eq. 23.26 can be added as a source term in the momentum equation as

$$S_i^2 = -\frac{\langle k \rangle \bar{v}_i'}{\langle \bar{v}_m' \bar{v}_m' \rangle} \frac{df_k}{dt} \qquad (23.29)$$

Multiplying S_i^2 by $\bar{v}_i'$ and time averaging gives

$$-\frac{\langle \langle k \rangle \bar{v}_i' \bar{v}_i' \rangle}{\langle \bar{v}_m' \bar{v}_m' \rangle} \frac{df_k}{dt} \simeq -\langle k \rangle \frac{df_k}{dt} \qquad (23.30)$$

Equation 23.30 is equal to the time average of the first term in Eq. 23.26 as it should.

In [166], the second term on the right side of Eq. 23.24 is represented by introducing an additional turbulent viscosity, ν_{tr}, in a diffusion term in the momentum equation as

$$\frac{\partial}{\partial x_j} (\nu_{tr} \bar{s}_{ij}), \quad \bar{s}_{ij} = \frac{1}{2} \left(\frac{\partial \bar{v}_i}{\partial x_j} + \frac{\partial \bar{v}_j}{\partial x_i} \right) \qquad (23.31)$$

where

$$\nu_{tr} = \frac{P_{k_{tr}}}{|\bar{s}|^2}.$$

(23.32)

The term, $P_{k_{tr}}$, is computed as

$$P_{k_{tr}} = k_{tot}\frac{df_k}{dt}$$

(23.33)

$P_{k_{tr}}$ is an additional production term in the k equation, see Eq. 23.19. In [166], $P_{k_{tr}}$ is re-written using Eq. 23.23 as

$$P_{k_{tr}} = \frac{k}{f_k}\frac{df_k}{dt}$$

(23.34)

23.2.2 Modeling the Interface

The gradient of f_k across a RANS-LES interface gives rise to an additional term in the momentum equations and the k equation. These terms are included only when the flow goes from a RANS region to an LES region. The effect of these terms will reduce k and act as a forcing term in the momentum equations. Four different models are investigated.

23.2.2.1 Interface Model 1

This is based on the approach suggested in [166]. The additional turbulent viscosity, ν_{tr}, gives an additional production term, $P_{k_{tr}}$, in the k equation, see Eq. 23.34. Since we are interested in stimulating resolved turbulence in the LES region adjacent to the RANS region, only negative values of ν_{tr} are included. A negative ν_{tr} means physically transfer of kinetic energy from modeled to resolved. It is found that the magnitude of the positive values of ν_{tr} is actually larger than the magnitude of the negative ones, which means that $\langle\nu_{tr}\rangle > 0$. The negative values correspond to $df_k/dt < 0$ (see Eqs. 23.32, 23.33 and 23.34), i.e. when a fluid particle in a RANS region passes the interface into an adjacent LES region. However, ν_{tr} takes such large (negative) values that $\nu_t + \nu_{tr} < 0$. To stabilize the simulations, it was found necessary to introduce a limit $\nu_t + \nu_{tr} > 0$ in the diffusion term in the momentum equation. No such limit is used in the k equation, and hence $P_k + P_{k_{tr}}$ is allowed to go negative.

23.2.2.2 Interface Model 2

This model is identical to Model 1 except that Eq. 23.33 is used instead of Eq. 23.34. k_{tot} in Eq. 23.33 is defined as

$$k_{tot} = k + \frac{1}{2}\langle\bar{v}_i'\bar{v}_i'\rangle_{r.a}$$

(23.35)

where subscript $r.a.$ denotes running average. Is is averaged in all homogeneous directions including time (note that time is not a homogeneous direction in decaying grid turbulence). Since k_{tot} is mostly larger than k/f_k [165], this approach will give a larger magnitude of the (negative) production than Model 1. It is found in [147] that this modification is of utmost importance.

23.2.2.3   Interface Model 3

The right side of Eq. 23.25 is added to the k equation, but only when the flow goes from a RANS region to an LES region (i.e. $df_k/dt < 0$), i.e.

$$P_{k_{tr}} = k_{tot} \min\left(\frac{df_k}{dt}, 0\right) \qquad (23.36)$$

where k_{tot} is computed as in Eq. 23.35. The production term $P_{k_{tr}} < 0$ which means that it reduces k as it should. The sum of the S_i^1 and S_i^2 terms (see Eqs. 23.27 and 23.29) in the momentum equations read

$$S_i = -\min\left(\frac{df_k}{dt}, 0\right)\left(0.5 + \frac{k}{\langle \bar{v}_m' \bar{v}_m' \rangle_{r.a.}}\right) \bar{v}_i' \qquad (23.37)$$

Since $df_k/dt < 0$, the source S_i has the same sign as $\bar{v}_i'$; this means that the source enhances the resolved turbulence as it should.

It may be noted that df_k/dt in Eq. 23.36 assumes the correct (i.e. negative) sign irrespectively of the orientation of the RANS-LES interface. Consider, for example, the RANS-LES interfaces at the lower and upper wall in fully-developed channel flow (Fig. 23.3). For these interfaces, the gradient of f_k in Eq. 23.36 reads $\bar{v}\partial f_k/\partial y$. When a fluid particles at the lower interface goes from the RANS region to the LES region, $\bar{v} > 0$ and $\partial f_k/\partial y < 0$ so that $\bar{v}\partial f_k/\partial y < 0$ as intended. Also for the upper interface we get $\bar{v}\partial f_k/\partial y < 0$ since $\bar{v} < 0$ and $\partial f_k/\partial y > 0$. For non-cartesian grids the material derivative, $df_k/dt < 0$, has to be formulated in local grid coordinates.

It is however found that the forcing often becomes too strong when S_i is added to the momentum equation. The effect of adding or neglecting S_i in the momentum equations is evaluated, see [147].

The differences between Model 3 and 2 are that

- When $S_i = 0$, no explicit modification is made in the momentum equation in Model 3 (recall that $-\nu < \nu_{tr} < 0$ is used in the momentum equation in Models 1 and 2).

- Model 2 (and Model 1) may need regularization in case $|\bar{s}| \to 0$ in the denominator of $\nu_{t_{tr}}$ in Eq. 23.33. No such regularization, however, is used here. It can be argued that the commutation term in Model 3 is introduced in a more physical way compared to Models 1 and 2 where artificially negative viscosities are used.

23.2.2.4   Interface Model 4

This interface model was developed in [165] for horizontal interfaces. The modeled turbulent kinetic energy in the LES region adjacent to the interface is reduced by setting the usual convection and diffusion fluxes of k at the interface to zero. New fluxes are introduced in which the interface condition is set to $k_{int} = f_k k_{RANS}$ ($f_k = 0.4$), where k_{RANS} is the k value in the cell located in the URANS region adjacent to the interface. No modification is made for the convection and diffusion of ε across the interface. The implementation is presented in Section 23.1.1. It is described in the next section.

23.3 A new formulation of f_k for the PANS model

It is natural to link f_k to the mesh resolution and in that aim several proposals have been made on how to compute f_k. Girimaji and Abdol-Hamid [162] proposed one way to compute f_k:

$$f_k = C_\mu^{-1/2} \left(\frac{\Delta}{L_t} \right)^{2/3}, L_t = \frac{k_{tot}^{3/2}}{\varepsilon} \qquad (23.38)$$

using $\Delta = \Delta_{min}$, the smallest grid cell size. Basara *et al.* also used f_k prescribed from Eq. 23.38, however taking the geometric average $\Delta = (\Delta V)^{1/3}$. [167] they have made a slightly different proposal which reads

$$f_k = \frac{\Delta}{L_t} \qquad (23.39)$$

More recently, in [168] they derived an expression from the Kolmogorov energy spectrum which reads

$$f_k = 1 - \left[\frac{(\Lambda/\Delta)^{2/3}}{0.23 + (\Lambda/\Delta)^{2/3}} \right]^{9/2} \qquad (23.40)$$

Recently, Davidson and Friess [169] proposed a new formulation for f_k. It is based on the H-equivalence introduced by Friess *et al.* (2015). In this formulation the expression of f_k is derived to mimic DES. This new formulation behaves very much like "classic DES", even though tthe two formulations use different mechanisms to separate modeled and resolved scales. They show very similar performance in separated flows as well as in attached boundary layers. Moreover, the new formulation exhibits similar robustness features as DES.

23.3.1 f_k derived from the equivalence criterion

In [170] a relation between f_k and the grid step is derived, through the establishment of a statistical equivalence between DES and PITM. To that aim, they performed perturbation analyses about the equilibrium states, representing small variation of the energy partition. They did the analysis with and without considering inhomogeneity. That derivation is summarized here in a homogeneous framework, as a first step. Let us first consider the PANS/PITM equations. For equilibrium turbulence $d\tau/dt = 0$ where $\tau = k/\varepsilon$, Eq. 23.19 gives

$$\begin{aligned} \frac{d\tau}{dt} &= \frac{1}{\varepsilon} \frac{dk}{dt} - \frac{k}{\varepsilon^2} \frac{d\varepsilon}{dt} = \frac{1}{\varepsilon} \left(P^k + D^k - \varepsilon \right) \\ &- \frac{k}{\varepsilon^2} \left(C_{\varepsilon 1} \frac{\varepsilon}{k} P^k + D^\varepsilon - C_{\varepsilon 2}^* \frac{\varepsilon^2}{k} \right) = 0 \end{aligned} \qquad (23.41)$$

where D^k and D^ε denote the diffusion term for k and ε, respectively. For local homogeneous turbulence (i.e. $D^k = D^\varepsilon = 0$), it can be written

$$\begin{aligned} \gamma(C_{\varepsilon 1} - 1)Sk &= (C_{\varepsilon 2}^* - 1)\varepsilon \\ \gamma &= \frac{P^k}{Sk}, \quad S = (2\bar{s}_{ij}\bar{s}_{ij})^{1/2} \end{aligned} \qquad (23.42)$$

The quantities that are affected by the partition between modeled and resolved turbulence (i.e. f_k) in Eq. 23.42 are γ, S, k and $C_{\varepsilon 2}^*$.[5] Differentiation of Eq. 23.42, by

---

[5] ε is independent of f_k provided that no dissipation is resolved, which corresponds to $f_\varepsilon = 1$

considering infinitesimal perturbations $\delta\gamma$, δS, δk and $\delta C_{\varepsilon2}^*$ of the variables, yields:

$$\delta\gamma Sk + \delta S\gamma k + \delta k\gamma S = \frac{\delta C_{\varepsilon2}^*\varepsilon}{C_{\varepsilon1} - 1} \tag{23.43}$$

so that

$$\frac{\delta\gamma}{\gamma} + \frac{\delta S}{S} + \frac{\delta k}{k} = \frac{\delta C_{\varepsilon2}^*\varepsilon}{(C_{\varepsilon1} - 1)\gamma Sk} = \frac{\delta C_{\varepsilon2}^*}{C_{\varepsilon2}^* - 1} \tag{23.44}$$

Equation 23.44 was derived for the PANS/PITM equations. Now we repeat the derivation for the DES equations. The differences between DES and PITM/PANS are that in DES (i) $C_{\varepsilon2}^* = C_{\varepsilon2}$ is constant and (ii) the dissipation term in the equation for modeled energy k is replaced with $\psi\varepsilon$, i.e.

$$\frac{dk}{dt} = \frac{\partial}{\partial x_j}\left[\left(\nu + \frac{\nu_t}{\sigma_k}\right)\frac{\partial k}{\partial x_j}\right] + P_k - \psi\varepsilon \tag{23.45}$$

$$\psi = \max\left(1, \frac{k^{3/2}/\varepsilon}{C_{DES}\Delta_{max}}\right), \quad \Delta_{max} = \max(\Delta x_1, \Delta x_2, \Delta x_3) \tag{23.46}$$

$$\frac{d\varepsilon}{dt} = \frac{\partial}{\partial x_j}\left[\left(\nu + \frac{\nu_t}{\sigma_\varepsilon}\right)\frac{\partial\varepsilon}{\partial x_j}\right] + C_{\varepsilon1}P_k\frac{\varepsilon}{k} - C_{\varepsilon2}\frac{\varepsilon^2}{k}$$

Assuming $d\tau/dt = 0$ and local homogeneous turbulence gives

$$\gamma(C_{\varepsilon1} - 1)Sk = (C_{\varepsilon2} - \psi)\varepsilon \tag{23.47}$$

We differentiate so that

$$\frac{\delta\gamma}{\gamma} + \frac{\delta S}{S} + \frac{\delta k}{k} = -\frac{d\psi\varepsilon}{(C_{\varepsilon1} - 1)Sk\gamma} = -\frac{d\psi}{C_{\varepsilon2} - \psi} \tag{23.48}$$

Equations 23.43 and 23.48 describe how $C_{\varepsilon2}^*$ and ψ depend on variations in γ, S and k. The parameters $C_{\varepsilon2}^*$ and ψ vary from $C_{\varepsilon2}$ and 1 (RANS values), respectively, to $C_{\varepsilon2}^*$ and $\psi(\Delta)$ (LES values). Combining Eqs. 23.43 and 23.48 and integrating from RANS to LES conditions ($C_{\varepsilon2}^*$ and ψ)

$$\int_{C_{\varepsilon2}}^{C_{\varepsilon2}^*} \frac{dC_{\varepsilon2}^*}{C_{\varepsilon2}^* - 1} = \int_1^\psi -\frac{d\psi}{C_{\varepsilon2} - \psi} \Rightarrow$$
$$\ln\left(\frac{C_{\varepsilon2}^* - 1}{C_{\varepsilon2} - 1}\right) = \ln\left(\frac{C_{\varepsilon2} - \psi}{C_{\varepsilon2} - 1}\right) \tag{23.49}$$

By using the expression for $C_{\varepsilon2}^*$ in Eq. 23.19 (with $f_2 = f_\varepsilon = 1$), and ensuring that $0 < f_k \le 1$ we finally get

$$f_k = \max\left[0, \min\left(1, 1 - \frac{\psi - 1}{C_{\varepsilon2} - C_{\varepsilon1}}\right)\right] \tag{23.50}$$

where ψ is given by Eq. 23.46. This model is evaluated in [169]. It gives much better results than the old PANS model and very similar results to the DES model. What is the advantage of the new PANS model vs. the DES model? The PANS model is based on a rigorous derivation whereas DES is based on an ad-hoc modification of RANS models.

24 The PITM model

PITM is an acronym for Partially Integrated Transport Model [146, 171].

24.1 RANS mode

Consider homogeneous turbulence, e.g. decay of grid generated turbulence, see Section 3.4 in [26] and Fig. 11.2. The k and ε equations can for this flow is simplified as

$$\frac{dk}{dt} = P^k - \varepsilon \tag{24.1}$$

$$\frac{d\varepsilon}{dt} = \frac{\varepsilon}{k}(c_{\varepsilon 1}P^k - c_{\varepsilon 2}\varepsilon) \tag{24.2}$$

where $d/dt = \bar{v}_1 d/dx$. The dissipation can be estimated as

$$\varepsilon = c\frac{k^{3/2}}{L_t} \tag{24.3}$$

Differentiation of Eq. 24.3 gives

$$\frac{d\varepsilon}{dt} = c\frac{3}{2}\frac{k^{1/2}}{L_t}\frac{dk}{dt} - c\frac{k^{3/2}}{L_t^2}\frac{dL_t}{dt} \tag{24.4}$$

Inserting Eq. 24.1 into Eq. 24.4

$$\frac{d\varepsilon}{dt} = c\frac{3}{2}\frac{k^{1/2}}{L_t}(P^k - \varepsilon) - c\frac{k^{3/2}}{L_t^2}\frac{dL_t}{dt}$$

and using Eq. 24.3 gives

$$\frac{d\varepsilon}{dt} = \frac{3}{2}\frac{\varepsilon}{k}(P^k - \varepsilon) - \frac{\varepsilon}{L_t}\frac{dL_t}{dt} = \frac{3}{2}\frac{P^k - \varepsilon}{T} - \frac{T}{L_t}\frac{dL_t}{dt}\frac{\varepsilon^2}{k} \tag{24.5}$$

where $T = k/\varepsilon$. Comparing Eqs. 24.5 and 24.2 we find that

$$C_{\varepsilon 1} = 1.5 \quad \text{and} \quad C_{\varepsilon 2} = C_{\varepsilon 1} + \frac{T}{L_t}\frac{dL_t}{dt} \tag{24.6}$$

24.2 LES mode

Now let's transform the RANS $k - \varepsilon$ model above to an SGS $k - \varepsilon$ model. In the RANS model, k represents all turbulence. In an SGS model, the modeled turbulent kinetic energy, k_{sgs}, represents scales with wavelength larger that the cut-off, κ_c, see Fig. 18.6. The viscous dissipation is the same in RANS and LES. The production P^k is replaced by $P_{k_{sgs}} = \varepsilon_{sgs}$ (see Fig. 18.6). The time scale, T, is replaced by $T_{sgs} = k_{sgs}/\varepsilon$ since the time scale of the small scales is different (it is smaller) than that of the large scales. Now, Eq. 24.5 can be written as

$$\frac{d\varepsilon}{dt} = C_{\varepsilon 1,sgs}\frac{\varepsilon\varepsilon_{sgs}}{k_{sgs}} - C_{\varepsilon 2,sgs}\frac{\varepsilon^2}{k_{sgs}}$$

$$C_{\varepsilon 2,sgs} = \frac{3}{2} + \frac{T_{sgs}}{L_t}\frac{dL_t}{dt} = \frac{3}{2} + \frac{T}{L_t}\frac{dL_t}{dt}\frac{k_{sgs}}{k_{tot}} \tag{24.7}$$
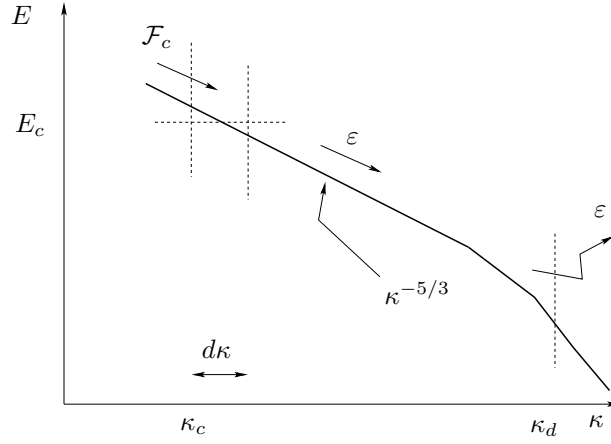
Figure 24.1: Spectral energy balance in PITM. Homogeneous turbulence.

where k_{tot} denotes the total turbulence (i.e. resolved and SGS). Note that L is not replaced by L_{sgs}, because Eq. 24.3 is still a valid estimate ε.

Let's introduce a new dissipative length scale of wavenumber κ_d which is much larger than κ_c

$$\kappa_d - \kappa_c = \xi \frac{\varepsilon}{k_{sgs}^{3/2}} \qquad (24.8)$$

The constant is very large since $\kappa_c \ll \kappa_d$; thus we can write

$$\kappa_d \simeq \xi \frac{\varepsilon}{k_{sgs}^{3/2}} \qquad (24.9)$$

Consider spectral balance of k_{sgs} in homogeneous turbulence, see Fig. 24.1. When the cut-off does not move we get simply

$$\mathcal{F}_c = \varepsilon \qquad (24.10)$$

where $\mathcal{F}_c = \mathcal{F}(\kappa_c)$ denotes the spectral transfer from wavenumber range $[0, \kappa_c^-]$ into $[\kappa_c^+, \infty]$; note that $\kappa_d \simeq \infty$. Recall that k_{sgs} is the area below E in Fig. 24.1. see Eq. 18.23. When the cut-off does not move in time (which implies that dk_{sgs}/dt), then

$$\mathcal{F}_c = \varepsilon_{sgs} = P_{k_{sgs}} \qquad (24.11)$$

When κ_c is time dependent as, for example, in decaying homogeneous grid turbulence, see Eq. 24.1, we can set-up the balance of k_{sgs} when κ_c moves $d\kappa_c$ during the time interval dt, i.e.

$$dk_{sgs} = \mathcal{F}_c dt - E_c d\kappa_c - \varepsilon dt \qquad (24.12)$$

where $E_c d\kappa$ denotes the spectral energy in the slice $d\kappa_c$. Taking the time derivative of Eq. 24.12 we get

$$\frac{dk_{sgs}}{dt} = \mathcal{F}_c - E_c \frac{d\kappa_c}{dt} - \varepsilon \qquad (24.13)$$

Comparing Eq. 24.13 with Eq. 24.10 and 24.11, we find the spectral energy transfer, ε_{sgs}, at the cut-off, κ_c, is

$$\varepsilon_{sgs} = \mathcal{F}_c - E_c \frac{d\kappa_c}{dt} \qquad (24.14)$$

We can write a similar equation as Eq. 24.14 at wavenumber κ_d, i.e.

$$\varepsilon = \mathcal{F}_d - E_d \frac{d\kappa_d}{dt} \qquad (24.15)$$

where ε is the energy transfer rate across κ_d. Now derivate Eq. 24.9 with respect to time and insert Eq. 24.15

$$\frac{d}{dt}\left(\xi \frac{\varepsilon}{k_{sgs}^{3/2}}\right) = \frac{\mathcal{F}_d - \varepsilon}{E_d} \qquad (24.16)$$

It may be noted that both the nominator and denominator of the right side go to zero as $\kappa_d \to \infty$. The left side is re-written as

$$\xi\left[\frac{1}{k_{sgs}^{3/2}}\frac{d\varepsilon}{dt} - \frac{3}{2}k_{sgs}^{-5/2}\varepsilon\frac{dk_{sgs}}{dt}\right] \qquad (24.17)$$

With Eq. 24.13 we get

$$\xi\left[\frac{1}{k_{sgs}^{3/2}}\frac{d\varepsilon}{dt} - \frac{3}{2}k_{sgs}^{-5/2}\varepsilon\left(\mathcal{F}_c - E_c\frac{d\kappa_c}{dt} - \varepsilon\right)\right] \qquad (24.18)$$

Replacing the left side of Eq. 24.16 with Eq. 24.18 gives

$$\xi\left[\frac{1}{k_{sgs}^{3/2}}\frac{d\varepsilon}{dt} - \frac{3}{2}k_{sgs}^{-5/2}\varepsilon\left(\mathcal{F}_c - E_c\frac{d\kappa_c}{dt} - \varepsilon\right)\right] = \frac{\mathcal{F}_d - \varepsilon}{E_d} \qquad (24.19)$$

We get (using first Eq. 24.14 and then Eq. 24.9)

$$\frac{d\varepsilon}{dt} = k_{sgs}^{3/2}\frac{\mathcal{F}_d - \varepsilon}{\xi E_d} + \frac{3}{2}\frac{\varepsilon}{k_{sgs}}(\varepsilon_{sgs} - \varepsilon) = \varepsilon\frac{\mathcal{F}_d - \varepsilon}{\kappa_d E_d} + \frac{3}{2}\frac{\varepsilon}{k_{sgs}}(\varepsilon_{sgs} - \varepsilon) \qquad (24.20)$$

This equation can now be written

$$\frac{d\varepsilon}{dt} = \underbrace{\frac{3}{2}}_{C_{\varepsilon 1,sgs}}\frac{\varepsilon}{k_{sgs}}\varepsilon_{sgs} - \frac{\varepsilon^2}{k_{sgs}}\underbrace{\left[\frac{3}{2} - \frac{k_{sgs}}{\kappa_d E_d}\left(\frac{\mathcal{F}_d}{\varepsilon} - 1\right)\right]}_{C_{\varepsilon 2,sgs}} \qquad (24.21)$$

When $\kappa_c \to 0$ (RANS), then $k_{sgs} \to k_{tot}$ so that

$$C_{\varepsilon 1,sgs} \to C_{\varepsilon 1} \qquad (24.22)$$

$$C_{\varepsilon 2,sgs} \to C_{\varepsilon 2} = \frac{3}{2} - \frac{k_{tot}}{\kappa_d E_d}\left(\frac{\mathcal{F}_d}{\varepsilon} - 1\right) \qquad (24.23)$$

It may be noted that both the term in the parenthesis and E_d go to zero as $\kappa_d \to \infty$. Inserting Eq. 24.23 in the expression for $C_{\varepsilon 2,sgs}$ in Eq. 24.21 gives

$$\begin{aligned} C_{\varepsilon 2,sgs} &= \frac{3}{2} - \frac{k_{sgs}}{k_{tot}}\frac{k_{tot}}{\kappa_d E_d}\left(\frac{\mathcal{F}_d}{\varepsilon} - 1\right) = \frac{3}{2} + \frac{k_{sgs}}{k_{tot}}\left(C_{\varepsilon 2} - \frac{3}{2}\right) \\ &= C_{\varepsilon 1} + \frac{k_{sgs}}{k_{tot}}(C_{\varepsilon 2} - C_{\varepsilon 1}) \end{aligned} \qquad (24.24)$$

When $k_{sgs}/k_{tot} \to 0$ (only a small part of the turbulent kinetic energy is modeled), the PITM model is in LES mode, i.e. $C_{\varepsilon 2,sgs} \to C_{\varepsilon 1}$. Then $C_{\varepsilon 2,sgs}$ is reduced which

increases ε and reduces the modeled turbulent kinetic energy and the turbulent viscosity. On the other hand, when $k_{sgs}/k_{tot} \to 1$ (everything is modeled), then the PITM model is in RANS mode (i.e. a usual RANS $k - \varepsilon$ model).

It should be noted that this model is very similar to the PANS model. Indeed, Eq. 24.24 is identical to the expression for $C_{\varepsilon2}^*$, see Eq. 23.15 (provided that no dissipative scales are resolved so that $f_\varepsilon = 1$), i.e.

$$C_{\varepsilon2,sgs} = C_{\varepsilon1} + f_k \left(C_{\varepsilon2} - C_{\varepsilon1} \right) \qquad (24.25)$$

In both models the $C_{\varepsilon2}$ coefficients are modified. The only difference between the PANS and PITM models is that the diffusion coefficients in the k and ε are modified in the former model, see Eq. 23.19.

In [146] they do not use k_{sgs}/k_{tot} to compute $C_{\varepsilon2,sgs}$. Instead they compute it using the ratio of the integral and the modeled lengthscales as

$$C_{\varepsilon2} = C_{\varepsilon1} + \frac{0.42}{1 + \gamma(L_t/\Delta)^{2/3}}$$

where $L_t = k_{tot}^{3/2}/\varepsilon$ and $\gamma = 0.42$.

25 Hybrid LES/RANS for Dummies

25.1 Introduction

FLUID flow problems are governed by the Navier-Stokes equations

$$\frac{\partial v_i}{\partial t} + \frac{\partial v_i v_j}{\partial x_j} = -\frac{1}{\rho}\frac{\partial p}{\partial x_i} + \nu\frac{\partial^2 v_i}{\partial x_j \partial x_j} \tag{25.1}$$

where v_i denotes the velocity vector, p is the pressure and ν and ρ are the viscosity and density of the fluid, respectively. In turbulent flow, the velocity and pressure are unsteady and v_i and p include all turbulent motions, often called eddies. The spatial scale of these eddies vary widely in magnitude where the largest eddies are proportional to the size of the largest physical length (for example the boundary layer thickness, δ, in case of a boundary layer). The smallest scales are related to the eddies where dissipation takes place, i.e. where the kinetic energy of the eddies is transformed into internal energy causing increased temperature. The ratio of the largest to the smallest eddies increases with Reynolds number, $Re = |v_i|\delta/\nu$. This has the unfortunate consequence – unless one is a fan of huge computer centers – that it is computationally extremely expensive to solve the Navier-Stokes equations for large Reynolds numbers.

25.1.1 Reynolds-Averaging Navier-Stokes equations: RANS

In order to be able to solve the Navier-Stokes equations with a reasonable computational cost, the velocity vector and the pressure are split into a time-averaged part ($\langle v_i \rangle$ and $\langle p \rangle$) and a fluctuating part (v_i' and p'), i.e. $v_i = \langle v_i \rangle + v_i'$, $p = \langle p \rangle + p'$. The resulting equation is called the RANS (Reynolds-Averaging Navier-Stokes) equations

$$\begin{aligned}
\frac{\partial \langle v_i \rangle \langle v_j \rangle}{\partial x_j} &= -\frac{1}{\rho}\frac{\partial \langle p \rangle}{\partial x_i} + \nu\frac{\partial^2 \langle v_i \rangle}{\partial x_j \partial x_j} - \frac{\partial \langle v_i' v_j' \rangle}{\partial x_j} \\
&= -\frac{1}{\rho}\frac{\partial \langle p \rangle}{\partial x_i} + \frac{\partial}{\partial x_j}\left((\nu + \nu_t)\frac{\partial \langle v_i \rangle}{\partial x_j}\right)
\end{aligned} \tag{25.2}$$

The last term on the first line is called the Reynolds stress and it is unknown and must be modeled. All turbulent fluctuation are modeled with a turbulence model and the results when solving Eq. 25.2 are highly dependent on the accuracy of the turbulence model. On the right side of Eq. 25.2 the unknown Reynolds stresses are expressed by a turbulence model in which a new unknown variable is introduced which is called the turbulent viscosity, ν_t. The ratio of ν_t to ν may be of the order of 1000 or larger. In industry today, CFD (Computationally Fluid Dynamics) based on finite volume methods is used extensively to solve the RANS equations, Eq. 25.2.

25.1.2 Large Eddy Simulations: LES

A method more accurate than RANS is LES (Large Eddy Simulations) in which only the small eddies (fluctuations whose eddies are smaller than the computational cell) are modeled with a turbulence model. The LES equations read

$$\begin{aligned}
\frac{\partial \bar{v}_i}{\partial t} + \frac{\partial \bar{v}_i \bar{v}_j}{\partial x_j} &= -\frac{1}{\rho}\frac{\partial \bar{p}}{\partial x_i} + \nu\frac{\partial^2 \bar{v}_i}{\partial x_j \partial x_j} - \frac{\partial \tau_{ij}}{\partial x_j} \\
&= -\frac{1}{\rho}\frac{\partial \bar{p}}{\partial x_i} + \frac{\partial}{\partial x_j}\left((\nu + \nu_{sgs})\frac{\partial \bar{v}_i}{\partial x_j}\right)
\end{aligned} \tag{25.3}$$

Note that the time dependence term (the first term on the left side of the first line) has been retained, because the large, time dependent turbulent (i.e. the resolved) fluctuations are part of $\bar{v}_i$ and $\bar{p}$ and are not modeled with the turbulence model. The last term on the first line includes the Reynolds stresses of the small eddies, which are called SGS (sub-grid stresses). This term must also – as in Eq. 25.2 – be modeled, and at the second line it has been modeled with a SGS turbulent viscosity, ν_{sgs}. The difference of ν_{sgs} compared to ν_t in Eq. 25.2 is that it includes only the effect of the *small* eddies. The ratio of ν_{sgs} to ν is of the order of 1 to 100. However, the ratio of the resolved to the modeled turbulence, $|\bar{v}_i'\bar{v}_j'|/|\tau_{ij}|$ (see Eqs. 25.2 and 25.3) is much larger than one. Hence, LES is much more accurate than RANS because only a small part of the turbulence is modeled with the turbulence SGS model whereas in RANS all turbulence is modeled. The disadvantage of LES is that it is *much* more expensive than RANS because a finer mesh must be used and because the equations are solved in four dimensions (time and three spatial directions) whereas RANS can be solved in steady state (no time dependence).

When the flow near walls is of importance, is turns out that LES is prohibitively expensive because very fine cells must be used there. The reason is entirely due to physics: near the walls, the spatial scales of the "large" turbulent eddies which should be resolved by LES are in reality rather small. Furthermore, their spatial scales get smaller for increasing Reynolds number. Much research has the last ten years been carried out to circumvent this problem. All proposed methods combines RANS and LES where RANS is used near walls and LES is used some distance away from the walls, see Fig. 25.1. These methods are called Detached Eddy Simulation (DES), hybrid LES/RANS or zonal LES/RANS. The focus here is zonal LES/RANS.

25.1.3   Zonal LES/RANS

Equations 25.2 and 25.3 can be written in a same form as

$$\frac{\partial \bar{v}_i}{\partial t} + \frac{\partial \bar{v}_i \bar{v}_j}{\partial x_j} = -\frac{1}{\rho}\frac{\partial \bar{p}}{\partial x_i} + \frac{\partial}{\partial x_j}\left((\nu + \nu_T)\frac{\partial \bar{v}_i}{\partial x_j}\right) \qquad (25.4)$$

Near the walls, a RANS turbulence model is used for the turbulent viscosity, i.e. $\nu_T = \nu_t$ and away from the walls an LES turbulence model is employed, i.e. $\nu_T = \nu_{sgs}$. Note that the time dependence term is now retained also in the RANS region: near the wall we are using an *un*steady RANS, i.e. URANS.

Above, we have describe how to use the zonal LES/RANS method for flows near walls. Another form of zonal LES/RANS is *embedded* LES, in which an LES region is embedded in a RANS region. One example is prediction of aeroacoustic noise created by the turbulence around an external mirror on a vehicle [116]. The flow around the vehicle can be computed with RANS, but in order to predict the noise in the region of the external mirror we must predict the large turbulence fluctuations and hence LES must be used in this region. In Section 25.4 we will present simulations using embedded LES in a simplified configuration represented by the flow in a channel in which RANS is used upstream of the interface and LES is used downstream of it, see Fig. 25.4.

25.2   The PANS $k - \varepsilon$ turbulence model

The PANS $k - \varepsilon$ model can be used to simulate wall-bounded flow at high Reynolds number as well as embedded LES. The turbulence model reads [144,145], see Eq. 23.19
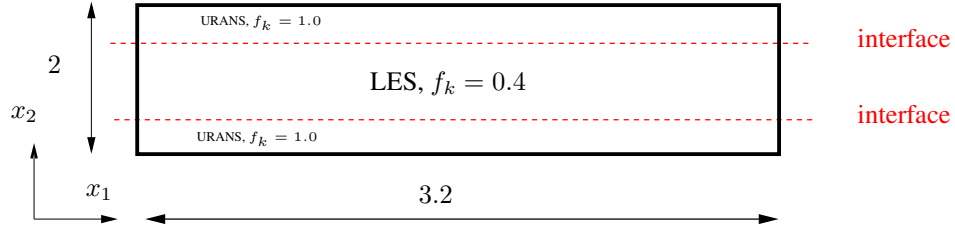
Figure 25.1: The LES and URANS regions. Fully developed channel flow. Periodic boundary conditions are applied at the left and right boundaries.

(here in a slightly simplified form to enhance readability)

$$\frac{\partial k}{\partial t} + \frac{\partial k \bar{v}_j}{\partial x_j} = \frac{\partial}{\partial x_j}\left[\left(\nu + \frac{\nu_T}{\sigma_k}\right)\frac{\partial k}{\partial x_j}\right] + P^k - \varepsilon \tag{25.5}$$

$$\frac{\partial \varepsilon}{\partial t} + \frac{\partial \varepsilon \bar{v}_j}{\partial x_j} = \frac{\partial}{\partial x_j}\left[\left(\nu + \frac{\nu_T}{\sigma_\varepsilon}\right)\frac{\partial \varepsilon}{\partial x_j}\right] + C_{\varepsilon 1} P^k \frac{\varepsilon}{k} - C_{\varepsilon 2}^* \frac{\varepsilon^2}{k} \tag{25.6}$$

$$C_{\varepsilon 2}^* = C_{\varepsilon 1} + f_k(C_{\varepsilon 2} - C_{\varepsilon 1}), \quad C_{\varepsilon 1} = 1.5, \quad C_{\varepsilon 2} = 1.9 \tag{25.7}$$

$$\nu_T = C_\mu \frac{k^2}{\varepsilon}, \quad C_\mu = 0.09 \tag{25.8}$$

Note that k and ε are always positive. The key elements in the present use of the PANS $k - \varepsilon$ model are highlighted in red. When f_k in Eq. 25.7 is equal to one, the model acts as a standard $k - \varepsilon$ RANS model giving a large turbulent viscosity. When f_k is decreased (to 0.4 in the present study), $C_{\varepsilon 2}^*$ in Eq. 25.7 decreases. As a result

- ε increases because the destruction term (last term in Eq. 25.6 which is the main sink term) in the ε equation decreases,

- k decreases because ε (last term in Eq. 25.5) is the main sink term in the k equation increases, and

- ν_T in Eq. 25.8 decreases because k decreases and ε increases.

Hence, the turbulence model in Eqs. 25.5–25.8 acts as a RANS turbulence model (large turbulent viscosity) when $f_k = 1$ and it acts as an LES SGS turbulence model (small turbulent viscosity) when $f_k = 0.4$.

25.3 Zonal LES/RANS: wall modeling

25.3.1 The interface conditions

The interface plane (see Fig. 25.1) separates the URANS regions near the walls and the LES region in the core region. In the LES region $f_k = 0.4$ and in the URANS region $f_k = 1$. In the former region, the turbulent viscosity ν_T should be an SGS viscosity and in the latter region it should be an RANS viscosity. Hence ν_T must decrease rapidly when going from the URANS region to the LES region. This is achieved by setting the usual convection and diffusion fluxes of k at the interface to zero. New fluxes are introduced using smaller SGS values [165].

(a) Velocities   (b) Resolved shear stresses
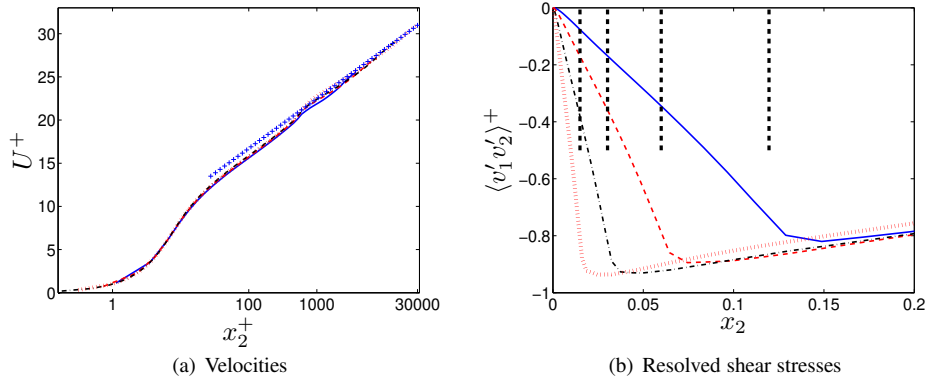
Figure 25.2: Velocities and resolved shear stresses. $(N_x \times N_z) = (64 \times 64)$ ——— : $Re_\tau = 4\,000$; — — : $Re_\tau = 8\,000$; — · — : $Re_\tau = 16\,000$; ////: $Re_\tau = 32\,000$.

25.3.2 Results

Fully developed channel flow is computed for Reynolds numbers $Re_\tau = u_\tau\delta/\nu = 4\,000, 8\,000, 16\,000$ and $32\,000$. The baseline mesh has 64×64 cells in the streamwise (x_1) and spanwise (x_3) directions. The size of the domain is $x_{1,max} = 3.2$, $x_{2,max} = 2$ and $x_{3,max} = 1.6$ ($\delta = u_\tau = 1$). The grid in the x_2 direction varies between 80 and 128 cells depending on Reynolds number. The interface is set to $x_2^+ \simeq 500$ for all grids.

The velocity profiles and the resolved shear stresses are presented in Fig. 25.2. As can be seen, the predicted velocity profiles are in good agreement with the log-law which represents experiments. Figure 25.2b presents the resolved shear stresses. The interface is shown by thick dashed lines and it moves towards the wall for increasing Reynolds number since it is located at $x_2^+ \simeq 500$ for all Reynolds numbers.

The turbulent viscosity profiles are shown in Fig. 25.3 for three different resolutions in the $x_1 - x_3$ plane. It is interesting to note that the turbulent viscosity is not affected by the grid resolution. Hence, the model yields *grid independent* results contrary to other LES/RANS models.

The turbulent viscosity (Fig. 25.3) is sharply reduced when going across the interface from the URANS region to the LES region and the resolved fluctuations (the Reynolds shear stress in Fig. 25.2b) increase. This shows that the model is switching from RANS mode to LES mode as it should. More detailed results can be found in [165].

25.4 Zonal LES/RANS: embedded LES

25.4.1 The interface conditions

The interface plane is now vertical, see Fig. 25.4. The interface conditions for k and ε are treated in the same way as in Section 25.3.1. The difference is now that "inlet" turbulent fluctuations must be added to the LES $\bar{v}_i$ equations (Eq. 25.3) to trigger the flow into turbulence-resolving mode. Anisotropic synthetic turbulent fluctuations are used [172, 173].

(a) $Re_\tau = 4000$. ——— : $(N_x \times N_z) = (64 \times 64)$; ▬ ▬ : $(N_x \times N_z) = (32 \times 32)$; ▬ ▪ ▬ : $(N_x \times N_z) = (128 \times 128)$

(b) $(N_x \times N_z) = (64 \times 64)$. ——— : $Re_\tau = 4\,000$; ▬ ▬ : $Re_\tau = 8\,000$; ▬ ▪ ▬ : $Re_\tau = 16\,000$; ////: $Re_\tau = 32\,000$.
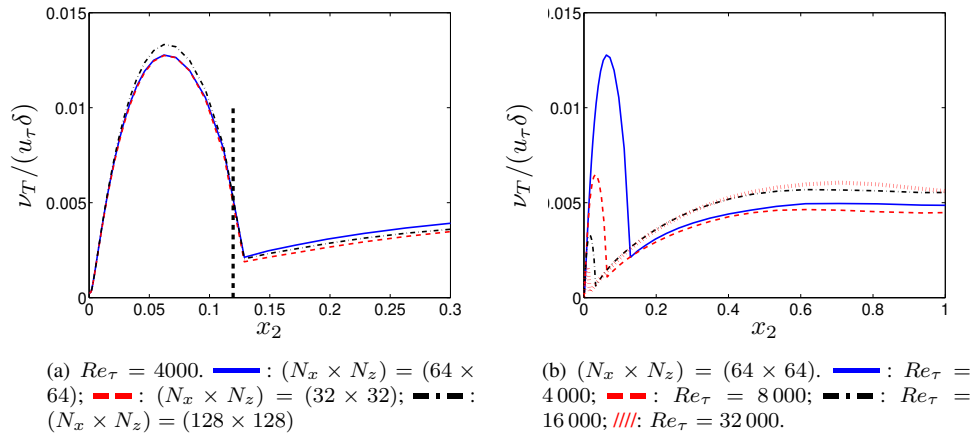
Figure 25.3: Turbulent viscosity.
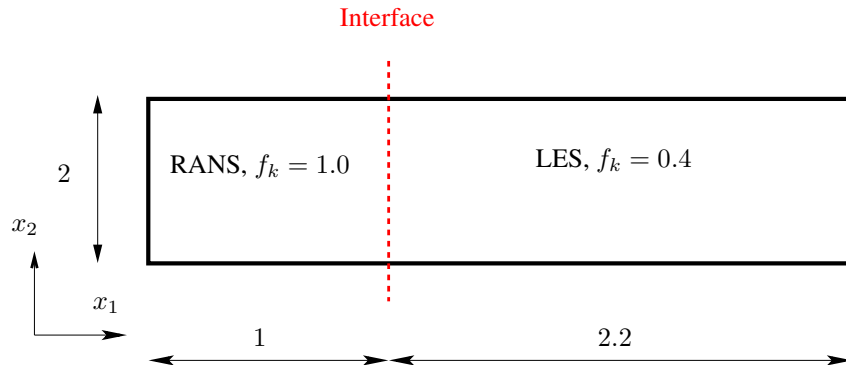
Figure 25.4: The LES and RANS regions. The left boundary is an inlet and the right boundary is an outlet.

(a) Velocities. ——— $x_1 = 0.19$; ▬ ▬ $x_1 = 1.25$; ▬ ▪ ▬ $x_1 = 3$. The log-law is plotted in symbols.

(b) ▬ ▬ : Turbulent viscosity (right x_2 axis); ——— : maximum streamwise fluctuations (left x_2 axis)
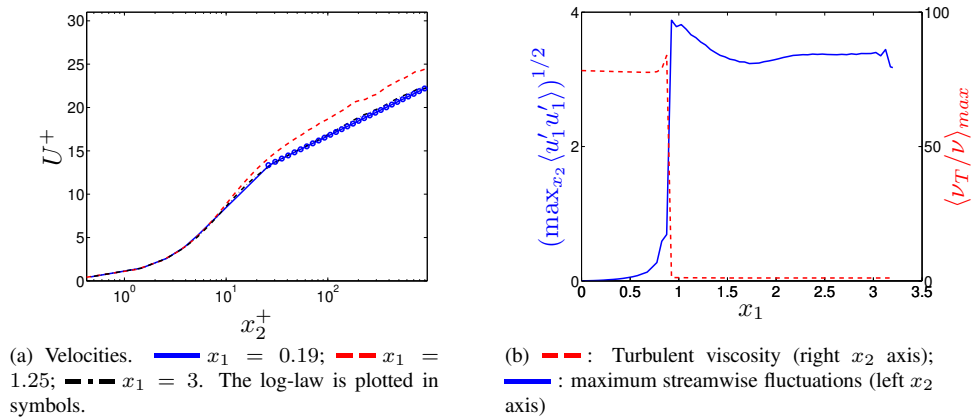
Figure 25.5: Channel flow with inlet and outlet. (a) Velocities; (b) maximum resolved streamwise turbulent fluctuations and turbulent viscosity versus x_1.

25.4.2 Results

The Reynolds number for the channel flow is $Re_\tau = 950$. With a $3.2 \times 2 \times 1.6$ domain, a mesh with $64 \times 80 \times 64$ cells is used in the streamwise (x_1), the wall-normal (x_2) and the spanwise (x_3) direction, see Fig. 25.4. Inlet conditions at $x = 0$ are created by computing fully developed channel flow with the PANS $k - \varepsilon$ model in RANS mode (i.e. with $f_k = 1$).

Figure 25.5a presents the mean velocity and the resolved shear stresses at three streamwise locations, $x_1 = 0.19$, 1.25 and 3 (recall that the interface is located at $x_1 = 1$). At $x_1 = 3$, the predicted velocity agrees very well with the experimental log-law profile.

The resolved streamwise velocity fluctuations are zero in the RANS region, as they should (Fig. 25.5b), and the maximum resolved values increase sharply over the interface thanks to the imposed synthetic turbulent "inlet" fluctuations. The turbulent viscosity is reduced at the interface from its peak RANS value of approximately 80 to a small LES value of approximately one (these values are both fairly low because of the low Reynolds number). Hence, it is seen that the present model successfully switches from RANS to LES across the interface. The results are presented in more detail in [165].

26   Commutation terms in the k and ω equations

In embedded LES, part of the flow is treated by RANS and part by LES. Here we are interested in a configuration where the upstream region is treated by RANS and the downstream by LES, and the interface is vertical, parallel to the inlet. We denote the interface between the two regions as "the RANS-LES interface" located at x_{R-L}, see Figs.25.4, 26.1 and 26.2. The transition region in which the predicted flow is in between RANS and LES is often called the *grey area*, a problem described in [174]. When the flow goes from a RANS region to an LES region through the RANS-LES interface, it should – in order to minimize the grey area – switch as quickly as possible from RANS mode to LES mode.

Hamda [175] showed that, when the filter size (i.e. the grid) is non-uniform, a commutation error appears in SGS models based on transport equations. He found by analyzing DNS channel data that this commutation term is large at interfaces between RANS and LES. Here we show how to apply the commutation term derived in [175] at RANS-LES interfaces. We present a method in which commutations terms are added in the k and ω equations in order to quickly switch from RANS te LES.

The two-equation zonal $k - \omega$ hybrid RANS-LES model of [176] is employed. In the LES region, the model reads

$$\frac{\partial k}{\partial t} + \frac{\partial \bar{v}_i k}{\partial x_i} = P^k - f_k \frac{k^{3/2}}{\ell_t} + \frac{\partial}{\partial x_j}\left[\left(\nu + \frac{\nu_t}{\sigma_k}\right)\frac{\partial k}{\partial x_j}\right] \qquad (26.1)$$

$$\frac{\partial \omega}{\partial t} + \frac{\partial \bar{v}_i \omega}{\partial x_i} = C_{\omega_1} f_\omega \frac{\omega}{k} P^k - C_{\omega 2}\omega^2 + \frac{\partial}{\partial x_j}\left[\left(\nu + \frac{\nu_t}{\sigma_\omega}\right)\frac{\partial \omega}{\partial x_j}\right] + C_\omega \frac{\nu_t}{k}\frac{\partial k}{\partial x_j}\frac{\partial \omega}{\partial x_j} \qquad (26.2)$$

$$\nu_t = f_\mu \frac{k}{\omega}, \quad P^k = \nu_t\left(\frac{\partial \bar{v}_i}{\partial x_j} + \frac{\partial \bar{v}_j}{\partial x_i}\right)\frac{\partial \bar{v}_i}{\partial x_j}, \quad \ell_t = \Psi_{PDH} C_{LES} \Delta_{dw}$$

$$\Psi_{PDH} = \min\left[10, f_k\left(\frac{f_\omega}{f_\mu}\right)^{3/4}\right], \quad \Delta_{max} = \max\{\Delta x, \Delta y, \Delta z\} \qquad (26.3)$$

$$\Delta_{dw} = \min\left(\max\left[C_{dw} d_w, C_w \Delta_{max}, \Delta_{nstep}\right], \Delta_{max}\right)$$

where d_w denotes the distance to the nearest wall and Δ_{step} is the grid step size in the wall-normal direction. The damping functions read

$$f_k = 1 - 0.722 \cdot \exp\left[-\left(\frac{R_t}{10}\right)^4\right], \quad f_\omega = 1 + 4.3 \cdot \exp\left[-\left(\frac{R_t}{1.5}\right)^{1/2}\right]$$

$$f_\mu = 0.025 + \left\{1 - \exp\left[-\left(\frac{R_t}{10}\right)^{3/4}\right]\right\}\left\{0.975 + \frac{0.001}{R_t}\cdot\exp\left[-\left(\frac{R_t}{200}\right)^2\right]\right\}.$$

The turbulent Reynolds number is defined as $R_t = k/(\nu\omega)$. The length scale, Δ_{dw}, is taken from the IDDES model [163]. In the RANS regions, $\ell_t = k^{1/2}/(C_k\omega)$. The constants read $\sigma_k = 0.8$, $\sigma_w = 1.35$, $C_k = 0.09$ $C_{\omega 1} = 0.42$, $C_{\omega 2} = 0.075$, $C_\omega = 0.75$, $C_{LES} = 0.7$ and $C_{dw} = 0.15$.

The difference between Eqs. 26.1 and 26.2 in the RANS and LES regions can be summarized as follows: in RANS regions, the RANS lengthscale, $\ell_t = k^{1/2}/(C_k\omega)$, is used in the dissipation term in the k equation and, in LES regions, the filter length scale, Δ_{dw}, is used.
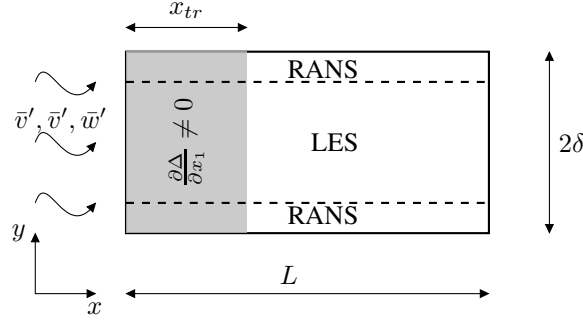
Figure 26.1: Channel flow.
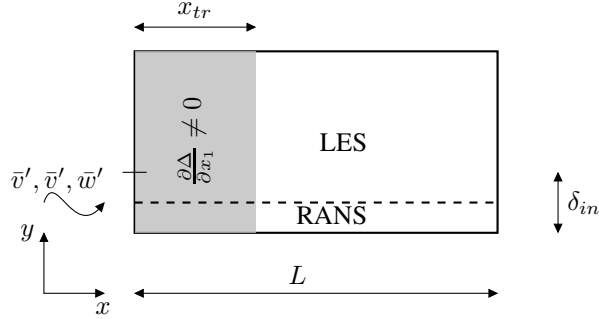
Figure 26.2: Boundary layer flow.

When the filter size in LES varies in space, an additional term appears in the momentum equation because the spatial derivatives and the filtering do not commute. For the convective term in Navier-Stokes, for example, we get

$$\overline{\frac{\partial v_i v_j}{\partial x_j}} = \frac{\partial}{\partial x_j}(\overline{v_i v_j}) + \mathcal{O}\left((\Delta x)^2\right).$$

Ghosal & Moin [80] show that the error is proportional to $(\Delta x)^2$ and, since this error is of the same order as the discretization error of most finite volume methods, it is usually neglected.

However, in zonal[6] hybrid RANS-LES, the length scale at the RANS-LES interface changes abruptly from a RANS length scale to an LES length scale. Hamda [175] estimated the commutation error at RANS-LES interfaces and found that it is large. The commutation term for the divergence of a flux, q_i, reads

$$\overline{\frac{\partial q_i}{\partial x_i}} = \frac{\partial \bar{q}_i}{\partial x_i} - \frac{\partial \Delta}{\partial x_i}\frac{\partial \bar{q}_i}{\partial \Delta} \tag{26.4}$$

The derivation of Eq. 26.4 is giben in [177] For the k equation, the commutation term

---

[6]by "zonal", we imply that the interface is chosen at a location where the RANS and LES length scales differ

in Eq. 26.4 reads [175]

$$\overline{\frac{\partial u_i k}{\partial x_i}} = \frac{\partial \bar{v}_i k}{\partial x_i} - \frac{\partial \Delta}{\partial x_i} \frac{\partial \bar{v}_i k}{\partial \Delta} \tag{26.5}$$

Consider a fluid particle in a RANS region moving in the x_1 direction and passing across a RANS-LES interface. The filter width decreases across the interface, i.e.

$$\frac{\partial \Delta}{\partial x_1} \simeq \frac{\Delta_{LES} - \Delta_{RANS}}{\Delta x_1} < 0 \tag{26.6}$$

and

$$\frac{\partial \bar{v}_1 k}{\partial \Delta} \simeq \frac{u_1 k_{LES} - u_1 k_{RANS}}{\Delta_{LES} - \Delta_{RANS}} > 0 \tag{26.7}$$

which means that the last term on the right-hand side of Eq. 26.5 gives a positive contribution on the left side of the k equation, Eq. 26.1; on the right side of Eq. 26.1, it gives a negative contribution. Hence, the additional term in Eq. 26.5 at a RANS-LES interface reduces k, as expected. To obtain the right hand of Eqs. 26.6 and 26.7, the derivatives on the left side of the equations have been estimated by simple finite-difference expressions, i.e.

$$\frac{df}{dx} \simeq \frac{\Delta f}{\Delta x} \tag{26.8}$$

It may be noted that the idea of adding an additional source term in the k equation due to a commutation error is similar to the proposal in [166]; they use a commutation term based on the gradient of f_k in the PANS model. This idea was later used by the present author at RANS-LES interfaces [147].

To find the corresponding term in the ω equation, let us start by looking at the ε equation. What happens with ε when a fluid particle moves from a RANS region into an LES region? The answer is, nothing. The dissipation is the same in a RANS region as in an LES region. This is best seen by looking at the k_{sgs} equation

$$\frac{\partial k_{sgs}}{\partial t} + \frac{\partial \bar{v}_i k_{sgs}}{\partial x_i} = P^{k_{sgs}} + \frac{\partial}{\partial x_j} \left[\left(\nu + \frac{\nu_{sgs}}{\sigma_k} \right) \frac{\partial k_{sgs}}{\partial x_j} \right] - \varepsilon. \tag{26.9}$$

The dissipation term, ε, in Eq. 26.9 is the same as the dissipation term in Eq. 26.1 unless the resolution is very fine (close to DNS). Then much of the dissipation is resolved, reducing the production term, $P^{k_{sgs}}$. However, this kind of resolution is not realistic.

Now consider the ω equation. It is derived by transformation of the k and ε equations to an ω equation as

$$\frac{d\omega}{dt} = \frac{d}{dt}\left(\frac{\varepsilon}{C_k k} \right) = \frac{1}{C_k k} \frac{d\varepsilon}{dt} + \frac{\varepsilon}{C_k} \frac{d(1/k)}{dt} = \frac{1}{C_k k} \frac{d\varepsilon}{dt} - \frac{\omega}{k} \frac{dk}{dt} \tag{26.10}$$

The right-hand side shows that the source terms in the ω equation correspond to those in the ε equation multiplied by $1/(C_k k)$ together with those in the k equation multiplied by $-\omega/k$. Hence, the source term due to the commutation error in the ω equation is the commutation term in Eq. 26.5 multiplied by $-\omega/k$ so that

$$\overline{\frac{\partial u_i \omega}{\partial x_i}} = \frac{\partial \bar{v}_i \omega}{\partial x_i} - \frac{\partial \Delta}{\partial x_i} \frac{\partial \bar{v}_i \omega}{\partial \Delta} = \frac{\partial \bar{v}_i \omega}{\partial x_i} + \frac{\omega}{k} \frac{\partial \Delta}{\partial x_i} \frac{\partial \bar{v}_i k}{\partial \Delta} \tag{26.11}$$

Assuming again a flow in the x_1 direction from a RANS region to an LES region, we find that the second term on the right-hand side of Eq. 26.11 is negative since

$\partial \Delta / \partial x_1 < 0$ (see Eq. 26.6) and $\partial \bar{v}_1 k / \partial \Delta > 0$ (see Eq. 26.7) so that the commutation term in Eq. 26.11 is positive/negative on the right/left-side of the ω equation (Eq. 26.2). This means that the commutation term in Eq. 26.11 will increase ω when moving from a RANS region to an LES region. Hence the source terms in the k and ω equations both contribute to reducing the turbulent viscosity, which is an effect we are looking for at RANS-LES interfaces: a reduced turbulent viscosity will promote growth of resolved turbulence on the LES side of an interface.

The results using the commutation terms are presented in [178, 179].

27 Inlet boundary conditions

IN RANS it is sufficient to supply profiles of the mean quantities such as velocity and temperature plus the turbulent quantities (e.g. k and ε). However, in unsteady simulations (LES, URANS, DES . . .) the time history of the velocity and temperature need to be prescribed; the time history corresponds to turbulent, resolved fluctuations. In some flows it is critical to prescribe reasonable turbulent fluctuations, but in many flows it seems to be sufficient to prescribe constant (in time) profiles [130, 180].

There are different ways to create turbulent inlet boundary conditions. One way is to use a pre-cursor DNS or well resolved LES of channel flow. This method is limited to fairly low Reynolds numbers and it is difficult (or impossible) to re-scale the DNS fluctuations to higher Reynolds numbers.

Another method based partly on synthesized fluctuations is the vortex method [181]. It is based on a superposition of coherent eddies where each eddy is described by a shape function that is localized in space. The eddies are generated randomly in the inflow plane and then convected through it. The method is able to reproduce first and second-order statistics as well as two-point correlations.

A third method is to take resolved fluctuations at a plane downstream of the inlet plane, re-scale them and use them as inlet fluctuations.

Below we present a method of generating synthesized inlet fluctuations.

27.1 Synthesized turbulence

The method described below was developed in [100, 182, 183] for creating turbulence for generating noise. It was later further developed for inlet boundary conditions [172, 184, 185].

A turbulent fluctuating velocity fluctuating field (whose average is zero) can be expressed using a Fourier series, see Section 5.3 and Eq. H.17. Let us re-write this formula as

$$a_n \cos(nx) + b_n \sin(nx) =$$
$$c_n \cos(\alpha_n) \cos(nx) + c_n \sin(\alpha_n) \sin(nx) = c_n \cos(nx - \alpha_n) \tag{27.1}$$

where $a_n = c_n \cos(\alpha)$, $b_n = c_n \sin(\alpha_n)$. The new coefficient, c_n, and the phase angle, α_n, are related to a_n and b_n as

$$c_n = \left(a_n^2 + b_n^2\right)^{1/2} \quad \alpha_n = \arctan\left(\frac{b_n}{a_n}\right) \tag{27.2}$$

A general form for a turbulent velocity field can thus be written as

$$\mathbf{v}'(\mathbf{x}) = 2 \sum_{n=1}^{N} \hat{u}^n \cos(\boldsymbol{\kappa}^n \cdot \mathbf{x} + \psi^n)\boldsymbol{\sigma}^n \tag{27.3}$$

where $\hat{u}^n$, ψ^n and σ_i^n are the amplitude, phase and direction of Fourier mode n. The synthesized turbulence at one time step is generated as follows.

27.2 Random angles

The angles φ^n and θ^n determine the direction of the wavenumber vector $\boldsymbol{\kappa}$, see Eq. 27.3 and Eq. 27.1; α^n denotes the direction of the velocity vector, $\mathbf{v}'$. For more details, see Appendix N.
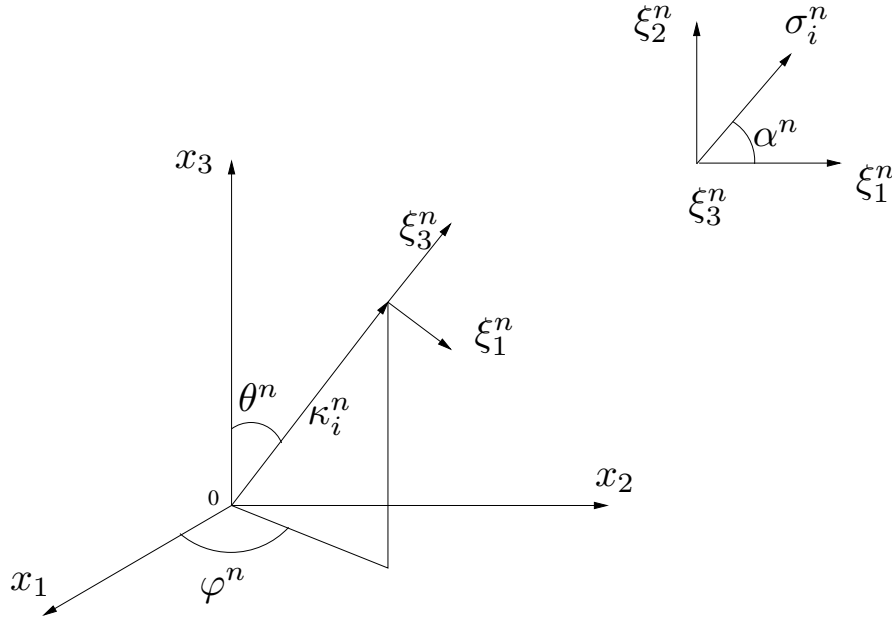
Figure 27.1: The wave-number vector, κ_i^n, and the velocity unit vector, σ_i^n, are orthogonal (in physical space) for each wave number n.

27.3 Highest wave number

Define the highest wave number based on mesh resolution $\kappa_{max} = 2\pi/(2\Delta)$ (see Section 18.5), where Δ is the grid spacing. Often the smallest grid spacing near the wall is small, and then a slightly larger values may be chosen. The fluctuations are generated on a grid with equidistant spacing (or on a weakly stretched mesh), $\Delta\eta = x_{2,max}/N_2$, $\Delta x_3 = x_{3,max}/N_3$, where η denotes the wall-normal direction and N_2 and N_3 denote the number of cells in the x_2 and x_3 direction, respectively. The fluctuations are set to zero at the wall and are then interpolated to the inlet plane of the CFD grid (the $x_2 - x_3$ plane).

27.4 Smallest wave number

Define the smallest wave number from $\kappa_1 = \kappa_e/p$, where $\kappa_e = \alpha 9\pi/(55L_t)$, $\alpha = 1.453$. The turbulent length scale, L_t, may be estimated in the same way as in RANS simulations, i.e. $L_t \propto \delta$ where δ denotes the inlet boundary layer thickness. In [172, 184, 185] it was found that $L_t \simeq 0.1\delta_{in}$ is suitable.

Factor p should be larger than one to make the largest scales larger than those corresponding to κ_e. A value $p = 5$ is suitable.

27.5 Divide the wave number range

Divide the wavenumber space, $\kappa_{max} - \kappa_1$, into N modes, equally large, of size $\Delta\kappa$.

27.6 von Kármán spectrum

A modified von Kármán spectrum is chosen, see Eq. 27.4 and Fig. 27.2. The amplitude $\hat{u}^n$ of each mode in Eq. 27.3 is then obtained from

$$\hat{u}^n = (E(\kappa)\Delta\kappa)^{1/2}$$
$$E(\kappa) = c_E \frac{u_{rms}^2}{\kappa_e} \frac{(\kappa/\kappa_e)^4}{[1+(\kappa/\kappa_e)^2]^{17/6}} e^{[-2(\kappa/\kappa_\eta)^2]} \tag{27.4}$$
$$\kappa = (\kappa_i \kappa_i)^{1/2}, \quad \kappa_\eta = \varepsilon^{1/4}\nu^{-3/4}$$

The coefficient c_E is obtained by integrating the energy spectrum over all wavenumbers to get the turbulent kinetic energy, i.e.

$$k = \int_0^\infty E(\kappa)d\kappa \tag{27.5}$$

which gives [84]

$$c_E = \frac{4}{\sqrt{\pi}} \frac{\Gamma(17/6)}{\Gamma(1/3)} \simeq 1.453 \tag{27.6}$$

where

$$\Gamma(z) = \int_0^\infty e^{-z'} x^{z-1} dz' \tag{27.7}$$

27.7 Computing the fluctuations

Having $\hat{u}^n$, κ_j^n, σ_i^n and ψ^n, allows the expression in Eq. 27.3 to be computed, i.e.

$$v_1' = 2\sum_{n=1}^N \hat{u}^n \cos(\beta^n)\sigma_1$$
$$v_2' = 2\sum_{n=1}^N \hat{u}^n \cos(\beta^n)\sigma_2 \tag{27.8}$$
$$v_3' = 2\sum_{n=1}^N \hat{u}^n \cos(\beta^n)\sigma_3$$
$$\beta^n = k_1^n x_1 + k_2^n x_2 + k_3^n x_3 + \psi^n$$

where $\hat{u}^n$ is computed from Eq. 27.4.

In this way inlet fluctuating velocity fields (v_1', v_2', v_3') are created at the inlet x_2-x_3 plane.

The code for generating the isotropic fluctuations can be downloaded here
`http://www.tfd.chalmers.se/~lada/projects/inlet-boundary-conditions/proright.ht`

27.8 Introducing time correlation

A fluctuating velocity field is generated each time step as described above. They are independent of each other and their time correlation will thus be zero. This is non-physical. To create correlation in time, new fluctuating velocity fields, $\mathcal{V}_1'$, $\mathcal{V}_2'$, $\mathcal{V}_3'$, are
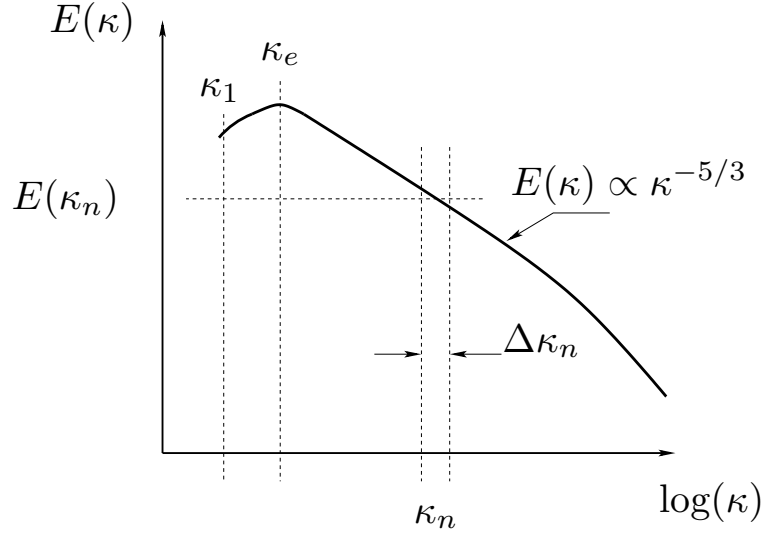
Figure 27.2: Modified von Kármán spectrum

computed based on an asymmetric time filter

$$
\begin{aligned}
(\mathcal{V}_1')_m &= a(\mathcal{V}_1')_{m-1} + b(v_1')_m \\
(\mathcal{V}_2')_m &= a(\mathcal{V}_2')_{m-1} + b(v_2')_m \\
(\mathcal{V}_3')_m &= a(\mathcal{V}_3')_{m-1} + b(v_3')_m
\end{aligned}
\tag{27.9}
$$

where m denotes the time step number and

$$
a = \exp(-\Delta t/T_{int})
\tag{27.10}
$$

where Δt and T_{int} denote the computational time step and the integral time scale, respectively. The second coefficient is taken as

$$
b = (1 - a^2)^{0.5}
\tag{27.11}
$$

which ensures that $\langle \mathcal{V}_1'^2 \rangle = \langle v_1'^2 \rangle$ ($\langle \cdot \rangle$ denotes averaging). The time correlation of two time instants will be equal to

$$
\exp(-\hat{t}/T_{int})
\tag{27.12}
$$

where $\hat{t}$ is the time separation and thus Eq. 27.9 is a convenient way to prescribe the turbulent time scale of the fluctuations. For more detail, see Section 27.8. The inlet boundary conditions are prescribed as (we assume that the inlet is located at $x_1 = 0$ and that the mean velocity is constant in the spanwise direction, x_3)

$$
\begin{aligned}
\bar{v}_1(0, x_2, x_3, t) &= V_{1,in}(x_2) + v_{1,in}'(x_2, x_3, t) \\
\bar{v}_2(0, x_2, x_3, t) &= V_{2,in}(x_2) + v_{2,in}'(x_2, x_3, t) \\
\bar{v}_3(0, x_2, x_3, t) &= V_{3,in}(x_2) + v_{3,in}'(x_2, x_3, t)
\end{aligned}
\tag{27.13}
$$

where $v_{1,in}' = (\mathcal{V}_1')_m$, $v_{2,in}' = (\mathcal{V}_2')_m$ and $v_{3,in}' = (\mathcal{V}_3')_m$ (see Eq. 27.9). The mean inlet profiles, $V_{1,in}$, $V_{2,in}$, $V_{3,in}$, are either taken from experimental data, a RANS
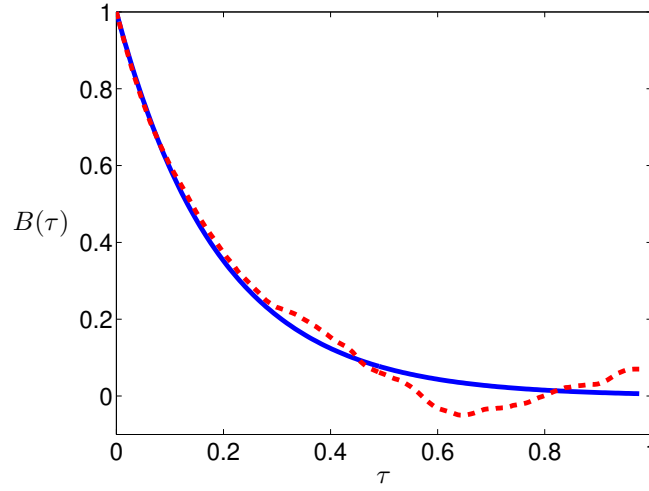
Figure 27.3: Auto correlation, $B(\tau) = \langle v_1'(t)v_1'(t-\tau)\rangle_t$ (averaged over time, t). ▬▬ : Eq. 27.12; ▬ ▬ : computed from synthetic data, $(\mathcal{V}_1')^m$, see Eq. 27.9.

solution or from the law of the wall; for example, if $V_{2,in} = V_{3,in} = 0$ we can estimate $V_{1,in}$ as [186]

$$V_{1,in}^+ = \begin{cases} x_2^+ & x_2^+ \le 5 \\ -3.05 + 5\ln(x_2^+) & 5 < x_2^+ < 30 \\ \frac{1}{\kappa}\ln(x_2^+) + B & x_2^+ \ge 30 \end{cases} \tag{27.14}$$

where $\kappa = 0.4$ and $B = 5.2$.

The method to prescribed fluctuating inlet boundary conditions have been used for channel flow [172], for diffusor flow [180] as well as for the flow over a bump and an axisymmetric hill [187].

Equation 27.9 introduces a time correlation with an integral time scale T_{int}. In order to understand Eq. 27.10, Equation 27.9 is written for $m = N \ldots 1$ where N denotes number of time steps

$$\begin{aligned}
\mathcal{U}_N' &= a\mathcal{U}_{N-1}' + bu_N' \\
\mathcal{U}_{N-1}' &= a\mathcal{U}_{N-2}' + bu_{N-1}' \\
\mathcal{U}_{N-2}' &= a\mathcal{U}_{N-3}' + bu_{N-2}' \\
&\vdots \\
\mathcal{U}_3' &= a\mathcal{U}_2' + bu_3' \\
\mathcal{U}_2' &= a\mathcal{U}_1' + bu_2' \\
\mathcal{U}_1' &= a\mathcal{U}_0' + bu_1'
\end{aligned} \tag{27.15}$$

With $\mathcal{U}'_0 = 0$ we get

$$
\begin{aligned}
\mathcal{U}'_1 &= bu'_1 \\
\mathcal{U}'_2 &= abu'_1 + bu'_2 \\
\mathcal{U}'_3 &= a^2bu'_1 + abu'_2 + bu'_3 \\
\mathcal{U}'_4 &= a^3bu'_1 + a^2bu'_2 + abu'_3 + bu'_4 \\
\mathcal{U}'_5 &= a^4bu'_1 + a^3bu'_2 + a^2bu'_3 + abu'_4 + bu'_5
\end{aligned}
\tag{27.16}
$$

which can be written as

$$
\mathcal{U}'_m = b \sum_{k=1}^{m} a^{m-k} u'_k
\tag{27.17}
$$

Let's show that $\langle \mathcal{U}'^2 \rangle = \langle u'^2 \rangle$. Equation 27.17 gives

$$
\langle \mathcal{U}'^2 \rangle = \frac{1}{m} \sum_{k=1}^{m} \mathcal{U}'_k \mathcal{U}'_k = \frac{b^2}{m^2} \sum_{k=1}^{m} a^{m-k} u'_k \sum_{i=1}^{m} a^{m-i} u'_i
\tag{27.18}
$$

Recall that the synthetic fields u'_k and u'_i are independent which means that $\langle u'_k u'_i \rangle = 0$ for $k \neq i$. Hence

$$
\langle \mathcal{U}'^2 \rangle = \frac{b^2}{m} \sum_{k=1}^{m} a^{2(m-k)} u'_k u'_k = \langle u'^2 \rangle (1 - a^2) \sum_{k=1}^{m} a^{2k}
\tag{27.19}
$$

replacing a with b using Eq. 27.11. The requirement is that $\langle \mathcal{U}'^2 \rangle = \langle u'^2 \rangle$ and hence

$$
(1 - a^2) \sum_{k=1}^{m} a^{2k} = (1 - a^2) \sum_{k=1}^{m} c^k = 1
\tag{27.20}
$$

must be satisfied. The sum $\sum_{k=1}^{m} c^k$ has for large m the value $S_m = 1/(1 - c) = 1/(1 - a^2)$ which shows that the requirement in Eq. 27.20 is satisfied.

The time correlation between many time steps with time step separation $m - n = r \geq 0$ reads

$$
\begin{aligned}
\langle \mathcal{U}'\mathcal{U}' \rangle_r &= \frac{b^2}{(m-r)n} \sum_{p=1}^{n} a^{n-p} u'_p \sum_{k=1}^{m-r} a^{m-k} u'_k \\
&= \frac{b^2}{m-r} \sum_{k=1}^{m-r} a^{2(m-k)} a^r u'^2_k = \langle u'u' \rangle a^r
\end{aligned}
\tag{27.21}
$$

using Eqs. 27.19 and 27.20. The factor a^r is given by the correlation between u'_k and u'_{k-r}, see Eq. 27.17. Inserting Eq. 27.10 into Eq. 27.21 we get the normalized autocorrelation

$$
B_{11}(\hat{t})_{norm} = \frac{\langle \mathcal{U}'\mathcal{U}' \rangle_r}{\langle u'^2 \rangle} = \exp(-\hat{t}/T_{int})
\tag{27.22}
$$

where $\hat{t} = r\Delta t$. The integral time scale can be computed from the autocorrelation as (see Eq. 10.11)

$$
\begin{aligned}
T_{int} &= \int_0^{\infty} B_{11}^{norm}(\hat{t}) d\hat{t} = \int_0^{\infty} \exp(-\hat{t}/T_{int}) d\hat{t} \\
&= \left[-T_{int} \exp(-\hat{t}/T_{int}) \right]_0^{\infty} = -T_{int}(0 - 1) = T_{int}
\end{aligned}
\tag{27.23}
$$

This shows that the one-sided filter in Eq. 27.9 introduces an integral time scale T_{int} as prescribed by the definition of a in Eq. 27.10. The integral time scale can be taken as $T_{int} = L_{int}/U_b$ using Taylor's hypothesis, where U_b and L_{int} denote the inlet bulk velocity and the integral length scale, respectively.

27.9   Anisotropic Synthetic Turbulent Fluctuations

Isotropic fluctuations are generated above. However, turbulence is generally anisotropic. The method for generating anisotropic turbulence is presented in [100, 173, 182, 188] and below it is described in detail.

The method can be summarized by the following steps.

1. A Reynolds stress tensor, $\langle v_i' v_j' \rangle$, is taken from DNS data for turbulent channel flow. Since the generated turbulence is homogeneous, it is sufficient to choose one location of the DNS data. The Reynolds stresses at $y^+ \simeq 16$ of the DNS channel data at $Re_\tau = 590$ [189] are used. Here $\langle v_1' v_1' \rangle$ – and hence the degree of anisotropy – is largest. The stress tensor reads

$$\langle v_i' v_j' \rangle = \begin{bmatrix} 7.67 & -0.662 & 0 \\ -0.662 & 0.32 & 0 \\ 0 & 0 & 1.50 \end{bmatrix} \qquad (27.24)$$

2. The principal directions (the eigenvectors, see Fig. 27.4), $\hat{e}_i^*$, are computed for the $\langle v_i' v_j' \rangle$ tensor, see Section 27.9.1. The eigenvalues are normalized so that their sum is equal to three. This ensures that the kinetic energy of the synthetic fluctuations does not change during transformation.

3. Isotropic synthetic fluctuations, $u_{i,iso}'$, are generated in the principal directions of $\langle u_i' u_j' \rangle$.

4. Now make the isotropic fluctuations non-isotropic according to $\langle v_i' v_j' \rangle$. This is done by multiplying the isotropic synthetic fluctuations in the $\hat{e}_i^*$ directions by the square-root of the normalized eigenvalues, $\sqrt{\lambda^{(i)}}_{norm}$. In Section 27.9.2 this is done by multiplying the unit vector σ_i^{*n} by $\sqrt{\lambda^{(i)}}_{norm}$, see Eq. 27.28 and Fig. 27.5. This gives a new field of fluctuations

$$\begin{aligned} (u_1')_{aniso} &= \sqrt{\lambda_{norm}^{(1)}} \, (u_1')_{iso} \\ (u_2')_{aniso} &= \sqrt{\lambda_{norm}^{(2)}} \, (u_2')_{iso} \\ (u_3')_{aniso} &= \sqrt{\lambda_{norm}^{(3)}} \, (u_3')_{iso} \end{aligned} \qquad (27.25)$$

The wavenumber vector, κ_j, is divided by $\sqrt{\lambda^{(i)}}$ to ensure that the $(u_i')_{aniso}$ velocity field is divergence free, i.e.

$$\sigma_j^* \kappa_j^* = \sqrt{\lambda_{norm}^{(j)}} \sigma_j \sqrt{\frac{1}{\lambda_{norm}^{(j)}}} \kappa_j = \sigma_j \kappa_j = 0, \qquad (27.26)$$

see Eq. N.3. Note that there is still no correlation between the $(u_i')_{aniso}$ fluctuations, which means that the shear stresses are zero (for example, $\langle (u_1' u_2')_{aniso} \rangle = 0$).

5. The $(u_i')_{aniso}$ fluctuations are transformed to the computational coordinate system, x_i; these anisotropic fluctuations are denoted $(u_i')_{synt}$. The transformation reads

$$(u_i')_{synt} = R_{ij}(u_j')_{aniso} \qquad (27.27)$$

where R_{ij} is the transformation matrix which is defined be the eigenvectors, see Section 27.9.1. The $(u_i')_{synt}$ fluctuations are now used in Eq. 27.9 replacing $v_{i.in}'$.

The Reynolds stress tensor of the synthetic anisotropic fluctuations is now identical to the DNS Reynolds stress tensor, i.e. $\langle (u_i'u_j')_{synt} \rangle = \langle v_i'v_j' \rangle$

6. Since the $u_{i,synt}'$ are homogeneous, the Reynolds stresses, $\langle u_{i,synt}'u_{j,synt}' \rangle$, have constant values in the inlet plane. One can choose to scale the inlet fluctuations by a k profile taken from DNS, experiments or a RANS simulation.

The Python/Matlab/Octave code for generating isotropic or anisotropic fluctuations can be downloaded [190].

27.9.1 Eigenvalues and eigenvectors

The normalized eigenvalues and eigenvectors may conveniently be computed with Python/Matlab/Octave as

```
stress=[7.6684 -6.6206e-01 0; ...
-6.6206e-01 3.1974e-01 0; ...
0 0 1.4997];
diag_sum=trace(stress)/3
stress=stress/diag_sum % ensures that the sum
                       % of the eigenvalues=3

[R,lambda] = eig(stress)

v_1_temp=[R(1,1);R(2,1); R(3,1)];
v_2_temp=[R(1,2);R(2,2); R(3,2)];
v_3_temp=[R(1,3);R(2,3); R(3,3)];

lambda_1_temp=lambda(1,1);
lambda_2_temp=lambda(2,2);
lambda_3_temp=lambda(3,3);
```

where `stress` is taken from Eq. 27.24. Python/Matlab/Octave defines the smallest eigenvalue as the first one and the largest as the last. Here we define the first eigenvalue (streamwise direction) as the largest and the second (wall-normal direction) as the smallest, i.e.

```
v1=v3_temp;
v2=v1_temp;
v3=v2_temp;

lambda_1=lambda_3_temp;
lambda_2=lambda_1_temp;
lambda_3=lambda_2_temp;
```
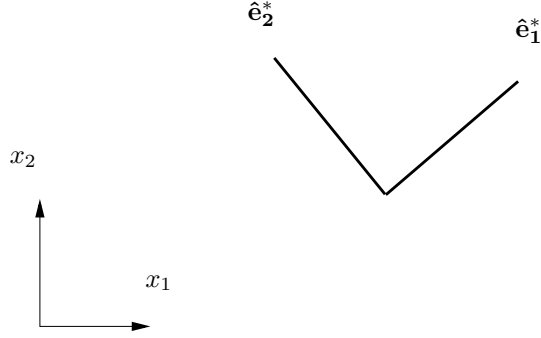
Figure 27.4: Eigenvectors $\hat{\mathbf{e}}_1^*$ and $\hat{\mathbf{e}}_2^*$. x_1 and x_2 denote streamwise and wall-normal direction, respectively.
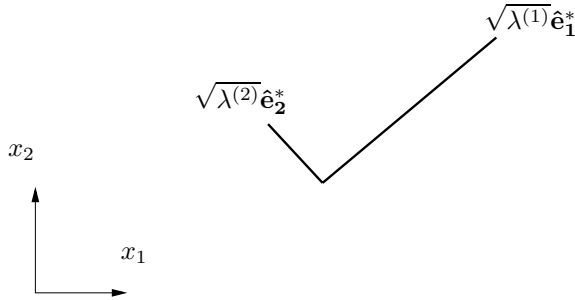
Figure 27.5: Eigenvectors multiplied by the eigenvalues. x_1 and x_2 denote streamwise and wall-normal direction, respectively. $\sqrt{\lambda^{(1)}}$ and $\sqrt{\lambda^{(2)}}$ define RMS of $(u_1')_{aniso}$ and $(u_2')_{aniso}$, respectively.

Make sure that Python/Matlab/Octave has defined the first eigenvector in the first or the third quadrant, and the second eigenvector in the second or the fourth quadrant, see Fig. 27.4. If not, change sign on some of the eigenvector components.

```
% switch sign on 12 and 21 to fix the above requirements
v1_new(2)=-v1_new(2);
v2_new(1)=-v2_new(1);
```

27.9.2 Synthetic fluctuations in the principal coordinate system

The equation for generating the synthetic fluctuations in the principal coordinate system, $(u_i')_{aniso}$, is similar to Eq. 27.3. The difference is that we now do it in the transformed coordinate system, and hence we have to involve the eigenvector matrix, R_{ij}, and the eigenvalues, $\lambda^{(i)}$. The equation reads [182, 188]

$$\mathbf{u}'_{aniso}(\mathbf{x}^*) = 2 \sum_{n=1}^{N} \hat{u}^n \cos(\boldsymbol{\kappa}^{*n} \cdot \mathbf{x}^* + \psi^n)\boldsymbol{\sigma}^{*n}$$

$$\boldsymbol{\kappa}^{*n} = \kappa_i^{*n} = \sqrt{\frac{1}{\lambda^{(i)}}}R_{ji}\kappa_j^n, \quad \boldsymbol{\sigma}^{*n} = \sigma_i^{*n} = \sqrt{\lambda^{(i)}}R_{ji}\sigma_j^n \tag{27.28}$$

The superscript $*$ denotes the principal coordinates.

28 Overview of LES, hybrid LES-RANS and URANS models

DIRECT Numerical Simulation (DNS) is the most accurate method available. In DNS we solve the unsteady, 3D Navier-Stokes equations (see Eq. 2.9) numerically without any turbulence model. This gives the exact solution of the flow field in time and space. We can afford to do DNS only for low Reynolds number. The higher the Reynolds number gets, the finer the grid must be because the smallest turbulent length and time scales, which we must resolve in DNS, decrease with $Re^{-3/4}$ and $Re^{-1/2}$, respectively, see Eq. 5.16. Hence the cell size in each coordinate direction of our CFD grid must decrease with $Re^{-3/4}$ and the time step must decrease with $Re^{-1/2}$. Let's take an example. If the Reynolds number increases by a factor of two, the number of cells increases by **DNS**

$$\underbrace{\Delta Re^{3/4}}_{\text{x-direction}}\underbrace{\Delta Re^{3/4}}_{\text{y-direction}}\underbrace{\Delta Re^{3/4}}_{\text{z-direction}}\underbrace{\Delta Re^{1/2}}_{\text{time}} = \Delta Re^{11/4} = 2^{11/4} = 6.7 \qquad (28.1)$$

Above we assume that the lengthscales are reduced when the Reynolds numbers is increased. This implies that we assume that the Reynolds number is increased due to an increase in velocity or a decrease in viscosity. We can, of course, also consider the change of Reynolds number by changing the size of the object. For example, it is affordable to compute the flow around a small car such as those we played with as kids (for this car of, say, length of $5cm$, the Reynolds number is very small). As we increase the size of the car we must increase the number of cells (the smallest cells cannot be enlarged, because the smallest turbulent scales will not increase). Also the time step cannot be increased, but we must compute longer time (i.e. increase the number of timesteps) in order to capture the largest time scales (assuming that the velocity of the small and the large car is the same).

Having realized that DNS is not feasible, we turn to LES, see Section 18. Here, the smallest scales are modeled, and only the eddies that are larger than the grid are resolved by the (filtered) Navier-Stokes. With LES, we can make the smallest grid cells somewhat larger (the cell side, say, $2 - 3$ times larger). **LES**

However, it is found that LES needs very fine resolution near walls, see Section 21. To find an approximate solution to this problem we use RANS near the walls and LES away from the walls. The models which we have looked at are DES (Section 20), hybrid LES-RANS (Section 21), SAS (Section 22) and PANS (Section 23); see also Section 25 where PANS and Zonal PANS are discussed.

As stated above, the LES must at high Reynolds number be combined with a URANS treatment of the near-wall flow region. In the literature, there are different methods for bridging this problem such as Detached Eddy Simulation (DES) [138, 154, 163] hybrid LES/RANS [191] and Scale-Adapted Simulations (SAS) [192, 193] (for a review, see [194]). The two first classes of models take the SGS length scale from the cell size whereas the last (SAS) involves the von Kármán lengthscale.

The DES, hybrid LES/RANS and the SAS models have one thing in common: in the LES region, the turbulent viscosity is reduced. This is achieved in different ways. In some models, the turbulent viscosity is reduced indirectly by reducing the dissipation term in the k equation, see Eq. 20.8, as in two-equation DES [195]. In other models, such as the two-equation XLES model [142] and in the one-equation hybrid LES-RANS [100], it is accomplished by reducing the length scale in both the expression for

the turbulent viscosity as well as for the dissipation term in the k equation, see Eq. 21.2 and Table 21.1.

In the partially averaged Navier-Stokes (PANS) model [144] and the Partially Integrated Transport Model (PITM) [146, 171], the turbulent viscosity is reduced by decreasing the destruction term in the dissipation (ε) equation which increases ε, see Eq. 23.15. This decreases the turbulent viscosity in two ways: first, the turbulent viscosity is reduced because of the enhancement of ε ($\nu_t = c_\mu k^2/\varepsilon$, see Eq. 23.6), and, second, the turbulent kinetic energy (k) decreases because of the increased dissipation term, ε. In the SAS model based on the $k - \omega$ model, the turbulent viscosity is reduced by an additional source term, P_{SAS}, see Eq. 22.5, in the ω equation. The source term is activated by resolved turbulence; in steady flow it is inactive. When the momentum equations are in turbulence-resolving mode, P_{SAS} increases which increases ω. This decreases the turbulent viscosity in two ways: first, directly, because ω appears in the denominator in the expression for the turbulent viscosity, ν_t, and, second, because k is reduced due to the increased dissipation term $\beta^* k\omega$.

The PANS model and the PITM models are very similar to each other although their derivations are completely different. The only difference in the models is that in the PANS model the turbulent diffusion coefficients in the k and ε equations are modified. These two models do not use the filter width, and can hence be classified as URANS models. On the other hand, a large part of the turbulence spectrum is usually resolved which is in contrast to standard URANS models. PANS and PITM models have in [194] been classified as second-generation URANS models, or 2G-URANS models.

A short description of the models are given here.

DES. A RANS models is used near the walls and LES is used away from the walls. The interface is usually defined automatic. In the original DES the entire boundary layer is covered by RANS. However, when the grid is refined in streamwise and spanwise directions, the interface moves closer to the wall. When a large part of the boundary layer is covered by LES, it is called WM-LES (Wall-Modeled **WM-LES** LES). The LES lengthscale is the filterwidth.

Hybrid LES-RANS. The difference between DES and hybrid LES-RANS is that the original DES covers the entire boundary layer by RANS whereas hybrid LES-RANS treats most of the boundary layer in LES mode. Hybrid LES-RANS and WM-LES can be considered to be the same thing. The LES lengthscale is the filterwidth.

PANS, PITM. These models are able to operate both in LES and RANS mode. In LES mode the models do not use the filterwidth as a lengthscale. Hence they are usually defined as an URANS model (defined below). Since the models usually aim at resolving a substantial part of the turbulence spectrum, they can be defined as a second-generation URANS model (a 2G-URANS model [194]).

SAS. This is also a model that can operate both in LES and RANS mode. In unsteady mode the model does not use the filterwidth as a lengthscale. In unsteady mode this model usually resolved less turbulence than the other models mentioned above; hence it can be classified as an URANS model (first generation).

URANS. A RANS model is used in unsteady mode. In unsteady mode the model does not use the filterwidth as a lengthscale. Unless the flow is prone to go unsteady,

the results will be steady (i.e. same as RANS). Usually a RANS model developed for steady flow is used. Only a small part of the turbulence is resolved.

The models listed above can be ranked in terms of accuracy and CPU cost:

1. **Hybrid LES-RANS, PANS, PITM, WM-LES.** Highest accuracy and CPU cost

2. **DES.**

3. **SAS.**

4. **URANS.** Lowest accuracy and CPU cost

29 Best practice guidelines (BPG)

In the early days of CFD, different CFD codes used to give different results. Even if the same grid and the same turbulence model were used, there could be substantial differences between the results. The reasons to these differences could be that the turbulence model was not implemented in exactly the same way in the two codes, or that the discretization scheme in one code was more diffusive than in the other. There could be small differences in the implementation of the boundary conditions in the two codes.

Today the situation is much improved. Two different CFD codes usually give the same results on the same grid. The main reason for this improved situation is because of workshops and EU projects where academics, engineers from industry and CFD software vendors regularly meet and discuss different aspects of CFD. Test cases with mandatory grids, boundary conditions, turbulence models etc are defined and the participants in the workshops and EU projects carry out CFD simulations for these test cases. Then they compare and discuss their results.

29.1 EU projects

Four EU projects in which the author has taken part can be mentioned

LESFOIL: Large Eddy Simulation of Flow Around Airfoils
http://www.tfd.chalmers.se/˜lada/projects/lesfoil/proright.html

FLOMANIA: Flow Physics Modelling: An Integrated Approach
http://cfd.mace.manchester.ac.uk/flomania/

DESIDER: Detached Eddy Simulation for Industrial Aerodynamics
http://cfd.mace.manchester.ac.uk/desider

ATAAC: Advanced Turbulence Simulation for Aerodynamic Application Challenges
http://cfd.mace.manchester.ac.uk/ATAAC/WebHome

29.2 Ercoftac workshops

Workshops are organized by Ercoftac (**E**uropean **R**esearch **C**ommunity **O**n **F**low, **T**urbulence **A**nd **C**ombustion). The Special Interest Group Sig15 is focused on evaluating turbulence models. The outcome from all workshop are presented

here
http://www.ercoftac.org/fileadmin/user_upload/bigfiles/sig15/database/index.html

Ercoftac also organizes workshops and courses on Best Practice Guidelines. The publication *Industrial Computational Fluid Dynamics of Single-Phase Flows* can be ordered on

Ercoftac www page
http://www.ercoftac.org/publications/ercoftac_best_practice_guidelines/single-phase_flows_spf/

29.3 Ercoftac Classical Database

A *Classical Database*, which includes some 100 experimental investigations, can be found at

Ercoftac's www page

http://www.ercoftac.org/products_and_services/classic_collection_database

29.4 ERCOFTAC QNET Knowledge Base Wiki

The QNET is also the responsibility of Ercoftac. Here you find descriptions of how CFD simulations of more than 60 different flows were carried out. The flows are divided into

Application Areas. These are sector disciplines such as Built Environment, Chemical and Process Engineering, External Aerodynamics, Turbomachinery, Combustion and Heat Transfer etc. Each Application Area is comprised of Application Challenges. These are realistic industrial test cases which can be used to judge the competency and limitations of CFD for a given Application Area.

Underlying Flow Regimes. These are generic, well-studied test cases capturing important elements of the key flow physics encountered across the Application Areas.

For more information, visit

ERCOFTAC QNET Knowledge Base Wiki

http://www.ercoftac.org/products_and_services/wiki/

A   TME226 Lecture Notes

A.1   Lecture 1

¶See Section 1.1, Eulerian, Lagrangian, material derivative

Lagrangian-Eulerian

►Lagrangian approach

- The (fluid) particle is described by its initial position, X_i, and time, t

- In other words we "label" a particle with X_i and then follow it.

- The variation of T is expressed as dT/dt.

►Eulerian approach

- We look a point, x_i, and see what happens.

- Hence T depends on both x_i and t

- The chain rule gives $\dfrac{dT}{dt} = \dfrac{\partial T}{\partial t} + \dfrac{dx_i}{dt}\dfrac{\partial T}{\partial x_i} = \dfrac{\partial T}{\partial t} + v_i\dfrac{\partial T}{\partial x_i}$

$$\blacktriangleright \quad \underbrace{\frac{dT}{dt}}_{\text{material change}} = \frac{\partial T}{\partial t} + \frac{dx_j}{dt}\frac{\partial T}{\partial x_j} = \underbrace{\frac{\partial T}{\partial t}}_{\text{local change}} + \underbrace{v_j\frac{\partial T}{\partial x_j}}_{\text{convective change}}$$

¶See Section 1.2, What is the difference between $\dfrac{dv_2}{dt}$ and $\dfrac{\partial v_2}{\partial t}$?

Difference between $\dfrac{dv_2}{dt}$ and $\dfrac{\partial v_2}{\partial t}$?
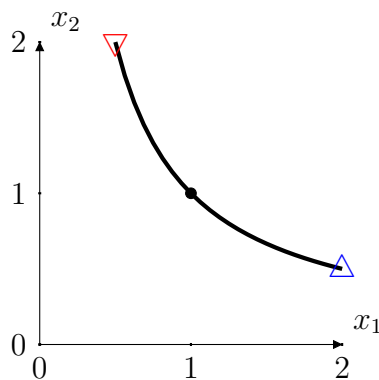
Flow path $x_2 = 1/x_1$. The filled circle shows the point $(x_1, x_2) = (1, 1)$. $\triangledown$: start ($t = \ln(0.5)$); $\triangle$: end ($t = \ln(2)$).

$$x_1 = \exp(t), \quad x_2 = \exp(-t) \tag{A.1}$$

and hence $x_2 = 1/x_1$. The flow is steady (in Eulerian coordinates).

▶Equation A.1 gives the velocities

$$v_1^L = \frac{dx_1}{dt} = \exp(t), \quad v_2^L = \frac{dx_2}{dt} = -\exp(-t) \tag{A.2}$$

Eqs. A.1 and A.2 give

$$v_1^E = x_1, \quad v_2^E = -x_2$$

Note that $v_i^L = v_i^E$ but $v_i^L = v_i^L(t)$ and $v_i^E = v_i^E(x_1, x_2)$.

▶Time derivatives of the v_2 velocity:

$$\frac{dv_2^L}{dt} = \exp(-t)$$

$$\frac{dv_2^E}{dt} = \frac{\partial v_2^E}{\partial t} + v_1^E \frac{\partial v_2^E}{\partial x_1} + v_2^E \frac{\partial v_2^E}{\partial x_2} = 0 + x_1 \cdot 0 - x_2 \cdot (-1) = x_2$$

Of course $\dfrac{dv_2}{dt} = \dfrac{dv_2^E}{dt} = \dfrac{dv_2^L}{dt} = x_2 = \exp(-t)$.

▶Consider the point $(x_1, x_2) = (1, 1)$. The velocity at this point does not change in time; hence $\dfrac{\partial v_2^E}{\partial t} = 0$.

▶If we however travel with the particle then the v_2 velocity changes with time, i.e. $\dfrac{dv_2^L}{dt} = \dfrac{dv_2}{dt} = 1$ (it increases, i.e. it gets less negative with time).

¶See Section B, Introduction to tensor notation

▶a: A tensor of zeroth rank (scalar)

▶a_i: A tensor of first rank (vector) $a_i = (2, 1, 0)$

▶a_{ij}: A tensor of second rank (tensor)

$$\sigma_{ij} = \begin{pmatrix} \sigma_{11} & \sigma_{12} & \sigma_{13} \\ \sigma_{21} & \sigma_{22} & \sigma_{23} \\ \sigma_{31} & \sigma_{32} & \sigma_{33} \end{pmatrix}$$

$\sigma_{ij} = \sigma_{ji}$.

What is a tensor?

▶A tensor is a *physical* quantity. It is independent of the coordinate system. The tensor of rank one (vector) b_i below

is physically the same expressed in the coordinate system (x_1, x_2)
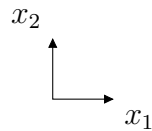
where $b_i = (1/\sqrt{2}, 1/\sqrt{2}, 0)^T$ and in the coordinate system $(x_{1'}, x_{2'})$
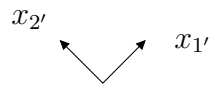
where $b_{i'} = (1, 0, 0)^T$. The tensor is the same even if its *components* are different.

¶See Section 1.3, Viscous stress, pressure
▶The momentum balance equation derived in the continuum mechanics lectures reads

$$\boxed{\rho \dot{v}_i - \sigma_{ji,j} - \rho f_i = 0}$$

We write it as

$$\rho \frac{dv_i}{dt} = \frac{\partial \sigma_{ji}}{\partial x_j} + \rho f_i \qquad (A.3)$$
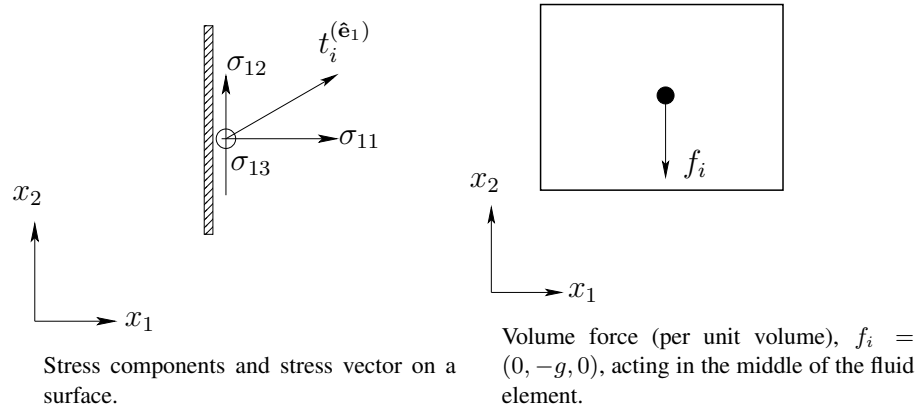
Stress components and stress vector on a surface.

Volume force (per unit volume), $f_i = (0, -g, 0)$, acting in the middle of the fluid element.

Stress tensor, volume (gravitation) force and stress vector, $t_i^{(\hat{\mathbf{e}}_1)}$.

- σ_{ij} denotes the stress tensor. Stress is force per unit area. The surface stress vector is computed as

$$t_i^{(\hat{\mathbf{n}})} = \sigma_{ji} n_j$$

 where $\hat{\mathbf{n}} = n_j$ is the normal vector of the surface.

- volume forces, f_i

▶The stress tensor, σ_{ij}, is split into one part which includes pressure, P, and one which includes viscous stresses (friction)

$$\sigma_{ij} = -P\delta_{ij} + \tau_{ij}$$

where $P = -\dfrac{1}{3}\sigma_{kk}$.

A constitutive relation can be derived for the stress tensor which reads

$$\sigma_{ij} = -P\delta_{ij} + 2\mu S_{ij} - \frac{2}{3}\mu S_{kk}\delta_{ij}$$
$$\tau_{ij} = 2\mu S_{ij} - \frac{2}{3}\mu S_{kk}\delta_{ij} \tag{A.4}$$
$$S_{ij} = \frac{1}{2}\left(\frac{\partial v_i}{\partial x_j} + \frac{\partial v_j}{\partial x_i}\right)$$

▶This expression includes the velocity gradients. Before we insert Eq. A.4 into Eq. A.3, we will look at the velocity gradient tensor, $\dfrac{\partial v_i}{\partial x_j}$, in some detail.

¶See Section 1.4, Strain rate tensor, vorticity

$$\frac{\partial v_i}{\partial x_j} = \frac{1}{2}\left(\underbrace{\frac{\partial v_i}{\partial x_j} + \frac{\partial v_i}{\partial x_j}}_{2\partial v_i/\partial x_j} + \underbrace{\frac{\partial v_j}{\partial x_i} - \frac{\partial v_j}{\partial x_i}}_{=0}\right)$$

$$= \frac{1}{2}\left(\frac{\partial v_i}{\partial x_j} + \frac{\partial v_j}{\partial x_i}\right) + \frac{1}{2}\left(\frac{\partial v_i}{\partial x_j} - \frac{\partial v_j}{\partial x_i}\right) = S_{ij} + \Omega_{ij}$$

►The vorticity reads

$$\boldsymbol{\omega} = \boldsymbol{\nabla} \times \mathbf{v}$$

$$\omega_i = \epsilon_{ijk}\frac{\partial v_k}{\partial x_j}$$

►The vorticity represents rotation of a fluid particle. Inserting the expression for S_{ij} and Ω_{ij} gives

$$\omega_i = \epsilon_{ijk}(S_{kj} + \Omega_{kj}) = \epsilon_{ijk}\Omega_{kj} \tag{A.5}$$

where we used the fact that the product of a symmetric, S_{kj}, and an antisymmetric tensor, ϵ_{ijk}, is zero.

►Now let's invert Eq. A.5. We start by multiplying it with $\varepsilon_{i\ell m}$ so that

$$\varepsilon_{i\ell m}\omega_i = \varepsilon_{i\ell m}\epsilon_{ijk}\Omega_{kj} \tag{A.6}$$

- ϵ_{ijk} is the permutation tensor.
  - It is one if ijk is equal to 123 or any cyclic permutation, i.e. $\varepsilon_{123} = \varepsilon_{312} = \varepsilon_{231} = 1$.
  - Switch two indices and it is equal to minus one, i.e, $\varepsilon_{132} = \varepsilon_{213} = \varepsilon_{132} = -1$.
  - If two indices are equal, then ϵ_{ijk} is zero.

- δ_{ij} is the unit or identity tensor. It is one if ijk are equal and zero otherwise, i.e.
  - $\delta_{11} = \delta_{22} = \delta_{33} = 1$
  - $\delta_{12} = \delta_{13} = \delta_{21} = \delta_{23} = \delta_{31} = \delta_{32} = 0$

Using the ε-δ-identity (see Section C) on the right side of Eq. A.6 gives

$$\varepsilon_{i\ell m}\epsilon_{ijk}\Omega_{kj} = (\delta_{\ell j}\delta_{mk} - \delta_{\ell k}\delta_{mj})\Omega_{kj} = \Omega_{m\ell} - \Omega_{\ell m} = 2\Omega_{m\ell}$$

Inserted in Eq. A.6 we get

$$\Omega_{m\ell} = \frac{1}{2}\varepsilon_{i\ell m}\omega_i = \frac{1}{2}\varepsilon_{\ell m i}\omega_i = -\frac{1}{2}\varepsilon_{m\ell i}\omega_i$$

where we first used cyclic permutation of $\varepsilon_{i\ell m}$, then used the fact that $\varepsilon_{i\ell m}$ is anti-symmetric.

►Actually, it is easier to invert Eq. A.5 component-by-component. For ω_3 we get

$$\omega_3 = \epsilon_{3jk}\frac{\partial v_k}{\partial x_j} = \epsilon_{321}\frac{\partial v_1}{\partial x_2} + \epsilon_{312}\frac{\partial v_2}{\partial x_1}$$
$$= -\frac{\partial v_1}{\partial x_2} + \frac{\partial v_2}{\partial x_1} = \left(\frac{\partial v_2}{\partial x_1} - \frac{\partial v_1}{\partial x_2}\right) = -2\Omega_{12}$$

¶See Section 1.5, Product of a symmetric and antisymmetric tensor
►The product of a symmetric, a_{ji}, and antisymmetric tensor, b_{ji}, is zero

$$a_{ij}b_{ij} = a_{ji}b_{ij} = -a_{ji}b_{ji},$$

where we used

2nd expression $a_{ij} = a_{ji}$ (symmetric)

last expression $b_{ij} = -b_{ji}$ (antisymmetric)

Indices i and j are dummy indices $\Rightarrow$

$$a_{ij}b_{ij} = -a_{ij}b_{ij}$$

This expression says that $A = -A$ which can be only true if $A = 0$ and hence $a_{ij}b_{ij} = 0$.

¶See Section 1.6, Deformation, rotation
►Rotation of a fluid particle ($\omega_3 > 0$, $\Omega_{12} < 0$) during time Δt
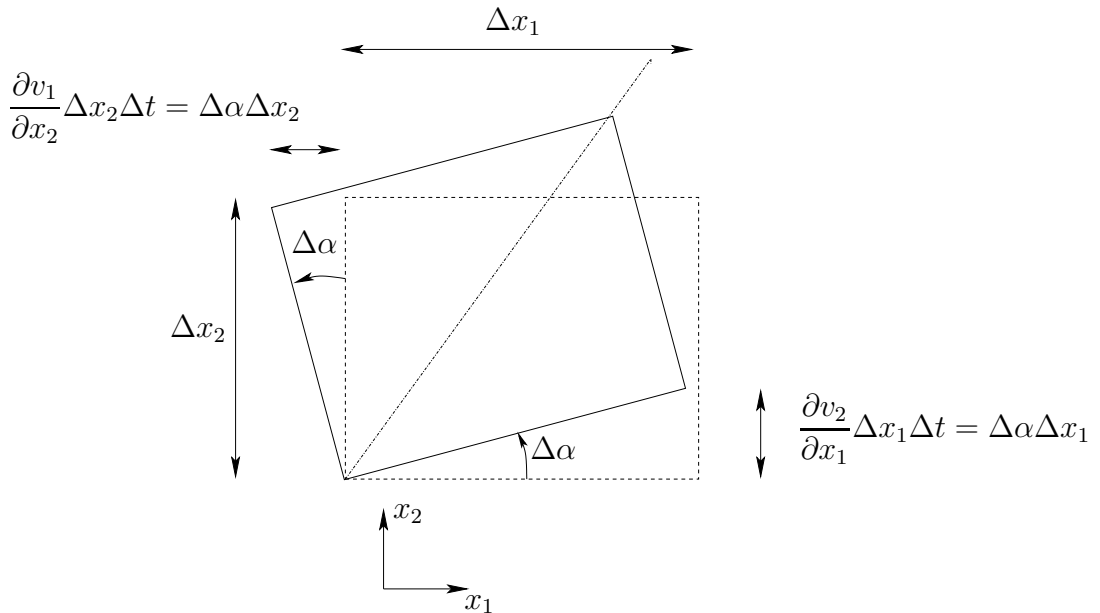
- angle rotation per unit time: $\frac{\Delta \alpha}{\Delta t} \simeq d\alpha/dt = -\partial v_1/\partial x_2 = \partial v_2/\partial x_1$

- if fluid element does not rotate as a solid body, we take the average $d\alpha/dt = (\partial v_2/\partial x_1 - \partial v_1/\partial x_2)/2$.

- Hence, the vorticity $\omega_3 = \partial v_2/\partial x_1 - \partial v_1/\partial x_2$ can be interpreted as twice the average rotation of the horizontal edge and vertical edge

▶Deformation of a fluid particle by shear during time Δt. Here $\partial v_1/\partial x_2 = \partial v_2/\partial x_1$ so that $S_{12} = (\partial v_1/\partial x_2 + \partial v_2/\partial x_1)/2 = \partial v_1/\partial x_2 > 0$.
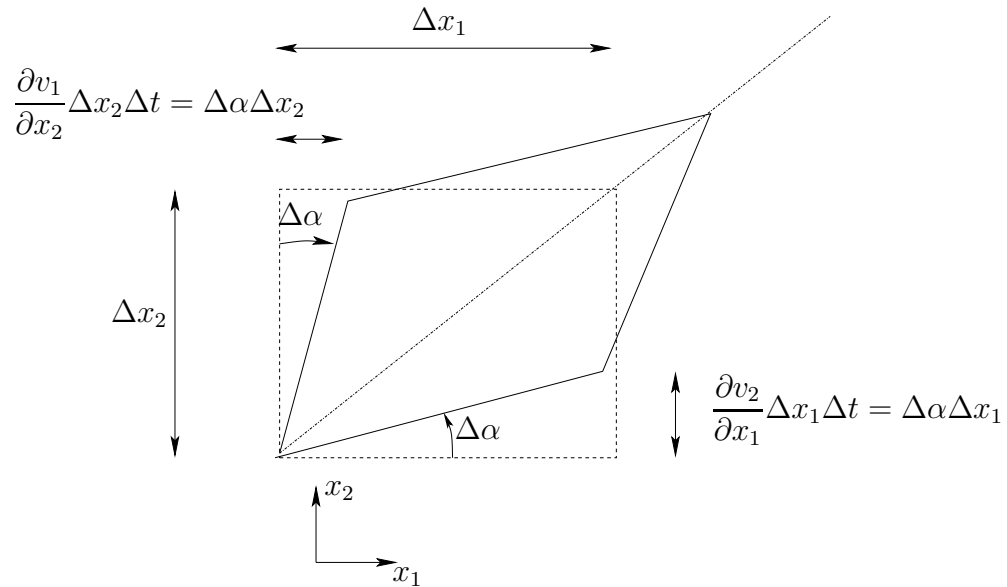
▶Deformation of a fluid particle by elongation during time Δt. Here $S_{11} = \partial v_1/\partial x_1 > 0$

$$\Delta x_1$$

$$\frac{\partial v_1}{\partial x_1}\Delta x_1 \Delta t$$

$$\Delta x_2$$

x_2

x_1
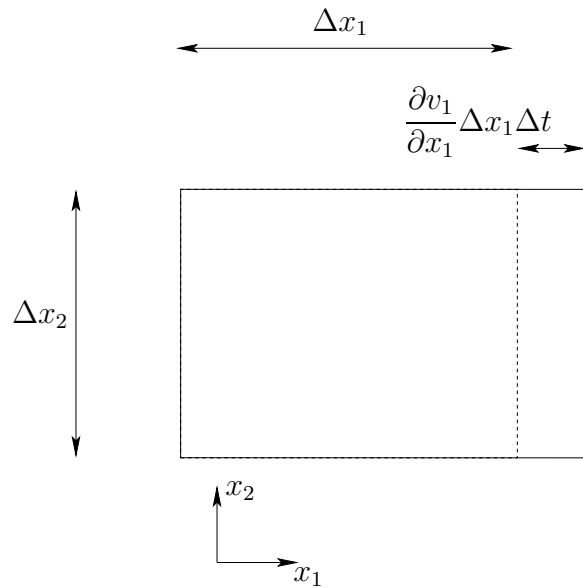
¶See Section 1.7, Irrotational and rotational flow

▶Flows are often classified based on rotation: they are *rotational* ($\omega_i \neq 0$) or *irrotational* ($\omega_i = 0$)

¶See Section 1.7.1, Ideal vortex line

▶Consider the ideal vortex line

$$\Phi = \frac{\Gamma \theta}{2\pi}, \quad v_k = \frac{\partial \Phi}{\partial x_k}, \quad v_\theta = \frac{\Gamma}{2\pi r}, \quad v_r = 0$$

v_θ

θ

x_2

r

θ x_1
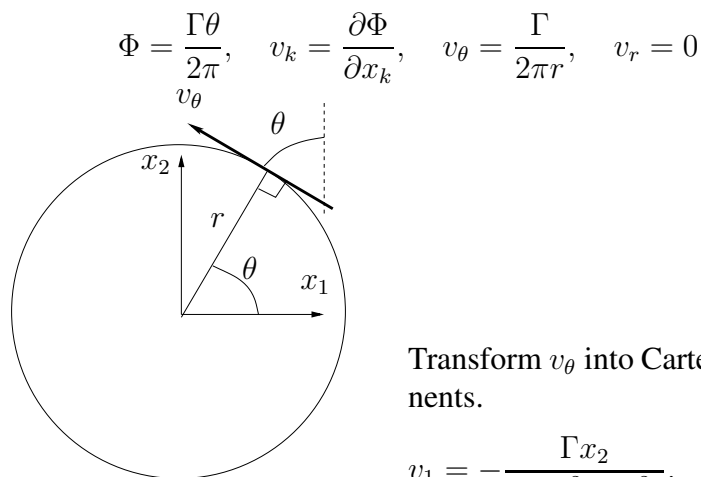
Transform v_θ into Cartesian components.

$$v_1 = -\frac{\Gamma x_2}{2\pi(x_1^2 + x_2^2)}, \quad v_2 = \frac{\Gamma x_1}{2\pi(x_1^2 + x_2^2)}.$$

$$\frac{\partial v_1}{\partial x_2} = -\frac{\Gamma}{2\pi}\frac{x_1^2 - x_2^2}{(x_1^2 + x_2^2)^2}, \quad \frac{\partial v_2}{\partial x_1} = \frac{\Gamma}{2\pi}\frac{x_2^2 - x_1^2}{(x_1^2 + x_2^2)^2}$$

$$\Rightarrow \omega_3 = \frac{\partial v_2}{\partial x_1} - \frac{\partial v_2}{\partial x_1} = 0$$
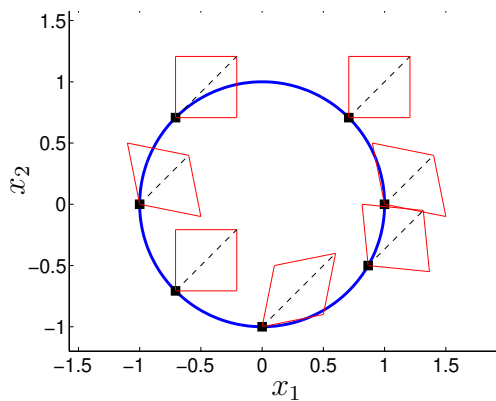
The fluid particle (i.e. its diagonal) does not rotate. The locations of the fluid particle is indicated by black, filled squares. The diagonals are shown as black dashed lines. The fluid particle is shown at $\theta = 0$, $\pi/4$, $3\pi/4$, π, $5\pi/4$, $3\pi/2$ and $-\pi/6$.

¶See Section 1.7.2, Shear flow

▶Consider shear flow with $v_1 = cx_2^2$, $v_2 = 0$, see figure below. The vorticity is computed as

$$\omega_1 = \omega_2 = 0, \quad \omega_3 = \frac{\partial v_2}{\partial x_1} - \frac{\partial v_1}{\partial x_2} = -2cx_2$$

Hence the flow is rotational
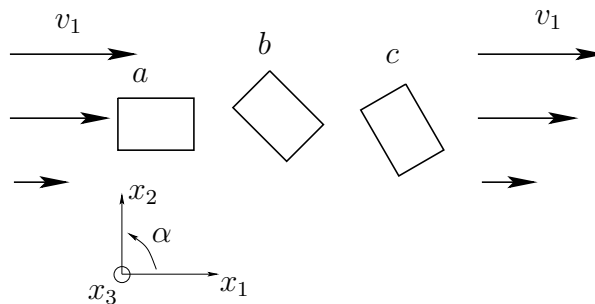
The fluid particles rotate according to the figure above (rotating in negative direction).

¶See Section 1.8, Eigenvalues and eigenvectors: physical interpretation

▶Eigenvalues and and eigenvectors: physical interpretation
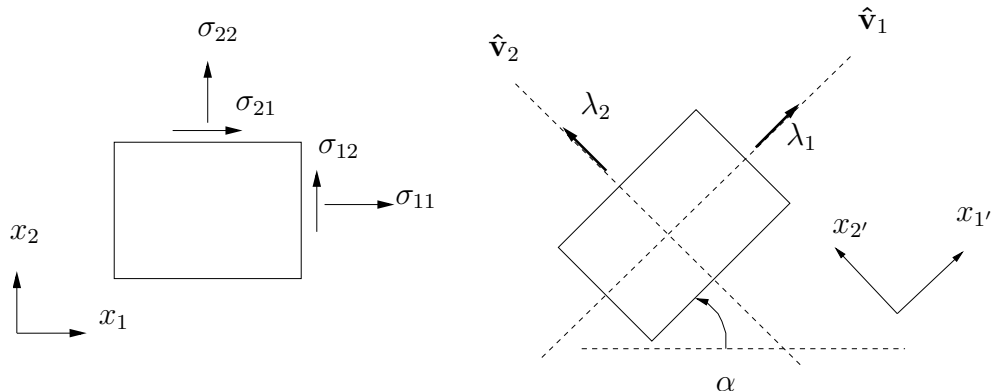
- A two-dimensional fluid element.

    - Left: in original state;
    - right: rotated to principal coordinate directions.
    - $\lambda_1 = \sigma_{1'1'}$ and $\lambda_2 = \sigma_{2'2'}$ denote eigenvalues;
    - $\hat{\mathbf{v}}_1$ and $\hat{\mathbf{v}}_2$ denote unit eigenvectors.

A.2 Lecture 2

¶See Section 2.1.1, The continuity equation
►The continuity equation

$$\frac{d\rho}{dt} + \rho\frac{\partial v_i}{\partial x_i} = 0 \quad \text{incompressible flow gives} \quad \frac{\partial v_i}{\partial x_i} = 0$$

¶See Section 2.1.2, The momentum equation
►The momentum equation

$$\sigma_{ij} = -P\delta_{ij} + 2\mu S_{ij} - \frac{2}{3}\mu S_{kk}\delta_{ij}$$

$$\rho\frac{dv_i}{dt} = \frac{\partial\sigma_{ji}}{\partial x_j} + \rho f_i = -\frac{\partial P}{\partial x_i} + \frac{\partial}{\partial x_j}\left(2\mu S_{ij} - \frac{2}{3}\mu\frac{\partial v_k}{\partial x_k}\delta_{ij}\right) + \rho f_i$$

$$= -\frac{\partial P}{\partial x_i} + \frac{\partial}{\partial x_j}\left(2\mu S_{ij}\right) - \frac{2}{3}\frac{\partial}{\partial x_i}\left(\mu\frac{\partial v_k}{\partial x_k}\right) + \rho f_i$$

Note that the stress tensor, σ_{ij}, depends only on S_{ij} (deformation), not on Ω_{ij} (rotation).

►Incompressible flow gives

$$\rho\frac{dv_i}{dt} = \frac{\partial\sigma_{ji}}{\partial x_j} + \rho f_i = -\frac{\partial P}{\partial x_i} + \frac{\partial}{\partial x_j}\left(2\mu S_{ij}\right) + \rho f_i$$

►Incompressible and constant μ give

$$\rho\frac{dv_i}{dt} = -\frac{\partial P}{\partial x_i} + \mu\frac{\partial^2 v_i}{\partial x_j\partial x_j} + \rho f_i$$

¶See Section 2.2, The energy equation
►The energy equation

$$\rho\underbrace{\frac{du}{dt}}_{\text{energy change}} = \underbrace{\sigma_{ji}\frac{\partial v_i}{\partial x_j}}_{\text{exchange of work}} \underbrace{-\frac{\partial q_i}{\partial x_i}}_{\text{exchange of heat}} \tag{A.7}$$

$$q_i = -k\frac{\partial T}{\partial x_i}$$

$$\sigma_{ij} = -P\delta_{ij} + 2\mu S_{ij} - \frac{2}{3}\mu S_{kk}\delta_{ij}$$

►We have

$$\frac{\partial v_i}{\partial x_j} = S_{ij} + \Omega_{ij}, \quad S_{ij} = \frac{1}{2}\left(\frac{\partial v_i}{\partial x_j} + \frac{\partial v_j}{\partial x_i}\right), \quad \Omega_{ij} = \frac{1}{2}\left(\frac{\partial v_i}{\partial x_j} - \frac{\partial v_j}{\partial x_i}\right)$$

$$\sigma_{ij}\frac{\partial v_i}{\partial x_j} = \sigma_{ij}(S_{ij} + \Omega_{ij}) = \sigma_{ij}S_{ij}$$

This gives (See Eq. 2.15)

$$\sigma_{ij}\frac{\partial v_i}{\partial x_j} = \left\{-P\delta_{ij} + 2\mu S_{ij} - \frac{2}{3}\mu\frac{\partial v_k}{\partial x_k}\delta_{ij}\right\}\frac{\partial v_i}{\partial x_j}$$

$$= \left\{-P\delta_{ij} + 2\mu S_{ij} - \frac{2}{3}\mu\frac{\partial v_k}{\partial x_k}\delta_{ij}\right\}(S_{ij} + \Omega_{ij}) = -P\frac{\partial v_i}{\partial x_i} + 2\mu S_{ij}S_{ij} - \frac{2}{3}\mu S_{kk}S_{ii}$$

Insert into Eq. A.7 gives

$$\underbrace{\rho\frac{du}{dt}}_{\Delta U} = \underbrace{-P\frac{\partial v_i}{\partial x_i}}_{Rev} + \underbrace{2\mu S_{ij}S_{ij} - \frac{2}{3}\mu S_{kk}S_{ii}}_{\Phi} + \underbrace{\frac{\partial}{\partial x_i}\left(k\frac{\partial T}{\partial x_i}\right)}_{Q}$$

▶During time, dt, the following happens:

ΔU: Change of inner energy of the fluid

Rev: Reversible work done by the fluid (compression or expansion)

Φ: Irreversible work (dissipation) done by the fluid

Q: Exchange of heat to the fluid

▶Incompressible flow (low speed, $|v_i| < \frac{1}{3}$speed of sound)

$$du = c_p dT, \quad \rho c_p\frac{dT}{dt} = \Phi + \frac{\partial}{\partial x_i}\left(k\frac{\partial T}{\partial x_i}\right)$$

Φ important for lubricant oils
▶For gases and "usual" liquids (i.e. not lubricant oils) we get (k is constant), see Eq. 2.18

$$\frac{dT}{dt} = \alpha\frac{\partial^2 T}{\partial x_i\partial x_i}, \quad \alpha = \frac{k}{\rho c_p}, \quad Pr = \frac{\nu}{\alpha}$$

¶See Section 2.3, Transformation of energy
▶k equation (multiply the momentum eq. with v_i)

$$\rho v_i\frac{dv_i}{dt} - v_i\frac{\partial\sigma_{ji}}{\partial x_j} - v_i\rho f_i = 0$$

The first term on the left side can be re-written (Trick 2, see Eq. 8.4)

$$\rho v_i\frac{dv_i}{dt} = \frac{1}{2}\rho\frac{d(v_i v_i)}{dt} = \rho\frac{dk}{dt}$$

$(v_i v_i/2 = v^2/2 = k)$ so that

$$\rho\frac{dk}{dt} = v_i\frac{\partial\sigma_{ji}}{\partial x_j} + \rho v_i f_i$$

Re-write the stress-velocity term so that (see Eq. 2.23)

$$\rho\frac{dk}{dt} = \frac{\partial v_i\sigma_{ji}}{\partial x_j} - \sigma_{ji}\frac{\partial v_i}{\partial x_j} + \rho v_i f_i$$

►Compare with the equation for inner energy

$$\rho\frac{du}{dt} = \sigma_{ji}\frac{\partial v_i}{\partial x_j} - \frac{\partial q_i}{\partial x_i}$$

¶See Section 2.4, Left side of the transport equations
►Left-hand side ($\Psi = v_i, u, T\ldots$)

$$\rho\frac{d\Psi}{dt} = \rho\frac{\partial\Psi}{\partial t} + \rho v_j\frac{\partial\Psi}{\partial x_j}$$

$$= \rho\frac{\partial\Psi}{\partial t} + \rho v_j\frac{\partial\Psi}{\partial x_j} + \Psi\underbrace{\left(\frac{d\rho}{dt} + \rho\frac{\partial v_j}{\partial x_j}\right)}_{=0}$$

$$= \underline{\rho\frac{\partial\Psi}{\partial t}} + \underbrace{\rho v_j\frac{\partial\Psi}{\partial x_j}} + \Psi\left(\underline{\frac{\partial\rho}{\partial t}} + \underbrace{v_j\frac{\partial\rho}{\partial x_j}} + \underbrace{\rho\frac{\partial v_j}{\partial x_j}}\right) = \frac{\partial\rho\Psi}{\partial t} + \frac{\partial\rho v_j\Psi}{\partial x_j}$$

¶See Section 3.1, The Rayleigh problem

►The Rayleigh problem

The plate moves to the right with speed V_0 for $t > 0$.
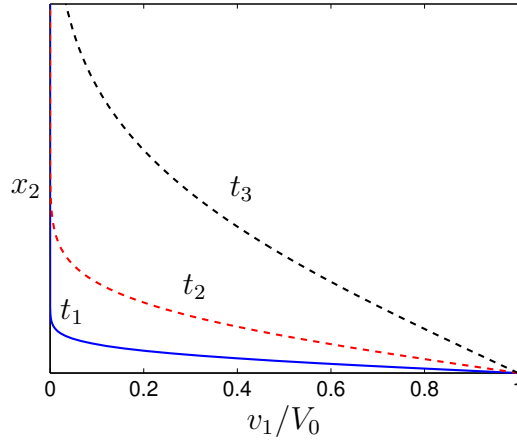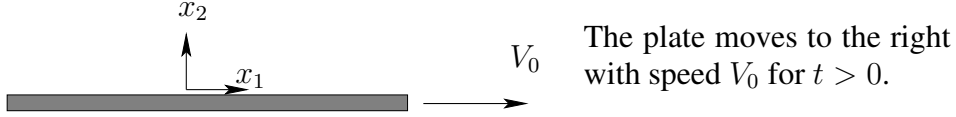
►The v_1 velocity at three different times. $t_3 > t_2 > t_1$.

Simplificatons: $\partial v_1/\partial x_1 = \partial v_3/\partial x_3 = 0 \Rightarrow \partial v_2/\partial x_2 = 0 \Rightarrow v_2 \equiv 0$.

$$\frac{\partial v_1}{\partial t} = \nu \frac{\partial^2 v_1}{\partial x_2^2}$$

►Similarity solution: the number of independent variables is reduced by one, from two (x_2 and t) to one (η).

$$\eta = \frac{x_2}{2\sqrt{\nu t}}, \quad \frac{\partial v_1}{\partial t} = \frac{dv_1}{d\eta}\frac{\partial \eta}{\partial t} = -\frac{x_2 t^{-3/2}}{4\sqrt{\nu}}\frac{dv_1}{d\eta} = -\frac{1}{2}\frac{\eta}{t}\frac{dv_1}{d\eta}$$

$$\frac{\partial v_1}{\partial x_2} = \frac{dv_1}{d\eta}\frac{\partial \eta}{\partial x_2} = \frac{1}{2\sqrt{\nu t}}\frac{dv_1}{d\eta}$$

$$\frac{\partial^2 v_1}{\partial x_2^2} = \frac{\partial}{\partial x_2}\left(\frac{\partial v_1}{\partial x_2}\right) = \frac{\partial}{\partial x_2}\left(\frac{1}{2\sqrt{\nu t}}\frac{dv_1}{d\eta}\right) = \frac{1}{2\sqrt{\nu t}}\frac{\partial}{\partial x_2}\left(\frac{dv_1}{d\eta}\right) = \frac{1}{4\nu t}\frac{d^2 v_1}{d\eta^2}$$

We get (see Eq. 3.6)

$$f = \frac{v_1}{V_0}, \quad \frac{d^2 f}{d\eta^2} + 2\eta\frac{df}{d\eta} = 0$$

►Boundary conditions

$$v_1(x_2, t = 0) = 0 \Rightarrow f(\eta \to \infty) = 0$$
$$v_1(x_2 = 0, t) = V_0 \Rightarrow f(\eta = 0) = 1$$
$$v_1(x_2 \to \infty, t) = 0 \Rightarrow f(\eta \to \infty) = 0$$

The solution reads (see Eq. 3.11)

$$f(\eta) = 1 - \text{erf}(\eta), \quad \eta = \frac{x_2}{2\sqrt{\nu t}}, \quad f = \frac{v_1}{V_0} \tag{A.8}$$
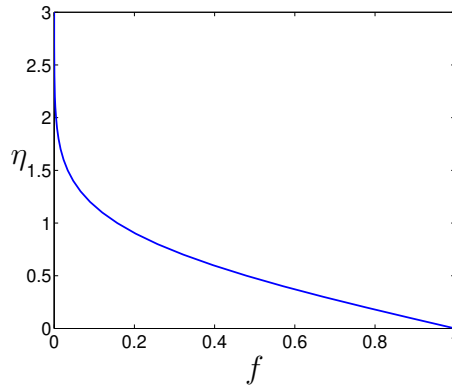
The velocity, $f = v_1/V_0$, given by Eq. A.8.

▶Boundary layer thickness defined by $v_1 = 0.01V_0$ (it would be $v_1 = 0.99V_0$ in an ordinary boundary layer). The figure above gives (for $f = 0.01$) $\eta = 1.8$ so that

$$\eta = 1.8 = \frac{\delta}{2\sqrt{\nu t}} \quad \Rightarrow \delta = 3.6\sqrt{\nu t}$$

$$\delta_{air} = 10.8cm$$
$$\delta_{water} = 2.8cm$$

¶See Section 3.2.1, Curved plates
▶The inlet part of a channel. $P_2 > P_1$
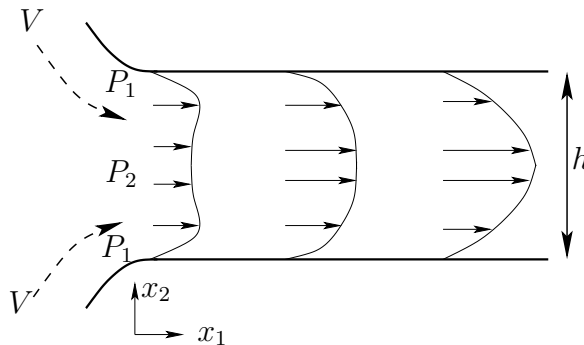
¶See Section 3.2.2, Flat plates
▶Fully developed incompressible flow in a channel. 2D and steady.
$\frac{\partial v_1}{\partial x_1} = \frac{\partial v_2}{\partial x_1} = \frac{\partial v_3}{\partial x_3} = v_3 = 0$.

$$\frac{\partial v_i}{\partial x_i} = 0 \quad \Rightarrow \frac{\partial v_2}{\partial x_2} = 0 \quad \Rightarrow v_2 = C_1(x_1) \quad \Rightarrow v_2 \equiv 0$$

►The Navier-Stokes for v_1 $(g_i = (0, -g, 0))$

$$\cancel{\frac{\partial v_1}{\partial t}}^0 + \cancel{v_1 \frac{\partial v_1}{\partial x_1}}^0 + \cancel{v_2} \frac{\partial v_1}{\partial x_2} = -\frac{\partial P}{\partial x_1} + \mu \left(\cancel{\frac{\partial^2 v_1}{\partial x_1^2}}^0 + \frac{\partial^2 v_1}{\partial x_2^2} \right) + \cancel{\rho g_1}^0 \Rightarrow \mu \frac{\partial^2 v_1}{\partial x_2^2} = \frac{\partial P}{\partial x_1}$$

The Navier-Stokes for v_2 gives

$$\cancel{\frac{\partial v_2}{\partial t}}^0 + \cancel{v_1 \frac{\partial v_2}{\partial x_1}}^0 + \cancel{v_2 \frac{\partial v_2}{\partial x_2}} = -\frac{\partial P}{\partial x_2} + \mu \left(\cancel{\frac{\partial^2 v_2}{\partial x_1^2}}^0 + \cancel{\frac{\partial^2 v_2}{\partial x_2^2}}^0 \right) - \rho g$$

$$\Rightarrow 0 = -\frac{\partial P}{\partial x_2} - \rho g \quad \Rightarrow P = -\rho g x_2 + C_1(x_1) = -\rho g x_2 + p(x_1)$$

$$\Rightarrow -\frac{\partial P}{\partial x_1} = -\frac{\partial p}{\partial x_1} \quad (p = p(x_1) \text{ is pressure at lower wall})$$

►The Navier-Stokes for v_1 (replacing $\partial P/\partial x_1$ by $\partial p/\partial x_1$, see Eq. 3.24)

$$0 = -\frac{\partial p}{\partial x_1} + \mu \frac{\partial^2 v_1}{\partial x_2^2} \quad \Rightarrow \mu \underbrace{\frac{\partial^2 v_1}{\partial x_2^2}}_{f(x_2)} = \underbrace{\frac{\partial p}{\partial x_1}}_{f(x_1)}$$

$$\Rightarrow \frac{\partial^2 v_1}{\partial x_2^2} = \frac{\partial p}{\partial x_1} = \text{const}$$

Integrate twice gives $v_1 = -\dfrac{h}{2\mu} \dfrac{dp}{dx_1} x_2 \left(1 - \dfrac{x_2}{h} \right)$

¶See Section 3.3, Two-dimensional boundary layer flow over flat plate
►2D boundary layer

$$v_1 \frac{\partial v_1}{\partial x_1} + v_2 \frac{\partial v_1}{\partial x_2} = \nu \frac{\partial^2 v_1}{\partial x_2^2}, \quad \frac{\partial p}{\partial x_2} = 0, \quad \frac{\partial v_1}{\partial x_1} + \frac{\partial v_2}{\partial x_2} = 0$$

(note that both terms on the left side are retained)
Streamfunction Ψ

$$v_1 = \frac{\partial \Psi}{\partial x_2}, \quad v_2 = -\frac{\partial \Psi}{\partial x_1}$$

The continuity equation is automatically satisfied

$$\frac{\partial v_1}{\partial x_1} + \frac{\partial v_2}{\partial x_2} = \frac{\partial^2 \Psi}{\partial x_1 \partial x_2} - \frac{\partial^2 \Psi}{\partial x_2 \partial x_1} = 0$$

Inserting the streamfunction into the streamwise momentum equation

$$\frac{\partial \Psi}{\partial x_2}\frac{\partial^2 \Psi}{\partial x_1 \partial x_2} - \frac{\partial \Psi}{\partial x_1}\frac{\partial^2 \Psi}{\partial x_2^2} = \nu \frac{\partial^3 \Psi}{\partial x_2^3}$$

Similarity solution: $x_1, x_2 \rightarrow \xi; \Psi \rightarrow g(\xi)$.

$$\xi = \left(\frac{V_{1,\infty}}{\nu x_1}\right)^{1/2} x_2, \quad \Psi = (\nu V_{1,\infty} x_1)^{1/2} g$$

First we need the derivatives $\partial\xi/\partial x_1$ and $\partial\xi/\partial x_2$

$$\frac{\partial \xi}{\partial x_1} = -\frac{1}{2}\left(\frac{V_{1,\infty}}{\nu x_1}\right)^{1/2}\frac{x_2}{x_1} = -\frac{\xi}{2x_1}, \quad \frac{\partial \xi}{\partial x_2} = \left(\frac{V_{1,\infty}}{\nu x_1}\right)^{1/2} = \frac{\xi}{x_2}$$

$$\frac{\partial \Psi}{\partial x_1} = \frac{\partial}{\partial x_1}\left((\nu V_{1,\infty} x_1)^{1/2}\right) g + (\nu V_{1,\infty} x_1)^{1/2} g' \frac{\partial \xi}{\partial x_1}$$

$$= \frac{1}{2}\left(\frac{\nu V_{1,\infty}}{x_1}\right)^{1/2} g - (\nu V_{1,\infty} x_1)^{1/2} g' \frac{\xi}{2x_1}$$

$$\ldots \Rightarrow -\frac{1}{2}gg'' + g''' = 0$$

This is Blasius solution (from his PhD thesis in 1907). The numerical solution is given in Table 3.1.

A.3   Lecture 3

¶See Section 4.1, Vorticity and rotation
►Vorticity
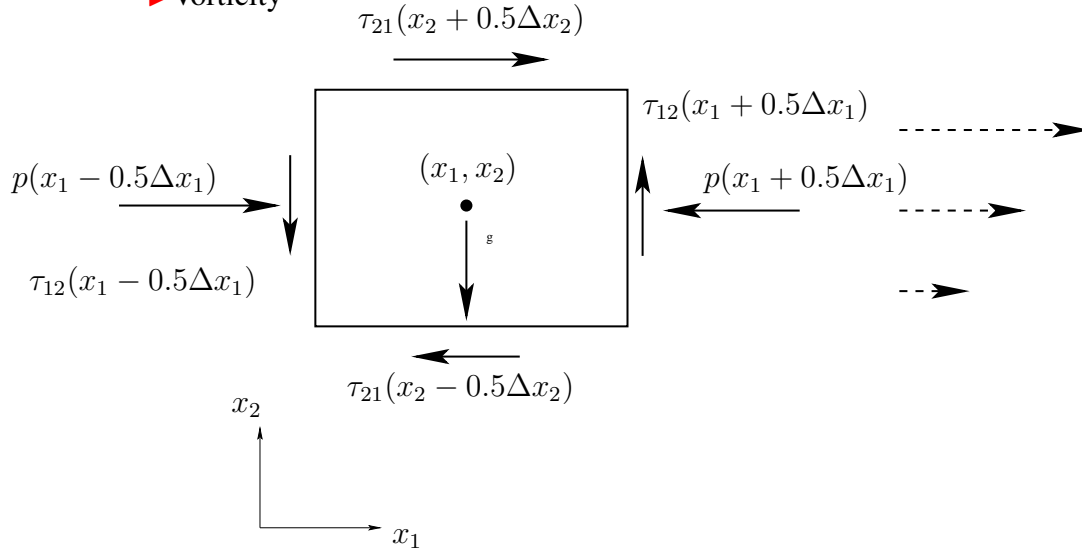
Surface forces. $\partial\tau_{12}/\partial x_1 = 0$, $\partial\tau_{21}/\partial x_2 > 0$.

$$\rho\frac{dv_i}{dt} = -\frac{\partial P}{\partial x_i} + \boxed{\frac{\partial\tau_{ji}}{\partial x_j}} = -\frac{\partial P}{\partial x_i}\boxed{-\mu\varepsilon_{inm}\frac{\partial\omega_m}{\partial x_n}} \qquad (A.9)$$

►change in vorticity $\Leftrightarrow$ change in shear stresses

- irrotational flow $\Leftrightarrow$

- potential flow $\Leftrightarrow$

- no change in ω_i (often $\omega_i = 0$)

►As a first step for deriving the ω_i transport eq., let's re-write the left-side of N-S:

$$v_j\frac{\partial v_i}{\partial x_j} = v_j(S_{ij} + \Omega_{ij}) = v_j\left(S_{ij} - \frac{1}{2}\varepsilon_{ijk}\omega_k\right)$$

Inserting $S_{ij} = (\partial v_i/\partial x_j + \partial v_j/\partial x_i)/2$ and multiplying by two gives

$$2v_j\frac{\partial v_i}{\partial x_j} = v_j\left(\frac{\partial v_i}{\partial x_j} + \frac{\partial v_j}{\partial x_i}\right) - \varepsilon_{ijk}v_j\omega_k \qquad (A.10)$$

The second term on the right side can be written as (Trick 2)

$$v_j\frac{\partial v_j}{\partial x_i} = \frac{1}{2}\frac{\partial(v_j v_j)}{\partial x_i}$$

With Eq. A.10 Navier-Stokes can be written (see Eq. 4.12)

$$\frac{\partial v_i}{\partial t} + \underbrace{\frac{\partial \frac{1}{2}v^2}{\partial x_i}}_{\text{no rotation}} - \underbrace{\varepsilon_{ijk}v_j\omega_k}_{\text{rotation}} = -\frac{1}{\rho}\frac{\partial P}{\partial x_i} + \nu\frac{\partial^2 v_i}{\partial x_j \partial x_j} + f_i \qquad (A.11)$$

▶Now we will derive the transport eq. for $\omega_p = \varepsilon_{pqi}\partial v_i/\partial x_q$. Multiply the Navier-Stokes equation by $\varepsilon_{pqi}\partial/\partial x_q$ so that

$$\varepsilon_{pqi}\frac{\partial^2 v_i}{\partial t \partial x_q} + \varepsilon_{pqi}\frac{\partial^2 k}{\partial x_i \partial x_q}^{\!\!\!0} - \varepsilon_{pqi}\varepsilon_{ijk}\frac{\partial v_j\omega_k}{\partial x_q}$$
$$= -\varepsilon_{pqi}\frac{1}{\rho}\frac{\partial^2 P}{\partial x_i \partial x_q}^{\!\!\!0} + \nu\varepsilon_{pqi}\frac{\partial^3 v_i}{\partial x_j \partial x_j \partial x_q} + \varepsilon_{pqi}\frac{\partial g_i}{\partial x_q}^{\!\!\!0} \qquad (A.12)$$

- Term on line 1: zero because a-sym & sym tensor

- 1st term in line 2: zero because a-sym & sym tensor

- last term: zero because g_i is constant

Re-write unsteady and viscous terms in Eq. A.12:

$$\varepsilon_{pqi}\frac{\partial^2 v_i}{\partial t \partial x_q} = \frac{\partial}{\partial t}\left(\varepsilon_{pqi}\frac{\partial v_i}{\partial x_q}\right) = \frac{\partial \omega_p}{\partial t}$$

$$\nu\varepsilon_{pqi}\frac{\partial^3 v_i}{\partial x_j \partial x_j \partial x_q} = \nu\frac{\partial^2}{\partial x_j \partial x_j}\left(\varepsilon_{pqi}\frac{\partial v_i}{\partial x_q}\right) = \nu\frac{\partial^2 \omega_p}{\partial x_j \partial x_j}$$

Inserted in Eq. A.12 gives

$$\frac{\partial \omega_p}{\partial t} - \varepsilon_{pqi}\varepsilon_{ijk}\frac{\partial v_j\omega_k}{\partial x_q} = \nu\frac{\partial^2 \omega_p}{\partial x_j \partial x_j}$$

▶Transport equation for the vorticity (see Eq. 4.20)

$$\frac{\partial \omega_p}{\partial t} + v_k\frac{\partial \omega_p}{\partial x_k} = \underline{\omega_k\frac{\partial v_p}{\partial x_k}} + \nu\frac{\partial^2 \omega_p}{\partial x_j \partial x_j}$$

Underlined term: vortex stretching/tilting term (a source/sink), see Eq. 4.21

$$\omega_k\frac{\partial v_p}{\partial x_k} = \begin{cases} \omega_1\dfrac{\partial v_1}{\partial x_1} + \omega_2\dfrac{\partial v_1}{\partial x_2} + \omega_3\dfrac{\partial v_1}{\partial x_3}, & p = 1 \\[2mm] \omega_1\dfrac{\partial v_2}{\partial x_1} + \omega_2\dfrac{\partial v_2}{\partial x_2} + \omega_3\dfrac{\partial v_2}{\partial x_3}, & p = 2 \\[2mm] \omega_1\dfrac{\partial v_3}{\partial x_1} + \omega_2\dfrac{\partial v_3}{\partial x_2} + \omega_3\dfrac{\partial v_3}{\partial x_3}, & p = 3 \end{cases}$$

Vortex stretching and vortex tilting
►Vortex stretching

$$\frac{\partial v_1}{\partial x_1} > 0$$

x_2

x_1
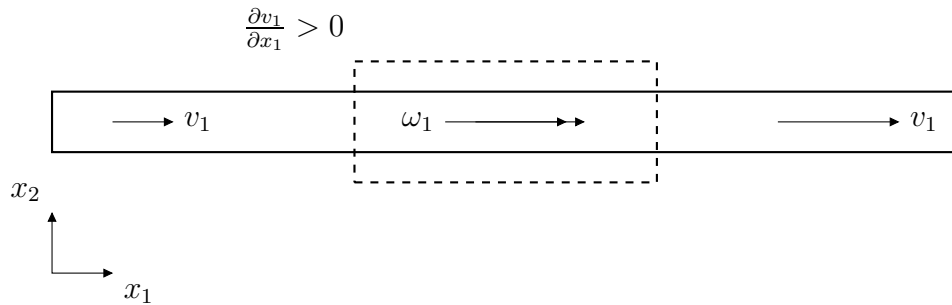
Assume $\dfrac{\partial v_1}{\partial x_1} > 0$: the term $\omega_1 \dfrac{\partial v_1}{\partial x_1}$ will increase ω_1

►Vortex tilting/deflection

$v_1(x_2)$, $\quad \frac{\partial v_1}{\partial x_2} > 0$

x_2

x_1
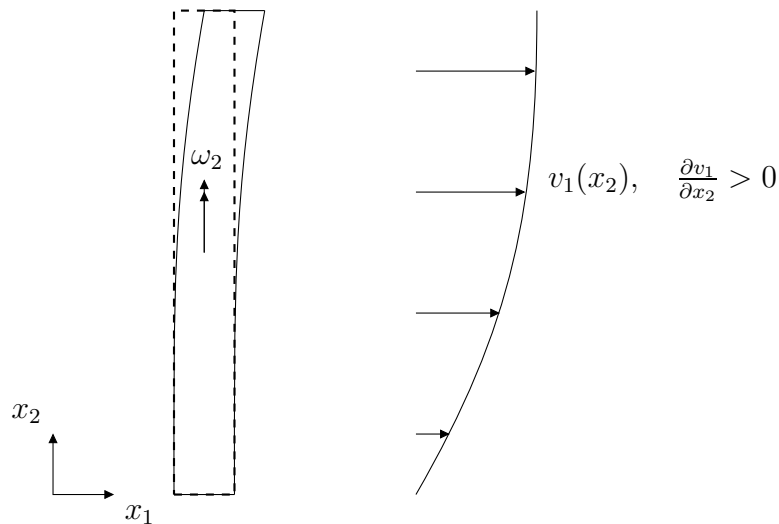
Assume $\dfrac{\partial v_1}{\partial x_2} > 0$: the term $\omega_2 \dfrac{\partial v_1}{\partial x_2}$ will increase ω_1

¶See Section 4.3, The vorticity transport equation in two dimensions
►2D flow: $v_i = (v_1, v_2, 0)$, $\omega_i = (0, 0, \omega_3)$ and $\dfrac{\partial}{\partial x_3} = 0$

Now the vortex stretching/tilting term $\omega_k \dfrac{\partial v_p}{\partial x_k} = \omega_3 \dfrac{\partial v_p}{\partial x_3} = 0$

The 2D ω_3 equation reads (see Eq. 4.22)

$$\frac{\partial \omega_3}{\partial t} + v_k \frac{\partial \omega_3}{\partial x_k} = \nu \frac{\partial^2 \omega_3}{\partial x_j \partial x_j}$$

▶Consider fully developed channel flow (see Eq. 4.23)

heat conduction $0 = k \dfrac{\partial^2 T}{\partial x_2^2}$

vorticity diffusion $0 = \nu \dfrac{\partial^2 \omega_3}{\partial x_2^2}$
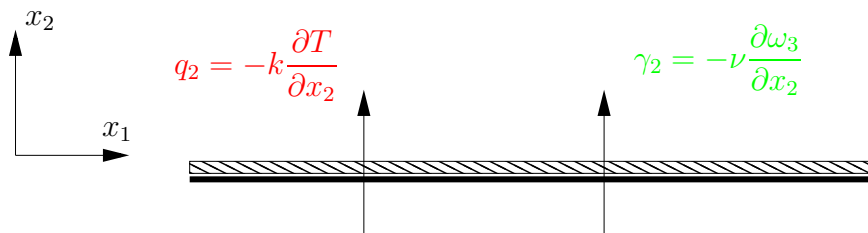
Temperature: $q_2 = 0 \Rightarrow$ no temperature (increase)
Vorticity: $\gamma_2 = 0 \Rightarrow$ no vorticity (increase). In the self-similar region of a boundary layer this is true because $\partial p / \partial x_1 = 0$; for channel flow $\gamma_2 \neq 0$

¶See Section 4.3.1, Boundary layer thickness from the Rayleigh problem
▶Rayleigh problem: $\delta(t) = 3.6\sqrt{\nu t}$ was presented for the temperature equation. It can also be used for the vorticity equation.
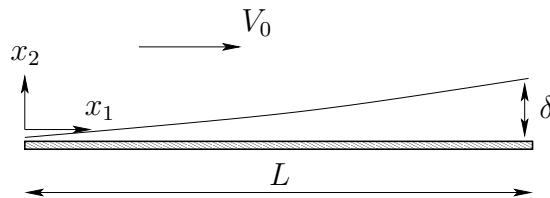
Boundary layer thickness $\delta \propto \sqrt{\dfrac{L\nu}{V}} = L\sqrt{\dfrac{\nu}{VL}} \Rightarrow \dfrac{\delta}{L} \propto \sqrt{\dfrac{1}{Re_L}}$

A.4 Lecture 4

Potential flow

¶See Section 4.4, Potential flow
►Define a potential

$$v_i = \partial \Phi / \partial x_i \qquad (A.13)$$

Then the vorticity is zero

$$\omega_i = \epsilon_{ijk} \frac{\partial v_k}{\partial x_j} = \epsilon_{ijk} \frac{\partial^2 \Phi}{\partial x_j \partial x_k} = 0$$

The continuity eq. reads

$$0 = \frac{\partial v_i}{\partial x_i} = \frac{\partial}{\partial x_i} \left(\frac{\partial \Phi}{\partial x_i} \right) = \frac{\partial^2 \Phi}{\partial x_i \partial x_i} \qquad (A.14)$$

►Derive the Bernoulli eq. The N-S reads (see Eqs. A.9 and A.11)

$$\frac{\partial v_i}{\partial t} + \underbrace{\frac{\partial \frac{1}{2}v^2}{\partial x_i}}_{\text{no rotation}} - \underbrace{\varepsilon_{ijk} v_j \omega_k}_{\text{rotation}} = -\frac{1}{\rho}\frac{\partial p}{\partial x_i} - \nu \varepsilon_{inm} \frac{\partial \omega_m}{\partial x_n} + g_i$$

In potential flow, $\omega_i = 0$. Insert Φ (Eq. A.13) and a gravitation potential $(g_i = -\partial \mathcal{X}/\partial x_i)$

$$\frac{\partial}{\partial x_i} \left(\frac{\partial \Phi}{\partial t} \right) + \frac{\partial \frac{1}{2}v^2}{\partial x_i} + \frac{1}{\rho}\frac{\partial p}{\partial x_i} + \frac{\partial \mathcal{X}}{\partial x_i} = 0$$

Integration gives (see Eq. 4.32)

$$\frac{\partial \Phi}{\partial t} + \frac{1}{2}v^2 + \frac{p}{\rho} + \mathcal{X} = const$$

Replacing $\mathcal{X} = -g_3 x_3 = gh$ gives the Bernoulli eq.

¶See Section 4.4.2, Complex variables for potential solutions of plane flows
►Complex functions.
The derivative of a complex function, f, by a complex variable, z ($f = u + iv$ and $z = x + iy$) is defined only if the derivatives in the real and imaginary directions are the same, i.e.

$$\frac{df}{dz} = \lim_{\Delta z \to 0} \frac{f(z_0 + \Delta z) - f(z_0)}{\Delta z}$$

$$= \lim_{\Delta x \to 0} \frac{f(x_0 + \Delta x, iy_0) - f(x_0, iy_0)}{\Delta x} = \lim_{\Delta y \to 0} \frac{f(x_0, iy_0 + i\Delta y) - f(x_0, iy_0)}{i\Delta y}.$$

$$(A.15)$$
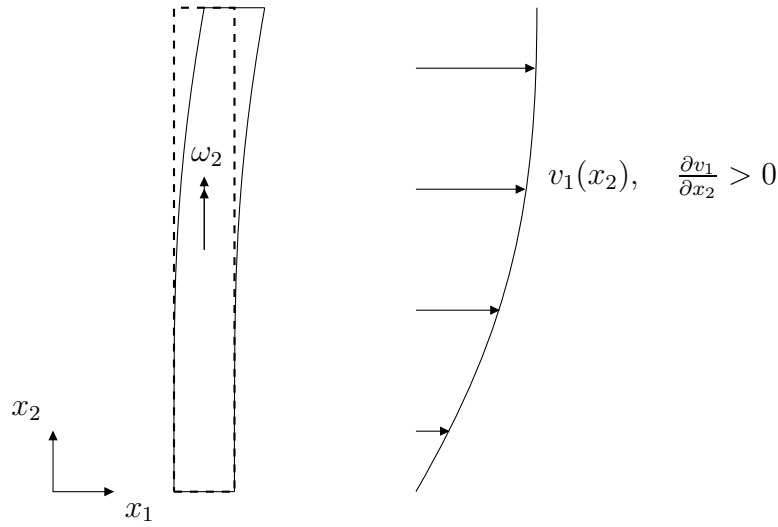
which means that

$$\frac{\partial f}{\partial x} = \frac{1}{i}\frac{\partial f}{\partial y} = -i\frac{\partial f}{\partial y} \qquad (A.16)$$

Inserting $f = u + iv$ in Eq. A.16 gives

$$\frac{\partial u}{\partial x} + i\frac{\partial v}{\partial x} = -i\frac{\partial u}{\partial y} - i^2\frac{\partial v}{\partial y} = -i\frac{\partial u}{\partial y} + \frac{\partial v}{\partial y}$$

We get (see Eq. 4.38)

$$\frac{\partial u}{\partial x} = \frac{\partial v}{\partial y}, \quad \frac{\partial u}{\partial y} = -\frac{\partial v}{\partial x}$$

which are called the *Cauchy-Riemann* equations.

▶A complex function in polar coordinates: $z = re^{i\theta} = r(\cos\theta + i\sin\theta)$

▶Fluid dynamics: define a complex potential $f = \Phi + i\Psi$ where Ψ is the streamfunction (recall the $v_1 = \frac{\partial\Psi}{\partial y}$ and $v_2 = -\frac{\partial\Psi}{\partial x}$, see Eq. 3.44). We want f to be differentiable: hence Eq. A.4 must hold (replace u and v with Φ and Ψ)

$$\frac{\partial\Phi}{\partial x} = \frac{\partial\Psi}{\partial y}, \quad \frac{\partial\Phi}{\partial y} = -\frac{\partial\Psi}{\partial x}, \qquad (A.17)$$

which is satisfied (first relation = v_1, second = v_2).

Φ satisfies Laplace eq. (see Eq. A.14). Since $\omega_3 = 0$, this applies also for Ψ

$$\frac{\partial^2\Psi}{\partial x_1^2} + \frac{\partial^2\Psi}{\partial x_2^2} = -\frac{\partial v_2}{\partial x_1} + \frac{\partial v_1}{\partial x_2} = -\omega_3 = 0$$

Hence, f also satisfies Laplace eq.

We have now defined a complex function, $f = \Phi + i\Psi$ which satisfies Laplace eq and which has a physical meaning in fluid dynamics.

¶See Section 4.4.3, $f \propto z^n$

1. Now we "guess"/dream up a complex function $f = \Phi + i\Psi$

2. then we check if it satisfies the Laplace equation (i.e. the continuity equation, 4.28 and that the flow is inviscid, $\omega_3 = 0$, Eq. 4.41)

3. then we find out if f corresponds to a meaningful fluid flow situation

▶We guess $f = C_1 z^n = C_1 r^n e^{in\theta} = C_1 r^n (\cos(n\theta) + i\sin(n\theta))$

Check that it satisfies Laplace eq. (it does, see Eq. 4.47) $\nabla^2 f = \frac{1}{r}\frac{\partial}{\partial r}\left(r\frac{\partial f}{\partial r}\right) + \frac{1}{r^2}\frac{\partial^2 f}{\partial \theta^2}$

¶See Section 4.4.3.1, *Parallel flow*
▶Parallel flow, $n = 1$. $f = C_1 z = V_\infty z = V_\infty(x + iy)$
The streamfunction, Ψ, is the imaginary part of f, i.e. $\Psi = V_\infty y = V_\infty r \sin(n\theta)$ which gives

$$v_1 = \frac{\partial \Psi}{\partial y} = V_\infty, \quad v_2 = -\frac{\partial \Psi}{\partial x} = 0$$
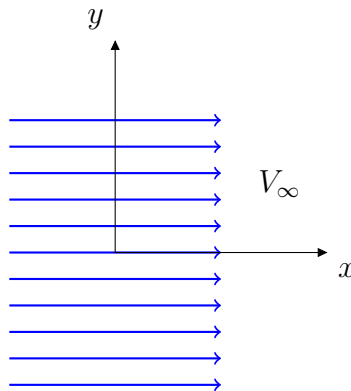
¶See Section 4.4.4, Analytical solutions for a line source
▶Line source

$$f = \frac{\dot{m}}{2\pi}\ln z = \frac{\dot{m}}{2\pi}\ln\left(re^{i\theta}\right) = \frac{\dot{m}}{2\pi}\left(\ln r + \ln\left(e^{i\theta}\right)\right) = \frac{\dot{m}}{2\pi}\left(\ln r + i\theta\right)$$
$$\text{(A.18)}$$

Check that it satisfies Laplace eq. (it does, see 4.58)

$$v_r = \frac{1}{r}\frac{\partial \Psi}{\partial \theta} = \frac{\dot{m}}{2\pi r}$$

$$v_\theta = -\frac{\partial \Psi}{\partial r} = 0$$
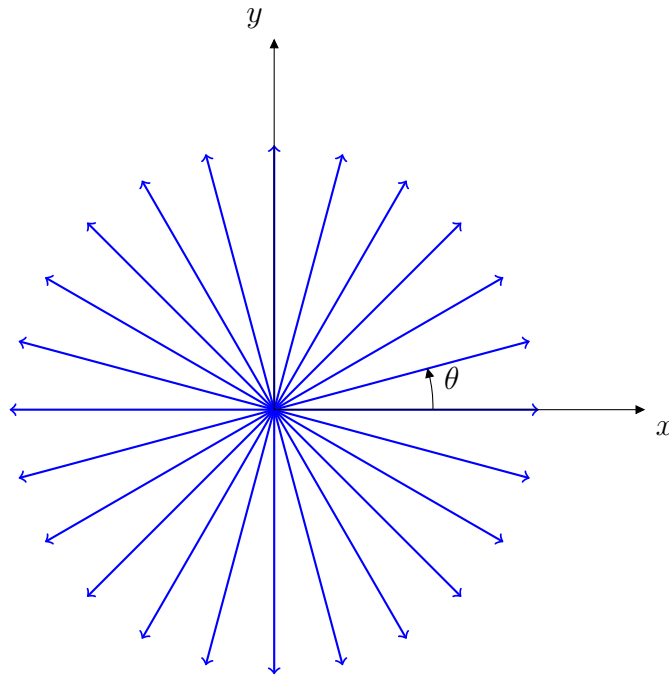
¶See Section 4.4.5, Analytical solutions for a vortex line
►Vortex line

$$f = -i\frac{\Gamma}{2\pi}\ln z = -i\frac{\Gamma}{2\pi}\ln\left(re^{i\theta}\right) = -i\frac{\Gamma}{2\pi}\left(\ln r + \ln\left(e^{i\theta}\right)\right) = \frac{\Gamma}{2\pi}\left(-i\ln r + \theta\right)$$

Check if it satisfies Laplace eq. (it does, see 4.58)

$$v_r = \frac{1}{r}\frac{\partial \Psi}{\partial \theta} = 0, \quad v_\theta = -\frac{\partial \Psi}{\partial r} = \frac{\Gamma}{2\pi r}$$
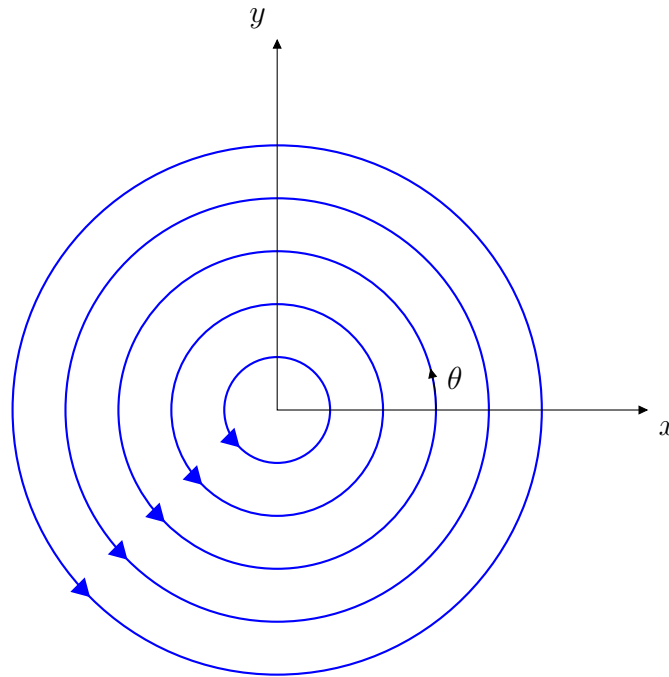
¶See Section 4.4.6, Analytical solutions for flow around a cylinder
▶Doublet: take a line source ($\dot{m} > 0$) a line sink ($\dot{m} < 0$) with a separation ε: let $\varepsilon \to 0$ which gives

$$f = \frac{\mu}{\pi z} = \frac{V_\infty r_0^2}{z}$$

where $r_0^2 = \mu/(\pi V_\infty)$. Add parallel flow ($f = V_\infty z$) gives cylinder flow

$$f = \frac{V_\infty r_0^2}{z} + V_\infty z = \frac{V_\infty r_0^2}{re^{i\theta}} + V_\infty re^{i\theta} = V_\infty \left(\frac{r_0^2}{r} e^{-i\theta} + re^{i\theta} \right)$$

$$= V_\infty \left(\frac{r_0^2}{r}(\cos\theta - i\sin\theta) + r(\cos\theta + i\sin\theta) \right)$$

The streamfunction reads (imaginary part)

$$\Psi = V_\infty \left(r - \frac{r_0^2}{r} \right) \sin\theta$$

and we get the velocity components

$$v_r = \frac{1}{r}\frac{\partial\Psi}{\partial\theta} = V_\infty \left(1 - \frac{r_0^2}{r^2} \right) \cos\theta, \quad v_\theta = -\frac{\partial\Psi}{\partial r} = -V_\infty \left(1 + \frac{r_0^2}{r^2} \right) \sin\theta$$
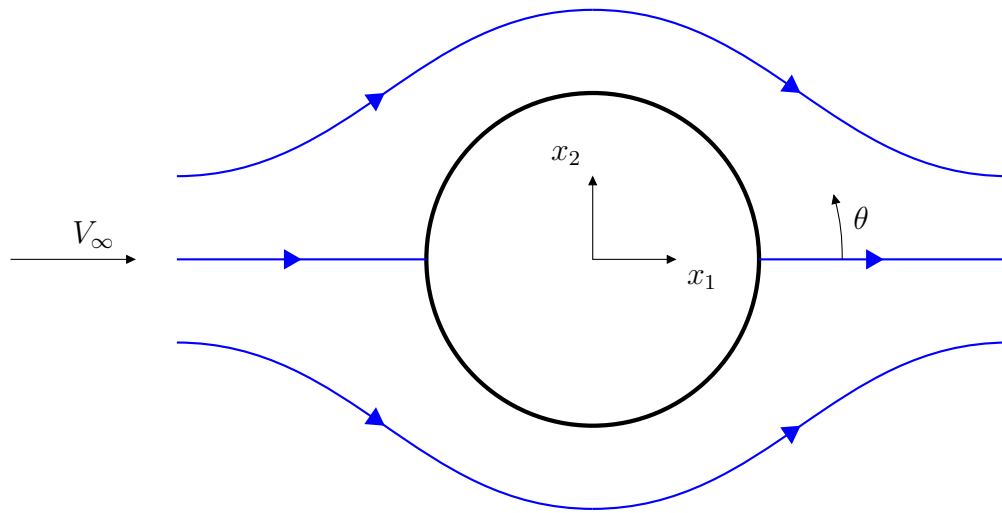
¶See Section 4.4.7, Analytical solutions for flow around a cylinder with circulation
►Flow around a cylinder with circulation, Γ
We have f for a cylinder. Now we add f for a vortex line

$$f = V_\infty \left(\frac{r_0^2}{r}(\cos\theta - i\sin\theta) + r(\cos\theta + i\sin\theta) \right) - i\frac{\Gamma}{2\pi}\ln z$$

The imaginary part gives the streamfunction

$$\Psi = V_\infty \left(r - \frac{r_0^2}{r} \right)\sin\theta - \frac{\Gamma}{2\pi}\ln r$$

We get the velocity components as

$$v_r = \frac{1}{r}\frac{\partial\Psi}{\partial\theta} = V_\infty\left(1 - \frac{r_0^2}{r^2}\right)\cos\theta, \quad v_\theta = -\frac{\partial\Psi}{\partial r} = -V_\infty\left(1 + \frac{r_0^2}{r^2}\right)\sin\theta + \frac{\Gamma}{2\pi r}$$
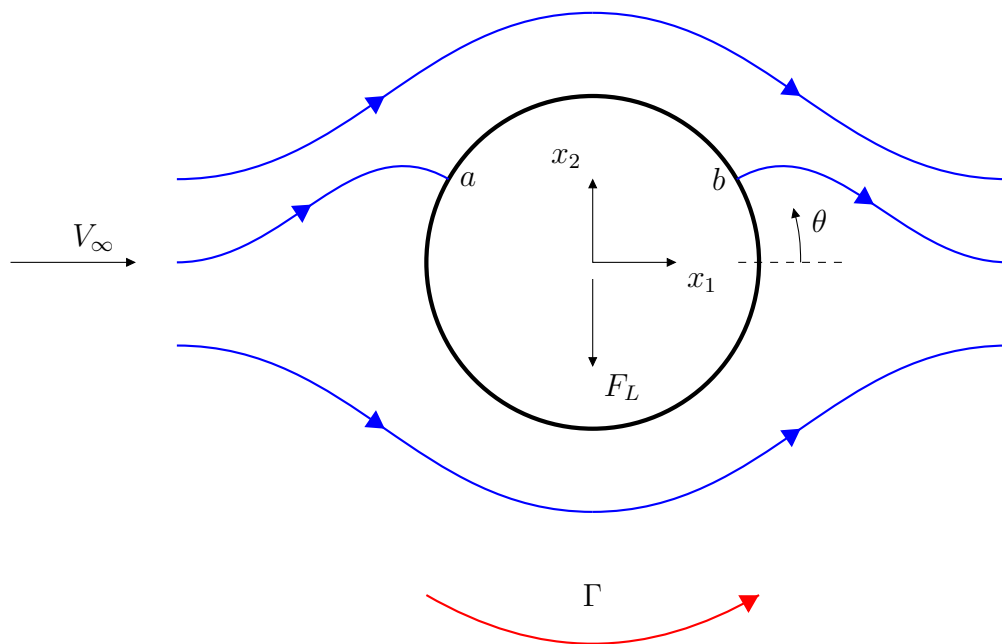
The velocity at the surface, $r = r_0$, reads

$$v_{r,s} = 0$$

$$v_{\theta,s} = -2V_\infty \sin\theta + \frac{\Gamma}{2\pi r_0}$$

▶Location of the stagnation points, i.e. where $v_{\theta,s} = 0$. We get

$$2V_\infty \sin\theta_{stag} = \frac{\Gamma}{2\pi r_0} \Rightarrow \theta_{stag} = \arcsin\left(\frac{\Gamma}{4\pi r_0 V_\infty}\right)$$

$$\Gamma_{max} = 4\pi V_\infty r_0.$$

▶The pressure is obtained from Bernoulli equation as (see Eq. 4.73)

$$C_p = 1 - \frac{v_{\theta,s}^2}{V_\infty^2} = 1 - \left(-2\sin\theta + \frac{\Gamma}{2\pi r_0 V_\infty}\right)^2$$

$$= 1 - 4\sin^2\theta + \frac{4\Gamma\sin\theta}{2\pi r_0 V_\infty} - \left(\frac{\Gamma}{2\pi r_0 V_\infty}\right)^2$$

▶Integration of C_p gives drag $F_D = 0$ and lift $F_L = -\rho V_\infty \Gamma$.

¶See Section 4.4.7.1, *The Magnus effect*
▶The Magnus' effect: three applications
▶Table tennis: loop
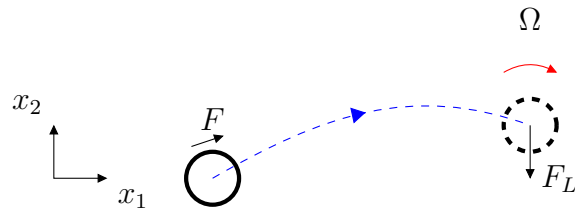
▶Free-kick
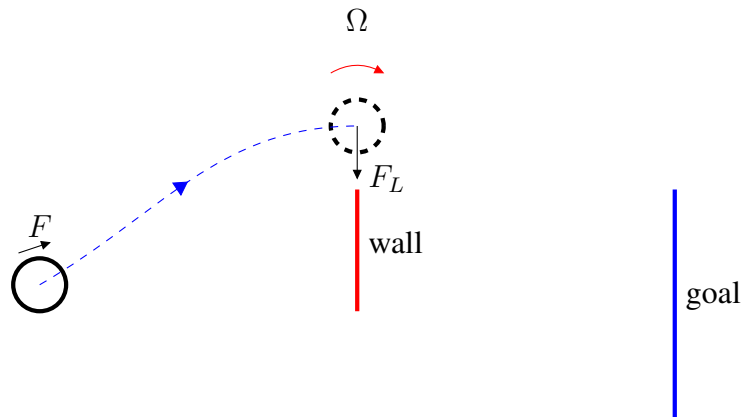
▶Flettner rotors: the Magus effect $\Rightarrow$ propulsion force of $F_L \cos(\alpha)$
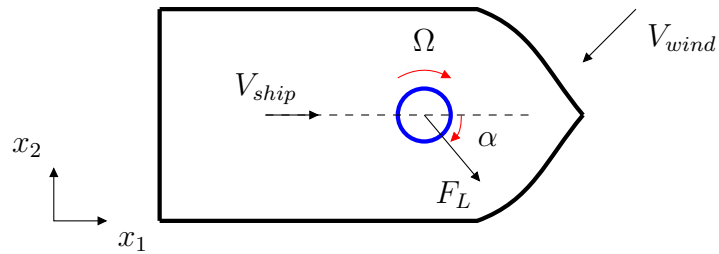
¶See Section 4.4.8, The flow around an airfoil
▶Airfoil flow
▶The boundary layers, $\delta(x_1)$, and the wake illustrated in red.
▶Lift force $F_L = -\rho V_\infty \Gamma$
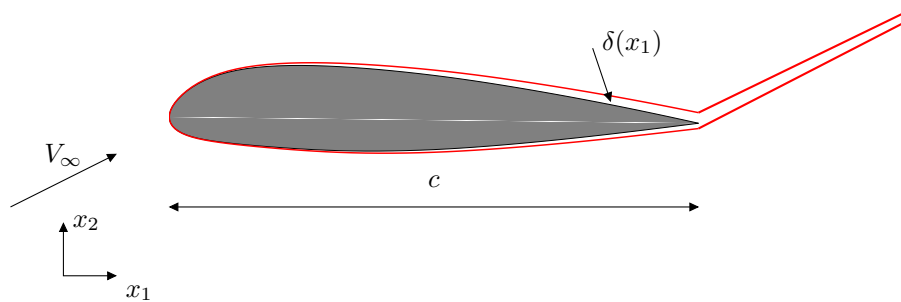
Figure A.1: Airfoil. The boundary layers, $\delta(x_1)$, and the wake illustrated in red. $x_1 = 0$ and $x_1 = c$ at leading and trailing edge, respectively.
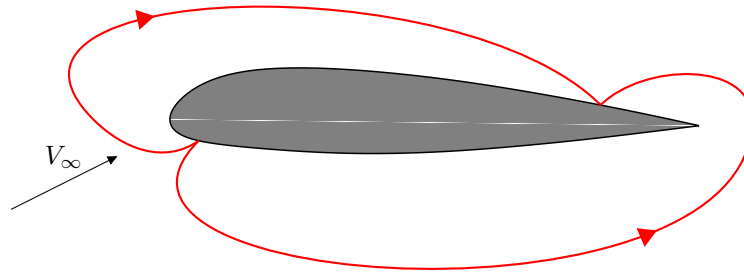
Figure A.2: Airfoil. Streamlines from potential flow. Rear stagnation point at the upper surface (suction side).

A.5   Lecture 5

¶See Section 5, Turbulence
▶Turbulence
▶$v_i = \bar{v}_i + v_i'$, is irregular and consists of eddies of different size
▶increases diffusivity
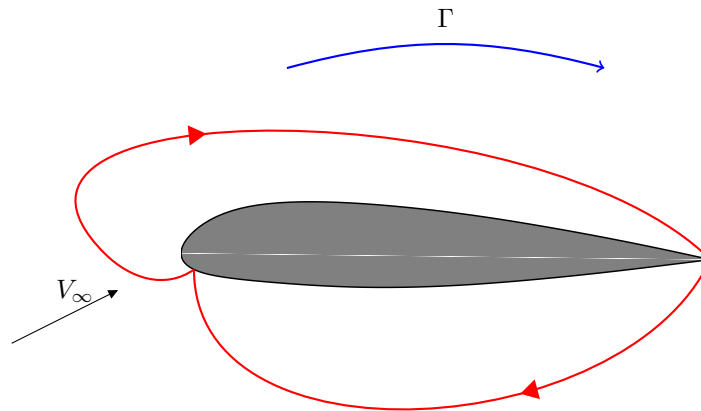
Figure A.3: Airfoil. Streamlines from potential flow with added circulation. Rear stagnation point at the trailing edge.

▶occurs at large Reynolds numbers. Pipes: $Re_D = \dfrac{VD}{\nu} \simeq 2300$; boundary layers: $Re_x = \dfrac{VL}{\nu} \simeq 500\,000$.

▶is three-dimensional

▶is dissipative. Kinetic energy, $v_i' v_i'/2$, in the small (dissipative) eddies

are transformed into thermal energy (increases temperature).

flow of kinetic energy

large scales

intermediate scales

dissipative scales

►Dissipation $\varepsilon = \nu \overline{\dfrac{\partial v_i'}{\partial x_j} \dfrac{\partial v_i'}{\partial x_j}}$

All kinetic energy (say 90%) is finally dissipated at the smallest (dissipative) scales.

►Kinetic energy dissipative at small scales determined by ε, ν

$$
\begin{array}{ccc}
v_\eta & = & \nu^a & \varepsilon^b \\
[m/s] & = & [m^2/s] & [m^2/s^3]
\end{array}
$$
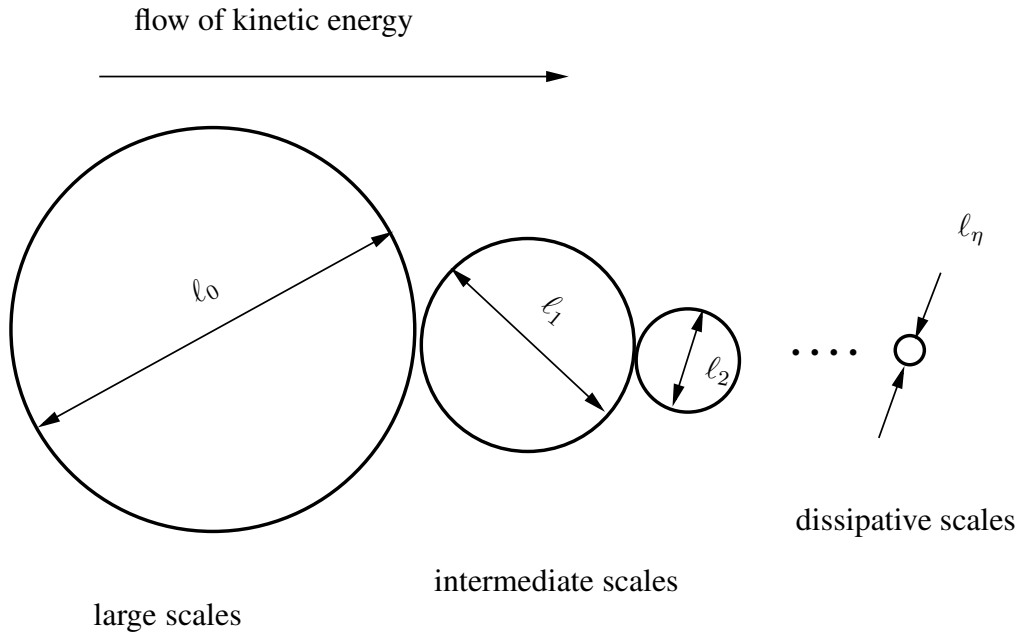
$$
\begin{aligned}
1 &= 2a + 2b, \quad [m] \\
-1 &= -a - 3b, \quad [s]
\end{aligned}
$$

►This gives the Kolmogorov scales (see Eq. 5.5)

$$
v_\eta = (\nu\varepsilon)^{1/4}, \; \ell_\eta = \left(\frac{\nu^3}{\varepsilon}\right)^{1/4}, \; \tau_\eta = \left(\frac{\nu}{\varepsilon}\right)^{1/2}
$$

►Any periodic function, f, can be expressed as a Fourier series

$$
f(x) = \frac{1}{2}a_0 + \sum_{n=1}^{\infty}(a_n \cos(\kappa_n x) + b_n \sin(\kappa_n x)), \quad f = v, \quad \kappa_n = \frac{n\pi}{L}
$$

$$a_n = \frac{1}{L} \int_{-L}^{L} f(x) \cos(\kappa_n x) dx$$

$$b_n = \frac{1}{L} \int_{-L}^{L} f(x) \sin(\kappa_n x) dx$$

Parseval's formula states that (average over all eddies)

$$\int_{-L}^{L} v'^2(x) dx = \frac{L}{2} a_0^2 + L \sum_{n=1}^{\infty} (a_n^2 + b_n^2)$$

Time-averaging (average of over time instants):

$$\overline{v'^2} = \frac{1}{2T} \int_{-T}^{T} v'^2 dt$$

►Spectrum for turbulent kinetic energy, k

$$P^k = -\overline{v_i' v_j'} \frac{\partial \bar{v}_i}{\partial x_j}$$

$$E(\kappa_n) \propto a_n^2 + b_n^2$$

$$k = \int_0^\infty E(\kappa)d\kappa = \sum_0^\infty E(\kappa_n)\Delta\kappa_n$$

$$P^k = -\overline{v_i'v_j'}\frac{\partial \bar{v}_i}{\partial x_j}$$

The turbulence spectrum is divided into three regions:

  I. Large eddies carry most of the turbulent kinetic energy. They extract energy from the mean flow.

 II. Inertial subrange. Independent of both large eddies (mean flow) and viscosity.

III. Dissipation range. Isotropic eddies ($\overline{v_i'v_j'} = c_1\delta_{ij}$) described by the Kolmogorov scales.

▶Turb. kinetic energy in Region II depends on ε and eddy size $1/\kappa$.

$$\begin{array}{ccccc} E & = & \kappa^a & & \varepsilon^b \\ [m^3/s^2] & = & [1/m] & & [m^2/s^3] \end{array}$$

$$3 = -a + 2b, \quad [m]$$
$$-2 = -3b, \quad [s]$$

$b = 2/3, a = -5/3$ so that

$$E(\kappa) = \text{const.} \cdot \varepsilon^{\frac{2}{3}}\kappa^{-\frac{5}{3}}$$

▶This is called Kolmogorov spectrum or $-5/3$ law
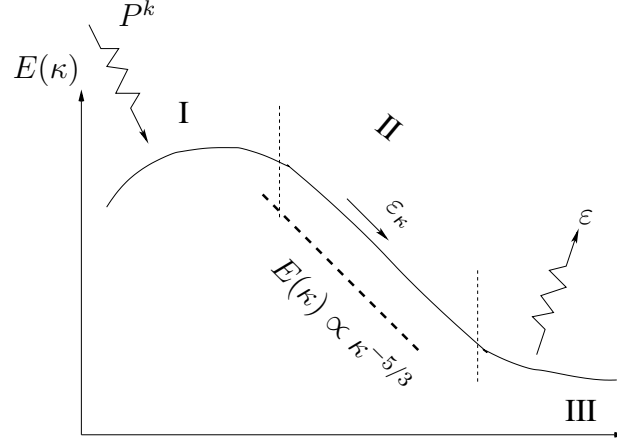
▶Small-scale turbulence is isotropic (see Section 5.3): $\overline{v_1'^2} = \overline{v_2'^2} = \overline{v_3'^2}$.
Not true instantaneously, i.e. $v_1' \neq v_2' \neq v_3'$.

Isotropy: if a coordinate direction is switched (i.e. rotated 180°), nothing should change. $\Rightarrow \overline{v_1'v_2'}$ in both coordinate directions must be the same. $\Rightarrow \overline{v_1'v_2'} = (\overline{v_1'v_2'})_{180^o} = -\overline{v_1'v_2'} = 0$.

▶On tensor form: $\overline{v_i'v_j'} = \text{const.}\delta_{ij}$

$$\varepsilon_\kappa \sim \frac{v_\kappa^2}{\ell_\kappa/v_\kappa} \sim \frac{v_\kappa^3}{\ell_\kappa} \sim \frac{v_0^3}{\ell_0}$$

▶Relation between largest and smallest scales ($Re = v_0\ell_0/\nu$)

$$\frac{v_0}{v_\eta} = (\nu\varepsilon)^{-1/4}v_0 = \left(\nu v_0^3/\ell_0\right)^{-1/4}v_0 = (v_0\ell_0/\nu)^{1/4} = Re^{1/4}$$

$$\frac{\ell_0}{\ell_\eta} = \left(\frac{\nu^3}{\varepsilon}\right)^{-1/4}\ell_0 = \left(\frac{\nu^3\ell_0}{v_0^3}\right)^{-1/4}\ell_0 = \left(\frac{\nu^3}{v_0^3\ell_0^3}\right)^{-1/4} = Re^{3/4}$$

$$\frac{\tau_o}{\tau_\eta} = \left(\frac{\nu\ell_0}{v_0^3}\right)^{-1/2}\tau_0 = \left(\frac{v_0^3}{\nu\ell_0}\right)^{1/2}\frac{\ell_0}{v_0} = \left(\frac{v_0\ell_0}{\nu}\right)^{1/2} = Re^{1/2}$$

• This explains why DNS (Direct Numerical Simulation) is too expensive at high Re numbers: a doubling of Re number $\Rightarrow$

$$\underbrace{2^{3/4}}_{x_1\ dir} \times \underbrace{2^{3/4}}_{x_2\ dir} \times \underbrace{2^{3/4}}_{x_3\ dir} \times \underbrace{2^{1/2}}_{time} = 2^{11/4} \simeq 7 \qquad (A.19)$$

times increase in computational effort

A.6 Lecture 6

¶See Section 6, Turbulent mean flow
►The continuity and the N-S for incompr. flow with const. μ

$$\frac{\partial v_i}{\partial x_i} = 0, \quad \rho\frac{\partial v_i}{\partial t} + \rho\frac{\partial v_i v_j}{\partial x_j} = -\frac{\partial p}{\partial x_i} + \mu\frac{\partial^2 v_i}{\partial x_j \partial x_j}$$

Decompose the variables and time average

$$v_i = \bar{v}_i + v'_i, \quad p = \bar{p} + p'$$

$$\frac{\partial \overline{\bar{v}_i + v'_i}}{\partial x_i} = \frac{\partial \overline{\bar{v}_i}}{\partial x_i} + \frac{\overset{0}{\cancel{\partial \overline{v'_i}}}}{\cancel{\partial x_i}} = \frac{\partial \bar{v}_i}{\partial x_i}$$

$$\frac{\partial \overline{v_i v_j}}{\partial x_j} = \frac{\partial}{\partial x_j}\left\{\overline{(\bar{v}_i + v'_i)(\bar{v}_j + v'_j)}\right\} = \frac{\partial}{\partial x_j}\left(\overline{\bar{v}_i\bar{v}_j} + \overline{\bar{v}_i v'_j} + \overline{\bar{v}_j v'_i} + \overline{v'_i v'_j}\right)$$

$$= \frac{\partial}{\partial x_j}\left(\overline{\bar{v}_i\bar{v}_j} + \overline{\bar{v}_i\cancel{v'_j}}^{\,0} + \overline{\bar{v}_j\cancel{v'_i}}^{\,0} + \overline{v'_i v'_j}\right) = \frac{\partial \bar{v}_i\bar{v}_j}{\partial x_j} + \frac{\partial \overline{v'_i v'_j}}{\partial x_j}$$

►The steady RANS (Reynolds-Averaged Navier-Stokes) equations, see Eq. 6.9

$$\frac{\partial \bar{v}_i}{\partial x_i} = 0, \quad \rho\frac{\partial \bar{v}_i\bar{v}_j}{\partial x_j} = -\frac{\partial \bar{p}}{\partial x_i} + \frac{\partial}{\partial x_j}\underbrace{\left(\mu\frac{\partial \bar{v}_i}{\partial x_j} - \rho\overline{v'_i v'_j}\right)}_{\tau_{ij,tot}}$$

¶See Section 6.1.1, Boundary-layer approximation
►RANS in developing boundary layer flow

$$\bar{v}_2 \ll \bar{v}_1,\ \frac{\partial \bar{v}_1}{\partial x_1} \ll \frac{\partial \bar{v}_1}{\partial x_2},$$

$$\rho\bar{v}_1\frac{\partial \bar{v}_1}{\partial x_1} + \rho\bar{v}_2\frac{\partial \bar{v}_1}{\partial x_2} = -\frac{\partial \bar{p}}{\partial x_1} + \frac{\partial}{\partial x_2}\underbrace{\left[\mu\frac{\partial \bar{v}_1}{\partial x_2} - \rho\overline{v'_1 v'_2}\right]}_{\tau_{tot}}$$

►Left side: each term include one large ($\bar{v}_1$ and $\partial/\partial x_2$) and one small ($\bar{v}_2$ and $\partial/\partial x_1$) part

¶See Section 6.2, Wall region in fully developed channel flow
►RANS in fully developed channel flow

$$0 = \underbrace{-\frac{\partial \bar{p}}{\partial x_1}}_{f(x_1)} + \underbrace{\frac{\partial}{\partial x_2}\left(\mu\frac{\partial \bar{v}_1}{\partial x_2} - \rho\overline{v'_1 v'_2}\right)}_{g(x_2)} = -\frac{\partial \bar{p}}{\partial x_1} + \frac{\partial \tau_{tot}}{\partial x_2}$$

Integration from $x_2 = 0$ to x_2 gives

$$\tau_{tot}(x_2) - \tau_w = \frac{\partial \bar{p}}{\partial x_1} x_2 \Rightarrow \tau_{tot} = \tau_w + \frac{\partial \bar{p}}{\partial x_1} x_2 = \tau_w \left(1 - \frac{x_2}{\delta}\right)$$

Last equality: $-\dfrac{\partial \bar{p}}{\partial x_1} = \dfrac{\tau_w}{\delta}$ (force balance)

► lower half of channel
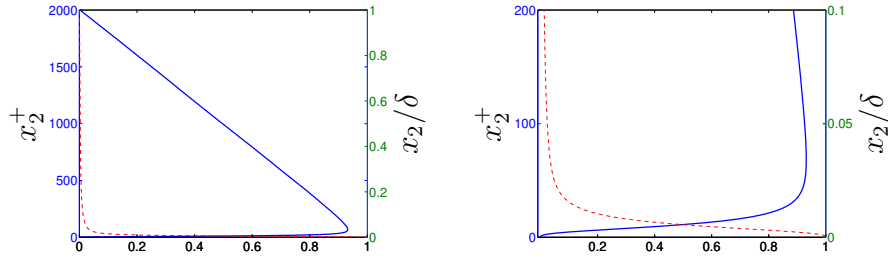
a) full view   b) zoom

——— : $-\rho \overline{v_1' v_2'} / \tau_w$; — — : $\mu(\partial \bar{v}_1 / \partial x_2) / \tau_w$.

► The different wall regions
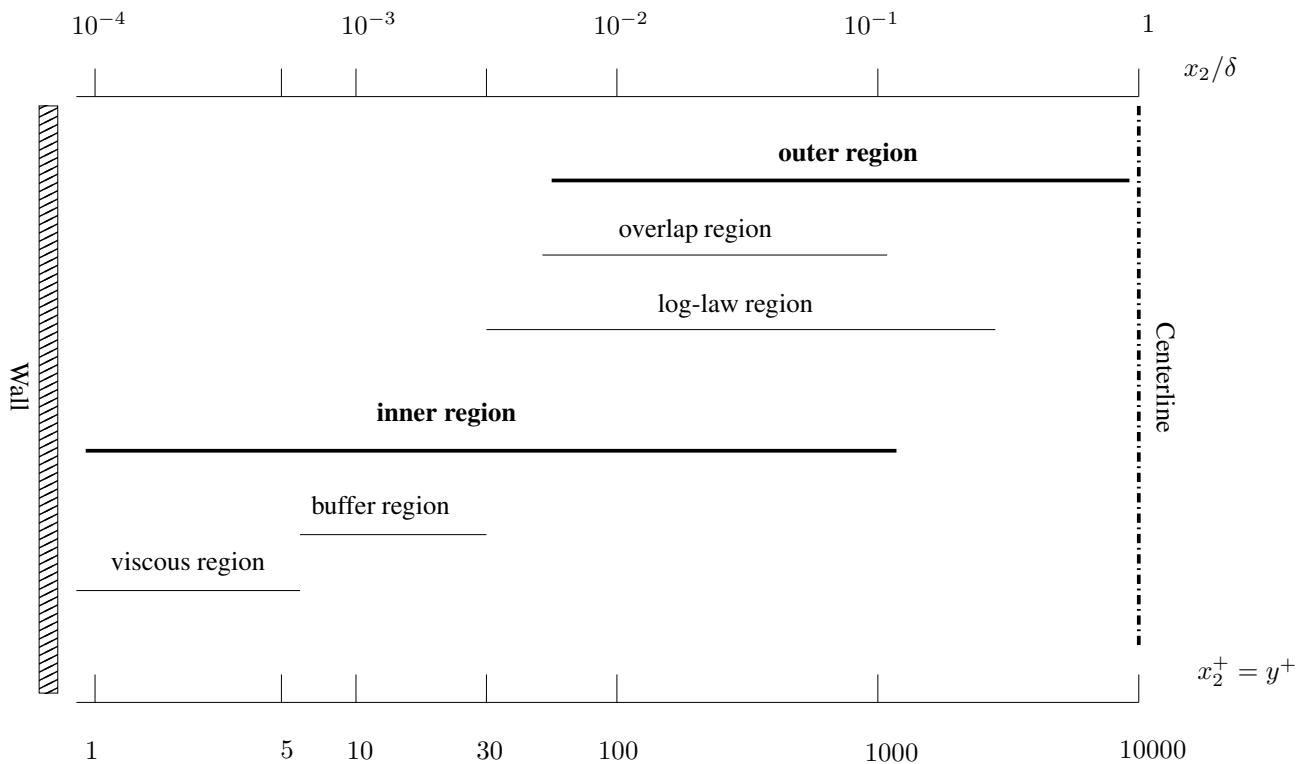
► Wall shear stress (see Eq. 6.21)

$$\tau_w = \mu \frac{\partial \bar{v}_1}{\partial x_2}\bigg|_w \equiv \rho u_\tau^2 \Rightarrow u_\tau = \left(\frac{\tau_w}{\rho}\right)^{1/2}, \quad x_2^+ = \frac{x_2 u_\tau}{\nu}$$

▶The linear velocity law

$$\frac{\partial \bar{v}_1}{\partial x_2}\bigg|_w = \frac{\tau_w}{\mu} = \frac{\rho u_\tau^2}{\mu} = \frac{u_\tau^2}{\nu}$$

Integration gives (recall that both ν and u_τ^2 are constant), see Eq. 6.23

$$\bar{v}_1 = \frac{1}{\nu}u_\tau^2 x_2 + C_1 = \frac{1}{\nu}u_\tau^2 x_2 \quad \text{or} \quad \bar{v}_1^+ = x_2^+$$

▶The log-law (turbulent region), see Eq. 6.32
Velocity scale: u_τ; length scale: $\ell \propto x_2 \Rightarrow \ell = \kappa x_2$

$$\frac{\partial \bar{v}_1}{\partial x_2} = \frac{u_\tau}{\kappa x_2} \Rightarrow \frac{\partial \bar{v}_1/u_\tau}{\partial(x_2 u_\tau/\nu)} = \frac{1}{\kappa(x_2 u_\tau/\nu)}$$

$$\Rightarrow \frac{\partial \bar{v}_1^+}{\partial x_2^+} = \frac{1}{\kappa x_2^+} \Rightarrow \bar{v}_1^+ = \frac{1}{\kappa}\ln x_2^+ + B$$
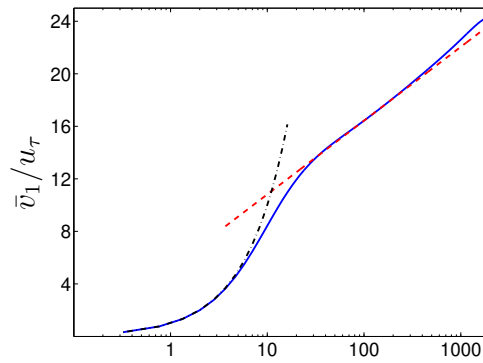
Velocity profiles in fully developed channel flow.

▶N.B. $\bar{v}_{1,centerline}/u_\tau = 24 \quad \Rightarrow$ good estimate for u_τ ($\bar{v}_{1,centerline}/u_\tau$ increases weakly with Reynolds number)
Example: channel flow (or boundary layer), $x_2^+ = 1$ gives

water: $x_2 = \nu x_2^+/u_\tau = 1 \cdot 10^{-6} \cdot 1/(1/24) = 2.4 \cdot 10^{-5} m = 2.4 \cdot 10^{-2} mm$

air: $x_2 = \nu x_2^+/u_\tau = 15 \cdot 1^{-6} \cdot 1/(1/24) = 3.6 \cdot 10^{-4} m = 3.6 \cdot 10^{-1} mm$

- δ/x_2 (at $x_2^+ = 1$) is an estimate of ratio of largest to smallest turbulent length scales (δ is boundary layer thickness or channel half width)

- estimate of ε: u_τ^3/δ

¶See Section 6.3, Reynolds stresses in fully developed channel flow
▶Symmetry plane of channel flow $\tau_{32,tot} = \tau_{32} - \rho\overline{v_3' v_2'}$

x_2

$\tau_{32,tot}$

x_3
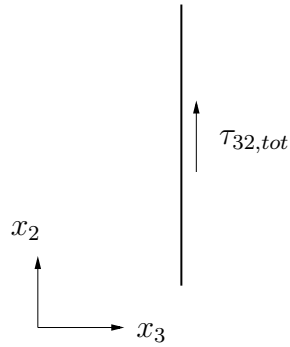
$$\tau_{32} = \mu\left(\frac{\partial \bar{v}_3}{\partial x_2} + \frac{\partial \bar{v}_2}{\partial x_3}\right) = 0, \quad \rho\overline{v_3' v_2'} = -\mu_t\left(\frac{\partial \bar{v}_3}{\partial x_2} + \frac{\partial \bar{v}_2}{\partial x_3}\right) = 0$$

because $\bar{v}_3 = \partial/\partial x_3 = 0$ (note that $\overline{v_3' v_3'} \neq 0$)
▶Normal Reynolds stresses
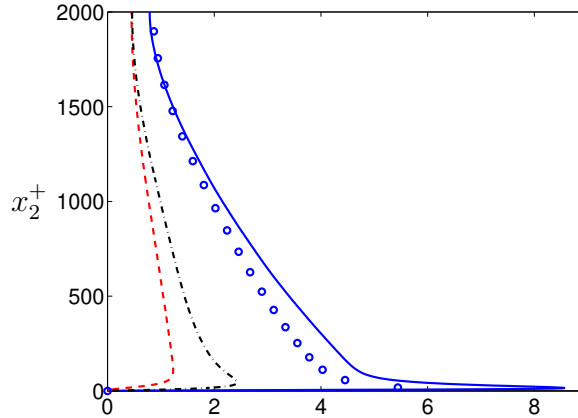
$\boldsymbol{-\!\!-}$: $\rho\overline{v_1'^2}/\tau_w$; $\boldsymbol{-\,-}$: $\rho\overline{v_2'^2}/\tau_w$; $\boldsymbol{-\!\cdot\!-}$: $\rho\overline{v_3'^2}/\tau_w$
▶Forces on a fluid element

$$0 = -\frac{\partial \bar{p}}{\partial x_1} + \frac{\partial}{\partial x_2}\left(\mu\frac{\partial \bar{v}_1}{\partial x_2} - \rho\overline{v_1' v_2'}\right)$$
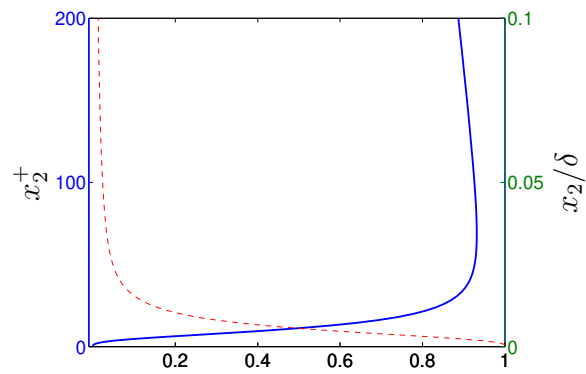
Shear stresses. ———— : $-\rho\overline{v'_1 v'_2}/\tau_w$; — — — : $\mu(\partial \bar{v}_1/\partial x_2)/\tau_w$.
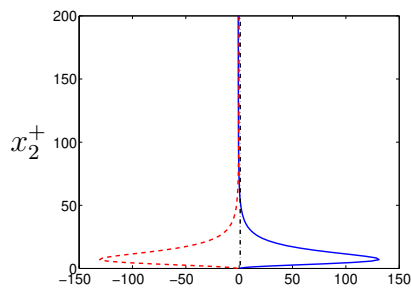
Near the wall
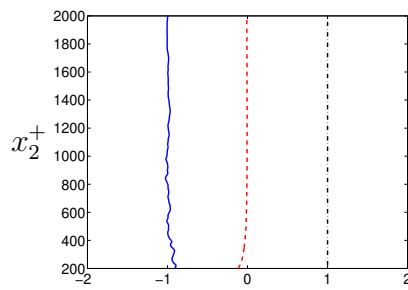
Far from the wall

Gradient of shear stresses. ———— : $-\rho(\partial\overline{v'_1 v'_2}/\partial x_2)/\tau_w$; — — — : $\mu(\partial^2 \bar{v}_1/\partial x_2^2)/\tau_w$; — ∙ — : $-(\partial\bar{p}/\partial x_1)/\tau_w$.

►Forces in a boundary layer. The red (dashed line) and the blue (solid line) fluid particle are located at $x_2^+ \simeq 400$ and $x_2^+ \simeq 20$, respectively
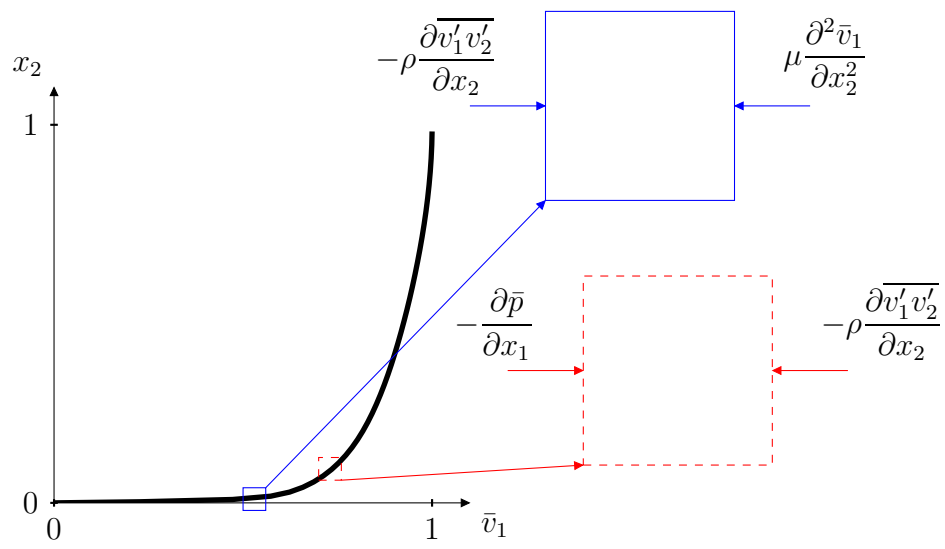
A.7   Lecture 7

¶See Section 8.1, Rules for time averaging
►Time averaging

$$\bar{v} = \frac{1}{2T} \int_{-T}^{T} v \, dt. \tag{A.20}$$

►What is the difference between $\overline{v_1' v_2'}$ and $\overline{v_1'} \, \overline{v_2'}$? Using A.20 we get

$$\overline{v_1' v_2'} = \frac{1}{2T} \int_{-T}^{T} v_1' v_2' \, dt.$$

whereas

$$\overline{v_1'} \, \overline{v_2'} = \left(\frac{1}{2T} \int_{-T}^{T} v_1' \, dt \right) \left(\frac{1}{2T} \int_{-T}^{T} v_1' \, dt \right)$$

(which is zero)

►What is the difference between $\overline{v_1'^2}$ and $\overline{v_1'}^2$? Using A.20 we get

$$\overline{v_1'^2} = \frac{1}{2T} \int_{-T}^{T} v'^2 \, dt.$$

whereas

$$\overline{v_1'}^2 = \left(\frac{1}{2T} \int_{-T}^{T} v' \, dt \right)^2.$$

(which is zero)

►Show that $\overline{\bar{v}_1 v_1'^2} = \bar{v}_1 \overline{v_1'^2}$. Using A.20 we get

$$\overline{\bar{v}_1 v_1'^2} = \frac{1}{2T} \int_{-T}^{T} \bar{v}_1 v_1'^2 \, dt$$

and since $\bar{v}$ does not depend on t we can take it out of the integral as

$$\bar{v}_1 \frac{1}{2T} \int_{-T}^{T} v_1'^2 \, dt = \bar{v}_1 \overline{v_1'^2}$$

►Show that $\overline{\bar{v}_1} = \bar{v}_1$. Using A.20 we get

$$\overline{\bar{v}_1} = \frac{1}{2T} \int_{-T}^{T} \bar{v}_1 \, dt$$

and since $\bar{v}$ does not depend on t we can take it out of the integral as

$$\bar{v}_1 \frac{1}{2T} \int_{-T}^{T} dt = \bar{v}_1 \frac{1}{2T} 2T = \bar{v}_1$$

▶RANS (see Eq. 6.9)

$$\rho\frac{\partial \bar{v}_i \bar{v}_j}{\partial x_j} = -\frac{\partial \bar{p}}{\partial x_i} + \frac{\partial}{\partial x_j}\left(\mu\frac{\partial \bar{v}_i}{\partial x_j} - \rho\overline{v_i' v_j'}\right)$$

¶See Section 11.6, The Boussinesq assumption
▶The RANS equations read (see Eq. 6.10)

$$\rho\frac{\partial \bar{v}_i \bar{v}_j}{\partial x_j} = -\frac{\partial \bar{p}}{\partial x_i} + \frac{\partial}{\partial x_j}\left(\mu\frac{\partial \bar{v}_i}{\partial x_j} - \rho\overline{v_i' v_j'}\right)$$

- The last term, the Reynolds stress, is unknown.

- It must be modeled

- This is called the *closure problem*

- We need a **turbulence model**

▶Write the diffusion term above for incompressible flow and without assuming constant viscosity (see Eq. 2.5)

$$\frac{\partial}{\partial x_j}\left\{\nu\left(\frac{\partial \bar{v}_i}{\partial x_j} + \frac{\partial \bar{v}_j}{\partial x_i}\right) - \overline{v_i' v_j'}\right\} \tag{A.21}$$

We want to replace $\overline{v_i' v_j'}$ by a turbulent viscosity, ν_t:

$$\frac{\partial}{\partial x_j}\left\{(\nu + \nu_t)\left(\frac{\partial \bar{v}_i}{\partial x_j} + \frac{\partial \bar{v}_j}{\partial x_i}\right)\right\} \tag{A.22}$$

Identification of Eqs. A.21 and A.22 gives (see Eq. 11.32)

$$-\overline{v_i' v_j'} = \nu_t\left(\frac{\partial \bar{v}_i}{\partial x_j} + \frac{\partial \bar{v}_j}{\partial x_i}\right)$$

This equation is not valid upon contraction. Hence (see Eq. 11.33)

$$\overline{v_i' v_j'} = -\nu_t\left(\frac{\partial \bar{v}_i}{\partial x_j} + \frac{\partial \bar{v}_j}{\partial x_i}\right) + \frac{1}{3}\delta_{ij}\overline{v_k' v_k'} = -2\nu_t \bar{s}_{ij} + \frac{2}{3}\delta_{ij}k \tag{A.23}$$

ν: different for different fluids (air, water, ...)

ν_t: depends on the flow, i.e. $\nu_t = \nu_t(x_i)$

¶See Section 8.2, The Exact k Equation

▶$k = \overline{v_i'v_i'}/2$ appears in the expression for the turbulence viscosity. The first step is to derive the k equation. Start by the N-S for v_i', multiply by v_i' and time average

$$\overline{v_i'\frac{\partial}{\partial x_j}\left[v_iv_j - \bar{v}_i\bar{v}_j\right]} =$$

$$\underbrace{-\frac{1}{\rho}\overline{v_i'\frac{\partial}{\partial x_i}\left[p - \bar{p}\right]}}_{\textbf{IV}} + \underbrace{\nu\overline{v_i'\frac{\partial^2}{\partial x_j\partial x_j}\left[v_i - \bar{v}_i\right]}}_{\textbf{V}} + \underbrace{\overline{\frac{\partial\overline{v_i'v_j'}}{\partial x_j}v_i'}}_{\textbf{VI}}$$

Using $v_j = \bar{v}_j + v_j'$, the left side can be rewritten as

$$\overline{v_i'\frac{\partial}{\partial x_j}\left[(\bar{v}_i + v_i')(\bar{v}_j + v_j') - \bar{v}_i\bar{v}_j\right]} = \overline{v_i'\frac{\partial}{\partial x_j}\left[\underbrace{\bar{v}_iv_j'}_{\textbf{I}} + \underbrace{v_i'\bar{v}_j}_{\textbf{II}} + \underbrace{v_i'v_j'}_{\textbf{III}}\right]}.$$

▶Term I is rewritten as

$$\overline{v_i'\frac{\partial}{\partial x_j}\left(\bar{v}_iv_j'\right)} = \overline{v_i'v_j'}\frac{\partial\bar{v}_i}{\partial x_j} + \overline{\bar{v}_iv_i'\underbrace{\frac{\partial v_j'}{\partial x_j}}_{\text{cont.eq.}}}^{\;0} = \overline{v_i'v_j'}\frac{\partial\bar{v}_i}{\partial x_j}$$

▶Term II

$$\overline{v_i'\frac{\partial}{\partial x_j}\left(v_i'\bar{v}_j\right)} \underset{\text{cont. eq.}}{=} \overline{\bar{v}_jv_i'\frac{\partial v_i'}{\partial x_j}} \underset{\text{Trick 2}}{=} \bar{v}_j\frac{\partial}{\partial x_j}\left(\frac{\overline{v_i'v_i'}}{2}\right) = \bar{v}_j\frac{\partial k}{\partial x_j}$$

▶Term III

$$\overline{v_i'\frac{\partial}{\partial x_j}\left(v_i'v_j'\right)} \underset{\text{cont. eq.}}{=} \overline{v_j'\left(v_i'\frac{\partial v_i'}{\partial x_j}\right)} \underset{\text{Trick 2}}{=} \overline{v_j'\frac{\partial}{\partial x_j}\left(\frac{v_i'v_i'}{2}\right)} \underset{\text{cont. eq.}}{=} \frac{\partial}{\partial x_j}\left(\frac{\overline{v_j'v_i'v_i'}}{2}\right)$$

▶First term on the right side (Term IV)

$$-\frac{1}{\rho}\overline{v_i'\frac{\partial p'}{\partial x_i}} \underset{\text{cont. eq.}}{=} -\frac{1}{\rho}\frac{\partial\overline{p'v_i'}}{\partial x_i}$$

▶Second term on the right side (Term V)

$$\nu\overline{v_i'\frac{\partial^2 v_i'}{\partial x_j\partial x_j}} \underset{\text{Trick 1}}{=} \nu\overline{\frac{\partial}{\partial x_j}\left(\frac{\partial v_i'}{\partial x_j}v_i'\right)} - \nu\overline{\frac{\partial v_i'}{\partial x_j}\frac{\partial v_i'}{\partial x_j}} \underset{\text{Trick 2}}{=}$$

$$\nu\overline{\frac{\partial}{\partial x_j}\left(\frac{1}{2}\left(\frac{\partial v_i'v_i'}{\partial x_j}\right)\right)} - \nu\overline{\frac{\partial v_i'}{\partial x_j}\frac{\partial v_i'}{\partial x_j}} = \nu\frac{\partial^2 k}{\partial x_j\partial x_j} - \nu\overline{\frac{\partial v_i'}{\partial x_j}\frac{\partial v_i'}{\partial x_j}}$$

►Third term on the right side (Term VI)

$$\overline{\frac{\partial \overline{v_i' v_j'}}{\partial x_j} v_i'} = \overline{\frac{\partial \overline{v_i' v_j'}}{\partial x_j}}\,\overline{v_i'} = 0$$

►We finally get (see Eq. 8.14)

$$\underbrace{\frac{\partial \bar{v}_j k}{\partial x_j}}_{\text{I}} = \underbrace{-\overline{v_i' v_j'}\frac{\partial \bar{v}_i}{\partial x_j}}_{\text{II}} - \underbrace{\frac{\partial}{\partial x_j}\left[\frac{1}{\rho}\overline{v_j' p'} + \frac{1}{2}\overline{v_j' v_i' v_i'} - \nu\frac{\partial k}{\partial x_j}\right]}_{\text{III}} - \underbrace{\nu\overline{\frac{\partial v_i'}{\partial x_j}\frac{\partial v_i'}{\partial x_j}}}_{\text{IV}}$$

The terms have the following meaning.

I. Convection.

II. Production, P^k. The large turbulent scales extract energy from the mean flow. It is largest for small wavenumbers. It can be written as $P^k = -\overline{v_i' v_j'}\bar{S}_{ij}$, see Eq. 8.15. Hence only $\bar{S}_{ij}$ creates turbulence, not $\bar{\Omega}_{ij}$

III. The two first terms represent **turbulent diffusion** by pressure-velocity fluctuations, and velocity fluctuations, respectively. The last term is viscous diffusion.

IV. Dissipation, ε. It is largest for high wavenumbers,
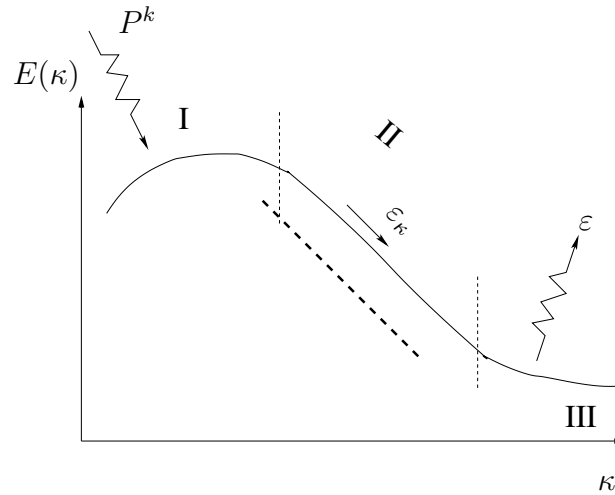
►The transport equation for k in symbolic form reads (see Eq. 8.16)

$$C^k = P^k + D^k - \varepsilon$$

¶See Section 8.3, The Exact k Equation: 2D Boundary Layers
▶In 2D boundary-layer flow, $\partial/\partial x_2 \gg \partial/\partial x_1$, $\bar{v}_2 \ll \bar{v}_1$, we get

$$\frac{\partial \bar{v}_1 k}{\partial x_1} + \frac{\partial \bar{v}_2 k}{\partial x_2} = -\overline{v_1' v_2'} \frac{\partial \bar{v}_1}{\partial x_2} - \frac{\partial}{\partial x_2} \left[\frac{1}{\rho} \overline{p' v_2'} + \frac{1}{2} \overline{v_2' v_i' v_i'} - \nu \frac{\partial k}{\partial x_2} \right] - \nu \overline{\frac{\partial v_i'}{\partial x_j} \frac{\partial v_i'}{\partial x_j}}$$

a) Zoom near the wall; b) Outer region. ──: P^k; ---: $-\varepsilon$; ▽: $-\partial \overline{v'p'}/\partial x_2$; +: $-\partial \overline{v_2' v_i' v_i'/2}/\partial x_2$; ○: $\nu \partial^2 k/\partial x_2^2$.
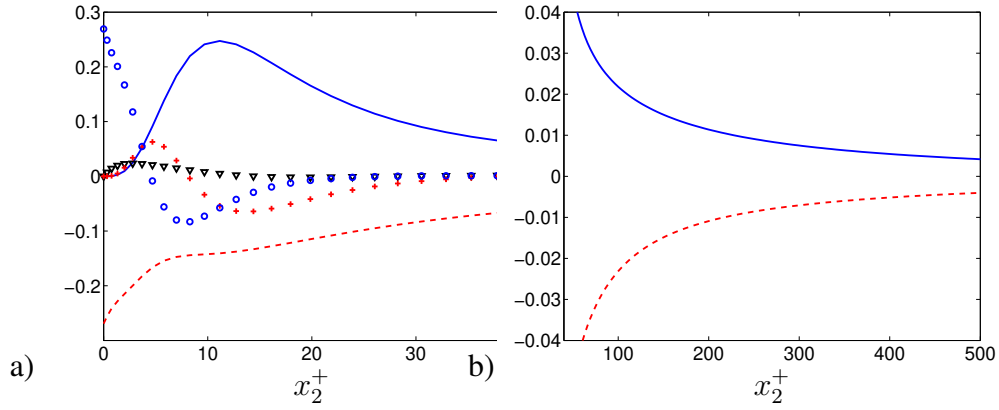
▶The production term $-\overline{v_1' v_2'} \dfrac{\partial \bar{v}_1}{\partial x_2}$
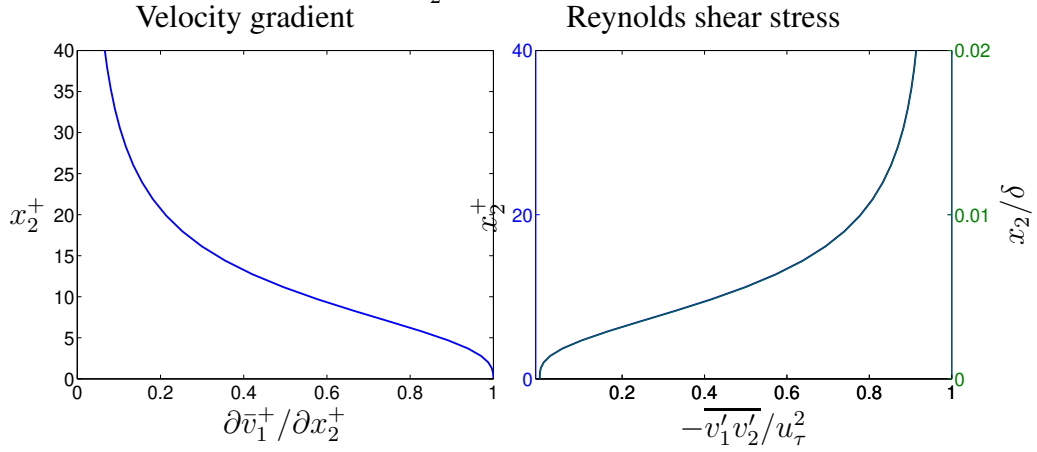
A.8 Lecture 8

¶See Section 8.6, The transport equation for $\bar{v}_i\bar{v}_i/2$

▶The main source term in k eq is the production term, P^k. This means that k gets energy via P^k. From where?

▶Answer: from $K = \bar{v}_i\bar{v}_i/2$. Let's derive the transport eq. for K.
Multiply the RANS equations by $\bar{v}_i$ so that

$$\underbrace{\bar{v}_i\left(\frac{\partial \bar{v}_i\bar{v}_j}{\partial x_j}\right)}_{\text{I}} = \bar{v}_i\left(\underbrace{-\frac{1}{\rho}\frac{\partial \bar{p}}{\partial x_i}}_{\text{II}} + \underbrace{\nu\frac{\partial^2 \bar{v}_i}{\partial x_j \partial x_j}}_{\text{III}} - \underbrace{\frac{\partial \overline{v_i' v_j'}}{\partial x_j}}_{\text{IV}}\right)$$

Term I:

$$\bar{v}_i\frac{\partial \bar{v}_i\bar{v}_j}{\partial x_j} = \bar{v}_i\bar{v}_j\frac{\partial \bar{v}_i}{\partial x_j} + \bar{v}_i\bar{v}_i\cancelto{0}{\frac{\partial \bar{v}_j}{\partial x_j}} = \frac{1}{2}\bar{v}_j\frac{\partial \bar{v}_i\bar{v}_i}{\partial x_j} = \frac{\partial \bar{v}_j K}{\partial x_j}$$

Term II:

$$-\bar{v}_i\frac{\partial \bar{p}}{\partial x_i} \quad \text{main source term in, for example, channel flow} \quad \left(-\bar{v}_1\frac{\partial \bar{p}}{\partial x_1} > 0\right)$$

Term III:

$$\nu\bar{v}_i\frac{\partial}{\partial x_j}\left(\frac{\partial \bar{v}_i}{\partial x_j}\right) = \nu\frac{\partial}{\partial x_j}\left(\underbrace{\bar{v}_i\frac{\partial \bar{v}_i}{\partial x_j}}_{\partial/\partial_j(\bar{v}_i\bar{v}_i/2)}\right) - \nu\frac{\partial \bar{v}_i}{\partial x_j}\frac{\partial \bar{v}_i}{\partial x_j} = \nu\frac{\partial^2 K}{\partial x_j \partial x_j} - \nu\frac{\partial \bar{v}_i}{\partial x_j}\frac{\partial \bar{v}_i}{\partial x_j}.$$

Term IV:

$$-\bar{v}_i\frac{\partial \overline{v_i' v_j'}}{\partial x_j} = -\frac{\partial \bar{v}_i\overline{v_i' v_j'}}{\partial x_j} + \overline{v_i' v_j'}\frac{\partial \bar{v}_i}{\partial x_j}.$$

▶$K = \frac{1}{2}\bar{v}_i\bar{v}_i$ eq. (see Eq. 8.36)

$$\frac{\partial \bar{v}_j K}{\partial x_j} = \underbrace{\overline{v_i' v_j'}\frac{\partial \bar{v}_i}{\partial x_j}}_{-P^k,\ \text{sink}} \underbrace{-\frac{\bar{v}_i}{\rho}\frac{\partial \bar{p}}{\partial x_i}}_{\text{source}} - \frac{\partial}{\partial x_j}\left(\bar{v}_i\overline{v_i' v_j'} - \nu\frac{\partial K}{\partial x_j}\right) \underbrace{-\nu\frac{\partial \bar{v}_i}{\partial x_j}\frac{\partial \bar{v}_i}{\partial x_j}}_{\varepsilon_{mean},\ \text{sink}}$$

▶$k = \frac{1}{2}\overline{v_i' v_i'}$ eq. (see Eq. 8.14)

$$\frac{\partial \bar{v}_j k}{\partial x_j} = \underbrace{-\overline{v_i' v_j'}\frac{\partial \bar{v}_i}{\partial x_j}}_{P^k,\ \text{source}} - \frac{\partial}{\partial x_j}\left[\frac{1}{\rho}\overline{v_j' p'} + \frac{1}{2}\overline{v_j' v_i' v_i'} - \nu\frac{\partial k}{\partial x_j}\right] \underbrace{-\nu\overline{\frac{\partial v_i'}{\partial x_j}\frac{\partial v_i'}{\partial x_j}}}_{\varepsilon,\ \text{sink}}$$
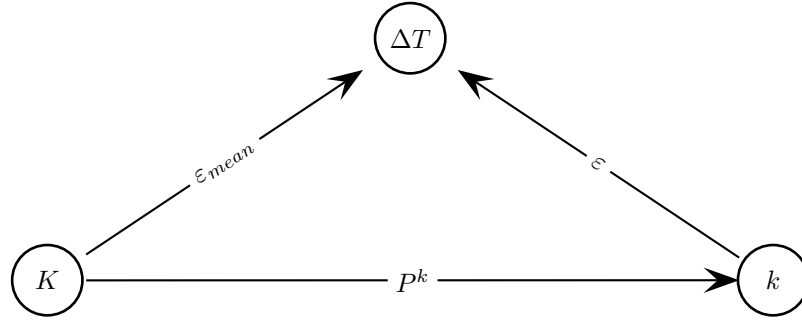
Figure A.4: Transfer of energy between mean kinetic energy (K), turbulent kinetic energy (k) and internal energy (denoted as an increase in temperature, ΔT). $K = \frac{1}{2}\bar{v}_i\bar{v}_i$ and $k = \frac{1}{2}\overline{v'_iv'_i}$.

¶See Section 11.5, The ε equation
▶Now we need to model the turbulent viscosity, see Eq. A.23. It is estimated as a turbulent velocity fluctuation times a turbulent length scale

$$\nu_t \propto \mathcal{U}\mathcal{L}$$

The velocity scale is taken as $k^{1/2}$. Recall that we have an estimate for the dissipation as $\varepsilon \propto \mathcal{U}^3/\mathcal{L}$, see Eq. 5.14. This gives $\mathcal{L} \propto k^{3/2}/\varepsilon$ which gives

$$\nu_t = C_\mu \frac{k^2}{\varepsilon}$$

where $C_\mu = 0.09$.

¶See Section 11.7.1, Production terms
▶We need modelled k and ε eqns. The exact k eq. reads (see Eq. 8.14)

$$\frac{\partial \bar{v}_j k}{\partial x_j} = -\overline{v'_iv'_j}\frac{\partial \bar{v}_i}{\partial x_j} - \frac{\partial}{\partial x_j}\left[\frac{1}{\rho}\overline{v'_jp'} + \frac{1}{2}\overline{v'_jv'_iv'_i} - \nu\frac{\partial k}{\partial x_j}\right] - \nu\overline{\frac{\partial v'_i}{\partial x_j}\frac{\partial v'_i}{\partial x_j}}$$
$$(A.24)$$

▶Production term needs to be modelled.

$$P^k = -\overline{v'_iv'_j}\frac{\partial \bar{v}_i}{\partial x_j} = \nu_t\left[\left(\frac{\partial \bar{v}_i}{\partial x_j} + \frac{\partial \bar{v}_j}{\partial x_i}\right) - \frac{2}{3}\delta_{ij}k\right]\frac{\partial \bar{v}_i}{\partial x_j} = 2\nu_t\bar{s}_{ij}\bar{s}_{ij}$$

▶Also the diffusion term needs to be modeled. Example: heat flux is modelled as (see Eq. 11.35)
$$\overline{v'_i\theta'} = -\frac{\nu_t}{\sigma_t}\frac{\partial \bar{\theta}}{\partial x_i}$$

▶The diffusion term in k eq, Eq. A.24, is modelled as

$$\frac{1}{2}\overline{v'_j v'_i v'_i} = -\frac{\nu_t}{\sigma_k}\frac{\partial k}{\partial x_j} \Rightarrow -\frac{1}{2}\frac{\partial \overline{v'_j v'_i v'_i}}{\partial x_j} = \frac{\partial}{\partial x_j}\left(\nu_t \frac{\partial k}{\partial x_j}\right)$$

¶See Section 11.8, The $k - \varepsilon$ model
►Modelled k equation

$$\frac{\partial k}{\partial t} + \bar{v}_j \frac{\partial k}{\partial x_j} = 2\nu_t \bar{s}_{ij}\bar{s}_{ij} + \frac{\partial}{\partial x_j}\left\{\left(\nu + \frac{\nu_t}{\sigma_k}\right)\frac{\partial k}{\partial x_j}\right\} - \varepsilon$$

►ε equation

$$C^\varepsilon = P^\varepsilon + D^\varepsilon - \Psi^\varepsilon$$

Use the same source terms as in k equation and add turbulent time-scale ε/k to get the right dimensions:

$$P^\varepsilon - \Psi^\varepsilon = \frac{\varepsilon}{k}(c_{\varepsilon 1}P^k - c_{\varepsilon 2}\varepsilon)$$

►The final form of the modelled ε equation (see Eq. 11.98)

$$\frac{\partial \varepsilon}{\partial t} + \bar{v}_j \frac{\partial \varepsilon}{\partial x_j} = \frac{\varepsilon}{k}(c_{\varepsilon 1}P^k - c_{\varepsilon 2}\varepsilon) + \frac{\partial}{\partial x_j}\left[\left(\nu + \frac{\nu_t}{\sigma_\varepsilon}\right)\frac{\partial \varepsilon}{\partial x_j}\right]$$

►Note that we have here omitted the buoyancy terms (they are included in Eqs. 11.97 and 11.98)

▶Summary of the $k - \varepsilon$ model.

- The Reynolds stress tensor, $\overline{v_i' v_j'}$, needs to be modeled, see Eq. 6.10

- We use the Boussinsq assumption, see Eq. 11.33, to replace the unknown $\overline{v_i' v_j'}$ with the turbulent viscosity, ν_t (a new unknown).

- We make a model for ν_t , see Eq. 11.99, which includes k and ε

- We formulate modeled equations for k (Eq. 11.97) and ε (Eq. 11.98)

- Now we have closed Eq. 6.10. The equations we need to solve are

    - The time-averaged continuity equation (Eq. 6.9)
    - Three time-averaged Navier-Stokes equations (Eq. 6.10)
    - Two equations for k and ε (Eq. 11.97) and ε (Eq. 11.98)
    - The equation for turbulent viscosity, $\nu_t = C_\mu k^2 / \varepsilon$ (Eq. 11.99)

A.9 Lecture 9

¶See Section 11.14, Wall boundary conditions
▶Two options for treating the wall boundary conditions.

- Coarse mesh near the walls. Assume that the logarithmic law applies. This is called *wall functions*

- Fine mesh. Modify the turbulence models to account for the viscous effects. This is called *Low-Reynolds number models*

¶See Section 11.14.1, Wall Functions
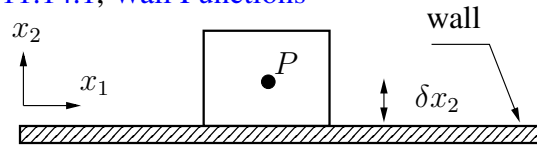
Wall-adjacent cell.

▶When using wall-functions, we don't resolve the boundary layer. The first cell center (the wall-adjacent) is placed in the log-law region ($30 < x_2^+ < 400$) and we *assume* that the velocity follows the log-law
▶The log-law reads (see Eq. 6.32)

$$\frac{\bar{v}_1}{u_\tau} = \frac{1}{\kappa} \ln \left(\frac{u_\tau x_2}{\nu} \right) + B$$

It is re-written as

$$\frac{\bar{v}_1}{u_\tau} = \frac{1}{\kappa} \ln \left(\frac{E u_\tau x_2}{\nu} \right), \quad E = 9.0, \quad B = \frac{1}{\kappa} \ln E$$

Friction velocity is computed as (see Eq. 11.144)

$$u_\tau = \frac{\kappa \bar{v}_{1,P}}{\ln(E u_\tau \delta x_2 / \nu)}$$

(subscript P denotes the wall-adjacent cell) It is obtained by iteration. Then $\tau_w = \rho u_\tau^2$ is used a force wall boundary condition.

▶B.c. for k and ε. In the log-region, the production and dissipation in the k eq. balance each other (see Fig. 8.3b) which gives (see Eq. 11.145)

Boundary along a flat plate. Energy balance in k equation.
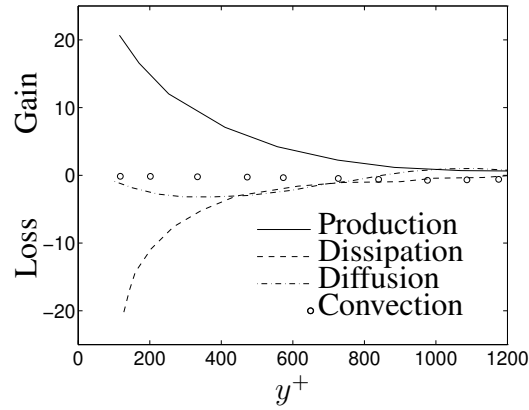
$$0 = P^k - \rho\varepsilon = \mu_t \left(\frac{\partial \bar{v}_1}{\partial x_2}\right)^2 - \rho\varepsilon. \tag{A.25}$$

In the log-region (see Fig. 6.3b)

$$\tau_w = -\rho\overline{v_1' v_2'} = \mu_t \frac{\partial \bar{v}_1}{\partial x_2} \tag{A.26}$$

Inserting Eq. A.26 into Eq. A.25 gives

$$0 = \frac{\overline{v_1' v_2'}^2}{\nu_t} - \varepsilon = \frac{u_\tau^2}{\nu_t} - \varepsilon$$

which with $\nu_t = C_\mu k^2/\varepsilon$ gives (see Eq. 11.149)

$$k_P = C_\mu^{-1/2} u_\tau^2, \quad C_\mu = 0.09$$

▶ε.

- Velocity gradient in log-region: when deriving the log-law we assumed (see Eq. 6.27): $\partial\bar{v}_1/\partial x_2 \simeq u_\tau/(\kappa x_2)$

- Shear stress in log-region $-\overline{v_1' v_2'} \simeq u_\tau^2$, see Eq. 6.25 and Fig. 6.3

Eq. A.25 gives (see Eq. 11.150)

$$\varepsilon_P = P^k = \frac{u_\tau^3}{\kappa\delta x_2}$$

¶See Section 11.14.2, Low-Re Number Turbulence Models
►In Low-Re number models we *resolve* the boundary layer, i.e. we use a refined grid near the wall. The wall-adjacent cell at $x_2^+ < 1$. B.c. for velocity is $v_i = 0$.

However, the turbulence near the wall is not fully turbulent: the viscous effect is large. We must modify the turbulence model.

►We start by analyzing the turbulence near the wall. Make a Taylor expansion of the fluctuating velocity, v_i', near the wall (also valid for $\bar{v}_i$)

$$
\begin{aligned}
v_1' &= a_0 + a_1 x_2 + a_2 x_2^2 + \dots \\
v_2' &= b_0 + b_1 x_2 + b_2 x_2^2 + \dots \\
v_3' &= c_0 + c_1 x_2 + c_2 x_2^2 + \dots
\end{aligned}
\tag{A.27}
$$

At the wall, $v_1' = v_2' = v_3' = 0$ which gives $a_0 = b_0 = c_0$.
Furthermore $\partial v_1'/\partial x_1 = \partial v_3'/\partial x_3 = 0$: continuity equation gives $\partial v_2'/\partial x_2 = 0$ so that $b_1 = 0$. Equation A.27 now reads

$$
\begin{aligned}
v_1' &= a_1 x_2 &+& a_2 x_2^2 + \dots \\
v_2' &= && b_2 x_2^2 + \dots \\
v_3' &= c_1 x_2 &+& c_2 x_2^2 + \dots
\end{aligned}
\tag{A.28}
$$

Using Eq. A.28 we can write

$$
\begin{aligned}
\overline{v_1'^2} &= \overline{a_1^2} x_2^2 + \dots &&= \mathcal{O}(x_2^2) \\
\overline{v_2'^2} &= \overline{b_2^2} x_2^4 + \dots &&= \mathcal{O}(x_2^4) \\
\overline{v_3'^2} &= \overline{c_1^2} x_2^2 + \dots &&= \mathcal{O}(x_2^2) \\
\overline{v_1' v_2'} &= \overline{a_1 b_2} x_2^3 + \dots &&= \mathcal{O}(x_2^3) \\
k &= \overline{(a_1^2 + c_1^2)} x_2^2 + \dots &&= \mathcal{O}(x_2^2) \\
\partial \bar{v}_1/\partial x_2 &= \overline{a_1} + \dots &&= \mathcal{O}(x_2^0) \\
\partial v_1'/\partial x_2 &= a_1 + \dots &&= \mathcal{O}(x_2^0) \\
\partial v_2'/\partial x_2 &= 2b_2 x_2 + \dots &&= \mathcal{O}(x_2^1) \\
\partial v_3'/\partial x_2 &= a_1 + \dots &&= \mathcal{O}(x_2^0)
\end{aligned}
\tag{A.29}
$$

¶See Section 11.14.3, Low-Re $k - \varepsilon$ Models
►Now let's compare the exact and the modeled k eq. near the wall
The exact k eq. (see Eq. 8.14)

$$\rho\bar{v}_1\frac{\partial k}{\partial x_1} + \rho\bar{v}_2\frac{\partial k}{\partial x_2} = \underbrace{-\rho\overline{v_1'v_2'}\frac{\partial\bar{v}_1}{\partial x_2}}_{\mathcal{O}(x_2^3)} - \frac{\partial\overline{p'v_2'}}{\partial x_2} \underbrace{- \frac{\partial}{\partial x_2}\left(\frac{1}{2}\overline{\rho v_2'v_i'v_i'}\right)}_{\mathcal{O}(x_2^3)}$$

$$+ \mu\frac{\partial^2 k}{\partial x_2^2} \underbrace{- \mu\overline{\frac{\partial v_i'}{\partial x_j}\frac{\partial v_i'}{\partial x_j}}}_{\mathcal{O}(x_2^0)}$$

The modeled k eq. (see Eq. 11.97)

$$\rho\bar{v}_1\frac{\partial k}{\partial x_1} + \rho\bar{v}_2\frac{\partial k}{\partial x_2} = \underbrace{\mu_t\left(\frac{\partial\bar{v}_1}{\partial x_2}\right)^2}_{\mathcal{O}(x_2^4)} + \underbrace{\frac{\partial}{\partial x_2}\left(\frac{\mu_t}{\sigma_k}\frac{\partial k}{\partial x_2}\right)}_{\mathcal{O}(x_2^4)}$$

$$+ \mu\frac{\partial^2 k}{\partial x_2^2} - \underbrace{\rho\varepsilon}_{\mathcal{O}(x_2^0)}$$

We used $\nu_t = C_\mu\dfrac{k^2}{\varepsilon} = \dfrac{\mathcal{O}(x_2^4)}{\mathcal{O}(x_2^0)} = \mathcal{O}(x_2^4)$

- the exact and the modeled dissipation term behave in the same way

- this is not true for the production term and the turbulent diffusion term

▶To make the modeled production term behave as $\mathcal{O}(x_2^3)$, replace C_μ with $C_\mu f_\mu$ (damping function) where $f_\mu \propto \mathcal{O}(x_2^{-1})$

This fixes also the modeled turb. diffusion term

▶Now we look at the modeled ε eq. (see Eq. 11.160)

$$\underbrace{\rho\bar{v}_1\frac{\partial\varepsilon}{\partial x_1}}_{\mathcal{O}(x_2^1)} + \underbrace{\rho\bar{v}_2\frac{\partial\varepsilon}{\partial x_2}}_{\mathcal{O}(x_2^2)} = \underbrace{C_{\varepsilon 1}\frac{\varepsilon}{k}P^k}_{\mathcal{O}(x_2^1)} + \underbrace{\frac{\partial}{\partial x_2}\left(\frac{\mu_t}{\sigma_\varepsilon}\frac{\partial\varepsilon}{\partial x_2}\right)}_{\mathcal{O}(x_2^2)}$$

$$+ \underbrace{\mu\frac{\partial^2\varepsilon}{\partial x_2^2}}_{\mathcal{O}(x_2^0)} - \underbrace{C_{\varepsilon 2}\rho\frac{\varepsilon^2}{k}}_{\mathcal{O}(x_2^{-2})}$$

where we assumed that the production term P^k has been suitable modified so that $P^k = \mathcal{O}(x_2^3)$. The only terms that are non-zero when $x_2 \to 0$ are the viscous diffusion term and the destruction term.

▶But they can't balance each other since the first is $\propto \mathcal{O}(x_2^0)$ and the second $\propto \mathcal{O}(x_2^{-2})$.

We fix this by multiplying the destruction term by $f_2 \propto \mathcal{O}(x_2^2)$

¶See Section 11.14.5, Different ways of prescribing ε at or near the wall
▶Boundary condition for k (since $v_i' \to 0$ near the wall)

$$k = 0$$

▶Boundary condition for ε: look at the k eq. near the wall. The only non-vanishing terms are

$$0 = \mu \frac{\partial^2 k}{\partial x_2^2} - \rho \varepsilon. \tag{A.30}$$

which gives (see Eq. 11.164)

$$\varepsilon_{wall} = \nu \frac{\partial^2 k}{\partial x_2^2}.$$

▶Eq. A.30 can be used to get alternative boundary conditions of ε. Exact form of the dissipation term near the wall reads (see Eq. 8.24)

$$\varepsilon = \nu \left\{ \overline{\left(\frac{\partial v_1'}{\partial x_2} \right)^2 + \left(\frac{\partial v_3'}{\partial x_2} \right)^2} \right\}$$

where we have assumed $\partial/\partial x_2 \gg \partial/\partial x_1 \simeq \partial/\partial x_3$ and $\partial v_1'/\partial x_2 \simeq \partial v_3'/\partial x_2 \gg \partial v_2'/\partial x_2$. Taylor expansion gives (see Eq. A.28)

$$\varepsilon = \nu \left(\overline{a_1^2} + \overline{c_1^2} \right) + \dots \tag{A.31}$$

The turbulent kinetic energy (see Eq. A.28)

$$k = \frac{1}{2} \left(\overline{a_1^2} + \overline{c_1^2} \right) x_2^2 + \dots \tag{A.32}$$

so that

$$\left(\frac{\partial \sqrt{k}}{\partial x_2} \right)^2 = \frac{1}{2} \left(\overline{a_1^2} + \overline{c_1^2} \right) + \dots \tag{A.33}$$

Eqs. A.31 and A.33 gives

$$\varepsilon_{wall} = 2\nu \left(\frac{\partial \sqrt{k}}{\partial x_2} \right)^2 .$$

►Often the following boundary condition is used (see Eq. 11.170)

$$\varepsilon_{wall} = \frac{2\nu k}{x_2^2} \tag{A.34}$$

where we have assumed $a_1 = c_1$ in Eqs. A.31 and A.32 so that

$$\varepsilon = 2\nu \overline{a_1^2}$$
$$k = \overline{a_1^2 x_2^2}$$

which gives Eq. A.34.

- **Summary of the low-Re number model.**

  - Fine mesh near the wall. The first cell center is located at $x_2^+ \lesssim 1$.
  - This means that standard wall b.c. can be used, i.e. $\bar{v}_1 = \bar{v}_2 = \bar{v}_3 = k = 0$.
  - There are different options for the wall b.c. for ε: usually $\varepsilon_P = 2\nu k/(x_2^2)$ is prescribed for the wall-adjacent cells

- **Summary of wall-functions.**

  - Coarse mesh near the wall. The first cell center is located at $30 \lesssim x_2^+ \lesssim 400$. The point is located in the log region.
  - Friction velocity, u_τ, computed from the log-law.
  - A force/area b.c. is used for the wall-parallel velocity component: $\tau_w = \rho u_\tau^2$
  - In the log-region we know that the k equation can be simplified as $0 = P^k - \varepsilon$ which gives $k_P = C_\mu^{-1/2} u_\tau^2$ (k_P is prescribed for the wall-adjacent cells)
  - We use the simplified k equation also for ε: $0 = P^k - \varepsilon$ gives $\varepsilon_P = u_\tau^3/(\kappa x_2)$ (ε_P is prescribed for the wall-adjacent cells)

B Introduction to tensor notation

The convection-diffusion equation for temperature reads

$$\frac{\partial}{\partial x_1}\left(\rho v_1 T\right) + \frac{\partial}{\partial x_2}\left(\rho v_2 T\right) + \frac{\partial}{\partial x_3}\left(\rho v_3 T\right) =$$
$$\frac{\partial}{\partial x_1}\left(\Gamma\frac{\partial T}{\partial x_1}\right) + \frac{\partial}{\partial x_2}\left(\Gamma\frac{\partial T}{\partial x_2}\right) + \frac{\partial}{\partial x_3}\left(\Gamma\frac{\partial T}{\partial x_3}\right)$$

Using tensor notation it can be written as

$$\boxed{\frac{\partial}{\partial x_j}\left(\rho v_j T\right) = \frac{\partial}{\partial x_j}\left(\Gamma\frac{\partial T}{\partial x_j}\right)}$$

The Navier-Stokes equation reads (incompressible and $\mu = const.$)

$$\frac{\partial}{\partial x_1}\left(v_1 v_1\right) + \frac{\partial}{\partial x_2}\left(v_2 v_1\right) + \frac{\partial}{\partial x_3}\left(v_3 v_1\right) =$$
$$-\frac{1}{\rho}\frac{\partial p}{\partial x_1} + \nu\left(\frac{\partial^2 v_1}{\partial x_1^2} + \frac{\partial^2 v_1}{\partial x_2^2} + \frac{\partial^2 v_1}{\partial x_3^2}\right)$$

$$\frac{\partial}{\partial x_1}\left(v_1 v_2\right) + \frac{\partial}{\partial x_2}\left(v_2 v_2\right) + \frac{\partial}{\partial x_3}\left(v_3 v_2\right) =$$
$$-\frac{1}{\rho}\frac{\partial p}{\partial x_2} + \nu\left(\frac{\partial^2 v_2}{\partial x_1^2} + \frac{\partial^2 v_2}{\partial x_2^2} + \frac{\partial^2 v_2}{\partial x_3^2}\right)$$

$$\frac{\partial}{\partial x_1}\left(v_1 v_3\right) + \frac{\partial}{\partial x_2}\left(v_2 v_3\right) + \frac{\partial}{\partial x_3}\left(v_3 v_3\right) =$$
$$-\frac{1}{\rho}\frac{\partial p}{\partial x_3} + \nu\left(\frac{\partial^2 v_3}{\partial x_1^2} + \frac{\partial^2 v_3}{\partial x_2^2} + \frac{\partial^2 v_3}{\partial x_3^2}\right)$$

Using tensor notation it can be written as

$$\boxed{\frac{\partial}{\partial x_j}\left(v_j v_i\right) = -\frac{1}{\rho}\frac{\partial p}{\partial x_i} + \nu\frac{\partial^2 v_i}{\partial x_j \partial x_j}}$$

a: A tensor of zeroth rank (scalar)

a_i: A tensor of first rank (vector) $\quad a_i = (2, 1, 0)$

a_{ij}: A tensor of second rank (tensor)

A common tensor in fluid mechanics (and solid mechanics) is the stress tensor σ_{ij}

$$\sigma_{ij} = \begin{pmatrix} \sigma_{11} & \sigma_{12} & \sigma_{13} \\ \sigma_{21} & \sigma_{22} & \sigma_{23} \\ \sigma_{31} & \sigma_{32} & \sigma_{33} \end{pmatrix}$$

It is symmetric, i.e. $\sigma_{ij} = \sigma_{ji}$. For fully, developed flow in a 2D channel (flow between infinite plates) σ_{ij} has the form:

$$\sigma_{12} = \sigma_{21} = \mu \frac{dv_1}{dx_2}$$

and the other components are zero. As indicated above, the coordinate directions (x_1, x_2, x_3) correspond to (x, y, z), and the velocity vector (v_1, v_2, v_3) corresponds to (u, v, w).

B.1 What is a tensor?

A tensor is a *physical* quantity. Consequently it is independent of which coordinate system. The tensor of rank one (vector) b_i below

is physically the same expressed in the coordinate system (x_1, x_2)
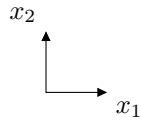
where $b_i = (1/\sqrt{2}, 1/\sqrt{2}, 0)^T$ and in the coordinate system $(x_{1'}, x_{2'})$
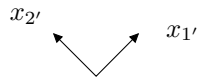
where $b_{i'} = (1, 0, 0)^T$. The tensor is the same even if its *components* are different.

The stress tensor σ_{ij} is a physical quantity which expresses the stress experienced by the fluid (or the solid); this stress is the same irrespective of coordinate system.

B.2 Examples of equations using tensor notation

B.2.1 Newton's second law

$$m\frac{d^2\mathbf{x}}{dt^2} = \mathbf{F}$$

which on component form reads

$$
\begin{aligned}
m\frac{d^2x_1}{dt^2} &= F_1 \\
m\frac{d^2x_2}{dt^2} &= F_2 \\
m\frac{d^2x_3}{dt^2} &= F_3.
\end{aligned}
\tag{B.1}
$$

On tensor notation:

$$m\frac{d^2x_i}{dt^2} = F_i$$

When an index appears once in each term (a free index) it indicates that the whole equation should be applied in each coordinate direction, cf. Eq. B.1.

B.2.2 Divergence $\nabla \cdot \mathbf{v} = 0$

The equation above reads

$$\frac{\partial v_1}{\partial x_1} + \frac{\partial v_2}{\partial x_2} + \frac{\partial v_3}{\partial x_3} = 0 \;\Leftrightarrow\; \sum_{i=1}^{3} \frac{\partial v_i}{\partial x_i} = 0 \tag{B.2}$$

In tensor notation the following rule is introduced: if an index appears twice (a dummy index) within a term, we should apply summation over this index. Normally the summation is taken from 1 to 3 (the three coordinate directions). If our coordinate system is 2D, the summation goes, of course, only from 1 to 2.

Equation B.2 is thus written as

$$\frac{\partial v_i}{\partial x_i} = 0. \tag{B.3}$$

Note that, since the dummy index implies a summation over each term, it can be interchanged against any index, i.e.

$$\frac{\partial v_k}{\partial x_k} = 0.$$

is exactly the same equation as Eq. B.3. Equation B can, for example, be written as

$$\frac{\partial}{\partial x_\ell}\left(v_\ell v_m\right) = -\frac{1}{\rho}\frac{\partial p}{\partial x_m} + \nu\frac{\partial v_m^2}{\partial x_k \partial x_k}$$

where different dummy indices have been used (ℓ and k); this is perfectly correct, because the summation is carried out for each term separately. What is not allowed, however, it to choose the dummy index same as the free index, i.e. for the equation above we are not allowed to use m as a dummy index.

B.2.3 The left-hand side of Navier-Stokes $v_\ell \partial v_m / \partial x_\ell$

For simplicity, let's assume 2D. The left-hand side of the equation above includes both a free index (m) and a dummy index (ℓ). Let's first write out the summation on component form so that

$$v_1 \frac{\partial v_m}{\partial x_1} + v_2 \frac{\partial v_m}{\partial x_2}.$$

The free index indicates that the equation should be written in each coordinate direction (x_1 and x_2 in this case, since we have assumed 2D flow), cf. Eq. B.1, i.e.

$$v_1 \frac{\partial v_1}{\partial x_1} + v_2 \frac{\partial v_1}{\partial x_2}$$
$$v_1 \frac{\partial v_2}{\partial x_1} + v_2 \frac{\partial v_2}{\partial x_2}$$

B.3 Contraction

If two free indices are set equal, they are turned into dummy indices, and the rank of the tensor is decreased by two. This is called *contraction*.If the tensor equation

$$a_{ij} = b_j c d_i - f_{ij}$$

is contracted, the result is

$$a_{ii} = b_i c d_i - f_{ii}.$$

For a tensor of rank two, a_{ij}, contraction is simply summation of the diagonal elements, i.e. $a_{11} + a_{22} + a_{33}$.

B.4 Two Tensor Rules

B.4.1 The summation rule

A summation over a dummy index corresponds to a scalar product or a divergence; it should not appear more than twice. The following expressions are not valid:

$$a_{kkk} = 0, \ a_{iik}b_{ij} = d_{kj}, \ a_i b_i c_i = d$$

B.4.2 Free Index

In an expression the free index (indices) must be the same in all terms The following expressions are not valid:

$$a_{ikk} = b_j, \ c_i a_i b_j = d_k, \ a_{ij}d_{jk} = c_{im}$$

B.5 Special Tensors

B.5.1 Kroenecker's δ (identity tensor)

It is defined as

$$\delta_{ij} = \begin{cases} 1 & i = j \\ 0 & i \neq j \end{cases}$$

Contraction of δ_{ij} yields

$$\delta_{ii} = \delta_{11} + \delta_{22} + \delta_{33} = 3$$

Another example of contraction can now be given. We have the expression for the turbulent stress tensor based on the Boussinesq hypothesis (see Eq. 11.33)

$$\rho\overline{v'_i v'_j} = -\mu_t \left(\frac{\partial \bar{v}_i}{\partial x_j} + \frac{\partial \bar{v}_j}{\partial x_i} \right) + \frac{2}{3}\delta_{ij}\rho k. \tag{B.4}$$

Contraction gives

$$\rho\overline{u_i u_i} = -2\mu_t \frac{\partial \bar{v}_i}{\partial x_i} + \frac{2}{3}\delta_{ii}\rho k = -2\mu_t \frac{\partial \bar{v}_i}{\partial x_i} + 2\rho k.$$

For incompressible flow the first term on the right-hand side is zero (due to continuity) so that

$$\overline{u_i u_i} = 2k,$$

which actually is the definition of k. Thus Eq. B.4 is valid upon contraction; this should always be the case. As can be seen, contraction of Eq. B.4 corresponds simply to the sum of the diagonal components (elements 11, 22 & 33).

B.5.2   Levi-Civita's ε_{ijk} (permutation tensor)

It is defined as

$$\varepsilon_{ij} = \begin{cases} 1 & \text{if } (i,j,k) \text{ are cyclic permutations of } (1,2,3) \\ 0 & \text{if at least two indices are equal} \\ -1 & \text{otherwise} \end{cases} \tag{B.5}$$

Examples:

$$\varepsilon_{123} = 1, \; \varepsilon_{132} = -1, \; \varepsilon_{113} = 0$$
$$\varepsilon_{312} = 1, \; \varepsilon_{321} = -1, \; \varepsilon_{233} = 0$$

B.6   Symmetric and antisymmetric tensors

A tensor a_{ij} is symmetric if $a_{ij} = a_{ji}$.

A tensor b_{ij} is antisymmetric if $b_{ij} = -b_{ji}$. It follows that for an antisymmetric tensor all diagonal components must be zero (for example, $b_{11} = -b_{11} \Rightarrow b_{11} = 0$).

The (inner) product of a symmetric and antisymmetric tensor is always zero. This can be shown as follows:

$$a_{ij}b_{ij} = a_{ji}b_{ij} = -a_{ji}b_{ji} = -a_{ij}b_{ij},$$

where we first used the fact that $a_{ij} = a_{ji}$ (symmetric), then that $b_{ij} = -b_{ji}$ (antisymmetric), and finally we interchanged the indices i and j, since they are dummy indices. Thus the product must be zero.

This can of course also be shown be writing out $a_{ij}b_{ij}$ on component form, i.e.

$$a_{ij}b_{ij} = a_{11}b_{11} + a_{12}b_{12} + a_{13}b_{13} + \ldots + a_{32}b_{32} + a_{33}b_{33} = 0$$

By inserting

$$a_{12} = a_{21}, \quad a_{13} = a_{31}, \quad a_{23} = a_{32}$$
$$b_{11} = b_{22} = b_{33} = 0$$
$$b_{12} = -b_{21}, \quad b_{13} = -b_{31}, \quad b_{23} = -b_{32}$$

the relation above, i.e. $a_{ij}b_{ij} = 0$, is verified.

B.7 Vector Product

The vector cross product

$$\mathbf{c} = \mathbf{a} \times \mathbf{b}$$

is on tensor notation written

$$c_i = \varepsilon_{ijk} a_j b_k. \qquad (B.6)$$

This is easily shown by writing it on component form. Using Sarrus' rule we get

$$\mathbf{c} = \begin{pmatrix} \mathbf{x} & \mathbf{y} & \mathbf{z} \\ a_1 & a_2 & a_3 \\ b_1 & b_2 & b_3 \end{pmatrix} = (a_2 b_3 - a_3 b_2, a_3 b_1 - a_1 b_3, a_1 b_2 - a_2 b_1)^T$$

We find that the first component of Eq. B.6 is

$$\begin{aligned} c_1 = \varepsilon_{1jk} a_j b_k &= \\ &= \varepsilon_{111} a_1 b_1 + \varepsilon_{112} a_1 b_2 + \varepsilon_{113} a_1 b_3 \\ &+ \varepsilon_{121} a_2 b_1 + \varepsilon_{122} a_2 b_2 + \varepsilon_{123} a_2 b_3 \\ &+ \varepsilon_{131} a_3 b_1 + \varepsilon_{132} a_3 b_2 + \varepsilon_{133} a_3 b_3 \\ &= \varepsilon_{123} a_2 b_3 + \varepsilon_{132} a_3 b_2 = a_2 b_3 - a_3 b_2. \end{aligned}$$

Recall that ε_{ijk} is zero if any two indices are equal (see Eq. B.5, p. 323).

B.8 Derivative Operations

B.8.1 The derivative of a vector $\mathbf{B}$:

Tensor notation   Vector notation
$$\frac{\partial B_i}{\partial x_j}$$
grad($\mathbf{B}$) or $\nabla \mathbf{B}$

The result is a tensor of rank two (rank of B_i plus one)

B.8.2 The gradient of a scalar a:

Tensor notation   Vector notation
$$\frac{\partial a}{\partial x_j}$$
grad(a) or ∇a

The result is a *vector*.

B.8.3   The divergence of a vector B:

Tensor notation   Vector notation

$$\frac{\partial B_j}{\partial x_j}$$ $\text{div}(\mathbf{B})$ or $\nabla \cdot \mathbf{B}$

The result is a *scalar.*

B.8.4   The curl of a vector B:

Tensor notation   Vector notation

$$\varepsilon_{ijk}\frac{\partial B_k}{\partial x_j}$$ $\text{curl}(\mathbf{B})$ or $\nabla \times \mathbf{B}$

The result is a *vector.*

B.8.5   The Laplace operator on a scalar a:

Tensor notation   Vector notation

$$\frac{\partial^2 a}{\partial x_j \partial x_j}$$ $\nabla \cdot (\nabla a) = \nabla^2 a$

The result is a *scalar.*

B.9   Integral Formulas

Stokes theorem

$$\oint_C \mathbf{B} \cdot d\mathbf{x} = \int_S (\nabla \times \mathbf{B}) \cdot d\mathbf{S},$$

where the surface S is bounded by the line C. On tensor notation:

$$\oint_C B_i dx_i \quad \text{or} \quad \int_S \varepsilon_{ijk}\frac{\partial B_k}{\partial x_j}dS_i.$$

Gauss theorem

$$\int_S \mathbf{B} \cdot d\mathbf{S} = \int_V \nabla \cdot \mathbf{B}dV,$$

where the volume V is bounded by the surface S. On tensor notation:

$$\int_S B_i dS_i \quad \text{or} \quad \int_V \frac{\partial B_i}{\partial x_i}dV$$

B.10   Multiplication of tensors

Two tensors can be multiplied in two ways: either the number of free indices is reduced by two (inner product), or it is unchanged (outer product). The product

$$a_{ijk}b_{k\ell} = c_{ij\ell}$$

represents an inner product; the rank of the product is the sum of the rank of the two tensors $(3 + 2 = 5)$ on the left-hand side minus two $(5 - 3 = 2)$. An outer product between the two tensors reads

$$a_{ijk}b_{m\ell} = d_{ijk\ell m}.$$

Now the rank of the resulting tensor $d_{ijk\ell m}$ (rank 5) is the sum of the rank of the two tensors $(3 + 2 = 5)$.

C   TME226: $\epsilon - \delta$ identity

THE $\epsilon - \delta$ identity reads

$$\epsilon_{inm}\epsilon_{mjk} = \epsilon_{min}\epsilon_{mjk} = \epsilon_{nmi}\epsilon_{mjk} = \delta_{ij}\delta_{nk} - \delta_{ik}\delta_{nj}$$

In Table C.1 the components of the $\epsilon - \delta$ identity are given.

i	n	j	k	$\epsilon_{inm}\epsilon_{mjk}$	$\delta_{ij}\delta_{nk} - \delta_{ik}\delta_{nj}$
1	2	1	2	$\epsilon_{12m}\epsilon_{m12} = \epsilon_{123}\epsilon_{312} = 1 \cdot 1 = 1$	$1 - 0 = 1$
2	1	1	2	$\epsilon_{21m}\epsilon_{m12} = \epsilon_{213}\epsilon_{312} = -1 \cdot 1 = -1$	$0 - 1 = -1$
1	2	2	1	$\epsilon_{12m}\epsilon_{m21} = \epsilon_{123}\epsilon_{321} = 1 \cdot -1 = -1$	$0 - 1 = -1$
1	3	1	3	$\epsilon_{13m}\epsilon_{m13} = \epsilon_{132}\epsilon_{213} = -1 \cdot -1 = 1$	$1 - 0 = 1$
3	1	1	3	$\epsilon_{31m}\epsilon_{m13} = \epsilon_{312}\epsilon_{213} = 1 \cdot -1 = -1$	$0 - 1 = -1$
1	3	3	1	$\epsilon_{13m}\epsilon_{m31} = \epsilon_{132}\epsilon_{231} = -1 \cdot 1 = -1$	$0 - 1 = -1$
2	3	2	3	$\epsilon_{23m}\epsilon_{m23} = \epsilon_{231}\epsilon_{123} = 1 \cdot 1 = 1$	$1 - 0 = 1$
3	2	2	3	$\epsilon_{32m}\epsilon_{m23} = \epsilon_{321}\epsilon_{123} = -1 \cdot 1 = -1$	$0 - 1 = -1$
2	3	3	2	$\epsilon_{23m}\epsilon_{m32} = \epsilon_{231}\epsilon_{132} = 1 \cdot -1 = -1$	$0 - 1 = -1$

Table C.1: The components of the $\epsilon - \delta$ identity which are non-zero.

D   TME226 Assignment 1 in 2020: laminar flow in a channel

$\mathbf{Y}$OU will get results of a developing two-dimensional channel flow (i.e. flow between two parallel plates), see Fig. D.1. The flow is steady and incompressible. The simulations have been done with Calc-BFC [196]. The inlet boundary condition (left boundary) is $v_1 = V_{in} = 0.9$. The height of the channel is $h = 0.01m$ and $L = 0.6385m$; the fluid is air of 20^oC.

You'll use data from a coarse DNS. Although some of the data are probably not fully accurate, in this exercise we consider the data to be exact. You can use Matlab, Octave or Python. Both Octave and Python are open-source software. Octave is a Matlab clone. Many large Swedish industries prefer engineers to use Python instead of Matlab due to Matlab's high license fees

- First, find out and write down the governing equations (N.B:. you cannot assume that the flow is fully developed).

From the course www page `http://www.tfd.chalmers.se/~lada/MoF/`, download the data file `channel_flow_data.dat` and the m-file `channel_flow.m` which reads the data and plot some results. Open Python or Matlab/Octave and execute `channel_flow`.

Open `channel_flow.m` in an editor and make sure that you understand it. There are three field variables, v_1, v_2 and p; the corresponding Python/Matlab/Octave arrays are `v1_2d`, `v2_2d` and `p_2d`. The grid is 199×28, i.e. $ni = 199$ grid points in the x_1 direction and $nj = 28$ grid points in the x_2 direction. The field variables are stored at these grid points. We denote the first index as i and the second index as j, i.e. `v1_2d(i,j)`. Hence in Python

`v1_2d[:,0]` are the v_1 values at the lower wall;

`v1_2d[:,nj-1]` are the v_1 values at the upper wall;

`v1_2d[0,:]` are the v_1 values at the inlet;

`v1_2d[ni-1,:]` are the v_1 values at the outlet;

and in Matlab/Octave

`v1_2d(:,1)` are the v_1 values at the lower wall;

`v1_2d(:,nj)` are the v_1 values at the upper wall;

`v1_2d(1,:)` are the v_1 values at the inlet;

`v1_2d(ni,:)` are the v_1 values at the outlet;

The work should be carried out in groups of two (you may also do it on your own, but we don't recommend it). At the end of this Assignment the group should write and submit a report (in English). Divide the report into sections corresponding to the sections D.1 – D.9. In some sections you need to make derivations; these should clearly be described and presented. Present the results in each section with a figure (or a numerical value). The results should also be discussed and – as far as you can – explained.
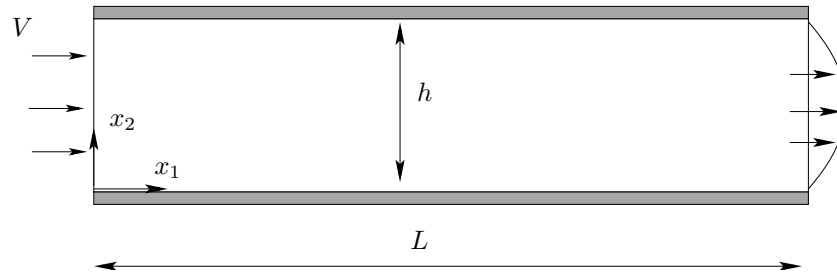
Figure D.1: Flow between two plates (not to scale).

It is recommended (but the not required) that you use LATEX (an example of how to write in LATEXis available on the course www page). You find LATEX here. You can also use LATEX on-line.

D.1   Fully developed region

Fully developed conditions mean that the flow does not change in the streamwise direction, i.e. $\partial v_1/\partial x_1 = 0$. If we define "fully developed" as the location where the velocity gradient in the center becomes smaller than 0.01, i.e. $|\partial v_1/\partial x_1| < 0.01$, how long distance from the inlet does the flow become fully developed?

Another way to define fully developed conditions can be the x_1 position where the centerline velocity has reached, for example, 99% of its final value. What x_1 value do you get?

In Section 3.2.2, a distance taken from the literature is given. How well does this agree with your values?

In the fully developed region, compare the velocity profile with the analytical profile (see Section 3.2.2).

Look at the vertical velocity component, v_2. What value should it take in the fully developed region (see Section 3.2.2)? What value does it take (at $x_2 = h/4$, for example)?

D.2   Wall shear stress

On the lower wall, the wall shear stress, $\tau_{w,L}$ (index L denotes <u>L</u>ower), is computed as

$$\tau_{w,L} \equiv \tau_{21,w,L} = \mu \frac{\partial v_1}{\partial x_2}\bigg|_L \tag{D.1}$$

Recall that $\tau_{12} = \mu(\partial v_1/\partial x_2 + \partial v_2/\partial x_1)$ (see Eqs. 2.10) but at the wall $\partial v_2/\partial x_1 = 0$; Plot $\tau_{w,L}$ versus x_1. Why does it behave as it does?

Now we will compute the wall shear stress at the upper wall, $\tau_{w,U}$. If you use Eq. D.1, you get the incorrect sign. Instead, use Cauchy's formula (see Fig. 1.3 and [1], Chapt. 4.2)

$$t_i^{(\hat{\mathbf{n}})} = \tau_{ji}n_j \tag{D.2}$$

which is a general way to compute the stress vector on a surface whose (outward pointing) normal vector is $\hat{\mathbf{n}} = n_j$. The expression for τ_{ij} can be found in Eqs. 1.9 and 2.4; recall that the flow in incompressible. On the top wall, the normal vector points *out* from the surface (i.e. $n_j = (0, -1, 0)$). Use Eq. D.2 to compute the wall shear

stress at the upper wall. Plot the two wall shear stresses in the same figure. How do they compare? In the fully developed region, compare with the analytical value (see Eq. 3.30).

D.3   Inlet region

In the inlet region the flow is developing from its inlet profile ($v_1 = V = 0.9$) to the fully developed profile somewhere downstream. The v_1 velocity is decelerated in the near-wall regions, and hence the v_1 velocity in the center must increase due to continuity. Plot v_1 in the center and near the wall as a function of x_1. Plot also $\partial v_1/\partial x_1$. If you, for a fixed x_1, integrate v_1, i.e.

$$\xi(x_1) = \int_0^h v_1(x_1, x_2)dx_2$$

what do you get? How does $\xi(x_1)$ vary in the x_1 direction? How should it vary?

D.4   Wall-normal velocity in the developing region

In Section D.3 we found that, in the developing region, v_1 near the walls decreases for increasing x_1. What about v_2? How do you explain the behaviour of v_2?

D.5   Vorticity

Do you expect the flow to be *irrotational* anywhere? Let's find out by computing the vorticity vector ω_i, see Section 1.4 (note that only one component of ω_i is non-zero). Plot it in the fully developed region as ω_3 vs. x_2. Where is it largest? Plot the vorticity also in the inlet and developing regions; what happens with the vorticity in the inlet region? Now, *is* the flow rotational anywhere? Why? Why not?

D.6   Deformation

In Section 1.6, we divided the velocity gradient into a strain-rate tensor, S_{ij}, and a vorticity tensor, Ω_{ij}. Since the flow is two-dimensional, we have only two off-diagonal terms (which ones?). Plot and compare one of the off-diagonal term of S_{ij} and Ω_{ij}. Where are they largest? Why? What is the physical meaning of S_{ij} and Ω_{ij}, respectively? Compare Ω_{ij} with the vorticity, ω_i, you plotted in Section D.5. Are they similar? Any comment?

D.7   Dissipation

Compute and plot the dissipation, $\Phi = \tau_{ji}\partial v_i/\partial x_j$, see Eq. 2.15. What is the physical meaning of the dissipation? Where do you expect it to be largest? Where is it largest? Any difference it its behaviour in the inlet region compared to in the fully developed region?

   The dissipation appears as a source term in the equation for internal energy, see Eq. 2.15. This means that dissipation increases the internal energy, i.e. the temperature. This is discussed in some detail at p. 29.

   Use Eq. 2.17 to compute the temperature increase that is created by the flow (i.e. by dissipation). Start by integrating the dissipation over the entire computational domain. Next, re-write the left side on conservative form (see Section 2.4) and then apply the

Gauss divergence theorem, See Section 3.2.3. Assume that the upper and the lower wall are adiabatic; furthermore we can neglect the heat flux by conduction, q_1, (see Eq. 2.14) at the inlet and outlet.

Compute the increase in bulk temperature, T_b, from inlet to outlet. The bulk temperature is defined as

$$T_b = \frac{\int_0^h v_1 T \, dx_2}{\int_0^h v_1 \, dx_2} \tag{D.3}$$

When you compute the convective flux in Eq. 2.12 at the outlet, for example, you get

$$\int_0^h v_1 T \, dx_2$$

which indeed is very similar to the bulk temperature in Eq. D.3.

D.8 Eigenvalues

Compute and plot the eigenvalues of the viscous stress tensor, τ_{ij}. Use the Python command np.linalg.eig or the Matlab/Octave command eig. If you have computed the four elements of the τ_{ij} matrix you can use the following commands in Python

```
tau=[tau_11 tau_12; tau_21 tau_22]
lambda,n=np.linalg.eig(tau)
```

and in Matlab/Octave

```
tau=[tau_11 tau_12; tau_21 tau_22];
[n,lambda]=eig(tau);
```

where n and lambda denote eigenvalues and eigenvectors, respectively. Note that tau_11, tau_12, tau_21, tau_22 are scalars and hence the coding above must be inserted in for loops.

What is the physical meaning of the eigenvalues (see Chapter 1.8)? Pick an x_1 location where the flow is fully developed. Plot one eigenvalue as a $x - y$ graph (eigenvalue versus x_2). Plot also the four stress components, τ_{ij}, versus x_2. Is (Are) anyone(s) negligible? How does the largest component of τ_{ij} compare with the largest eigenvalue? Any thoughts? And again: *what is the physical meaning of the eigenvalues?*

D.9 Eigenvectors

Compute and plot the eigenvectors of τ_{ij}. Recall that at each point you will get two eigenvectors, perpendicular to each other. It is enough to plot one of them. An eigenvector is, of course, a vector. Use the Python command plt.quiver or the Matlab/Octave command quiver to plot the field of the eigenvectors. Recall that the sign of the eigenvector is not defined (for example, both $\hat{\mathbf{v}}_1$ and $-\hat{\mathbf{v}}_1$ in Fig. 1.11 at p. 24 are eigenvectors).

Recall that the stress vector, $t_i^{(\hat{\mathbf{n}})}$, (see Eq. D.2 and Fig. 1.3) can be computed as the product of the eigenvalues and eigenvectors. Do that as a vector plot [7]. In regions where the eigenvalues are close to zero, the eigenvectors have no meaning.

Try to analyze why the eigenvectors behave as they do. '

---

[7]If you plot it over the entire region, you'll see nothing; make a zoom

E   TME226 Assignment 1: laminar flow in a boundary layer

$\mathbf{Y}$OU will get results of a developing two-dimensional boundary-layer flow (i.e. flow along a flat plate, see Fig. E.1). The flow is steady and incompressible. The simulations have been done with CALC-BFC [196] using the QUICK discretizatin scheme [197]. The height of the domain is $H = 1.289m$, $L = 2.461m$ and $x_0 = 0.19m$; the fluid is air of 20^oC and $V_{1,\infty} = 1m/s$. The mesh has 252×200 grid points, i.e. $ni = 252$ points in the x_1 direction and $nj = 200$ points in the x_2 direction.

Inlet boundary, $x_1 = -x_0$ (i=1)

$v_1 = V_{1,\infty} = 1$, $v_2 = 0$.

Lower boundary, $x_2 = 0$ (j=1)

$x_1 \leq 0$, i$\leq$ i=i_lower_sym: $v_2 = \partial v_1/\partial x_2 = 0$, i.e. a symmetry boundary condition

$x_1 > 0$, i> i=i_lower_sym: $v_1 = v_2 = 0$, i.e. a wall

Outlet, $x_1 = L$ (i=ni)

Neumann boundary conditions are used, i.e. $\partial v_1/\partial x_1 = \partial v_2/\partial x_1 = 0$.

Upper boundary, $x_2 = H$ (j=nj)

$v_2 = \partial v_1/\partial x_2 = 0$, i.e. a symmetry boundary condition

You'll use data from a coarse DNS. Although some of the data are probably not fully accurate, in this exercise we consider the data to be exact. You can use Matlab, Octave or Python. Both Octave and Python are open-source software. Octave is a Matlab clone. Many large Swedish industries prefer engineers to use Python instead of Matlab due to Matlab's high license fees

- First, find out and write down the governing equations

From the course www page `http://www.tfd.chalmers.se/~lada/MoF/`, download the data files `boundary_layer_data.dat`, `xc.dat`, `yc.dat` and `blasius.dat` and the m-file `boundary_layer.m` which reads the data and plot some results. Download also the file with the Blasius solution, `blasius.dat`. Open Python or Matlab/Octave and execute `boundary_layer`

Open `boundary_layer` in an editor and make sure that you understand it. There are three field variables, v_1, v_2 and p; the corresponding Python/Matlab/Octave arrays are `u2d`, `v2d` and `p2d`. The field variables are stored at the cell centers denoted `xp,yp`. We denote the first index as i and the second index as j, i.e. `u2d(i,j)`. Hence in Python

- `u2d[:,0]` are the v_1 values at the lower boundary

  - i$\leq$ i=i_lower_sym: symmetric boundary condition
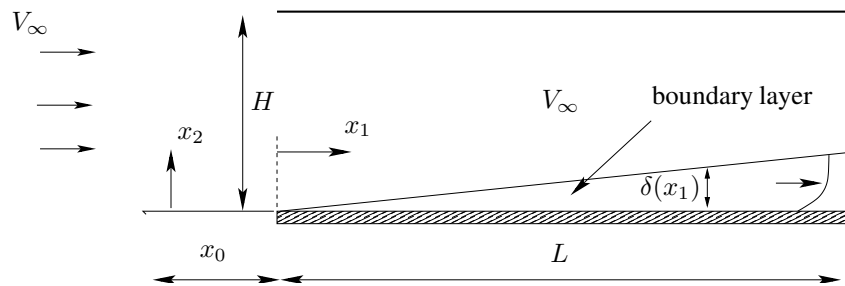
Figure E.1: Flow along a flat plate (not to scale). The leading edge is located at $x = 0$.

> > – i> i=i_lower_sym: wall

- u2d[:,nj-1] are the v_1 values at the upper boundary;

- u2d[0,:] are the v_1 values at the inlet;

- u2d[ni-1,:] are the v_1 values at the outlet;

and in Matlab/Octave

- u2d(:,1) are the v_1 values at the lower boundary

> > – i≤ i=i_lower_sym: symmetric boundary condition
> > – i> i=i_lower_sym: wall

- u2d(:,nj) are the v_1 values at the upper boundary;

- u2d(1,:) are the v_1 values at the inlet;

- u2d(ni,:) are the v_1 values at the outlet;

The work should be carried out in groups of two (you may also do it on your own, but we don't recommend it). At the end of this Assignment the group should write and submit a report (in English). Divide the report into sections corresponding to the sections E.1 – E.10. In some sections you need to make derivations; these should clearly be described and presented. Present the results in each section with a figure (or a numerical value). The results should also be discussed and – as far as you can – explained.

It is recommended (but the not required) that you use LATEX (an example of how to write in LATEXis available on the course www page). You find LATEX here. You can also use LATEX on-line.

E.1 Velocity profiles

The flat plate starts at $x_1 = 0$. What happens with the streamwise velocity, v_1, near the wall as you go downstream from $x_1 = 0$? Why does v_1 behave as it does? What happens with v_2? Does the behavior of v_2 has anything to do with v_1?

Plot profiles of v_1 vs. x_2 at a couple of x_1 locations.

Now plot $v_1/V_{1,\infty}$ vs. ξ, see Eq. 3.48 and compare with Blasius solution, see Table 3.1 (the Blasius solution is loaded in boundary_layer.m). Note that when

you compute ξ you must use x_1, x_2 and ν from the Navier-Stokes solution. Plot also $v_2/V_{1,\infty}$.

Compare $v_1/V_{1,\infty}$ and $v_2/V_{1,\infty}$ with Blasius solution; $v_{1,Blasius}/V_{1,\infty}$ is taken from the data file and $v_{2,Blasius}/V_{1,\infty}$ is obtained from Eqs. 3.44 and 3.50.

E.2 Boundary layer thickness

Look at the v_1 profiles vs. x_2 you plotted at different x_1 locations in Section E.1. The boundary layer gets thicker and thicker as you go downstream, right? The boundary layer thickness, δ, can be defined in many ways. One way is the boundary layer thickness at the x_2 value where the local velocity is 99% of the freestream velocity; this boundary layer thickness is denoted δ_{99}.

Compute and plot δ_{99} vs. x_1 and compare it with the Blasius solution

$$\delta_{99,Blasius} = 5 \left(\frac{\nu x_1}{V_{1,\infty}} \right)^{1/2} \tag{E.1}$$

The disadvantage of δ_{99} is that this definition is entirely dependent on the behavior of the velocity profile near the edge of the boundary layer. There are two other, more stable, definitions of boundary layer thickness, the *displacement* thickness, δ^*, and the *momentum* thickness, θ; they are defined as

$$\delta^* = \int_0^\infty \left(1 - \frac{v_1}{V_{1,\infty}} \right) dx_2$$
$$\theta = \int_0^\infty \frac{v_1}{V_{1,\infty}} \left(1 - \frac{v_1}{V_{1,\infty}} \right) dx_2 \tag{E.2}$$

The upper limit of the integrals is infinity. If you look carefully at the velocity profiles which you plotted in Section E.1, you find that v_1 has a maximum outside the boundary layer. We don't want to carry out the integration in Eq. E.2 outside of this maximum, because this will give an incorrect estimate of $\delta^*_{Blasius}$ and $\theta_{Blasius}$. Hence, terminate the integration when `u2d(i,j+1) < u2d(i,j)`. Plot δ^* and θ vs. x_1 and compare with the Blasius solution

$$\delta^*_{Blasius} = 1.721 \left(\frac{\nu x_1}{V_{1,\infty}} \right)^{1/2}$$
$$\theta_{Blasius} = 0.664 \left(\frac{\nu x_1}{V_{1,\infty}} \right)^{1/2}$$

E.3 Velocity gradients

Compute and plot $\partial v_1/\partial x_2$ vs. x_2 at a couple of x_1 locations. How does this velocity derivative change as you move downstream along the plate? Do you see any connection with the change of the boundary layer thickness with x_1 and the change of $\partial v_1/\partial x_2$ with x_1?

In boundary layer approximations, we assume that $v_2 \ll v_1$ and $\partial v_1/\partial x_2 \gg \partial v_1/\partial x_1$: are these assumptions satisfied in this flow?

E.4 Skinfriction

The skinfriction, C_f, is a dimensionless wall shear stress defined as

$$C_f = \frac{\tau_w}{\frac{1}{2}\rho V_{1,\infty}^2} \tag{E.3}$$

The wall shear stress, τ_w, is the same as $\tau_{12} = \tau_{21}$, see Eq. 2.10, at the wall. Furthermore, what about $\partial v_2/\partial x_1$ in Eq. 2.10? Where is it largest? Plot C_f vs. x_1 and compare it with the Blasius solution

$$C_{f,Blasius} = \frac{0.664}{\sqrt{V_{1,\infty}x_1/\nu}}$$

C_f decreases vs. x_1 and δ increases vs. x_1: do you see any connection?

E.5 Vorticity

Do you expect the flow to be *irrotational* anywhere? Let's find out by computing the vorticity vector, ω_i, see Section 1.4 (note that one velocity gradient in ω_i is very small). Plot the vorticity above the plate vs. x_2 at a couple of x_1 locations. Where is it largest? Plot the vorticity also upstream of the plate. Now, *is* the flow rotational anywhere? Why? Why not?

E.6 Deformation

In Section 1.6, we divided the velocity gradient into a strain-rate tensor, S_{ij}, and a vorticity tensor, Ω_{ij}. Since the flow is two-dimensional, we have only two off-diagonal terms (which ones?). Plot and compare one of the off-diagonal term of S_{ij} and Ω_{ij}. Where are they largest? Why? What is the physical meaning of S_{ij} and Ω_{ij}, respectively? Compare Ω_{ij} with the vorticity, ω_i, which you plotted in Section E.5. Are they similar? Any comment?

E.7 Dissipation

Compute and plot the dissipation, $\Phi = \tau_{ji}\partial v_i/\partial x_j$, see Eq. 2.15. The viscous stress tensor is given in Eq. 2.10. What is the physical meaning of the dissipation? Where is it largest? How large is it upstream the plate?

The dissipation appears as a source term in the equation for internal energy, see Eq. 2.15. This means that dissipation increases the internal energy, i.e. the temperature. This is discussed in some detail at p. 29.

Use Eq. 2.17 to compute the temperature increase that is created by the flow (i.e. by dissipation). Start by integrating the dissipation over the entire computational domain. Next, re-write the left side on conservative form (see Section 2.4) and then apply the Gauss divergence theorem. see Section 3.2.3. Assume that the lower ($x_2 = 0$) and the upper ($x_2 = H$) boundaries are adiabatic; furthermore we can neglect the heat flux by conduction, q_1, (see Eq. 2.14) at the inlet and outlet.

Compute the increase in bulk temperature, T_b, from inlet to outlet. The bulk temperature is defined as

$$T_b = \frac{\int_0^H v_1 T dx_2}{\int_0^H v_1 dx_2} \tag{E.4}$$

When you compute the convective flux in Eq. 2.12 at the outlet, for example, you get

$$\int_0^H v_1 T dx_2$$

which indeed is very similar to the bulk temperature in Eq. E.4.

E.8   Eigenvalues

Compute and plot the eigenvalues of the viscous stress tensor, τ_{ij}. Use the Python command np.linalg.eig or the Matlab/Octave command eig. If you have computed the four elements of the τ_{ij} matrix you can use the following commands in Python

```
tau=[tau_11 tau_12; tau_21 tau_22];
n,lambda=np.linalg.eig(tau);
```

and in Matlab/Octave

```
tau=[tau_11 tau_12; tau_21 tau_22];
[n,lambda]=eig(tau);
```

where n and lambda denote eigenvalues and eigenvectors, respectively.

where n and lambda denote eigenvalues and eigenvectors, respectively. Note that tau_11, tau_12, tau_21, tau_22 are scalars and hence the coding above must be inserted in for loops.

What is the physical meaning of the eigenvalues (see Chapter 1.8)? Pick an x_1 location above the plate. Plot one eigenvalue as a $x - y$ graph (eigenvalue versus x_2). Plot also the four stress components, τ_{ij}, versus x_2. Is (Are) anyone(s) negligible? How does the largest component of τ_{ij} compare with the largest eigenvalue? Any thoughts? And again: *what is the physical meaning of the eigenvalues?*

E.9   Eigenvectors

Compute and plot the eigenvectors of τ_{ij}. Recall that at each point you will get two eigenvectors, perpendicular to each other. It is enough to plot one of them. An eigenvector is, of course, a vector. Use the Python command plt.quiver or Matlab/Octave command quiver to plot the field of the eigenvectors. Recall that the sign of the eigenvector is not defined (for example, both $\hat{\mathbf{v}}_1$ and $-\hat{\mathbf{v}}_1$ in Fig. 1.11 at p. 24 are eigenvectors).

Recall that the stress vector, $t_i^{(\hat{\mathbf{n}})}$, (see Eq. D.2 and Fig. 1.3) can be computed as the product of the eigenvalues and eigenvectors. Do that as a vector plot [8]. In regions where the eigenvalues are close to zero, the eigenvectors have no meaning.

Try to analyze why the eigenvectors behave as they do.

E.10   Terms in the v_1 equation

The Navier-Stokes equation for v_1 includes only three terms, see Eq. 3.42. The left side and the right side of this equation must be equal. Let's verify that. Plot the three terms vs. x_2 at a couple of x_1 locations. Plot also the sum of the terms, i.e. check if the left side and the right side of Eq. 3.42 are equal: are they? If not, what could be

---

[8]If you plot it over the entire region, you'll see nothing; make a zoom

the reason? Recall that in Eq. 3.42 we assume that $\partial p/\partial x_1 = 0$. Maybe it is not zero? Plot it and check! If it's not zero, what could be the reason?

How large is $\partial^2 v_1/\partial x_2^2$ at the wall? How large should it be? (<u>Hint:</u> which other terms in the v_1 equation are non-zero?). How large is the gradient of vorticity, $\partial \omega/\partial x_2$, at the wall? Look at the discussion in connection to Eq. 4.25.

F   TME226, Assignment 2: Turbulent flow using STAR-CCM+

IN this task, a commercial CFD software (STAR-CCM+ 12.06.011) will be used. The task is to do simulation of a two-dimensional hill flow. Several turbulence models will be used and the results will be compared with experimental data. Before doing the task, it is recommended to first do one of the tutorials in the User Guide (Version 12.06) of STAR-CCM+. The tutorial which is similar to this task is the "Steady Flow: Backward Facing Step".

You can do the assignment on your own or in a group of two. It is recommended (but the not required) that you use LaTeX (an example of how to write in LaTeXis available on the course www page). You find LaTeX here. You can also use LaTeX on-line.

F.1   Backward Facing Step Tutorial

This tutorial is a good bridge before doing different cases. Here are some steps to access the tutorial:

1. Open a terminal window. In the terminal window, type starccm+

2. To start a new simulation, click **File → New**

3. Tick the Power-On-Demand box and fill the license box with the POD Key.

4. Download the tutorial instruction and data from the course homepage

F.2   2D Hill Flow
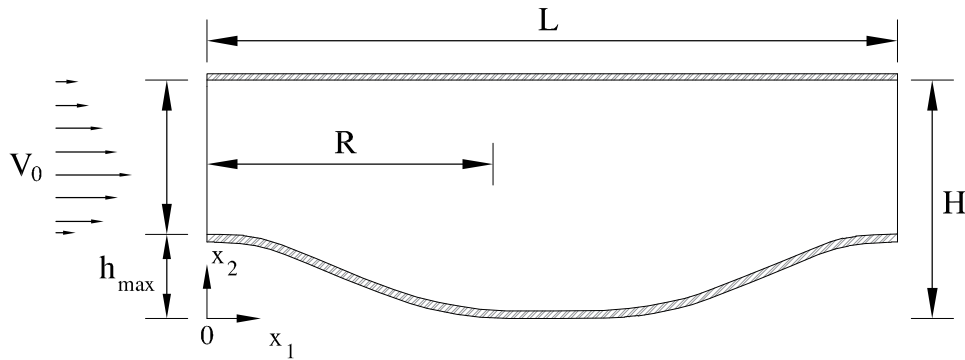
Figure F.1: flow over two consecutive hills

In this case, a two-dimensional, steady and incompressible flow over two consecutive hills mounted on the bottom of the channel will be studied. The height of the channel is $H = 151.75\ mm$. The maximum height and length of each hill are $h_{max} = 50$ mm and $R = 192.8\ mm$, respectively. The space between each of the consecutive hills is $9.0h_{max}$. The fluid is water of $20°$ Celsius and the Reynolds number (Re = 37000) is based on the mean centerline velocity at inlet and the inlet channel height. The inlet boundary condition (left boundary) is imposed as the velocity profile of the

fully-developed channel flow in the absence of the hills. The case is built based on the paper [198]. Please read this paper.

F.3   Steady Flow: 2D Hill Flow Tutorial

1. Start the STAR-CCM+

   - Open a terminal window → type starccm+

2. Create a new simulation

   - Click the new simulation icon (left icon of the system toolbar) → tick the Power-On-Demand (POD) box.
   - In the **Process Options** section, choose **Serial** (default option) mode. DO NOT change it to any other options.
   - Fill the POD box with the POD Key and then press OK button.

3. Importing the Geometry and Mesh

   - Select **File** → **Import** → **Import Volume Mesh** from the menu bar.
   - In the *Open* window, navigate to the stored location and select the file *2dHill.ccm*
   - Click the **Open** button to import the mesh file.
   - Save the new simulation as *2dHill.sim*

4. Visualizing the Imported Mesh

   - Right-click the node **Scenes** in the explorer pane (to the left) and then select **New Scene** → **Mesh**. The mesh can be seen in a scene in the graphics window.
   - The edges of the square are boundaries. By clicking on each edge in the graphics window, a label with its name appears on the graphics window. The node corresponding to the selected edge (boundary) is also highlighted in the explorer pane, **Regions** → **Fluid** → **Boundaries**.

5. Setting Up the Physics Models

   - Expand the node **Continua**.
   - Edit the default continuum (**Physics 1**) including appropriate physical models for the simulation. Right-click the node **Physics 1** and then in the new window, click **Select models**:
     - In the left-bottom of the window **Physics 1 Model Selection**, untick the Auto-select recommended models. Choose the required models as:
     - Time box: Steady
     - Material box: Liquid
     - Flow box: Segregated flow
     - Equation of State box: Constant Density
     - Viscous Regime box: Turbulent
     - Turbulence box: Reynolds-Averaged Navier-Stokes*

- – Reynolds-Averaged Turbulence box: K-Epsilon Turbulence model
- – K-Epsilon Turbulence Models box: AKN K-Epsilon Low-Re
- – Choose desired sub-model(s) for the selected turbulence model in the K-Epsilon Damped Low Re Wall Treatment box: Low y+ Wall Treatment
- – Close the window **Physics 1 Model Selection**

- • Turning the color of the node **Physics 1**, from gray to blue, indicates that sufficient models have been activated.

- • Expand the node **Physics 1**, go to **Initial Conditions** → **Turbulence Specification**.

- • In the properties window, set the *Method* to be the same as the selected turbulence model.

- • Save the simulation.

6. Setting Fluid Properties

- • Go to the node **Continua** → **Physics 1** → **Models** → **Liquid** → **Water** → **Material Properties** → **Density** → **Constant** → *Value* = 998.29 kg/m^3.

- • Go to the node **Continua** → **Physics 1** → **Models** → **Liquid** → **Water** → **Material Properties** → **Dynamic Viscosity** → **Constant** → *Value* = 0.001003 $Pa - s$.

7. Importing Inlet and Measurement Data

- • Go to the node **Tools** → **Tables**.

- • Right click on **Tables** and select **New Table** → **File Table**.

- • In the *Open* window, navigate to the stored location and select all **.xy* files.

- • Click the **Open** button to import all data.

8. Setting Boundary Conditions and Values

- • Expand the node **Regions** and go to **Fluid** → **Boundaries**.

- • Inlet
  - – Click on the node **Inlet**. In the properties window, change the *Type* from `Wall` to `Velocity Inlet`.
  - – Expand the node **Inlet** and go to **Physics Conditions** → **Turbulence Specification**.
  - – In the properties window, set the *Method* to be the same as the selected turbulence model, e.g. `K+Epsilon`.
  - – Under the node **Inlet**, go to **Physics Conditions** → **Velocity Specification**.
  - – In the properties window, set the *Method* to be `Components`.
  - – In case of choosing `K+Epsilon` turbulence model, in the node **Inlet**, go to **Physics Values** and select **Turbulent Dissipation Rate**.
  - – In the properties window, set the *Method* to be `Table(x,y,z)`.
  - – **Table(x,y,z)** is created under **Turbulent Dissipation Rate**.

- Click on **Table(x,y,z)**. In the properties window, set the *Table* to be `inletProfile` and *Table:Data* to be `Epsilon`.
- In the node **Inlet**, go to **Physics Values** and select **Turbulent Kinetic Energy**.
- In the properties window, set the *Method* to be `Table(x,y,z)`.
- **Table(x,y,z)** is created under **Turbulent Kinetic Energy**.
- Click on **Table(x,y,z)**. In the properties window, set the *Table* to be `inletProfile.xy` and *Table:Data* to be `K`.
- In the node **Inlet**, go to **Physics Values** and select **Velocity**.
- In the properties window, set the *Method* to be `Table(x,y,z)`.
- **Table(x,y,z)** is created under **Velocity**.
- Click on **Table(x,y,z)**. In the properties window, set the *Table* to be `inletProfile.xy`. Similarly, set *Table: X-Data*, *Table: Y-Data* and *Table: Z-Data* to be `U`, `V` and `W`, respectively.

- Outlet
  - Click on the node **Outlet**. In the properties window, change the *Type* from `Wall` to `Pressure Outlet`.

- Save the simulation.

9. Setting the Solver Parameters and Stopping Criteria

- Solvers
  - Expand the node **Solvers** and keep the default settings.
  - To Extract more variables from the simulation (e.g., Kolmogorov Length Scale), expand the node related to the selected turbulence model (e.g., K-Epsilon Turbulence).
  - In the properties window, tick *Temporary Storage Retained*.
  - By enabling *Temporary Storage Retained*, additional scalar, vector and tensor variables are appeared in the node **Tools** → **Field Functions**.

- Stopping Criteria
  - Expand the node **Stopping Criteria** and select **Maximum Steps**.
  - In the properties window, set *Maximum Steps* to 2000.
  - Again, go to the node **Solvers** → **Steady** → **Stopping Criteria** → **Maximum Steps**. Check that in the properties window, the value of **Maximum Steps** must be greater than or equal to the value of **Maximum Steps** in the node **Stopping Criteria**.
  - Change *Logical Rule* to `And`.
  - A new stopping criterion may be also created as:
    (a) Right click on the node **Stopping Criteria** and select **New Monitor Criterion**.
    (b) In the Select Monitor window, Choose your interested Monitor(s) (e.g., X-Momentum) and press the **OK** button. A new sub-node, **X-Momentum Criterion** is created.
    (c) Go to **X-Momentum Criterion**. In the properties window, set *Criterion Option* to `Minimum` and change *Logical Rule* to `And`.

    (d) Go to **X-Momentum Criterion** → **Minimum Limit**. In the properties window, set *Minimum Value* equal to `1.0E-4`.

10. Initializing and Running the Simulation

    - Go to the menu bar and click **Solution** → **Initialize Solution**. Generally, you may specify initial conditions through the node **Continua** → **Physics 1** → **Initial Conditions**.

    - Again, go to the menu bar and click **Solution** → **Run** to execute the simulation.

    - After running, the Residuals plot is shown automatically in the graphics Window.

    - You may stop the simulation process (before the stopping criteria are satisfied) by clicking **Solution** → **Stop Iterating** in the menu bar. By clicking **Solution** → **Run**, the simulation will be run again.

11. Visualizing the Solution. This is optional. You can do all plotting in Python or Matlab/Octave (see Item 14)

    - Right click on the node **Scenes**, and select **New Scene** → **Scalar**.

    - A new sub-node **Scalar Scene 1** is created under the node **Scenes**.

    - Expand **Scalar Scene 1** and go to **Displayers** → **Scalar 1**.

    - Expand the sub-node **Scalar 1** and then click **Scalar Field**.

    - In the properties window in front of *Function*, click `<Select Function>` to open Scalar Field-Function window.

    - Scroll down, expand the node `Velocity` and select `Magnitude`.

12. Creating Parts (Plane, Line or Probe) to Extract Simulation Data

    - Right click on the node **Derived Parts** and select **New Part** → **Probe** → **Line**.

    - In Create Line Probe window, set the parameters as:

Property	Value
Input Parts	`[Fluid]`
Point 1	`[0.10, 0.0, 0.0]`
Point 2	`[0.10, 0.16, 0.0]`
Resolution	`200`
Display	`No Displayer`

    - Click on **Create** button and then **Close**.

    - In the node **Derived Parts**, a new sub-node, **Line Probe** is created.

    - Right-click on **Line Probe** and rename it to *x/h=2*.

    - *x/h=a* means the streamwise station at $x = h_{max}*a$ (h_{max}=50 mm). For instance, *x/h=2* indicates the streamwise station at *x=2*50 mm=0.1 m* (See the *Point 1* and *Point 2* in the above table).

    - Do the same procedure for other streamwise stations (same as the measurement locations), i.e. *xh1.xy, xh2.xy, ... and xh8.xy*.

13. Plotting Simulation Data.

- Right-click on the node **Plot** and select **New Plot** → **XY Plot**.
- In the node **Plot**, a new sub-node displayed as **XY Plot 1** is created.
- Rename it to *U@x/h=2*
- Set the parameters as:

Node			Property	Value
U@x/h=2			Parts	`[x/h=2]`
X Type			X-Axis	`Bottom Axis`
			Data Type	`Scalar`
	Scalar Function		Field Function	`Velocity[i]`
Y Types			——	——
	Y Type 1		Y-Axis	`Left Axis`
			Data Type	`Direction`
			Smooth Values	✓
	Vector Quantity		Value	`[0,1,0]`
		Line Style	Style	——
		Symbol Style	Shape	`○`

- To add the measurement data to compare with the simulation results, go to the node **Plots** → **U@x/h=2** → **Data Series**.
- Right-click on **Data Series** and then click **Add Data**.
- In the **Add Data Providers to Plot** window, select the measurement file corresponds to the location you have chosen for the simulation. As an example, we choose **xh2**.
- A new sub-node, **xh2** is created. Click on it.
- In the properties window, set *X Column*, *X-Axis*, *Y Column* and *Y-Axis* equal to U, `Bottom Axis`, y and `Left Axis`, respectively.
- You may change line and symbol style for the measurement plot different than the ones for simulation.
- To extract the plot data as a table (in *.csv format), right-click on the node **Plot** → **U@x/h=2** and then click **Export**.
- Choose an appropriate file name and storage location, then press Save button.

14. Extracting Simulation Field Data as Table for Python/Matlab/Octave

- Go to the node **Tools** → **Tables**.
- Right click on the node **New Table**, and select **XYZ Internal Table**.
- The sub-node **XYZ Internal Table** is created under the node **Table**.
- Set the parameters as the table below.

Node		Property	Value
XYZ Internal Table		Scalars	`Cell Index`
			`Velocity[i]`
			`Velocity[j]`
			`Pressure`
			`Turbulent Kinetic Energy`
			`Turbulent Dissipation Rate`
			`Turbulent Viscosity`
		Parts	`[Fluid]`
		Data on Vertices	
	Update	Enabled	✓
		Auto Extract	✓
		Trigger	`None`

- Right-click on **XYZ Internal Table**, then click on **Extract** and **Export...**, respectively.
- Specify an appropriate file name and storage location, then press Save button.

15. Loading data in Python/Matlab/Octave

- Use Python/Matlab/Octave to read the extracted data from STAR-CCM+.
- Download the experimental data from the course homepage.
- At the course homepage, you can download a file (`pl_vect`) which reads the simulation and experimental data and plot some results.
- Change the **open('output_standard-keps-low-re.csv')** in the Python script `pl_vect.py` or in the **fileName=sprintf('*.csv')** in the Matlab/Octave script (`pl_vect.m`) according to the name of *"csv"* file which you have generated from the STAR-CCM+ simulation.
- Make sure you put all files (extracted table in `*.csv` format from STAR-CCM+ and the measurement data in `*.xy` format), in the directory where you execute `pl_vect`.

Open Python or Matlab/Octave in an editor and execute `pl_vect`. There are six field variables, $\bar{v}_1$, $\bar{v}_2$, p, k, ϵ, and ν_t; the corresponding Python/Matlab/Octave arrays are `v1_2d`, `v2_2d`, `p_2d`, `k_2d`, `e_2d` and `mut_2d`, respectively. The grid is 200 × 202, i.e. $ni = 200$ cells in the x_1 direction and $nj = 202$ cells in the x_2 direction. The field variables are stored at the center of these cells. We denote the first index as i and the second index as j, i.e. `v1_2d(i,j)`.

Hence in Python

`v1_2d[:,0]` are the $\bar{v}_1$ values at the lower wall;
`v1_2d[:,nj-1]` or `v1_2d[:,-1]` are the $\bar{v}_1$ values at the upper wall;
`v1_2d[0,:]` are the $\bar{v}_1$ values at the inlet;
`v1_2d[ni-1,:]` or `v1_2d[-1,:]` are the $\bar{v}_1$ values at the outlet;

and in Matlab/Octave

`v1_2d(:,1)` are the $\bar{v}_1$ values at the lower wall;
`v1_2d(:,nj)` are the $\bar{v}_1$ values at the upper wall;
`v1_2d(1,:)` are the $\bar{v}_1$ values at the inlet;
`v1_2d(ni,:)` are the $\bar{v}_1$ values at the outlet;

F.3.1 Pressure

Execute the `pl_vect` file with Python/Matlab/Octave. It plots the contours of $\bar{v}_1$, the velocity vector field and the $\bar{v}_1$ profile along x_2 at $x_1 = 1$ comparing with experiments. As you can see, there is a large recirculation region where the flow goes backwards.

▶ Plot a contour plot of the pressure. Where is it high and low and why? (think of the Bernoulli equation, see Eq. 4.34)

The Bernoulli equation describes one-dimensional flow (inviscid, without friction). Let's compare the pressure from STAR-CCM+ and the Bernoulli equation. Since the 2D hill geometry is horizontal, then the gravity term does not contribute in the Bernoulli equation. Then you must make the velocity from STAR-CCM+ one-dimensional.

▶ Compute the bulk velocity (at each x_1 station)

$$V_b = \frac{1}{h(x_1)} \int_{x_{2,min}}^{x_{2,max}} \bar{v}_1 dx_2 \tag{F.1}$$

where $h(x_1) = x_{2,max} - x_{2,min}$ is the local height of the channel. Then compute the pressure from Bernoulli equation (Eq. 4.34). Compare it with the bulk STAR-CCM+ pressure computed similar to the bulk velocity in Eq. F.1. Compare the pressure drop from inlet to outlet for STAR-CCM+ and the Bernoulli equation. Why do they differ? How large is the pressure drop from the Bernoulli equation? How large should it be?
<u>hint:</u> the domain is symmetric in the x_1 direction.

How large is the pressure drop in terms of dynamic pressure, i.e. $\rho V_{b,inlet}^2/2$? How large is it compared to pipe flow pressure drop? In pipe flow, you may compute the friction factor (f_D) either from **Turbulent regime/Smooth-pipe regime** equation or from Figure 2. Then you can compute the pressure drop (Δp) from the first equation (Darcy-Weisbach equation) in pipe flow.

The pressure drop is usually an important engineering quantity. A large pressure drop means a large, expensive pump. You have used the AKN K-Epsilon turbulence model. How dependent are your results on the choice of turbulence model?

▶ Try some other turbulence models. Does the flow change a lot? And, more important, how much does the pressure drop change? This part is **optional**.

F.3.2 Skinfriction

The skinfriction, C_f, is an important concept in fluid dynamics. It is a non-dimensional wall shear stress which is defined as

$$C_f = \frac{\tau_w}{0.5\rho V_b^2} \tag{F.2}$$

where V_b is the bulk velocity (which is the same at all x_1 planes due to continuity). The bulk velocity at any x_1 plane is defined in Eq. F.1. The wall shear stress is defined in Eq. 6.16.

● We must first extract data for the bottom wall

- Go to the node **Tools** → **Tables**.

- Right-click on the node **New Table**, and select **XYZ Internal Table**.

- The sub-node **XYZ Internal Table** is created under the node **Table**.

- Set the parameters as the table below.

Node		Property	Value
XYZ Internal Table		Scalars	Ustar
			Wall Y+
			Wall Shear Stress Magnitude
		Parts	[Fluid Bottom]
		Data on Vertices	
	Update	Enabled	✓
		Auto Extract	✓
		Trigger	None

- Right-click on **XYZ Internal Table**, then click on **Extract** and **Export...**, respectively.

- Specify an appropriate file name and storage location, then press Save button.

Now create another **XYZ Internal Table** table for the top wall.

▶ First, load the two exported files from STAR-CCM+ (bottom and top wall). Then plot the skinfriction along the top and bottom walls.

F.3.3 Vorticity

In the first assignment you computed the vorticity in laminar flow. Now you will do it for turbulent flow. The velocity gradients are computed in pl_vect using the function dphidx_dy.

▶ Compute $\bar{\omega}_3$, see Eq. 1.12. Where is it largest? (cf. Fig 8.4). In the first assignment we could identify a region of inviscid flow (no vorticity). What about this case?

F.3.4 Turbulent viscosity

You have computed a turbulent flow with a turbulence model. We have said that the turbulent viscosity is much larger than the viscous one.

▶ Plot the ratio μ_t/μ as a contour plot. What is the maximum turbulent viscosity? Where?

• When you use another turbulence model, does the maximum value change? This part is **optional**.

• Plot μ_t/μ versus x_2 also as x-y graphs at a couple of x_1 stations. Plot μ_t/μ also versus $x_2^+ = u_\tau x_2/\nu$ for the bottom wall (you have exported u_τ (Ustar) at the bottom wall in Section F.3.2). Please note that in $x_2^+ = u_\tau x_2/\nu$, x_2 is the wall distance. Zoom also in near the wall. Does the turbulent viscosity go to zero at the wall as it should?

F.3.5 Diffusion

You have computed a turbulent flow with a turbulence model. You have learnt – hopefully – that the turbulent diffusion in channel flow is much larger than the usual physical (viscous) diffusion (except very close to the wall), see Fig. 6.6. Channel flow is essentially two attached boundary layer whereas the hill flow includes recirculation regions.

▶ Compute the viscous and turbulent diffusion terms in the $\bar{v}_1$ equation (see the expression for both viscous and turbulent diffusions in Eq. 11.31). Plot them in x-y graphs at a couple of x_1 stations (choose one x_1 station at the top of a hill). Plot them also versus x_2^+ for the bottom wall. Compare with Fig. 6.6. Do you see the same behaviour as in in channel flow?
<u>Hint:</u> Use the function dphidx_dy when computing the derivative of $\partial \bar{v}_1/\partial x_2$ and $\mu_t \partial \bar{v}_1/\partial x_2$.

F.3.6 Production

The production term, P^k, in the k equation is usually a large term (see Figs. 8.3 and 11.6). When a source is large, it usually also means that the variable in question is large (see Section 9.1), i.e. when P^k is large so is k. If this is not the case, it means simply that other terms are larger. Now let's see how strong the relation between k and P^k is.

▶ Plot k and P^k as contour plots. (The k exists in the *csv* file extracted from your STAR-CCM+ simulation. You only need to compute P^k according to Eq. 11.39). Is there any strong relation?

The turbulent viscosity is computed as $\mu_t = \rho C_\mu k^2/\varepsilon$. There is a fair chance that μ_t is large where P^k is large.

▶ Plot μ_t as a contour plot. Is there any strong relation between μ_t and P^k?

F.3.7 Wall boundary conditions for ε

The wall boundary conditions for ε are discussed in Section 11.14.5. The boundary condition for the turbulent kinetic energy is simply $k = 0$. The boundary condition for ε is given by Eq. 11.170 which means that ε is set to that value at the wall-adjacent cells. Please note that x_2^+ in Eq. 11.170 is the wall distance and k is the value at the wall-adjacent cells.

▶ Compare ε from STAR-CCM+ at the wall-adjacent cells with Eq. 11.170 (both upper and lower wall). Do they agree?

F.3.8 Near-wall behaviour of f_μ

In Section 11.14.3 we show that the f_μ damping function near the wall actually must be an augmentation function, see Eq. 11.159. The f_μ damping function in the AKN model reads (see Eq. 1798 in Section *Damping Functions* in the STAR-CCM+ User guide)

$$f_\mu = \left[1 - \exp\left(-\frac{x_2^*}{14}\right)\right]^2 \left\{1 + \frac{5}{R_t^{3/4}}\exp\left[-\left(\frac{R_t}{200}\right)^2\right]\right\} \tag{F.3}$$

where $R_t = k^2/(\nu\varepsilon)$ and $x_2^* = (\varepsilon\nu)^{1/4}x_2/\nu$. Show mathematically that $f_\mu = \mathcal{O}(x_2^{-1})$.
<u>Hint:</u> Taylor expansion gives $1 - \exp(-x) = x - x^2 \dots$

F.3.9   Compare with experiments

The measurement data at seven x_1 locations can be download from the course home-page. Each file consists of seven columns that are x_2, $\bar{v}_1$, $\bar{v}_2$, $\overline{v_1'^2}$, $\overline{v_2'^2}$, $\overline{v_1'v_2'}$ and x_3, respectively. Since it is a 2D case, the x_3 values are zero. The predicted $\bar{v}_1$ velocity is compared with experiments at $x_1 = h_{max}$ ($xh1.xy$) in `pl_vect`.

▶ Compare $\bar{v}_1$ with experiment and the other six locations.

The agreement between predictions and experiments is not good. The main reason is that you are simulating the flow over only one hill. The inlet boundary conditions are taken from another CFD simulation of an infinite long channel (periodic boundary conditions were used).

In the experiments they use ten hills. The object is to achieve a periodic flow where the time-averaged flow is identical between two hills. In the CFD simulations one can then use *periodic* boundary conditions.

▶ Change the boundary conditions at the inlet and outlet boundaries to *periodic* boundary conditions. Compare the $\bar{v}_1$ velocities with experiments. This part is **optional**.

- Change **Inlet-Outlet** boundary conditions to **Periodic** boundary conditions

    – Expand **Regions/Fluid/Boundaries**

    – Press Ctrl key and choose **Inlet** and **Outlet**. Right-click and select **Create Interface**

    – You have now created an interface and need to change type and topology

    – Expand **Interface**

    – Right-click on **Interface 1** and select **Edit**

    – Change **Type** to **Fully-Developed Interface**

    – Change **Topology** to **Periodic**

    – Expand **Interface 1/Physics Condition** and click on **Fully Developed Condition** and select **Mass Flow Rate**

    – Expand **Interface 1/Physics Values** and click on **Mass Flow Rate** and set an appropriate value. To get the mass flow rate you can integrate the inlet velocity profile in `pl_vect`.

G TME226 Assignment 2: turbulent flow (2017)

IN this exercise you will use data from a Direct Numerical Simulation (DNS) for fully developed channel flow. In DNS the unsteady, three-dimensional Navier-Stokes equations are solved numerically. The Re number based on the friction velocity and the half channel width is $Re_\tau = u_\tau h/\nu = 500$ ($h = \rho = u_\tau = 1$ so that $\nu = 1/Re_\tau$).

A $96 \times 96 \times 96$ mesh has been used. The streamwise, wall-normal and spanwise directions are denoted by x (x_1), y (x_2) and z (x_3) respectively. The cell size in x and z directions are $\Delta x = 0.0654$ and $\Delta z = 0.0164$. Periodic boundary conditions were applied in the x and z direction (homogeneous directions). All data have been made non-dimensional by u_τ and ρ.

You can do the assignment on your own or in a group of two. You should write a report where you analyze the results following the headings G.1–G.12. It is recommended (but the not required) that you use LATEX (an example of how to write in LATEXis available on the course www page). You can download LATEX at here.

G.1 Time history

At the course home page `http://www.tfd.chalmers.se/~lada/MoF/` you find a file `u_v_time_4nodes.dat` with the time history of v_1 and v_2. The file has eight columns of v_1 and v_2 at four nodes: $x_2/h = 0.0039$, $x_2/h = 0.0176$, $x_2/h = 0.107$ and $x_2/h = 0.47$. With $u_\tau = 1$ and $\nu = 1/Re_\tau = 1/500$ this correspond to $x_2^+ = 1.95$, $x_2^+ = 8.8$, $x_2^+ = 53.5$ and $x_2^+ = 235$. The sampling time step is $\Delta t = 0.0033$ (every second time step). The four points are located in the viscous sublayer, the buffer layer and in the logarithmic layer, see Fig. 6.2 at p. 83.

Use Matlab. You can also use Octave. Octave is a Matlab clone which can be downloaded for free here both on Linux and Windows. Start the program `pl_time.m` which loads and plots the time history of v_1. Start Matlab and run the program `pl_time`. Recall that the velocities have been scaled with the friction velocity u_τ, and thus what you see is really v_1/u_τ. The time history of v_1 at $x_2/h = 0.0176$ and $x_2/h = 0.107$ are shown. Study the time history of the blue line ($x_2/h = 0.0176$) more in detail. Make a zoom between, for example, $t = 10$ and $t = 11$ and $v_{1,min} = 3$ and $v_{1,min} = 21$. This is conveniently done with the command

```
axis([10 11 3 21])
```

In order to see the value at each sampling time step, change the plot command to

```
plot(t,u2,'b-',t,u2,'bo')
```

Use this technique to zoom, to look at the details of the time history. Alternatively, you can use the zoom buttons above the figure.

Plot v_1 for all four nodes. How does the time variation of v_1 vary for different positions? Plot also v_2 at the four different positions. What is the differences between v_1 and v_2?

G.2 Time averaging

Compute the average of the v_1 velocity at node 2. Add the following code (before the plotting section)

```
umean=mean(u2)
```

Here the number of samples is $n = 5000$ (the entire `u2` array). Find out how many samples must be used to get a correct mean value. Start by trying with 100 samples as

```
umean_100=mean(u2(1:100))
```

What is the maximum and minimum value of v_1? Compare those to the mean.

Do the same exercise for the other three nodes.

Compute and plot also the instantaneous fluctuations; v_1' at node 1, for example, is computed as

```
u1_mean=mean(u1);
u1_fluct=u1-u1_mean;
```

G.3 Mean flow

All data in the data files below have been stored every $10th$ time step.

Download the file `uvw_inst_small.mat`, `y.dat` and the Matlab file `pl_vel.m` which reads the data files. The data file includes v_1, v_2 and v_3 from the same DNS as above, but now you are given the time history of all x_2 nodes at one chosen x_1 and x_3 node. There are $nj = 98$ nodes in the x_2 direction; node 1 and nj are located at the lower and upper wall, respectively.

Your data are instantaneous. Compute the mean velocity. Plot it both as linear-linear plot and a log-linear plot (cf. Fig. 6.4).

In the log-linear plot, use x_2^+ for the wall distance. Include the linear law, $v_1^+ = x_2^+$, and the log law, $v_1^+ = \kappa^{-1} \ln x_2^+ + B$ ($\kappa = 0.41$ is the von Kármán constant and $B = 5.2$). How far out from the wall does the velocity profile follow the linear law? At what x_2^+ does it start to follow the log-law?

Compute the bulk velocity

$$V_{1,b} = \frac{1}{2h} \int_0^{2h} \bar{v}_1 dx_2 \tag{G.1}$$

(recall that h denote half the channel width) What is the Reynolds number based on $V_{1,b}$ and centerline velocity, $V_{1,c}$, respectively?

G.4 The time-averaged momentum equation

Let us time average the streamwise momentum equation. Since the flow is fully developed and two dimensional we get

$$0 = -\frac{1}{\rho}\frac{\partial \bar{p}}{\partial x_1} + \nu \frac{\partial^2 \bar{v}_1}{\partial x_2^2} - \frac{\partial \overline{v_1' v_2'}}{\partial x_2} \tag{G.2}$$

This equation is very similar to fully developed laminar flow, see Eq. 3.24; the difference is that we now have an additional term which is the derivative of the Reynolds shear stress. Recall that all terms in the equation above represent *forces* (per unit mass). Let us investigate how these forces (the pressure gradient, the viscous term and the Reynolds stress term) affect fluid particles located at different x_2 locations. Compute and plot the three terms. (the file `uvw_inst_small.mat` does not include $\bar{p}$; set $\partial \bar{p}/\partial x = -1$.)

y(j+1)

n

yc(j)

y(j)

Δx_2

yc(j-1)

s

y(j-1)
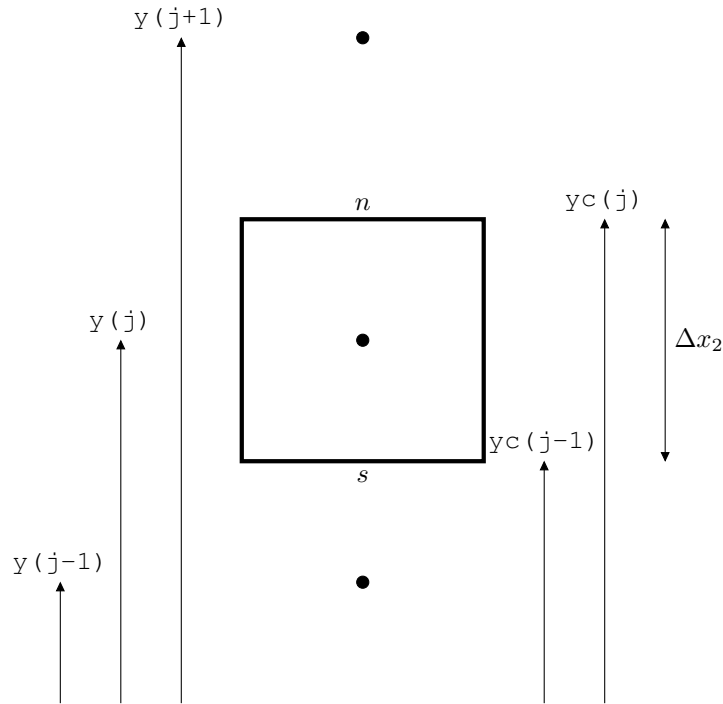
Figure G.1: Control volume. Its south (s) and north (n) faces are located at `yc(j-1)` and `yc(j)`, respectively. The cell center, marked by a black bullet, is located at `y(j)`.

If a term is positive it means that it pushes the fluid particle in the positive x_1 direction. What about the viscous term? Is it always negative? Where is it largest? At that point? Which term balances it? How large is the third term? The pressure term should be a *driving* force. Where is the Reynolds shear stress positive and where is it negative?

G.5 The gradient

In Section G.4 you needed to compute the gradient of the velocities, e.g. $\partial \bar{v}_1 / \partial x_2$. Presumably, you used the Matlab command

```
dudy=gradient(u1d,y);
```

Now you should compute $\partial \bar{v}_1 / \partial x_2$ yourself, i.e. without using the Matlab command `gradient`. Make a `for` loop and compute $\partial \bar{v}_1 / \partial x_2$ as $\Delta \bar{v}_1 / \Delta x_2$. Recall that the grid is non-equidistant, i.e. Δx_2 is not constant, see Fig. G.1. Make sure that your $\partial \bar{v}_1 / \partial x_2$ gives exactly the same values as the Matlab command `gradient`, also at the boundaries ($j = 1$ and $j = nj$).

Hint: compute first the face values of $\bar{v}_1$ ($\bar{v}_{1,n}$ and $\bar{v}_{1,s}$) using linear interpolations (you cannot use weight factors of 0.5 since Δx_2 is not constant). Then compute $\Delta \bar{v}_1 / \Delta x_2$ as $(\bar{v}_{1,n} - \bar{v}_{1,s})/(x_{2,n} - x_{2,s})$ where subscript n and s denote north and south, respectively. Recall that the variable `yc` in `pl_vel.m` denotes x_2 at the faces.

Compute also the second derivate, $\partial^2 \bar{v}_1 / \partial x_2^2$, without using the Matlab command `gradient`. Compare this result with what you get with the `gradient`, i.e.

```
dudy=gradient(u1d,y);
d2udy2=gradient(dudy,y);
```

Hint: compute first the face values of $\partial \bar{v}_1/\partial x_2$.

G.6 Wall shear stress

Compute the wall shear stress at both walls. They should be equal. Are they?

G.7 Resolved stresses

In Section G.3 you computed the mean velocities. From the instantaneous and the mean velocity, you can compute the fluctuations as

$$v_i' = v_i - \bar{v}_i \tag{G.3}$$

Now you can easily compute all stresses $\overline{v_i' v_j'}$. Plot the normal stresses in one figure and the shear stresses in one figure (plot the stresses over the entire channel, i.e. from $x_2 = 0$ to $x_2 = 2h$). Which shear stresses are zero?

G.8 Fluctuating wall shear stress

In the same way as the velocity, the wall shear stress can be decomposed into a mean value and a fluctuation, i.e.

$$\tau_{w,inst} = \mu \frac{\partial v_1}{\partial x_2}, \quad \tau_w = \mu \frac{\partial \bar{v}_1}{\partial x_2} \tag{G.4}$$

where the first expression is the instantanous wall shear stress and the second is the time-averaged. In general, any fluctuating variable, ϕ, can be decomposed into a mean and fluctuation as $\phi = \bar{\phi} + \phi'$. The root-mean-square (RMS) is then defined as

$$\phi_{rms} = \left(\overline{\phi'^2}\right)^{1/2} \tag{G.5}$$

Compute the RMS of the wall shear stress. This is a measure of the fluctuating tangential force on the wall due to turbulence. If heat transfer is involved, the fluctuating temperature at the wall inducing fluctuating heat transfer may be damaging to the material of the walls causing material fatigue. This is probably the most common form of fluid-solid interaction.

G.9 Production terms

In order to understand why a stress is large, it is useful to look at its transport equation, see Eq. 9.12. Usually, a stress is large when its production term, P_{ij}, is large (there may be exceptions when other terms, such as the diffusion term, are largest). Plot the production terms for all non-zero stresses across the entire channel. Which ones are zero (or close to)? Does any production term change sign at the centerline? If so, what about the sign of the corresponding shear stress plotted in Section G.7?

G.10 Pressure-strain terms

The pressure-strain term reads (see Eq. 9.14)

$$\Pi_{ij} = \overline{\frac{p'}{\rho} \left(\frac{\partial v_i'}{\partial x_j} + \frac{\partial v_j'}{\partial x_i} \right)} \tag{G.6}$$

Our data are obtained from incompressible simulations, in which the pressure may vary unphysically in time ($\partial p / \partial t$ does not appear in the equations). Hence, we prefer to compute the velocity-pressure as gradient term

$$\Pi_{ij}^p = -\overline{\frac{v_i'}{\rho} \frac{\partial p'}{\partial x_j}} - \overline{\frac{v_j'}{\rho} \frac{\partial p'}{\partial x_i}}, \tag{G.7}$$

see the second line in Eq. 9.3. The pressure diffusion term in the $\overline{v_2'^2}$ equation – which is the difference between Eqs. G.6 and G.7 (the two first terms in Eq. 9.8) – is small except very close to the wall (see Figs. 9.4 and 9.6). Hence, the difference between Π_{ij}^p and Π_{ij} is small.

Download the data file p_inst_small.mat and the Matlab file pl_press_strain.m which reads the data file. The time histories of the pressure along five x_2 lines [(x_1, x_2, x_3), $(x_1 \pm \Delta x_1, x_2, x_3)$ and $(x_1, x_2, x_3 \pm \Delta x_3)$] are stored in this file. This allows you to compute all the three spatial derivatives of p'. Using the velocities stored in uvw_inst_small.mat (see Section G.3), you can compute all the terms in Eq. G.7.

Plot the pressure strain, Π_{ij}^p, for the three normal stresses and the shear stress across the channel. For which stresses is it negative and positive? Why?

Which term Π_{ij}^p is the largest source and sink term, respectively?

G.11 Dissipation

The physical meaning of dissipation, ε, is transformation of turbulent kinetic energy into internal energy, i.e. increased temperature.

Download the files y_half.dat, diss_inst.mat and the Matlab file pl_diss.m which reads it. The data file includes the time history of the velocities along five x_2 lines [(x_1, x_2, x_3), $(x_1 \pm \Delta x_1, x_2, x_3)$ and $(x_1, x_2, x_3 \pm \Delta x_3)$] so that you can compute all spatial derivatives. The data cover only the lower half of the channel. Compute and plot

$$\varepsilon = \nu \overline{\frac{\partial v_i'}{\partial x_k} \frac{\partial v_i'}{\partial x_k}} \tag{G.8}$$

see Eq. 8.14. Where is it largest? In which equation does this quantity appear?

Let us now consider the equations for the mean kinetic energy, $K = \bar{v}_i \bar{v}_i / 2$ (Eq. 8.36) and turbulent kinetic energy, $k = \overline{v_i' v_i'}/2$ (Eq. 8.14). The dissipation in the K equation reads

$$\varepsilon_{mean} = \nu \frac{\partial \bar{v}_i}{\partial x_k} \frac{\partial \bar{v}_i}{\partial x_k} \tag{G.9}$$

The flow of kinetic energy between K, k and ΔT is illustrated in Fig. 8.6 The dissipations, ε and ε_{mean}, are defined in Eqs. G.8 and G.9, respectively. Compute and plot also ε_{mean} and P^k. Which is large and which is small? How is the major part of the kinetic energy transformed from K to ΔT? Is it transformed via k or directly from K to ΔT?

G.12   Do something fun!

You have been provided with a lot of data which you have analyzed in many ways. Now think of some other way to analyze the data. There are many interesting things yet to be analyzed!
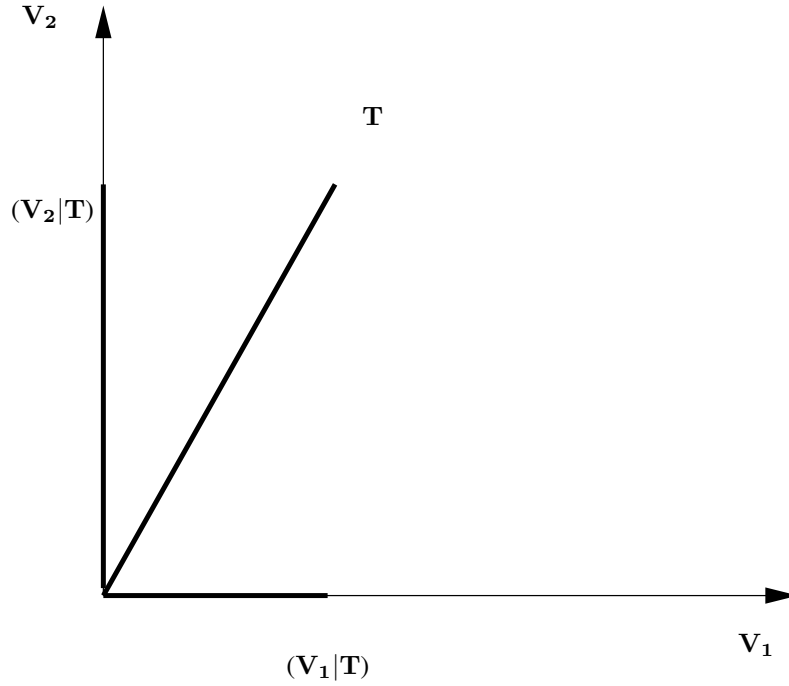
Figure H.1: Scalar product.

H TME226: Fourier series

Hᴇʀᴇ a brief introduction to Fourier series extracted from [199] is given.

H.1 Orthogonal functions

Consider three vectors, $\mathbf{V_1}$, $\mathbf{V_2}$, $\mathbf{V_3}$, in physical space which form an orthogonal base in $\mathbf{R}^3$ (i.e. their scalar products are zero). Let us call them *basis functions*. Any vector, $\mathbf{T}$, in $\mathbf{R}^3$ can now be expressed in these three vectors, i.e.

$$\mathbf{T} = c_1\mathbf{V}_1 + c_2\mathbf{V}_2 + c_3\mathbf{V}_3 \tag{H.1}$$

see Fig. H.1. Now define the scalar product of two vectors, $\mathbf{a}$ and $\mathbf{b}$, as $\mathbf{a} \cdot \mathbf{b} = (\mathbf{a}|\mathbf{b})$. The coordinates, c_i, can be determined by making a scalar product of Eq. H.1 and $\mathbf{V_i}$ which gives

$$\begin{aligned}(\mathbf{T}|\mathbf{V}_i) &= (c_1\mathbf{V}_1|\mathbf{V}_i) + (c_2\mathbf{V}_2|\mathbf{V}_i) + (c_3\mathbf{V}_3|\mathbf{V}_i) \\ &= (c_1\mathbf{V}_1|\mathbf{V}_1) + (c_2\mathbf{V}_2|\mathbf{V}_2) + (c_3\mathbf{V}_3|\mathbf{V}_3) \\ &= c_1|\mathbf{V}_1|^2 + c_2|\mathbf{V}_2|^2 + c_3|\mathbf{V}_3|^2 = c_i|\mathbf{V}_i|^2\end{aligned} \tag{H.2}$$

where $|\mathbf{V}_i|$ denotes the length of $\mathbf{V}_i$; the second line follows because of the orthogonality of $\mathbf{V}_i$. Hence the coordinates, c_i, are determined by

$$c_i = (\mathbf{T}|\mathbf{V}_i)/|\mathbf{V}_i|^2 \tag{H.3}$$

Now let us define an infinite (∞-dimensional) functional space, $\mathbf{B}$, with orthogonal basis functions $\{g\}_1^\infty$. The "scalar product" of two functions, f and g_n, is defined as

$$(f|g_n) = \int_a^b f(x)g_n(x)dx \tag{H.4}$$

Then, in a similar way to Eq. H.1, any function can, over the interval $[a, b]$, be expressed as

$$f = \sum_{n=1}^\infty c_n g_n \tag{H.5}$$

As above, we must now find the "coordinates", c_n (cf. the coordinates, c_i, in Eq. H.1). Multiply, as in Eq. H.2, f with the basis functions, g_i, i.e.

$$(f|g_i) = \sum_{n=1}^\infty c_n(g_n|g_i) \tag{H.6}$$

Since we know that all g_n are orthogonal, Eq. H.6 is non-zero only if $i = n$, i.e.

$$\begin{aligned}(f|g_i) &= (c_1 g_1|g_i) + (c_2 g_2|g_i) \ldots c_i(g_i|g_i) \ldots c_{i+1}(g_{i+1}|g_i) \ldots = \\ &= c_i(g_i|g_i) = c_i||g_i||^2\end{aligned} \tag{H.7}$$

Similar to Eq. H.3, the "coordinates" can be found from (switch from index i to n)

$$c_n = (f|g_n)/||g_n||^2 \tag{H.8}$$

The "coordinates", c_n, are called the *Fourier* coefficients to f in system $\{g\}_1^\infty$ and $||g_n||$ is the "length" of g_n (cf. $|\mathbf{V}_i|$ which is the length of $\mathbf{V}_i$ in Eq. H.3), i.e.

$$||g_n|| = (g_n|g_n)^{1/2} = \left(\int_a^b g_n(x)g_n(x)dx\right)^{1/2} \tag{H.9}$$

Let us now summarize and compare the basis functions in physical space and the basis functions in functional space.

1. Any vector in $\mathbf{R}^3$ can be expressed in the orthogonal basis vectors $\mathbf{V}_i$

2. The length of the basis vector, $\mathbf{V}_i$, is $|\mathbf{V}_i|$

3. The coordinates of $\mathbf{V}_i$ are computed as $c_i = (\mathbf{T}|\mathbf{V}_i)/|\mathbf{V}_i|^2$

1. Any function in $[a, b]$ can be expressed in the orthogonal basis functions g_n

2. The length of the basis function, g_n, is $||g_n||$

3. The coordinates of g_n are computed as $c_n = (f|g_n)/||g_n||^2$

H.2 Trigonometric functions

Here we choose g_n as trigonometric functions which are periodic in $[-\pi, \pi]$. The question is now how to choose the orthogonal function system $\{g\}_1^\infty$ on the interval $[-\pi, \pi]$. In mathematics, we usually start by doing an intelligent "guess", and then we prove that it is correct. So let us "guess" that the trigonometric series

$$[1, \sin x, \cos x, \sin(2x), \ldots, \sin(nx), \cos(nx), \ldots] \tag{H.10}$$

is an orthogonal system. The function system in Eq. H.10 can be defined as

$$g_n(x) = \begin{cases} \phi_k(x), & \text{for } n = 2k = 2, 4, \ldots \\ \psi_k(x), & \text{for } n = 2k+1 = 1, 3, \ldots \end{cases} \tag{H.11}$$

where $\phi_k(x) = \sin(kx)$ ($k = 1, 2, \ldots$) and $\psi_k(x) = \cos(kx)$ ($k = 0, 1, \ldots$). Now we need to show that they are orthogonal, i.e. that the integral of the product of any two functions ϕ_k and ψ_k is zero on $\mathbf{B}[-\pi, \pi]$ and we need to compute their "length" (i.e. their norm).

Orthogonality of ψ_n and ψ_k

$$
\begin{aligned}
(\psi_n|\psi_k) &= \int_{-\pi}^{\pi} \cos(nx)\cos(kx)dx = \frac{1}{2}\int_{-\pi}^{\pi} \left[\cos((n+k)x) + \cos((n-k)x)\right] dx \\
&= \frac{1}{2}\left[\frac{1}{n+k}\sin((n+k)x) + \frac{1}{n-k}\sin((n-k)x)\right]_{-\pi}^{\pi} = 0 \ \text{ for } \ k \neq n
\end{aligned}
\tag{H.12}
$$

H.2.1 "Length" of ψ_k

$$
(\psi_k|\psi_k) = ||\psi_k||^2 = \int_{-\pi}^{\pi} \cos^2(kx)dx = \left[\frac{x}{2} + \frac{1}{4k}\sin(2kx)\right]_{-\pi}^{\pi} = \pi \ \text{ for } \ k > 0
$$

$$
(\psi_0|\psi_0) = ||\psi_0||^2 = \int_{-\pi}^{\pi} 1 \cdot dx = 2\pi
$$

$$\tag{H.13}$$

H.2.2 Orthogonality of ϕ_n and ψ_k

$$
\begin{aligned}
(\phi_n|\psi_k) &= \int_{-\pi}^{\pi} \sin(nx)\cos(kx)dx = \frac{1}{2}\int_{-\pi}^{\pi} \left[\sin((n+k)x) + \sin((n-k)x)\right] dx \\
&= -\frac{1}{2}\left[\frac{1}{n+k}\cos((n+k)x) + \frac{1}{n-k}\cos((n-k)x)\right]_{-\pi}^{\pi} = 0
\end{aligned}
\tag{H.14}
$$

because $\cos((n+k)\pi) = \cos(-(n+k)\pi)$ and $\cos((n-k)\pi) = \cos(-(n-k)\pi)$.

H.2.3 Orthogonality of ϕ_n and ϕ_k

$$
\begin{aligned}
(\phi_n|\phi_k) &= \int_{-\pi}^{\pi} \sin(nx)\sin(kx)dx = \frac{1}{2}\int_{-\pi}^{\pi} \left[\cos((n-k)x) - \cos((n+k)x)\right] dx \\
&= \frac{1}{2}\left[\frac{1}{n-k}\sin((n-k)x) - \frac{1}{n+k}\sin((n+k)x)\right]_{-\pi}^{\pi} = 0 \ \text{ for } \ k \neq n
\end{aligned}
\tag{H.15}
$$

H.2.4 "Length" of ϕ_k

$$
(\phi_k|\phi_k) = ||\phi_k||^2 = \int_{-\pi}^{\pi} \sin^2(kx)dx = \left[\frac{x}{2} - \frac{1}{4k}\sin(2kx)\right]_{-\pi}^{\pi} = \pi \ \text{ for } \ k \geq 1
$$

$$\tag{H.16}$$

H.3 Fourier series of a function

Now that we have proved that $\{g\}_1^\infty$ in Eq. H.11 forms an orthogonal system of functions, we know that we can express any periodic function, f (with a period of 2π) in $\{g\}_1^\infty$ as

$$f(x) = c + \sum_{n=1}^{\infty}(a_n \cos(nx) + b_n \sin(nx)) \tag{H.17}$$

where x is a spatial coordinate. The Fourier coeffients are given by

$$b_n = (f|\phi_n)/||\phi_n||^2 = \frac{1}{\pi}\int_{-\pi}^{\pi} f(x)\sin(nx)dx \tag{H.18a}$$

$$a_n = (f|\psi_n)/||\psi_n||^2 = \frac{1}{\pi}\int_{-\pi}^{\pi} f(x)\cos(nx)dx \tag{H.18b}$$

$$c = (f|\psi_0)/||\psi_0||^2 = \frac{1}{2\pi}\int_{-\pi}^{\pi} f(x)dx \tag{H.18c}$$

where $n > 0$. If we set $c = a_0/2$, then a_0 is obtained from Eq. H.18b, i.e.

$$f(x) = \frac{a_0}{2} + \sum_{n=1}^{\infty}(a_n \cos(nx) + b_n \sin(nx)) \tag{H.19a}$$

$$b_n = (f|\phi_n)/||\phi_n||^2 = \frac{1}{\pi}\int_{-\pi}^{\pi} f(x)\sin(nx)dx \tag{H.19b}$$

$$a_n = (f|\psi_n)/||\psi_n||^2 = \frac{1}{\pi}\int_{-\pi}^{\pi} f(x)\cos(nx)dx \tag{H.19c}$$

Note that $a_0/2$ corresponds to the average of f. Taking the average of f (i.e. integrating f from $-\pi$ to π) and dividing with the integration length, 2π, gives (see Eq. H.19a)

$$\bar{f} = \frac{1}{2\pi}\int_{-\pi}^{\pi} f(x)dx = \frac{1}{2\pi}\frac{a_0}{2}\cdot 2\pi = \frac{a_0}{2} \tag{H.20}$$

Hence, if $\bar{f} = 0$ then $a_0 = 0$.

H.4 Derivation of Parseval's formula

Parseval's formula reads

$$\int_{-\pi}^{\pi}(f(x))^2 dx = \frac{\pi}{2}a_0^2 + \pi\sum_{n=1}^{\infty}(a_n^2 + b_n^2) \tag{H.21}$$

We will try to prove this formula. Assume that we want to approximate the function f as well as possible with an orthogonal series

$$\sum_{n=1}^{\infty} a_n g_n \tag{H.22}$$

Now we want to prove that the Fourier coefficients are the best choice to minimize the difference

$$||f - \sum_{n=1}^{N} a_n g_n|| \tag{H.23}$$

Later we will let $N \to \infty$. Using the definition of the norm and the laws of scalar product we can write

$$||f - \sum_{n=1}^{N} a_n g_n||^2 = \left(f - \sum_{n=1}^{N} a_n g_n \middle| f - \sum_{k=1}^{N} a_k g_k \right)$$

$$= (f|f) - \sum_{n=1}^{N} a_n (f|g_n) - \sum_{k=1}^{N} a_k (f|g_k) + \sum_{n=1}^{N} \sum_{k=1}^{N} a_n a_k (g_n|g_k) = \qquad \text{(H.24)}$$

$$= (f|f) - 2\sum_{n=1}^{N} a_n (f|g_n) + \sum_{n=1}^{N} a_n^2 (g_n|g_n)$$

because of the orthogonality of the function system, $\{g\}_1^N$. Expressing f in the second term using the Fourier coefficients c_n (see Eqs. H.5 and H.8) gives

$$(f|f) - 2\sum_{n=1}^{N} a_n c_n (g_n|g_n) + \sum_{n=1}^{N} a_n^2 (g_n|g_n)$$

$$= ||f||^2 + \sum_{n=1}^{N} ||g_n||^2 \left(a_n^2 - 2a_n c_n \right) \qquad \text{(H.25)}$$

$$= ||f||^2 + \sum_{n=1}^{N} ||g_n||^2 \left(a_n - c_n \right)^2 - \sum_{n=1}^{N} ||g_n||^2 c_n^2$$

The left side of Eq. H.24 is thus minimized if the coefficients a_n are chosen as the Fourier coefficients, c_n so that

$$||f - \sum_{n=1}^{N} a_n g_n||^2 = ||f||^2 - \sum_{n=1}^{N} ||g_n||^2 c_n^2 \qquad \text{(H.26)}$$

The left side must always be positive and hence

$$\sum_{n=1}^{N} ||g_n||^2 c_n^2 \leq ||f||^2 = \int_{-\pi}^{\pi} (f(x))^2 dx \quad \text{for all } N \qquad \text{(H.27)}$$

As N is made larger, the magnitude of the left side increases, and its magnitude gets closer and closer to that of the right side, but it will always stay smaller than $||f||^2$. This means that the series on the left side is *convergent*. Using the Fourier coefficients in Eq. H.19 and letting $N \to \infty$ it can be shown that we get equality of the left and right side, which gives Parseval's formula,

$$||f||^2 \equiv \int_{-\pi}^{\pi} (f(x))^2 dx = \sum_{n=1}^{N} ||g_n||^2 c_n^2 = ||\psi_0|| \left(\frac{a_0^2}{2} \right) + \sum_{n=1}^{N} ||\psi_n|| a_n^2 + ||\phi_n|| b_n^2$$

$$= 2\pi \left(\frac{a_0^2}{2} \right) + \pi \sum_{n=1}^{N} a_n^2 + b_n^2 = \frac{\pi}{2} a_0^2 + \pi \sum_{n=1}^{\infty} (a_n^2 + b_n^2)$$

Note that 2π and π on the second line are the "length" of $||g_n||$, i.e. the length of $||\psi_0||$, $||\psi_n||$ and $||\phi_n||$ (see Sections H.2.1 and H.2.4).

Appendix R describes in detail how to create energy spectra from two-point correlations.

H.5   Complex Fourier series

Equation H.19 gives the Fourier series of a real function. It is more convenient to express a Fourier series in complex variables even if the function f itself is real. On complex form it reads

$$f(x) = \sum_{n=-\infty}^{\infty} c_n \exp(\imath nx)) \tag{H.28a}$$

$$c_n = \frac{1}{2\pi} \int_{-\pi}^{\pi} f(x)\exp(-\imath nx)dx \tag{H.28b}$$

where the Fourier coefficients, c_n, are complex. Below we verify that if f is real, then Eq. H.28 is equivalent to Eq. H.19. The Fourier coefficients, c_n, read – assuming that f is real – according to Eq. H.28

$$c_n = \frac{1}{2\pi} \int_{-\pi}^{\pi} f(x)(\cos(nx) - \imath \sin(nx))dx = \frac{1}{2}(a_n - \imath b_n), \quad n > 0 \tag{H.29}$$

where a_n and b_n are given by Eq. H.19. For negative n in Eq. H.28 we get

$$c_{-n} = c_n^* = \frac{1}{2\pi} \int_{-\pi}^{\pi} f(x)(\cos(nx) + \imath \sin(nx))dx = \frac{1}{2}(a_n + \imath b_n), \quad n > 0 \tag{H.30}$$

where c_n^* denotes the complex conjugate. For $n = 0$, Eq. H.28 reads

$$c_0 = \frac{1}{2\pi} \int_{-\pi}^{\pi} f(x)dx = \frac{1}{2}a_0 \tag{H.31}$$

see Eq. H.19. Inserting Eqs. H.29, H.30 and H.31 into Eq. H.28 gives

$$f(x) = \frac{1}{2}a_0 + \frac{1}{2}\sum_{n=1}^{\infty}(a_n - \imath b_n)\exp(\imath nx) + (a_n + \imath b_n)\exp(-\imath nx)$$

$$= \frac{1}{2}a_0 + \frac{1}{2}\sum_{n=1}^{\infty}(a_n - \imath b_n)(\cos(nx) + \imath \sin(nx)) + (a_n + \imath b_n)(\cos(nx) - \imath \sin(nx))$$

$$= \frac{1}{2}a_0 + \sum_{n=1}^{\infty} a_n \cos(nx) - \imath^2 b_n \sin(nx) = \frac{1}{2}a_0 + \sum_{n=1}^{\infty} a_n \cos(nx) + b_n \sin(nx)$$

$$\tag{H.32}$$

which verifies that the complex Fourier series for a real function f is indeed identical to the usual formulation in Eq. H.19 although the Fourier coefficients, c_n, are complex. One advantage of Eq. H.28 over the formulation in Eq. H.19 is that we don't need any special definition for the first Fourier coefficient, a_0. The trick in the formulation in Eq. H.28 is that the imaginary coefficients for negative and positive n cancel whereas the real coefficients add. This means that the real coefficients are multiplied by a factor two except the first coefficient, a_0, which makes up for the factor $\frac{1}{2}$ in front of a_0 in Eq. H.19.

I   TME226: Why does the energy spectrum, E, have such strange dimensions?

THE energy spectrum, E, has the strange dimension v^2/ℓ. The reason is that it is a spectral *density* so that the kinetic energy, $k = \overline{v'_i v'_i}$, is computed by integrating over all wavenumbers, see Eq. 5.10. The energy spectrum is a spectral density function in a similar way as $f_v(v)$ in Eq. 7.2; the difference is that $f_v(v)$ in Eq. 7.2 is the first *moment*. Equation 7.5 defines the second moment. The dimension of $f_v(v)$ in Eq. 7.2 and $f_{v'}(v')$ in Eq. 7.5 is one over velocity.

Since we have chosen to express the energy spectrum as a function of the wavenumber, dimension analysis gives $E \propto \kappa^{-5/3}$, see Eqs. 5.12 and 5.13. A similar dimension analysis for the kinetic energy of v' gives $v'^2_\kappa \propto \kappa^{-2/3}$. However, integrating v'^2_κ over all wavenumbers does not give any useful integral quantity.

The integral of the energy spectrum in the inertial region can be estimated as (see Eqs. 5.10 and 5.13)

$$k = C_K \varepsilon^{\frac{2}{3}} \int_{\kappa_1}^{\kappa_2} \kappa^{-\frac{5}{3}} d\kappa \tag{I.1}$$

We could also express E as a function of the turbulent length scale of the eddies, ℓ_κ ($\kappa = 2\pi/\ell_\kappa$, see Eq. 5.7). The energy spectrum is then integrated as

$$k = \int_{\kappa_1}^{\kappa_2} \underbrace{E(\kappa) d\kappa}_{[m^2]} = C_K \varepsilon^{\frac{2}{3}} \int_{\kappa_1}^{\kappa_2} \underbrace{\kappa^{-\frac{5}{3}}}_{\kappa^{-2/3}} d\kappa$$

$$= C_K \varepsilon^{\frac{2}{3}} \int_{\kappa_1}^{\kappa_2} \kappa^{-\frac{5}{3}} \frac{d\kappa}{d\ell_\kappa} d\ell_\kappa = -C_K 2\pi \varepsilon^{\frac{2}{3}} \int_{\ell_1}^{\ell_2} \kappa^{-\frac{5}{3}} \ell_\kappa^{-2} d\ell_\kappa \tag{I.2}$$

$$= C_K \left(\frac{\varepsilon}{2\pi} \right)^{\frac{2}{3}} \int_{\ell_2}^{\ell_1} \underbrace{\ell_\kappa^{-\frac{1}{3}}}_{\ell_\kappa^{2/3}} d\ell_\kappa = \int_{\ell_2}^{\ell_1} \underbrace{E^\ell(\ell_\kappa) d\kappa}_{[m^2]}$$

As can be seen, the energy spectrum $E^\ell(\ell_\kappa)$ obeys the $-1/3$ law and $E(\kappa)$ obeys the $-5/3$ law. However, as mentioned above, v'^2_κ varies as $\kappa^{-2/3}$ (or $\ell_\kappa^{2/3}$).

I.1   Energy spectrum for an ideal vortex

The velocity field for an ideal vortex is given by $v_\theta = \Gamma/(2\pi r)$, $v_r = 0$, see Eq. 1.27 and Fig. 1.8, where Γ denotes the circulation. The kinetic energy, k, for the vortex between $r = R_1$ and $r = R_2$ is obtained by integrating $v_\theta^2/2$ from R_1 to R_2, i.e.

$$k = \frac{1}{8\pi^2(R_2 - R_1)} \int_{R_1}^{R_2} \frac{\Gamma dr}{r^2} \tag{I.3}$$

From this we can define a kinetic energy spectrum as

$$E^{ideal}(r) = \frac{\Gamma}{8\pi^2(R_2 - R_1)r^2} \tag{I.4}$$

so that

$$k = \int_{R_1}^{R_2} E^{ideal}(r) dr \tag{I.5}$$

Equation I.4 shows that $E^{ideal} \propto r^{-3}$. As in the previous section, we find that the dependence of k on the radius is one degree higher, i.e. $k = v_\theta^2/2 \propto r^{-2}$.

I.2   An example

Let's generate a fluctuating velocity, v', using a Fourier series. For simplicity we make it symmetric so that only the cosine part needs to be used. We make it with four terms. It reads then (see Eq. H.19)

$$
\begin{aligned}
v'(x) = a_1^{0.5} \cos\left(\frac{2\pi}{L/1}x\right) + a_2^{0.5} \cos\left(\frac{2\pi}{L/2}x\right) \\
+ a_3^{0.5} \cos\left(\frac{2\pi}{L/3}x\right) + a_4^{0.5} \cos\left(\frac{2\pi}{L/4}x\right)
\end{aligned}
\tag{I.6}
$$

where the wavenumber n in Eq. H.19 corresponds to $2\pi/(L/m)$ with $m = (1, 2, 3, 4)$. The first coefficient, $a_0 = 0$, in Eq. H.19 because the mean of the fluctuation v' is zero, i.e.

$$
\int_0^L v'dx = 0
\tag{I.7}
$$

Equation Eq. I.6 is *continuous*, i.e. it is given for any $x/L = [0, 1]$. In unsteady CFD simulations we are always dealing with discrete points, i.e. a computational grid. Hence, let's express Eq. I.6 for $N = 16$ discrete points with $\Delta x = 1/(N-1)$ as

$$
\begin{aligned}
v'(x) = a_1^{0.5} \cos\left(\frac{2\pi(n-1))}{N/1}\right) + a_2^{0.5} \cos\left(\frac{2\pi(n-1))}{N/2}\right) \\
+ a_3^{0.5} \cos\left(\frac{2\pi(n-1))}{N/3}\right) + a_4^{0.5} \cos\left(\frac{2\pi(n-1))}{N/4}\right)
\end{aligned}
\tag{I.8}
$$

where $(n-1)/N = x/L$ and $n = [1, N]$.

Now we want v' in Eq. I.8 to have an energy spectrum of $-5/3$. Parseval's formula, Eq. H.21, tells us that the kinetic energy of an eddy of wavenumber κ is simply the square of its Fourier coefficient. Hence we let the ratio of the a_k coefficients in Eq. I.8 decrease as $m^{-5/3}$, i.e. (for simplicity we set $a_1 = 1$)

$$
a_1 = 1 \quad a_2 = 2^{-5/3}, \quad a_3 = 3^{-5/3}, \quad a_4 = 4^{-5/3}
\tag{I.9}
$$

Figure I.1 shows how v' varies over x/L. The four terms in E. I.8 shown in Fig. I.1 can be regarded as the velocity fluctuations at one time instant of four eddies of length-scale L, $L/2$, $L/3$ and $L/4$. The period of the four terms is L, $L/2$, $L/3$, and $L/4$ corresponding to wavenumber $2\pi/L$, $2 \cdot 2\pi/L$, $3 \cdot 3\pi/L$ and $4 \cdot 2\pi/L$.

Now let's make a DFT of v' to get the energy spectrum (see Matlab code in Section I.3). In DFT, the integral in Eq. H.18

$$
b_m = \frac{1}{\pi} \int_{-\pi}^{\pi} v'(x) \cos(\kappa x)dx = \frac{1}{\pi} \int_{-\pi}^{\pi} v'(x) \cos\left(\frac{2\pi mx}{L}\right) dx
\tag{I.10}
$$

(where $b_m = a_m^{1/2}$) is replaced by a summation over discrete points, i.e.

$$
B_m = \frac{1}{N} \sum_{n=1}^{N} v'(x) \cos\left(\frac{2\pi m(n-1)}{N}\right)
\tag{I.11}
$$

where $(n-1)/N = x/L$ (note that $m = 0$ corresponds to the mean, which is zero, see Eq. I.7). Note that B_m (denoted by W_cos in the Matlab file) is half as large
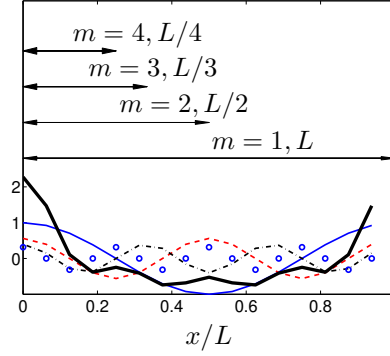
Figure I.1: v' in Eq. I.8 vs. x/L. ——— : term 1 ($m = 1$); ▬ ▬ : term 2 ($m = 2$); ▬ ▪ ▬ : term 3 ($m = 3$); ○: term 4 ($m = 4$); thick line: v'. Matlab code is given in Section I.3.

(a) Dashed thick line shows $\kappa^{-5/3}$.

(b) Dashed thick line shows $\kappa^{-1/3}$.
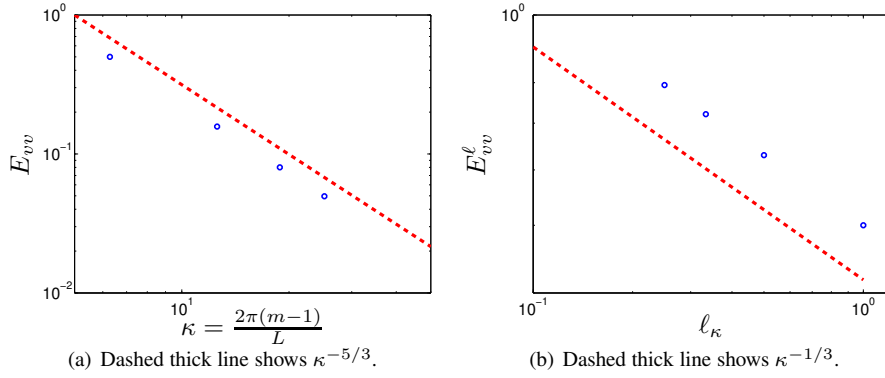
Figure I.2: Energy spectrum of v'. ○: $E_{vv} = B_m^2$. Matlab code is given in Section I.3.

as $a_1^{1/2} \dots a_4^{1/2}$ (but twice as many) because B_m includes both legs of the symmetric spectrum.

Now plot the energy spectrum, $E_{vv} = B_m^2$ versus wavenumber, see Fig. I.2a. It can be seen that it decays as $\kappa^{-5/3}$ as expected (recall that we chose the Fourier coefficients, a_m, to achieve this). The total energy is now computed as

$$\langle v'^2 \rangle_x = \sum_{m=1}^{N} B_m^2 = \sum_{m=1}^{N} E_{vv}(m) \tag{I.12}$$

where $\langle \cdot \rangle_x$ denotes averaging over x.

Figure I.2b shows the computed energy spectrum, $E^\ell(\ell_\kappa)$, versus eddy size, see Matlab code in Section I.3. It decays as $\ell_\kappa^{-1/3}$ as it should, see Eq. I.2.

I.3 An example: Matlab code

```
close all
clear all


% number of cells
```

```
N=16;
L=1;

n=1:1:N;
x_over_L=(n-1)/N;

%  E_vv=m^(-5/3)
a1=1;
a2=2^(-5/3);
a3=3^(-5/3);
a4=4^(-5/3);


for i=1:N
  arg2(i)=2*pi*(i-1)/N;
  arg2(i)=2*pi*x_over_L(i);
  v(i)=a1^0.5*cos(arg2(i))+a2^0.5*cos(2*arg2(i))+a3^0.5*cos(3*arg2(i))+a4^0.5*c
end

% take DFT
W_cos=zeros(1,N);
W_sin=zeros(1,N);
for m=1:N
for i=1:N
  a=v(i);
  arg1=2*pi*(m-1)*(i-1)/N;
  W_cos(m)=W_cos(m)+a*cos(arg1)/N;
  W_sin(m)=W_sin(m)+a*sin(arg1)/N;
end
end

% Note that all elements of W_sin are zero since v(i) is symmetric

%****************************************************************
figure(1)
f1=a1^0.5*cos(arg2);
f2=a2^0.5*cos(2*arg2);
f3=a3^0.5*cos(3*arg2);
f4=a4^0.5*cos(4*arg2);
plot(x_over_L,f1,'linew',2)
hold
plot(x_over_L,f2,'r--','linew',2)
plot(x_over_L,f3,'k-.','linew',2)
plot(x_over_L,f4,'o','linew',2)
plot(x_over_L,v,'k-','linew',4)


h=gca
set(h,'fontsi',[20])
xlabel('x')
```

```
ylabel('y')
axis([0 1 -1 3])
print vprim_vs_L.ps -depsc2


%
%***************************************************************
%
figure(2)
%
% the power spectrum is equal to W*conj(W) = W_cos^2+W_sin^2
PW=W_cos.^2+W_sin.^2;

mx=2*pi*(n-1)/L;


% plot power spectrum; plot only one side of the symmetric spectrum and
% multiply by two so that all energy is accounted for
plot(mx(1:N/2),2*PW(1:N/2),'bo','linew',2)
hold
h=gca
set(h,'xscale','log')
set(h,'yscale','log')
axis([5 50 0.01 1])

% plot -5/3 line
xxx=[5 50];
yynoll=1;
yyy(1)=yynoll;
yyy(2)=yyy(1)*(xxx(2)/xxx(1))^(-5/3);
plot(xxx,yyy,'r--','linew',4)


% compute the average of energy in physical space
int_phys=0;
for i=1:N
    int_phys=int_phys+v(i).^2/N;
end

% compute the average of energy in wavenumber space
int_wave=0;
for i=1:N
    int_wave=int_wave+PW(i);
end

set(h,'fontsi',[20])
xlabel('x')
ylabel('y')
print spectra_vs_kappa.ps -depsc2
%
```

```
%*****************************************************************
%
figure(3)

% compute the length corresponding the wavenumber
lx=2*pi./mx;

% multiply PW by lx^(-2) to get the energy spectrum E(lx)
PW_L=PW.*lx.^(-2);

% plot power spectrum
plot(lx(1:N/2),2*PW_L(1:N/2),'bo','linew',2)
hold
h=gca
set(h,'xscale','log')
set(h,'yscale','log')

axis([0.1 1.2 0.4 1])

% plot -1/3 line
xxx=[0.1 1]
yynoll=0.9;
yyy(1)=yynoll;
yyy(2)=yyy(1)*(xxx(2)/xxx(1))^(-1/3);
plot(xxx,yyy,'r--','linew',4);

set(h,'fontsi',[20])
xlabel('x')
ylabel('y')
print spectra_vs_L.ps -depsc2
```

J TME226 Learning outcomes 2020

TME226 Learning outcomes 2020: Lecture 1

1. Explain the difference between Lagrangian and Eulerian description of the motion of a fluid particle.

2. Consider the flow in Section 1.2. Show that $\partial v_1/\partial t$ is different from dv_1/dt.

3. Watch the on-line lecture *Eulerian and Lagrangian Description* at
   http://www.tfd.chalmers.se/~lada/MoF/flow_viz.html

   i. The first part (approx. the first 12 minutes) describes the difference between Lagrangian and Eulerian points and velocities.

   ii. The formula $\dfrac{\partial T}{\partial t} + v_i\dfrac{\partial T}{\partial x_i}$ is nicely explained in (after approx. 12 minutes) where the example is the flow in a river

4. Show which stress components, σ_{ij}, that act on a Cartesian surface whose normal vector is $n_i = (1, 0, 0)$. Show also the stress vector, $t_i^{\hat{n}}$. (see Eq. D.2 and Fig. 1.3 and the Lecture notes of Ekh [2])

5. Show that the product of a symmetric and an antisymmetric tensor is zero.

6. Explain the physical meaning of diagonal and off-diagonal components of S_{ij}

7. Explain the physical meaning of Ω_{ij}

8. What is the definition of irrotational flow?

9. What is the physical meaning of irrotational flow?

10. Derive the relation between the vorticity vector and the vorticity tensor

11. Start from Eq. 1.16 and express the vorticity tensor as a function of the vorticity vector (Eq. 1.18)

12. Explain the physical meaning of the eigenvectors and the eigenvalues of the stress tensor (see Section 1.8 and the Lecture notes of Ekh [2])

13. Watch the on-line lecture *Vorticity, part 1* at
    http://www.tfd.chalmers.se/~lada/MoF/flow_viz.html

    i. What is a vortex line?

    ii. The teacher talks of ω_A and ω_B, where $\omega = 0.5(\omega_A + \omega_B)$; what does it denote? (cf. Fig. 1.4 in the eBook)

    iii. The teacher shows the rotating tank (after 3 minutes into the movie). He puts the vorticity meter into the tank. The flow in the tank moves like a solid body. How does the vorticity meter move? This is a curved flow with vorticity.

    iv. The teacher puts the vorticity meter into a flow in a straight channel (near a wall). What happens with the vorticity meter? (cf. Fig. 1.10)

v. After 4:20 minutes, the teacher shows the figure of a boundary layer. He says that one of the "vorticity legs" (ω_A in Item 13ii above) is parallel to the wall; what does he say about ω_B? What conclusion does is draw about ω? This is a straight flow with vorticity.

vi. After 4:30 minutes, the teacher introduces a spiral vortex tank (in the eBook this is called an ideal vortex). How does the vortex meter behave? (cf. Fig. 1.8 in the eBook). How does the teacher explain that the vorticity is zero (look at the figure he talks about after 6 minutes); the explanation uses the fact that the tangential velocity, v_θ, is inversely proportional to the radius, r, see Eq. 1.29 in the eBook.

vii. After 8:40 minutes, the teacher puts the vorticity meter at different locations in the boundary layer; he puts it near the solid wall, a bit further out and finally at the edge of the boundary layer. How does the vorticity meter move at the different locations? Where is the vorticity smallest/largest? Explain why.

viii. After 10:35, the vortex meter is shown in the spiral vortex tank. What happens with the vorticity when we get very close to the center? Does it still remain zero? What happens with the tangential velocity? (see Eq. 1.29)

ix. The teachers explains the concept of circulation, Γ, and its relation to vorticity (cf. Eqs. 1.23 and 1.25).

x. What is a vortex core?

xi. How large is the vorticity and the circulation in the rotating tank?

xii. How large is the vorticity and the circulation in the spiral vortex tank? Does it matter if you include the center?

xiii. The teacher presents a two-dimensional wing. Where is the pressure low and high, respectively? The Bernoulli equation gives then the velocity; where is it high and low, respectively? The velocity difference creates a circulation, Γ.

xiv. After 15:25 minutes, the teacher looks at the rotating tank again. He starts to rotate the tank; initially there is only vorticity near the outer wall. As time increases, vorticity (and circulation) spread toward the center. Finally, the flow in the entire tank has vorticity (and circulation). This illustrates that as long as there is an imbalance in the shear stresses, vorticity (and circulation) is changed (usually created), see Figs. 1.10 and 4.1.

14. Vortex lines are shown in experiments in the on-line lecture *Vorticity, part 2* (18 minutes into the movie) at
http://www.tfd.chalmers.se/~lada/MoF/flow_viz.html

15. Show that the vorticity is non-zero in a boundary layer, see Section 1.7.2 (see also Item 13iv above)

16. Show that the vorticity is zero in an ideal vortex (see Item 13vi above)
Hint:

$$v_1 = -v_\theta \frac{x_2}{(x_1^2 + x_2^2)^{1/2}}$$
$$v_2 = v_\theta \frac{x_1}{(x_1^2 + x_2^2)^{1/2}}$$

TME226 Learning outcomes 2020: Lecture 2

1. Derive the Navier-Stokes equation, Eq. 2.5 (use the formulas in the Formula sheet which can be found on the course www page)

2. Simplify the Navier-Stokes equation for incompressible flow and constant viscosity (Eq. 2.9)

3. Derive the transport equation for the internal energy, u, Eq. 2.15 (again, use the Formula sheet). What is the physical meaning of the different terms?

4. Simplify the transport equation for internal energy to the case when the flow is incompressible (Eq. 2.18).

5. Derive the transport equation for the kinetic energy, $v_i v_i/2$, Eq. 2.23. What is the physical meaning of the different terms?

6. Explain the energy transfer between kinetic energy, k, and internal energy, u

7. Show how the left side of the transport equations can be written on conservative and non-conservative form

8. Starting from the Navier-Stokes equations (see Formula sheet), derive the flow equation governing the Rayleigh problem expressed in f and η; what are the boundary conditions in time (t) and space (x_2); how are they expressed in the similarity variable η?

9. Show how the boundary layer thickness can be estimated from the Rayleigh problem using f and η (Fig. 3.3)

TME226 Learning outcomes 2020: Lecture 3

1. Explain the flow physics at the entrance (smooth curved walls) to a plane channel (Fig. 3.5). Watch also the on-line lecture *Pressure field and acceleration* (22 minutes into the movie) at
   `http://www.tfd.chalmers.se/˜lada/MoF/flow_viz.html`

2. Explain the flow physics in a channel bend (Fig. 3.6). Watch also the on-line lecture *Pressure field and acceleration*
   `http://www.tfd.chalmers.se/˜lada/MoF/flow_viz.html`.

   (a) at 28 minutes into the movie the teacher discusses how the pressure varies in a fixed-body rotation flow

   (b) at 16 minutes into the movie the teacher discusses how the pressure varies for the flow in a bend.

3. Explain the flow physics in a channel bend (Fig. 3.6).

4. Derive the flow equations for fully developed flow between two parallel plates, i.e. fully developed channel flow (Eqs. 3.18, 3.22 and 3.26)

5. Show that the continuity equation is automatically satisfied in 2D when the velocity is expressed in the streamfunction, Ψ

6. Starting from Eq. 3.42, derive the equation for two-dimensional boundary-layer flow expressed in the streamfunction (Eq. 3.46).

7. Derive the Blasius equation, Eq. 3.54. Start from Eq. 3.46

TME226 Learning outcomes 2020: Lecture 4

1. Explain (using words and a figure) why vorticity can be created only by an imbalance (i.e. a gradient) of shear stresses. Explain why pressure and the gravity force cannot create vorticity.

2. The incompressible Navier-Stokes equation can be re-written on the form

$$\frac{\partial v_i}{\partial t} + \underbrace{\frac{\partial k}{\partial x_i}}_{\text{no rotation}} - \underbrace{\varepsilon_{ijk} v_j \omega_k}_{\text{rotation}} = -\frac{1}{\rho}\frac{\partial p}{\partial x_i} + \nu \frac{\partial^2 v_i}{\partial x_j \partial x_j} + f_i$$

   Derive the transport equation (3D) for the vorticity vector, Eq. 4.20

3. Show that the divergence of the vorticity vector, ω_i, is zero

4. Explain vortex stretching and vortex tilting. The vortex stretching can be shown in experiments,

5. Watch the on-line lecture *Vorticity, part 2* (11 minutes into the movie) at
   http://www.tfd.chalmers.se/~lada/MoF/flow_viz.html

6. Show that the vortex stretching/tilting term is zero in two-dimensional flow

7. Derive the 2D equation transport equation (Eq. 4.22) for the vorticity vector from the 3D transport equation (Eq. 4.20)

8. Show the similarities between the vorticity and temperature transport equations in fully developed flow between two parallel plates

9. Use the diffusion of vorticity to show that $\frac{\delta}{\ell} \propto \sqrt{\frac{\nu}{U\ell}} = \sqrt{\frac{1}{Re}}$ (see Fig. 4.4 and Eq. 3.14).

10. Watch the on-line lecture *Boundary layers* at
    http://www.tfd.chalmers.se/~lada/MoF/flow_viz.html

    i. Consider the flow over the flat plate (after two minutes) . How does the boundary layer thickness change when we move downstream?

    ii. What value does the fluid velocity take at the surface? What is this boundary conditions called: slip or no-slip? How do they define the boundary layer thickness?

    iii. How is the wall shear stress defined? How does it change when we move downstream? (how does this compare with the channel/boundary layer flow in TME226 Assignment 1?)

    iv. How is the circulation, Γ, defined? (cf. with Eq. 1.23) How is it related to vorticity? How do they compute Γ for a unit length ($> \delta$) of the boundary layer? How large is it? How does it change when we move downstream on the plate?

v. Where is the circulation (i.e. the vorticity) created? Where is the vorticity created in "your" channel/boundary layer flow (TME226 Assignment 1)? The vorticity is created at different locations in the flat-plate boundary layer and in the channel flow: can you explain why? (hint: in the former case

$$\frac{\partial p}{\partial x_1} = \mu \frac{\partial^2 v_1}{\partial x_2^2}\bigg|_{wall} = 0,$$

but not in the latter; this has an implication for $\gamma_{2,wall}$ [see Section 4.3])

vi. How do they estimate the boundary layer thickness? (cf. Section. 4.3.1)

11. Watch the on-line lecture *Boundary layers* 10 minutes into the movie
    http://www.tfd.chalmers.se/˜lada/MoF/flow_viz.html

    i. How does the boundary layer thickness change at a given x when we increase the velocity? Explain why.

    ii. Consider the flow in a contraction: what happens with the boundary layer thickness after the contraction?

    iii. Why is the vorticity level higher after the contraction?

    iv. Is the wall shear stress lower or higher after the contraction? Why?

    v. Consider the flow in a divergent channel (a diffusor): what happens with the boundary layer thickness and the wall shear stress?

    vi. What happens when the angle of the diffusor increases?

    vii. What do we mean by a "separated boundary layer"? How large is the wall shear stress at the separation point?

    viii. The second part of the movie deals with turbulent flow: we'll talk about that in the next lecture (and the remaining ones).

TME226 Learning outcomes 2020: Lecture 5

1. Derive the Bernoulli equation (Eq. 4.32)
   <u>Hint:</u> The gravitation term is first expressed as a potential $g_i = -\partial\hat{\Phi}/\partial x_i$.

2. Consider the derivative of the complex function $(f(z + z_0) - f(z))/z_0$ where $z = x + iy$ and $f = u + iv$. The derivative of f must be independent in which coordinate direction the derivative is taken (either along the real or the imaginary axis). Show that this leads to the *Cauchy-Riemann* equations

$$\frac{\partial u}{\partial x} = \frac{\partial v}{\partial y}, \quad \frac{\partial u}{\partial y} = -\frac{\partial v}{\partial x}$$

3. Show that in inviscid flow, both the velocity potential and the streamfunction satisfy the Laplace equation.

4. Consider the complex potential $f = \Phi + i\Psi$. Show that $f = C_1 z^n$ satisfies the Laplace equation. Derive the velocity polar components for $n = 1$ and $n = 2$. What physical flow do these two cases correspond to?

5. Look at *Potential flow* at Wikipedia

   (a) Figure 1 shows the streamfunction around an airfoil. Recall that the Bernoulli equation applies for a streamline.

   (b) Figure 2 shows the streamfunction for plane flow ($n = 1$) and a doublet ($n = -1$, separation ε, see Section 4.4.6)

   (c) Figure 3 shows the streamfunction for cylinder flow

   (d) Figure 4 shows the flow around a blunt corner, $n = 1/2$ (streamlines in blue and potential lines in cerise)

   (e) Figure 5 shows the flow around a sharp corner, $n = 2/3$ (streamlines in blue and potential lines in cerise)

   (f) Figure 6 shows parallel flow, $n = 1$ (streamlines in blue and potential lines in cerise)

   (g) Figure 7 shows flow along a corner (angle larger than 90°), $n = 3/2$ (streamlines in blue and potential lines in cerise)

   (h) Figure 8 shows flow in a 90° corner, i.e. stagnation flow, see Section 4.4.3.2, $n = 2$ (streamlines in blue and potential lines in cerise)

   (i) Figure 9 shows flow in a corner (angle smaller than 90°), $n = 3$ (streamlines in blue and potential lines in cerise)

   (j) Figure 10 shows flow for a doublet (separation $\varepsilon = 0$, see Section 4.4.6, $n = -1$ (streamlines in blue and potential lines in cerise)

6. Derive the polar velocity components for the complex potential $f = \dot{m}\ln z/(2\pi)$ and $f = -i\Gamma\ln z/(2\pi)$ (Γ denotes circulation). What does the physical flow look like? Show that they satisfy the Laplace equation.

7. A doublet is a combination of a radial sink and source and its complex potential reads $f = \mu/(\pi z)$. Combine it with the potential for parallel flow ($f = V_\infty z$). Derive the resulting velocity field around a cylinder (in polar components).
   <u>Hint:</u> the radius is defined as $r_0^2 = \mu/(\pi V_\infty)$.

8. Consider the potential flow around a cylinder. Show that the radial velocity is zero at the surface. Use the Bernoulli equation to get the surface pressure. Show that the drag and lift forces are zero. Where are the stagnation points located?

9. Add the complex potential of a vortex line, $f = -i\Gamma \ln z/(2\pi)$ (Γ denotes circulation) to the complex potential for cylinder flow. Compute the polar velocity components. Where are the stagnation points located? What happens with the location of the stagnation point(s) when the circulation becomes very large? How is the lift of the cylinder computed (which applies for any body).

10. What is the Magnus effect? Explain the three applications in the text: why is it efficient to use loops in table tennis? Why does the Magnus effect help a football player get the ball around the wall (of players) when making a free-kick? How does the Magnus effect help propulsing a ship using Flettner rotors. To look at old and new installations of Flettner rotors, see Wikipedia.

11. Consider the inviscid flow around an airfoil, see Fig. 4.19. In inviscid theory it would look like Fig. 4.20. What has been done to achieve the flow in Fig. 4.21? How is the lift computed?

12. Watch the on-line lecture *Boundary layers (17 minutes into the movie* at
http://www.tfd.chalmers.se/~lada/MoF/flow_viz.html

   i. The flow is "tripped" into turbulence. How?

   ii. When the flow along the lower wall of the diffusor is tripped into turbulent flow, the separation region is suppressed. Try to explain why.

   iii. Two boundary layers – one on each side of the plate – are shown. The upper one is turbulent and the lower one is laminar. What is the difference in the two velocity profiles? (cf. my figures in the 'summary of lectures') Explain the differences.

   iv. Why is the turbulent wall shear stress larger for the turbulent boundary layer? What about the amount of circulation (and vorticity) in the laminar and turbulent boundary layer? How are they distributed?

   v. Consider the airfoil: when the boundary layer on the upper (suction) side is turbulent, stall occurs at a higher angle of incidence compared when the boundary layer is laminar. Why?

   vi. Vortex generator are place on the suction side in order prevent or delay separation. Try to explain why separation is delayed.

TME226 Learning outcomes 2020: Lecture 6

1. What characterizes turbulence? Explain the characteristics. What is the life time of a turbulent eddy?

2. Explain the cascade process. How large are the largest scales? What is dissipation? What dimensions does it have? Which eddies extract energy from the mean flow? Why are these these eddies "best" at extracting energy from the mean flow?

3. What are the Kolmogorov scales? Use dimensional analysis to derive the expression for the velocity scale, v_η, the length scale, ℓ_η and the time scale, τ_η.

4. Make a figure of the energy spectrum. The energy spectrum consists of three subregions: which? Describe their characteristics. Show the flow of turbulent kinetic energy in the energy spectrum. Given the energy spectrum, $E(\kappa)$, how is the turbulent kinetic energy, k, computed? Use dimensional analysis to derive the $-5/3$ Kolmogorov law.

5. What does isotropic turbulence mean? What about the shear stresses?

6. Show how the ratio of the large eddies to the dissipative eddies depends on the Reynolds number (see Eq. 5.16). Using these estimations, you can show how the number of cells in DNS (Direct Numerical Simulations) depends on Reynolds number (see eBook).

7. Watch the on-line lecture *Turbulence* at
http://www.tfd.chalmers.se/˜lada/MoF/flow_viz.html

    i. Why does the irregular motion of wave on the sea not qualify as turbulence?

    ii. How is the turbulence syndrome defined?

    iii. The movie shows laminar flow in a pipe. The viscosity is decreased, and the pressure drop (i.e. the resistance, the drag, the loss) decreases. Why? The viscosity is further decreased, and the pressure drop increases. Why? How does the characteristics of the water flow coming out of the pipe change due to the second decrease of viscosity?

    iv. It is usually said that the flow in a pipe gets turbulent at a Reynolds number of 2300. In the movie they show that the flow *can* remain laminar up to 8 000. How do they achieve that?

    v. Dye is introduced into the pipe. For laminar flow, the dye does not mix with the water; in turbulent flow it does. When the mixing occurs, what happens with the pressure drop?

8. Watch the on-line lecture *Turbulence* (10 minutes into the movie) at
http://www.tfd.chalmers.se/˜lada/MoF/flow_viz.html

    i. Draw a laminar and turbulent velocity profile for pipe flow. What is the main difference? In which flow is the wall shear stress $\tau_w = \mu \dfrac{\partial \bar{v}_1}{\partial x_2}$ largest, laminar or turbulent?

    ii. In turbulent flow, the velocity near the wall is larger than in laminar flow. Why?

iii. Discuss the connection between mixing and the cross-stream (i.e. v_2') fluctuations.

iv. Try to explain the increased pressure drop in turbulent flow with increased mixing.

v. The center part of the pipe is colored with blue dye and the wall region is colored with red dye: by looking at this flow, try to explain how turbulence creates a *Reynolds shear stress*.

vi. The red and blue dye nicely show the turbulent eddies (fluctuations)

vii. After 16 minutes, the flow in jets is consider. Two turbulent jet flows are shown, one at low Reynolds number and one at high Reynolds number. They look very similar in one way and very different in another way. Which scales are similar and which are different?

viii. he two turbulent jet flows have the same energy input and hence the same dissipation. Use this fact to explain why the smallest scales in the high Reynolds number jet must be smaller that those in the low Reynolds number jet.

ix. At the end of the presentation of the jet flow, they explain the *cascade process*.

x. Explain the analogy of a water fall (cascade of water, the water passes down the cascade) and the turbulent cascade process.

TME226 Learning outcomes 2020: Lecture 7

1. Use the decomposition $v_i = \bar{v}_i + v'_i$ to derive the time-averaged Navier-Stokes equation. A new terms appears: what is it called? Simplify the time-averaged Navier-Stokes equation for boundary layer flow. What is the total shear stress?

2. How is the friction velocity, u_τ, defined? Define x_2^+ and $\bar{v}_1^+$.

3. The wall region is divided into an inner and outer region. The inner region is furthermore divided into a viscous sublayer, buffer layer and log-layer. Make a figure and show where these regions are valid (Fig. 6.2)

4. Look at *Turbulent flow around a wing* at You Tube

   (a) At 1:07 minutes into the movie, they present the flow using the λ_2 criterion. This is the second eigenvalue of $S_{ij}^2 + \Omega_{ij}^2$ where $\lambda_1 > \lambda_2 > \lambda_3$. This criterion finds vortex cores i.e. the center of turbulent eddies

   (b) At 1:18 minutes they show the prescribed transition on the upper side (suction side)

   (c) At 1:42 minutes, for example, you can see turbulent vortex core in the outer part of the boundary layer

   (d) At 1:56 minutes, the incipient (the start of) separation near the trailing edge is shown

5. What are the relevant velocity and length scales in the viscous-dominated region $(x_2^+ \lesssim 5)$? Derive the linear velocity law in this region (Eq. 6.22). What are the suitable velocity and length scales in the inertial region (the fully turbulent region)? Derive the log-law for this region.

6. Consider fully developed turbulent channel flow. In which region (viscous sublayer, buffer layer or log-layer) does the viscous stress dominate? In which region is the turbulent shear stress large? Integrate the channel flow equations and show that the total shear stress varies as $1 - x_2/\delta$ (Eq. 6.20).

7. In fully developed turbulent channel flow, the time-averaged Navier-Stokes consists only of three terms. Make a figure and show how the velocity and Reynolds shear stress vary across the channel. After that, show how the three terms vary across the channel (Fig. 6.6). Which two terms balance each other in the outer region? Which term drives ("pushes") the flow in the x_1 direction? Which two terms are large in the inner region? Which term drives the flow?

TME226 Learning outcomes 2020: Lecture 8

1. Derive the exact transport equation for turbulent kinetic energy, k. Discuss the physical meaning of the different terms in the k equation. Which terms are transport terms? Which is the main source term? Main sink (i.e. negative source) term?

2. Watch the on-line lecture *Turbulence* (20 minutes into the movie) at
   http://www.tfd.chalmers.se/~lada/MoF/flow_viz.html

   i. The movie says that there is a similarity of the small scales in a channel flow and in a jet flow. What do they mean?

   ii. What happens with the small scales when the Reynolds number is increased? What happens with the large scales? Hence, how does the ratio of the large scales to the small scales change when the Reynolds number increases (see Eq. 5.16)

   iii. In decaying turbulence, which scales die first? The scenes of the clouds show this in a nice way.

   iv. Even though the Reynolds number may be large, there are a couple of physical phenomena which may inhibit turbulence and keep the flow laminar: mention three.

   v. Consider the flow in the channel where the fluid on the top (red) and the bottom (yellow) are separated by a horizontal partition. The two fluids are identical. Study how the two fluids mix downstream of the partition. In the next example, the fluid on the top is hot (yellow) and light, and the one at the bottom (dark blue) is cold (heavy); how do the fluids mix downstream of the partition, better or worse than in the previous example? This flow situation is called *stable stratification*. In the last example, the situation is reversed: cold, heavy fluid (dark blue) is moving on top of hot, light fluid (yellow). How is the mixing affected? This flow situation is called *unstable stratification*. Compare in meteorology where heating of the ground may cause unstable stratification or when *inversion* causes stable stratification. You can read about stable/unstable stratification in Section 12.1 at p. 159.

3. Given the exact k equation, give the equation for 2D boundary-layer flow (Eq. 8.24). All spatial derivatives are kept in the dissipation term: why? In the turbulent region of the boundary layer, the k equation is dominated by two terms. Which ones? Which terms are non-zero at the wall?

4. Where is the production term, $P^k = -\overline{v_1' v_2'} \partial \bar{v}_1 / \partial x_2$, largest? In order to explain this, show how $-\overline{v_1' v_2'}$ and $\partial \bar{v}_1 / \partial x_2$ vary near the wall.

TME226 Learning outcomes 2020: Lecture 9

1. Derive the exact transport equation for mean kinetic energy, K. Discuss the physical meaning of the different terms. One term appears in both the k and the K equations: which one? Consider the dissipation terms in the k and the K equations: which is largest near the wall and away from the wall, respectively?

2. Which terms in the k equation need to be modeled? Explain the physical meaning of the different terms in the k equation.

3. Show how the modeled production term in the $k - \varepsilon$ model is derived. Show how it can be expressed in $\bar{s}_{ij}$

4. Show how the turbulent diffusion (i.e. the term which includes the triple correlation) in the k equation is modeled.

5. Given the modeled k equation, derive the modeled ε equation.

6. How are the Reynolds stress tensor, $\overline{v'_i v'_j}$, and the turbulent heat flux vector, $\overline{v'_i \theta'}$, modeled in the Boussinesq approach?

7. Watch the on-line lecture *Pressure field and acceleration* at
   http://www.tfd.chalmers.se/˜lada/MoF/flow_viz.html

   i. The water flow goes through the contraction. What happens with the velocity and pressure. Try to explain.

   ii. Fluid particles become thinner and elongated in the contraction. Explain why.

   iii. In the movie they show that the acceleration along s, i.e. $\dfrac{dV_s^2/2}{ds}$, is related to the pressure gradient $\dfrac{dp}{ds}$. Compare this relation with the Bernoullii equation (Eq. 4.34)

8. Watch the on-line lecture *Pressure field and acceleration* (6 minutes into the movie) at
   http://www.tfd.chalmers.se/˜lada/MoF/flow_viz.html

   i. Water flow in a manifold (a pipe with many outlets) is presented. The pressure decreases slowly downstream. Why?

   ii. The bleeders (outlets) are opened. The pressure now increases in the downstream direction. Why?

   iii. What is the stagnation pressure? How large is the velocity at a stagnation point?

   iv. What is the static pressure? How can it be measured? What is the difference between the stagnation and the static pressures?

   v. A venturi meter is a pipe that consists of a contraction and an expansion (i.e. a diffusor). The bulk velocities at the inlet and outlet are equal, but still the pressure at the outlet is lower than that at the inlet. There is a pressure drop. Why?

vi. What happens with the pressure drop when there is a separation in the diffusor?

vii. They increase the speed in the venturi meter. The pressure difference in the contraction region and the outlet increases. Since there is atmospheric pressure at the outlet, this means that the pressure in the contraction region must decrease as we increase the velocity of the water. Finally the water starts to boil, although the water temperature may be around $10^{o}C$. This is called cavitation (this causes large damages in water turbines).

viii. Explain how suction can be created by blowing in a pipe.

9. Watch the on-line lecture *Pressure field and acceleration* (19 minutes into the movie) at
   http://www.tfd.chalmers.se/~lada/MoF/flow_viz.html

   i. What is the Coanda effect?

   ii. The water from the tap which impinges on the horizontal pipe attaches to the surface of the pipe because of the Coanda effect. How large is the pressure at the surface of the pipe relative to the surrounding pressure?

   iii. Explain the relation between streamline curvature and pressure (cf. Section 3.2.1).

   iv. At the end of the contraction, there is an adverse pressure gradient ($\partial p/\partial x > 0$). Explain why.

TME226 Learning outcomes 2020: Lecture 10

1. Two options are used for treating the wall boundary conditions: which ones? Explain the main features.

2. Consider wall functions. Show how the expression

$$u_\tau = \frac{\kappa \bar{v}_{1,P}}{\ln(E u_\tau \delta x_2 / \nu)}$$

   is obtained. What is the wall boundary condition for the velocity equation?

3. How is the k equation simplified in the log-law region? Show how the boundary condition

$$k_P = C_\mu^{-1/2} u_\tau^2$$

   for k is derived (wall functions).

4. Show how the boundary condition for ε

$$\varepsilon_P = P^k = \frac{u_\tau^3}{\kappa \delta x_2}$$

   is derived (wall functions).

5. How fine should the grid be near the wall when using a low-Reynolds number model? Why must the turbulence model be modified?

6. Use Taylor expansion (including boundary conditions and the continuity equation) to show how the three velocity components vary near the wall. Show then how $\bar{v}$, $\bar{v}$, $\overline{v_1'^2}$, $\overline{v_1'v_2'}$, ε, $\partial \bar{v}_1/\partial x_2$ and k vary near the wall.

7. The exact k equation reads

$$\rho \bar{v}_1 \frac{\partial k}{\partial x_1} + \rho \bar{v}_2 \frac{\partial \rho k}{\partial x_2} = -\rho \overline{v_1' v_2'} \frac{\partial \bar{v}_1}{\partial x_2} - \frac{\partial \overline{p' v_2'}}{\partial x_2} - \frac{\partial}{\partial x_2} \left(\frac{1}{2} \overline{\rho v_2' v_i' v_i'} \right)$$
$$+ \mu \frac{\partial^2 k}{\partial x_2^2} - \mu \overline{\frac{\partial v_i'}{\partial x_j} \frac{\partial v_i'}{\partial x_j}}$$

   Show how the production term, the viscous and turbulent diffusion terms and the dissipation vary near the wall.

8. The modeled k eq. reads

$$\rho \bar{v}_1 \frac{\partial k}{\partial x_1} + \rho \bar{v}_2 \frac{\partial \rho k}{\partial x_2} = \mu_t \left(\frac{\partial \bar{v}_1}{\partial x_2} \right)^2 + \frac{\partial}{\partial x_2} \left(\frac{\mu_t}{\sigma_k} \frac{\partial k}{\partial x_2} \right)$$
$$+ \mu \frac{\partial^2 k}{\partial x_2^2} - \rho \varepsilon$$

   Show how the production term, the turbulent diffusion term and the dissipation vary near the wall.

9. Looking at how the exact and the modelled terms in the k behave near walls, which terms need to modified? How?

10. The modeled ε eq. reads

$$\rho\bar{v}_1\frac{\partial\varepsilon}{\partial x_1} + \rho\bar{v}_2\frac{\partial\varepsilon}{\partial x_2} = C_{\varepsilon 1}\frac{\varepsilon}{k}P^k + \frac{\partial}{\partial x_2}\left(\frac{\mu_t}{\sigma_\varepsilon}\frac{\partial\varepsilon}{\partial x_2}\right)$$
$$+ \mu\frac{\partial^2\varepsilon}{\partial x_2^2} - C_{\varepsilon 2}\rho\frac{\varepsilon^2}{k}$$

Show how all terms behave as the wall is approached. Which terms do not go to zero. Do they balance each other? If not, what modification is needed?

11. In low-Reynolds number models, what is the boundary condition for k?

12. A boundary condition for ε can be derived (Eq. 11.165) by looking at the two terms in the k eq. that do not go to zero. Show this boundary condition.

13. Another boundary condition for ε

$$\varepsilon_{wall} = 2\nu\left(\frac{\partial\sqrt{k}}{\partial x_2}\right)^2$$

can be derived by using Taylor expansion. Derive the boundary condition above. A third b.c. for ε reads

$$\varepsilon_{wall} = 2\nu\frac{k}{x_2^2}$$

Show that this agrees with Taylor expansion.

K   MTF271 Lecture Notes

K.1   Lecture 1

¶See Section 11.1.1, Flow equations

▶Boussinesq approximation: density variation only in gravitation (buoyancy) term

$$\frac{\partial \rho_0 \bar{v}_i}{\partial t} + \frac{\partial}{\partial x_j}\left(\rho_0 \bar{v}_i \bar{v}_j\right) = -\frac{\partial \bar{p}}{\partial x_i} + \mu \frac{\partial^2 \bar{v}_i}{\partial x_j \partial x_j} - \frac{\partial \tau_{ij}}{\partial x_j} - \rho_0 \beta (\bar{\theta} - \theta_0) g_i$$

$$\bar{p} \text{ is hydrodynamic pressure: } \rho f_i \to (\rho - \rho_0) g_i$$

If we let density depend on pressure and temperature, differentiation gives

$$d\rho = \left(\frac{\partial \rho}{\partial \theta}\right)_p d\theta + \left(\frac{\partial \rho}{\partial p}\right)_\theta dp$$

Incompressible $\Rightarrow \partial \rho / \partial p = 0$

$$\beta = -\frac{1}{\rho_0}\left(\frac{\partial \rho}{\partial \theta}\right)_p \Rightarrow$$

$$d\rho = -\rho_0 \beta d\theta \Rightarrow \rho - \rho_0 = -\beta \rho_0 (\theta - \theta_0)$$

$$\rho_0 f_i = (\rho - \rho_0) g_i = -\rho_0 \beta (\bar{\theta} - \theta_0) g_i$$

¶See Section 11.1.2, Temperature equation
▶Temperature equation

$$\frac{\partial \theta}{\partial t} + \frac{\partial v_i \theta}{\partial x_i} = \alpha \frac{\partial^2 \theta}{\partial x_i \partial x_i}$$

where $\alpha = k/(\rho c_p)$. Introducing $\theta = \bar{\theta} + \theta'$ gives the mean temperature equation

$$\frac{\partial \bar{v}_i \bar{\theta}}{\partial x_i} = \alpha \frac{\partial^2 \bar{\theta}}{\partial x_i \partial x_i} - \frac{\partial \overline{v_i' \theta'}}{\partial x_i}$$

▶Total (viscous plus turbulent) flux: momentum and temperature equation

$$\frac{q_{2,tot}}{\rho c_p} = \frac{q_{2,visc}}{\rho c_p} + \frac{q_{2,turb}}{\rho c_p} = \alpha \frac{\partial \bar{\theta}}{\partial x_2} - \overline{v_2' \theta'}, \quad \alpha = \frac{k}{\rho c_p}$$

$$\tau_{tot} = \tau_{visc} + \tau_{turb} = \mu \frac{\partial \bar{v}_1}{\partial x_2} - \rho \overline{v_1' v_2'}$$

Reynolds shear stress.
—— : $-\rho \overline{v_1' v_2'} / \tau_w$
- - - : $\mu(\partial \bar{v}_1 / \partial x_2) / \tau_w$.
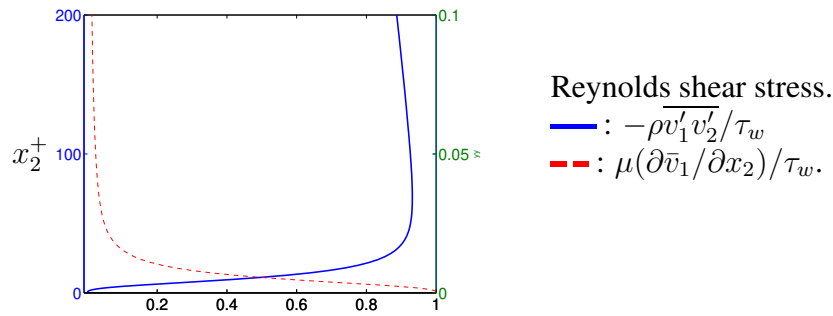
¶See Section 11.2, The exact $\overline{v_i' v_j'}$ equation
▶$\overline{v_i' v_j'}$-equation

$$\underbrace{\bar{v}_k \frac{\partial \overline{v_i' v_j'}}{\partial x_k}}_{C_{ij}} = \underbrace{-\overline{v_i' v_k'} \frac{\partial \bar{v}_j}{\partial x_k} - \overline{v_j' v_k'} \frac{\partial \bar{v}_i}{\partial x_k}}_{P_{ij}} + \underbrace{\overline{\frac{p'}{\rho} \left(\frac{\partial v_i'}{\partial x_j} + \frac{\partial v_j'}{\partial x_i} \right)}}_{\Pi_{ij}}$$

$$\underbrace{- \frac{\partial}{\partial x_k} \left[\overline{v_i' v_j' v_k'} + \frac{\overline{p' v_j'}}{\rho} \delta_{ik} + \frac{\overline{p' v_i'}}{\rho} \delta_{jk} \right]}_{D_{ij,t}} + \underbrace{\nu \frac{\partial^2 \overline{v_i' v_j'}}{\partial x_k \partial x_k}}_{D_{ij,\nu}}$$

$$\underbrace{- g_i \beta \overline{v_j' \theta'} - g_j \beta \overline{v_i' \theta'}}_{G_{ij}} \underbrace{- 2\nu \overline{\frac{\partial v_i'}{\partial x_k} \frac{\partial v_j'}{\partial x_k}}}_{\varepsilon_{ij}}$$

• Unknown terms

  Π_{ij} Pressure-strain

  $D_{ij,t}$ Turbulent diffusion

  ε_{ij} Dissipation

¶See Section 11.3, The exact $\overline{v_i'\theta'}$ equation

▶$\overline{v_i'\theta'}$ equation

$$\frac{\partial \theta'}{\partial t} + \frac{\partial}{\partial x_k}(v_k'\bar{\theta} + \bar{v}_k\theta' + v_k'\theta') = \alpha \frac{\partial^2 \theta'}{\partial x_k \partial x_k} + \frac{\partial \overline{v_k'\theta'}}{\partial x_k} \qquad \text{(K.1)}$$

$$\frac{\partial v_i'}{\partial t} + \frac{\partial}{\partial x_k}(v_k'\bar{v}_i + \bar{v}_k v_i' + v_k'v_i') = -\frac{1}{\rho}\frac{\partial p'}{\partial x_i} + \nu \frac{\partial^2 v_i'}{\partial x_k \partial x_k} + \frac{\partial \overline{v_i'v_j'}}{\partial x_k} - g_i\beta\theta'$$
$$\text{(K.2)}$$

Multiply Eq. K.1 with v_i' and multiply Eq. K.2 with θ', add them together and time average

$$\overline{v_i'\frac{\partial}{\partial x_k}(v_k'\bar{\theta} + \bar{v}_k\theta' + v_k'\theta') + \theta'\frac{\partial}{\partial x_k}(\bar{v}_i v_k' + \bar{v}_k v_i' + v_i'v_k')}$$
$$= -\frac{\overline{\theta'}\frac{\partial p'}{\partial x_i}}{\rho} + \alpha\overline{v_i'\frac{\partial^2 \theta'}{\partial x_k \partial x_k}} + \nu\overline{\theta'\frac{\partial^2 v_i'}{\partial x_k \partial x_k}} - g_i\beta\overline{\theta'\theta'}$$

$$\frac{\partial}{\partial x_k}\bar{v}_k\overline{v_i'\theta'} = \underbrace{-\overline{v_i'v_k'}\frac{\partial \bar{\theta}}{\partial x_k} - \overline{v_k'\theta'}\frac{\partial \bar{v}_i}{\partial x_k}}_{P_{i\theta}} \underbrace{-\frac{\overline{\theta'}\frac{\partial p'}{\partial x_i}}{\rho}}_{\Pi_{i\theta}} \underbrace{-\frac{\partial}{\partial x_k}\overline{v_k'v_i'\theta'}}_{D_{i\theta,t}}$$
$$+ \underbrace{(\nu + \alpha)\frac{\partial^2 \overline{v_i'\theta'}}{\partial x_k \partial x_k}}_{D_{i\theta,\nu}} - \underbrace{(\nu + \alpha)\overline{\frac{\partial v_i'}{\partial x_k}\frac{\partial \theta'}{\partial x_k}}}_{\varepsilon_{i\theta}} \underbrace{-g_i\beta\overline{\theta'^2}}_{G_{i\theta}}$$

¶The original derivation is shown in Section 8.2. In 11.4, The k equation, we derive the k equation as follows

►Take the trace of the $\overline{v'_i v'_j}$ equation and divide by two

$$
\underbrace{\frac{\partial k}{\partial t} + \bar{v}_j \frac{\partial k}{\partial x_j}}_{C^k} = \underbrace{- \overline{v'_i v'_j} \frac{\partial \bar{v}_i}{\partial x_j}}_{P^k} \underbrace{- \nu \overline{\frac{\partial v'_i}{\partial x_j} \frac{\partial v'_i}{\partial x_j}}}_{\varepsilon}
$$

$$
\underbrace{- \frac{\partial}{\partial x_j} \left\{ \overline{v'_j \left(\frac{p'}{\rho} + \frac{1}{2} v'_i v'_i \right)} \right\}}_{D_t^k} + \underbrace{\nu \frac{\partial^2 k}{\partial x_j \partial x_j}}_{D_\nu^k} \underbrace{- g_i \beta \overline{v'_i \theta'}}_{G^k}
$$

- Unknown terms

  $\overline{v'_i v'_j}$ Reynolds stress in P^k

  D_t^k Turbulent diffusion

  ε Dissipation

¶See Section 11.6, The Boussinesq assumption
►The Boussinesq assumption: a model for $\overline{v'_i v'_j}$
The diffusion term of time-averaged Navier-Stokes

$$
\frac{\partial}{\partial x_j} \left\{ \nu \left(\frac{\partial \bar{v}_i}{\partial x_j} + \frac{\partial \bar{v}_j}{\partial x_i} \right) - \overline{v'_i v'_j} \right\} \Rightarrow \frac{\partial}{\partial x_j} \left\{ (\nu + \nu_t) \left(\frac{\partial \bar{v}_i}{\partial x_j} + \frac{\partial \bar{v}_j}{\partial x_i} \right) \right\}
$$

$$
\overline{v'_i v'_j} = -\nu_t \left(\frac{\partial \bar{v}_i}{\partial x_j} + \frac{\partial \bar{v}_j}{\partial x_i} \right) + \boxed{\frac{2}{3} \delta_{ij} k}
$$

$$
\nu_t \propto v'\ell = k^{1/2} \frac{k^{3/2}}{\varepsilon} = c_\mu \frac{k^2}{\varepsilon}
$$

K.2 Lecture 2

¶See Section 11.7.1, Production terms

▶Production term in k equation needs to be modelled.

$$P^k = -\overline{v_i'v_j'}\frac{\partial \bar{v}_i}{\partial x_j} = \nu_t\left[\left(\frac{\partial \bar{v}_i}{\partial x_j} + \frac{\partial \bar{v}_j}{\partial x_i}\right) - \frac{2}{3}\delta_{ij}\frac{\partial \bar{v}_k}{\partial x_k}\right]\frac{\partial \bar{v}_i}{\partial x_j} = 2\nu_t\bar{s}_{ij}\bar{s}_{ij}$$

▶The heat flux is needed to close the mean temperature equation, Eq. 11.9. It is modelled as (see Eq. 11.35)

$$\overline{v_i'\theta'} = -\alpha_t\frac{\partial \bar{\theta}}{\partial x_i}, \alpha_t = \frac{\nu_t}{\sigma_t}$$

▶Diffusion term in k eq, Eq. 11.23, must be modelled. Compare with heat conduction, Eq. 2.14:

$$q_i = -k\frac{\partial \bar{\theta}}{\partial x_i}.$$

Flux of k:

$$d_{j,t}^k = \frac{1}{2}\overline{v_j'v_i'v_i'} = -\frac{\nu_t}{\sigma_k}\frac{\partial k}{\partial x_j} \Rightarrow -\frac{1}{2}\frac{\partial \overline{v_j'v_i'v_i'}}{\partial x_j} = \frac{\partial}{\partial x_j}\left(\frac{\nu_t}{\sigma_k}\frac{\partial k}{\partial x_j}\right)$$

¶See Section 11.8, The $k - \varepsilon$ model
▶Modelled k equation

$$\frac{\partial k}{\partial t} + \bar{v}_j\frac{\partial k}{\partial x_j} = 2\nu_t\bar{s}_{ij}\bar{s}_{ij} + \frac{\partial}{\partial x_j}\left\{\left(\nu + \frac{\nu_t}{\sigma_k}\right)\frac{\partial k}{\partial x_j}\right\} + g_i\beta\frac{\nu_t}{\sigma_\theta}\frac{\partial \bar{\theta}}{\partial x_i} - \varepsilon$$

¶See Section 11.5, The ε equation
▶ε equation

$$C^\varepsilon = P^\varepsilon + D^\varepsilon + G^\varepsilon - \Psi^\varepsilon$$

Use the same source terms as in k equation and add turbulent time-scale ε/k to get the right dimensions:

$$P^\varepsilon - \Psi^\varepsilon + G^\varepsilon = \frac{\varepsilon}{k}(c_{\varepsilon 1}P^k - c_{\varepsilon 2}\varepsilon + c_{\varepsilon 3}G^k)$$

▶The final form modelled ε equation

$$\frac{\partial \varepsilon}{\partial t} + \bar{v}_j\frac{\partial \varepsilon}{\partial x_j} = \frac{\varepsilon}{k}(c_{\varepsilon 1}P^k - c_{\varepsilon 2}\varepsilon + c_{\varepsilon 3}G^k) + \frac{\partial}{\partial x_j}\left[\left(\nu + \frac{\nu_t}{\sigma_\varepsilon}\right)\frac{\partial \varepsilon}{\partial x_j}\right]$$

¶See Section 11.7.3, Dissipation term, ε_{ij}

▶The dissipation term, ε_{ij}, in the $\overline{v_i' v_j'}$ equation (eq. 11.11), is modeled as follows:

Small-scale turbulence is isotropic

1. $\overline{v_1'^2} = \overline{v_2'^2} = \overline{v_3'^2}$.

2. All shear stresses are zero $\Rightarrow$

$$\varepsilon_{ij} = \frac{2}{3}\varepsilon\delta_{ij} \tag{K.3}$$

¶See Section 11.7.4, Slow pressure-strain term

▶The pressure-strain term is the last unknown term that need to be modelled in the $\overline{v_i' v_j'}$ equation, Eq. 11.11. We start with the slow pressure-strain term
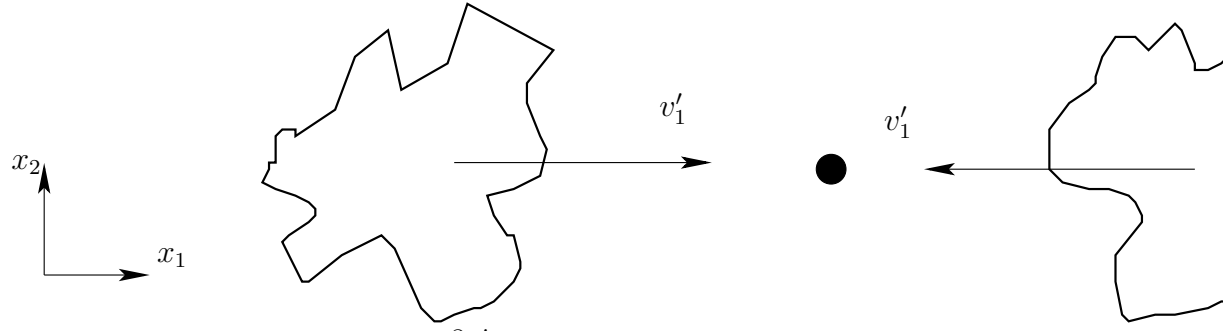
$\partial v_1'/\partial x_1 < 0$ and $p' > 0$ so that $p'\dfrac{\partial v_1'}{\partial x_1} < 0$

$$\frac{\partial v_2'}{\partial x_2} > 0, \quad \frac{\partial v_3'}{\partial x_3} > 0$$

If this happens then
$$\overline{v_1'^2} > \overline{v_2'^2}, \overline{v_1'^2} > \overline{v_3'^2}$$

$$\overline{p'\frac{\partial v_1'}{\partial x_1}} \propto -\frac{\rho}{2t}\left[\left(\overline{v_1'^2} - \overline{v_2'^2}\right) + \left(\overline{v_1'^2} - \overline{v_3'^2}\right)\right] = -\frac{\rho}{t}\left[\overline{v_1'^2} - \frac{1}{2}\left(\overline{v_2'^2} + \overline{v_3'^2}\right)\right]$$

$$= -\frac{\rho}{t}\left[\frac{3}{2}\overline{v_1'^2} - \frac{1}{2}\left(\overline{v_1'^2} + \overline{v_2'^2} + \overline{v_3'^2}\right)\right] = -\frac{\rho}{t}\left(\frac{3}{2}\overline{v_1'^2} - k\right)$$

$$\Phi_{ij,1} \equiv \overline{p'\left(\frac{\partial v_i'}{\partial x_j} + \frac{\partial v_j'}{\partial x_i}\right)} = -c_1\rho\frac{\varepsilon}{k}\left(\overline{v_i' v_j'} - \frac{2}{3}\delta_{ij}k\right) \tag{K.4}$$

see Eq. 11.57

¶See Eq. 11.2 at p. 133
►Decaying grid turbulence

a)
x_1

b)
x_3

►$\overline{v'_i v'_j}$ equation
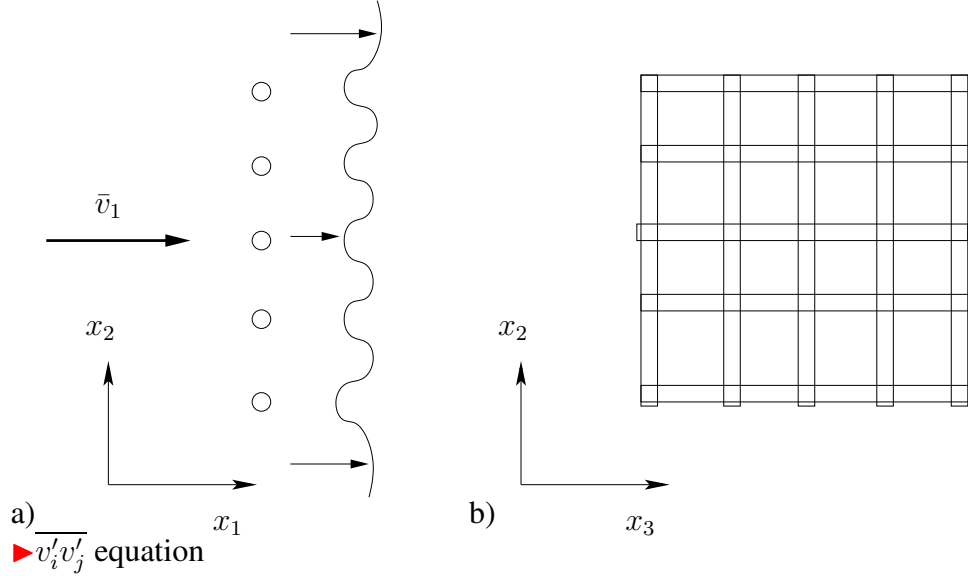
$$\bar{v}_1 \frac{d\overline{v'_i v'_j}}{dx_1} = \overline{\frac{p'}{\rho}\left(\frac{\partial v'_i}{\partial x_j} + \frac{\partial v'_j}{\partial x_i}\right)} - \varepsilon_{ij} \qquad \text{(K.5)}$$

stress tensor which is defined as

$$a_{ij} = \frac{\overline{v'_i v'_j}}{k} - \frac{2}{3}\delta_{ij} \qquad \text{(K.6)}$$

When isotropic, $a_{ij} = 0$. We introduce a_{ij} (Eq. K.6), $\phi_{ij,1}$ (Eq. K.4) and $\varepsilon_{ij} = (2/3)\delta_{ij}$ (Eq. K.3) into Eq. K.5 so that

$$\bar{v}_1 \left(\frac{d(ka_{ij})}{dx_1} + \delta_{ij}\frac{2}{3}\frac{dk}{dx_1}\right) = \underline{-c_1 \varepsilon a_{ij} - \frac{2}{3}\delta_{ij}\varepsilon}$$

Using $\bar{v}_1 \frac{dk}{dx_1} = -\varepsilon$ gives

$$\bar{v}_1 \frac{da_{ij}}{dx_1} = \underline{-c_1 \frac{\varepsilon}{k}a_{ij} - \frac{2}{3}\delta_{ij}\frac{\varepsilon}{k}} + \frac{\varepsilon}{k}a_{ij} + \frac{2}{3}\delta_{ij}\frac{\varepsilon}{k} = \frac{\varepsilon}{k}a_{ij}(1-c_1)$$

$da_{ij}/dx < 0$ (the turbulence becomes isotropic) $\Rightarrow c_1 > 1$.

K.3 Lecture 3

¶See Section 11.7.5, Rapid pressure-strain term
►Pressure strain: rapid part
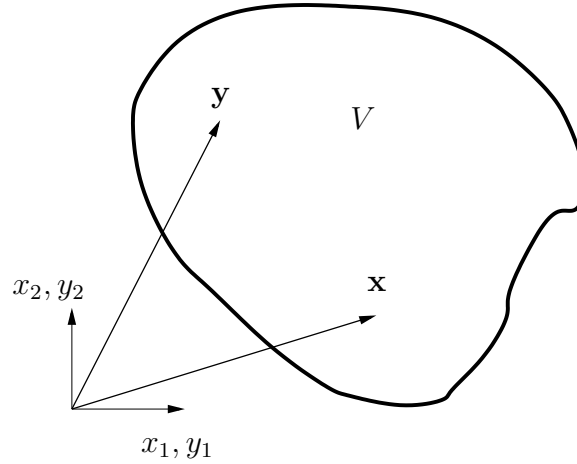
1. Take the divergence of the incompressible Navier-Stokes equation assuming constant viscosity (see Eq. 6.6) i.e. $\dfrac{\partial}{\partial x_i}\left(v_j\dfrac{\partial v_i}{\partial x_j}\right)=\ldots$
   $\Rightarrow$ Equation **A**.

2. Take the divergence of the incompressible time-averaged Navier-Stokes equation assuming constant viscosity (see Eq. 6.10) i.e. $\dfrac{\partial}{\partial x_i}\left(\bar{v}_j\dfrac{\partial \bar{v}_i}{\partial x_j}\right)=\ldots \Rightarrow$ Equation **B**.

Eq. A - Eq. B gives

$$\frac{1}{\rho}\frac{\partial^2 p'}{\partial x_j \partial x_j}=-\underbrace{2\frac{\partial \bar{v}_i}{\partial x_j}\frac{\partial v'_j}{\partial x_i}}_{\text{rapid term}}-\underbrace{\frac{\partial^2}{\partial x_i \partial x_j}\left(v'_i v'_j - \overline{v'_i v'_j}\right)}_{\text{slow term}} \qquad \text{(K.7)}$$

$$\frac{\partial^2 \varphi}{\partial x_j \partial x_j}=f$$

►There exists an exact analytical solution given by Green's formula (derived from Gauss divergence law)

$$\varphi(\mathbf{x})=-\frac{1}{4\pi}-\int_V \frac{f(\mathbf{y})dy_1 dy_2 dy_3}{|\mathbf{y}-\mathbf{x}|}$$

where $dy_1 dy_2 dy_3 = dV = d\mathbf{y}^3$. The integral is carried out for all points,

$\mathbf{y}$, in volume V.

$$p'(\mathbf{x}) = \frac{\rho}{4\pi} \int_V \left[2 \underbrace{\frac{\partial \bar{v}_i(\mathbf{y})}{\partial y_j} \frac{\partial v'_j(\mathbf{y})}{\partial y_i}}_{\text{rapid term}} \right.$$

$$\left. + \underbrace{\frac{\partial^2}{\partial y_i \partial y_j} \left(v'_i(\mathbf{y})v'_j(\mathbf{y}) - \overline{v'_i(\mathbf{y})v'_j(\mathbf{y})} \right)}_{\text{slow term}} \right] \frac{d\mathbf{y}^3}{|\mathbf{y} - \mathbf{x}|} \qquad (K.8)$$

▶Now make two assumptions in Eq. K.8:

i) the turbulence is homogeneous which means that the last term in square brackets is zero.

ii) the variation of $\partial \bar{v}_i / \partial x_j$ in space is small because $\partial \bar{v}_i / \partial x_j$ varies much more slowly $\partial v'_j(\mathbf{y}) / \partial y_i$

Assumption *i)* $\Rightarrow$ last term in the integral in Eq. 11.68 is zero, i.e.

$$\frac{\partial^2 \overline{v'_i v'_j}}{\partial y_i \partial y_j} = 0$$

Assumption *ii)* $\Rightarrow$ mean velocity gradient moved outside the integral.
  ▶multiply Eq. K.8 with $\partial v'_i / \partial x_j + \partial v'_j / \partial x_i$ and average:

$$\frac{1}{\rho} \overline{p'(\mathbf{x}) \left(\frac{\partial v'_i(\mathbf{x})}{\partial x_j} + \frac{\partial v'_j(\mathbf{x})}{\partial x_i} \right)}$$

$$= \frac{\partial \bar{v}_k(\mathbf{x})}{\partial x_\ell} \frac{1}{2\pi} \int_V \underbrace{\overline{\left(\frac{\partial v'_i(\mathbf{x})}{\partial x_j} + \frac{\partial v'_j(\mathbf{x})}{\partial x_i} \right) \frac{\partial v'_\ell(\mathbf{y})}{\partial y_k}} \frac{d\mathbf{y}^3}{|\mathbf{y} - \mathbf{x}|}}_{M_{ijk\ell}} \qquad (K.9)$$

$$+ \underbrace{\frac{1}{4\pi} \int_V \overline{\left(\frac{\partial v'_i(\mathbf{x})}{\partial x_j} + \frac{\partial v'_j(\mathbf{x})}{\partial x_i} \right) \frac{\partial^2}{\partial y_k \partial y_\ell} \left(v'_k(\mathbf{y})v'_\ell(\mathbf{y}) \right)} \frac{d\mathbf{y}^3}{|\mathbf{y} - \mathbf{x}|}}_{A_{ij}}$$

Short form of Eq. K.9:

$$\overline{\frac{p'}{\rho} \left(\frac{\partial v'_i}{\partial x_j} + \frac{\partial v'_j}{\partial x_i} \right)} = A_{ij} + M_{ijk\ell} \frac{\partial \bar{v}_k}{\partial x_\ell} = \Phi_{ij,1} + \Phi_{ij,2}$$

• First term=slow term, $\Phi_{ij,1}$ (see Eq. 11.57),

• second term=rapid term, $\Phi_{ij,2}$ (index 2 denotes the rapid part).

$$\Phi_{ij,2} = -c_2\rho \left(P_{ij} - \frac{2}{3}\delta_{ij}P^k \right) \quad \text{IP model}$$

See Eq. 11.90.

¶See Section 11.7.6, Wall model of the pressure-strain term
►Wall models of pressure-strain:

$$\Phi_{ij} = \Phi_{ij,1} + \Phi_{ij,2} + \Phi_{ij,1w} + \Phi_{ij,2w}$$

$$\Phi_{22,1w} = -2c_{1w}\frac{\varepsilon}{k}\overline{v_2'^2}f, \quad f = \min\left\{\frac{k^{\frac{3}{2}}}{2.55|n_{i,w}(x_i - x_{i,w})|\varepsilon}, 1.0\right\}$$

Traceless $\Rightarrow$

$$\Phi_{11,1w} = \Phi_{33,1w} = c_{1w}\frac{\varepsilon}{k}\overline{v_2'^2}f$$

The wall model for the shear stress is set as

$$\Phi_{12,1w} = -\frac{3}{2}c_{1w}\frac{\varepsilon}{k}\overline{v_1'v_2'}f$$

The general form reads:

$$\Phi_{ij,1w} = c_{1w}\frac{\varepsilon}{k}\left(\overline{v_k'v_m'}n_{k,w}n_{m,w}\delta_{ij} - \frac{3}{2}\overline{v_k'v_i'}n_{k,w}n_{j,w} - \frac{3}{2}\overline{v_k'v_j'}n_{i,w}n_{k,w}\right)f$$

The analogous wall model for the rapid part reads

$$\Phi_{ij,2w} = c_{2w}\left(\Phi_{km,2}n_{k,w}n_{m,w}\delta_{ij} - \frac{3}{2}\Phi_{ki,2}n_{k,w}n_{j,w} - \frac{3}{2}\Phi_{kj,2}n_{i,w}n_{k,w}\right)f$$

¶See Section 11.9, The modeled $\overline{v_i' v_j'}$ equation with IP model

►We can finally formulate the **modelled** $\overline{v_i' v_j'}$ equation (with IP model), the Reynolds Stress Model (RSM)

$$\frac{\partial \overline{v_i' v_j'}}{\partial t} + \quad \text{(unsteady term)}$$

$$\bar{v}_k \frac{\partial \overline{v_i' v_j'}}{\partial x_k} = \quad \text{(convection)}$$

$$-\overline{v_i' v_k'} \frac{\partial \bar{v}_j}{\partial x_k} - \overline{v_j' v_k'} \frac{\partial \bar{v}_i}{\partial x_k} \quad \text{(production)}$$

$$-c_1 \frac{\varepsilon}{k} \left(\overline{v_i' v_j'} - \frac{2}{3} \delta_{ij} k \right) \quad \text{(slow part)}$$

$$-c_2 \left(P_{ij} - \frac{2}{3} \delta_{ij} P^k \right) \quad \text{(rapid part, IP model)}$$

$$+c_{1w} \rho \frac{\varepsilon}{k} \left[\overline{v_k' v_m'} n_k n_m \delta_{ij} - \frac{3}{2} \overline{v_i' v_k'} n_k n_j \right.$$

$$\left. - \frac{3}{2} \overline{v_j' v_k'} n_k n_i \right] f \quad \text{(wall, slow part)}$$

$$+c_{2w} \left[\Phi_{km,2} n_k n_m \delta_{ij} - \frac{3}{2} \Phi_{ik,2} n_k n_j \right.$$

$$\left. - \frac{3}{2} \Phi_{jk,2} n_k n_i \right] f \quad \text{(wall, rapid part, IP model))}$$

$$+\nu \frac{\partial^2 \overline{v_i' v_j'}}{\partial x_k \partial x_k} \quad \text{(viscous diffusion)}$$

$$+\frac{\partial}{\partial x_k} \left[\frac{\nu_t}{\sigma_k} \frac{\partial \overline{v_i' v_j'}}{\partial x_m} \right] \quad \text{(turbulent diffusion)}$$

$$-g_i \beta \overline{v_j' \theta'} - g_j \beta \overline{v_i' \theta'} \quad \text{(buoyancy production)}$$

$$-\frac{2}{3} \varepsilon \delta_{ij} \quad \text{(dissipation)}$$

¶See Section 11.10, Algebraic Reynolds Stress Model (ASM)

▶The <u>A</u>lgebraic Reynolds <u>S</u>tress <u>M</u>odel (ASM) is a simplified Reynolds Stress Model (RSM)

$$\text{RSM} : C_{ij} - D_{ij} = P_{ij} + \Phi_{ij} - \varepsilon_{ij}$$

$$k - \varepsilon :\ C^k - D^k = P^k - \varepsilon$$

Assumption in ASM:

$$C_{ij} - D_{ij} = \frac{\overline{v_i' v_j'}}{k} \left(C^k - D^k \right)$$

$$\Rightarrow P_{ij} + \Phi_{ij} - \varepsilon_{ij} = \frac{\overline{v_i' v_j'}}{k} \left(P^k - \varepsilon \right)$$

This gives

$$\overline{v_i' v_j'} = \frac{2}{3}\delta_{ij}k + \frac{k}{\varepsilon} \frac{(1 - c_2)\left(P_{ij} - \frac{2}{3}\delta_{ij}P^k\right) + \Phi_{ij,1w} + \Phi_{ij,2w}}{c_1 + P^k/\varepsilon - 1}$$

¶See Section 11.13, Boundary layer flow

▶We will now look at the source terms in the modelled $\overline{v_i' v_j'}$ equation (Eq. 11.101), for a special flow, namely the boundary layer flow. We have $\bar{v}_2 \simeq 0$, $\partial \bar{v}_1/\partial x_2 \gg \partial \bar{v}_1/\partial x_1$. The production term reads (Eq. 11.38)

$$P_{ij} = -\overline{v_i' v_k'}\frac{\partial \bar{v}_j}{\partial x_k} - \overline{v_j' v_k'}\frac{\partial \bar{v}_i}{\partial x_k}$$

In this special case we get:

$$P_{11} = -2\overline{v_1' v_2'}\frac{\partial \bar{v}_1}{\partial x_2}$$

$$P_{12} = -\overline{v_2'^2}\frac{\partial \bar{v}_1}{\partial x_2}$$

$$P_{22} = 0$$

$$\Phi_{22,1} = c_1 \frac{\varepsilon}{k}\left(\frac{2}{3}k - \overline{v_2'^2}\right) > 0$$

$$\Phi_{22,2} = c_2\frac{1}{3}P_{11} = -c_2\frac{2}{3}\overline{v_1' v_2'}\frac{\partial \bar{v}_1}{\partial x_2} > 0$$

$\varepsilon_{12} = 0$: No sink term in $\overline{v_1' v_2'}$ eq? Answer: the pressure strain terms $\Phi_{12,1}$ and $\Phi_{12,2}$ act as sink terms.

¶See Section 12.1, Stable and unstable stratification

▶Assume there is a non-constant temperature field and that the natural convection is important (no forced convection). We have then two different flow conditions, stable or unstable conditions.

We start with stable stratification for which $\partial\bar{\theta}/\partial x_3 > 0$.
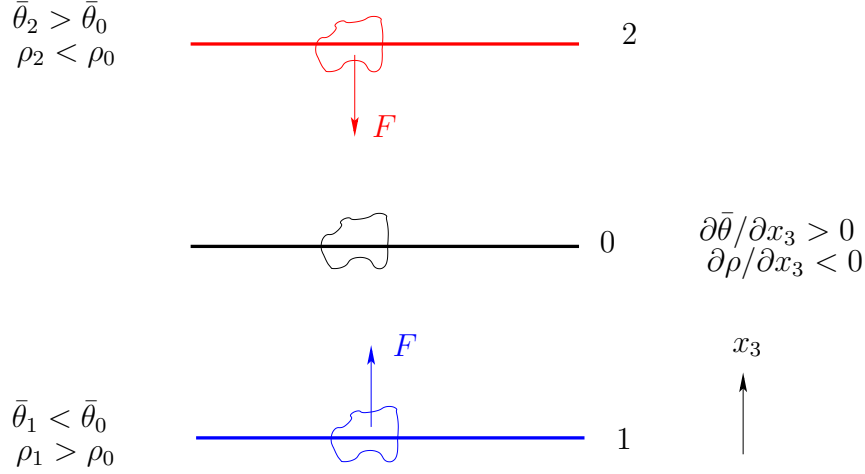
$$G_{ij} = -g_i\beta\overline{v'_j\theta'} - g_j\beta\overline{v'_i\theta'} \quad \Rightarrow \overline{v'^2_3} \text{ eq.:} \quad G_{33} = 2g\beta\overline{v'_3\theta'}$$

which is the source term in the $\overline{v'^2_3}$ eq (Eq. 11.101) due to buoyancy. Now we need $\overline{v'_3\theta'}$. Its main source term reads (see Eq. 11.22)

$$P_{3\theta} = -\overline{v'_3 v'_k}\frac{\partial\bar{\theta}}{\partial x_k} - \overline{v'_k\theta'}\frac{\partial\bar{v}_3}{\partial x_k} = -\overline{v'^2_3}\frac{\partial\bar{\theta}}{\partial x_3} < 0$$

So

- $P_{3\theta} < 0 \Rightarrow \overline{v'_3\theta'} < 0$

- $\Rightarrow G_{33} < 0$

- which dampens $\overline{v'^2_3}$ (but not $\overline{v'^2_1}, \overline{v'^2_2}$) as it should.

▶$k - \varepsilon$ model. The buoyancy term reads (Eq. 12.3)

$$G^k = 0.5G_{ii} = -g_i\beta\overline{v'_i\theta'}, \quad \overline{v'_i\theta'} = -\frac{\nu_t}{\sigma_\theta}\frac{\partial\bar{\theta}}{\partial x_i}$$

For $g_i = (0, 0, -g)$ it reads $G^k = g\beta\overline{v'_3\theta'}$ which gives, using Eq. 11.35,

$$G^k = -g\beta\frac{\nu_t}{\sigma_\theta}\frac{\partial\bar{\theta}}{\partial x_3}$$

Hence $G^k < 0$ which dampens k (i.e. $\overline{v'^2_1}, \overline{v'^2_2}, \overline{v'^2_3}$).

K.4   Lecture 4

¶See Section 12.2, Curvature effects

▶Streamline curvature affects the turbulence. Let's look at an example where the streamlines are aligned with the θ axis. We assume inviscid flow (viscosity equal to zero) and express the Navier-Stokes eq. in polar coordinates:

$$v_r \text{ eq. with } \mu = 0: \quad \frac{\rho v_\theta^2}{r} - \frac{\partial p}{\partial r} = 0 \qquad \text{(K.10)}$$

$\partial v_\theta / \partial r > 0$. Hence $(v_\theta)_A > (v_\theta)_0$, which from Eq. K.10 gives $(\partial p / \partial r)_A > (\partial p / \partial r)_0$.
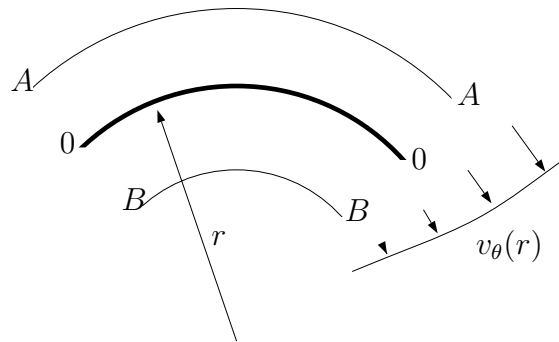
▶Now we will find out how well the effect of streamline curvature is modelled by RSM (and ASM). We choose a boundary layer flow in which the flow departs from the wall (see figure below).
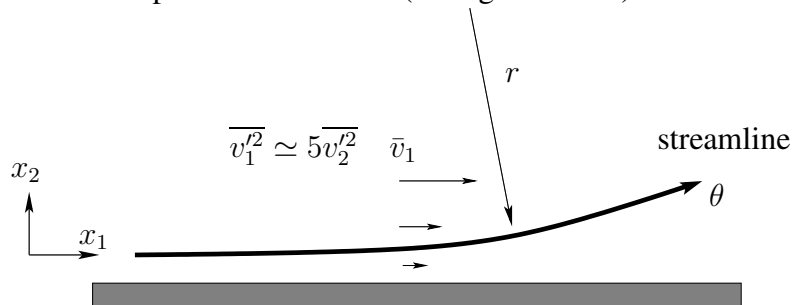
For this flow, the production terms read (boxed terms appear because

the boundary layer departs from the wall)

$$\text{RSM, } \overline{v_1'^2} - \text{eq.}: \quad P_{11} = -2\overline{v_1'v_2'}\frac{\partial \bar{v}_1}{\partial x_2} \tag{K.11a}$$

$$\text{RSM, } \overline{v_1'v_2'} - \text{eq.}: \quad P_{12} = \boxed{-\overline{v_1'^2}\frac{\partial \bar{v}_2}{\partial x_1}} - \overline{v_2'^2}\frac{\partial \bar{v}_1}{\partial x_2} \tag{K.11b}$$

$$\text{RSM, } \overline{v_2'^2} - \text{eq.}: \quad P_{22} = \boxed{-2\overline{v_1'v_2'}\frac{\partial \bar{v}_2}{\partial x_1}} \tag{K.11c}$$

$$k - \varepsilon \quad P^k = \nu_t \left\{ \left(\frac{\partial \bar{v}_1}{\partial x_2}\right) + \boxed{\left(\frac{\partial \bar{v}_2}{\partial x_1}\right)} \right\}^2 \tag{K.11d}$$

- $\frac{\partial \bar{v}_1}{\partial x_2} > 0, \frac{\partial \bar{v}_2}{\partial x_1} > 0$

- $-\overline{v_1'^2}\frac{\partial \bar{v}_2}{\partial x_1}$ increases $|P_{12}|$ (recall that $\overline{v_1'^2} \gg \overline{v_2'^2}$)

- $\Rightarrow |\overline{v_1'v_2'}|$ increases

- $\Rightarrow \overline{v_1'^2}$ and $\overline{v_2'^2}$ increase

- $\Rightarrow |P_{12}|$ increases even more (a positive feedback loop)

¶See Section 12.3, Stagnation flow
►Stagnation 2D flow
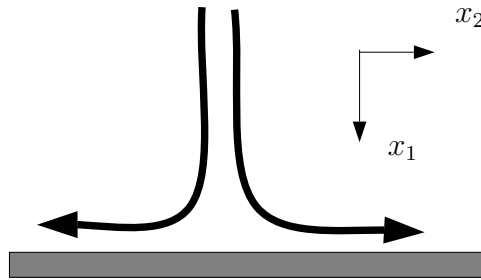
The flow pattern for stagnation flow.

$$RSM/ASM : 0.5\,(P_{11} + P_{22}) = -\overline{v_1'^2}\frac{\partial \bar{v}_1}{\partial x_1} - \overline{v_2'^2}\frac{\partial \bar{v}_2}{\partial x_2} = -\frac{\partial \bar{v}_1}{\partial x_1}(\overline{v_1'^2} - \overline{v_2'^2})$$

$$k - \varepsilon : P^k = 2\nu_t \left\{ \left(\frac{\partial \bar{v}_1}{\partial x_1}\right)^2 + \left(\frac{\partial \bar{v}_2}{\partial x_2}\right)^2 \right\}$$

For RSM/ASM, $\overline{v_1'^2} - \overline{v_2'^2}$ nearly cancels whereas for $k - \varepsilon$ they don't since the sum of squared velocity gradients is used.

¶See Section 13, Realizability
►Realizability

$$\overline{v_i'^2} \geq 0 \text{ for all } i$$

$$\frac{\left|\overline{v_i' v_j'}\right|}{\left(\overline{v_i'^2}\,\overline{v_j'^2}\right)^{1/2}} \leq 1 \text{ no summation over } i \text{ and } j, \ i \neq j$$

$$\overline{v_1'^2} = \frac{2}{3}k - 2\nu_t \frac{\partial \bar{v}_1}{\partial x_1} = \frac{2}{3}k - 2\nu_t \bar{s}_{11}$$

$\bar{s}_{11}$ largest in the principal coordinate directions. Hence, let's find the eigenvalues of $\bar{s}_{ij}$

$$\left|\bar{s}_{ij} - \delta_{ij}\lambda\right| = 0$$

which gives in 2D

$$\begin{vmatrix} \bar{s}_{11} - \lambda & \bar{s}_{12} \\ \bar{s}_{21} & \bar{s}_{22} - \lambda \end{vmatrix} = 0$$

The resulting equation characteristic equation is

$$\lambda^2 - I_1^{2D}\lambda + I_2^{2D} = 0$$

$$I_1^{2D} = \bar{s}_{ii} = 0 \quad \textbf{continuity equation}$$

$$I_2^{2D} = \frac{1}{2}(\bar{s}_{ii}\bar{s}_{jj} - \bar{s}_{ij}\bar{s}_{ij}) = \det(C_{ij}) = -\bar{s}_{ij}\bar{s}_{ij}/2$$

$$\lambda_{1,2} = \pm\left(-I_2^{2D}\right)^{1/2} = \pm\left(\frac{\bar{s}_{ij}\bar{s}_{ij}}{2}\right)^{1/2}$$

$$\overline{v_1'^2} = \frac{2}{3}k - 2\nu_t\lambda_1 = \frac{2}{3}k - 2\nu_t\left(\frac{\bar{s}_{ij}\bar{s}_{ij}}{2}\right)^{1/2} \Rightarrow \nu_t \leq \frac{k}{3|\lambda_1|} = \frac{k}{3}\left(\frac{2}{\bar{s}_{ij}\bar{s}_{ij}}\right)^{1/2}$$

In 3D

$$|\lambda_k| = k\left(\frac{2\bar{s}_{ij}\bar{s}_{ij}}{3}\right)^{1/2}$$

¶See Section 14, Non-linear Eddy-viscosity Models
▶Non-linear eddy-viscosity models

It is non-linear in velocity gradients. The advantage is better normal stresses and a certain ability to handle streamline curvature.

The anisotropy tensor is defined as ($-2/3 \leq a_{ij} \leq 2$, and $a_{ij} = 0$ for isotropic turbulence)

$$a_{ij} \equiv \frac{\overline{v_i' v_j'}}{k} - \frac{2}{3}\delta_{ij}$$

$$a_{ij} = \boxed{-2c_\mu \tau \bar{s}_{ij}}$$
$$+ c_1 \tau^2 \left(\bar{s}_{ik}\bar{s}_{kj} - \frac{1}{3}\bar{s}_{\ell k}\bar{s}_{\ell k}\delta_{ij} \right) + c_2 \tau^2 \left(\bar{\Omega}_{ik}\bar{s}_{kj} - \bar{s}_{ik}\bar{\Omega}_{kj} \right)$$
$$+ c_3 \tau^2 \left(\bar{\Omega}_{ik}\bar{\Omega}_{jk} - \frac{1}{3}\bar{\Omega}_{\ell k}\bar{\Omega}_{\ell k}\delta_{ij} \right) + c_4 \tau^3 \left(\bar{s}_{ik}\bar{s}_{k\ell}\bar{\Omega}_{\ell j} - \bar{\Omega}_{i\ell}\bar{s}_{\ell k}\bar{s}_{kj} \right)$$
$$+ c_5 \tau^3 \left(\bar{\Omega}_{i\ell}\bar{\Omega}_{\ell m}\bar{s}_{mj} + \bar{s}_{i\ell}\bar{\Omega}_{\ell m}\bar{\Omega}_{mj} - \frac{2}{3}\bar{\Omega}_{mn}\bar{\Omega}_{n\ell}\bar{s}_{\ell m}\delta_{ij} \right)$$
$$+ c_6 \tau^3 \bar{s}_{k\ell}\bar{s}_{k\ell}\bar{s}_{ij} + c_7 \tau^3 \bar{\Omega}_{k\ell}\bar{\Omega}_{k\ell}\bar{s}_{ij}$$
$$\bar{\Omega}_{ij} = \frac{1}{2} \left(\frac{\partial \bar{v}_i}{\partial x_j} - \frac{\partial \bar{v}_j}{\partial x_i} \right)$$

where $\tau = k/\varepsilon$ or $1/(c_\mu \omega)$.

$$\overline{v_1'^2} = \frac{2}{3}k + \frac{0.82}{12}k\tau^2 \left(\frac{\partial \bar{v}_1}{\partial x_2} \right)^2$$
$$\overline{v_2'^2} = \frac{2}{3}k - \frac{0.5}{12}k\tau^2 \left(\frac{\partial \bar{v}_1}{\partial x_2} \right)^2$$
$$\overline{v_3'^2} = \frac{2}{3}k - \frac{0.16}{12}k\tau^2 \left(\frac{\partial \bar{v}_1}{\partial x_2} \right)^2$$

K.5   Lecture 5

¶See Section 15, The V2F Model

►The V2F Model

Four equations are solved, k, ε (or ω), $\overline{v_2'^2}$ and f. The variable f is related to the pressure-strain term in the $\overline{v_2'^2}$ equation. The strength of this model is that it is better in modeling damping of the turbulence near walls.

The $\overline{v_2'^2}$ equation reads

$$\frac{\partial \rho \bar{v}_1 \overline{v_2'^2}}{\partial x_1} + \frac{\partial \rho \bar{v} \overline{v_2'^2}}{\partial x_2} = \frac{\partial}{\partial x_2}\left[(\mu + \mu_t)\frac{\partial \overline{v_2'^2}}{\partial x_2}\right] \underbrace{-2\overline{v_2' \partial p'/\partial x_2}}_{\Phi_{22}} -\rho\varepsilon_{22}$$

$$\frac{\partial \rho \bar{v}_1 \overline{v_2'^2}}{\partial x_1} + \frac{\partial \rho \bar{v}_2 \overline{v_2'^2}}{\partial x_2} = \frac{\partial}{\partial x_2}\left[(\mu + \mu_t)\frac{\partial \overline{v_2'^2}}{\partial x_2}\right] + \underbrace{\Phi_{22} - \rho\varepsilon_{22} + \rho\frac{\overline{v_2'^2}}{k}\varepsilon}_{fk} -\rho\frac{\overline{v_2'^2}}{k}\varepsilon$$

An equation is formulated for f (where Φ_{22} is taken as the Rotta & IP model, see Eqs. 11.57 and 11.90)

$$L^2\frac{\partial^2 f}{\partial x_2^2} - f = -\frac{\Phi_{22}}{k} - \frac{1}{T}\left(\frac{\overline{v_2'^2}}{k} - \frac{2}{3}\right), \quad T \propto \frac{k}{\varepsilon}, \quad L \propto \frac{k^{3/2}}{\varepsilon}$$

Far from wall $\frac{\partial^2 f}{\partial x_2^2} \simeq 0$ so that $-f \to -\frac{\Phi_{22}}{k} - \frac{1}{T}\left(\frac{\overline{v_2'^2}}{k} - \frac{2}{3}\right)$. Inserted in to the $\overline{v_2'^2}$ eq. above gives

$$\frac{\partial \rho \bar{v}_1 \overline{v_2'^2}}{\partial x_1} + \frac{\partial \rho \bar{v} \overline{v_2'^2}}{\partial x_2} = \frac{\partial}{\partial x_2}\left[(\mu + \mu_t)\frac{\partial \overline{v_2'^2}}{\partial x_2}\right] + \Phi_{22} - \rho\varepsilon_{22}$$

The $\overline{v_2'^2}$ eq. is retrieved. Hence the f eq. has a proper behavior far from walls.
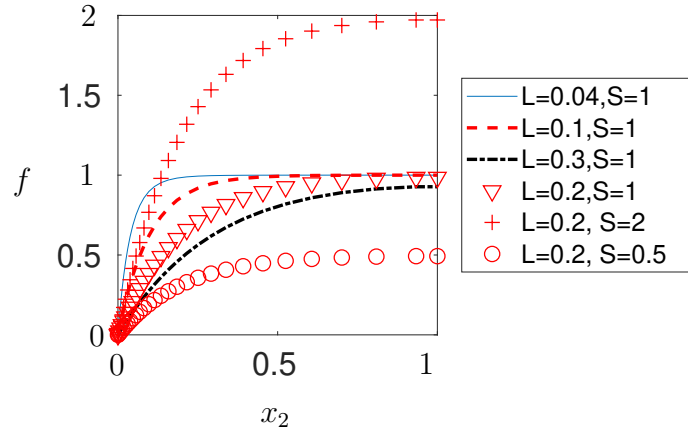
Solution of the equation $L^2\partial^2 f/\partial x_2^2 - f + S = 0$ for different L and S

▶V2F model. Wall boundary conditions

Near the wall, the $\overline{v_2'^2}$ equation reads (see Eq. 15.8)

$$0 = \nu\frac{\partial^2 \overline{v_2'^2}}{\partial x_2^2} + fk - \frac{\overline{v_2'^2}}{k}\varepsilon$$

Assume $f \simeq const$ and $\varepsilon \simeq const$ as $x_2 \Rightarrow 0$ Linear ODF

$$\overline{v_2'^2} = Ax_2^2 + \frac{B}{x_2} - \varepsilon f\frac{x_2^4}{20\nu^2}$$

Since $\overline{v_2'^2} = \mathcal{O}(x_2^4)$ as $x_2 \to 0$, $A = B = 0$, so we get

$$f = -\frac{20\nu^2}{\varepsilon}\frac{\overline{v_2'^2}}{x_2^4}$$

In 3D, the V2F model reads (see Eq. 15.9)

$$\frac{\partial \rho \bar{v}_j v^2}{\partial x_j} = \frac{\partial}{\partial x_j}\left[(\mu + \mu_t)\frac{\partial v^2}{\partial x_j}\right] + \rho fk - \rho\frac{v^2}{k}\varepsilon$$

$$L^2\frac{\partial^2 f}{\partial x_j \partial x_j} - f = -\frac{\Phi_{22}}{\rho k} - \frac{1}{T}\left(\frac{v^2}{k} - \frac{2}{3}\right)$$

$$\frac{\Phi_{22}}{\rho k} = \frac{C_1}{T}\left(\frac{2}{3} - \frac{v^2}{k}\right) + C_2\frac{P^k}{k}$$

P^k in the expression of Φ_{22} explains why v^2 is equal to $\overline{v_2'^2}$, $\overline{v_1'^2}$ or $\overline{v_3'^2}$ depending on orientation of the nearest wall, see text below Eq. 15.9

¶See Section 16, The SST Model

►The SST (Shear Stress Transport) model

1. Combination of a $k - \omega$ model (in the inner boundary layer) and $k - \varepsilon$ model (in the outer region of the boundary layer as well as outside of it);

2. A limitation of the shear stress in adverse pressure gradient regions.

►$\omega = \varepsilon/(\beta^* k) = \varepsilon/(c_\mu k)$. Use this to obtain an eq. for ω

$$\frac{d\omega}{dt} = \frac{d}{dt}\left(\frac{\varepsilon}{\beta^* k}\right) = \frac{1}{\beta^* k}\frac{d\varepsilon}{dt} - \frac{\varepsilon}{\beta^* k^2}\frac{dk}{dt} = \frac{1}{\beta^* k}\frac{d\varepsilon}{dt} - \frac{\omega}{k}\frac{dk}{dt}$$

►Production term

$$P_\omega = \frac{1}{\beta^* k}P_\varepsilon - \frac{\omega}{k}P^k = C_{\varepsilon 1}\frac{\varepsilon}{\beta^* k^2}P^k - \frac{\omega}{k}P^k = (C_{\varepsilon 1} - 1)\frac{\omega}{k}P^k$$

►Destruction term

$$\Psi_\omega = \frac{1}{\beta^* k}\Psi_\varepsilon - \frac{\omega}{k}\Psi_k = \frac{1}{\beta^* k}C_{\varepsilon 2}\frac{\varepsilon^2}{k} - \frac{\omega}{k}\varepsilon = (C_{\varepsilon 2} - 1)\beta^*\omega^2$$

►Viscous diffusion term

$$D_\omega^\nu = \frac{\nu}{\beta^* k}\frac{\partial^2\varepsilon}{\partial x_j^2} - \frac{\nu\omega}{k}\frac{\partial^2 k}{\partial x_j^2} = \frac{\nu}{k}\frac{\partial^2\omega k}{\partial x_j^2} - \frac{\nu\omega}{k}\frac{\partial^2 k}{\partial x_j^2}$$

$$= \frac{\nu}{k}\left[\frac{\partial}{\partial x_j}\left(\omega\frac{\partial k}{\partial x_j} + k\frac{\partial\omega}{\partial x_j}\right)\right] - \nu\frac{\omega}{k}\frac{\partial^2 k}{\partial x_j^2}$$

$$= \frac{2\nu}{k}\frac{\partial\omega}{\partial x_j}\frac{\partial k}{\partial x_j} + \frac{\partial}{\partial x_j}\left(\nu\frac{\partial\omega}{\partial x_j}\right)$$

The ω eq. (which really is an ε eq. when the $k - \varepsilon$ constants are used)

$$\frac{\partial}{\partial x_j}(\bar{v}_j \omega) = \frac{\partial}{\partial x_j}\left[\left(\nu + \frac{\nu_t}{\sigma_\omega}\right)\frac{\partial \omega}{\partial x_j}\right] + \alpha\frac{\omega}{k}P^k - \beta\omega^2 + \frac{2}{k}\left(\nu + \frac{\nu_t}{\sigma_\varepsilon}\right)\frac{\partial k}{\partial x_i}\frac{\partial \omega}{\partial x_i}$$
$$\alpha = C_{\varepsilon 1} - 1 = 0.44, \beta = (C_{\varepsilon 2} - 1)\beta^* = 0.0828$$

Inner region: $k - \omega$ coeff; outer region: $k - \varepsilon$ coeff. Blending function

$$F_1 = \tanh(\xi^4), \quad \xi \propto \frac{L_t}{x_n} = \frac{k^{1/2}}{\omega x_n}$$

$F_1 = 1$ in the near-wall region and $F_1 = 0$ in the outer region. The β-coefficient, for example, is computed as

$$\beta_{SST} = F_1\beta_{k-\omega} + (1 - F_1)\beta_{k-\varepsilon}$$

▶SST model. Limitation of shear stress.

The $k - \omega$ gives too high shear stress. The JK model based on $-\overline{v_1' v_2'} = a_1 k$ ($a_1 = c_\mu^{1/2}$) gives good results.

▶Two formulas for ν_t. $\Omega = \partial\bar{v}_1/\partial x_2$. Formulate JK model with Boussinesq.

$$\left.\begin{array}{ll} \text{JK Model:} & \nu_t = \frac{-\overline{v_1' v_2'}}{\Omega} = \frac{a_1 k}{\Omega} \\ k - \omega \text{ model:} & \nu_t = \frac{k}{\omega} = \frac{a_1 k}{a_1 \omega} \end{array}\right\} \nu_t = \frac{a_1 k}{\max(a_1\omega, F_2\Omega)}$$

F_2 (see Eq. 16.18) is one near walls and zero elsewhere

▶The idea is that

- the second part, $a_1 k/\Omega$ (which mimics the Johnson-King model), should be used in APG flow (where $P^k > \varepsilon$)

- the first part, k/ω (which corresponds to the usual Boussinesq model), should be in the remaining of the flow

K.6 Lecture 6

¶See Section 5, Turbulence

▶Turbulence

▶$v_i = \bar{v}_i + v_i'$, is irregular and consists of eddies of different size

▶increases diffusivity

x_2

turbulent

$\tau_w = \mu \dfrac{\partial v_1}{\partial x_2}$

laminar

x_1

$\tau_w = \mu \dfrac{\partial v_1}{\partial x_2}$

▶occurs at large Reynolds numbers. Pipes: $Re_D = \dfrac{VD}{\nu} \simeq 2300$;
boundary layers: $Re_x = \dfrac{VL}{\nu} \simeq 500\,000$.

▶is three-dimensional

▶is dissipative. Kinetic energy, $v_i'v_i'/2$, in the small (dissipative) ed-

dies are transformed into thermal energy (increases temperature).

flow of kinetic energy

dissipative scales

intermediate scales

large scales

►Dissipation $\varepsilon = \nu \overline{\dfrac{\partial v_i'}{\partial x_j} \dfrac{\partial v_i'}{\partial x_j}}$

All kinetic energy (say 90%) is finally dissipated at the smallest (dissipative) scales.

►Kinetic energy dissipative at small scales determined by ε, ν

$$
\begin{array}{ccccc}
v_\eta & = & \nu^a & & \varepsilon^b \\
[m/s] & = & [m^2/s] & & [m^2/s^3]
\end{array}
$$

$$
\begin{array}{ll}
1 = 2a + 2b, & [m] \\
-1 = -a - 3b, & [s]
\end{array}
$$

►This gives the Kolmogorov scales (see Eq. 5.5)

$$
v_\eta = (\nu\varepsilon)^{1/4}, \; \ell_\eta = \left(\frac{\nu^3}{\varepsilon}\right)^{1/4}, \; \tau_\eta = \left(\frac{\nu}{\varepsilon}\right)^{1/2}
$$

►Any periodic function, f, can be expressed as a Fourier series

$$
f(x) = \frac{1}{2}a_0 + \sum_{n=1}^{\infty}(a_n \cos(\kappa_n x) + b_n \sin(\kappa_n x)), \quad f = v, \quad \kappa_n = \frac{n\pi}{L}
$$

$$a_n = \frac{1}{L} \int_{-L}^{L} f(x) \cos(\kappa_n x) dx$$

—   — $$b_n = \frac{1}{L} \int_{-L}^{L} f(x) \sin(\kappa_n x) dx$$

Parseval's formula states that (average over all eddies)

$$\int_{-L}^{L} v'^2(x) dx = \frac{L}{2} a_0^2 + L \sum_{n=1}^{\infty} (a_n^2 + b_n^2)$$

Time-averaging (average of over time instants):

— $$\overline{v'^2} = \frac{1}{2T} \int_{-T}^{T} v'^2 dt$$

► Spectrum for turbulent kinetic energy, k

$$P^k = -\overline{v_i' v_j'} \frac{\partial \bar{v}_i}{\partial x_j}$$

$$E(\kappa_n) \propto a_n^2 + b_n^2$$

$$k = \int_0^\infty E(\kappa)d\kappa = \sum_0^\infty E(\kappa_n)\Delta\kappa_n$$

The turbulence spectrum is divided into three regions:

I. Large eddies carry most of the turbulent kinetic energy. They extract energy from the mean flow.

II. Inertial subrange. Independent of both large eddies (mean flow) and viscosity.

III. Dissipation range. Isotropic eddies ($\overline{v_i'v_j'} = c_1\delta_{ij}$) described by the Kolmogorov scales.

▶Turb. kinetic energy in Region II depend on ε and eddy size $1/\kappa$.

$$\begin{array}{ccc} E & = & \kappa^a \quad \varepsilon^b \\ [m^3/s^2] & = & [1/m] \quad [m^2/s^3] \end{array}$$

$$3 = -a + 2b, \quad [m]$$
$$-2 = -3b, \quad [s]$$

$b = 2/3, a = -5/3$ so that

$$E(\kappa) = \text{const.} \cdot \varepsilon^{\frac{2}{3}}\kappa^{-\frac{5}{3}}$$

▶This is called von Kármán spectrum or $-5/3$ law

$$\varepsilon_\kappa \sim \frac{v_\kappa^2}{\ell_\kappa/v_\kappa} \sim \frac{v_\kappa^3}{\ell_\kappa} \sim \frac{v_0^3}{\ell_0}$$

▶Relation between largest and smallest scales ($Re = v_0\ell_0/\nu$)

$$\frac{v_0}{v_\eta} = (\nu\varepsilon)^{-1/4}v_0 = \left(\nu v_0^3/\ell_0\right)^{-1/4}v_0 = (v_0\ell_0/\nu)^{1/4} = Re^{1/4}$$

$$\frac{\ell_0}{\ell_\eta} = \left(\frac{\nu^3}{\varepsilon}\right)^{-1/4}\ell_0 = \left(\frac{\nu^3\ell_0}{v_0^3}\right)^{-1/4}\ell_0 = \left(\frac{\nu^3}{v_0^3\ell_0^3}\right)^{-1/4} = Re^{3/4}$$

$$\frac{\tau_o}{\tau_\eta} = \left(\frac{\nu\ell_0}{v_0^3}\right)^{-1/2}\tau_0 = \left(\frac{v_0^3}{\nu\ell_0}\right)^{1/2}\frac{\ell_0}{v_0} = \left(\frac{v_0\ell_0}{\nu}\right)^{1/2} = Re^{1/2}$$

• This explains why DNS (Direct Numerical Simulation) is too expensive at high Re numbers: a doubling of Re number $\Rightarrow$

$$\underbrace{2^{3/4}}_{x_1\ dir} \times \underbrace{2^{3/4}}_{x_2\ dir} \times \underbrace{2^{3/4}}_{x_3\ dir} \times \underbrace{2^{1/2}}_{time} = 2^{11/4} \simeq 7$$

times increase in computational effort

▶Why dissipation only at small scales?

• Let's show that $\varepsilon = \nu\overline{\dfrac{\partial v_i'}{\partial x_j}\dfrac{\partial v_i'}{\partial x_j}}$ gets larger the smaller the scales.

• The velocity gradient for an eddy can be estimated as (see Eq. 8.17)

$$\left(\frac{\partial v}{\partial x}\right)_\kappa \propto \frac{v_\kappa}{\ell_\kappa} \propto \left(v_\kappa^2\right)^{1/2}\kappa$$

Energy spectrum gives

$$E(\kappa) \propto k_\kappa/\kappa \propto v_\kappa^2/\kappa \propto \kappa^{-5/3} \quad \Rightarrow \quad v_\kappa^2 \propto \kappa^{-2/3}$$

We get

$$\left(\frac{\partial v}{\partial x}\right)_\kappa \propto \left(\kappa^{-2/3}\right)^{1/2} \kappa \propto \kappa^{-1/3}\kappa \propto \kappa^{2/3}$$

- Hence ε gets larger the smaller the scales.

K.7 Lecture 7

¶See Section 18, Large Eddy Simulations

▶LES

<u>in RANS:</u>

$$\langle \Phi \rangle = \frac{1}{2T} \int_{-T}^{T} \Phi(t) dt, \quad \Phi = \langle \Phi \rangle + \Phi', \quad \langle \Phi' \rangle = 0$$

<u>in LES:</u>

$$\bar{\Phi}(x,t) = \frac{1}{\Delta x} \int_{x-0.5\Delta x}^{x+0.5\Delta x} \Phi(\xi,t) d\xi, \quad \Phi = \bar{\Phi} + \Phi'', \quad \overline{\Phi''} \neq 0$$

$$\frac{\partial \bar{v}_i}{\partial t} + \frac{\partial}{\partial x_j} (\bar{v}_i \bar{v}_j) = -\frac{1}{\rho} \frac{\partial \bar{p}}{\partial x_i} + \nu \frac{\partial^2 \bar{v}_i}{\partial x_j \partial x_j} - \frac{\partial \tau_{ij}}{\partial x_j}, \quad \tau_{ij} = \overline{v_i v_j} - \bar{v}_i \bar{v}_j$$

▶Filter and derivative (see Eq. 18.4)

$$\overline{\frac{\partial p}{\partial x_i}} = \frac{1}{V} \int_V \frac{\partial p}{\partial x_i} dV \overset{?}{=} \frac{\partial}{\partial x_i} \left(\frac{1}{V} \int_V p dV \right) = \frac{\partial \bar{p}}{\partial x_i}$$

$$\overline{\frac{\partial p}{\partial x_i}} = \frac{\partial}{\partial x_i} \left(\frac{1}{V} \int_V p dV \right) + \mathcal{O}\left((\Delta x)^2 \right) = \frac{\partial \bar{p}}{\partial x_i} + \mathcal{O}\left((\Delta x)^2 \right)$$

▶Non-linear term (see Eq. 18.5)

$$\overline{\frac{\partial v_i v_j}{\partial x_j}} = \frac{\partial}{\partial x_j}(\overline{v_i v_j}) + \mathcal{O}\left((\Delta x)^2 \right)$$

$$\text{Left side}: \frac{\partial}{\partial x_j}(\overline{v_i v_j}) \underline{- \frac{\partial}{\partial x_j}(\overline{v_i v_j}) + \frac{\partial}{\partial x_j}(\bar{v}_i \bar{v}_j)} = \frac{\partial}{\partial x_j}(\bar{v}_i \bar{v}_j)$$

$$\text{Right side}: \underline{-\frac{\partial}{\partial x_j}(\overline{v_i v_j}) + \frac{\partial}{\partial x_j}(\bar{v}_i \bar{v}_j)} = -\frac{\partial \tau_{ij}}{\partial x_j}$$

$$\blacktriangleright \frac{\partial \bar{v}_i}{\partial t} + \frac{\partial}{\partial x_j} (\bar{v}_i \bar{v}_j) = -\frac{1}{\rho} \frac{\partial \bar{p}}{\partial x_i} + \nu \frac{\partial^2 \bar{v}_i}{\partial x_j \partial x_j} - \frac{\partial \tau_{ij}}{\partial x_j}$$

$$\tau_{ij} = \overline{v_i v_j} - \bar{v}_i \bar{v}_j$$

▶Filtering twice (used for turbulence modeling), see Eq. 18.6

$$\bar{\bar{v}}_I = \frac{1}{\Delta x} \int_{-\Delta x/2}^{\Delta x/2} \bar{v}(\xi) d\xi = \frac{1}{\Delta x} \left(\int_{-\Delta x/2}^{0} \bar{v}(\xi) d\xi + \int_{0}^{\Delta x/2} \bar{v}(\xi) d\xi \right) =$$

$$= \frac{1}{\Delta x} \left(\frac{\Delta x}{2} \bar{v}_A + \frac{\Delta x}{2} \bar{v}_B \right) \cdot = \frac{1}{2} \left[\left(\frac{1}{4} \bar{v}_{I-1} + \frac{3}{4} \bar{v}_I \right) + \left(\frac{3}{4} \bar{v}_I + \frac{1}{4} \bar{v}_{I+1} \right) \right]$$

$$= \frac{1}{8} \left(\bar{v}_{I-1} + 6\bar{v}_I + \bar{v}_{I+1} \right) \neq \bar{v}_I$$

¶See Section 18.3, Resolved & SGS scales
▶Resolved & SGS scales (GS & SGS)
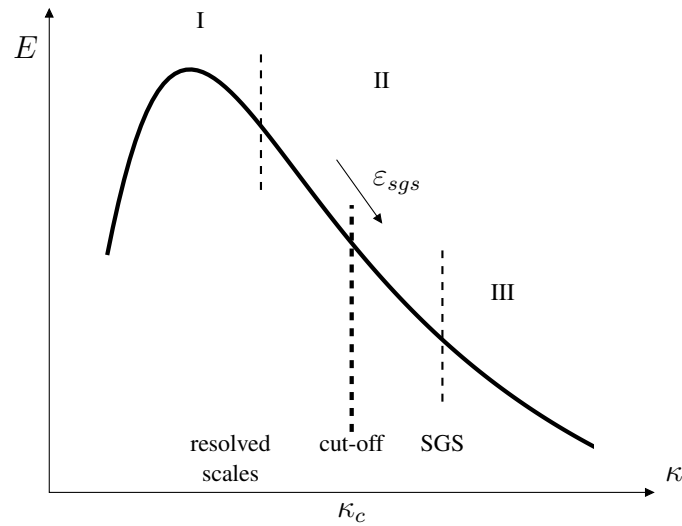
I= large scales; II= $-5/3$ range; III= dissipation range; $\kappa \leq \kappa_c$= Grid Scales; $\kappa > \kappa_c$= Sub-Grid Scales

¶See Section 18.5, Highest resolved wavenumbers
▶Physical and wavenumber space.
A Fourier series (see Appendix H)

$$v_1'(x) = \sum_{n=-\infty}^{\infty} c_n \exp(\imath\kappa_n x_1))$$
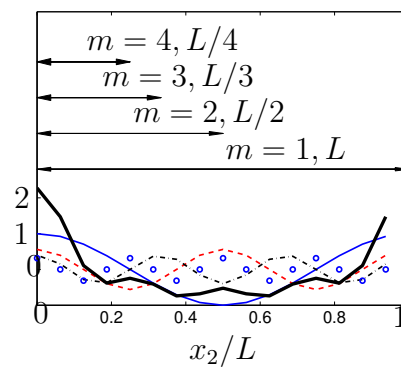
v_2' vs. x_2/L. ━━ : term 1 ($m = 1$); ━ ━ : term 2 ($m = 2$); ━ ∙ ━ : term 3 ($m = 3$); ○: term 4 ($m = 4$); ▬ : v_2'=term1+term2+term3+term4. Matlab code is given in Section I.3.

We construct v_2' as a sum of four Fourier components

$$v_2'(x_2) = b_1 \cos\left(\frac{2\pi}{L/1}x_2\right) + b_2 \cos\left(\frac{2\pi}{L/2}x_2\right) + b_3 \cos\left(\frac{2\pi}{L/3}x_2\right) + b_4 \cos\left(\frac{2\pi}{L/4}x_2\right)$$

One period=two cells   One period=four cells
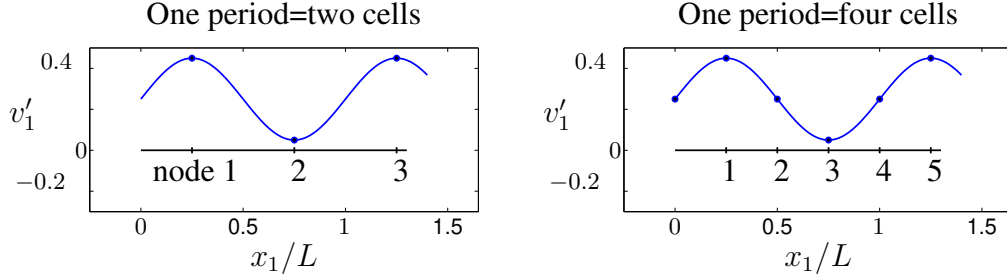
$$v_1' = \sin(\kappa_c x_1)$$

two cells : $\kappa_c 2\Delta x_1 = 2\pi \Rightarrow \kappa_c = 2\pi/(2\Delta x_1) = \pi/\Delta x_1$

four cells : $\kappa_c 4\Delta x_1 = 2\pi \Rightarrow \kappa_c = 2\pi/(4\Delta x_1) = \pi/(2\Delta x_1)$

¶See Section 18.6, Subgrid model
▶Smagorinsky Subgrid model

$$\tau_{ij} - \frac{1}{3}\delta_{ij}\tau_{kk} = -\nu_{sgs}\left(\frac{\partial \bar{v}_i}{\partial x_j} + \frac{\partial \bar{v}_j}{\partial x_i}\right) = -2\nu_{sgs}\bar{s}_{ij}$$

$$\nu_{sgs} = (C_S\Delta)^2\sqrt{2\bar{s}_{ij}\bar{s}_{ij}} \equiv (C_S\Delta)^2\,|\bar{s}|$$

$$\Delta = (\Delta V_{IJK})^{1/3}$$

$|\bar{s}|$ stems from the production term in the k eq., $|\bar{s}^2| = 2\bar{s}_{ij}\bar{s}_{ij}$

¶See Section 18.21, One-equation k_{sgs} model
▶One-equation model

$$\frac{\partial k_{sgs}}{\partial t} + \frac{\partial}{\partial x_j}(\bar{v}_j k_{sgs}) = \frac{\partial}{\partial x_j}\left[(\nu + \nu_{sgs})\frac{\partial k_{sgs}}{\partial x_j}\right] + P_{k_{sgs}} - \varepsilon$$

$$\nu_{sgs} = c_k\Delta k_{sgs}^{1/2}, \quad P_{k_{sgs}} = 2\nu_{sgs}\bar{s}_{ij}\bar{s}_{ij}, \quad \varepsilon = C_\varepsilon\frac{k_{sgs}^{3/2}}{\Delta}$$

¶See Section 18.8, Energy path
►Energy path
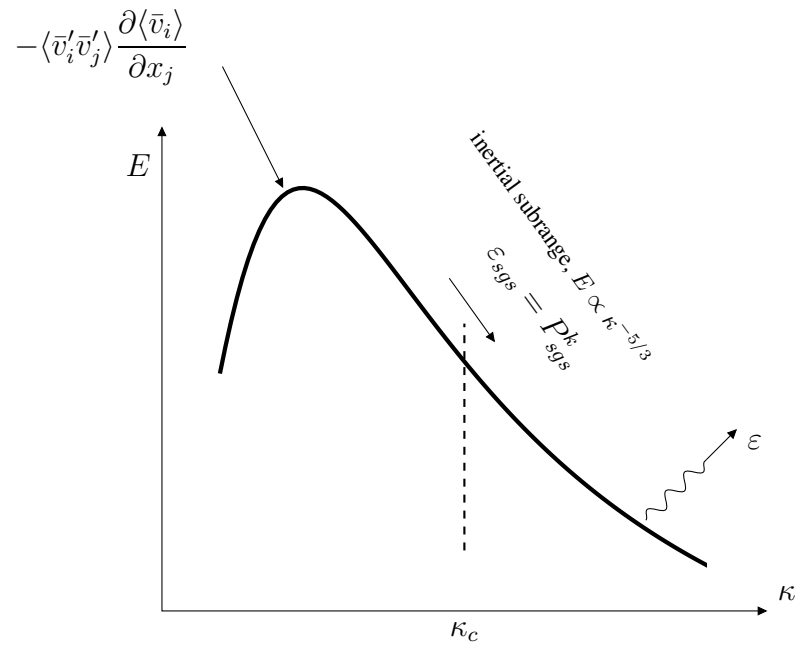
¶See Section 18.9, SGS kinetic energy
►SGS kinetic energy

$$v_i = \langle v_i \rangle + v_i', \quad v_i = \bar{v}_i + v_i'' = \langle \bar{v}_i \rangle + \bar{v}_i' + v_i''$$

$$k \equiv \frac{1}{2}\langle v_i' v_i' \rangle = \int_0^\infty E(\kappa)d\kappa, \quad k_{sgs} \equiv \frac{1}{2}\langle v_i'' v_i'' \rangle = \int_{\kappa_c}^\infty E(\kappa)d\kappa$$

$$\bar{k} \equiv \frac{1}{2}\langle \bar{v}_i' \bar{v}_i' \rangle = \int_0^{\kappa_c} E(\kappa)d\kappa, \quad \bar{K} \equiv \frac{1}{2}\langle \bar{v}_i \rangle \langle \bar{v}_i \rangle$$

$$K = \frac{1}{2}\langle v_i \rangle \langle v_i \rangle$$

K.8   Lecture 8

¶See Section 18.11, The dynamic model

▶The dynamic model. C is <u>computed</u>. Test filter, $\widehat{\Delta} = 2\Delta$

$$\frac{\partial \widehat{\overline{v}}_i}{\partial t} + \frac{\partial}{\partial x_j}\left(\widehat{\overline{v}}_i \widehat{\overline{v}}_j\right) = -\frac{1}{\rho}\frac{\partial \widehat{\overline{p}}}{\partial x_i} + \nu \frac{\partial^2 \widehat{\overline{v}}_i}{\partial x_j \partial x_j} - \frac{\partial T_{ij}}{\partial x_j} \qquad \text{(K.12)}$$

$$T_{ij} = \widehat{\overline{v_i v_j}} - \widehat{\overline{v}}_i \widehat{\overline{v}}_j$$

$$\begin{aligned}
\frac{\partial \widehat{\overline{v}}_i}{\partial t} + \frac{\partial}{\partial x_j}\left(\widehat{\overline{v}}_i \widehat{\overline{v}}_j\right) &= -\frac{1}{\rho}\frac{\partial \widehat{\overline{p}}}{\partial x_i} + \nu \frac{\partial^2 \widehat{\overline{v}}_i}{\partial x_j \partial x_j} - \frac{\partial \widehat{\tau}_{ij}}{\partial x_j} \\
&\quad - \frac{\partial}{\partial x_j}\underbrace{\left(\widehat{\overline{v_i \overline{v}_j}} - \widehat{\overline{v}}_i \widehat{\overline{v}}_j\right)}_{\mathcal{L}_{ij}}
\end{aligned}$$

(K.13)

Identification of Eqs. K.12 and K.13 gives

$$T_{ij} = \widehat{\overline{v_i \overline{v}_j}} - \widehat{\overline{v}}_i \widehat{\overline{v}}_j + \widehat{\tau}_{ij} = \mathcal{L}_{ij} + \widehat{\tau}_{ij}, \quad \frac{1}{3}\delta_{ij}T_{kk} = \frac{1}{3}\delta_{ij}\mathcal{L}_{kk} + \frac{1}{3}\delta_{ij}\widehat{\tau}_{kk}$$
(K.14)

Smag.model for both grid and test level SGS stresses:

$$\tau_{ij} - \frac{1}{3}\delta_{ij}\tau_{kk} = -2C\Delta^2 |\bar{s}|\bar{s}_{ij} \qquad \text{(K.15)}$$

$$T_{ij} - \frac{1}{3}\delta_{ij}T_{kk} = -2C\widehat{\Delta}^2 |\widehat{\overline{s}}|\widehat{\overline{s}}_{ij} \qquad \text{(K.16)}$$

where

$$\widehat{\overline{s}}_{ij} = \frac{1}{2}\left(\frac{\partial \widehat{\overline{v}}_i}{\partial x_j} + \frac{\partial \widehat{\overline{v}}_j}{\partial x_i}\right), \ |\widehat{\overline{s}}| = \left(2\widehat{\overline{s}}_{ij}\widehat{\overline{s}}_{ij}\right)^{1/2}$$

¶See Section 18.12, The test filter

►The test filter

test filter

grid filter

$$\Delta x \qquad \Delta x$$
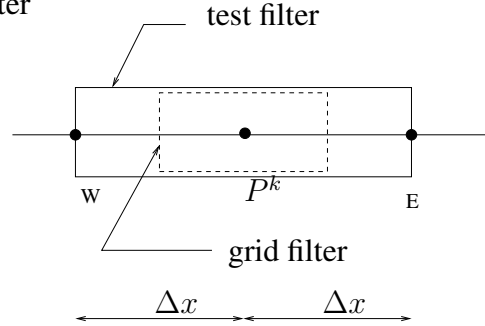
$\widehat{\bar{v}}$ is computed as $(\widehat{\Delta x} = 2\Delta x)$

$$\widehat{\bar{v}} = \frac{1}{2\Delta x} \int_W^E \bar{v}dx = \frac{1}{2\Delta x} \left(\int_W^P \bar{v}dx + \int_P^E \bar{v}dx \right)$$

$$= \frac{1}{2\Delta x} \left(\bar{v}_w \Delta x + \bar{v}_e \Delta x \right) = \frac{1}{2} \left(\frac{\bar{v}_W + \bar{v}_P}{2} + \frac{\bar{v}_P + \bar{v}_E}{2} \right)$$

$$= \frac{1}{4} \left(\bar{v}_W + 2\bar{v}_P + \bar{v}_E \right)$$

¶See Section 18.13, Stresses on grid, test and intermediate level

►Stresses

$E(\kappa)$

test filter   cut-off, grid filter

SGS grid scales

SGS test filter scales

I

II

III

resolved on test filter

resolved on grid filter

κ

$$\kappa = \pi/\widehat{\Delta} \qquad \kappa_c = \pi/\Delta$$
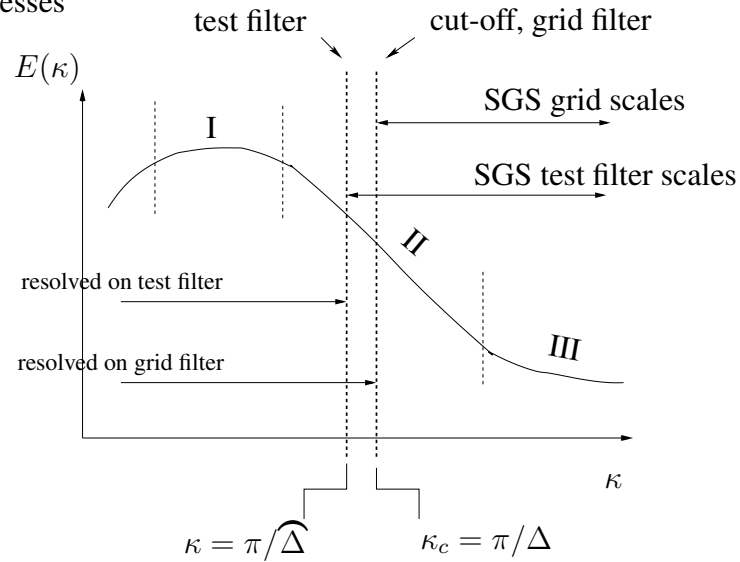
$$\tau_{ij} = \overline{v_i v_j} - \bar{v}_i \bar{v}_j \;\; \textbf{stresses with } \ell < \Delta$$

$$T_{ij} = \widehat{\overline{v_i v_j}} - \widehat{\bar{v}}_i \widehat{\bar{v}}_j \;\; \textbf{stresses with } \ell < \widehat{\Delta}$$

$$\mathcal{L}_{ij} = T_{ij} - \widehat{\tau}_{ij} \;\; \textbf{stresses with } \Delta < \ell < \widehat{\Delta}$$

Eqs. K.15. K.16 into Eq. K.14 gives

$$\mathcal{L}_{ij} - \frac{1}{3}\delta_{ij}\mathcal{L}_{kk} = -2C\left(\widehat{\Delta}^2 |\,\widehat{\bar{s}}\,|\,\widehat{\bar{s}}_{ij} - \widehat{\Delta^2|\bar{s}|\bar{s}_{ij}}\right)$$

Here we made the assumption $\widehat{C\Delta^2|\bar{s}|\bar{s}_{ij}} \simeq C\,\widehat{\Delta^2|\bar{s}|\bar{s}_{ij}}$. We get

$$\mathcal{L}_{ij} - \frac{1}{3}\delta_{ij}\mathcal{L}_{kk} + 2C\underbrace{\left(\widehat{\Delta}^2 |\,\widehat{\bar{s}}\,|\,\widehat{\bar{s}}_{ij} - \Delta^2\widehat{|\bar{s}|\bar{s}_{ij}}\right)}_{M_{ij}}$$ (K.17)

$$= \mathcal{L}_{ij} - \frac{1}{3}\delta_{ij}\mathcal{L}_{kk} + 2CM_{ij} = 0$$

$$Q = \left(\mathcal{L}_{ij} - \frac{1}{3}\delta_{ij}\mathcal{L}_{kk} + 2CM_{ij}\right)^2$$

Find a Q which best satisfies Eq. K.17 for all i, j

$$\frac{\partial Q}{\partial C} = 4M_{ij}\left(\mathcal{L}_{ij} + 2CM_{ij}\right) = 0, \quad \partial^2 Q/\partial C^2 = 8M_{ij}M_{ij} > 0$$

Note that $\frac{1}{3}\delta_{ij}\mathcal{L}_{kk}M_{ij} = \frac{1}{3}\mathcal{L}_{kk}M_{ii} = 0$ since $\widehat{\bar{s}}_{ii} = \bar{s}_{ii} = 0$ thanks to contiuity. We get

$$C = -\frac{\mathcal{L}_{ij}M_{ij}}{2M_{ij}M_{ij}}, \quad \text{stability problems: needs smoothing}$$

¶See Section 18.20, Numerical method

▶Numerical dissipation

$$\overrightarrow{\bar{v}_I}$$

$$I-1 \qquad I \qquad I+1$$
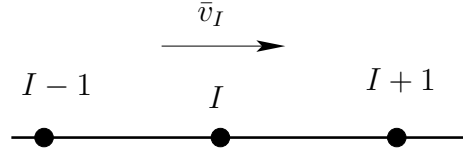
$$\bar{v}_I \left(\frac{\partial \bar{v}}{\partial x}\right)_{exact} = \bar{v}_I \left(\frac{\bar{v}_I - \bar{v}_{I-1}}{\Delta x} + \mathcal{O}\left(\Delta x\right)\right)$$

$$\bar{v}_{I-1} = \bar{v}_I - \Delta x \left(\frac{\partial \bar{v}}{\partial x}\right)_I + \frac{1}{2}(\Delta x)^2 \left(\frac{\partial^2 \bar{v}}{\partial x^2}\right)_I + \mathcal{O}\left((\Delta x)^3\right)$$

Insert this expression in the first equation:

$$\bar{v}\left(\frac{\partial \bar{v}}{\partial x}\right)_{exact} = \bar{v}\frac{\partial \bar{v}}{\partial x} - \underbrace{\frac{1}{2}\Delta x \bar{v}\frac{\partial^2 \bar{v}}{\partial x^2}}_{\mathcal{O}(\Delta x)} + \bar{v}\mathcal{O}\left((\Delta x)^2\right)$$

$$\text{diffusion term} = \frac{\partial}{\partial x}\left\{(\nu + \nu_{sgs} + \nu_{num})\frac{\partial \bar{v}}{\partial x}\right\}, \quad \varepsilon_{sgs+num} = 2(\nu_{sgs}+\nu_{num})\bar{s}_{ij}\bar{s}_{ij}$$

K.9 Lecture 9

¶See Section 18.15, Scale-similarity Models
▶Scale-similarity models

$$\tau_{ij} = \overline{v_i v_j} - \bar{v}_i \bar{v}_j = \overline{(\bar{v}_i + v_i'')(\bar{v}_j + v_j'')} - \bar{v}_i \bar{v}_j$$
$$= \underbrace{(\overline{\bar{v}_i \bar{v}_j} - \bar{v}_i \bar{v}_j)}_{L_{ij}} + \underbrace{\left[\overline{\bar{v}_i v_j''} + \overline{\bar{v}_j v_i''}\right]}_{C_{ij}} + \underbrace{\overline{v_i'' v_j''}}_{R_{ij}}$$

C_{ij} denotes <u>scale-similar</u> stresses

$$v_i = \bar{v}_i + v_i'' \Rightarrow \overline{v_j''} = \bar{v}_i - \bar{\bar{v}}_i$$

▶Scale-similarity model

$$C_{ij}^M = c_r(\bar{v}_i \bar{v}_j - \bar{\bar{v}}_i \bar{\bar{v}}_j) \tag{K.18}$$

The $C_{ij} = \overline{\bar{v}_i v_j''} + \overline{\bar{v}_j v_i''}$ and $L_{ij} = \overline{\bar{v}_i \bar{v}_j} - \bar{v}_i \bar{v}_j$ stresses are not Galilean invariant (but $C_{ij} + L_{ij}$ is). This is shown in an Appendix.

¶See Section 18.16, The Bardina Model
▶The Bardina model
The Bardina model reads (since C_{ij}^M was not sufficiently dissipative, a Smagorinsky model has to be added)

$$C_{ij}^M = c_r \overline{\bar{v}_i \bar{v}_j} - \bar{v}_i \bar{v}_j, \quad R_{ij}^M = -2C_S^2 \Delta^2 |\bar{s}| \bar{s}_{ij}$$

This is called a **mixed** model

¶See Section 18.22, Smagorinsky model derived from the k_{sgs} equation
▶Smagorinsky model derived from the one-equation model

• Small isotropic scales: production = dissipation

$$P_{k_{sgs}} = 2\nu_{sgs} \bar{s}_{ij} \bar{s}_{ij} = \nu_{sgs} |\bar{s}|^2 = \varepsilon$$

Replace ε by ν_{sgs} and Δ.

$\nu_{sgs} = \varepsilon^a (C_S \Delta)^b \Rightarrow a = 1/3, b = 4/3 \Rightarrow \nu_{sgs} = (C_S \Delta)^{4/3} \varepsilon^{1/3} \Rightarrow \varepsilon = \nu_{sgs}^3 \Delta^{-4}/C_S$

which gives

$$\nu_{sgs} = (C_s \Delta)^2 |\bar{s}|$$

¶See Section 18.26, Resolution requirements
▶In LES we resolve *large* scales. Near the wall, the "large" scales are not that large $\Rightarrow$ very expensive to resolve these "large" scales.

$\Delta x_1^+ \simeq 100,\ \Delta x_{2,min}^+ \simeq 1,\ \Delta x_3^+ \simeq 30 \quad \Rightarrow$ VERY expensive (see Eq. 18.67)

▶Outer region of the boundary layer (i.e. the logarithmic layer) the resolution can be expressed in boundary layer thickness, δ.

$\delta/\Delta x_1 = 10 - 20$, $\delta/\Delta x_3 = 20 - 40$ and $x_2^+ < 1$, see Eq. 18.68

There are many ways to estimate resolution (see Assignment in Section T.7):

1. Ratio between viscous and modelled turbulent viscosity (not recommended in [128, 129]). This quantity does not say much about how good the LES resolution is. It tells us how close the LES is to a DNS.

2. Ratio between modeled and total shear stress (recommended in [128, 129]).

3. Ratio between modeled and total turbulent kinetic energy (recommended in [200]).

4. Integral lengthscale fro two-point correlations (they are explained below). If the ratio is larger than, say, 16, the resolution is sufficient. The integral lengthscale is computed from This is recommended in [128, 129].

5. Ratio of boundary-layer thickness, δ to Δx and Δz. This is a measure of the resolution in the log-law region.

¶See Section 10.1, Two-point correlations

$$B_{11}(x_1^A, x_1^C) = \overline{v_1'(x_1^A)v_1'(x_1^C)}$$

Often, expressed as

$$B_{11}(x_1^A, \hat{x}_1) = \overline{v_1'(x_1^A)v_1'(x_1^A + \hat{x}_1)}$$

where $\hat{x}_1 = x_1^C - x_1^A$ is the separation distance between point A and C.

Two-point correlation.

Small integral length scale
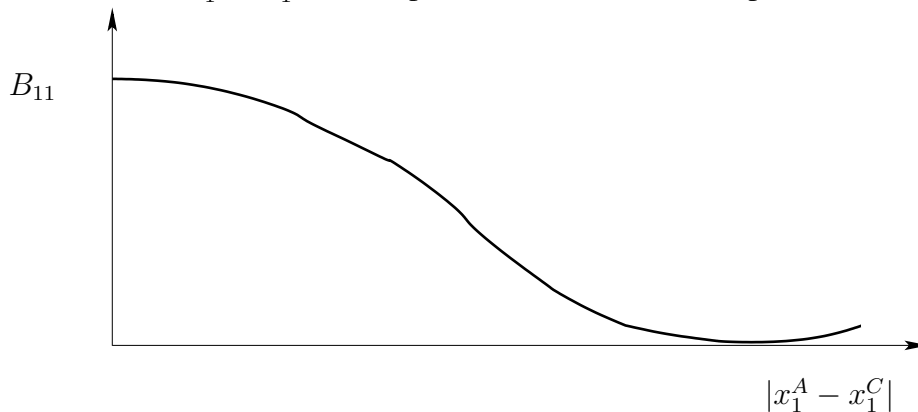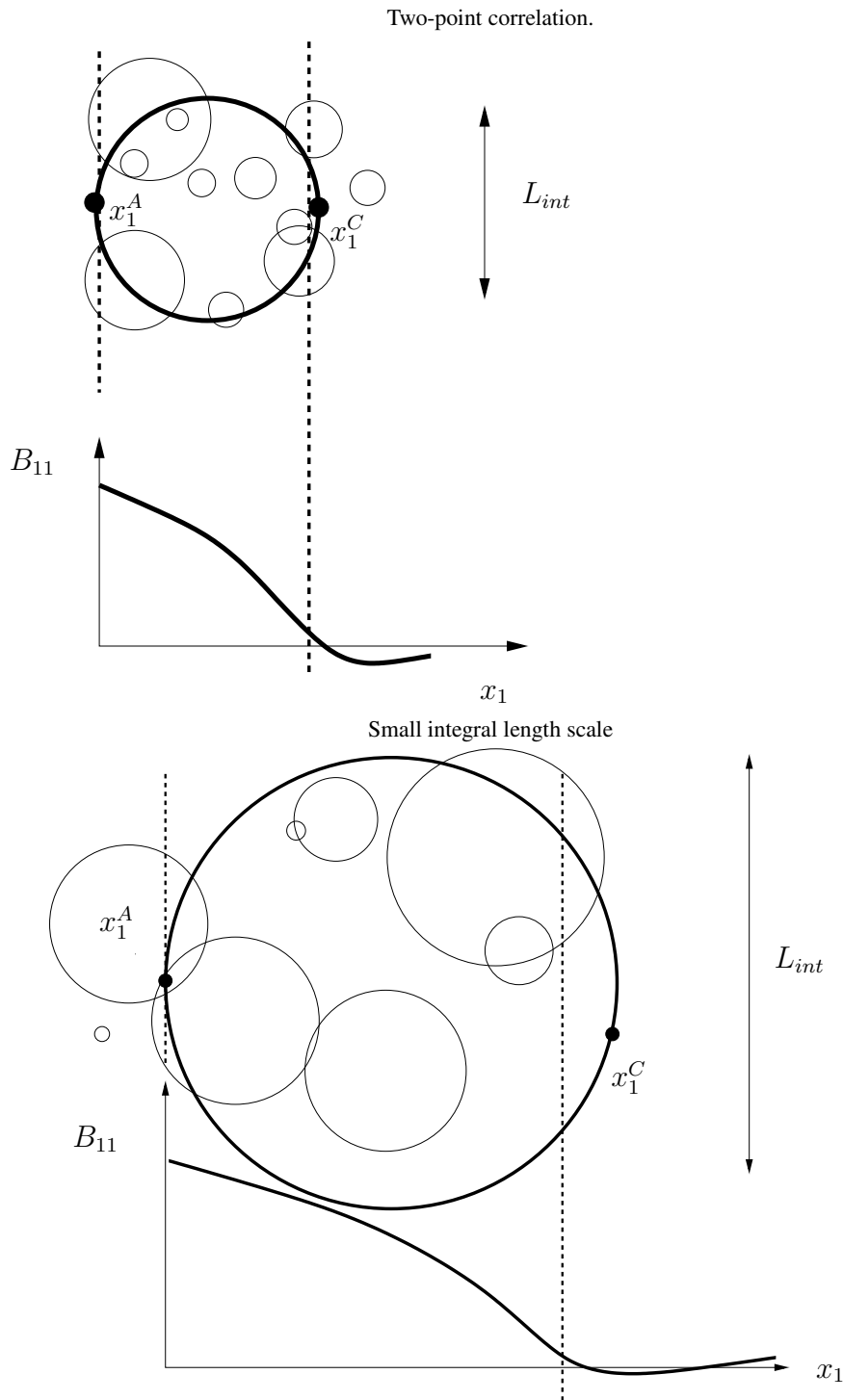
The circles show different eddy sizes. The circle with a thick line shows a large energetic eddy whose size corresponds to the integral lengthscale.

- if we move point A and C closer to each other, B_{11} increases; when A=C, then $B_{11} = \overline{v'^2}(x_1^A)$,

- When C moves further and further away from A, $\Rightarrow B_{11} \to 0$

- The normalized two-point correlation reads

$$B_{11}^{norm}(x_1^A, \hat{x}_1) = \frac{1}{v_{1,rms}(x_1^A)v_{1,rms}(x_1^A + \hat{x}_1)} \overline{v_1'(x_1^A)v_1'(x_1^A + \hat{x}_1)}$$

▶Integral length scale is then computed as

$$L_{int} = \int_0^\infty B_{11}^{norm}(\hat{x}_1)d\hat{x}_1 \qquad \text{(K.19)}$$

¶See Section 10.2, Auto correlation
▶Auto correlation is a "two-point correlation in time" which reads (see Eq. 10.8)

$$B_{11}(t^A, \hat{t}) = \overline{v_1'(t^A)v_1'(t^A + \hat{t})}$$

$\hat{t} = t^C - t^A$ is time separation between time A and C.
▶In analogy to L_{int} (Eq. K.19), the *integral time scale*, T_{int}, is defined (see Eq. 10.11)

$$T_{int} = \int_0^\infty B_{11}^{norm}(\hat{t})d\hat{t}$$

▶Integral timescale is used an Assignment (see Section Q.3) for finding time samples that are *independent* (i.e. the time between the samples is at least one integral timescale).

¶See Section 18.20.1, RANS vs. LES

►Numerical method: RANS vs. LES

	RANS	**LES**
Domain	2D or 3D	always 3D
Time domain	steady or unsteady	always unsteady
Space discretization	2nd order upwind	central differencing
Time discretization	1st order	2nd order (e.g. C-N)
Turbulence model	$\geq$ two-equations	zero- or one-equation

►**Start** and **end** time averaging. $t_{end} - t_{start} \simeq 100H/\langle \bar{v} \rangle_{center}$
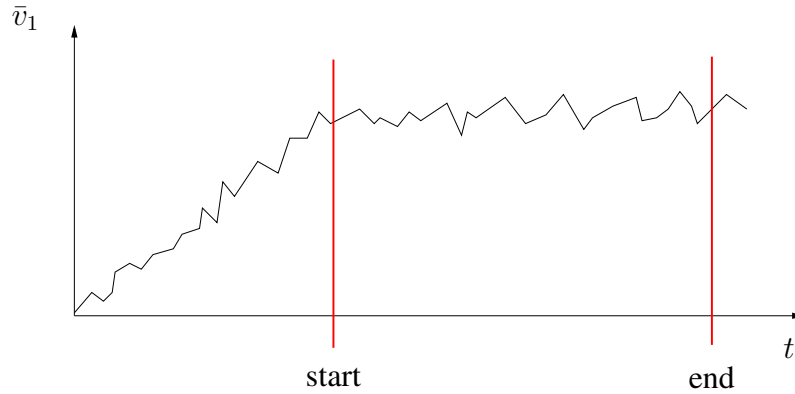
¶See Section 19, URANS: Unsteady RANS

▶URANS. The usual Reynolds decomposition is employed

$$\bar{v}(t) = \frac{1}{2T} \int_{t-T}^{t+T} v(t)dt, \ v = \bar{v} + v''$$

URANS eqns=RANS, but with the unsteady term retained

$v, \ \bar{v}, \ \langle\bar{v}\rangle$

$\langle\bar{v}\rangle$

t
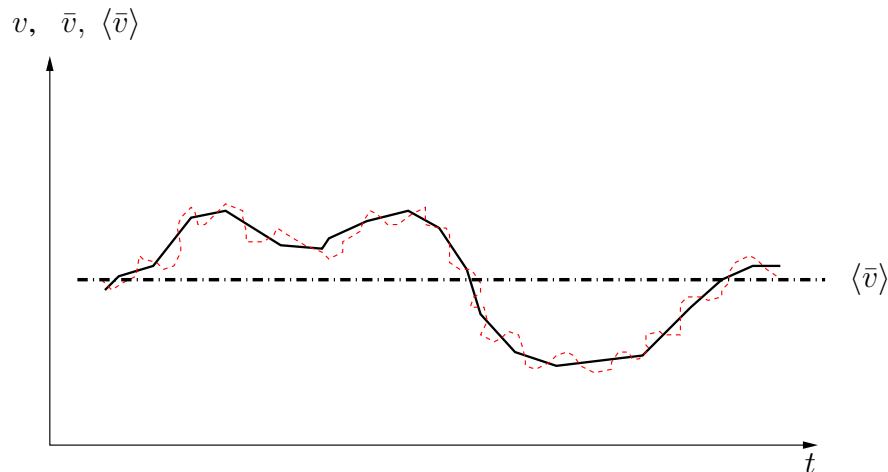
- Decomposition of velocities: $v = \bar{v} + v'' = \langle\bar{v}\rangle + \bar{v}' + v''$. ▬▬ : $\bar{v}$; ▬ ▬ : v; ▬·▬ $\langle\bar{v}\rangle$.

- In theory, T should be $\ll$ resolved time scale. This is called *scale separation*. In practice, it is seldom satisfied.

- RANS turbulence models are used: one should choose a model with small dissipation (i.e. small ν_t) in order to not kill/dampen resolved turbulence. Reynolds-stress turbulence models best (but very expensive), see Eq. 11.101. The EARSM (Section 11.11) and non-linear eddy-viscosity models (Section 14) also seem to give less dissipation. Probably because the weaker connection between $\bar{s}_{ij}$ and $\overline{v_i'v_j'}$ which reduced P^k.

- Modelled dissipation (turbulence model) and numerical dissipation (discretization scheme) may be of equal importance

¶See Section 20, DES: Detached-Eddy-Simulations

▶DES=<u>D</u>etached <u>E</u>ddy <u>S</u>imulations: Use RANS near walls and LES away from walls

The S-A one-equation model (RANS) reads

$$\frac{d\rho\tilde{\nu}_t}{dt} = \frac{\partial}{\partial x_j}\left(\frac{\mu+\mu_t}{\sigma_{\tilde{\nu}_t}}\frac{\partial\tilde{\nu}_t}{\partial x_j}\right) + \text{cr. term} + P - C_{w1}\rho f_w\left(\frac{\tilde{\nu}_t}{d}\right)^2, \quad d = x_n$$

►Replace d with $\tilde{d}$:

$$\left(\frac{\tilde{\nu}_t}{d}\right)^2 \Rightarrow \left(\frac{\tilde{\nu}_t}{\tilde{d}}\right)^2, \quad \tilde{d} = \min\{C_{DES}\Delta, d\}, \quad \Delta = \max\{\Delta x_1, \Delta x_3, \Delta x_3\}$$

►This is the DES S-A one-equation model

¶See Section 20.1, DES based on two-equation models
►Two-equation DES models
$k - \varepsilon$ RANS

$$C^k = D^k + P^k - \varepsilon, \quad C^\varepsilon = D^\varepsilon + P^\varepsilon - \Psi$$

$k - \varepsilon$ DES (modify ε_T)

$$C^k = D^k + P^k - \varepsilon \Rightarrow C^k = D^k + P^k - \varepsilon_T, \quad \varepsilon_T = \max\left(\varepsilon, C_\varepsilon \frac{k^{3/2}}{\Delta}\right)$$

$k - \varepsilon$ DES (modify ν_T and ε_T)

$$C^k = D^k + P^k - \varepsilon_T, \quad C^\varepsilon = D^\varepsilon + P^\varepsilon - \Psi^\varepsilon, \quad \nu_t = k^{1/2}\ell_t$$

1. $\varepsilon_T = \max\left(\varepsilon, C_\varepsilon \frac{k^{3/2}}{\Delta}\right)$: $\varepsilon_T \uparrow \Rightarrow \nu_t, k \downarrow$ in LES region

2. $\ell_t = \min\left(C_\mu \frac{k^{3/2}}{\varepsilon}, C_k \Delta\right) \Rightarrow \nu_t$ decreases in LES region

K.10   Lecture 10

¶See Section 20.2, DES based on the $k - \omega$ SST model
$k - \omega$ SST DES (modify $\beta^* k \omega$)

$$C^k = D^k + P^k - F_{DES}\beta^* k\omega, \quad F_{DES} = \max\left\{\frac{L_t}{C_{DES}\Delta}, 1\right\} = \max\left\{\frac{k^{1/2}}{\beta^*\omega C_{DES}\Delta}, 1\right\}$$

Dissip. term $\beta^* k\omega = \dfrac{k^{3/2}}{L_t} \Rightarrow$ the $k - \omega$ SST-DES model gives
$F_{DES}\beta^* k\omega = \dfrac{k^{3/2}}{C_{DES}\Delta}$ in the LES region

¶See Section 20.3, DDES
▶It may occur that the F_{DES} term switches to LES in the boundary layer
because Δx_1 is too small (Δx_3 is usually smaller than Δx_1)
Hence boundary layer is treated in LES mode with too a coarse mesh $\Rightarrow$
poorly resolved LES $\Rightarrow$ inaccurate predictions.
▶The solution is DDES (Delayed DES)
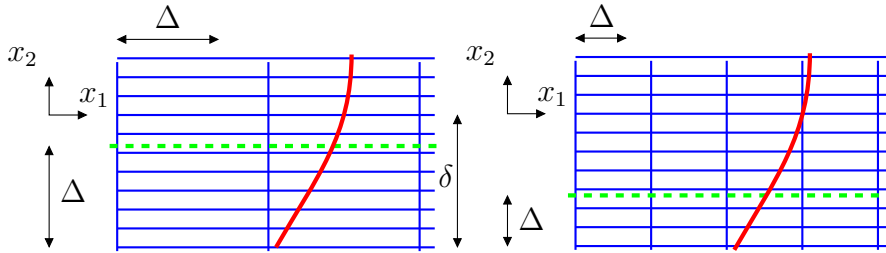
Grid (in blue) and a velocity profile (in red). RANS-LES interface is shown by the dashed-green
line. $C_{DES} = 0.67$

- The left grid above is a good DES mesh because (see Eq. 20.4)
  $\ell_t = \min\left(C_\mu \frac{k^{3/2}}{\varepsilon}, C_{DES}\Delta\right) = C_{DES}\Delta = C_{DES}\Delta x_1 \simeq \delta$ (see
  dashed green line) $\rightarrow$ the entire boundary layer is modeled by
  RANS.

- The grid on the right is a poor DES grid because $\ell_t =$
  $\min\left(C_\mu \frac{k^{3/2}}{\varepsilon}, C_{DES}\Delta\right) = C_{DES}\Delta = C_{DES}\Delta x_1 \ll \delta$ (see dashed
  green line) $\rightarrow$ the outer part of the boundary layer is in LES mode
  (and the LES resolution requirements may not be satisfied)

▶In DDES, F_{DES} is computed as (see Eq. 20.9)

$$F_{DDES} = \max\left\{\frac{L_t}{C_{DES}\Delta}(1 - F_S), 1\right\}$$

where F_S ($F_S = 1$ in the boundary layer) is taken as F_1 or F_2 (see Eqs. 16.12 and 16.18) of the SST model.

¶See Section 21, Hybrid LES-RANS

DES: The entire boundary layer is modelled with URANS

Hybrid LES-RANS: Only the inner part (RANS-LES interface at the inner part of the log region) is modelled with URANS. This is also called **WM-LES** (WM=Wall-modelled)

▶Hybrid LES-RANS *wall*

URANS region

LES region

x_2 URANS region

wall $x_{2,ml}^+$

x_1
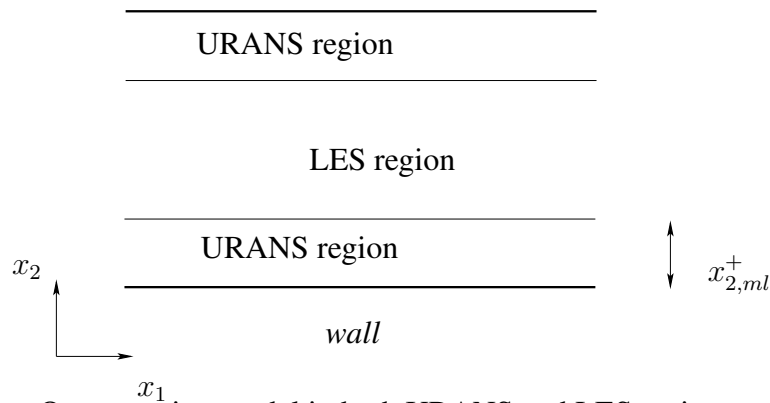
One-equation model in both URANS and LES region

$$\frac{\partial k_T}{\partial t} + \frac{\partial}{\partial x_j}(\bar{v}_j k_T) = \frac{\partial}{\partial x_j}\left[(\nu + \nu_T)\frac{\partial k_T}{\partial x_j}\right] + P_{k_T} - C_\varepsilon \frac{k_T^{3/2}}{\ell}$$

$$P_{k_T} = -\tau_{ij}\bar{s}_{ij}, \quad \tau_{ij} = -2\nu_T\bar{s}_{ij}, \quad \nu_T \propto k^{1/2}\ell$$

Inner region ($x_2 \leq x_{2,ml}$): $\ell \propto \kappa x_2$; outer region: $\ell = \Delta$

¶See Section 22, The SAS model

►The SAS model: This is a method to improve URANS. If the flow tries to go unsteady in URANS, P^k increases so that ν_t increases and the flow goes back to steady state. The objective of SAS is to reduce ν_t when the equations want to go into unsteady, resolving turbulence mode (LES mode).

$$L_{vK,3D} = \kappa \frac{|\partial \bar{v}_1/\partial y|}{|\partial^2 \bar{v}_1/\partial x_2^2|}$$

$$L_{vK,1D} = \kappa \frac{|\partial \langle \bar{v}_1 \rangle/\partial y|}{|\partial^2 \langle \bar{v}_1 \rangle/\partial x_2^2|}$$
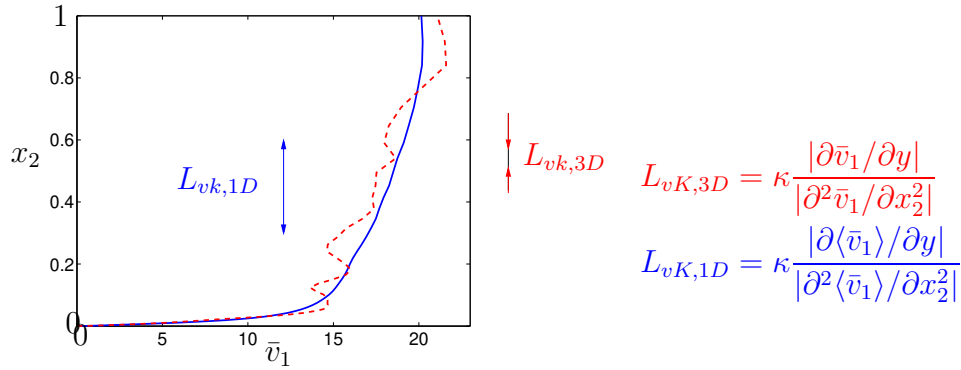
Solid line: $L_{vk,1D}$; dashed line: $L_{vk,3D}$

►An additional source term, P_{SAS}, is introduced in the ω equation. $P_{SAS} \propto \frac{L_t}{L_{vK,3D}}$.

$$L_t \propto \frac{k^{1/2}}{\omega}, \quad L_{vK,3D} = \kappa \frac{|\bar{s}|}{|U''|}, \quad U'' = \left(\frac{\partial^2 \bar{v}_i}{\partial x_j \partial x_j} \frac{\partial^2 \bar{v}_i}{\partial x_k \partial x_k} \right)^{0.5}$$

►The von Kármán length scale is used to detect unsteadiness; when it happens:

- the P_{SAS} term increases

- $\rightarrow \omega$ increases

- $\rightarrow \nu_t$ and k decrease

- $\rightarrow$ mom.eqns go into (or stay in) unsteady mode

►In URANS, resolved fluctuations may be damped.

K.11 Lecture 11

¶See Section 23, The PANS Model
▶PANS: Partial-Averaging Navier-Stokes. It is a hybrid LES-RANS model and it is based on the $k - \varepsilon$ model.

- $f_k = k/k_{tot}$ and $f_\varepsilon = \varepsilon/\varepsilon_{tot}$ denote the ratio of modelled to total $k_{tot} = k + k_{res}$ and ε_{tot}, respectively.

- $f_\varepsilon < 1$ means that part of the dissipation is resolved. This occurs only for DNS-like resolution. Hence, in practice $f_\varepsilon = 1$

- For DNS, $f_k \to 0$; for RANS, $f_k = 1$ and for LES it is in-between

▶Derivation of k equation

- Multiply the RANS ($k_{tot} = k_{RANS}$) equation ($k_{tot} = k + k_{res}$), Eq. 11.97, by f_k

Left side

$$f_k \left\{ \frac{\partial k_{tot}}{\partial t} + \bar{V}_j \frac{\partial k_{tot}}{\partial x_j} \right\} = \frac{\partial k}{\partial t} + \bar{V}_j \frac{\partial k}{\partial x_j} \simeq \frac{\partial k}{\partial t} + \bar{v}_j \frac{\partial k}{\partial x_j}$$

where V_j is the RANS velocity and f_k assumed constant (non-constant f_k is accounted for in Section 23.1.1).
Right side, diffusion term

$$f_k \left\{ \frac{\partial}{\partial x_j} \left[\left(\nu + \frac{\nu_{t,tot}}{\sigma_k} \right) \frac{\partial k_{tot}}{\partial x_j} \right] \right\} = \frac{\partial}{\partial x_j} \left[\left(\nu + \frac{\nu_{t,tot}}{\sigma_k} \right) \frac{\partial k}{\partial x_j} \right] = \frac{\partial}{\partial x_j} \left[\left(\nu + \frac{\nu_t}{\sigma_{ku}} \right) \frac{\partial k}{\partial x_j} \right]$$

where $\sigma_{ku} = \sigma_k f_k^2 / f_\varepsilon$ and $\nu_t = c_\mu k^2 / \varepsilon$ because $\nu_{t,tot} = c_\mu k_{tot}^2 / \varepsilon_{tot}$ and $\nu_t = c_\mu k^2 / \varepsilon$.
Right side, production and dissipation term
$P^{k,tot}$ and ε_{tot} are replaced by P_k and ε, i.e.

$$f_k \left(P^{k,tot} - \varepsilon_{tot} \right) = P^k - \varepsilon \Rightarrow P^{k,tot} = \frac{1}{f_k} (P^k - \varepsilon) + \frac{\varepsilon}{f_\varepsilon} \qquad \text{(K.20)}$$

The k eqn can now be written (see Eq. 23.9)

$$\frac{\partial k}{\partial t} + \frac{\partial (k\bar{v}_j)}{\partial x_j} = \frac{\partial}{\partial x_j} \left[\left(\nu + \frac{\nu_t}{\sigma_{ku}} \right) \frac{\partial k}{\partial x_j} \right] + P^k - \varepsilon$$

▶Derivation of ε equation
Left side

$$f_\varepsilon \left\{ \frac{\partial \varepsilon_{tot}}{\partial t} + \bar{V}_j \frac{\partial \varepsilon_{tot}}{\partial x_j} \right\} = \frac{\partial \varepsilon}{\partial t} + \bar{V}_j \frac{\partial \varepsilon}{\partial x_j} \simeq \frac{\partial \varepsilon}{\partial t} + \bar{v}_j \frac{\partial \varepsilon}{\partial x_j}$$

f_ε assumed constant
Right side, diffusion term

$$f_\varepsilon \left\{ \frac{\partial}{\partial x_j} \left[\left(\nu + \frac{\nu_{t,tot}}{\sigma_\varepsilon} \right) \frac{\partial \varepsilon_{tot}}{\partial x_j} \right] \right\} = \frac{\partial}{\partial x_j} \left[\left(\nu + \frac{\nu_{t,tot}}{\sigma_\varepsilon} \right) \frac{\partial \varepsilon}{\partial x_j} \right] = \frac{\partial}{\partial x_j} \left[\left(\nu + \frac{\nu_t}{\sigma_{\varepsilon u}} \right) \frac{\partial \varepsilon}{\partial x_j} \right]$$

production and destruction terms (use Eq. K.20, $k_{tot} = k/f_k$, $\varepsilon_{tot} = \varepsilon/f_\varepsilon$)

$$f_\varepsilon \left\{ C_{\varepsilon 1} P^{k,tot} \frac{\varepsilon_{tot}}{k_{tot}} - C_{\varepsilon 2} \frac{\varepsilon_{tot}^2}{k_{tot}} \right\} = C_{\varepsilon 1} \frac{\varepsilon f_k}{k} \left(\frac{1}{f_k}(P^k - \varepsilon) + \frac{\varepsilon}{f_\varepsilon} \right) - C_{\varepsilon 2} \frac{\varepsilon^2 f_k}{f_\varepsilon k}$$

$$= C_{\varepsilon 1} \frac{\varepsilon}{k} P^k - C_{\varepsilon 1} \frac{\varepsilon^2}{k} + C_{\varepsilon 1} \frac{\varepsilon^2 f_k}{k f_\varepsilon} - C_{\varepsilon 2} \frac{\varepsilon^2 f_k}{f_\varepsilon k} = C_{\varepsilon 1} \frac{\varepsilon}{k} P^k - C_{\varepsilon 2}^* \frac{\varepsilon^2}{k}$$

where

$$C_{\varepsilon 2}^* = C_{\varepsilon 1} + \frac{f_k}{f_\varepsilon}(C_{\varepsilon 2} - C_{\varepsilon 1}) = 1.5 + \frac{f_k}{f_\varepsilon}(1.9 - 1.5)$$

The ε eqn can now be written (see Eq. 23.9)

$$\frac{\partial \varepsilon}{\partial t} + \frac{\partial (\varepsilon \bar{v}_j)}{\partial x_j} = \frac{\partial}{\partial x_j} \left[\left(\nu + \frac{\nu_t}{\sigma_{\varepsilon u}} \right) \frac{\partial \varepsilon}{\partial x_j} \right] + C_{\varepsilon 1} P^k \frac{\varepsilon}{k} - C_{\varepsilon 2}^* \frac{\varepsilon^2}{k}$$

- When $f_k = 1$, the PANS eqns are in RANS mode

- When $f_k < 1$ (say, $f_k = 0.4$) then:

  - $C_{\varepsilon 2}^* \dfrac{\varepsilon^2}{k}$ is reduced
  - $\Rightarrow \varepsilon$ is increased
  - $\Rightarrow k$ and ν_t are decreased
  - $\Rightarrow$ the momentum eqns go into LES mode.

K.12 Lecture 12

¶See Section 27.1, Synthesized turbulence

▶In LES and DES the large-scale turbulence is resolved: hence, turbulent fluctuations should be provided as inlet boundary conditions

▶Synthetic fluctuations is one method. The inlet velocity can be written as a Fourier series

$$\mathbf{v}'(\mathbf{x}) = 2 \sum_{n=1}^{N} \hat{u}^n \cos(\boldsymbol{\kappa}^n \cdot \mathbf{x} + \psi^n) \boldsymbol{\sigma}^n$$

¶See Section 27.2, Random angles

$p(\varphi^n) = 1/(2\pi)$	$0 \le \varphi^n \le 2\pi$
$p(\psi^n) = 1/(2\pi)$	$0 \le \psi^n \le 2\pi$
$p(\theta^n) = 1/2 \sin(\theta)$	$0 \le \theta^n \le \pi$
$p(\alpha^n) = 1/(2\pi)$	$0 \le \alpha^n \le 2\pi$

Probability distributions of the random variables. α^n is the angle for $\boldsymbol{\sigma}^n$.
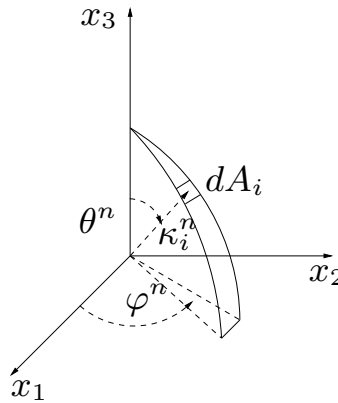
The probability of a randomly selected direction of a wave in wave-space is the same for all dA_i on the shell of a sphere.

Compute the wavenumber vector, κ_j^n, using the angles above (see Section N).

$$\kappa_1^n = \sin(\theta^n) \cos(\varphi^n)$$
$$\kappa_2^n = \sin(\theta^n) \sin(\varphi^n)$$
$$\kappa_3^n = \cos(\theta^n)$$

▶Amplitude $\hat{u}^n$ related to energy spectrum: $\hat{u}^n = (E(\kappa)\Delta\kappa)^{1/2}$, see below.

$$\hat{u}^2/(\Delta\kappa) = E(\kappa)$$
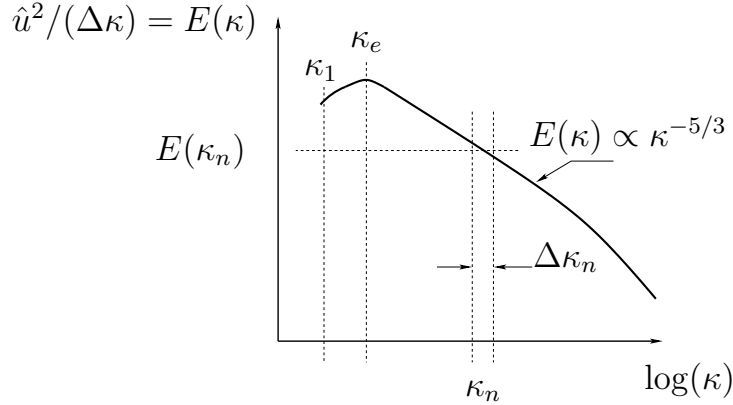
- Usually we generate energy spectra from turbulent fluctuations. Here we do the opposite: we prescribe a spectrum and generate turbulent fluctuations. A $-5/3$ spectrum is assumed (see Section 27.6): this gives the amplitude $\hat{u}^n$ for wavenumber κ_n

- Highest wave number (see Section 27.3): $\kappa_{max} = 2\pi/2\Delta$ from the cell size, $\Delta = \min(\Delta x_2)$

- Most energetic wave number (see Section 27.4): $\kappa_e \propto 1/L_t$ from the integral turbulent length scale. $\kappa_1 = \kappa_e/p$ where $p = 5$

- Smallest wave number (see Section 27.4): $\kappa_{min} = \kappa_e/2$, $\Delta\kappa = (\kappa_{max} - \kappa_{min})/N \Rightarrow \kappa_1 = \kappa_{min}, \kappa_2 = \kappa_1 + \Delta\kappa, \ldots \kappa_N = \kappa_{max}$

- Number of wave numbers: N

- Now the fluctuations are computed (see Section 27.7)

$$
\begin{aligned}
v_1' &= 2\sum_{n=1}^{N} \hat{u}^n \cos(\beta^n)\sigma_1 \\
v_2' &= 2\sum_{n=1}^{N} \hat{u}^n \cos(\beta^n)\sigma_2 \\
v_3' &= 2\sum_{n=1}^{N} \hat{u}^n \cos(\beta^n)\sigma_3 \\
\beta^n &= k_1^n x_1 + k_2^n x_2 + k_3^n x_3 + \psi^n
\end{aligned}
\tag{K.21}
$$

where $\hat{u}^n = (E(\kappa)\Delta\kappa)^{1/2}$, see Eq. 27.4.

- With this method synthetic turbulent fluctuations are generated at the inlet plane for M time steps.

¶See Section 27.8, Introducing time correlation

►However, the synthetic fluctuations are not correlated in time. An asymmetric time filter is used $(\mathcal{V}_1')^m = a(\mathcal{V}_1')^{m-1} + b(v_1')^m$

- The coefficient a is related to the turbulent integral timescale, $\mathcal{T}$, as $a = \exp(-\Delta t/\mathcal{T})$

- The coefficient b is computed as $b = (1 - a^2)^{1/2}$ which ensures that $\mathcal{V}_{1,rms}' = v_{1,rms}'$

- Finally, the turbulent synthetic fluctuations are superimposed to the inlet mean velocity.

¶See Section 23.2.1, The Interface Condition

▶Embedded LES and inlet b.c. for k and ε using PANS

- embedded LES: an LES region (e.g. the side mirror, see figure below) is embedded in a steady RANS simulation.

- LES is used around the mirror in order to compute aeroacoustic sources (wind noise)

- Additional boundary conditions are needed at the inlet region of LES, both synthetic fluctuations and LES values of k and ε

Windscreen
A-pillar
Plenum
Duck tail
Hood

y z
  x

Beltline
Side window
Side mirror
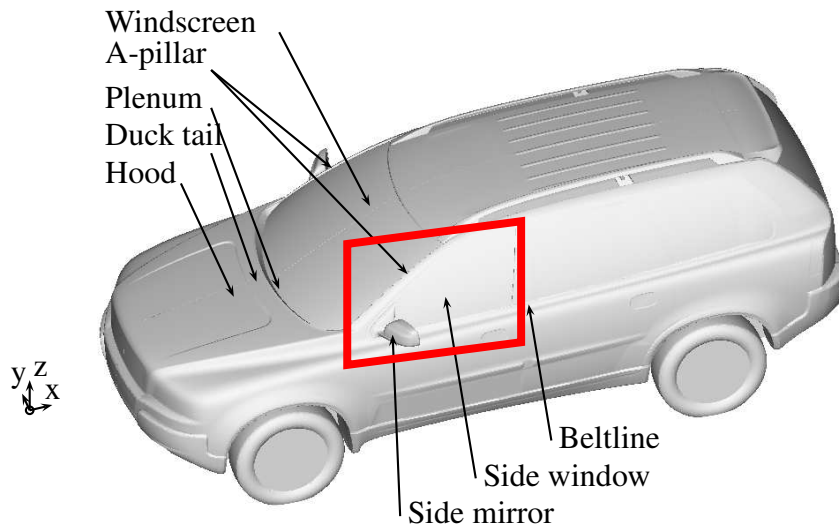
Vehicle geometry (from [116]). Red region shows embedded LES region

▶In the PANS model we assumed that f_k is constant, see Eq. 23.22.

$$f_k \frac{dk_{tot}}{dt} = \frac{d(f_k k_{tot})}{dt} = \frac{dk}{dt} \qquad \text{(K.22)}$$

where $f_k = k/k_{tot}$, $k_{tot} = k_{res} + k$ (recall that $k = k_{model}$)

- PANS is used as a hybrid RANS-LES model ($f_k = 1$ in the RANS region, and f_k is smaller in the LES region)

- A gradient of f_k appears at the RANS-LES interface since f_k varies in space; Eq. K.22 is replaced by

$$f_k \frac{dk_{tot}}{dt} = \frac{d(f_k k_{tot})}{dt} - k_{tot} \frac{df_k}{dt} = \frac{dk}{dt} - k_{tot} \frac{df_k}{dt} \qquad \text{(K.23)}$$

- Hence, an extra term, $-k_{tot}df_k/dt$ (see Eq. 23.25), appears on the left side (opposite sign on right side) of the k eq,

- Since $df_k/dt < 0$, this is a sink term $\rightarrow$ reduction of k

- Since we add a sink term to the k eq., we must add a source term to the resolved k eq, i.e. to the k_{res} eq.

- This is done by adding a term to the mom. eq.
  $-(0.5 + \langle k \rangle / \langle \bar{v}'_m \bar{v}'_m \rangle)\bar{v}'_i df_k/dt$
  see Eqs. 23.27, 23.29 $\rightarrow -\langle k + 0.5\bar{v}'_i\bar{v}'_i \rangle)df_k/dt$ (see Eq. 23.28, 23.30) in the k_{res} eq.

The URANS and the LES regions near a wall (horizontal interface).

Embedded LES. RANS-LES interface at x_I.   RANS-LES interface at inlet.
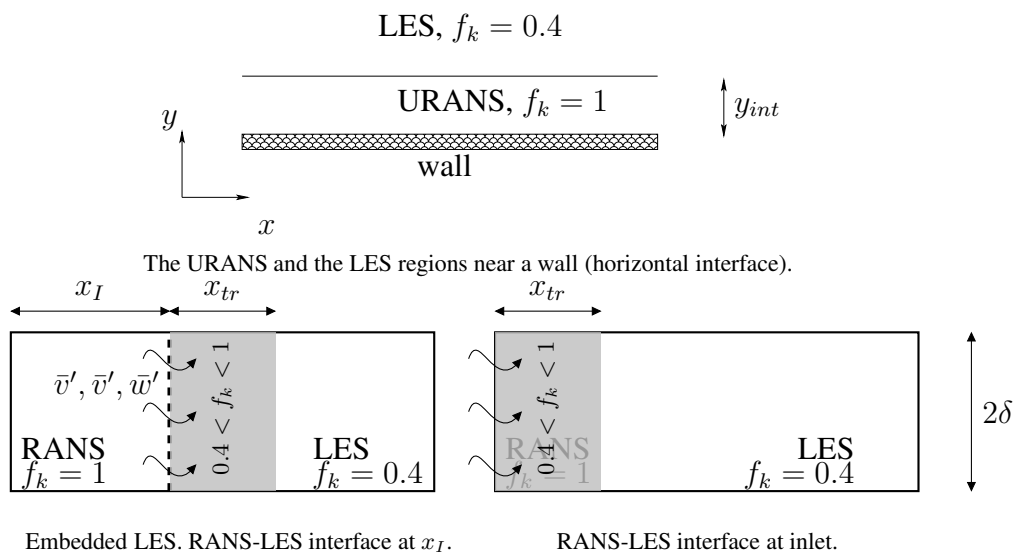
f_k varies linearly in the gray area (width x_{tr}) from 1 to 0.4.

▶Summary

- Add synthetic fluct. at inlet and embedded surfaces

- Use RANS values of k and ε

- The source terms in the k (and in the momentum) equations will quickly reduce k from RANS values to LES values

- No source terms are needed for ε because it is the same for RANS and LES

L MTF271: Some properties of the pressure-strain term

IN this Appendix we will investigate some properties of $a_{ijk\ell}$ in Eq. 11.77 at p. 137. Introduce the two-point correlation function

$$B_{j\ell}(\mathbf{r}) = \overline{v'_j(\mathbf{x})v'_\ell(\mathbf{x}+\mathbf{r})}$$

Define the point $\mathbf{x}' = \mathbf{x} + \mathbf{r}$ so that

$$B_{j\ell}(\mathbf{r}) = \overline{v'_j(\mathbf{x}'-\mathbf{r})v'_\ell(\mathbf{x}')} = \overline{v'_\ell(\mathbf{x}')v'_j(\mathbf{x}'-\mathbf{r})} = B_{\ell j}(-\mathbf{r})$$

We get

$$\frac{\partial B_{j\ell}(\mathbf{r})}{\partial r_i} = -\frac{\partial B_{\ell j}(-\mathbf{r})}{\partial r_i} \Rightarrow \frac{\partial^2 B_{j\ell}(\mathbf{r})}{\partial r_k \partial r_i} = \frac{\partial^2 B_{\ell j}(-\mathbf{r})}{\partial r_k \partial r_i} \tag{L.1}$$

Since Eq. L.1 in the definition of $a_{ijk\ell}$ in Eq. 11.77 is integrated over $\mathbf{r}^3$ covering both $\mathbf{r}$ and $-\mathbf{r}$ (recall that v'_ℓ and v'_j are separated by $\mathbf{r}$), $a_{ijk\ell}$ is symmetric with respect to index j and ℓ, i.e.

$$a_{ijk\ell} = a_{i\ell kj} \tag{L.2}$$

Green's third formula (it is derived from Gauss divergence law) reads

$$\varphi(\mathbf{x}) = -\frac{1}{4\pi} \int_V \frac{\nabla^2 \varphi}{|\mathbf{y}-\mathbf{x}|} d\mathbf{y}^3 \tag{L.3}$$

where the boundary integrals have been omitted. Setting $\varphi = \overline{v'_\ell v'_j}$ in Eq. L.3 gives

$$\overline{v'_j v'_\ell} = -\frac{1}{4\pi} \int_V \frac{\partial^2 \overline{v'_\ell v'_j}}{\partial x_i \partial x_i} \frac{d\mathbf{y}^3}{|\mathbf{y}-\mathbf{x}|} = \frac{1}{2} a_{iji\ell} \tag{L.4}$$

where the last equality is given by Equation 11.77.

M MTF271: Galilean invariance

B ELOW we repeat some of the details of the derivation given in [91]. Galilean invariance means that the equations do not change if the coordinate system is moving with a constant speed V_k. Let's denote the moving coordinate system by $*$, i.e.

$$x_k^* = x_k + V_k t, \; t^* = t, \; \bar{v}_k^* = \bar{v}_k + V_k \tag{M.1}$$

By differentiating a variable $\phi = \phi(t^*, x_i^*)$ we get

$$
\begin{aligned}
\frac{\partial \phi(x_i, t)}{\partial x_k} &= \frac{\partial x_j^*}{\partial x_k} \frac{\partial \phi}{\partial x_j^*} + \frac{\partial t^*}{\partial x_k} \frac{\partial \phi}{\partial t^*} = \frac{\partial \phi}{\partial x_k^*} \\
\frac{\partial \phi(x_i, t)}{\partial t} &= \frac{\partial x_k^*}{\partial t} \frac{\partial \phi}{\partial x_k^*} + \frac{\partial t^*}{\partial t} \frac{\partial \phi}{\partial t^*} = V_k \frac{\partial \phi}{\partial x_k^*} + \frac{\partial \phi}{\partial t^*}.
\end{aligned}
\tag{M.2}
$$

From Eq. M.2 is it easy to show that the Navier-Stokes (both with and without filter) is Galilean invariant [91, 201]. Transforming the material derivative from the (t, x_i)-coordinate system to the (t^*, x_i^*)-coordinate system gives

$$
\begin{aligned}
\frac{\partial \phi}{\partial t} + v_k \frac{\partial \phi}{\partial x_k} &= \frac{\partial \phi}{\partial t^*} + V_k \frac{\partial \phi}{\partial x_k^*} + (v_k^* - V_k) \frac{\partial \phi}{\partial x_k^*} \\
&= \frac{\partial \phi}{\partial t^*} + v_k^* \frac{\partial \phi}{\partial x_k^*},
\end{aligned}
$$

It shows that the left hand side does not depend on whether the coordinate system moves or not, i.e. it is Galilean invariant.

Now, let's look at the Leonard term and the cross term. Since the filtering operation is Galilean invariant [91], we have $\bar{v}_k^* = \bar{v}_k + V_k$ and consequently also $v_k''^* = v_k''$. For the Leonard and the cross term we get (note that since V_i is constant $V_i = \bar{V}_i = \overline{\bar{V}_i}$)

$$
\begin{aligned}
L_{ij}^* &= \overline{\bar{v}_i^* \bar{v}_j^*} - \bar{v}_i^* \bar{v}_j^* = \overline{(\bar{v}_i + V_i)(\bar{v}_j + V_j)} - (\bar{v}_i + V_i)(\bar{v}_j + V_j) \\
&= \overline{\bar{v}_i \bar{v}_j} + \overline{\bar{v}_i} V_j + \overline{\bar{v}_j} V_i - \bar{v}_i \bar{v}_j - \bar{v}_i V_j - V_i \bar{v}_j \\
&= \overline{\bar{v}_i \bar{v}_j} - \bar{v}_i \bar{v}_j + V_j(\overline{\bar{v}_i} - \bar{v}_i) + V_i(\overline{\bar{v}_j} - \bar{v}_j) \\
&= L_{ij} - V_j \overline{v_i''} - V_i \overline{v_j''}
\end{aligned}
\tag{M.3}
$$

$$
\begin{aligned}
C_{ij}^* &= \overline{\bar{v}_i^* v_j''^*} + \overline{\bar{v}_j^* v_i''^*} = \overline{(\bar{v}_i + V_i) v_j''} + \overline{(\bar{v}_j + V_j) v_i''} = \\
&= \overline{\bar{v}_i v_j''} + \overline{v_j''} V_i + \overline{\bar{v}_j v_i''} + \overline{v_i''} V_j = C_{ij} + \overline{v_j''} V_i + \overline{v_i''} V_j
\end{aligned}
$$

From Eq. M.3 we find that the Leonard term and the cross term are different in the two coordinate systems, and thus the terms are not Galilean invariant. However, note that the sum is, i.e.

$$L_{ij}^* + C_{ij}^* = L_{ij} + C_{ij}. \tag{M.4}$$

The requirement for the Bardina model to be Galilean invariant is that the constant must be one, $c_r = 1$ (see Eq. 18.47). This is shown by transforming both the exact C_{ij} (Eq. 18.45) and the modelled one, C_{ij}^M (i.e. Eq. 18.46). The exact form of C_{ij} transforms as in Eq. M.3. The Bardina term transforms as

$$
\begin{aligned}
C_{ij}^{*M} &= c_r(\bar{v}_i^* \bar{v}_j^* - \overline{\bar{v}}_i^* \overline{\bar{v}}_j^*) \\
&= c_r \left[(\bar{v}_i + V_i)(\bar{v}_j + V_j) - \overline{(\bar{v}_i + V_i)} \, \overline{(\bar{v}_j + V_j)} \right] \\
&= c_r \left[\bar{v}_i \bar{v}_j - \overline{\bar{v}_i \bar{v}_j} - (\overline{\bar{v}}_i - \bar{v}_i) V_j - (\overline{\bar{v}}_j - \bar{v}_j) V_i \right] \\
&= C_{ij}^M + c_r \left[\overline{v''}_i V_j + \overline{v''}_j V_i \right].
\end{aligned}
\tag{M.5}
$$

As is seen, $C_{ij}^{*M} \neq C_{ij}^{M}$, but here this does not matter, because provided $c_r = 1$ the modelled stress, C_{ij}^{M}, transforms in the same way as the exact one, C_{ij}. Thus, as for the exact stress, C_{ij} (see Eq. M.4), we have $C_{ij}^{*M} + L_{ij}^{*} = C_{ij}^{M} + L_{ij}$. Note that in order to make the Bardina model Galilean invariant the Leonard stress *must* be computed explicitly.

N MTF271: Computation of wavenumber vector and angles

FOR each mode n, create random angles φ^n, α^n and θ^n (see Figs. N.1 and 27.1) and random phase ψ^n. The probability distributions are given in Table N.1. They are chosen so as to give a uniform distribution over a spherical shell of the direction of the wavenumber vector, see Fig. N.1.

N.1 The wavenumber vector, κ_j^n
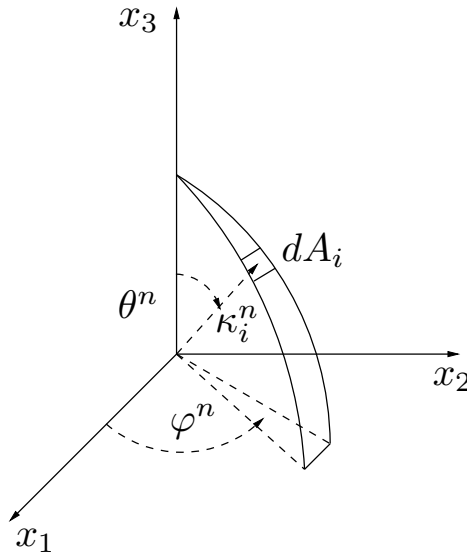
Figure N.1: The probability of a randomly selected direction of a wave in wave-space is the same for all dA_i on the shell of a sphere.

Compute the wavenumber vector, κ_j^n, using the angles in Section N according to Fig. N.1, i.e.

$$\begin{aligned}
\kappa_1^n &= \sin(\theta^n)\cos(\varphi^n) \\
\kappa_2^n &= \sin(\theta^n)\sin(\varphi^n) \\
\kappa_3^n &= \cos(\theta^n)
\end{aligned} \tag{N.1}$$

$p(\varphi^n) = 1/(2\pi)$	$0 \leq \varphi^n \leq 2\pi$
$p(\psi^n) = 1/(2\pi)$	$0 \leq \psi^n \leq 2\pi$
$p(\theta^n) = 1/2\sin(\theta)$	$0 \leq \theta^n \leq \pi$
$p(\alpha^n) = 1/(2\pi)$	$0 \leq \alpha^n \leq 2\pi$

Table N.1: Probability distributions of the random variables.

κ_i^n	σ_i^n	α^n
$(1,0,0)$	$(0,0,-1)$	0
$(1,0,0)$	$(0,1,0)$	90
$(0,1,0)$	$(0,0,-1)$	0
$(0,1,0)$	$(-1,0,0)$	90
$(0,0,1)$	$(0,1,0)$	0
$(0,0,1)$	$(-1,0,0)$	90

Table N.2: Examples of value of κ_i^n, σ_i^n and α^n from Eqs. N.1 and N.4.

N.2 Unit vector σ_i^n

Continuity requires that the unit vector, σ_i^n, and κ_j^n are orthogonal. This can be seen by taking the divergence of Eq. 27.3 which gives

$$\boldsymbol{\nabla} \cdot \mathbf{v}' = 2 \sum_{n=1}^{N} \hat{u}^n \cos(\boldsymbol{\kappa}^n \cdot \mathbf{x} + \psi^n) \boldsymbol{\sigma}^n \cdot \boldsymbol{\kappa}^n \tag{N.2}$$

i.e.

$$\sigma_i^n \kappa_i^n = 0 \tag{N.3}$$

(superscript n denotes Fourier mode n). Hence, σ_i^n will lie in a plane normal to the vector κ_i^n, see Fig. 27.1. This gives

$$\begin{aligned} \sigma_1^n &= \cos(\varphi^n) \cos(\theta^n) \cos(\alpha^n) - \sin(\varphi^n) \sin(\alpha^n) \\ \sigma_2^n &= \sin(\varphi^n) \cos(\theta^n) \cos(\alpha^n) + \cos(\varphi^n) \sin(\alpha^n) \\ \sigma_3^n &= -\sin(\theta^n) \cos(\alpha^n) \end{aligned} \tag{N.4}$$

The direction of σ_i^n in this plane (the $\xi_1^n - \xi_2^n$ plane) is randomly chosen through α^n. Table N.2 gives the direction of the two vectors in the case that κ_i is along one coordinate direction and $\alpha = 0$ and $\alpha = 90^o$.

O MTF271: 1D and 3D energy spectra

$\mathbf{T}$HE general two-point correlation B_{ij} of v_i' and v_j' (see Eq. 10.2) can be expressed by the energy spectrum tensor as [84, Chapter 3] (see Eq. H.28a)

$$B_{ij}(x_1, x_2, x_3)) = \int_{-\infty}^{+\infty} \Psi_{ij}(\boldsymbol{\kappa}) \exp(\imath\kappa_m \hat{x}_m) d\kappa_1 d\kappa_2 d\kappa_3 \qquad (O.1)$$

where $\hat{x}_m$ and κ_m are the separation vector the two points and the wavenumber vector, respectively. The complex Fourier transform $\exp(\imath\kappa_m \hat{x}_m)$ is defined in Appendix H (see Eq. 18.11). The two-point correlation, B_{ij}, and the energy spectrum tensor, Ψ_{ij}, form a Fourier-transform pair (see Eq. H.28b)

$$\Psi_{ij}(\boldsymbol{\kappa}) = \frac{1}{(2\pi)^3} \int_{-\infty}^{+\infty} B_{ij}(\hat{\boldsymbol{x}}) \exp(-\imath\kappa_m r_m) d\hat{x}_1 d\hat{x}_2 d\hat{x}_3 \qquad (O.2)$$

The separation between the two points is described by a general three-dimensional vector, $\hat{x}_m$. Both in experiments and in LES it is usually sufficient to study the two-point correlation and the energy spectra along a line. Hence, one-dimensional energy spectra, $E_{ij}(\kappa)$, which are a function of *scalar* wavenumber, κ (κ_1, κ_2 or κ_3), are often used. They are formed by integrating over a wavenumber plane; the energy spectrum for the wavenumber κ_1, for example, reads

$$E_{ij}(\kappa_1) = \frac{1}{2} \int_{-\infty}^{+\infty} \Psi_{ij}(\boldsymbol{\kappa}) d\kappa_2 d\kappa_3 \qquad (O.3)$$

A factor of two is included because $E \propto \Psi_{ii}/2$ is used to define a energy spectrum for the turbulent kinetic energy $k = \overline{v_i' v_i'}/2$, see Eqs. O.8 and O.10. Note that the maximum magnitude of the wavenumber vector contributing to $E_{ij}(\kappa_1)$ is very large since it includes all κ_2 and κ_3, i.e. $-\infty < \kappa_2 < \infty$ and $-\infty < \kappa_3 < \infty$. The one-dimensional two-point correlation, $B_{ij}(\hat{x}_1)$, for example, and the one-dimensional spectrum, $E_{ij}(\kappa_1)$, form a Fourier-transform pair, i.e.

$$B_{ij}(\hat{x}_1) = \frac{1}{2} \int_{-\infty}^{+\infty} E_{ij}(\kappa_1) \exp(\imath\kappa_1 \hat{x}_1) d\kappa_1 \qquad (O.4)$$

$$E_{ij}(\kappa_1) = \frac{2}{2\pi} \int_{-\infty}^{+\infty} B_{ij}(\hat{x}_1) \exp(-\imath\kappa_1 \hat{x}_1) d\hat{x}_1 \qquad (O.5)$$

where E_{ij} is *twice* the Fourier transform of B_{ij} because of the factor two in Eq. O.3. The diagonal components of the two-point correlation tensor are real and symmetric and hence the antisymmetric part of $\exp(-\imath\kappa_1 \hat{x}_1)$ – i.e. the sinus part – is zero and Eqs. O.4 and O.5 are simplified as

$$B_{ij}(\hat{x}_1) = \frac{1}{2} \int_{-\infty}^{+\infty} E_{ij}(\kappa_1) \cos(\kappa_1 \hat{x}_1) d\kappa_1 = \int_0^{\infty} E_{ij}(\kappa_1) \cos(\kappa_1 \hat{x}_1) d\kappa_1$$

$$E_{ij}(\kappa_1) = \frac{1}{\pi} \int_{-\infty}^{+\infty} B_{ij}(\hat{x}_1) \cos(\kappa_1 \hat{x}_1) d\hat{x}_1 = \frac{2}{\pi} \int_0^{+\infty} B_{ij}(\hat{x}_1) \cos(\kappa_1 \hat{x}_1) d\hat{x}_1$$

$$(O.6)$$

for $i = j$. The Reynolds stress $\rho \overline{v_1'^2}$, for example, is equal to the two-point correlation tensor ρB_{ij} with with zero separation distance. The $\overline{v_1'^2}$ can be computed both from the

three-dimensional spectrum (Eq. O.1) and one-dimensional spectrum (Eq. O.6)

$$
\begin{aligned}
\overline{v_1'^2} &= B_{11}(x_1, 0, 0) = \int_{-\infty}^{+\infty} \Psi_{11}(\boldsymbol{\kappa})d\kappa_1 d\kappa_2 d\kappa_3 \\
\overline{v_1'^2} &= B_{11}(0) = \int_0^{\infty} E_{11}(\kappa_1)d\kappa_1
\end{aligned}
\tag{O.7}
$$

Hence the turbulent kinetic energy, $k = \overline{v_i' v_i'}/2$, an be written as

$$
k = \frac{1}{2} \int_{-\infty}^{+\infty} \Psi_{ii}(\boldsymbol{\kappa})d\kappa_1 d\kappa_2 d\kappa_3
\tag{O.8}
$$

$$
k = \frac{1}{2} \int_0^{\infty} E_{11}(\kappa_1)\kappa_1 + \frac{1}{2} \int_0^{\infty} E_{22}(\kappa_2)\kappa_2 + \frac{1}{2} \int_0^{\infty} E_{33}(\kappa_3)d\kappa_3
\tag{O.9}
$$

The integral in Eq. O.8 has no directional dependence: it results in a scalar, k. Instead of integrating over $d\kappa_1 d\kappa_2 d\kappa_3$ we can integrate over a shell with radius $\kappa = (\kappa_i \kappa_i)^{1/2}$ and letting the radius go from zero to infinity, i.e.

$$
k = \frac{1}{2} \int_0^{\infty} 4\pi\kappa^2 \Psi_{ii} d\kappa
\tag{O.10}
$$

where $4\pi\kappa^2$ is the surface area of the shell. We now define an energy spectrum, $E(\kappa) = 2\pi\kappa^2 \Psi_{ii}$ so that

$$
k = \int_0^{\kappa} E(\kappa)d\kappa.
\tag{O.11}
$$

The energy spectrum $E_{11}(\kappa_1)$, for example, corresponds to the square of the Fourier coefficient of the velocity fluctuation (see Parseval's formula, Eq. H.4), i.e.

$$
E_{11}(\kappa_1) = \hat{v}_1^2(\kappa_1)
\tag{O.12}
$$

Below the properties of the three energy spectra are summarized.

- The three-dimensional spectrum tensor, $\Psi_{ij}(\boldsymbol{\kappa})$, is a tensor which is a function of the wavenumber vector.

- The one-dimensional spectrum, $E_{ij}(\kappa_1)$, is a tensor which is a function of a scalar (one component of κ_m).

- The energy spectrum, $E(\kappa)$, is a scalar which is a function of the length of the wavenumber vector, $|\boldsymbol{\kappa}| \equiv \kappa$.

O.1   Energy spectra from two-point correlations

In connection to Eqs. O.4, O.5 and O.6 we stated that the one-dimensional energy spectra and the two-point correlations form Fourier-transform pairs. The proof is given in this section. The energy spectrum is given by the square of the Fourier coefficients, see Parseval's formula, Eq. H.4. Let $\hat{u}$ be the Fourier coefficient of the velocity fluctuation u' in the x direction which is periodic with period $2L$. Take the covariance of the

Fourier coefficients, $\hat{u}(\kappa')$ and $\hat{u}(\kappa)$ where κ and κ' denote two different wavenumbers and x and x' denote two points separated in the x directions so that

$$
\begin{aligned}
\langle \hat{u}(\kappa)\hat{u}(\kappa')\rangle &= \left\langle \frac{1}{2L}\int_{-L}^{L} u(x)\exp(-\imath\kappa x)dx \frac{1}{2L}\int_{-L}^{L} u(x')\exp(-\imath\kappa' x')dx' \right\rangle \\
&= \left\langle \frac{1}{4L^2}\int_{-L}^{L}\int_{-L}^{L} u(x)u(x')\exp(-\imath(\kappa x + \kappa' x'))dx dx' \right\rangle
\end{aligned}
\tag{O.13}
$$

where $\langle\cdot\rangle$ denotes averaging over time; this equation corresponds to Eq. O.4 except the factor of two. Since we are performing a Fourier transform in x we must assume that this direction is homogeneous, i.e. all averaged turbulence quantities are independent of x and the two-point correlation is not dependent of x (or x') but only on the separation distance $x - x'$, see discussion in connection to Eq. 10.6 on p. 117. Hence we replace x' by $x + x''$ so that

$$
\begin{aligned}
\langle \hat{u}(\kappa)\hat{u}(\kappa')\rangle &= \left\langle \frac{1}{4L^2}\int_{-L}^{L}\left(\int_{-L-x}^{L-x} u(x)u(x+x'')\exp(-\imath(\kappa x + \kappa'(x + x'')))dx''\right) dx \right\rangle \\
&= \left\langle \frac{1}{2L}\int_{-L}^{L}\exp(-\imath(\kappa+\kappa')x)\left(\frac{1}{2L}\int_{-L-x}^{L-x} B_{11}(x'')\exp(-\imath\kappa' x'')dx''\right) dx \right\rangle
\end{aligned}
\tag{O.14}
$$

The second integral (in parenthesis) is the Fourier transform (which corresponds to the Fourier *coefficient* in discrete space, see Eq. H.28b) of the two-point correlation B_{11}, i.e.

$$
\langle \hat{u}(\kappa)\hat{u}(\kappa')\rangle = \left\langle \hat{B}_{11}(x'')\frac{1}{2L}\int_{-L}^{L}\exp(-\imath(\kappa+\kappa')x))dx \right\rangle
\tag{O.15}
$$

where $\hat{B}_{11}$ denotes the Fourier transform of B_{11} (cf. O.5) and since it does not depend on the spatial coordinate it has been moved out of the integral. Furthermore, $\hat{B}_{11}$ is real and symmetric since B_{11} is real and symmetric. The remaining integral in Eq. O.15 includes trigonometric function with wavelengths κ and κ'. They are orthogonal functions, see Appendix H, and the integral of these functions is zero unless $\kappa = \kappa'$. The integral in Eq. O.15 for $\kappa = \kappa'$ is evaluated as (see "length of of ψ_k" in Appendix H, Eq. H.13, and use $\psi_1 = \cos(2\pi x/L)$)

$$
\begin{aligned}
(\psi_1|\psi_1) = ||\psi_1||^2 &= \int_{-L}^{L}\cos^2\left(\frac{2\pi x}{L}\right) dx \\
&= \left[\frac{x}{2} + \frac{L}{8\pi}\sin\left(\frac{4\pi x}{L}\right)\right]_{-L}^{L} = L
\end{aligned}
\tag{O.16}
$$

In the same way, the "length of of ϕ_k" in Eq. H.16 is also L. Equation O.15 can now be written

$$
\langle \hat{u}(\kappa)\hat{u}(\kappa)\rangle = \frac{1}{2L}(L + L)\langle \hat{B}_{11}(x)\rangle = \langle \hat{B}_{11}(x)\rangle
\tag{O.17}
$$

Hence, it is seen that the Fourier transform of a two-point correlation (in this example $\langle B_{11}(x_1)\rangle$) indeed gives the corresponding one-dimensional energy spectrum (in this example $E_{11}(\kappa_1) = \langle(\hat{u}(\kappa))^2\rangle$).

P MTF271, Assignment 1: Reynolds averaged Navier-Stokes

P.1 Part I: Data of Two-dimensional flow

YOU can do the assignment on your own or in a group of two. It is recommended (but the not required) that you use LaTeX (an example of how to write in LaTeXis available on the course www page). You find LaTeX at here. You can also use LaTeX on-line.

You'll use data from a coarse DNS. Although some of the data are probably not fully accurate, in this exercise we consider the data to be exact. You can use Matlab, Octave or Python. Both Octave and Python are open-source software. Octave is a Matlab clone. Many large Swedish industries prefer engineers to use Python instead of Matlab due to Matlab's high license fees.

Use Matlab/Octave/Python to read data files of the mean flow ($\bar{v}_1$, $\bar{v}_2$, $\bar{p}$) and turbulent quantities. ($\overline{v_1'^2}$, $\overline{v_2'^2}$, $\overline{v_3'^2}$ and $\overline{v_1'v_2'}$). You will analyze one of the following flows:

Case 1: Flow over a wavy wall (small wave) [202, 202]. $Re = 10\,000$ ($\nu = 1 \cdot 10^{-4}$, $\rho = 1$) based on the bulk velocity in the channel at $x = 0$ and the channel height.

Case 2: Flow over a wavy wall (large wave) [202, 202]. $Re = 10\,000$ ($\nu = 1 \cdot 10^{-4}$, $\rho = 1$) based on the bulk velocity in the channel at $x = 0$ and the channel height.

Case 3: Flow over a hill $Re = 10\,595$ ($\nu = 1/10595$, $\rho = 1$) based on the bulk velocity in the channel at $x = 0$ and the channel height.

Case 4: Flow over two hills $Re = 10\,595$ ($\nu = 1/10595$, $\rho = 1$) based on the bulk velocity in the channel at $x = 0$ and the channel height.

Periodic boundary conditions are imposed in streamwise (x_1) and spanwise (x_3) directions in all flows.

Get the case the case number by register in a group at Canvas. Download the data from
`http://www.tfd.chalmers.se/~lada/comp_turb_model`. At the www-page you can download a py-file (`pl_vect.py`) or m-file (`pl_vect.m`) which read the data and plots the vector field and the pressure contours. You must also download the function `dphidx_dy.py` or `dphidx_dy.m` which compute the gradients, see Section P.2. Make sure you put this function in the directory where you execute `pl_vect.py.` or `pl_vect.m`.

The report, along with the Matlab/Octave/Python files(s), should be submitted electronically at Canvas; the deadline can be found in the time table.

Report: See the following as a guideline to discuss the results. Write a flowing report, so the reader does not need the assignment. Discuss all plots based on reasonability. If you figure out deviations from the expected outcome discuss them. You should discuss all figures; if you have nothing to write about a figure, don't include it.

P.1.1 Analysis

Study the flow. In which regions do you expect the turbulence to be important? Let's find out. The two-dimensional time-averaged Navier-Stokes for the x_1 momentum

reads (the density is set to one, i.e. $\rho = 1$)

$$\frac{\partial \bar{v}_1 \bar{v}_1}{\partial x_1} + \frac{\partial \bar{v}_1 \bar{v}_2}{\partial x_2} = -\frac{\partial \bar{p}}{\partial x_1} + \nu \frac{\partial^2 \bar{v}_1}{\partial x_1^2} - \frac{\partial \overline{v_1'^2}}{\partial x_1} + \nu \frac{\partial^2 \bar{v}_1}{\partial x_2^2} - \frac{\partial \overline{v_1' v_2'}}{\partial x_2}$$

$$\frac{\partial \bar{v}_1 \bar{v}_2}{\partial x_1} + \frac{\partial \bar{v}_2 \bar{v}_2}{\partial x_2} = -\frac{\partial \bar{p}}{\partial x_2} + \nu \frac{\partial^2 \bar{v}_2}{\partial x_1^2} - \frac{\partial \overline{v_1' v_2'}}{\partial x_1} + \nu \frac{\partial^2 \bar{v}_2}{\partial x_2^2} - \frac{\partial \overline{v_2'^2}}{\partial x_2}$$

(P.1)

Recall that all the terms on the right-hand side represent x_1 components of forces per unit volume.

P.1.2 The momentum equations

The files pl_vect.py, pl_vect.m loads the data file and plots the profiles of $\overline{v_1'^2}$ at some x stations, the velocity vector field and a contour plot of velocity gradient $\partial \bar{v}_1 / \partial x_2$. Choose two x_1 locations (vertical grid lines), one without recirculation (close to the left boundary, for example) and one grid line where there is a recirculation region.

Assignment 1.1. Plot the stresses along vertical grid lines at these two locations using the Python plt.plot(x,y) or Matlab/Octave command plot(x,y). Please make sure that in your report the numbering on the axis and the text in the legend is large enough; you can use the command

```
h1=gca;
set(h1,'fontsize',[20]) %the number '20' gives the fontsize
```

The size of the labels and the title is similarly controlled by

```
xlabel('x/H','fontsize',[20])
ylabel('y/H','fontsize',[20])
title('velocity','fontsize',[20])
```

Assignment 1.2. Compute and plot all terms in Eq. P.1 (see Fig. 6.6). You will need to compute the derivatives of e.g. $\bar{v}_1$ and $\bar{p}$. In pl_vect.m and pl_vect.py the function dphidx_dy is used to compute $\partial \bar{v}_1 / \partial x_1$ and $\partial \bar{v}_1 / \partial x_2$. Use this function to compute all derivatives that you need. To enhance readability you may omit the small terms or use two plots per vertical grid line. Make also a zoom near the walls. For example, for a $x - y$ plot

```
plot(u,y,'linew',2) % linewidth=2
```

you may want to zoom in on y=[0 0.01] and u=[-0.1 0.4]; this is achieved by

```
axis([-0.1 0.4 0 0.01])
```

The 'axis' command can be used together with any plot, e.g. with 'surf' and 'quiver'.

Which terms are negligible? Can you explain why they are negligible?

What about the viscous terms: where do they play an important role?

Use the Taylor expansion for the fluctuating terms and show analytically, which terms are non-zero *at* the wall. Compare with the DNS results and explain derivations.

So far we have looked at the $\bar{v}_1$-momentum equation. The database corresponds to a two-dimensional flow. Now let's think of the forces as vectors. The gradient of the normal stresses in the $x_1 - x_2$ plane represents the force vector (see Eq. P.1)

$$\mathbf{F}_N = \left(-\frac{\partial \overline{v_1'^2}}{\partial x_1}, -\frac{\partial \overline{v_2'^2}}{\partial x_2} \right) \tag{P.2}$$

and the corresponding force vector due to the shear stresses reads (see Eq. P.1)

$$\mathbf{F}_S = \left(-\frac{\partial \overline{v_1' v_2'}}{\partial x_2}, -\frac{\partial \overline{v_1' v_2'}}{\partial x_1} \right) \tag{P.3}$$

Find the first term in Eqs. P.2 and P.3 in the $\bar{v}_1$ momentum equation, Eq. P.1. Consider the second line in Eq. P.1 which is the $\bar{v}_2$ equation and find the other two terms in Eqs. P.2 and P.3. Note that $\mathbf{F}_N$ and $\mathbf{F}_S$ are forces per unit volume ($[N/m^3]$).

Assignment 1.3. Plot the vector field $\mathbf{F}_N$ to learn something about its properties. When $\overline{v_2'^2}$ reaches a maximum or a minimum along a grid line normal to the wall, what happens with the vector field $\mathbf{F}_N$? Zoom-in on interesting regions.

Assignment 1.4. Plot also vector fields of the shear stress, $\mathbf{F}_S$ (see Eq. P.3), the pressure gradient and the viscous terms. Zoom up in interesting regions.

P.1.3   The turbulent kinetic energy equation

The exact transport equation for the turbulent kinetic energy, k, reads

$$\frac{\partial}{\partial x_j} \left(\bar{v}_j k \right) = \nu \frac{\partial^2 k}{\partial x_j \partial x_j} + P^k + D_k - \varepsilon$$
$$P^k = -\overline{v_i' v_j'} \frac{\partial \bar{v}_i}{\partial x_j} \tag{P.4}$$

Assignment 1.5. Plot the production term along the two grid lines (see Fig. 8.3). Explain why it is large at some locations and small at others. The production term consists of the sum of four terms, two of which involve the shear stress while the other include the normal stresses. Compare the contributions due the shear stress and the normal stresses.

Assignment 1.6. Plot the dissipation and compare it with the production. Do you have local equilibrium (i.e. $P^k \simeq \varepsilon$) anywhere? Take ε from 2D RANS simulation.

P.1.4 The Reynolds stress equations

The modeled transport equation for the Reynolds stresses can be written as

$$
\frac{\partial}{\partial x_k}\left(\bar{v}_k \overline{v_i' v_j'}\right) = \nu \frac{\partial^2 \overline{v_i' v_j'}}{\partial x_k \partial x_k} + P_{ij} + \Phi_{ij} + D_{ij} - \varepsilon_{ij}
$$
$$
P_{ij} = -\overline{v_i' v_k'}\frac{\partial \bar{v}_j}{\partial x_k} - \overline{v_j' v_k'}\frac{\partial \bar{v}_i}{\partial x_k}
$$
(P.5)

The pressure-strain term, Φ_{ij}, use the models in Eqs. 11.91, 11.57, 11.90, 11.95 and 11.96.

1. In the damping function, f (see Eq. 11.92), $|n_{k,w}(x_k - x_{k,w})|$ denotes the distance to the nearest wall. If, for example, a lower wall is the closest wall to node (I, J), then

$$
|n_{k,w}(x_k - x_{k,n})| = \left\{(x(I,J) - x(I,1))^2 + (y(I,J) - y(I,1))^2\right\}^{1/2} \quad \text{(P.6)}
$$

   Note that you have to search through all wall nodes to find which wall node gives the smallest value. The damping function, f, involves k and ε. These should be taken from the 2D RANS simulation (they are loaded in `pl_vect.py` and `pl_vect.m`).

2. If we assume, again, that the lower wall is the closest wall to cell (I, J) and that the lower wall is horizontal, then $n_{i,w} = (0, 1)$. To compute $n_{i,w}$ for the general case (see Eqs. 11.95 and 11.96), compute first the vector which is parallel to the wall, $s_{i,w}$, and then compute $n_{i,w}$ from $s_{i,w}$ (see Eq. P.11)

3. The diffusion terms D_{ij} and D^ε can be modeled using the Generalized Gradient Diffusion Hypothesis GGDH of [203]

$$
D_{ij} = \frac{\partial}{\partial x_m}\left(c\,\overline{u_k u_m}\frac{k}{\varepsilon}\frac{\partial \overline{v_i' v_j'}}{\partial x_k}\right)
$$
(P.7)

   This diffusion model can cause numerical problems, and the GGDH is then replaced by a simple eddy viscosity model

$$
D_{ij} = \frac{\partial}{\partial x_m}\left(\frac{\nu_t}{\sigma_k}\frac{\partial \overline{v_i' v_j'}}{\partial x_m}\right), \quad \nu_t = C_\mu k^2/\varepsilon
$$
(P.8)

   The following constants should be used:

$$
(c_\mu, c_1, c_2, c_{1w}, c_{2w}, \sigma_k) = (0.09, 1.5, 0.6, 0.5, 0.3, 1)
$$

4. The dissipation is modelled as (see Section 11.7.3)

$$
\varepsilon_{ij} = \frac{2}{3}\varepsilon\delta_{ij}
$$

Assignment 1.7. Choose two stresses. Plot the different terms in the equations for one vertical grid line fairly close to the inlet (not too close!). Looks at the corresponding plot for channel flow, see Fig. 9.1. Use the simple eddy viscosity model for the

turbulent diffusion term. Use k and ε from the 2D RANS simulation. If the figure becomes too crowdy, use two plots per vertical grid line or simply omit terms that are negligible. Try to explain why some terms are large and vice versa. Usually, a stress is large in locations where its production (or pressure-strain) term is large. Is that the case for you?

Assignment 1.8. Compute the stresses using the Boussinesq assumption, i.e $\overline{v'_i v'_j} = -2\nu_t \bar{s}_{ij} + (2k/3)\delta_{ij}$ where $\nu_t = c_\mu k^2/\varepsilon$. Use k and ε from the 2D RANS simulation. Compare the eddy-viscosity stresses with two of the Reynolds stresses from the database. Make also a zoom-in near walls.

When using the Boussinesq assumption the production of turbulent kinetic energy (use k and ε from the 2D RANS simulation)

$$P^k = 2\nu_t \bar{s}_{ij} \bar{s}_{ij} \tag{P.9}$$

is always positive. The exact production of turbulent kinetic energy (see Eq. P.4) is usually positive. It can however become negative.

Assignment 1.9. Compute the exact production in Eq. P.4 in the entire domain to investigate if the production is negative anywhere. If so, explain why (for physical explanation, see Item II at p. 97).

The reason why the eddy-viscosity production in Eq. P.9 must be positive is that neither ν_t nor $\bar{s}_{ij}\bar{s}_{ij}$ can go negative. Another way to explain this fact is that the modeled Reynolds stress, $\overline{v'_i v'_j}$, and the strain rate tensor, $\bar{s}_{ij}$ are parallel. To find out to what degree the exact Reynolds stress and the strain rate are parallel, one can compute the eigenvectors.

Assignment 1.10. The realizability concept is discussed in Section 13. It is shown that the Boussinesq assumption can give unphysical negative normal Reynolds stresses (if $\partial \bar{v}_1/\partial x_1$ in Eq. 13.2 is very large then $\overline{v'^2_1}$ goes negative). A remedy is presented in Section 13 in which the turbulent viscosity is limited using the eigenvalues of the strain-rate tensor, $\bar{s}_{ij}$, see Eq. 13.12. Compute the eigenvalues of $\bar{s}_{ij}$ in the entire domain. Check if the limiter in Eq. 13.12 reduces ν_t along the two vertical lines you previously chose. Find out where in the entire domain the limiter has largest effect. Is this region a stagnation region? (the object of Eq. 13.12 is to limit ν_t in stagnation regions, see Section 12.3).

P.2 How to compute derivatives on a curvi-linear mesh

In this section we describe how the derivatives on a curvi-linear grid are computed in the provided Python dphidx_dy.py or Matlab function dphidx_dy.m. On a Cartesian grid it is more convenient to use the built-in Python/Matlab/Octave function gradient, but the approach used below works for all meshes, including Cartesian ones.

The data you have been given, x_1 and x_2 and all variables, are stored at the grid points, i.e. at $(x_{1,sw}, x_{2,sw})$, $(x_{1,se}, x_{2,se})$, $(x_{1,nw}, x_{2,nw})$ and $(x_{1,ne}, x_{2,ne})$. When you need a variable, say v_1, at the center of the cell, compute it as

$$v_{1,P} = \frac{1}{4}(v_{1,sw} + v_{1,se} + v_{1,nw} + v_{1,ne}) \tag{P.10}$$
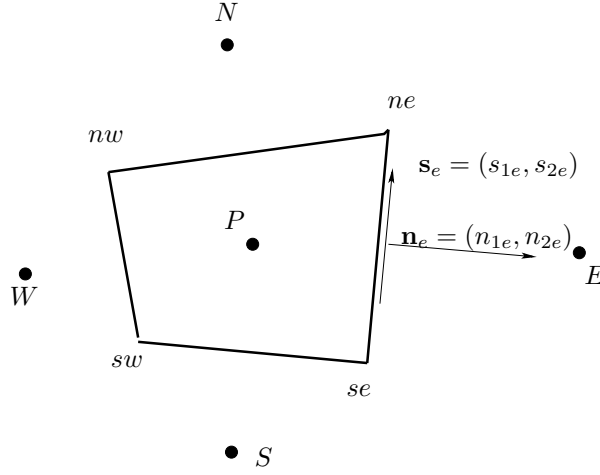
Figure P.1: *Control volume. The velocity v_1 is stored at the corners (ne, nw, ...). Coordinates x_1, x_2 are given at the corners (ne, nw, ...).*

Let's compute $\partial v_1/\partial x_1$. In order to do that we use Gauss' law over a control volume centered at face e (dashed control volume in Fig. P.1). The divergence theorem for a scalar, ϕ, reads

$$\int_V \frac{\partial \phi}{\partial x_i} dV = \int_A \phi n_i dA$$

To compute $\partial v_1/\partial x_1$ we set $\phi = v_1$ and $i = 1$ which gives

$$\int_V \frac{\partial v_1}{\partial x_1} dV = \int_A v_1 n_1 dA$$

Assuming that $\partial v_1/\partial x_1$ is constant in the volume V we obtain

$$\frac{\partial v_1}{\partial x_1} = \frac{1}{V} \int_A v_1 n_1 dA$$

In discrete form we can write (see Fig. P.1)

$$\left(\frac{\partial v_1}{\partial x_1}\right) = \frac{1}{V} \sum_{i=e,n,w,w} (v_1 n_1 A)_i =$$

$$\frac{1}{V} \left\{ (v_1 A n_1)_e + (v_1 A n_1)_n + (v_1 A n_1)_w + (v_1 A n_1)_s \right\}$$

P.2.1   Geometrical quantities

It is useful to first compute the unit vectors **s** along the control volume. For the east face, for example, we get

$$s_{1e} = \frac{x_{1,ne} - x_{1,se}}{d_e}$$

$$s_{2e} = \frac{x_{2,ne} - x_{2,se}}{d_e}$$

$$d_e = \sqrt{(x_{1,ne} - x_{1,se})^2 + (x_{2,ne} - x_{2,se})^2}$$

(note that the area of the east face A_e is equal to d_e since $\Delta z = 1$). The relation between the normal vector **n**, **s** and the unit vector in the z-direction

$$\mathbf{s} \cdot \mathbf{n} = 0$$
$$\mathbf{s} \times \hat{z} = \mathbf{n},$$

gives us the normal vector for the east face as

$$n_{1e} = s_{2e}$$
$$n_{2e} = -s_{1e}. \tag{P.11}$$

P.3   Part II: StarCCM+

In this task, a commercial CFD software (StarCCM+ 11.02.009) will be used. The task is to do simulation of an asymmetric diffuser. Several turbulence models will be used and the results will be compared with experimental data. Before doing the task, it is recommended to first do one of the tutorials in the StarCCM+. The tutorial is the steady backward facing step tutorial. The tutorials can be found in the StarCCM+ user guide.

P.3.1   Backward Facing Step Tutorial

This tutorial is a good bridge before doing the asymmetric diffuser case. Here are some steps to access the tutorial:

1. Open a terminal window. In the terminal window, type starccm+

2. To start a new simulation, click File → new simulation

3. Tick the Power-On-Demand box and fill the license box with the POD code.

4. Download the tutorial instruction and data from the course homepage

Assignment 1.11 Continue to work on the backward facing step flow. Choose a new turbulence model (right click on `Continua/Fluid` and select `Select models ....` Untick `All y+ Wall treatment` and then untick the turbulence model. Now you can choose a new turbulence model. Run a couple different turbulence model and compare the results. A short recirculation region is usually connected to high turbulence in the shear layer bounding the recirculation region.

P.3.2 Asymmetric diffuser case

In this case 2D Asymmetric diffuser will be studied. The Reynolds number (Re = 20000) is based on the bulk velocity and the inlet channel height. The case is built based on these references. It is highly recommended to read these references before doing the case :

1. Ercoftac case 8.2: Flow through an asymmetric plane diffuser Description.

2. El-Behery & Hamed [204]

3. Buice & Eaton [205]

4. Davidson [160].

P.3.3 Brief instruction to begin the asymmetric diffuser case

1. Start the StarCCM+

   - Open a terminal window → type StarCCM+

2. Create a new simulation

   - Click the new simulation icon → tick the power on demand box
   - Fill the license box with the POD license

3. Draw the geometry

   - Follow and modify the geometry in the ercoftac case 8.2
   - Create a new 3D-CAD Models
   - Create a new sketch on XY plane
   - Start by drawing the asymmetric diffuser without the radius
   - Right click on each lines and apply vertical / horizontal constraint accordingly
   - Set the diffuser angle to 10 degree
   - Set the length of each lines. Use H = 1 m. Length of the inlet = 60H. Length of the diffuser = 21H. Length of the outlet = 22H. Do not need to set the height of the outlet.
   - Create a fillet on the beginning and end of the diffuser line. (R = 9.7H)
   - Set your base point (which is the point where the channel start to bend) at X = 0 and Y = 3.7 m
   - Extrude the sketch 1 m for easier renaming
   - Rename the faces accordingly (inlet, outlet, top, bottom, leftside, rightside)

4. Create a new geometry part. (The same way as in backward facing step tutorial)

5. Assign parts to regions. (The same way as in backward facing step tutorial)

6. Set the boundary condition accordingly. Inlet = velocity inlet; Outlet = pressure outlet; leftside = symmetry plane; rightside = symmetry plane.

7. Create directed mesh

   - Right click on the operation → new → directed mesh → body1 → OK
   - Expand operations → Right click on the directed mesh → edit
   - Add rightSide as a source surfaces and leftSide as target surfaces
   - Right click on source meshes → new source mesh → patch mesh → body1 → OK
   - Click auto populate feature edges icon
   - Change the mode from patch topology into patch mesh
   - Click the inlet line
     - Number of divisions = 80
     - Type = two sided hyperbolic
     - Spacing start and end = 3e-4 m
   - Click the top line
     - Number of divisions = 421
     - Type = constant
   - Right click on the mesh distributions → create new volume distribution. Set the number of layers = 2
   - Close the directed mesh and execute the directed mesh

8. Create 2D Mesh

   - Go to Menu bar → Mesh → Convert to 2D → Delete 3D regions after conversion → OK

9. Select turbulence model

   - Right click on Physics 1 2D → Select model
   - In the new window select:
     (a) Untick the auto-select recommended models
     (b) Two dimensional
     (c) Steady
     (d) Gas
     (e) Segregated flow
     (f) Constant Density
     (g) Turbulent
     (h) Reynolds-Averaged Navier-Stokes
     (i) Choose turbulence model that you want to use.

10. Set the Gas properties

   - Expand Physics 1 folder → Gas → Air → Material Properties → Dynamic Viscosity → Constant → Value = $6E - 5 Pa - s$

11. Set the boundary condition

   - Go to Regions.

- In the properties window, check that mesh continuum is parts meshes. Check that physics continuum is physics 1 2D
- Expand Body 1 2D → Boundaries → Inlet
  (a) Physics Conditions → Velocity Specification → Method → Components
  (b) Physics Values → Velocity → value → [1,0,0] m/s

12. Extract more data from the simulation (for example: Turbulent kinetic energy production)

   - Expand Solvers folder → go to every subfolder and tick temporary storage retained if you find one

13. Set the stopping criteria

   - For Reynolds Stress Model, use the default setting of the stopping criteria
   - For the rest of the model use instruction below
   - Disabled the maximum iteration criteria
   - Create new stopping criteria
     (a) Right click on the Report folder → go to New Report → click Pressure Drop
     (b) In the Pressure Drop 1 properties window. High Pressure = Outlet. Low Pressure = Inlet.
   - Right click on the Pressure Drop 1 → click on create monitor and plot from report
   - Right click on the Stopping criteria folder →choose create new criterion → create from monitor → click on Pressure Drop 1 monitor
   - In the Pressure Drop 1 Monitor criterion properties window
     (a) Criterion option = Asymptotic
     (b) Click on Asymptotic limit
   - set [max-min] value = $1E-4$ → Number of samples = 100

14. Create a scalar scene to show the result

   - Go to Scenes folder → New Scene → Scalar
   - Right click on the select function → select velocity [i]

15. Create planes to extract the results at the same location as the experimental data

   - Right click on Derived Parts folder → New Part → Section → Plane
   - Input Parts → Select → All the region
   - Set normal → $x = 1, y = 0, z = 0$
   - Display → New Geometry Displayer
   - Specify the x-coordinate according to the experimental data (see below)
   - Click Apply for each of the x-coordinate
     (a) $X - 6 = -5.87m$

(b) $X03 = 2.59m$

(c) $X06 = 5.98m$

(d) $X14 = 13.56m$

(e) $X17 = 16.93m$

(f) $X20 = 20.32m$

(g) $X24 = 23.71m$

(h) $X27 = 27.09m$

(i) $X30 = 30.48m$

(j) $X34 = 33.87m$

16. Create the X-Y plot to monitor the result

- Right click on Plots folder → choose New Plot → click on X-Y Plot
- On the new X-Y Plot properties window, go to Parts → select all the derived parts
- Expand the X-Y Plot 1

    (a) X-type → Type = Scalar → Scalar Function → Field Function = Velocity[i]

    (b) Y-types → Y Type 1
        - Type = Direction; smooth values
        - Vector Quantity → Value = [0,1,0]
        - Go to each Plane Section and change the X Offset accordingly

17. Insert experimental data

- Download the experimental data from the course homepage
- Expand Tools folder
- Right click on Tables folder → choose Create a New Table → click File Table → Load all the experimental data
- Go back to X-Y plot 1 monitor → right click on Data Series folder → Add Data → Select all the experimental data
- Expand Data series folder → select all the experimental data by click the first data hold shift button and click the last data → right click on the highlighted area → click swap column

18. Run the simulation

- Go to Solution → Run
- Other method: click icon which show a running man.

19. Collecting the simulation data

- After the simulation has reached its stopping criteria → Right click on XY plot 1 → Export → Save with appropriate name
- Add the simulation data to other simulation as you add experimental data

Assignment 1.12. Look at the results. How large is the pressure recovery (i.e. how much does the pressure increase from inlet to outlet).

Assignment 1.13. Choose a new turbulence model. Run the same turbulence models as for the back- step case and compare the results. Are the results different? Where do the difference appear? In the plane channel upstream of the diffuser? Compare turbulent quantities such a k and ν_t (or if you chose to use a Reynolds stress model, compare the shear stresses $\overline{v_1' v_2'}$. If the recirculation region is different, the reason is maybe connected to the turbulence level in the shear layer above the recirculation region. Or maybe the reason is that the incoming boundary layers are different. In the backstep flow, you found that one turbulence model was better than the other one(s). Is the same turbulence model best for this flow? Make other interesting comparisons!

Q   MTF271, Assignment: LES, $Re_\tau = 1\,000$

Y OU can do the assignment on your own or in a group of two. You will receive data from a DNS of fully developed flow in a channel. It is recommended (but not required) that you use LATEX (an example of how to write in LATEXis available on the course www page). You can download LATEX at here. You can also use LATEX on-line.

You can use Matlab, Octave or Python. Both Octave and Python are open-source software. Octave is a Matlab clone. Many large Swedish industries prefer engineers to use Python instead of Matlab due to Matlab's high license fees.

The report, along with the Matlab/Octave/Python files(s), should be submitted electronically.

The equations that have been solved are

$$\frac{\partial v_i}{\partial x_i} = 0$$

$$\frac{\partial v_i}{\partial t} + \frac{\partial}{\partial x_j}(v_i v_j) = \delta_{i1} - \frac{\partial p}{\partial x_i} + \frac{1}{Re_\tau}\frac{\partial^2 v_i}{\partial x_j \partial x_j} \tag{Q.1}$$

The Re number based on the friction velocity and the half channel width is $Re_\tau = u_\tau h/\nu = 1\,000$ ($h = \rho = u_\tau = 1$ so that $\nu = 1/Re_\tau$).

A $192 \times 160 \times 192$ mesh has been used. The streamwise, wall-normal and spanwise directions are denoted by x (x_1), y (x_2) and z (x_3) respectively. The cell size in x and z directions are $\Delta x = 0.0327$ and $\Delta z = 0.00818$. Periodic boundary conditions were applied in the x and z direction (homogeneous directions). The size of the domain is (L, h, Z_{max}) in (x, y, z), see Fig .Q.1.

Q.1   Time history

At the www-page

    http://www.tfd.chalmers.se/~lada/comp_turb_model/

you find a file u_v_time_4nodes_re1000.dat with the time history of u and v. The file has eight columns of u and v at four nodes: $y/\delta = 0.00463$, $y/\delta = 0.0144$, $y/\delta = 0.0727$ and $y/\delta = 0.25$. With $u_\tau = 1$ and $\nu = 1/Re_\tau = 1/1000$ this correspond to $y^+ = 4.6$, $y^+ = 14$, $y^+ = 67$ and $y^+ = 253$. The time step is 0.0008178

Download the Matlab/Octave program pl_time.m or the Pythonb file pl_time.py which load and plot the time history of u. Run the program pl_time. Recall that the velocities have been scaled with the friction velocity u_τ, and thus what you see is really u/u_τ. The time history of u at $y/\delta = 0.014$ and $y/\delta = 0.067$ are shown. Study the time history of the blue line ($y/\delta = 0.014$) in greater detail. Make a zoom between, for example, $t = 1$ and $t = 2$ and $u_{min} = 3$ and $u_{min} = 21$. This is conveniently done with the Python commands

```
plt.axis([1,2,3,21])
plt.plot(t,u2,'b-o')
```

or the Matlab/Octave commands

```
axis([1 2 3 21])
plot(t,u2,'b-o')
```

Use this technique to zoom and to look at the details of the time history. Alternatively, you can use the zoom buttons above the figure.

Plot u for all four nodes. How does the time variation of u vary for different positions? Why? Plot also v at the four different positions. What is the difference between u and v?

Q.2 Time averaging

Compute the average of the u velocity at node 2. Add the following code (before the plotting section) for Python

```
umean=np.mean(u2)
```

or in Matlab/Octave

```
umean=np.mean(u2)
```

Here the number of samples is $n = 10000$ (the entire `u2` array). Find out how many samples must be used to get a correct mean value. Start by trying with 100 samples as in Python

```
umean_100=plt.mean(u2(0:100))
```

or in Matlab/Octave

```
umean_100=mean(u2(1:100))
```

Do the same exercise for the other three nodes.

Q.3 Auto correlation

Auto correlation is defined in Section 10.2. Compute the autocorrelation for u' at Node 1 using the Python command

```
1_fluct=u1-np.mean(u1)
two_uu_1=np.correlate(u1_fluct,u1_fluct,'full')
# find max
nmax=np.argmax(two_uu_1)
# and its value
two_max=np.max(two_uu_1)
```

or in Matlab/Octave

```
imax=500;
two_uu_1=autocorr(u1,imax);
```

In Octave, it should be `xcorr`; download the file `pl_time_re1000_with_xcorr.m`. Maybe you need to download the `signal` package. In Ubuntu you type

```
sudo apt-get install octave-signal
```

Then you load the package by typing (in Octave)

```
pkg load signal
```

Finally, use the commands

```
u_fluct=u2-mean(u2);
two_uu_1=xcorr(u_fluct,imax,'coeff');
```

where the option "coeff" means that the autocorrelation is normalized by RMS, i.e. R/(rms(x).rms(y)).

Above, we set the maximum separation in time to $imax = 500$ (i.e. we carry out the integration in Eq. 10.11 not to infinity, but to $imax \cdot \Delta t$). Note that the `autocorr` command returns the normalized autocorrelation, i.e. B_{11}^{norm}, see Eq. 10.10. Plot the autocorrelation as in Python as

```
plt.plot(t[0:imax},two_uu_1[0:imax},'b-')
plt.xlabel('t')
plt.ylabel('$B_{11}^{norm}$')
```

or in Matlab/Octave

```
plot(t(1:imax),two_uu_1(1:imax),'linewidth',2)
xlabel('t')
ylabel('$B_{11}^{norm}$','Interpreter','latex')
handle=gca
set(handle,'fontsize',[20])
```

Note that if you have created `two_uu_1t` with `xcorr` you get the correlation for negative times as well. Then you should plot it as

```
 plot(t(1:imax+1),two_uu_1(imax+1:end))
```

For large time separation you find that the autocorrelation oscillates around zero. This is numerical noise. You should carry out the integration in Eq. 10.11 only up to the point when the autocorrelation goes negative. If is does not go negative, terminate the integration at the time separation when the autocorrelation starts to increase. Compute the integral time scale T_{int} in Python as

```
dt=t(1);
int_T_1=np.trapz(two_uu_1)*dt;
```

or in Matlab/Octave

```
dt=t(1);
int_T_1=trapz(two_uu_1)*dt;
```

Again, if you have used `two_uu_1` you should integrate from $imax + 1$ to *end*.

Plot the normalized autocorrelation and compute the integral time scales also for the other three points. Where is T_{int} large and small, respectively? Try to explain why.

In Section Q.2 you time averaged the velocities to get the mean value. You investigated how few samples you could use. In reality it is not only the number of samples that is relevant, but also that they are *independent*. To find out if two samples are independent, it is convenient to use the integral time scale, T_{int}. If the samples are separated by T_{int} seconds they are independent. Hence, re-do the averaging you

did in Section Q.2 but use samples every T_{int} second. The theoretical estimate of the statistical error varies with number of independent samples, N, as

$$error = \frac{1}{\sqrt{N}} \frac{v_{1,rms}}{\langle v_1 \rangle} \qquad (Q.2)$$

We see that the statistical error decreases as $N^{-1/2}$, provided that the samples are *independent*.

Let us use Taylor's frozen turbulence hypothesis to compute the integral length scale. This hypothesis assumes that – if the turbulence level is not too strong – the velocity fluctuation at point x and time t is the same as that at time $(t - \tau)$ at point $(x - \xi)$ where $\tau = (x - \xi)/\langle u \rangle$ (it takes time τ for the particle to travel from point $(x - \xi)$ to point x with a velocity $\langle u \rangle$). The hypothesis assumes that the turbulence is frozen between point $(x - \xi)$ and x. When we want to find the velocity fluctuation at point $(x - \xi)$ at time $(t - \tau)$ we can instead take it at point x at time t. The Taylor hypothesis makes it possible to compute the integral lengthscale from the integral timescale as (see Eq. 10.12)

$$L_{int} = \langle u \rangle \int_0^\infty B_{11}^{norm}(\hat{t})d\hat{t} = \langle u \rangle T_{int} \qquad (Q.3)$$

Compute the integral lengthscale.

Q.4   Probability density/histogram

Histogram (also called probability density function, PDF) can give additional useful information, see Section 7. With a probability density, f_v, of the v velocity, the mean velocity is computed as

$$\langle v \rangle = \int_{-\infty}^\infty v f_v(v) dv \qquad (Q.4)$$

Normalize the probability density function so that

$$\int_{-\infty}^\infty f_v(v) dv = 1 \qquad (Q.5)$$

Here we integrate over v. The mean velocity can of course also be computed by integrating over time, as we do when we define a time average. Compute the PDF in Python as

```
u3_fluct=u3-np.mean(u3)
pdf3,u3_pdf=np.histogram(u3_fluct, bins=20, density=True)
```

and in Matlab/Octave as

```
u3_fluct=u3-mean(u3);
[pdf3 u3_pdf]= hist(u3_fluct,20);
```

Here we have divided u_3 into 20 bins which span the variation of u_3, i.e. $[\min(u_3), \max(u_3)]$. The variable *pdf*3 is a vector of length 20 whose elements gives the number of samples in each bin. Plot the histogram in Python as

```
fig4 = plt.figure("Figure 4")
plt.clf()
plt.plot(u3_pdf[0:-1],pdf3,'b-')
plt.xlabel('$u_3^\prime$')
plt.ylabel('PDF')
```

and in Matlab/Octave as

```
norm3=sum(pdf3)*(u3_pdf(2)-u3_pdf(1));
plot(u3_pdf,pdf3/norm3,'linewidth',2)
xlabel('u3')
ylabel('PDF')
handle=gca
set(handle,'fontsize',[20])
```

where $norm3$ is the integral in Eq. 7.3. You find that the PDF is rather symmetric. Compute and plot the PDFs of the points close to the wall and you will find that they are more skewed. Skewness, S, is a variable that quantify the skewness and it is defined as

$$S_{v'} = \frac{1}{v_{rms}^3} \int_{-\infty}^{\infty} v'^3 f_{v'}(v')dv'$$

Compute it in Python as

```
urms3=np.std(u3_fluct)
S=np.mean(u3_fluct**3)/urms3**3
```

and in Matlab/Octave as

```
urms3=std(u3_fluct);
S=mean(u3_fluct.^3)/urms3^3;
```

where $urms3 = \langle u'^2 \rangle^{1/2}$ at Node 3. Verify that the magnitude of S is large close to the wall. What does a negative skewness mean physically? (cf. Fig. 7.2) Do you have any explanation why the skewness increases as we go closer to the wall?

Q.5 Frequency spectrum

One way to verify that the LES you have performed resolves the turbulence properly, is to look at the spectra of the resolved turbulence. One can analyze the time history of a variable at a point. You do a FFT of that signal to get the Fourier coefficients a_i and then plot a_i^2. Then you get the frequency spectrum, i.e. how much energy resides in each frequency. The other way to do it is to look at the instantaneous velocity along a grid line, and do a FFT of that signal. Then you get the energy spectrum as a function of the wave number, i.e. the inverse of the wave length. In this case you must average over many instants to get a reasonably smooth spectrum.

The Python file `pl_spectrum.py` (corresponding Matlab file is `pl_spectrum.m`) makes a FFT of the time history of fluctuating velocity, u', ($u = \langle u \rangle + u'$) and plots a_i^2. The same data file as in the previous exercise is used (`u_v_time_4nodes.dat`). They use the Python/Matlab function `pwelch`. Run the program `pl_spectrum`

As we mentioned in the eBook, in a well-resolved LES we want to have the cut-off in the inertial subrange where the kinetic energy decays as the wave number (or frequency) up to the power of $-5/3$. No $-5/3$ region can be seen. There are probably two reasons for than: too coarse a grid and too low Reynolds number.

There are two useful frequencies you can use to get a feeling for the frequencies in the plotted energy spectrum. First, we have the integral timescale which we computed in Section Q.3. This corresponds to the frequency $f_{int} = 1/T_{int}$. Second, we have the frequency related to the streamwise spacing, i.e. the time it takes for a fluid particle to flow past a cell. This is $f_{\Delta x} = \langle v_1 \rangle / \Delta x_1$. Where are f_{int} and $f_{\Delta x}$ in the spectrum?

(a) $x_1 - x_2$ plane.

(b) $x_2 - x_3$ plane.
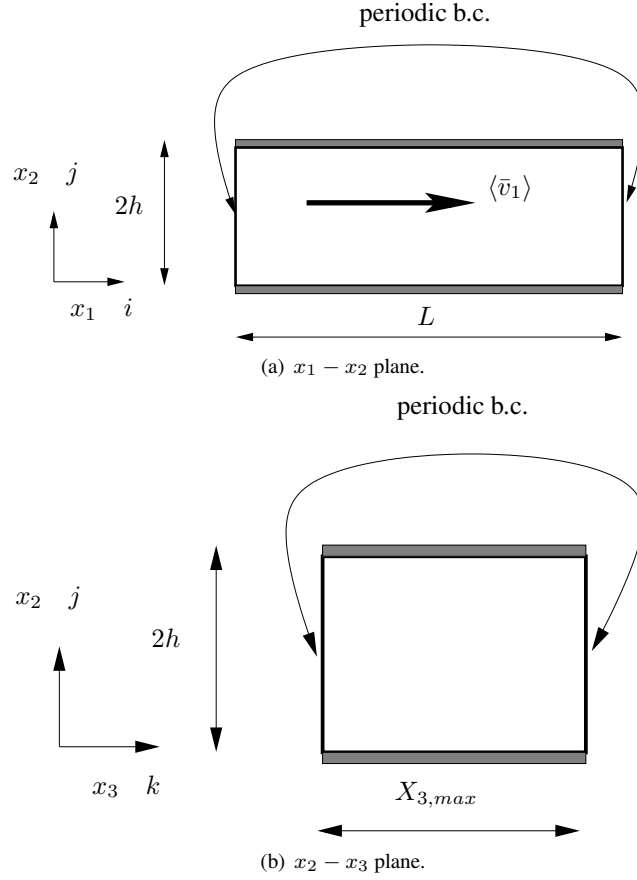
Figure Q.1: Channel domain.

Plot the spectra for the three other points (make changes in pl_spectrum.m).

It should be mentioned that spectra may not be a reliable measure of resolution [128, 129]. Two-point correlations are usually better.

Q.6 Backstep

If you want, you can now also study time histories in a backward facing step, see Fig. Q.2. It is data from LES [206] using PANS. The inlet Reynolds number is $Re_\theta = 3\,600$. The inlet height is $\delta_{inlet} = 1$, see Fig. Q.2, and it is covered by 55 cells.

A precursor RANS using the AKN model [47] is carried out from which U_{RANS}, V_{RANS} and k_{RANS} are obtained at $Re_\theta = 3\,600$. The time-varying inlet velocities are then computed as $\bar{v}_{in} = U_{RANS} + u'_{synt}$, $\bar{v}_{in} = V_{RANS} + v'_{synt}$, $\bar{w}_{in} = w'_{synt}$ where $u'_{i,synt}$ denotes anisotropic synthetic fluctuations that were obtained using the same procedure as in [207]. The synthetic fluctuations are scaled with $k_{RANS}/k_{RANS,max}$. The inlet modeled turbulent kinetic energy and its dissipation are computed as $k_{in} = f_k k_{RANS}$, $\varepsilon_{in} = C_\mu^{3/4} k_{in}^{3/2}/\ell_{sgs}$, $\ell_{sgs} = C_s \Delta$, $\Delta = V^{1/3}$ [207] ($C_s = 0.05$). The grid has $336 \times 152 \times 64$ cells in the streamwise (x), wall-normal (y) and spanwise (z) direction, respectively.
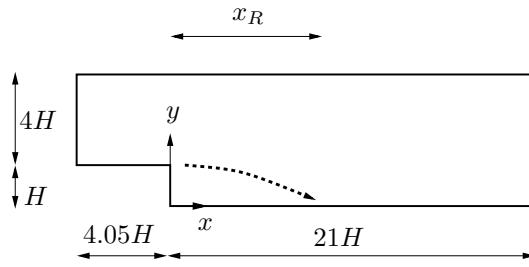
Figure Q.2: Backstep domain.

	x/H	y/H	i	j
$u1$	3.3	0.037	96	15
$u2$	8.7	0.037	150	15
$u3$	18.7	0.037	250	15
$u4$	3.3	0.85	96	30
$u5$	8.7	0.85	150	30
$u6$	18.7	0.85	250	30
$u7$	-3.94	1.017	15	66
$v1$	3.3	0.85	96	15
$v2$	8.7	0.85	150	15
$v3$	18.7	0.85	250	15

Table Q.1: Backstep. Data points.

Time histories of $\bar{v}$ and $\bar{v}$ have been recorded at 6 points, see Table Q.1. Downstream the step, the flow re-attaches at $x = x_R \simeq 6H$, see Fig. Q.2.

This flow is much more exiting than the channel flow which you studied above. Look at the time histories, compute PDF:s and integral time and length scales! Use the Python (`pl_time_backstep.py`) or Matlab file (`pl_time_backstep.m`); they read the file `utime_backstep.dat` which includes the time histories at the points shown in Table Q.1. It can be noted that point 7 is very close to the inlet and close to the wall ($y^+ \simeq 17$). Points $4 - 6$ are located in the outer region of the boundary layer ($\delta \simeq 1$).

Q.7   Channel flow: resolved stresses

Now we return to the channel flow. At the www-page (`http://www.tfd.chalmers.se/~lada/comp_turb_m`) you find data files. The data files include the instantaneous variables u (v_1), v (v_2), w (v_3) and p (made non-dimensional by u_τ and ρ); the files are `u3d_re1000.mat`, `v3d_re1000.mat`, `w3d_re1000.mat`, `p3d_re1000.mat`). You find a Python/Matlab/Octave program at the www-page which read the data and computes the mean velocity. The data files are Matlab binary files.

We decompose the instantaneous variables in time-averaged and fluctuating quantities as

$$v_i = \langle v_i \rangle + v_i', \ p = \langle p \rangle + p'$$

The symbol $\langle . \rangle$ denotes averaging in the homogeneous directions x and z. Note that in reality $\langle . \rangle$ always denote time averaging. It is only in this special academic test case where we have *three* homogeneous directions (x, z, t) where we can – in addition to

time averaging – also can use x and z averaging. Compute the six stresses of the stress tensor, $\langle v_i' v_j' \rangle$. Use the definition to compute the stresses, for example

$$
\begin{aligned}
\langle v_1' v_2' \rangle &= \langle (v_1 - \langle v_1 \rangle)(v_2 - \langle v_2 \rangle) \rangle \\
&= \langle v_1 v_2 \rangle - \langle v_1 \langle v_2 \rangle \rangle - \langle v_2 \langle v_1 \rangle \rangle + \langle \langle v_1 \rangle \langle v_2 \rangle \rangle \\
&= \langle v_1 v_2 \rangle - 2 \langle v_1 \rangle \langle v_2 \rangle + \langle v_1 \rangle \langle v_2 \rangle = \langle v_1 v_2 \rangle - \langle v_1 \rangle \langle v_2 \rangle.
\end{aligned}
\tag{Q.6}
$$

Wait with analysis of the results until you have done next part.

Q.8 Resolved production and pressure-strain

Compute the production term and the pressure-strain terms

$$
P^k = -\langle v_1' v_2' \rangle \frac{\partial \langle v_1 \rangle}{\partial x_2}
$$

$$
P_{11} = -2 \langle v_1' v_2' \rangle \frac{\partial \langle v_1 \rangle}{\partial x_2}
$$

$$
P_{12} = -\langle v_2' v_2' \rangle \frac{\partial \langle v_1 \rangle}{\partial x_2}
$$

$$
\Phi_{11} = 2 \left\langle p' \frac{\partial v_1'}{\partial x_1} \right\rangle
$$

$$
\Phi_{12} = \left\langle p' \frac{\partial v_1'}{\partial x_2} \right\rangle + \left\langle p' \frac{\partial v_2'}{\partial x_1} \right\rangle
$$

$$
\Phi_{22} = 2 \left\langle p' \frac{\partial v_2'}{\partial x_2} \right\rangle
$$

When computing the gradient of, for example, v_1, use the Python command

```
dudx, dudy, dudz=np.gradient(u3d,dx,y,dz,edge_order=2)
```

or the Matlab command

```
[dudy dudx dudz]=gradient(u3d,y,x,z);
```

Do the production terms and the pressure-strain term appear as you had expected? (see the previous course TME226).

Now analyze the fluctuations in the previous subsection. Which stresses do you think are symmetric with respect to the centerline? or anti-symmetric? What's the reason?

When averaging, we use only one time step. If we would use many more time steps – or, in general, if we let $T \to \infty$ when time averaging, e.g.

$$
\langle \phi \rangle = \lim_{T \to \infty} \frac{1}{2T} \int_{-T}^{+T} \phi \, dt
$$

then some of the stresses would be identical zero (now they are small): which ones? Why?
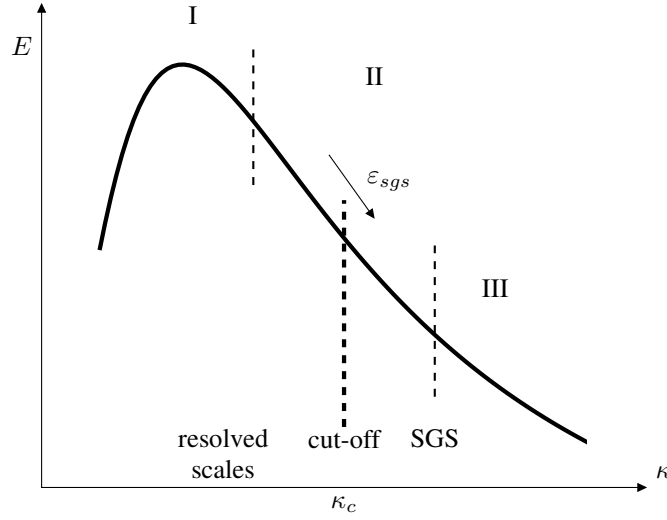
Figure Q.3: Spectrum with cut-off.

Q.9 Filtering

Plot v_1 and v_2 along x_1 at two different x_2 values at $x_3 = x_{3,max}/2$.

1. Filter v_1 and v_2 to get $\bar{v}_1$ and $\bar{v}_2$ using a 1D box-filter (in the x_1 direction) with filter width $\Delta = 2\Delta x_1$ (this corresponds to a test filter, see Eq. 18.31). Compare $\bar{v}_1$ and $\bar{v}_2$ with v_1 and v_2.

2. Do the same thing again but with a filter width of $\Delta = 4\Delta x_1$ (now you must derive the expression on your own!). Discuss the differences between no filter, $\Delta = 2\Delta x_1$ and $\Delta = 4\Delta x_1$.

In LES we almost always assume that the filter width is equal to the control volume (i.e. we use an *implicit* filter). Above, in Item 1 and 2 you have just carried out *explicit* filtering. This type of filtering is used in the scale-similarity model, see Section 18.15.

Repeat Item 1, but now for a 2D filter (x_1 and x_3 direction); the formula for a 3D filter is given in Eq. 18.35. Compare the results along the same lines as in Item 1 and 2.

Q.10 SGS stresses: Smagorinsky model

Compute the SGS stress τ_{12} from the Smagorinsky model, which reads

$$
\begin{aligned}
&\tau_{ij} = -2\nu_{sgs}\bar{s}_{ij}, \quad \nu_{sgs} = (C_s f_\mu \Delta)^2 \sqrt{2\bar{s}_{ij}\bar{s}_{ij}} \\
&\bar{s}_{ij} = \frac{1}{2}\left(\frac{\partial \bar{v}_i}{\partial x_j} + \frac{\partial \bar{v}_j}{\partial x_i}\right) \\
&f_\mu = 1 - \exp(-x_2^+/26)
\end{aligned}
\tag{Q.7}
$$

The filtered velocities, $\bar{v}_i$, are taken from Section Q.9 using the 2D filter (in x_1 and x_3); we should really have used a 3D filter, but in order to keep it simple, we use the 2D filter. The constant $C_s = 0.1$.

As an alternative to the damping function, f_μ, one can compute the filter length as

$$\Delta = \min\{\kappa n, \Delta\} \qquad \text{(Q.8)}$$

where n is the distance to the nearest wall and $\kappa = 0.4$ (von Kàrmàn constant). In this case you should set $f_\mu = 1$.

Compare the SGS stress $\langle \tau_{12} \rangle$ with the resolved stress $\langle u'v' \rangle$ and compare the SGS viscosity with the physical one. Use wall damping both according to Eqs. Q.7 and Q.8. Plot them across the channel. Any thoughts?

Q.11 SGS stresses: WALE model

Repeat the Task in Section Q.10, but now for the WALE model by [208], which reads

$$g_{ij} = \frac{\partial \bar{v}_i}{\partial x_j}, \; g_{ij}^2 = g_{ik} g_{kj}$$

$$\bar{s}_{ij}^d = \frac{1}{2} \left(g_{ij}^2 + g_{ji}^2 \right) - \frac{1}{3} \delta_{ij} g_{kk}^2 \qquad \text{(Q.9)}$$

$$\nu_{sgs} = (C_m \Delta)^2 \frac{\left(\bar{s}_{ij}^d \bar{s}_{ij}^d \right)^{3/2}}{\left(\bar{s}_{ij} \bar{s}_{ij} \right)^{5/2} + \left(\bar{s}_{ij}^d \bar{s}_{ij}^d \right)^{5/4}}$$

with $C_m = 0.325$ which corresponds to $C_s = 0.1$.

Q.12 Dissipations

Compute the dissipation

$$\varepsilon = \nu \left\langle \frac{\partial v_i'}{\partial x_j} \frac{\partial v_i'}{\partial x_j} \right\rangle$$

and plot ε across the channel.

In LES we introduce a filter which is assumed to cut off the spectrum at κ_c in the inertial region, see Fig. Q.3. At cut-off, kinetic energy is extracted from the resolved flow by the SGS dissipation ε_{sgs}. Since the cut-off is assumed to be located in the inertial sub-range (II), the SGS dissipation is at high Re numbers equal to the dissipation.

Introduce a 2D filter ($2\Delta x_1$ and $2\Delta x_3$) as in Sections Q.9 and Q.10 and filter all velocities to obtain $\bar{v}_1$, $\bar{v}_2$ and $\bar{v}_3$. Compute the SGS stresses from the definition

$$\tau_{ij} = \overline{v_i v_j} - \bar{v}_i \bar{v}_j \qquad \text{(Q.10)}$$

and compute the SGS dissipation

$$\varepsilon_{sgs} = - \left\langle \tau_{ij} \frac{\partial \bar{v}_i}{\partial x_j} \right\rangle \qquad \text{(Q.11)}$$

Now, what is the relation between ε_{sgs} and ε? Considering the cascade process, what did you expect?

Recall that when we do traditional Reynolds decomposition, the production term in the equation for turbulent kinetic energy appears as a sink term in the equation for the mean kinetic energy, see Eq. 8.36. This is the case also in LES, but now we have a decomposition into time-averaged filtered velocity, $\langle \bar{v}_i \rangle$, resolved fluctuation, $\bar{v}_i'$, and SGS fluctuation, v_i'', i.e.

$$v_i = \bar{v}_i + v_i'' = \langle \bar{v}_i \rangle + \bar{v}_i' + v_i'' \qquad \text{(Q.12)}$$

Now we have three equations for kinetic energy: $\bar{K} = \frac{1}{2}\langle \bar{v}_i \rangle \langle \bar{v}_i \rangle$, $\bar{k} = \frac{1}{2}\langle \bar{v}'_i \bar{v}'_i \rangle$ and $k_{sgs} = \frac{1}{2}\langle v''_i v''_i \rangle$. The flow of kinetic energy can be illustrated as in Figs. Q.4 and Q.5 (cf. Fig. 20 in [100])
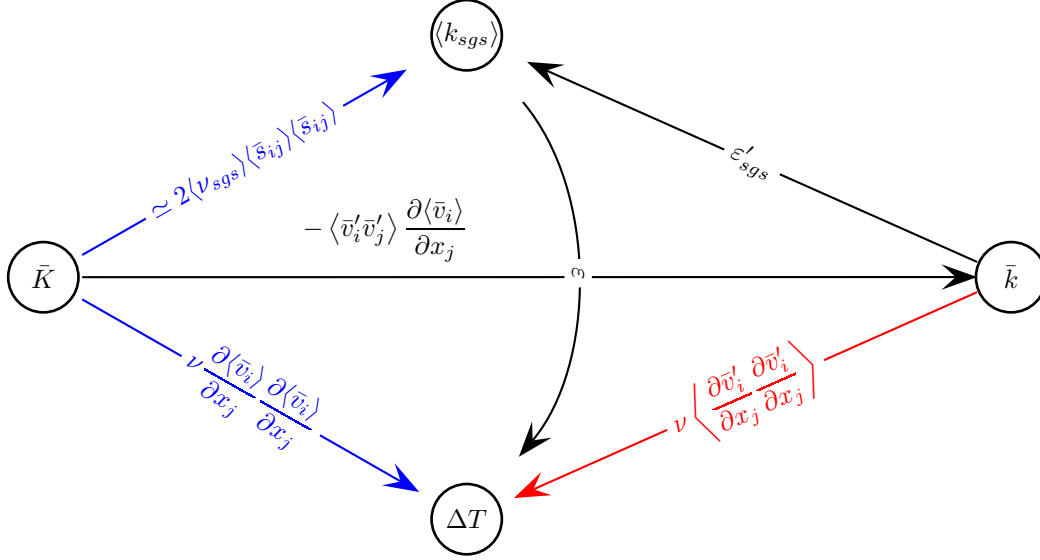
Figure Q.4: Transfer of kinetic turbulent energy. $\bar{K} = \frac{1}{2}\langle \bar{v}_i \rangle \langle \bar{v}_i \rangle$ and $\bar{k} = \frac{1}{2}\langle \bar{v}'_i \bar{v}'_i \rangle$ denote time-averaged kinetic and resolved turbulent kinetic energy, respectively. ΔT denotes increase in internal energy, i.e. dissipation. The cascade process assumes that the term in red is negligible (see also Fig. 8.2). The terms in blue show viscous and the SGS dissipation of the mean flow which is not included in the cascad process.

The transport equation for $\langle \frac{1}{2}\bar{v}'_i \bar{v}'_i \rangle$ is derived in [23]. (can be downloaded from `www.tfd.chalmers.se/˜lada`).

When deriving the k_{sgs} equation, no decomposition into time-averaged, $\langle \bar{v}_i \rangle$, and resolved fluctuations, $\bar{v}'_i$, is made. Hence the SGS dissipation in Eq. Q.11 appears as an instantaneous production term in the equation for k_{sgs} [101, 102] (can be downloaded from `www.tfd.chalmers.se/˜lada`).

Plot (along x_2), compare and discuss the five dissipations (see Figs. Q.4 and Q.5)

$\langle \bar{v}'_1 \bar{v}'_2 \rangle \dfrac{\partial \langle \bar{v}_1 \rangle}{\partial x_2}$: dissipation (which is equal to production with minus sign) by resolved
  turbulence in the $\bar{K}$ equation

$\varepsilon'_{sgs} = \left\langle \left(\nu_{sgs} \dfrac{\partial \bar{v}_i}{\partial x_j} \dfrac{\partial \bar{v}_i}{\partial x_j} \right)' \right\rangle \simeq \left\langle \nu_{sgs} \dfrac{\partial \bar{v}'_i}{\partial x_j} \dfrac{\partial \bar{v}'_i}{\partial x_j} \right\rangle$: SGS dissipation term in the $\bar{k}$ equation. This is the *modelled* SGS dissipation.

The exact SGS dissipation is computed as (since ε'_{sgs} is a product of two fluctuating quantities, we compute it with the same formula as in Eq. Q.6)

$$\varepsilon'_{sgs} = \left\langle -\tau'_{ij} \dfrac{\partial \bar{v}'_i}{\partial x_j} \right\rangle = -\left\langle \tau_{ij} \dfrac{\partial \bar{v}_i}{\partial x_j} \right\rangle + \langle \tau_{ij} \rangle \dfrac{\partial \langle \bar{v}_i \rangle}{\partial x_j} = \varepsilon_{sgs} + \langle \tau_{ij} \rangle \dfrac{\partial \langle \bar{v}_i \rangle}{\partial x_j} \quad \text{(Q.13)}$$

see Eq. Q.11. Note that ε'_{sgs} is defined using the *fluctuating* velocity gradient
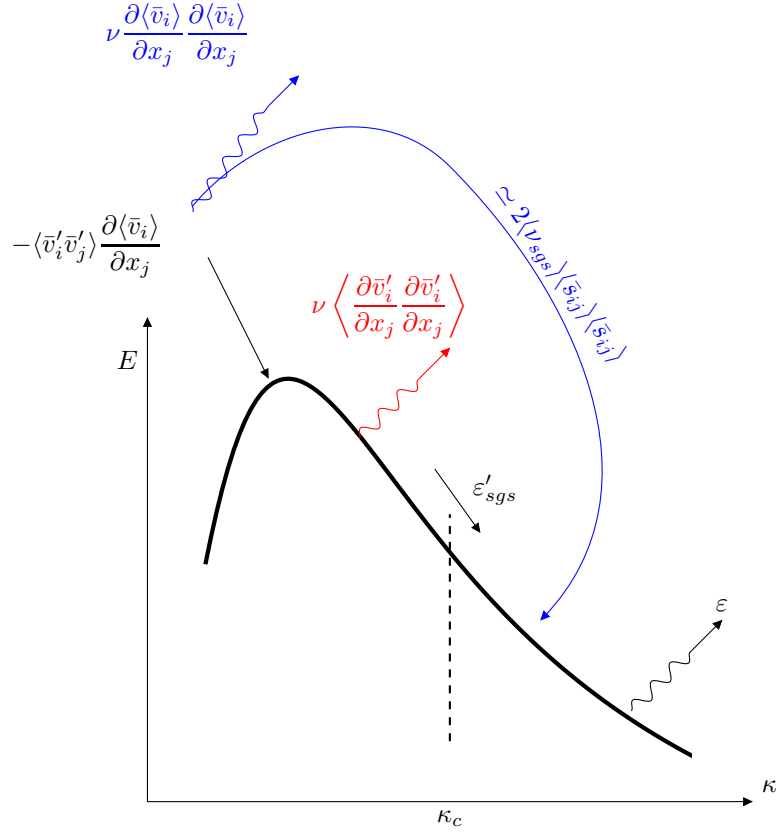
Figure Q.5: Energy spectrum. Transfer of kinetic energy. The cascade process assumes that the term in red is negligible (see also Fig. 8.2). The terms in blue show viscous and the SGS dissipation of the mean flow which is not included in the cascad process.

(see [23][9]), contrary to $\varepsilon_{sgs} = P_{k_{sgs}}$ in Eq. Q.11. The difference between ε_{sgs} and ε'_{sgs} is that the former includes the SGS dissipation from the mean kinetic energy; using the Boussinesq assumption, the last term in Eq. Q.13 reads

$$\langle \tau_{ij} \rangle \frac{\partial \langle \bar{v}_i \rangle}{\partial x_j} = \langle -2\nu_{sgs} \bar{s}_{ij} \rangle \langle \bar{s}_{ij} \rangle \simeq -2 \langle \nu_{sgs} \rangle \langle \bar{s}_{ij} \rangle \langle \bar{s}_{ij} \rangle \tag{Q.14}$$

see Figs. Q.4 and Q.5.

$\nu \left\langle \dfrac{\partial \bar{v}'_i}{\partial x_j} \dfrac{\partial \bar{v}'_i}{\partial x_j} \right\rangle$**:** viscous dissipation term in the $\bar{k}$ equation

$\left\langle \nu_{sgs} \dfrac{\partial \bar{v}_1}{\partial x_2} \right\rangle \dfrac{\partial \langle \bar{v}_1 \rangle}{\partial x_2} \simeq \langle \nu_{sgs} \rangle \left(\dfrac{\partial \langle \bar{v}_1 \rangle}{\partial x_2} \right)^2$**:** SGS dissipation term in the $\bar{K}$ equation. This corresponds to $2\langle \nu_{sgs} \bar{s}_{ij} \rangle \langle \bar{s}_{ij} \rangle$ in Figs. Q.4 and Q.5. This is seen by re-writing the production term

$$\left\langle \nu_{sgs} \left(\frac{\partial \bar{v}_i}{\partial x_j} + \frac{\partial \bar{v}_j}{\partial x_i} \right) \right\rangle \left\langle \frac{\partial \bar{v}_i}{\partial x_j} \right\rangle = 2 \langle \nu_{sgs} \bar{s}_{ij} \rangle \langle \bar{s}_{ij} \rangle \tag{Q.15}$$

---

[9]can be downloaded from course home page

see Eq. 11.39. In fully-developed channel flow, the left side reads

$$\left\langle \nu_{sgs} \frac{\partial \bar{v}_1}{\partial x_2} \right\rangle \frac{\partial \langle \bar{v}_1 \rangle}{\partial x_2} \tag{Q.16}$$

Q.13 Test filtering

Above the filtered velocities were computed using the filter width $\Delta = 2\Delta x_1$. In dynamic models, we often define the test filter as twice the usual filter, i.e. $\widehat{\Delta} = 2\Delta$. Use this definition (1D filter, i.e. $\widehat{\Delta} = 4\Delta x_1$) to compute the dynamic Leonard stress $\langle \mathcal{L}_{12} \rangle$ from the definition

$$\mathcal{L}_{ij} = \widehat{\overline{v_i v_j}} - \widehat{\overline{v}}_i \, \widehat{\overline{v}}_j \tag{Q.17}$$

and compare it (across the channel) with the resolved stress $\langle \bar{v}_1' \bar{v}_2' \rangle$ and the SGS stress $\langle \tau_{12} \rangle$ defined in Eq. Q.10. Do you expect the magnitude of stresses to be similar?

Q.14 Near-wall behavior

What is the near-wall behavior of $\langle v_1 \rangle$, $\langle v_1'^2 \rangle$ and $\langle v_2'^2 \rangle$ (i.e., for v_1, what is m in $\langle v_1 \rangle = \mathcal{O}(x_2^m)$). In order to estimate m, plot the quantities in log-log coordinates. Do the quantities exhibit the near-wall behaviour that you expected?

Q.15 Two-point correlations

The two-point correlation for u'

$$B_{11}(x_2, \zeta_m) = \frac{1}{192 \times 192} \sum_{I=1}^{192} \sum_{K=1}^{192} v_1'(x_1^I, x_2, x_3^K) v_1'(x_1^I, x_2, x_3^K - \zeta_m) \tag{Q.18}$$

where x_3^K and ζ_m are the spanwise locations of the two points. Take advantage of the fact that the flow is periodic, but be careful when integrating the correlation above in the x_3 direction. We have 192 cells in the x_3 direction. If, for example, $\zeta_m = 2\Delta x_3$, and one of the points (x_3^1) is at $K = 1$ then the other $(x_3^1 - 2\Delta)$ is at $K = 95$.

Plot the two-point correlation at a couple of x_2 positions. When plotting two-point correlations, it is no point showing both symmetric parts; show only half of it (cf. the two-point correlations in Section 10.1 and Fig. R.1).

Compute and plot the integral length scale, $\mathcal{L}_1$, which is defined by

$$\mathcal{L}_1(x_2) = \frac{1}{v_{1,rms}^2} \int_0^\infty B_{11}(x_2, \zeta_1) d\zeta_1. \tag{Q.19}$$

Compute also $\mathcal{L}_3$, which is defined as

$$\mathcal{L}_3(x_2) = \frac{1}{v_{3,rms}^2} \int_0^\infty B_{33}(x_2, \zeta_3) d\zeta_3. \tag{Q.20}$$

What's the difference between $\mathcal{L}_1$ and $\mathcal{L}_3$? Did you expect this difference?

Q.16 Energy spectra, optional

The energy spectrum of any second moment can be obtained by taking the FFT of the corresponding two-point correlation. You can find some details on how to use Pythons FFT in Appendix R.

If you have computed the Fourier coefficients properly, the sum of all coefficients should give the energy. The reason is that the Fourier coefficients correspond to the energy spectrum, and if we integrate the energy spectrum over all wave numbers we get the total energy. When we take the FFT of Eq. Q.18, for example, we get

$$\hat{B}_{11}(\kappa_z) = FFT(B_{11})$$

and summation gives

$$v_{1,rms}^2 = \sum_1^N \hat{B}_{11}/N \tag{Q.21}$$

see Appendix R.

Plot the energy spectra at a couple of x_2 locations. When plotting two energy spectrum, it is no point showing both symmetric parts; show only half of it (cf. the energy spectrum in Fig. R.5 b). Confirm that Eq. Q.21 is satisfied.

Q.17 Something fun

Think of an interesting turbulent quantity and plot it and analyze it!

R MTF271: Compute energy spectra from LES/DNS data using Python

R.1 Introduction

WHEN analyzing DNS or LES data, we are interested to look at the energy spectra. From these we can find out in which turbulence scales (i.e. at which wave numbers) the fluctuating kinetic turbulent energy reside. By taking the Fourier transform of the time signal (a fluctuating turbulent velocity) and then taking the square of the Fourier coefficients we obtain the energy spectrum versus frequency.

If we want to have the energy spectrum versus wavenumber there are two options; either we

1. Fourier transform N instantaneous signals in space and then time average the N Fourier transforms, or

2. we Fourier transform a (time-averaged) two-point correlation, $B_{33}(\hat{x}_3)$.

Option 1 and 2 is really only a question when we time average. In Option 1, we take first FFT and then time average. In 2, we first time average and then take FFT.

Here we will use Option 2. The two-point correlation, $B_{33}(\hat{x}_3)$ is defined as (see Eq. 10.2)

$$B(x_3, \hat{x}_3) = \langle v_3'(x_3 - \hat{x}_3) v_3'(x_3) \rangle \tag{R.1}$$

where $\hat{x}_3$ is the separation between the two points. Here we assume that x_3 is an homogeneous direction so that B_{33} is independent of x_3, i.e. $B_{33} = B_{33}(\hat{x}_3)$. The two-point correlation for an infinite channel flow is shown in Fig. R.1. On discrete form the expression for B_{33} reads

$$B_{33}(k\Delta z) = \frac{1}{M} \sum_{m=1}^{M} v_3'(x_3 - k\Delta z) v_3'(x_3) \tag{R.2}$$

where m denotes summation in homogeneous directions (i.e. time plus spatial homogeneous directions).

In the following section we give a simple example how to use Python to Fourier transform a signal where we know the answer. Then we show how to derive the energy spectrum from a spatial two-point correlation. Finally, some comments are given on how to create an energy spectrum versus frequency from an autocorrelation (i.e. from a two-point correlation in time).

R.2 An example of using FFT

Here we will present a simple example. Consider the function

$$u = 1 + \cos(2\pi x/L) = 1 + \cos(2\pi(n-1)/N) \tag{R.3}$$

where $L = 3$ is the length of the domain and $N = 16$ is the number of discrete points, see Fig. R.2. Let's use this function as input vector for the discrete Fourier transform (DFT) using Python. The function u is symmetric, so we expect the Fourier coefficients

to be real. In Python the DFT of u is defined as

$$U(k) = \sum_{n=1}^{N} u_n \exp\left\{\frac{-\imath 2\pi(k-1)(n-1)}{N}\right\} \tag{R.4}$$

$$1 \le k \le N$$

where k is the non-dimensional wavenumber and $\imath = \sqrt{-1}$. The ratio $(n-1)/N$ corresponds to the physical coordinate, x, in the the continuous FFT

$$U^c(\kappa) = \frac{1}{L}\int_{-L}^{L} u(x)\exp(-\imath\kappa x)dx, \quad \kappa = 2\pi/L \tag{R.5}$$

Note that the discrete Fourier $U(k)$ coefficients in Eq. R.4 must be divided by N, i.e. $U(k)/N$, in order to correspond to the Fourier coefficients U^c (N corresponds to L in Eq. R.5). Furthermore, it can be noted that in Eq. R.4 the period $[0, 2\pi]$ is used whereas the formulation in Eq. R.5 is based on the interval $[-\pi, \pi]$.

In Python, we generate the function u in Eq. R.3 using the commands

```
mport numpy as np
import math
import matplotlib.pyplot as plt
N=16
n = np.linspace(1,N,N,dtype=int)
u=1.+np.cos(2.*pi*(n-1)/N)
```

The u function is shown in Fig. R.2. 16 nodes are used; node 1 is located at $x = 0$ and node 16 is located at $15L/16$.

Now we take the discrete Fourier transform of u. Type
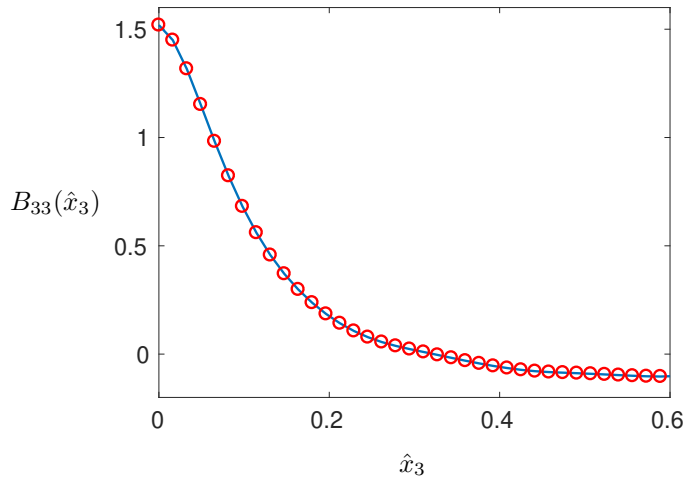
Figure R.1: Two-point correlation, $B(\hat{x}_3) = \langle v_3'(x_3 - \hat{x}_3)v_3'(x_3)\rangle$, of DNS data in channel flow taken from [100].
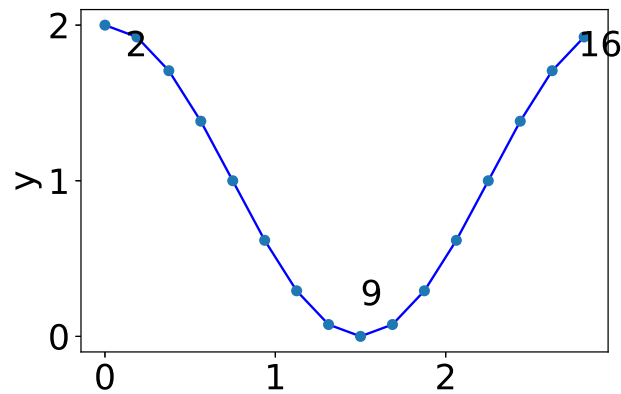
Figure R.2: The u function.

```
U=sci.fft(u)
```

Instead of using the built-in `fft` command in Python we can program Eq. R.4 directly in Python as

```
U=zeros(1,N);
for k=1:N
for n=1:N
  arg1=2*pi*(k-1)*(n-1)/N;
  U(k)=U(k)+u(n)*cos(-arg1);
end
end
```

```
# take FFT
U=np.zeros(N)
for kp in range (N):
   for np in range (N):
      arg1=2.*pi*kp*np/N
      U[kp]=U[kp]+u[np]*math.cos(arg1)
```

Note that since u is symmetric, we have only used $\cos(-x) = \cos(x)$ (the symmetric part of $\exp(-\imath x)$).

The resulting Fourier coefficients are shown in Fig. R.3. Since the function u includes only one cosine function and a mean (which is equal to one) only three Fourier coefficient are non-zero. Two of them, $U(2)/N = 0.5$, $U(16)/N = 0.5$, correspond to the cosine functions (there must be two since U is symmetric). For $k = 2$ we have

$$\cos(2\pi(n-1)/N)$$

and for $k = N$

$$\cos((N-1)2\pi(n-1)/N) = \cos(-2\pi(n-1)/N) = \cos(2\pi(n-1)/N)$$

(a) Versus non-dimensional wavenumber, k.

(b) Versus wavenumber, κ.
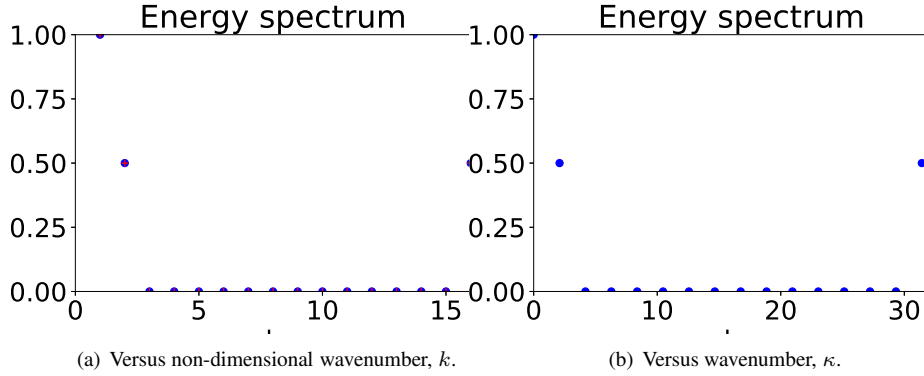
Figure R.3: The U/N Fourier coefficients.

which corresponds to $\cos(2\pi x/L)$ in Eq. R.3. It can be noted that the interval $[k = N/2 + 1, N = 9, 16]$ corresponds to the negative, symmetric part of the wavenumbers in the physical formulation (cf. Eqs. R.4 and R.5). The first Fourier coefficient corresponds – as always – to the mean of u, i.e. $U(1)/N = \langle u \rangle$. This is easily verified from Eq. R.4 by inserting $k = 1$. The remaining coefficients are zero.

In Fig. R.3, U/N is plotted versus non-dimensional wavenumber, k, and versus wavenumber $\kappa = 2\pi(n-1)/L$.

The energy, $\langle u^2 \rangle$, of the signal in Fig. R.2 can be computed as

$$\langle u^2 \rangle = \frac{1}{L} \int_0^L u^2(x)dx = \sum_{n=1}^{N} u_n^2/N = 1.5 \tag{R.6}$$

In wavenumber space the energy is – according to Parseval's formula, see Eq. H.4 – equal to the integral of the square of the Fourier coefficients, i.e.

$$\langle u^2 \rangle = \frac{1}{L} \int_0^\infty U^2(\kappa)d\kappa = \frac{1}{N} \sum_{n=1}^{N} U_n^2/N = 1.5 \tag{R.7}$$

see Fig. R.3.

R.3 Energy spectrum from the two-point correlation

Now that we have learnt how to use the FFT command in Python, let's use it on our two-point correlation in Eq. R.1 and Fig. R.1. Equation R.4 reads

$$\hat{B}_{33}(k) = \sum_{n=1}^{N} B_{33}(n) \exp\left\{ \frac{-\imath 2\pi(k-1)(n-1)}{N} \right\} \tag{R.8}$$

The simulations in [100] have been carried out with periodic boundary conditions in x_3 direction (and x_1), and hence $B_{33}(\hat{x}_3)$ is symmetric, see Fig. R.4. Thus, it is sufficient to use the cosine part of Eq. R.8, i.e.

$$\hat{B}_{33}(k) = \sum_{n=1}^{N} B_{33}(n) \cos\left\{ \frac{2\pi(k-1)(n-1)}{N} \right\} \tag{R.9}$$
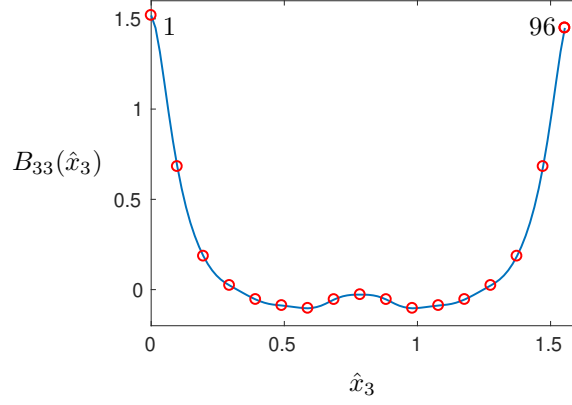
Figure R.4: Periodic two-point correlation, $B_{33}(\hat{x}_3) = \langle v_3'(x_3)v_3'(x_3 + \hat{x}_3)\rangle$, of DNS data in channel flow taken from [100].

(a) Linear-linear scale   (b) Log-log scale
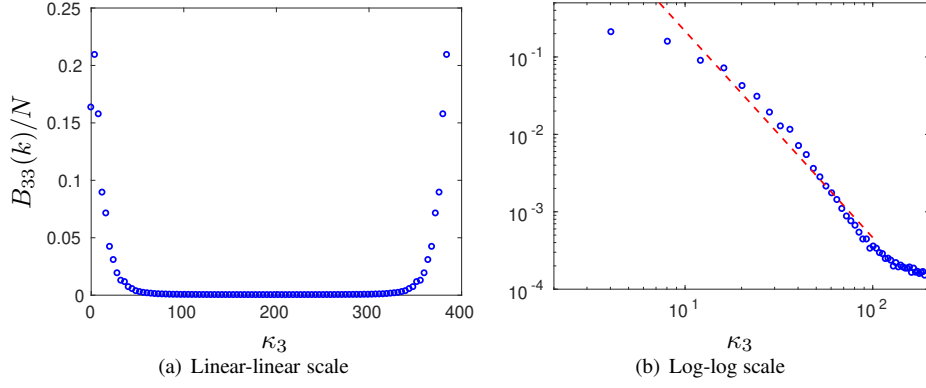
Figure R.5: The energy spectrum of $\overline{v_3'^2}$ versus wavenumber, κ_3. Dashed line in b) show $-5/3$ slope. Taken from [100].

In Fig. R.5a the Fourier coefficients $\hat{B}_{33}\kappa_3$ are presented versus wavenumber $\kappa_3 = 2\pi(n-1)/x_{3,max}$, where $x_{3,max} \simeq 1.55$, see Fig. R.4. Figure R.5b shows the same energy spectra in log-log scale (only half of the spectrum is included), which is the common way to present energy spectra. The dashed line shows the $-5/3$ slope which indicates that the energy spectra from the DNS follows the Kolmogorov $-5/3$ decay.

As usual, the Fourier coefficient for the first non-dimensional wavenumber, i.e. $\hat{B}_{33}(1)/N$ is equal to the mean of B_{33}, i.e.

$$\langle B_{33}\rangle = \frac{1}{N}\sum_{n=1}^{N} B_{33}(n) \equiv \frac{1}{N}\hat{B}_{33}(1) \tag{R.10}$$

compare with Eq. R.9. Note that this is almost the same expression as that for the integral length scale which reads (see Eq. 10.6)

$$L_{int}(x_3) = \frac{1}{\overline{v_3'^2}}\int_0^\infty B_{33}(x_3, \hat{x}_3)d\hat{x}_3 = \frac{\langle B_{33}\rangle}{\overline{v_3'^2}} \tag{R.11}$$

Hence the integral length scale is related to the first Fourier mode as

$$L_{int} = \frac{\hat{B}_{33}(1)}{N\overline{v_3'^2}} \tag{R.12}$$

The two-point correlation for zero separation is equal to $\overline{v_3'^2}$, i.e. $B_{33}(0) = \overline{v_3'^2} = 1.51$. Another way to obtain $\overline{v_3'^2}$ is to integrate the energy spectrum in Fig. R.5, i.e.

$$\overline{v_3'^2} = \int_0^\infty \hat{B}_{33}(\kappa_3)d\kappa_3 = \frac{1}{N}\sum_{n=1}^N \hat{B}_{33}(n) = 1.51 \tag{R.13}$$

R.4 Energy spectra from the autocorrelation

When computing the energy spectra of the v_3' velocity, say, versus frequency, the time series of $v_3'(t)$ is commonly Fourier transformed and the energy spectrum is obtained by plotting the square of the Fourier coefficients versus frequency, f. We can also split the time signal into a number subsets, Fourier transform each subset and then average. In Python, the command np.pwelch is a convenient command which does all this.

In the previous section we computed the energy spectrum versus wavenumber by Fourier transforming the two-point correlation. We can use the same approach in time. First we create the autocorrelation $B_{33}(\tau) = \langle v_3'(t)v_3'(t + \tau)\rangle$ (this can be seen as a two-point correlation in time). Then $B_{33}(\tau)$ is Fourier transformed to get $\hat{B}_{33}(f)$ in the same way as in Section R.3.

S   MTF271, Assignment 2a: DES, DDES and SAS

IN this exercise you will evaluate PANS (Section 23), DES (Section 20), DDES (Section 20.3) and SAS (Section 22). You will use data from a S-DES (combination of steady RANS and DES). Only the DES data are provided here. The flow is fully developed channel flow. The data are taken from [209, 210] [10]. The Re number based on the friction velocity and the half channel width is $Re_\tau = u_\tau h/\nu = 8000$. The matching line is determined by the DES switch (Eq. 20.8). It turns out that is occurs at gridline number 21 at which $x_2^+ \simeq 144$, $x_2/\delta = 0.0175$.

A $32 \times 96 \times 32$ mesh has been used. The cell size in x_1 and x_3 directions are $\Delta x_1 = 0.05$ and $\Delta x_3 = 0.025$. Periodic boundary conditions were applied in the x_1 and x_3 direction (homogeneous directions). All data have been made non-dimensional by u_τ and ρ.

At the course www page you find data files with instantaneous flow fields (statistically independent). The data files include the instantaneous variables u (v_1), v (v_2), w (v_3) and k (made non-dimensional by u_τ and ρ).

You can use Matlab, Octave or Python. Both Octave and Python are open-source software. Octave is a Matlab clone. Many large Swedish industries prefer engineers to use Python instead of Matlab due to Matlab's high license fees.

Use one of the programs Python/Matlab/Octave to analyze the data. You find a Python/Matlab/Octave program at the www page which reads the data and computes the mean velocity. The data files are Matlab binary files.

You will also find a file with time history of u.

S.1   Time history

At the www page you find a file u_w_time_5nodes_sdes.dat with the time history of $\bar{v}_1$ and $\bar{v}_3$. The file has eleven columns of $\bar{v}_1$ and $\bar{v}_3$ at five nodes (and time): $x_2/\delta = 0.0028$ (node 10) , $x_2/\delta = 0.0203$, (node 22) $x_2/\delta = 0.0364$, (node 26) $x_2/\delta = 0.0645$ (node 30) and $x_2/\delta = 0.20$ (node 38) . Hence, two node is located in the URANS region, one at the interface and three nodes in the LES region. With $u_\tau = 1$ and $\nu = 1/Re_\tau = 1/8000$, this correspond to $x_2^+ = 23$, $x_2^+ = 168$, $x_2^+ = 302$, $x_2^+ = 535$ and $x_2^+ = 1659$, respectively. The sampling time step is $1.25E - 3$ (every time step). Use the Python/Matlab program pl_time_sdes to load and plot the time history of $\bar{v}_1$.

Recall that the velocities have been scaled with the friction velocity u_τ, and thus what you see is really $\bar{v}_1/u_\tau$. The time history of $\bar{v}_1$ at $x_2/\delta = 0.0203$ and $x_2/\delta = 0.0645$ are shown. To study the profiles in closer detail, use the axis-command in the same way as when you studied the DNS data.

Plot $\bar{v}_1$ for all five nodes. How does the time variation of $\bar{v}_1$ differ for different positions? Recall that the two points closest the wall are located in the URANS region and the other two are located in the LES region. In the URANS region the turbulent viscosity is much larger than in the LES region. How do you expect that the difference in ν_t affects the time history of $\bar{v}_1$?[11]. You should also keep in my mind that turbulent fluctuations are created by the mean flow gradient (i.e. the production). Small mean flow gradients means little or no creation of turbulence. Does the time history of $\bar{v}_1$ behave as you expect? What about $\bar{v}_3$?

---

[10]these papers can be downloaded from http://www.tfd.chalmers.se/~lada/allpaper.html

[11]Hint: small scales destroys/kills the large scales

Compute the autocorrelation (see Section 10.2) of the five points. In Python, you do

```
u1_fluct=u1-np.mean(u1)
two=np.correlate(u1_fluct,u1_fluct,'full')
# find max
nmax=np.argmax(two)
# and its value
two_max=np.max(two)
# two_max is symmwetric. Pick the right half and normalize
two_sym_norm=two[nmax:]/two_max
```

and in Matlab/Octave

```
imax=500;
two_uu_1_mat=autocorr(u1,imax);
```

Plot the autocorrelation in Python

```
fig1 = plt.figure("Figure 1")
imax=500;
plt.plot(t[0:imax],two_sym_norm[0:imax],'b-')
plt.xlabel('t')
plt.ylabel('$B_{uu}$')
```

or in Matlab/Octave

```
plot(t(1:imax),two_uu_1_mat(1:imax),'linew',2)
xlabel('t')
ylabel('B_{uu}')
handle=gca
set(handle,'fontsi',[20])
```

Above we set the maximum separation in time to 500 samples. For large time separation you find that the autocorrelation oscillates around zero. This is numerical noise. You should carry out the integration in Eq. 10.11 only up to the point when the autocorrelation goes negative. If is does not go negative, terminate the integration at the time separation when the autocorrelation starts to increase.

Compute the integral timescale in Pythons

```
dt=t(1);
int_T_1=np.trapz(two_sym_norm)*dt;
```

or in Matlab/Octave

```
dt=t(1);
int_T_1=np.trapz(two_uu_1_mat)*dt;
```

Compute the autocorrelation and integral timescale also for the other four points. Do you see any difference between the points in the URANS region and the LES region? What did you expect?
Hint: small-scale turbulence breaks up/destroys large eddies.

S.2 Mean velocity profile

After having performed a DES, we want to look at the time-averaged results. Use the file `pl_uvw_sdes` to look at the mean velocity profiles. `pl_uvw_sdes` reads the instantaneous $\bar{v}_1$ field and performs an averaging in the homogeneous directions x_1 and x_3. The time averaged velocity profile is compared with the log profile (markers). There are eight files with instantaneous values of $\bar{v}_1$ $\bar{v}_2$ and $\bar{v}_3$ which in the beginning of `pl_uvw_sdes` is merged into three 3D arrays, `u3d`, `v3d` and `w3d` of size $(8 * ni, nj, nk)$.

S.3 Resolved stresses

We want to find out how much of the turbulence that has been resolved and how much that has been modelled. Compute first `vmean` (this quantity should be very small, but if you had infinite number of samples it would be zero). Now compute $\langle v_1' v_2' \rangle$. Here's an example how to do in Python:

```
uv=np.zeros(nj)
for k in range (0,ni):
for j in range (0,nj):
for i in range (0,nk):
   ufluct=u3d[i,j,k]-umean[j]
   vfluct=v3d[i,j,k]-vmean[j]
   wfluct=w3d[i,j,k]-wmean[j]
   uv[j]=uv[j]+ufluct*vfluct

uv=uv/ni/nk
```

and in Matlab

```
uv=zeros(nj,1);
for k=1:nk
for j=1:nj
for i=1:ni
   ufluct=u3d(i,j,k)-umean(j);
   vfluct=v3d(i,j,k)-vmean(j);
   uv(j)=uv(j)+ufluct*vfluct;
end
end
end
uv=uv/ni/nk;
```

A much faster way is to use Python's built-in function

```
uvmean1=np.mean((u3d-umean[None,:,None])*(v3d-vmean[None,:,None]), axis=(0,2))
```

or Matlab's built-in function

```
uv=mean(mean(((u3d-umean).*(v3d-vmean)),3),1);
```

Plot it in a new figure (a figure is created by the command `figure(2)`).

S.4 Turbulent kinetic energy

The resolved turbulent kinetic energy is defined as

$$k_{res} = 0.5 \left(\langle v_1'^2 \rangle + \langle v_2'^2 \rangle + \langle v_3'^2 \rangle \right)$$

Plot and compare the resolved and modelled turbulent kinetic energies. Note that the modelled turbulent kinetic energy, k (te1_sdes.mat, te2_sdes.mat,...), can be downloaded from the www page and are loaded at the beginning of pl_uvw_sdes. Which is largest (modeled or resolved)? Which is largest in the URANS region and in the LES region, respectively? What about the sum? The magnitude of resolved and modelled turbulent kinetic energies is discussed on p. 115 in [165] in relation to Fig. 6 in [165].

S.5 The modelled turbulent shear stress

We have computed the resolved shear stress. Let's find the modelled shear stress. The modelled turbulent kinetic energy, k (file te1_sdes.mat, ...), and the specific dissipation, ω (file om1_sdes.mat, ...) will be used. Recall that $\nu = 1/8000$. Compute the turbulent viscosity as k/ω, see Eq. 26.3.

Compute the modelled shear stress from the Boussinesq assumption

$$\tau_{12} = -2\nu_t \bar{s}_{12} = -\nu_t \left(\frac{\partial \bar{v}_1}{\partial x_2} + \frac{\partial \bar{v}_2}{\partial x_1} \right)$$

To compute the velocity gradient, use the Python command

```
dudx, dudy, dudz=np.gradient(u3d,dx,y,dz)
```

or the Matlab command

```
[dudy dudx dudz]=gradient(u3d,y,x,z);
```

Plot $\langle \tau_{12} \rangle$ and compare with the resolved shear stress (see Section S.3). Are they smooth across the interface? Is the resolved shear stress large in the URANS region? Should it be large? Why/why not?

S.6 Location of interface in DES and DDES

As mentioned above, the interface in the present simulations is computed using the DES switch. Let's compare that with DES and DDES.

In SA-DES, the interface is defined as the location where the wall distance is equal to $C_{DES}\Delta$ where $\Delta = \max\{\Delta_x, \Delta_y, \Delta_z\}$, see Eq. 20.3.

In SST-DES, the location of the interface is computed using k and ω and compute the location where the switch of model takes place according to Eq. 20.8. How does the location compare with SA-DES?

In DDES, the boundary layer is shielded with a damping function. In SST-DES, the shielding function (see Eq. 20.9) may be one of the blending functions, F_1 or F_2 (see Eq. 20.5). Let's use F_2 as the shielding function as in [79]. Does DDES work, i.e. does it make the model to be in RANS mode in the entire boundary layer?

S.7 SAS turbulent length scales

Compute the 1D von Kármán length scale defined as

$$L_{vK,1D} = \kappa \left| \frac{\partial \langle \bar{v}_1 \rangle / \partial x_2}{\partial^2 \langle \bar{v}_1 \rangle / \partial x_2^2} \right| \tag{S.1}$$

where $\kappa = 0.41$ is the von Kármán constant. Note that you should take the derivatives of the *averaged* $\bar{v}_1$ velocity, i.e. of $\langle \bar{v}_1 \rangle$. How does it behave (i.e. what is n in $\mathcal{O}(x_2^n)$) in the fully turbulent region? What should n be?

When we're doing real 3D simulations, the first and second derivative must be defined in 3D. One way of defining the von Kármán length scale in 3D is [159, 160]

$$L_{vK,3D,inst} = \kappa \left| \frac{S}{U''} \right|$$
$$S = (2\bar{s}_{ij}\bar{s}_{ij})^{0.5} \tag{S.2}$$
$$U'' = \left(\frac{\partial^2 \bar{v}_i}{\partial x_j \partial x_j} \frac{\partial^2 \bar{v}_i}{\partial x_k \partial x_k} \right)^{0.5}$$

Plot the von Kármán length scale using Eqs. S.2 and S.2. Compare them with Eq. S.1. What's the difference? What effect do the different length scales give for P_{SAS} (i.e. T_1 in Eq. 22.5) and what effect does it give to ω?

Another way to compute the second derivative is [211]

$$U'' = \left(\frac{\partial^2 \bar{v}_i}{\partial x_j \partial x_k} \frac{\partial^2 \bar{v}_i}{\partial x_j \partial x_k} \right)^{0.5} \tag{S.3}$$

Plot and compare the von Kármán length scales using the second derivatives defined in Eqs. S.2 and S.3.

S.8 Anisotropic errors (optional)

Recently, Toosi & Johan Larsson [212] proposed a method for evaluating resolution. They propose to use a directionally small-scale (i.e., a directionally high-pass test filtered) field, $\bar{v}_i^{*(\mathbf{n})}$ defined as

$$\bar{v}_i^{*(\mathbf{n})} \equiv \bar{v} - \hat{\bar{v}}_i^{*(\mathbf{n})} \simeq \frac{-\Delta_{\mathbf{n}}^2}{4} \mathbf{n}^T \left(\nabla \nabla^T \bar{v}_i \right) \mathbf{n} \tag{S.4}$$

where $\mathbf{n}$ defines the direction along which the small-scale velocity is computed. The anisotropic error is then defined as

$$\mathcal{A}(\mathbf{n}) = \left(\left\langle \bar{v}_i^{*(\mathbf{n})} \bar{v}_i^{*(\mathbf{n})} \right\rangle \right)^{1/2} \tag{S.5}$$

In [212] they used the quantity as an indicated where the grid needed to be refined and in which direction. But it can also be used as a post-processing tool to evaluate if the grid is equally good (or bad) everywhere. Hence we want the error in Eq. S.5 to be as constant as possible in all grid direction and throughout the domain. Since our flow is homogeneous in x_1 and x_3 we need only to evaluate how inhomogeneous the error is in the x_2 direction. Furthermore, on structured grids we can compute Eq. S.4 using second velocity derivatives, i.e.

$$\bar{v}_i^{*(\mathbf{n})} \simeq -\frac{\Delta_{\mathbf{n}}^2}{4} \frac{\partial \bar{v}_i}{\partial x_n \partial x_n}, \text{ no summation over } n \tag{S.6}$$

where $\Delta_{\mathbf{n}}$ is equal to Δx, Δy or Δz. In order to take the anisotropic cells into account, the error should be multiplied by the cell volume [213]

$$\mathcal{A}(\mathbf{n})_V = \Delta x \Delta y \Delta z \left(\left\langle \bar{v}_i^{*(\mathbf{n})} \bar{v}_i^{*(\mathbf{n})} \right\rangle \right)^{1/2} \tag{S.7}$$

Plot $\mathcal{A}(\mathbf{n})_V$ and find out how constant and isotropic it is. Where does the mesh needs to be refined? In which direction(s)?

T   MTF271, Assignment 2b, recirculating flow: PANS, DES, DDES and SAS

I N this exercise you will use data from PANS and Zonal PANS SAS for for the flow over a hump. In Section S, a similar analysis is carried for channel flow. It may be interesting to do that assignment before this one.

The results of the hump simulations are presented in detail in [165, 173, 207] [12]
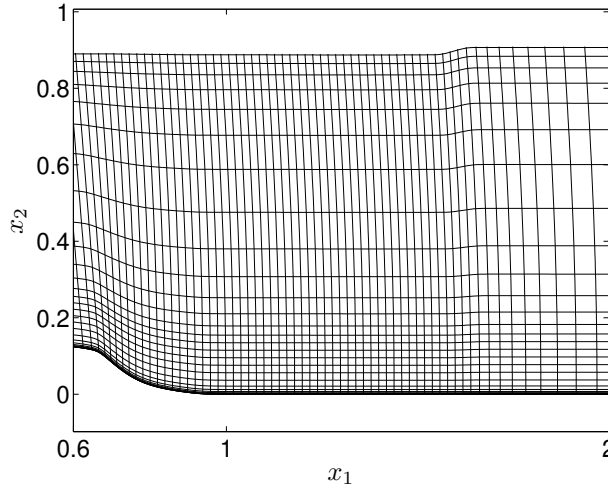
Figure T.1: Hump flow. Grid. Every 4th grid line is shown.

The Reynolds number of the hump flow is $Re_c = 936\,000$, based on the hump length, c, and the inlet mean velocity at the centerline, $U_{in,c}$. The grid is shown in Fig. T.1. Experiments were conducted by Greenblatt [214, 215]; they are also described in detail at http://cfdval2004.larc.nasa.gov/case3.html. The maximum height of the hump, h, and the channel height, H, are given by $H/c = 0.91$ and $h/c = 0.128$, respectively. The baseline mesh has $312 \times 120 \times 64$ cells with $Z_{max} = 0.2$.

There are side-wall effects (3D flow) near the side plates in the experiment. Hence, in order to compensate for the blockage effect of the side plates in the computation, the surface shape of the upper wall (above the hump) is modified and the upper wall is moved slightly indented, see Fig. T.1. The ratio of the local cross-sectional area of the side plates (facing the flow) to the cross sectional area of the tunnel enclosed by the side plates was computed. This ratio was used to scale the local height of the channel and thus modifying the contour shape of the upper wall.

Neumann conditions are used at the outflow section located at $x_1 = 4.2$. Slip conditions are used at the upper wall and symmetric boundary conditions are used on the spanwise boundaries. Inflow boundary (at $x_1 = 0.6$) conditions are taken from 2D RANS SST $k - \omega$ simulations carried out by the group of Prof. Strelets in St. Petersburg. The distributions of V_1 and V_2 at $x_1 = 0.6$ from the RANS simulation are used together with $V_3 = 0$ as mean inlet velocities to which the fluctuating velocity $\mathcal{V}'_1$, $\mathcal{V}'_2$ and $\mathcal{V}'_2$ are superimposed. The computed integral length scale for the synthetic inlet fluctuations is $\mathcal{L} \simeq 0.040$ and the integral time scale $\mathcal{T} \simeq 0.038$. It is noted that the

---

[12]these papers can be downloaded from http://www.tfd.chalmers.se/~lada/allpaper.html

prescribed inlet integral length scale is rather large [173] (approximately equal to the inflow boundary layer thickness). The reason is that synthetic fluctuations with a large integral length scale are efficient in generating resolved turbulent fluctuations [187].

At the course www page you find data files with time and spanwise averaged flow fields. You can use Matlab, Octave or Python. Both Octave and Python are open-source software. Octave is a Matlab clone. Many large Swedish industries prefer engineers to use Python instead of Matlab due to Matlab's high license fees.

Use one of the programs Python/Matlab/Octave to analyze the data. You find a Python/Matlab/Octave program at the www page which reads the data and computes the mean velocity. The data files are Matlab binary files.

Start by downloading `pl_vect_hump.py` or `pl_vect_hump.m`, `vectz_aiaa_paper.dat`, `xy_hump.dat` and `x065_off.dat` ... `x130_off.dat`. The py and m-files read the data files. The velocities, the square of the velocities and a number of other quantities are read. The resolved stresses are computed as in Eq. Q.6. Furthermore, the m file plots contours of $\langle v_1' v_1' \rangle$, the grid, a vector plot as well as $\langle \bar{v}_1 \rangle$ and $\langle v_2' v_2' \rangle$ at $x = 0.65$. The experimental values are also included in the plots at $x = 0.65$.

T.1 Discretization schemes

You will analyze results from two publications [173, 207]. You can also find slides for the two papers at here (titles: *Embedded LES using PANS, Hawaii 2011* and *Embedded LES using PANS (CDS)*). The main difference is that in [207] pure central differencing was used whereas in [173] a blend of 95% central differencing and 5% bounded second-order upwind scheme (van Leer scheme [216]) was employed. In both works, f_k was set to 0.4 in the entire region, which means that the PANS model was operating in LES mode everywhere.

Consider the plot of $\langle \bar{v}_1 \rangle$ (Figure 1) and $\langle v_2' v_2' \rangle$ (Figure 2) at $x = 0.65$. The velocity profile shows that the boundary layer extends up to $x_2 \simeq 0.17$. However, the $\langle v_2' v_2' \rangle$ exhibits large values outside the boundary layer; the peak value at $x_2 \simeq 0.24$ is almost 5 times larger than in the boundary layer. These fluctuations are nonphysical and stem from the use of central differencing.

Now plot $\langle v_2' v_2' \rangle$ at locations further downstream (choose the positions where experimental data exist, i.e. $x = 0$, $x = 0.80$, $x = 0.90$, $x = 1.0$, $x = 1.1$, $x = 1.2$ and $x = 1.3$); There are nonphysical fluctuations at the inlet. do they disappear further downstream? Compare with $\langle v_1' v_2' \rangle$ in Fig. 12 in [207]. The nonphysical fluctuations appear in the outer region where no physical resolved turbulence is present. Pure central differences sometimes give problems is flow regions like this. It is tempting to draw the conclusion that these nonphysical fluctuations are caused by the inlet synthetic fluctuations. However, when increasing the magnitude of the inlet synthetic fluctuations the magnitude of the nonphysical fluctuation diminishes, see Fig. 13a in [207].

Similar (much worse) problems with central differences were encountered in LES of the flow around an airfoil [115, 217]. Large nonphysical fluctuations were found in regions far from the airfoil; in these studies the problems were solved by using 100% van Leer scheme in the far-field regions.

In [173] the same simulations were carried out but now using a blend of central differencing (95%) and van Leer scheme (5%). Analyze these results by loading file `vectz_aiaa_journal.dat` in `pl_vect_hump.py` or `pl_vect_hump.m`.

Consider the resolved fluctuations: note how strongly they increase when going from the attached boundary layer ($x_1 = 0.65$) to the recirculating region, $0.8 \lesssim x \lesssim 1.2$. The peak of $\langle v_2' v_2' \rangle$, for example, increases from 0.0017 ($x_1 = 0.65$) to 0.046

($x_1 = 0.8$). This is the main reason why the nonphysical fluctuations at $x_1 = 0.65$ vanish quickly further downstream.

T.2 The modeled turbulent shear stress

As usual, when analyzing results of DES, PANS etc, we want to find out how much of the turbulence is modeled and how much is resolved. This gives an indication how well the turbulence has been resolved; if much turbulence is resolved it may be either good or bad. In recirculating regions it is usually good but it may be disastrous in boundary layer regions close to the wall if the mesh is not fine enough (this is the very reason why DDES was proposed, see Eq. 20.9). A suitable quantity to look at is the shear stress which is much more relevant than the turbulent kinetic energy; the shear stress is the largest diffusion term in the momentum equations, much larger than the normal stresses (at least in boundary layer flows).

Now plot the resolved (uv_2d) and the modelled shear stress (uv_model_2d) in the boundary layer region (e.g. $x = 0.65$) and the recirculating region (e.g. $x = 1$). Where is the modeled shear stress large and where is it small? Look at the other locations with experiments $(0.65 \ldots 1.30)$.

When you compare turbulent quantities here and below, note that it is interesting to compare turbulent quantities **only inside the turbulent boundary layer**. The flow is laminar outside the turbulent boundary. The find the thickness of the turbulent, find where ν_t/ν falls below one,

T.3 The turbulent viscosity

It may be interesting to look at the turbulent viscosity. Usually it is plotted scaled with ν, i.e. ν_t/ν. Plot the viscosity, ν_t/ν ((vis_2d-viscos)/viscos), vis_2d is the total viscosity, $\nu_{tot} = \nu + nu_t$) in the boundary layer and in the recirculating region. You find that the turbulent viscosity is large in the recirculation region, right? That might lead you to conclude that the turbulence is better resolved in the boundary layer than in the recirculating region. But that would be an incorrect conclusion. When estimating the influence of the modeled turbulence, we should not look at the turbulent viscosity because it does not appear as a term in the momentum equations; we should look at the ratio of modeled stresses to the resolved one, and, as mentioned in Section T.2, preferably the ratio of the modeled to the resolved shear stress [128, 129]. It would actually be even more relevant to look at the divergence of these terms, i.e.

$$\frac{\partial}{\partial x_j}\left(\left\langle \nu_t \frac{\partial \bar{v}_i}{\partial x_j} \right\rangle\right) \quad \text{and} \quad -\frac{\partial \langle v_i' v_j' \rangle}{\partial x_j} \tag{T.1}$$

because these are the terms that indeed appear in the momentum equations. Plot and compare the two terms in Eq. T.1.

You have noted that the turbulent viscosities are rather large; in the recirculation region ν_t/ν is larger than 100. Go back and load the results of [207] (vectz_aiaa_paper.dat).

Plot the turbulent viscosity for the two data sets. You find that the turbulent viscosity is much larger than for the data of [173]. It is true that the discretization schemes used in the two papers are slightly different, but that is not the reason. The difference stems from the fact that the turbulent Prandtl numbers in the k and ε equations were in the two papers set as

$$\sigma_k = 1.4, \quad \sigma_\varepsilon = 1.4 \quad [207] \tag{T.2}$$

$$\sigma_k = \frac{1.4}{f_k^2}, \quad \sigma_\varepsilon = \frac{1.4}{f_k^2} \quad [173] \tag{T.3}$$

Equation T.3 corresponds to the original PANS model. Recall that the turbulent diffusion in, for example, the k equation reads

$$\frac{\partial}{\partial x_j}\left(\frac{\nu_t}{\sigma_k}\frac{\partial k}{\partial x_j}\right) \tag{T.4}$$

Since $f_k = 0.4$, it means that the turbulent diffusion in the k and ε equations are $1/0.4^2 \simeq 6$ times larger in [173] than in [207]. The consequence is that peaks in k and ε (and also ν_t) are reduced in the former case compared to the latter (this is the physical role played by diffusion: it transports k from regions of high k to regions of low k). This explains why the peaks of k are much larger in [207] compared to in [173].

Hence, in the original PANS model (Eq T.3), the RANS turbulent viscosity appears in the turbulent diffusion of k (and ε), because the turbulent diffusion term reads (recall that $f_k = k/k_{total} = k/k_{RANS}$ where k_{RANS} denotes the turbulent kinetic energy in a RANS simulation)

$$\frac{\partial}{\partial x_j}\left(\frac{\nu_t}{f_k^2\sigma_k}\frac{\partial k}{\partial x_j}\right) = \frac{\partial}{\partial x_j}\left(\frac{c_\mu k^2}{\varepsilon f_k^2\sigma_k}\frac{\partial k}{\partial x_j}\right)$$
$$= \frac{\partial}{\partial x_j}\left(\frac{c_\mu k_{RANS}^2}{\varepsilon\sigma_k}\frac{\partial k}{\partial x_j}\right) = \frac{\partial}{\partial x_j}\left(\frac{\nu_{t,RANS}}{\sigma_k}\frac{\partial k}{\partial x_j}\right) \tag{T.5}$$

cf. Eqs. 18 and 19 in [145]. Thus the *total* (i.e. RANS) viscosity is responsible for the transport of the *modeled* turbulent kinetic energy.

T.4 Location of interface

The results analyzed above were from LES simulations [173, 207] (i.e. the PANS model was used in LES mode). Now we will analyze results from PANS where f_k is computed. In [169, 218] f_k is computed based on the DES model. We will use data obtained from this model but on a fine mesh (in the inlet and outlet region) and larger domain than in [169, 218]. Here we call the model D-PANS.

Run the file `pl_vect_hump_fine.py` (Python) or `pl_vect_hump_fine.m` (MAtlab/Octave) which loads the file `vectz_fine.dat`, `xy_hump_fine.dat`, and `x065_off.dat`. This mesh has $649 \times 110 \times 32$ cells with $Z_{max} = 0.2$ (the mesh is plotted in `pl_vect_hump_fine`). Recall that $\Delta z = 0.2/32$. Start by finding where the PANS model predicts the switch from RANS to LES (i.e where f_k goes from one down to, say, 0.4). f_k is computed in Eq. 16 in [169]. Plot location of the switch (the wall distance) versus x.

Plot f_k also at a couple of x_1 locations (0.65...1.30). Is it bigger or smaller than the prescribed values (0.4 and 1)? Compare it also with the definition of $f_k = k/k_{total}$ (cf. Fig. 26 in [165]).

In [219], f_k is computed as

$$f_k = c_\mu^{-1/2}\left(\frac{\Delta}{L_t}\right)^{2/3}, \quad L_t = \frac{k_{total}^{3/2}}{\langle\varepsilon\rangle} \tag{T.6}$$

where $k_{tot} = k_{res} + k$. Compare this f_k with f_k with D-PANS.

T.5 Location of interface in DES and DDES

Let's compare D-PANS with DES and DDES. In SA-DES, the interface is defined as the location where the wall distance is equal to $C_{DES}\Delta$ where $\Delta = \max\{\Delta_x, \Delta_y, \Delta_z\}$, see Eq. 20.3. How does this compare with switching locating defined by D-PANS?

Next, compare the DES lengthscale, $C_{DES}\Delta$, with the lengthscale of D-PANS, i.e. (see the definition of f_k and ψ in Eqs. 16, 11 and 12 in [169])

$$\ell_{PANS} = \frac{k^{3/2}}{\varepsilon} \tag{T.7}$$

see Eq. 20.4. Note that outside the boundary layer (i.e. in the inviscid region), ℓ_{PANS} becomes very large; the reason is that both k and ε are very small. Hence, plot the lengthscales only in the boundary layer. Plot the lengthscales at the usual experimental locations as well as at $x = 2$. It is also interesting to compare with the RANS lengthscale by replacing k with $g_{tot} = k + k_{res}$ in Eq. T.7.

In SST-DES, the location of the interface is computed using k and ω. Compute ω from $\varepsilon/(\beta^* k)$ and compute the location using Eq. 20.8. How does the location compare with D-PANS and SA-DES?

In DDES, the boundary layer is shielded with a damping function. In SST-DES, the shielding function (see Eq. 20.9) may be one of the blending functions, F_1 or F_2 (see Eq. 20.5). Let's use F_2 as the shielding function as in [79]. Does DDES work, i.e. does it make the model to be in RANS mode in the entire boundary layer? What about the separation region?

T.6 The SAS model

Learn about the SAS model in Section 22. The SAS model is based on the von Kármán lengthscale, Download `pl_sas_fine` which reads data files with instantaneous results. The files are

- `u1_pans_iddes,v1_pans_iddes,w1_pans_iddes`
- `u2_pans_iddes,v2_pans_iddes,w2_pans_iddes`
- `u3_pans_iddes,v3_pans_iddes,w3_pans_iddes`
- `u4_pans_iddes,v4_pans_iddes,w4_pans_iddes`
- `u5_pans_iddes,v5_pans_iddes,w5_pans_iddes`
- `u6_pans_iddes,v6_pans_iddes,w6_pans_iddes`
- `u7_pans_iddes,v7_pans_iddes,w7_pans_iddes`
- `u8_pans_iddes,v8_pans_iddes,w8_pans_iddes`

which include eight independent instantaneous velocity fields. Only the first two fields are loaded in `pl_sas_fine` (the lines where field 3-8 are loaded are commented). The more instantaneous velocity fields that are used, the better statistics and the smoother the plotted lines. When everything works, I recommend that you use more files (maybe all eight).

In the beginning of `pl_sas_fine`, all first and second velocity derivatives are computed. Compute the instantaneous von Kármán lengthscale $L_{vK,3D}$ using Eq. 22.3. Spanwise average and it at the positions of the experiments ($0.65\ldots 1.30$).

Recall that the idea of the SAS model is that the von Kármán lengthscale is smaller for an unsteady flow field than for a steady one. Compute the von Kármán lengthscale using the time-averaged velocity field (use the file `vectz_fine.dat`); note that $\langle \bar{v}_3 \rangle$ is zero since the time-averaged flow field is two dimensional). Compare it with $L_{vK,3D}$. Compare with $C_{DES}\Delta$ and the D-PANS lengthscale (Eq. T.7). Try also the alternative formulation of U'' in Eq. S.3.

The von Kármán lengthscale using the time-averaged velocity field is a RANS lengthscale. Therefor it is interesting to compare it with the RANS lengthscale $k_{res}^{3/2}/\varepsilon$ where k_{res} is the resolved turbulent kinetic energy and ε is the modelled dissipation (from the PANS $k-\varepsilon$ model). Note that what we denote as a 1D von Kármán lengtscale in Se

$$L_{vK,steady} = \kappa \frac{2\langle \bar{s}_{ij} \rangle \langle \bar{s}_{ij} \rangle}{U''_{mean}} \tag{T.8}$$

where

$$U''_{mean} = \left(\frac{\partial^2 \langle \bar{v}_i \rangle}{\partial x_j \partial x_j} \frac{\partial^2 \langle \bar{v}_i \rangle}{\partial x_k \partial x_k} \right)^{0.5} \tag{T.9}$$

For the hump flow, $\langle \bar{v}_3 \rangle = 0$ since the time-averaged flow is 2D. Note than in a CFD code, Eq. 22.3 and 22.2 are always used but when the flow is steady it is equal to Eqs. T.8 and T.9.

T.7 Different ways to evaluate resolution

In [128, 129] different ways to estimate the resolution of an LES were investigated. It is also discussed in Section 18.26. There are many ways to estimate resolution:

1. Ratio between viscous and modelled turbulent viscosity (not recommended in [128, 129]).
   Plot $\langle \nu_t \rangle / \nu$ at the positions $0.65 \ldots 1.30$. This quantity does not say much about how good the LES resolution is. It tells us how close the LES is to a DNS.

2. Ratio between modeled and total shear stress (recommended in [128, 129]).
   Plot $|\langle \tau_{12} \rangle / (\langle \tau_{12} \rangle + \langle \bar{v}_1' \bar{v}_2' \rangle)|$ at the positions $0.65 \ldots 1.30$. Compute the modeled shear stress from the Boussinesq approximation.

3. Ratio between modeled and total turbulent kinetic energy (recommended in [200]).
   Plot $\langle k_{model} \rangle / (\langle k_{model} \rangle + k_{res})$ ratio at the positions $0.65 \ldots 1.30$.

4. Anisotropic error.
   Plot the anisotropic error at the positions $0.65 \ldots 1.30, 2.00, 3.00$. This quantity should be as constant as possible. Some further instructions are given in Section T.7.1.

5. Two-point correlations.
   Plot the two-point correlations (recommended in [128, 129]). You find info on how to proceed in Section T.7.2

6. Ratio of boundary-layer thickness, δ to Δx and Δz. This is a measure of the resolution in the log-law region. It is commended that $10 < \delta/\Delta x < 20$ and $20 < \delta/\Delta z < 40$, see Section 18.26.

Plot $\delta/\Delta x$ and $\delta/\Delta z$ vs. x. One question arises: how the estimate the boundary-layer thickness. One useful definition is to define δ as the location where ν_t/ν falls below one.

In [200] he suggest that if $k_{model}/(k_{model} + k_{res}) < 0.2$ (ratio of modelled to total turbulence), then the turbulence is well resolved by the LES. Assume we make the same definition for the shear stress, i.e. $|\langle\tau_{12}\rangle/(\langle\tau_{12}\rangle + \langle\bar{v}'_1\bar{v}'_2\rangle)| < 0.2$.

Do these methods give similar results? Do you trust anyone more than the other? (<u>hint</u>: look at [129].

T.7.1 Anisotropic errors (optional)

You plotted this error estimate also for the channel flow, see Section S.8. You can use the first and second-order derivatives that you computed in Section T.6. The Δx and Δy needed in Eq. S.6 can be computed as

```
dx=diff(xp2d);
dx=repmat(dx,[1 1 nk-1]);
dx(ni,:)=dx(ni-1,:);

dy=diff(yp2d,1,2);
dy(:,nj)=dy(:,nj-1);
dy=repmat(dy,[1 1 nk-1]);
```

(Δz is constant). Only two sets of velocity fields are loaded, u1_pans_iddes.mat, ...w2_pans_iddes.mat. When everything works, use more velocity fields (possibly all eight) in order to get better statistics.

T.7.2 Two-point correlations

In Item 5 in Section T.7 you should compute two-point correlation. To do that, you will use data from another simulation of the hump flow presented in [169, 218]. Download the Pythons file pl_twocorr_computed_fk.py or the Matlab/Octave file pl_twocorr_computed_fk.m. They load a new grid with 305×109 grid points. The 3D grid has 32 cells in the spanwise direction ($z_{max} = 0.2$). pl_twocorr_computed_fk will also load time histories of the spanwise velocity $\bar{v}_3$ at $x = 0.65, 0.8, 1.1$ and $x = 1.3$ (files w_time_z65, w_time_z80, w_time_z110 and w_time_z130). These files include time histories at cell center $j = 10, 30, 50, 70, 90$ in the wall-normal direction at 16 positions in the x_3 direction. The time series are re-arranged into 3D arrays w_y_z_t_65(j,k,t), w_y_z_t_80(j,k,t), w_y_z_t_110(j,k,t) and w_y_z_t_130(j,k,t) where index j, k, t denote wall-normal direction, spanwise direction and time, respectively.

Now, use the time series to compute two-point correlations using the formulas given in Section 10.1. Equation 10.3 gives the two-point correlation of v'_1 at two points separated in the x_1 direction. In your case, you will compute the two-point correlation of v'_3 at two points separated in the x_3 direction, i.e. $B_{33}^{norm}(x_3^A, \hat{x}_3)$. Plot it at all x_1 positions ($x_1 = 0.65, 0.8, 1.1$ and 1.3) and at a couple of x_2 locations. Then compute the integral lengthscale, see Eq. 10.6. A good approximation of the integral lengthscale is usually the point in the two-point correlation where $B_{33}^{norm} \simeq 0.2$ (i.e. $\mathcal{L} \simeq \hat{x}_3$ where $B_{33}^{norm} \simeq 0.2$). Check if it is good approximation.

In [128, 129] it is recommended that in a good LES (or in the LES region of a DES/hybrid LES-RANS), the integral lengthscale should cover 8-16 cells, depending on how accurate the user wants her/his LES/DES to be.

Here are some hints on how to compute the two-point correlation. Start by computing it for one y location (=2) and one z separation, $2\Delta z$).

```
B33=0;
k=2;
for n=1:N % time average
  B33=B33+w(2,1,n)*w(2,1+k,n)/N
end
```

where $k = 2$ (because the separation is $2\Delta z$) and N is the number of time steps. Next, do it for all $k = 0, 1, \ldots 15$. And then normalize by w_{rms}^2 (or, easier, simply by `B33(1)`). Finally, do it for all five y locations.

U MTF271, Assignment: Embedded LES with PANS, channel flow
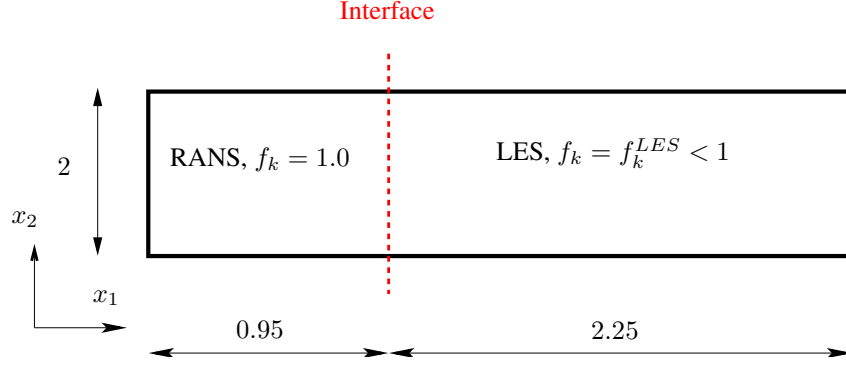
Figure U.1: Channel flow configuration. The interface separates the RANS and the LES regions.

IN this exercise you will use data from an embedded PANS of channel flow where RANS is used for $x < 0.95$ and LES is used for $x \geq 0.95$. The data are taken from [173]. The k_u (Eq. 23.9) and the ε_u (Eq. 23.16) equations are solved. The turbulent viscosity is computed from Eq. 23.6. The PANS model is a modified $k - \varepsilon$ model which can operate both in RANS mode and LES mode.

The Reynolds number for the channel flow is $Re_\tau = 950$ based on the friction velocity, u_τ, and half the channel width, δ. In the present simulations, we have set $\rho = 1$, $\delta = 1$ and $u_\tau \simeq 1$, see Fig. U.1. With a $3.2 \times 2 \times 1.6$ domain, a mesh with $64 \times 80 \times 64$ cells is used in, respectively, the streamwise (x), the wall-normal (y) and the spanwise (z) direction, see Fig. U.1. The resolution is approximately (the wall shear stress varies slightly along the wall) $48 \times (0.6 - 103) \times 24$ in viscous units. Inlet conditions at $x = 0$ are created by computing fully developed channel flow with the LRN PANS model in RANS mode (i.e. with $f_k = 1$). The RANS part extends up to $x_1 = 0.95$; downstream the equations operate in LES mode ((i.e. $f_k = 0.4$).

Anisotropic synthetic fluctuations are added at the interface. The interface condition for ε_u is computed with the baseline value $C_s = 0.07$, where k_{RANS} is taken at $x = 0.5$, see Fig. U.1. The modeled dissipation, ε_{inter}, is set from k_{inter} and an SGS length scale, ℓ_{sgs}, which is estimated from the Smagorinsky model as

$$\ell_{sgs} = C_s \Delta \tag{U.1}$$

and the interface condition for k_u is computed as

$$k_{inter} = f_k^{LES} k_{RANS} \tag{U.2}$$

with $f_k^{LES} = 0.4$. The interface conditions on k_u and ε_u will make the turbulent viscosity steeply decrease from its large values in the RANS region to much smaller values appropriate for the LES region.

U.1 Time history

At the www-page you find a file u_time_interior.dat with the time history of $\bar{v}_2$. The file has eight columns of $\bar{v}_2$ along two lines: $x_2 = 0.0139$ ($x_2^+ \simeq 13$) and

$x_2 = 0.24$ ($x_2^+ \simeq 230$); they are located at $x_1 = 0.775, 1.175, 1.675, 2.175$. The sampling time step is 0.000625 (every time step).

You can use Matlab, Octave or Python. Both Octave and Python are open-source software. Octave is a Matlab clone. Many large Swedish industries prefer engineers to use Python instead of Matlab due to Matlab's high license fees.

Use the Python/Matlab/Octave program `pl_time_pans` to load and plot the time history of $\bar{v}_2$.

The time history of $\bar{v}_2$ at $x_2 = 0.0139$ at $x_1 = 0.775$ and $x_1 = 1.675$ are shown. To study the profiles in closer detail, use the `axis`-command in the same way as when you studied the DNS data. Why is there such a big difference in the fluctuations?

If you're not interested in integral time scales, skip the rest of this section and proceed to Section U.2.

In `pl_time_pans`, figure 2, the autocorrelation is plotted. The autocorrelation is defined as

$$B(\tau) = \int_0^\infty v(t)v(t-\tau)dt \tag{U.3}$$

When prescribing the time correlation of the synthetic fluctuations, the integral timescale $\mathcal{T}$ is used. The integral time scale is defined as

$$\mathcal{T} = \int_0^\infty B^{norm}(\tau)d\tau \tag{U.4}$$

where $B^{norm} = B(\tau)/B(0)$ so that $B^{norm}(0) = 1$. The constant a is in [173] set to 0.954 and from Eq. 14 in [207] we can then compute the prescribed integral timescale. In the Python/Matlab/Octave file the integral timescale is computed from the autocorrelation.

Plot $\bar{v}_2$ for the other nodes and study the differences. Compute the autocorrelations and the integral timescales.

U.2 Resolved stresses

Now we will look at the time-averaged results. Use the file `pl_uuvvww_2d.m` to look at the mean quantities such as velocity, resolved and modeled stresses, turbulent viscosities etc. `pl_uuvvww_2d.m` reads the fields and transforms them into 2D arrays such as `u_2d`, `uu_2d`.

Run `pl_uuvvww_2d`. The resolved stresses $\langle \overline{v_1'^2} \rangle$ are plotted vs x_2 (figure 1) and vs. x_1 (figure 2). Two x_1 stations are shown in figure 1, $x_1 = 1.175$ and $x_1 = 2.925$. Plot the resolved stress also in the RANS region, i.e. for $x_1 < 0.95$. The $\langle \overline{v_1'^2} \rangle$ profiles are very different in the RANS region ($x_1 < 0.95$) and in the LES ($x_1 > 0.95$), aren't they? Why? This can also be seen in figure 2 where $\langle \overline{v_1'^2} \rangle$ is plotted vs. x_1

Now plot the resolved shear stresses, $\langle \overline{v_1'v_2'} \rangle$, both in the RANS region and in the LES region. You find the same difference between RANS and LES region as for $\langle \overline{v_1'^2} \rangle$, don't you?

U.3 Turbulent viscosity

Plot the turbulent viscosity vs. x_2 in both regions. Normalize it with $\langle \nu \rangle$, i.e. plot $\langle \nu_u \rangle / \nu$. Where is it large and where is it small? Why? Now plot it also vs. x_1. Something drastically happens at $x_1 = 0.95$, right?
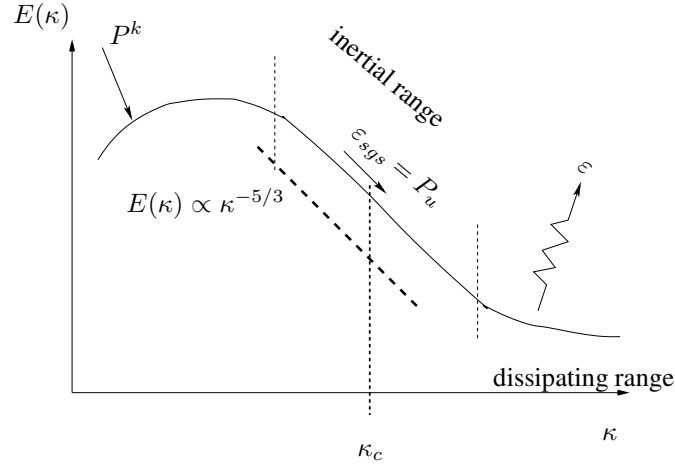
Figure U.2: Energy spectrum.

U.4 Modeled stresses

In Section U.2 you looked at the resolved Reynolds stresses. Now let's look at the *modeled* stresses. Compute the modeled Reynolds stresses from the Boussinesq assumption

$$\langle \overline{v_i' v_j'}_{mod} \rangle = -\langle \nu_u \rangle \left(\frac{\partial \langle \bar{v}_i \rangle}{\partial x_j} + \frac{\partial \langle \bar{v}_j \rangle}{\partial x_i} \right) + \frac{2}{3} \delta_{ij} \langle k_u \rangle \tag{U.5}$$

Compare the resolved and the modeled shear stress as well as the streamwise and the normal stresses in the RANS region and in the LES region.

U.5 Turbulent SGS dissipation

In an LES the resolved turbulent fluctuations can be represented by a energy spectrum as in Fig. U.2. The resolved turbulence extracts kinetic energy via the production term, P^k, which represents a source term in the k equation (Eq. 8.14) and a sink term in the $\bar{K}$ equation (Eq. 8.36). The energy flow is visualized in Fig. Q.4 where the energy in $\bar{K}$ mostly goes to resolved turbulence, $\bar{k}$, then to modeled turbulence, k_{sgs} (or k_u) and finally to internal energy via dissipation, ε_u.

In RANS mode, however, there is no resolved turbulence. Hence the kinetic energy goes directly from $\bar{K}$ to the modeled turbulence, k_u.

In the LES region, the production term in the k_u equation includes both mean and fluctuating strain rates since

$$P_u = \varepsilon_{sgs} = \left\langle \nu_u \left(\frac{\partial \bar{v}_i}{\partial x_j} + \frac{\partial \bar{v}_j}{\partial x_i} \right) \frac{\partial \bar{v}_i}{\partial x_j} \right\rangle$$

which is stored as `pksgs_2d`. Now consider the LES region. Investigate the relation between $P_u = \varepsilon_{sgs}$ and the production due to the resolved turbulence

$$P^k = -\langle \overline{v_i' v_j'} \rangle \frac{\partial \langle \bar{v}_i \rangle}{\partial x_j}$$

Compare also P^k in the LES region and in the RANS region.

In both the RANS and the LES region the process of viscous dissipation takes place via ε_u. Hence, plot also this quantity. Is the turbulence in local equilibrium, i.e. does the relation $P_u = \varepsilon_u$ hold?

V MTF271, Assignment 3: Hybrid LES-RANS, channel flow

$\mathbf{I}$N this exercise you will use data from a Hybrid LES-RANS for fully developed channel flow. The turbulence model is the same as in [100] (no forcing), but the domain and Reynolds number is taken from [220]. The Re number based on the friction velocity and the half channel width is $Re_\tau = u_\tau h/\nu = 8000$. 28 cells (29 nodes including the boundary) are located in the URANS region at each wall. The matching line is located at gridline number 29 at which $x_2^+ \simeq 500$, $x_2/\delta = 0.06$.

A $64 \times 96 \times 64$ mesh has been used. The cell size in x_1 and x_3 directions are $\Delta x_1 = 0.05$ and $\Delta x_3 = 0.025$. Periodic boundary conditions were applied in the x_1 and x_3 direction (homogeneous directions). All data have been made non-dimensional by u_τ and ρ.

The number of A4 pages in the report should not exceed 20. Font size must be $11pt$ or larger. The minium size of each figure must not be smaller than $7cm$.

At the course www page you find data files with instantaneous flow fields (statistically independent). The data files include the instantaneous variables u (v_1), v (v_2), w (v_3) and k_T (made non-dimensional by u_τ and ρ).

You can use Matlab, Octave or Python. Both Octave and Python are open-source software. Octave is a Matlab clone. Many large Swedish industries prefer engineers to use Python instead of Matlab due to Matlab's high license fees.

Use Python, Matlab or Octave to analyze the data. You find a Python/Matlab/Octave program at the www page which reads the data and computes the mean velocity. The data files are Matlab binary files. Since the data files are rather large, it is recommended that you do all tasks using only data files '1'. When everything works, then use also data files '2', '3' and '4', and average by use of all four files.

You will also find a file with time history of u.

V.1 Time history

At the www page you find a file u_v_time_4nodes_hybrid.dat with the time history of $\bar{v}_1$ and $\bar{v}_3$. The file has nine columns of $\bar{v}_1$ and $\bar{v}_3$ at four nodes (and time): $x_2/\delta = 0.0028$, $x_2/\delta = 0.015$, $x_2/\delta = 0.099$ and $x_2/\delta = 0.35$. Hence, two nodes are located in the URANS region and two nodes in the LES region. With $u_\tau = 1$ and $\nu = 1/Re_\tau = 1/8000$, this correspond to $x_2^+ = 22$, $x_2^+ = 120$, $x_2^+ = 792$ and $x_2^+ = 2800$, respectively. The sampling time step is $6.250E - 4$ (every time step). Use the Python/Matlab/Octave program pl_time_hybrid to load and plot the time history of $\bar{v}_1$.

Recall that the velocities have been scaled with the friction velocity u_τ, and thus what you see is really $\bar{v}_1/u_\tau$. The time history of $\bar{v}_1$ at $x_2/\delta = 0.015$ and $x_2/\delta = 0.35$ are shown. To study the profiles in closer detail, use the axis-command in the same way as when you studied the DNS data.

Plot $\bar{v}_1$ for all four nodes. How does the time variation of $\bar{v}_1$ differ for different positions? Recall that the two points closest the wall are located in the URANS region and the other two are located in the LES region. In the URANS region the turbulent viscosity is much larger than in the LES region. How do you expect that the difference in ν_t affects the time history of $\bar{v}_1$. Does the time history of $\bar{v}_1$ behave as you expect? What about $\bar{v}_2$?

Compute the autocorrelation of the four points

```
imax=500;
two_uu_1_mat=autocorr(u1,imax);
```

Above we set the maximum separation in time to 500 samples. Compute the integral timescale

```
dt=t(1);
int_T_1=trapz(two_uu_1_mat)*dt;
```

Plot the autocorrelation.

```
plot(t(1:imax),two_uu_1_mat(1:imax),'linew',2)
xlabel('t')
ylabel('B_{uu}')
handle=gca
set(handle,'fontsi',[20])
```

How does it compare to the integral timescale? Compute the autocorrelation and integral timescale also for the other three points. Do you see any difference between the points in the URANS region and the LES region?

V.2   Mean velocity profile

After having performed a hybrid LES-RANS, we want to look at the time-averaged results. Use the file pl_uvw_hybrid.m to look at the mean velocity profiles. pl_uvw_hybrid.m reads the instantaneous $\bar{v}_1$ field and performs an averaging in the homogeneous directions x_1 and x_3. The time averaged velocity profile is compared with the log profile (markers). There are four files with instantaneous values of $\bar{v}_1$. Use more than one file to perform a better averaging.

V.3   Resolved stresses

We want to find out how much of the turbulence that has been resolved and how much that has been modelled. Compute first vmean (this quantity should be very small, but if you use only one file this may not be the case due to too few samples). Now compute $\langle v_1' v_2' \rangle$. Here's an example how to do:

```
uv=zeros(nj,1);
for k=1:nk
for j=1:nj
for i=1:ni
   ufluct=u3d(i,j,k)-umean(j);
   vfluct=v3d(i,j,k)-vmean(j);
   uv(j)=uv(j)+ufluct*vfluct;
end
end
end
uv=uv/ni/nk;
```

Plot it in a new figure (a figure is created by the command figure(2)).
Compute also the resolved turbulent kinetic energy

$$k_{res} = 0.5 \left(\langle v_1'^2 \rangle + \langle v_2'^2 \rangle + \langle v_3'^2 \rangle \right)$$

and plot it in a new figure.

	URANS region	LES region
ℓ	$2.5n[1 - \exp(-0.2k_T^{1/2}n/\nu)]$	$\ell = \Delta = (\delta V)^{1/3}$
ν_T	$0.09 \cdot 2.5k_T^{1/2}n[1 - \exp(-0.014k_T^{1/2}n/\nu)]$	$0.07k_T^{1/2}\ell$

Table V.1: Expressions for ℓ and ν_T in the LES and URANS regions. n denotes the distance from the wall.

V.4 Turbulent kinetic energy

Now plot and compare the resolved and modelled turbulent kinetic energies. Note that the modelled turbulent kinetic energy, k_T (te1_hybrid.mat, te2_hybrid.mat, . . .), can be downloaded from the www page and loaded at the beginning of pl_uvw_hybrid.m. Which is largest? Which is largest in the URANS region and in the LES region, respectively? What about the sum? The magnitude of resolved and modelled turbulent kinetic energies is discussed in the last subsection in [100].

V.5 The modelled turbulent shear stress

We have computed the resolved shear stress. Let's find the modelled shear stress.

The modelled turbulent kinetic energy, k_T (file te1_hybrid.mat, . . .), will be used. Recall that $\nu = 1/8000$. Compute the turbulent viscosity according to Table V.1 and do the usual averaging. When computing Δ, you need the volume, δV, of the cells. It is computed as $\delta V = (\Delta x_1 \Delta x_2 \Delta x_3)$; Δx_1 and Δx_3 are constant and Δx_2 is stored in the array dy(j), look at the beginning of the m-file. Plot $\langle \nu_T \rangle / \nu$. Where is it large and where is it small? (Recall that the URANS region is located in the first 28 cells). Is it smooth? Do you need more samples? If so, use more files.

Compute the modelled shear stress from the Boussinesq assumption

$$\tau_{12} = -2\nu_T \bar{s}_{12} = -\nu_T \left(\frac{\partial \bar{v}_1}{\partial x_2} + \frac{\partial \bar{v}_2}{\partial x_1} \right)$$

Plot it and compare with the resolved shear stress (see Section V.3). Are they smooth across the interface? Is the resolved shear stress large in the URANS region? Should it be large? Why/why not?

V.6 Location of interface in DES and DDES

As mentioned above, the interface in the present simulations is prescribed along a fixed grid line (No 29). Let's compare that with DES and DDES.

In SA-DES, the interface is defined as the location where the wall distance is equal to $C_{DES}\Delta$ where $\Delta = \max \Delta_x, \Delta_y, \Delta_z$, see Eq. 20.3. How does this compare with gridline number 29?

In SST-DES, the location of the interface is computed using k and ω. Compute ω from ν_T and k as $\omega = \nu_T/k$) and compute the location using Eq. 20.8.

V.7 Turbulent length scales

Compute and plot the turbulent length scales given in Table V.1. Plot the ℓ_{SGS} and ℓ_{URANS} length scales in both regions. Which is largest? Any surprises? Compare them with Δx_2 and $(\Delta x_1 \Delta x_2 \Delta x_3)^{1/3}$. One would expect that $(\Delta x_1 \Delta x_2 \Delta x_3)^{1/3} < \ell_{URANS}$ everywhere. Is this the case?

W MTF271, Assignment 4: Synthetic inlet fluctuations

From the course www page, download the files, i.e. `angles`, `randf_1`, `randf_2`, `synt_main`.

   The file you should mainly concentrate is on `synt_main`. Study this file. The theory is covered in Section 27.

   You can use Matlab, Octave or Python. Both Octave and Python are open-source software. Octave is a Matlab clone. Many large Swedish industries prefer engineers to use Python instead of Matlab due to Matlab's high license fees.

W.1 `synt_main`

In Chapter 1 length scale, constants and the grid are defined. The inlet plane is assumed to be located at $x = $ const, i.e. the inlet plane is a $y - z$ ($j - k$) plane. For simplicity, constant grid spacing is used in the z direction and only one cell is used in the y direction ($nj = 2$).

Random numbers are used. A random generator needs a seed; ii is taken from the local time (the Python command `time` or the Matlab/Octave command `clock` (note that the seed must be negative, see `randf_2.m`). This means that a different random velocity field will be generated every time you run the code.

In Chapter 2 the loop over `nstep` realizations ("time steps") starts.

In Chapter 3 the loop over the inlet grid plane starts.

W.2 `angles`

In this file the angles φ^n, ψ^n, α^n and θ^n are computed for each wavenumber n by calling the function `rand1`.

W.3 `rand1.m`

In this file the upper and lower limits of the random numbers are set.

W.4 `rand2.m`

In this file random numbers are generated. The function corresponds to `ran1` in *Numerical Recipes in C: The Art of Scientific Computing*, Second Edition.

W.5 Mean values; randomness

Run the program `synt_main`. Random fields of u', v' and w' are created for 200 realizations. They are stored in the vectors the `ut`, `vt` and `wt`. Check the dimensions in Python by typing

    ut.shape

in Matlab/Octave

    size(ut)

at the Matlab prompt. You'll find that the dimension of `ut` is $(62, 200)$. It consists of 200 independent realizations of the u' field along the z axis (62 cells).

In plot 1 u' is shown vs. z. Run the program again. Is u' the same now? The answer is: no. The reason is that the random number generator is given a seed based on the clock. The seed is stored in the variable `iseed`. Set, for example,

```
iseed=-21
```

and run the code a couple of times. Now the same "random" field is created each run.

At the beginning of Chapter 4 in `synt_main` the mean of u', v' and w' are computed. They should be close to zero. They are, aren't they? They will get closer to zero the more realizations you use. You can try this by increasing the number of realizations (for example `nstep=400` in Chapter 1 in `synt_main`); note that it will take longer time to run the program.

W.6 RMS and shear stress

Compute the RMS (root-mean-square) of u', v' and w', i.e. u_{rms}, v_{rms} and w_{rms}. You can do this in Python as (we assume the that mean of u' is zero)

```
urms=0.
for n in range(1,nstep):
   for k in range(0,nk-1):
      urms=urms+ut[k,n]**2/nstep/(nk-1)

urms=urms**0.5
```

and in Matlab/Octave as

```
urms=0;
for n=1:nstep
for k=1:nk-1
   urms=urms+ut(k,n)^2/nstep/(nk-1);
end
end
urms=urms^0.5;
```

You can also use the Python command `np.var(ut[0:nk-1,1:])` or the Matlab/Octave command `u2_v=var(ut(:)))`.

Above we average over time and the z direction. u_{rms} should be equal to `up` which was set in Chapter 1 in `synt_main`. Is it? Again, the more time steps you use, the closer it will get. Compute also v_{rms} and w_{rms}. Since the turbulent field should be isotropic, we should get $u_{rms} = v_{rms} = w_{rms}$.

Furthermore, as the fluctuating field is isotropic, there should be no correlation between the three velocity components. Check if it's true. The correlation between u' and v' (i.e. $\langle u'v' \rangle$), for example, can be computed in Python as

```
uv=0
for n in range(1,nstep):
   for k in range(0,nk-1):
      uv=uv+ut[k,n]*vt[k,n]/nstep/(nk-1)
```

and in Matlab/Octave as

```
uv=0;
for n=1:nstep
for k=1:nk-1
   uv=uv+ut(k,n)*vt(k,n)/nstep/(nk-1);
end
end
```

W.7   Two-point correlations

When generating the fluctuating field we have prescribed a length scale, L_t (`sli=0.1*delta=0.05` in Chapter 1 in `synt_main`). Let's compute the length scale of our fluctuating field. The best way to do this is to compute the two-point correlation and then, maybe, the integral length scale.

The two-point correlation of u', for example, is defined as

$$B_{uu}(\zeta) = \frac{1}{u_{rms}^2} \int_{t=0}^{\infty} \int_{z=0}^{z_{max}} u(z,t)u(z-\zeta,t)dzdt \qquad (\text{W.1})$$

where ζ is the separation distance between the two points. Compute this in Python as

```
imax=min(50,nk)
two_uu=np.zeros(imax)
for it in range(1,nstep+1):
   for z in range(0,imax-1):#separation distance
      for k in range(0,nk-imax-1):
         i0=k+z
         two_uu[z]=two_uu[z]+ut[k,it]*ut[i0,it]
         if it == 1:
            print('i0=',i0,'k=',k,'z=',z,'two_uu',two_uu[z])
two_uu_org=two_uu
two_uu=two_uu/two_uu[0]   #normalize so that two_uu(1)=1


fig2 = plt.figure("Figure 2")
plt.clf() #clear the figure
plt.plot(zp[0:imax-1],two_uu[0:imax-1],'b-')
plt.xlabel('zeta')
plt.ylabel('two-uu')
plt.axis([0,0.2,-0.2,1.1])
```

and in Matlab/Octave as

```
imax=min(50,nk);
two_uu=zeros(imax,1);
for it=1:nstep
for z=1:imax
   zeta=z-1; %zeparation distance
   for k=1:nk-imax-2
      i0=k+zeta;
      two_uu(z)=two_uu(z)+ut(k,it)*ut(i0,it);
   end
```

```
end
end
two_uu=two_uu/two_uu(1); %normalize so that two_uu(1)=1

%% plot two_uu
figure(2)
zeta=zp(1:imax)-zp(1);
plot(zeta,two_uu(1:imax),'linewidth',2)
xlabel('zeta')
ylabel('two-uu')
axis([0 0.2 -0.2 1.1])
h=gca;
set(h,'fontsize',[20])
```

Run the program. The two-point correlation should approach zero for $\zeta > L_t$. Does it? (the integral length scale, L_t, corresponds to the integral of the two-point correlation (see Eq. W.2), i.e. it is equal to the area below the B_{uu}). Increase the length scale in Chapter 1 in synt_main. and run the program again. The two-point correlation should now increase (i.e. it should go to zero for a larger separation distance). Does it?

W.8 The integral length scale

A quantitative measure of the length scale is the integral length scale. It is defined from the two-point correlation

$$L_{int} = \int_0^\infty B_{uu}(\zeta)d\zeta \tag{W.2}$$

where we assume that B_{uu} has been normalized so that $B_{uu}(0) = 1$. Program this in Python as

```
L=0.
dz=zp[2]-zp[1]
for z in range(0,imax-1):
    if two_uu[z] < 0:
        break
    L=L+two_uu[z]*dz
```

and in Matlab as

```
Lint=0;
dz=zp(2)-zp(1);
for z=1:imax
    if two_uu(z) < 0
       break
    end
    Lint=Lint+two_uu(z)*dz;
end
```

The integral in Eq. W.2 should be carried out to infinity. Here we choose to stop when B_{uu} goes negative. This choice is somewhat arbitrary. Run the code. What L_{int} do you get? How does it compare with the prescribed L_t (Python/Matlab/Octave variable sli)? What happens if you increase the number of modes, N (Python/Matlab/Octave variable nmodes)?

W.9   Correlation in time

We have generated `nstep` *independent* velocity fields. Now we want to create a correlation between them, i.e. we will prescribe a time scale $\mathcal{T}$ that will create the autocorrelation $\exp(-\Delta t/\mathcal{T})$. The time scale should be proportional to $L_t/\mathcal{U}$, and we set it to $\mathcal{T} = 0.1\delta/u_\tau = 0.1 \cdot 0.5/1 = 0.05$. We can now compute the coefficients a and b as

$$a = \exp(-\Delta t/\mathcal{T}), \quad b = \sqrt{1 - a^2}$$

(see Section 27.8). With a time step of $\Delta t = 0.001$, this gives $a = 0.98$ and $b = 0.198$. The fluctuating inlet u' velocity for time step m is now obtained as

$$(\mathcal{U}')^m = a(\mathcal{U}')^{m-1} + b(u')^m \tag{W.3}$$

Program this in Python as

```
dt=0.001
t = np.linspace(0,dt*nstep,nstep+1)
a=np.exp(-dt/0.05)
b=(1-a**2)**0.5
uin_fluct=np.zeros(nstep+1)
k=0
uin_fluct[1]=ut[k,1]  #we generate the inlet fluctuations for one cell, and we
for n in range(2,nstep+1):
   uin_fluct[n] =  a*uin_fluct[n-1] + b*ut[k,n]

fig3 = plt.figure("Figure 3")
plt.clf() #clear the figure
plt.plot(t,uin_fluct,'b-')
plt.plot(t,ut[k,:],'r--')

plt.xlabel('z')
plt.ylabel('u-in-fluct')
```

or in Matlab/Octave as

```
dt=0.001;
t=dt:dt:nstep*dt;
a=exp(-dt/0.05);
b=(1-a^2)^0.5;
uin_fluct=zeros(nstep,1);
k=1;
m=1;
uin_fluct(1)=ut(k,1); % we generate the inlet fluctuations for one cell,
                      % and we choose k=1. The first time step, m=1,
                      % we set simply uin_fluct=ut
for m=2:nstep
   uin_fluct(m) =  a*uin_fluct(m-1) + b*ut(k,m);
end
%
figure(3)
hold off
```

```
plot(t,uin_fluct,'linewidth',2)
hold
plot(t,ut(k,:),'r--','linewidth',2)
xlabel('time')
ylabel('u-in-fluct')
hold
h=gca;
set(h,'fontsize',[20])
```

Run the code. Both $\mathcal{U}'$ (solid blue line) and u' (red dashed line) are plotted versus time. As you can see, the variation of $\mathcal{U}'$ is much smoother than that of u'; the latter fluctuates "wildly", i.e. randomly.

W.10 Autocorrelation in time

In Section W.7, we looked at the two-point correlation in space. Now let's look at the two-point correlation in *time*, defined as

$$B_{uu}^t(\tau) = \frac{1}{u_{rms}^2} \int_{t=0}^{\infty} u(t)u(t-\tau)dt$$

where τ is the separation distance in time between the two velocity signals.

So far, we have only generated 200 realizations of u'. This is not sufficiently long. Let's generate 2000 realizations; set `nstep=2000` in Chapter 1 in `synt_main`. This will require rather long computer time; to speed it up, decrease the number of cells in the z direction from $nk = 63$ to $nk = 3$ (do this in Chapter 1). Program the Python code as

```
nstep=2000
imax=200
two_uu_t=np.zeros(imax+1)
k=1
for tau in range(0,imax): # time separation
   for it in range(1,nstep-imax-1):
      i0=it+tau;
      two_uu_t[tau]=two_uu_t[tau]+uin_fluct[it]*uin_fluct[i0]
      if it == 1:
         print('it=',it,'i0=',i0,'tau',tau,'two_uu_t',two_uu_t[tau])
two_uu_t_org=two_uu_t
two_uu_t=two_uu_t/two_uu_t[0]  #normalize so that two_uu_t(1)=1
fig4 = plt.figure("Figure 3")
plt.clf() #clear the figure
plt.plot(t[0:imax-1],two_uu_t[0:imax-1],'b-')
plt.xlabel('tau')
plt.ylabel('two-uu-t')
plt.axis([0,0.2,-0.2,1.1])
```

or in Matlab

```
nstep=2000,
imax=200;
```

```
two_uu_t=zeros(imax,1);
for tt=1:imax
   tau=tt-1; %time separation
   for it=1:nstep-imax-2
      i0=it+tau;
      two_uu_t(tt)=two_uu_t(tt)+uin_fluct(it)*uin_fluct(i0);
   end
end
two_uu_t=two_uu_t/two_uu_t(1); %normalize _uu_t so that two_uu_t(1)=1

figure(4)
hold off
tau=t(1:imax)-t(1);
plot(tau,two_uu_t(1:imax),'linewidth',2)
xlabel('tau')
ylabel('two-uu-t')
hold
axis([0 0.2 -0.2 1.1])
h=gca;
set(h,'fontsize',[20])
```

Run the code. We have prescribed a time scale $\mathcal{T} = 0.05$ (see Section W.9). Does the autocorrelation behave as expected?

In Section W.8 we computed the integral length scale from the two-point correlation. In the same way you can compute the integral *time* scale from the autocorrelation. Do that.

W.11   Spectrum

We have generated fluctuations whose spectrum should follow the $-5/3$ spectrum. Let's find out if our generated fluctuations really do exhibit a $-5/3$ spectrum. In Section W.7 you created a two-point correlation for the fluctuations. In Section R it is described how to make energy spectra from two-point correlations. Read the Section carefully and try to create an energy spectrum from the two-point correlation you created in Section W.7. Be patient; it will take some time …

W.12   Anisotropic fluctuations

Now we will generate anisotropic fluctuations. Read the Section 27.9 carefully.

Download the Matlab file synt_main_aniso.m from the course www page. There are a few additional features in this file compared to synt_main.m.

Chapter 1 the eigenvalues and the eigenvectors are computed from the prescribed stress tensor.

Chapter 2 The eigenvalues are inverted

Chapter 3   1. σ_i and κ_j are transformed to the principal coordinate directions, i.e. σ_i^* and κ_j^*

        2. σ_i and κ_j are scaled with the eigenvectors. σ_i is modified so as to make the fluctuation anisotropic and κ_i is modified to ensure that the fluctuations satisfy the continuity equation.

3. The synthetic fluctuations are computed in the principal coordinate system

Chapter 4 The synthetic fluctuations are transformed from the principal coordinate system to the original coordinate system

Now run the code and generate the anisotropic fluctuations. Do the fluctuations agree with the prescribed stress tensor $\langle v_i' v_j' \rangle$?

Check if the anisotropy of the synthetic fluctuations agree with the prescribed anisotropy. Compute, for example, $\langle u_{synt}'^2 \rangle$ ni Python as

```
u2_synt=0
for t in range(1,nstep):
    for k in range(0,nk-1):
        u2_synt=u2_synt+ut[k,t]**2/nstep/nk
```

or in Matlab/Octave as

```
u2_synt=0;
for t=1:nstep
for k=1:nk
   u2_synt=u2_synt+ut(k,t)^2/nstep/nk;
end
end
```

It is much faster to use the Python command `u2_synt=np.var(ut)` or the Matlab commands, `u2_synt=mean(var(ut'))`. Now compare $\langle u_{synt}'^2 \rangle / \langle v_{synt}'^2 \rangle$ with the prescribed value `stress(1,1)/stress(2,2)`. The agreement is, with `nstep=500` within 2 percent. Increasing `nstep=500` leads to even better agreement.

Change the prescribed Reynolds tensor. The original choice is from channel data of $Re_\tau = 590$ at $y^+ \simeq 16$ where $\langle u'u' \rangle$ is largest. Let's take the Reynolds stress at $y^+ \simeq 116$ where

$$\langle v_i' v_j' \rangle = \left[\begin{array}{ccc} 2.96 & -0.77 & 0 \\ -0.77 & 1.04 & 0 \\ 0 & 0 & 1.55 \end{array} \right] \tag{W.4}$$

Change the `stress` variable in Chapter 1 in `synt_main_aniso.m` accordingly. Run the code. Make sure that the eigenvectors `v1_new` and `v2_new` are in the appropriate quadrants (see Chapter 2 in `synt_main_aniso.m`). Compare the anisotropic synthetic fluctuations with $\langle u'u' \rangle$.

So far we have used constant time-averaged fluctuations in space, i.e. we have assumed that the Reynolds stresses are not function of the space coordinate z in `synt_main_aniso.m`. One way to improve this is to scale the synthetic fluctuations with the turbulent kinetic energy, k_{RANS}, obtained from a RANS simulation or experiments. Download the file `k_RANS_4000.dat` which is k_{RANS} from a RANS simulation of channel flow at $Re_\tau = 4\,000$. Assume that `zp` in `synt_main_aniso.m` corresponds to the wall-normal coordinate in the channel. The `k_RANS_4000.dat` data have been interpolated to the `zp` coordinates and `max(zp)` corresponds to the center of the channel.

Make the profiles of the synthetic fluctuations the same as k_{RANS} by multiplying them with $k_{RANS}/k_{RANS,max}$. Then scale the synthetic fluctuations so that their kinetic energy, $k_{synt} = 0.5 \langle u'^2 + u'^2 + w'^2 \rangle$, is equal to k_{RANS}, i.e.

$$\int_0^h k_{synt} dz = \int_0^h k_{RANS} dz \tag{W.5}$$

where h denotes half channel height.

Above we have scaled the synthetic fluctuations with k. It is often better to scale them with the shear stress. This is done in Appendix X.

X MTF271, Assignment 5: synthetic anisotropic fluctuations using EARSM

In this assignment we will create anisotropic synthetic fluctuations. They will be scaled with a shear stress. We will solve the time-averaged Navier-Stokes for 2D fully-developed channel flow.

You can use Matlab, Octave or Python. Both Octave and Python are open-source software. Octave is a Matlab clone. Many large Swedish industries prefer engineers to use Python instead of Matlab due to Matlab's high license fees.

X.1 Mean flow

From the course www page
http://www.tfd.chalmers.se/~lada/comp_turb_model/
download `rans` and `tdma`. The Python or Matlab/octave script `rans` solves U with the PDH $k - \omega$ turbulence model [221]. Since the flow is fully developed 2D flow, it reduces to one dimension. Look at the code and try to understand what it is doing.

Open Python/Matlab/Octave and run the code. When the solution has converged, it program plots U and k as well as convergence history of k and ω (at a chosen point, `jmon`) and the wall shear stress. In this way you get an additional confirmation that the solution has converged.

At the end of `rans`, the results are written to file
`yp_u_k_om_vist_uv_yc_PDH_8000.dat`; the file includes seven columns with y (cell centers), U, k, ω, ν_t, $\overline{v'_1 v'_2}$ and y (grid lines).

X.2 Synthetic fluctuations

In this section, we will generate anisotropic synthetic fluctuations. The prodedure follows that given in [178].

1. A pre-cursor RANS simulation is made using `rans`

2. After having carried out the pre-cursor RANS simulation, the Reynolds stress tensor is computed using the EARSM model [36].

3. The Reynolds stress tensor is used as input for generating the anisotropic synthetic fluctuations. The integral length scale is set to 0.3δ.

4. Since the method of synthetic turbulence fluctuations assumes homogeneous turbulence, we can only use the Reynolds stress tensor in one point. We need to choose a relevant location for the Reynolds stress tensor. In a turbulent boundary layer, the Reynolds shear stress is by far the most important stress component. Hence, the Reynolds stress tensor is taken at the location where the magnitude of the turbulent shear stress is largest.

5. Finally, the synthetic fluctuations are scaled with $\left(|\overline{u'v'}| / |\overline{u'v'}|_{max} \right)^{1/2}_{RANS}$, which is obtain from the simulation with `rans`.

Download the files `angles`, `randf_1`, `randf_2`, `synt_main_earsm`.
The main code is `synt_main_earsm` for which some details are given below.

X.2.1   Chapter 1

- The file created by `rans` is read.

- The Reynolds shear stresses are computed using EARSM.

- The location where the magnitude of the shear stress is found (cell number 19).

- Using the stress tensor at cell number 19, the eigenvalues and the eigenvectors are computed.

X.2.2   Chapter 2-3

- Isotropic fluctuations are created in the directions of the eigenvectores (see Section W).

- The eigenvalues and the wavenumbers are scaled with the eigenvalues.

- The fluctuations are generated

X.3   Exercises

- Define your own channel flow case in `rans` (new Re number, new grid, . . .)

- Use another two-equation turbulence model, e.g. the standard Wilcox $k - \omega$ model. The model is presented in the report [26]. You can download it here

- Instead of using a two-equation turbulence model based on an eddy visacosity, use EARSM when solving the momentum equations. You find an implementation in the MSc thesis [222]. It can be downloaded here

- Compare isotropic and anisotropic fluctuations

- In `synt_main_earsm` we scale the fluctuations with the shear stress. In [147], the fluctuations are scaled with the modelled turbulent kinetic energy. Try this.
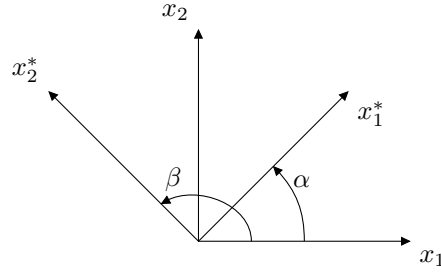
Figure Y.1: Transformation between the coordinate systems (x_{1*}, x_{2*}) and (x_1, x_2).

Y MTF271: Transformation of tensors

Y.1 Rotation from $x_{1*} - x_{2*}$ to $x_1 - x_2$

THE rotation of a vector from the x_{i*} coordinate system to x_i reads (see, e.g., Chapter 1 in [29])

$$u_i = b_{ij} u_{j*} \tag{Y.1}$$

where b_{ij} denotes the cosine between the axis

$$b_{ij} = \cos(x_i, x_{j*}) \tag{Y.2}$$

In Fig. Y.1, the b_{ij} is given by

$$
\begin{aligned}
b_{11} &= \cos\alpha, \quad b_{12} = \cos\beta = -\cos(\pi/2 - \alpha) = -\sin(\alpha) \\
b_{21} &= \cos(\pi/2 - \alpha) = \sin\alpha, \quad b_{22} = \cos\alpha
\end{aligned}
\tag{Y.3}
$$

The relations $b_{ik}b_{jk} = b_{ki}b_{kj} = \delta_{ij}$ are fulfilled as they should.

For a second-order tensor, the transformation reads

$$u_{ij} = b_{ik} b_{jm} u_{k*m*} \tag{Y.4}$$

As an example, set $\alpha = \pi/4$. Equation Y.3 gives

$$b_{11} = 1/\sqrt{2}, \quad b_{12} = -1/\sqrt{2}, \quad b_{21} = 1/\sqrt{2}, \quad b_{22} = 1/\sqrt{2} \tag{Y.5}$$

Inserting Eq. Y.5 into Eq. Y.4 gives

$$
\begin{aligned}
u_{11} &= b_{11}b_{11}u_{1*1*} + b_{12}b_{11}u_{2*1*} + b_{11}b_{12}u_{1*2*} + b_{12}b_{12}u_{2*2*} && \text{(Y.6a)} \\
&= \frac{1}{2}(u_{1*1*} - u_{2*1*} - u_{1*2*} + u_{2*2*}) \\
u_{12} &= b_{11}b_{21}u_{1*1*} + b_{12}b_{21}u_{2*1*} + b_{11}b_{22}u_{1*2*} + b_{12}b_{22}u_{2*2*} && \text{(Y.6b)} \\
&= \frac{1}{2}(u_{1*1*} - u_{2*1*} + u_{1*2*} - u_{2*2*}) \\
u_{21} &= b_{21}b_{11}u_{1*1*} + b_{22}b_{11}u_{2*1*} + b_{21}b_{12}u_{1*2*} + b_{22}b_{12}u_{2*2*} && \text{(Y.6c)} \\
&= \frac{1}{2}(u_{1*1*} + u_{2*1*} - u_{1*2*} - u_{2*2*}) \\
u_{22} &= b_{21}b_{21}u_{1*1*} + b_{22}b_{21}u_{2*1*} + b_{21}b_{22}u_{1*2*} + b_{22}b_{22}u_{2*2*} && \text{(Y.6d)} \\
&= \frac{1}{2}(u_{1*1*} + u_{2*1*} + u_{1*2*} + u_{2*2*})
\end{aligned}
$$

Y.2   Rotation from $x_1 - x_2$ to $x_{1*} - x_{2*}$

Now we do the same transformation as in Section Y.1 but backwards, i.e. from $x_1 - x_2$ to $x_{1*} - x_{2*}$. Consider fully developed flow in a channel, see Appendix D, for which

$$\frac{\partial v_1}{\partial x_1} = v_2 = 0 \tag{Y.7}$$

so that the strain-rate tensor, s_{ij}, reads

$$s_{11} = 0, \quad s_{12} = \frac{1}{2}\frac{\partial v_1}{\partial x_2}, \quad s_{21} = s_{12}, \quad s_{22} = 0 \tag{Y.8}$$

The x_1 and x_2 coordinates in Fig. Y.1 correspond now to the streamwise and wall-normal directions in the channel, respectively. Let the $x_{1*} - x_{2*}$ coordinate system denote the eigenvectors. The transformation from $x_1 - x_2$ to $x_{1*} - x_{2*}$ reads

$$s_{i*j*} = c_{ik}c_{jm}s_{km}, \quad c_{ij} = \cos(x_{i*}, x_j) \tag{Y.9}$$

where

$$\begin{aligned}c_{11} &= \cos\alpha, \quad c_{12} = \cos(\pi/2 - \alpha) = \sin\alpha\\ c_{21} &= \cos\beta = -\sin\alpha, \quad c_{22} = \cos\alpha\end{aligned} \tag{Y.10}$$

see Fig. Y.1. It can be seen that the relation $c_{ji} = b_{ij}$ is satisfied as it should. The eigenvectors for Eq. Y.8 are any two orthogonal vectors with angles $\pm\pi/4, \pm 3\pi/4$. Let us choose $\pi/4$ and $3\pi/4$ for which the transformation in Eq. Y.9 reads ($\alpha = \pi/4$)

$$s_{1*1*} = c_{11}c_{11}s_{11} + c_{12}c_{11}s_{21} + c_{11}c_{12}s_{12} + c_{12}c_{12}s_{22} \tag{Y.11a}$$

$$= \frac{1}{2}(s_{11} + s_{21} + s_{12} + s_{22})$$

$$s_{1*2*} = c_{11}c_{21}s_{11} + c_{12}c_{21}s_{21} + c_{11}c_{22}s_{12} + c_{12}c_{22}s_{22} \tag{Y.11b}$$

$$= \frac{1}{2}(-s_{11} - s_{21} + s_{12} + s_{22})$$

$$s_{2*1*} = c_{21}c_{11}s_{11} + c_{22}c_{11}s_{21} + c_{21}c_{12}s_{12} + c_{22}c_{12}s_{22} \tag{Y.11c}$$

$$= \frac{1}{2}(-s_{11} + s_{21} - s_{12} + s_{22})$$

$$s_{2*2*} = c_{21}c_{21}s_{11} + c_{22}c_{21}s_{21} + c_{21}c_{22}s_{12} + c_{22}c_{22}s_{22} \tag{Y.11d}$$

$$= \frac{1}{2}(s_{11} - s_{21} - s_{12} + s_{22})$$

The fully developed channel flow is obtained by inserting Eq. Y.8

$$s_{1*1*} = s_{12}, \quad s_{1*2*} = 0, \quad s_{2*1*} = 0, \quad s_{2*2*} = -s_{21} \tag{Y.12}$$

Since the off-diagonal elements are zero it confirms that the coordinate system $x_{1*} - x_{2*}$ with $\alpha = \pi/4$ is indeed a principal coordinate system. The eigenvalues, $\lambda^{(k)}$, of s_{ij} correspond to the diagonal elements in Eq. Y.12, i.e.

$$\lambda^{(1)} \equiv s_{1*1*} = s_{12} = \frac{1}{2}\frac{\partial v_1}{\partial x_2}, \quad \lambda^{(2)} \equiv s_{2*2*} = -s_{12} = -\frac{1}{2}\frac{\partial v_1}{\partial x_2} \tag{Y.13}$$

Y.3 Transformation of a velocity gradient

Consider the velocity gradient $A_{ij} = \partial v_i / \partial x_j$. Apply the transformation from the $x_1 - x_2$ system to the principal coordinate system $x_{1*} - x_{2*}$ in Eqs. Y.11a-Y.11d with $\alpha = \pi/4$

$$
\begin{aligned}
A_{1*1*} &= \frac{1}{2}(A_{11} + A_{21} + A_{12} + A_{22}) \\
A_{1*2*} &= \frac{1}{2}(-A_{11} - A_{21} + A_{12} + A_{22}) \\
A_{2*1*} &= \frac{1}{2}(-A_{11} + A_{21} - A_{12} + A_{22}) \\
A_{2*2*} &= \frac{1}{2}(A_{11} - A_{21} - A_{12} + A_{22})
\end{aligned}
\tag{Y.14}
$$

Insert Eq. Y.10 with $\alpha = \pi/4$ and replace A_{ij} by the velocity gradient use Eq. Y.7 (i.e. fully-developed channel flow)

$$
\frac{\partial v_{1*}}{\partial x_{1*}} = \frac{\partial v_{1*}}{\partial x_{2*}} = \frac{1}{2}\frac{\partial v_1}{\partial x_2}, \quad \frac{\partial v_{2*}}{\partial x_{1*}} = \frac{\partial v_{2*}}{\partial x_{2*}} = -\frac{1}{2}\frac{\partial v_1}{\partial x_2},
\tag{Y.15}
$$

It can be seen that $\partial v_{1*}/\partial x_{1*} = s_{1*1*}$ and $\partial v_{1*}/\partial x_{2*} + \partial v_{2*}/\partial x_{1*} = 2s_{1*2*} = 0$ (see Eqs. Y.13 and Y.15) as it should.

Z MTF271: Green's formulas

Ｉ N this appendix we will derive Green's three formulas from Gauss divergence law. In the last section we will derive the analytical solution to the Poisson equation. The derivations below are partly taken from [223].

Z.1 Green's first formula

Gauss divergence law reads

$$\int_V \frac{\partial F_i}{\partial x_i} dV = \int_S F_i n_i dS \tag{Z.1}$$

where S is the bounding surface of the volume, V, and n_i is the normal vector of S pointing out of V. Replacing F_i by $\varphi \dfrac{\partial \psi}{\partial x_i}$ gives

$$\int_V \frac{\partial}{\partial x_i} \left(\varphi \frac{\partial \psi}{\partial x_i} \right) dV = \int_S \varphi \frac{\partial \psi}{\partial x_i} n_i dS \tag{Z.2}$$

The left side is re-written as

$$\frac{\partial}{\partial x_i} \left(\varphi \frac{\partial \psi}{\partial x_i} \right) = \varphi \frac{\partial^2 \psi}{\partial x_i \partial x_i} + \frac{\partial \psi}{\partial x_i} \frac{\partial \varphi}{\partial x_i} \tag{Z.3}$$

which inserted in Eq. Z.2 gives

$$\int_V \varphi \frac{\partial^2 \psi}{\partial x_i \partial x_i} dV + \int_V \frac{\partial \psi}{\partial x_i} \frac{\partial \varphi}{\partial x_i} dV = \int_S \varphi \frac{\partial \psi}{\partial x_i} n_i dS \tag{Z.4}$$

This is Green's first formula.

Z.2 Green's second formula

Switching φ and ψ in Eq. Z.4 gives

$$\int_V \psi \frac{\partial^2 \varphi}{\partial x_i \partial x_i} dV + \int_V \frac{\partial \varphi}{\partial x_i} \frac{\partial \psi}{\partial x_i} dV = \int_S \psi \frac{\partial \varphi}{\partial x_i} n_i dS \tag{Z.5}$$

Subtract Eq. Z.5 from Z.4 gives

$$\int_V \left(\varphi \frac{\partial^2 \psi}{\partial x_i \partial x_i} - \psi \frac{\partial^2 \varphi}{\partial x_i \partial x_i} \right) dV = \int_S \left(\varphi \frac{\partial \psi}{\partial x_i} - \psi \frac{\partial \varphi}{\partial x_i} \right) n_i dS \tag{Z.6}$$

This is Green's second formula.

Z.3 Green's third formula

In Green's second formula, Eq. Z.6, set

$$\psi(\mathbf{r}) = \frac{1}{|\mathbf{r} - \mathbf{r}_P|} \tag{Z.7}$$

As usual we are considering a volume V with bounding surface S and normal vector n_i. Since function $\psi(\mathbf{r})$ is singular for $\mathbf{r} = \mathbf{r}_P$, consider a small sphere in V, see Fig. Z.1.
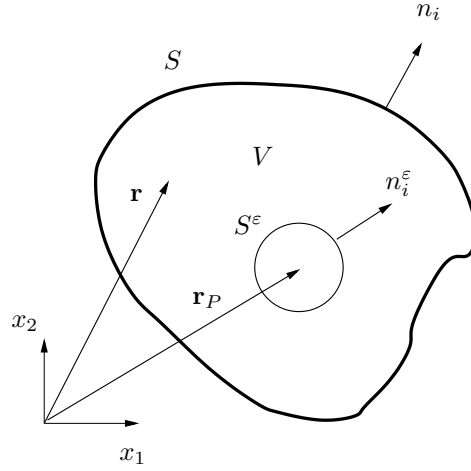
Figure Z.1: Green's third formula. A volume V with bounding surface S with normal vector n_i. In V there is a small sphere S^ε located at $\mathbf{r}_P$ with radius ε and normal vector n_i^ε.

In Eq. Z.6 we need the first and the second derivative of ψ. The first derivative of $1/r_i$ is computed as

$$\frac{\partial}{\partial x_i}\left(\frac{1}{r}\right) = -\frac{\partial r/\partial x_i}{r^2} = -\frac{r_i}{r^3} \tag{Z.8}$$

since the derivative of a distance X is a vector along the increment of the distance, i.e. $\partial X/\partial x_i = X_i/X$ where $X = |X_i|$. The second derivative is obtained as

$$\begin{aligned}
\frac{\partial^2}{\partial x_i \partial x_i}\left(\frac{1}{r}\right) &= -\frac{\partial}{\partial x_i}\left(\frac{r_i}{r^3}\right) = -\frac{\partial r_i}{\partial x_i}\left(\frac{1}{r^3}\right) + \frac{\partial r}{\partial x_i}\left(\frac{3r_i}{r^4}\right) \\
&= -3\left(\frac{1}{r^3}\right) + \frac{r_i}{r}\left(\frac{3r_i}{r^4}\right) = -\frac{3}{r^3} + \frac{r^2}{r}\left(\frac{3}{r^4}\right) = 0
\end{aligned} \tag{Z.9}$$

To get the right side on the second line we used the fact that $r_i r_i = r^2$. Now we replace $r_i = \mathbf{r}$ by $\mathbf{r} - \mathbf{r}_P = r_i - r_{P,i}$ in Eqs. Z.8 and Z.9 which gives

$$\begin{aligned}
\frac{\partial}{\partial x_i}\left(\frac{1}{|\mathbf{r} - \mathbf{r}_P|}\right) &= -\frac{r_i - r_{P,i}}{|\mathbf{r} - \mathbf{r}_P|^3} \\
\frac{\partial^2}{\partial x_i \partial x_i}\left(\frac{1}{|\mathbf{r} - \mathbf{r}_P|}\right) &= 0
\end{aligned} \tag{Z.10}$$

for $r_i \neq r_i^P$, i.e. for V excluding the sphere S^ε, see Fig. Z.1. Apply Green's second formula for this volume which has the bounding surfaces S and S^ε with normal vectors n_i (outwards) and n_i^ε (inwards), respectively. We get

$$\begin{aligned}
-\int_{V-S^\varepsilon} \frac{1}{|\mathbf{r} - \mathbf{r}_P|}\frac{\partial^2 \varphi}{\partial x_i \partial x_i} dV &= \int_S \left(-\varphi\frac{r_i - r_i^P}{|\mathbf{r} - \mathbf{r}_P|^3} - \frac{1}{|\mathbf{r} - \mathbf{r}_P|}\frac{\partial \varphi}{\partial x_i}\right) n_i dS \\
&+ \underbrace{\int_{S^\varepsilon} \left(-\varphi\frac{r_i - r_i^P}{|\mathbf{r} - \mathbf{r}_P|^3} - \frac{1}{|\mathbf{r} - \mathbf{r}_P|}\frac{\partial \varphi}{\partial x_i}\right)(-n_i^\varepsilon) dS}_{I_{S*}}
\end{aligned} \tag{Z.11}$$

where the volume integral is taken over the volume V but excluding the sphere S^ε, i.e. $V - S^\varepsilon$. Note the minus sign in front of the normal vector in the S^ε integral; this is

because the normal vector must point *out* of the volume $V - S^\varepsilon$, i.e. into the sphere, S^ε. In the sphere the normal vector, n_i^ε, correspond to the direction from point $\mathbf{r}_P$, i.e.

$$n_i^\varepsilon = \frac{\mathbf{r} - \mathbf{r}_P}{|\mathbf{r} - \mathbf{r}_P|} = \frac{r_i - r_{P,i}}{|r_i - r_{P,i}|} \tag{Z.12}$$

where we have normalized the vector $r_i - r_{P,i}$ in order to make its length equal to one. The length of the vector $r_i - r_{P,i}$ is the radius of sphere S^ε, i.e.

$$|\mathbf{r} - \mathbf{r}_P| = \varepsilon \tag{Z.13}$$

The surface area, dS, for sphere S^ε can be expressed in spherical coordinates as

$$dS = \varepsilon^2 \Omega = \varepsilon^2 \sin\theta d\theta d\alpha \tag{Z.14}$$

where Ω is the solid angle. Inserting Eqs. Z.12, Z.13 and Z.14 in the last integral in Eq. Z.11 gives

$$I_{S^\varepsilon} = \int_{S^\varepsilon} \left(\frac{\varphi}{\varepsilon^2} + \frac{r_i - r_{P,i}}{\varepsilon^2} \frac{\partial\varphi}{\partial x_i} \right) \varepsilon^2 d\Omega = \int_{S^\varepsilon} \left(\varphi + (r_i - r_{P,i}) \frac{\partial\varphi}{\partial x_i} \right) d\Omega \quad \text{(Z.15)}$$

To re-write this integral we will use the *mean value theorem* for integrals. In one dimension this theorem simply states that for the integral of a function, $g(x)$, over an interval $[a, b]$, there exists (at least) on point for which the the relation

$$\int_a^b g(x)dx = (a - b)g(x_Q) \tag{Z.16}$$

holds, where x_Q denotes a point on $[a, b]$. Applying this theorem to the integral in Eq. Z.15 gives

$$I_{S^\varepsilon} = \varphi(\mathbf{r}_Q) \int_{S^\varepsilon} d\Omega + \left[r_{Q,i} - r_{P,i}) \frac{\partial\varphi}{\partial x_i} (\mathbf{r}_Q) \right] \int_{S^\varepsilon} d\Omega \tag{Z.17}$$

where $\mathbf{r}_Q \equiv r_{Q,i}$ denotes a point on S^ε. As we let $Q \to P$, the radius, ε, of sphere S^ε goes to zero so that the integral in Eq. Z.17 reads

$$\lim_{\varepsilon \to 0} I_{S^\varepsilon} = 4\pi\varphi(\mathbf{r}_Q) \tag{Z.18}$$

since $\int_{S^\varepsilon} d\Omega = 4\pi$. Inserted in Eq. Z.11 gives

$$\varphi(\mathbf{r}_P) = -\frac{1}{4\pi} \int_V \frac{1}{|\mathbf{r} - \mathbf{r}_P|} \frac{\partial^2\varphi}{\partial x_i \partial x_i} dV$$
$$+ \frac{1}{4\pi} \int_S \varphi \frac{r_i - r_i^P}{|\mathbf{r} - \mathbf{r}_P|^3} n_i dS + \frac{1}{4\pi} \int_S \frac{1}{|\mathbf{r} - \mathbf{r}_P|} \frac{\partial\varphi}{\partial x_i} n_i dS \tag{Z.19}$$

This is Green's third formula.

The singularity $1/|\mathbf{r} - \mathbf{r}_P|$ in the volume integral in Eq. Z.19 is not a problem. Consider a small sphere with radius $r = |\mathbf{r}_a - \mathbf{r}_P|$ centered at point P. In spherical coordinates the volume element can then be expressed as

$$dV = r^2 \sin\theta dr d\theta d\alpha = r^2 dr d\Omega \tag{Z.20}$$

Hence it is seen that volume element dV goes to zero faster than the singularity $1/|\mathbf{r} - \mathbf{r}_P|$.

Z.4   Analytical solution to Poisson's equation

Poisson's equation reads

$$\frac{\partial^2 \varphi}{\partial x_j \partial x_j} = f \tag{Z.21}$$

where we assume that φ goes to zero at infinity and that the right side is limited. Green's third formula, Eq. Z.19, gives

$$
\begin{aligned}
\varphi(\mathbf{r}_P) = & -\frac{1}{4\pi} \int_V \frac{f(\mathbf{r})}{|\mathbf{r} - \mathbf{r}_P|} dV \\
& + \frac{1}{4\pi} \int_S \varphi \frac{r_i - r_i^P}{|\mathbf{r} - \mathbf{r}_P|^3} n_i dS + \frac{1}{4\pi} \int_S \frac{1}{|\mathbf{r} - \mathbf{r}_P|} \frac{\partial \varphi}{\partial x_i} n_i dS
\end{aligned}
\tag{Z.22}
$$

We choose the volume as a large sphere with radius R. Using Eqs. Z.12, Z.13 and Z.14, the first surface integral can be written as

$$\frac{1}{4\pi} \int_S \varphi \frac{r_i - r_i^P}{|\mathbf{r} - \mathbf{r}_P|^3} n_i dS = \frac{1}{4\pi R^2} \int_S \varphi n_i n_i dS = \frac{1}{4\pi} \int_S \varphi d\Omega \tag{Z.23}$$

using $n_i n_i = 1$. This integral goes to zero for large R since $\varphi \to 0$ as $R \to \infty$.

The second surface integral in Eq. Z.22 can be re-written using Eq. Z.13, Gauss divergence law and Eq. Z.21 as

$$
\begin{aligned}
\frac{1}{4\pi} \int_S \frac{1}{|\mathbf{r} - \mathbf{r}_P|} \frac{\partial \varphi}{\partial x_i} n_i dS & = \frac{1}{4\pi R} \int_S \frac{\partial \varphi}{\partial x_i} n_i dS \\
& = \frac{1}{4\pi R} \int_S \frac{\partial^2 \varphi}{\partial x_i \partial x_i} dV = \frac{1}{4\pi R} \int_V f dV
\end{aligned}
\tag{Z.24}
$$

This integral also goes to zero for large R since we have assumed that f is limited. Hence the final form of Eq. Z.22 reads

$$\varphi(\mathbf{r}_P) = -\frac{1}{4\pi} \int_V \frac{f(\mathbf{r})}{|\mathbf{r} - \mathbf{r}_P|} dV \tag{Z.25}$$

This is the analytical solution to Poisson's equation, Eq. Z.21.

AA   MTF271: Learning outcomes for 2020

Lecture 1-2

1. How is the buoyancy term, ρg_i, re-written in incompressible flow?

2. Show the principles how to derive the transport equation for $\overline{v'_i v'_j}$, Eq. 11.11 (see Section 11.2 on p. 121)

3. Derive the transport equation of $\overline{v'_i v'_j}$, Eq. 11.11 (see Section 9)

4. Given the transport equation of $\overline{v'_i v'_j}$, Eq. 11.11, derive the exact k equation (Eq. 11.4)

5. Given the transport equation for the temperature, θ, and the transport equation for $\bar{\theta}$, show the principles (in the same way as is done for the $\overline{v'_i v'_j}$ equation on Section 11.2 on p. 121) how to derive the transport equation for $\overline{v'_i \theta'}$, Eq. 11.22. Discuss the physical meaning of the different terms. Which terms need to be modeled?

6. What is the expression for the total heat flux that appears in the $\bar{\theta}$ equation?

7. Which terms in the $\overline{v'_i v'_j}$ equation need to be modeled? Explain the physical meaning of the different terms in the $\overline{v'_i v'_j}$ equation.

8. Show how the turbulent diffusion (i.e. the term which includes the triple correlation) in the k equation is modeled.

9. How is the production term modeled in the $k - \varepsilon$ model? Show how it can be expressed in $\bar{s}_{ij}$

10. Given the modeled k equation, derive the modeled ε equation.

11. Derive the Boussinesq assumption (see Section 11.6). How is the turbulent heat flux, $\overline{v'_i \theta'}$, modeled in the Boussinesq approach?

12. Discuss and show how the dissipation term, ε_{ij}, is modeled.

13. Use physical reasoning to derive a model for the diagonal components of the pressure-strain term (slow part).

14. Using physical reasoning, the model for the pressure-strain term above is formulated only for the normal streses. Show that if the model is expressed in the principal directions, then a model for the shear stress is also obtained.

15. The slow pressure-strain model reads $\Phi_{ij,1} = -c_1 \rho \frac{\varepsilon}{k} \left(\overline{v'_i v'_j} - \frac{2}{3} \delta_{ij} k \right)$. The anisotropy tensor is defined as $a_{ij} = \frac{\overline{v'_i v'_j}}{k} - \frac{2}{3} \delta_{ij}$. Show that for decaying grid turbulence, the model for the slow pressure-strain model indeed acts as to make the turbulence more isotropic if $c_1 > 1$.

16. Derive the exact Poisson equation for the pressure fluctuation, Eq. 11.65.

Lecture 3-4

1. For a Poisson equation

$$\frac{\partial^2 \varphi}{\partial x_j \partial x_j} = f$$

there exists an exact analytical solution

$$\varphi(\mathbf{x}) = -\frac{1}{4\pi} \int_V \frac{f(\mathbf{y})dy_1 dy_2 dy_3}{|\mathbf{y} - \mathbf{x}|} \qquad \text{(AA.1)}$$

Use Eqs. 11.65 and AA.1 to derive the exact analytical solution (Eq. 11.68) for the fluctuating pressure. Which are the "slow" and "rapid" terms? Why are they called "slow" and "rapid"?

2. Derive the algebraic stress model (ASM). What main assumption is made?

3. Show the physical reasoning leading to the modeled slow pressure strain term, $\Phi_{22,1w}$, for wall effects. What sign does it have? Give also the expressions for $\Phi_{11,1w}$ and $\Phi_{33,1w}$

4. The modeled slow and rapid pressure strain term read $\Phi_{ij,1} = -c_1 \rho \frac{\varepsilon}{k} \left(\overline{v_i' v_j'} - \frac{2}{3}\delta_{ij}k \right)$ and $\Phi_{ij,2} = -c_2 \left(P_{ij} - \frac{2}{3}\delta_{ij}P^k \right)$, respectively. Give the expression for the production terms, modeled pressure-strain terms and modeled dissipation terms for a simple boundary layer. In some stress equations there is no production terms nor any dissipation term. How come? Which is the main source term (or sink term) in these equations?

5. Describe the physical effect of stable stratification and unstable stratification on turbulence.

6. Consider buoyancy-dominated flow with x_3 vertically upwards. The production term for the $\overline{v_i' v_j'}$ and the $\overline{v_i' \theta'}$ equations read

$$G_{ij} = -g_i \beta \overline{v_j' \theta'} - g_j \beta \overline{v_i' \theta'}, \quad P_{i\theta} = -\overline{v_i' v_k'}\frac{\partial \bar{\theta}}{\partial x_k}$$

respectively (we assume that the velocity gradient is negligible). Show that the Reynolds stress model dampens and increases the vertical fluctuation in stable and unstable stratification, respectively, as it should. Show also that k in the $k - \varepsilon$ model is affected in the same way.

7. Watch the on-line lecture *Turbulence* (20 minutes into the movie) at
   http://www.tfd.chalmers.se/~lada/MoF/flow_viz.html

   i. Consider the flow in the channel where the fluid on the top (red) and the bottom (yellow) are separated by a horizontal partition. The two fluids are identical. Study how the two fluids mix downstream of the partition. In the next example, the fluid on the top is hot (yellow) and light, and the one at the bottom (dark blue) is cold (heavy); how do the fluids mix downstream of the partition, better or worse than in the previous example? This flow situation is called *stable stratification*. In the last example, the situation is reversed: cold, heavy fluid (dark blue) is moving on top of hot, light fluid

(yellow). How is the mixing affected? This flow situation is called *unstable stratification*. Compare in meteorology where heating of the ground may cause unstable stratification or when *inversion* causes stable stratification.

8. Consider streamline curvature for a streamline formed as a circular arc (convex curvature). Show that the turbulence is dampened if $\partial v_\theta / \partial r > 0$ and that it is enhanced if the sign of $\partial v_\theta / \partial r$ is negative.

9. Streamline curvature: now consider a boundary layer where the streamlines are curved away from the wall (concave curvature). Show that the Reynolds stress model gives an enhanced turbulence production (as it should) because of positive feedback between the production terms. Why is the effect of streamline curvature in the $k - \varepsilon$ model much smaller?

10. Consider stagnation flow. Show that in the Reynolds stress model, there is only a small production of turbulence whereas eddy-viscosity models (such as the $k - \varepsilon$ model) give a large production of turbulence.

11. What is a realizability constraint? There are two main realizability constraints, one on the normal and one on the shear stresses: give the form of these constraints.

12. Show that the Boussinesq assumption may give negative normal stresses. In which coordinate system is the risk largest for negative normal stresses? Derive an expression (2D) how to avoid negative normal stresses by reducing the turbulent viscosity (Eq. 13.12).
    <u>Hint:</u> the eigenvalues, λ_1, λ_2, are obtained from $|\bar{s}_{ij} - \delta_{ij}\lambda| = 0$, $I_2^{2D} = \frac{1}{2}(C_{ii}C_{jj} - C_{ij}C_{ij})$

13. What is a non-linear eddy-viscosity model? When formulating a non-linear model, the anisotropy tensor $a_{ij} = -2\nu_t \bar{s}_{ij}/k$ is often used. The three terms read

$$c_1 \tau^2 \left(\bar{s}_{ik}\bar{s}_{kj} - \frac{1}{3}\bar{s}_{\ell k}\bar{s}_{\ell k}\delta_{ij} \right)$$
$$+c_2 \tau^2 \left(\bar{\Omega}_{ik}\bar{s}_{kj} - \bar{s}_{ik}\bar{\Omega}_{kj} \right)$$
$$+c_3 \tau^2 \left(\bar{\Omega}_{ik}\bar{\Omega}_{jk} - \frac{1}{3}\bar{\Omega}_{\ell k}\bar{\Omega}_{\ell k}\delta_{ij} \right)$$

Show that each term has the same properties as a_{ij}, i.e. non-dimensional, traceless and symmetric.

Lecture 5

1. Which equations are solved in the V2F model?

2. The transport equation for $\overline{v_2'^2}$ reads (the turbulent diffusion term is modeled)

$$\frac{\partial \rho \bar{v}_1 \overline{v_2'^2}}{\partial x_1} + \frac{\partial \rho \bar{v} \overline{v_2'^2}}{\partial x_2} = \frac{\partial}{\partial x_2}\left[(\mu + \mu_t)\frac{\partial \overline{v_2'^2}}{\partial x_2}\right] \underbrace{-2\overline{v_2'\partial p'/\partial x_2}}_{\rho \Phi_{22}} -\rho \varepsilon_{22}$$

   Show how this equation is re-written in the V2F model.

3. The f equation in the V2F model reads

$$L^2 \frac{\partial^2 f}{\partial x_2^2} - f = -\frac{\Phi_{22}}{k} - \frac{1}{T}\left(\frac{\overline{v_2'^2}}{k} - \frac{2}{3}\right), \quad T \propto \frac{k}{\varepsilon}, \quad L \propto \frac{k^{3/2}}{\varepsilon}$$

   Explain how the magnitude of the right side and L affect f (Fig 15.1). How does f enter into the $\overline{v_2'^2}$ equation? Show that far from the walls, the V2F model (i.e. the f and the $\overline{v_2'^2}$ equation) returns to the $\overline{v_2'^2}$ equation in the Reynolds stress model. In the V2F model, the v^2 equation is solved: what is the difference between $\overline{v_2'^2}$ and v^2 (see the discussion in connection to Eq. 15.9)?

4. What does the acronym SST mean? The SST model is a combination of the $k - \varepsilon$ and the $k - \omega$ model. In which region is each model used and why? How is ω expressed in k and ε?

5. Derive a transport equation for ω from the k and ε transport equations; you only need to do the production, the destruction and the viscous diffusion terms.

6. In the SST model, two blending function, F_1 and F_2, are used; explain what is the object of F_1 or F_2.

7. What is the purpose of the shear stress limiter in the SST model? Show that the eddy-viscosity assumption gives too high a shear stress in APG since $P^k/\varepsilon \gg 1$ (Eq. 16.15).

Lecture 6

1. What characterizes turbulence? Explain the characteristics. What is a turbulent eddy?

2. Explain the cascade process. How large are the largest scales? What is dissipation? What dimensions does it have? Which eddies extract energy from the mean flow? Why are these these eddies "best" at extracting energy from the mean flow?

3. What are the Kolmogorov scales? Use dimensional analysis to derive the expression for the velocity scale, v_η, the length scale, ℓ_η and the time scale, τ_η.

4. Make a figure of the energy spectrum. The energy spectrum consists of three subregions: which? describe their characteristics. Show the flow of turbulent kinetic energy in the energy spectrum. Given the energy spectrum, $E(\kappa)$, how is the turbulent kinetic energy, k, computed? Use dimensional analysis to derive the $-5/3$ Kolmogorov law.

5. What does isotropic turbulence mean? What about the shear stresses?

6. How is the energy transfer from eddy-to-eddy, ε_κ, estimated? Show how the ratio of the large eddies to the dissipative eddies depends on the Reynolds number (see Eq. 5.16).

7. Show how the ratio of the large eddies to the dissipative eddies depends on the Reynolds number (see Eq. 5.16). Using these estimations, you can show how the number of cells in DNS (Direct Numerical Simulations) depends on Reynolds number (see eBook).

Lecture 7

1. Show the difference between volume averaging (filtering) in LES and time-averaging in RANS. Show that avereging once or twice is different in RANS and LES.

2. Consider the spatial derivative of the pressure in the filtered Navier-Stokes: show that the derivative can be moved outside the filtering integral (it gives an additional second-order term).

3. The filtered non-linear term has the form

$$\overline{\frac{\partial v_i v_j}{\partial x_j}}$$

Show that it can be re-written as

$$\frac{\partial \bar{v}_i \bar{v}_j}{\partial x_j}$$

giving an additional term

$$-\frac{\partial}{\partial x_j}(\overline{v_i v_j}) + \frac{\partial}{\partial x_j}(\bar{v}_i \bar{v}_j) = -\frac{\partial \tau_{ij}}{\partial x_j}$$

on the right side.

4. Consider a 1D finite volume grid. Carry out a second filtering of $\bar{v}$ at node I and show that $\bar{\bar{v}}_I \neq \bar{v}_I$.

5. Consider the energy spectrum. Show the three different regions (the large energy-containing scales, the $-5/3$ range and the dissipating scales). Where should the cut-off be located? Show where the SGS scales, grid (i.e resolved) scales and the cut-off, κ_c are located in the spectrum.

6. Show how a sinus wave $\sin(\kappa_c x)$ corresponding to cut-off is represented on a grid with two and four cells, respectively. How is κ_c related to the grid size Δx for these cases?

7. Watch the on-line lecture *Turbulence* at
   http://www.tfd.chalmers.se/~lada/MoF/flow_viz.html

8. Taking guidance from the RANS k equation, formulate the one-equation k_{sgs} equation

9. Derive the Smagorinsky model in two different ways (Sections 18.6 and 18.22)

10. Consider the energy spectrum and discuss the physical meaning of $P_{k_{sgs}}$ and ε_{sgs}.

11. Discuss the energy path in connection to the source and sink terms in the $\bar{k}$, $\bar{K}$ and the k_{sgs} equations, see Figs. Q.4 and Q.5.

12. Show how the velocity is decomposed in DNS and LES, both in physical space and wavennumber space (i.e. how are k, $\bar{k}$ and k_{sgs} computed from the energy spectrum?).

Lecture 8

1. Consider the dynamic model. What is a test filter? Grid and test filter Navier-Stokes equation and derive the relation

$$\widehat{\overline{v_i \bar{v}_j}} - \widehat{\overline{v}}_i \widehat{\overline{v}}_j + \widehat{\mathcal{T}}_{ij} = \mathcal{L}_{ij} + \widehat{\mathcal{T}}_{ij} = T_{ij} \qquad (AA.2)$$

Draw an energy spectrum and show which wavenumber range $\bar{k}$, k_{sgs}, $k_{sgs,test}$ cover.

2. Formulate the Smagorinsky model for the grid filter SGS stress, τ_{ij}, and the test filter SGS stress, T_{ij}. Use Eq. AA.2 and derive the relation [13]

$$\mathcal{L}_{ij} - \frac{1}{3}\delta_{ij}\mathcal{L}_{kk} = -2C\left(\widehat{\Delta}^2 |\widehat{\bar{s}}|\widehat{\bar{s}}_{ij} - \overline{\Delta^2|\bar{s}|\bar{s}_{ij}}\right)$$

3. The equation you derived above is a tensor equation for C. Use this relation and derive the final expression for the dynamic coefficient, C, Eq. 18.41.

4. Show that when a first-order upwind schemes is used for the convection term, an additional diffusion term and dissipation terms appear because of a numerical SGS viscosity

Lecture 9

1. We usually define the SGS stress tensor as $\tau_{ij} = \overline{v_i' v_j'} - \bar{v}_i \bar{v}_j$. In scale-similarity models, τ_{ij} is written as three different terms. Derive these three terms. What are they called? What does the word "scale-similar" mean? Two of the terms are not Galilean invariant: which ones? What *is* Galilean invariance?

2. Explain and discuss the two-point correlation and auto-correlation. How are the integral length and timescale defined?

3. What are the five main differences between a RANS finite volume CFD code and a LES finite volume CFD code? What do you need to consider in LES when you want to compute time-averaged quantities? (see Fig. 18.12). How can the integral time scale, T_{int}, be used?(see Section M.3)

4. When doing LES, how fine does the mesh need to be in the near-wall region? Why does it need to be that fine?

5. Describe URANS. How is the instantaneous velocity decomposed? What turbulence models are used? What is scale separation?

6. Mention four different ways to estimate the resolution of an LES that you have made; see Section 18.26 Which method is good/bad? Which is best?

7. What is DES? The destruction term in the RANS S-A model reads $\left(\dfrac{\tilde{\nu}_t}{d}\right)^2$; how is it computed in the S-A DES model?

---

[13] note that the test filter here covers Δ^2 (which is correct); Eq. 18.38 is not correct

8. How is the length scale computed in a $k - \varepsilon$ two-equation DES model? Where in a boundary layer does the DES model switch from RANS to LES?

9. The modified (reduced) length scale in two-equation DES models can be introduced in different ways. It it usually introduced in one transport equation. Which one and which term? Apart from this transport equation, it is sometimes used in a another equation. Which one? What is the effect on the modeled, turbulent quantities?

Lecture 10

1. Give a brief description of the $k - \omega$ SST DES model.

2. What is DDES? Why was it invented?

3. Describe hybrid LES-RANS based on a one-equation model.

4. Describe the SAS model. How is the von Kármán length scale defined? An additional source term is introduced in the ω equation: what is the form of this term? Describe how this source reduces the turbulent viscosity. When is the term large and small, respectively?

Lecture 11

1. What is the physical meaning of f_k in PANS?

2. Derive the PANS model.

3. The PANS equations are given in Eqs. 23.19. Assume that $f_\varepsilon = 1$. Consider the destruction term in the ε equation and the coefficient $C_{\varepsilon 2}^*$. Explain what happens if f_k is reduced from 1 (RANS mode) to $f_k = 0.4$ (LES mode).

4. Consider the PANS model: in the derivation, we assumed that f_k is constant. Relaxing that condition is useful when presccribing k and ε prescribed at inlet and at embedded RANS/LES interfaces. Derive the additional term in the k equation (Eq. 23.24). Show that the the sign of the gradient at the inlet (and embedded interface) does indeed give a reduction of k as it should.

Lecture 12

1. Give a short description of the method to generate synthetic turbulent inlet fluctuations; see Chapter 27 and first 13 slides in
   http://www.tfd.chalmers.se/~lada/slides/slides_inlet.pdf
   What form on the spectrum is assumed? How is the wavenumber, κ_e, for the energy-containing eddies, determined? How are the maximum and minimum wavelengths, κ_{max}, κ_{min}, determined? With this method, the generated shear stress is zero: why? How is the correlation in time achieved?

2. What is embedded LES? Give an example when we may use it.

AB   References

[1] J. N. Reddy. *An Introduction to Continuum Mechanics*. Cambridge University Press, New York, 2008.

[2] M. Ekh. Mechanics of solids & fluids – introduction to continuum mechanics. Report, Div. of Material and Computational Mechanics, Dept. of Applied Mechanics, Chalmers University of Technology, Göteborg, Sweden, 2017.

[3] H. Abedi. *Development of Vortex Filament Method for Wind Power Aerodynamics*. PhD thesis, Div. of Fluid Dynamics, Dept. of Applied Mechanics, Chalmers University of Technology, Göteborg, Sweden, 2016.

[4] J. Wojtkowiak and C.O. Popiel. Inherently linear annular-duct-type laminar flowmeter. *Journal of Fluids Engineering*, 128(1):196–198, 2006.

[5] H. Blasius. *Grenzschichten in Flüssigkeiten mit kleiner Reibung*. PhD thesis, University of Göttingen, Göttingen, Germany, 1907.

[6] W. H. Hager. Blasius: A life in research and education. *Experiments in Fluids*, 34:566–571, 2003.

[7] S. G. Krantz. *A Guide to Complex Variables*. Cambridge University Press, 2007.

[8] L. Qu, Ch. Norberg, L. Davidson, S.-H. Peng, and F. Wang. Quantitative numerical analysis of flow past a circular cylinder at Reynolds number between 50 and 200. *Journal of Fluids and Structures*, 39:347–370, 2013.

[9] S. Hong and T. Asai. Effect of panel shape of soccer ball on its flight characteristics. *Scientific Reports*, 4(5068), 2014.

[10] W. Zhang, R. Bensow, M. Golubev, and V Chernoray. Flow past a rotating finite length cylinder: numerical and experimental study. In *51st AIAA Aerospace Sciences Meeting including the New Horizons Forum and Aerospace Exposition, AIAA 2013-0987*, 2012.

[11] H. Abedi. Development of vortex filament method for aerodynamic loads on rotor blades. Thesis for licentiate of engineering, Div. of Fluid Dynamics, Dept. of Applied Mechanics, Chalmers University of Technology, Göteborg, Sweden, 2013.

[12] S. B. Pope. *Turbulent Flow*. Cambridge University Press, Cambridge, UK, 2001.

[13] H. Tennekes and J. L. Lumley. *A First Course in Turbulence*. The MIT Press, Cambridge, Massachusetts, 1972.

[14] P. Bradshaw. *Turbulence*. Springer-Verlag, Berlin, 1976.

[15] S. Hoyas and J. Jiménez. Scaling of the velocity fluctuations in turbulent channels up to $Re_\tau = 2003$. *Physics of Fluids A*, 18(011702), 2006.

[16] S. Hoyas and J. Jiménez. http://torroja.dmt.upm.es/ftp/channels/data/statistics/. 2006.

[17] Th. von Kármán. Mechanische ähnlichkeit und Turbulenz. *Nachrichten von der Gesellschaft der Wissenchaften zu Göttingen, Fachgruppe 1 (Mathematik)*, 5:58–76, 1930.

[18] J.M. Österlund. *Experimental Studies of Zero Pressure-Gradient Turbulent Boundary-Layer Flow*. PhD thesis, Department of Mechanics, Royal Institute of Technology, Stockholm, Sweden, 1999.

[19] M. Österlund, A.V. Johansson, H.M. Nagib, and M.H. Hites. Mean-flow characteristics of high Reynolds number turbulent boundary layers from two facilities. In *30th Fluid Dynamics Conference, 28 June-1 July, Norfolk, Virginia*, 1999.

[20] M. Österlund, A.V. Johansson, H.M. Nagib, and M.H. Hites. A note on the overlap region in turbulent boundary layers. *Physics of Fluids A*, 12(1):1–4, 2000.

[21] P. R. Spalart. Direct simulation of a turbulent boundary layer up to $R_\theta = 1410$. *Journal of Fluid Mechanics*, 187:61–98, 1988.

[22] A. A. Townsend. Equilibrium layers and wall turbulence. *Journal of Fluid Mechanics*, 11:97–120, 1961.

[23] L. Davidson. Transport equations in incompressible URANS and LES. Report 2006/01, Div. of Fluid Dynamics, Dept. of Applied Mechanics, Chalmers University of Technology, Göteborg, Sweden, 2006.

[24] K. Hanjalić. Advanced turbulence closure models: A view of current status and future prospects. *Int. J. Heat and Fluid Flow*, 15:178–203, 1994.

[25] D. C. Wilcox. *Turbulence Modeling for CFD*. DCW Industries, Inc., 5354 Palm Drive, La Cañada, California 91011, 2 edition, 1998.

[26] L. Davidson. An introduction to turbulence models. Technical Report 97/2, Dept. of Thermo and Fluid Dynamics, Chalmers University of Technology, Gothenburg, 1997.

[27] K. Hanjalić and B. E. Launder. A Reynolds stress model of turbulence and its application to thin shear flows. *Journal of Fluid Mechanics*, 52:609–638, 1972.

[28] J. C. Rotta. Statistische theorie nichthomogener turbulenz. *Zeitschrift für Physik*, 129:547–572, 1951.

[29] G. E. Mase. *Continuum Mechanics*. Schaum's Outline Series. McGraw-Hill, 1970.

[30] S. Fu, B. E. Launder, and D. P. Tselepidakes. Accomodating the effects of high strain rates in modelling the pressure-starin correlation. Technical Report TFD/87/5, UMIST, Mechanical Engineering Dept., 1987.

[31] B. E. Launder, G. J. Reece, and W. Rodi. Progress in the development of a Reynolds-stress turbulence closure. *Journal of Fluid Mechanics*, 68(3):537–566, 1975.

[32] D. Naot, A. Shavit, and M. Wolfshtein. Interactions between components of the turbulent velocity correlation tensor. *Israel J. Techn.*, 8:259, 1970.

[33] B. E. Launder. An introduction to single-point closure methodology. In T. B. Gatski, M.Y. Hussaini, and J. L. Lumpley, editors, *Simulation and Modeling of Turbulent Flows*, New York, 1996. Oxford University Press.

[34] M. M. Gibson and B. E. Launder. Ground effects on pressure fluctuations in the atmospheric boundary layer. *Journal of Fluid Mechanics*, 86:491–511, 1978.

[35] S. B. Pope. A more general effective-viscosity hypothesis. *Journal of Fluid Mechanics*, 472:331–340, 1975.

[36] S. Wallin and A. V. Johansson. A new explicit algebraic Reynolds stress model for incompressible and compressible turbulent flows. *Journal of Fluid Mechanics*, 403:89–132, 2000.

[37] A. J. Johansson and S. Wallin. A new explicit algebraic Reynolds stress model. In *Advances in Turbulence VI*, pages 31–34, Netherlands, 1996. Kluwer Academic Publishers.

[38] S. S. Girimaji. Fully-explicit and self-consistent algebraic Reynolds stress model. *Theoretical and Computational Fluid Dynamics*, 8:387–402, 1996.

[39] S. S. Girimaji. Improved algebraic Reynolds stress model for engineering flows. In W. Rodi and G. Bergeles, editors, *Engineering Turbulence Modelling and Measurements – ETMM3*, pages 121–129. Elsevier, 1996.

[40] S. Wallin. private communication. Dept. of Mechanics, KTH, 2017.

[41] A. A. Townsend. *The Structure of Turbulent Shear Flow*. Cambridge University Press, New York, second edition, 1976.

[42] G. Eitel-Amor, R. Orlu, and P. Schlatter. Simulation and validation of a spatially evolving turbulent boundary layers up to $Re_\theta = 8300$. *International Journal of Heat and Fluid Flow*, 47:57–69, 2014.

[43] J. Kim. The collaborative testing of turbulence models (organized by P. Bradshaw *et al.*). Data Disk No. 4 (also available at Ercoftac's www-server `http://fluindigo.mech.surrey.ac.uk/database`), 1990.

[44] V. C. Patel, W. Rodi, and G. Scheuerer. Turbulence models for near-wall and low Reynolds number flows: A review. *AIAA Journal*, 23:1308–1319, 1985.

[45] H. C. Chen and V. C. Patel. Near-wall turbulence models for complex flows including separation. *AIAA Journal*, 26:641–648, 1988.

[46] L. Davidson. Calculation of the turbulent buoyancy-driven flow in a rectangular cavity using an efficient solver and two different low reynolds number $k - \varepsilon$ turbulence models. *Numer. Heat Transfer*, 18:129–147, 1990.

[47] K. Abe, T. Kondoh, and Y. Nagano. A new turbulence model for predicting fluid flow and heat transfer in separating and reattaching flows - 1. Flow field calculations. *Int. J. Heat Mass Transfer*, 37(1):139–151, 1994.

[48] F. S. Lien and M. A. Leschziner. Low-Reynolds-number eddy-viscosity modelling based on non-linear stress-strain/vorticity relations. In W. Rodi and G. Bergeles, editors, *Engineering Turbulence Modelling and Experiments 3*, pages 91–100. Elsevier, 1996.

[49] N. N. Mansour, J. Kim, and P. Moin. Reynolds-stress and dissipation-rate budgets in a turbulent channel flow. *Journal of Fluid Mechanics*, 194:15–44, 1988.

[50] B. E. Launder and B. T. Sharma. Application of the energy dissipation model of turbulence to the calculation of flow near a spinning disc. *Lett. Heat and Mass Transfer*, 1:131–138, 1974.

[51] C. G. Speziale, R. Abid, and E. C. Anderson. Critical evaluation of two-equation models for near-wall turbulence. *AIAA Journal*, 30:324–331, 1992.

[52] P. Bradshaw. Effects of streamline curvature on turbulent flow. Agardograph progress no. 169, AGARD, 1973.

[53] W. Rodi and G. Scheuerer. Calculation of curved shear layers with two-equation turbulence models. *Physics of Fluids*, 26:1422–1435, 1983.

[54] B. E. Thompson and J. H. Whitelaw. Characteristics of a trailing-edge flow with turbulent boundary-layer separation. *Journal of Fluid Mechanics*, 157:305–326, 1985.

[55] L. Davidson. Prediction of the flow around an airfoil using a Reynolds stress transport model. *Journal of Fluids Engineering*, 117:50–57, 1995.

[56] P. A. Durbin. On the $k - 3$ stagnation point anomaly. *International Journal of Heat and Fluid Flow*, 17:89–90, 1996.

[57] J. Hult. *Cartesiska tensorer: Ett praktiskt fikonspråk*. Almqvist & Wiksell, 1972.

[58] J. L. Lumley. Computational modeling of turbulent flows. *Advances in Applied Mechanics*, 18:123–176, 1978.

[59] T. J. Craft and B. E. Launder. A Reynolds stress closure designated for complex geometries. *International Journal of Heat and Fluid Flow*, 17(3):245–254, 1996.

[60] T. J. Craft, B. E. Launder, and K. Suga. Prediction of turbulent transitional phenomena with a nonlinear eddy-viscosity model. *International Journal of Heat and Fluid Flow*, 18:15–28, 1997.

[61] T. B. Gatski and C. G. Speziale. On explicit algebraic stress models for complex turbulent flows. *Journal of Fluid Mechanics*, 154:59–78, 1993.

[62] T.-H. Shih, J. Zhu, and J. L. Lumley. A new Reynolds stress algebraic equation model. *Comput. Methods Appl. Engng.*, 125:287–302, 1995.

[63] P. A. Durbin. Near-wall turbulence closure modeling without damping functions. *Theoretical and Computational Fluid Dynamics*, 3:1–13, 1991.

[64] P. A. Durbin. Application of a near-wall turbulence model to boundary layers and heat transfer. *International Journal of Heat and Fluid Flow*, 14(4):316–323, 1993.

[65] A. Sveningsson. Analysis of the performance of different $\overline{v^2} - f$ turbulence models in a stator vane passage flow. Thesis for licentiate of engineering, Dept. of Thermo and Fluid Dynamics, Chalmers University of Technology, Göteborg, Sweden, 2003.

[66] K. Hanjalic, M. Popovacx, and M. Habziabdic. A robust near-wall elliptic relaxation eddy-viscosity turbulence model for CFD. *International Journal of Heat and Fluid Flow*, 2004.

[67] F-S Lien and G. Kalitzin. Computations of transonic flow with the v2f turbulence model. *International Journal of Heat and Fluid Flow*, 22(1):53–61, 2001.

[68] A. Sveningsson and L. Davidson. Assessment of realizability constraints in $\overline{v^2} - f$ turbulence models. *International Journal of Heat and Fluid Flow*, 25(5):785–794, 2004.

[69] A. Sveningsson and L. Davidson. Computations of flow field and heat transfer in a stator vane passage using the $\overline{v^2} - f$ turbulence model. Paper GT2004-53586, ASME TURBO EXPO 2004, Vienna, 2004.

[70] A. Sveningsson and L. Davidson. Computations of flow field and heat transfer in a stator vane passage using the $\overline{v^2} - f$ turbulence model. *Journal of Turbomachinery*, 127(3):627–634, 2005.

[71] A. Sveningsson. *Turbulence Transport Modelling in Gas Turbine Related Applications*. PhD thesis, Div. of Fluid Dynamics, Dept. of Applied Mechanics, Chalmers University of Technology, Göteborg, Sweden, 2006.

[72] L. Davidson, P. V. Nielsen, and A. Sveningsson. Modifications of the $v^2 - f$ model for computing the flow in a 3D wall jet. In K. Hanjalić, Y. Nagano, and M. J. Tummers, editors, *Turbulence Heat and Mass Transfer 4*, pages 577–584, New York, Wallingford (UK), 2003. begell house, inc.

[73] F. R. Menter. Two-equation eddy-viscosity turbulence models for engineering applications. *AIAA Journal*, 32:1598–1605, 1994.

[74] D. C. Wilcox. Reassessment of the scale-determining equation. *AIAA Journal*, 26(11):1299–1310, 1988.

[75] F. R. Menter. Influence of freestream values on $k - \omega$ turbulence model predictions. *AIAA Journal*, 30(6):1657–1659, 1992.

[76] A. Hellsten. New advanced $k - \omega$ turbulence model for high-lift aerodynamics. *AIAA Journal*, 43(9):1857–1869, 2005.

[77] J. Bredberg. On two-equation eddy-viscosity models. Report 01/8, can be downloaded from www.tfd.chalmers.se/~lada/allpaper.html, Dept. of Thermo and Fluid Dynamics, Chalmers University of Technology, 2001.

[78] P. Bradshaw, D. H. Ferriss, and N. P. Atwell. Calculation of boundary-layer development using the turbulent energy equation. *Journal of Fluid Mechanics*, 28:593–616, 1967.

[79] F. R. Menter, M. Kuntz, and R. Langtry. Ten years of industrial experience of the SST turbulence model. In K. Hanjalić, Y. Nagano, and M. J. Tummers, editors, *Turbulence Heat and Mass Transfer 4*, pages 624–632, New York, Wallingford (UK), 2003. begell house, inc.

[80] S. Ghosal and P. Moin. The basic equations for the large eddy simulation of turbulent flows in complex geometry. *J. Comp. Phys.*, 118:24–37, 1995.

[81] J. Smagorinsky. General circulation experiments with the primitive equations. *Monthly Weather Review*, 91:99–165, 1963.

[82] P. Moin and J. Kim. Numerical investigation of turbulent channel flow. *Journal of Fluid Mechanics*, 118:341–377, 1982.

[83] W. P. Jones and M. Wille. Large eddy simulation of a jet in a cross-flow. In *10th Symp. on Turbulent Shear Flows*, pages 4:1 – 4:6, The Pennsylvania State University, 1995.

[84] J. O. Hinze. *Turbulence*. McGraw-Hill, New York, 2nd edition, 1975.

[85] H. Schlichting. *Boundary-Layer Theory*. McGraw-Hill, New York, 7 edition, 1979.

[86] M. Germano, U. Piomelli, P. Moin, and W. H. Cabot. A dynamic subgrid-scale eddy viscosity model. *Physics of Fluids A*, 3:1760–1765, 1991.

[87] Y. Zang, R. L. Street, and J. R. Koseff. A dynamic mixed subgrid-scale model and its application to turbulent recirculating flows. *Physics of Fluids A*, 5:3186–3196, 1993.

[88] D. K. Lilly. A proposed modification of the Germano subgrid-scale closure method. *Physics of Fluids A*, 4:633–635, 1992.

[89] J. P. Boris, F. F. Grinstein, E. S. Oran, and R. L. Kolbe. New insights into large eddy simulation. *Fluid Dynamic Research*, 10:199–228, 1992.

[90] J. Bardina, J. H. Ferziger, and W. C. Reynolds. Improved subgrid scale models for large eddy simulation. AIAA 80-1357, Snomass, Colorado, 1980.

[91] C. G. Speziale. Galilean invariance of subgrid-scale stress models in the large-eddy simulation of turbulence. *Journal of Fluid Mechanics*, 156:55–62, 1985.

[92] M. Germano. A proposal for a redefinition of the turbulent stresses in the filtered Navier-Stokes equations. *Phys. Fluids A*, 7:2323–2324, 1986.

[93] L. Davidson. A dissipative scale-similarity model. In V. Armenio, B. Geurts, and J. Fröhlich, editors, *DLES7: Direct and Large-Eddy Simulations 7*, volume 13 of *ERCOFTAC series*, pages 261–266, 2010.

[94] C. Hirsch. *Numerical Computation of Internal and External Flows: Fundamentals of Numerical Discretization*, volume 1. John Wiley & Sons, Chichester, UK, 1988.

[95] L. Davidson. Hybrid LES-RANS: back scatter from a scale-similarity model used as forcing. *Phil. Trans. of the Royal Society A*, 367(1899):2905–2915, 2009.

[96] P. Emvin. *The Full Multigrid Method Applied to Turbulent Flow in Ventilated Enclosures Using Structured and Unstructured Grids*. PhD thesis, Dept. of Thermo and Fluid Dynamics, Chalmers University of Technology, Göteborg, 1997.

[97] L. Davidson and S.-H. Peng. Hybrid LES-RANS: A one-equation SGS model combined with a $k - \omega$ model for predicting recirculating flows. *International Journal for Numerical Methods in Fluids*, 43:1003–1018, 2003.

[98] S. V. Patankar. *Numerical Heat Transfer and Fluid Flow*. McGraw-Hill, New York, 1980.

[99] H. K. Versteegh and W. Malalasekera. *An Introduction to Computational Fluid Dynamics - The Finite Volume Method*. Longman Scientific & Technical, Harlow, England, 1995.

[100] L. Davidson and M. Billson. Hybrid LES/RANS using synthesized turbulent fluctuations for forcing in the interface region. *International Journal of Heat and Fluid Flow*, 27(6):1028–1042, 2006.

[101] L. Davidson. Large eddy simulation: A dynamic one-equation subgrid model for three-dimensional recirculating flow. In *11th Int. Symp. on Turbulent Shear Flow*, volume 3, pages 26.1–26.6, Grenoble, 1997.

[102] L. Davidson. Large eddy simulations: A note on derivation of the equations for the subgrid turbulent kinetic energies. Technical Report 97/11, Dept. of Thermo and Fluid Dynamics, Chalmers University of Technology, Gothenburg, 1997.

[103] A. Sohankar, L. Davidson, and C. Norberg. Large eddy simulation of flow past a square cylinder: Comparison of different subgrid scale models. *Journal of Fluids Engineering*, 122(1):39–47, 2000.

[104] A. Sohankar, L. Davidson, and C. Norberg. Erratum. *Journal of Fluids Engineering*, 122(3):643, 2000.

[105] S. Krajnović and L. Davidson. A mixed one-equation subgrid model for large-eddy simulation. *International Journal of Heat and Fluid Flow*, 23(4):413–425, 2002.

[106] S. Krajnović and L. Davidson. Large eddy simulation of the flow around a bluff body. *AIAA Journal*, 40(5):927–936, 2002.

[107] S. Krajnović. *Large Eddy Simulations for Computing the Flow Around Vehicles*. PhD thesis, Dept. of Thermo and Fluid Dynamics, Chalmers University of Technology, Göteborg, Sweden, 2002.

[108] J. Pallares and L. Davidson. Large-eddy simulations of turbulent flow in a rotating square duct. *Physics of Fluids*, 12(11):2878–2894, 2000.

[109] J. Pallares and L. Davidson. Large-eddy simulations of turbulent heat transfer in stationary and rotating square duct. *Physics of Fluids*, 14(8):2804–2816, 2002.

[110] S. Krajnović and L. Davidson. Numerical study of the flow around the bus-shaped body. *Journal of Fluids Engineering*, 125:500–509, 2003.

[111] S. Krajnović and L. Davidson. Flow around a simplified car. part I: Large eddy simulations. *Journal of Fluids Engineering*, 127(5):907–918, 2005.

[112] S. Krajnović and L. Davidson. Flow around a simplified car. part II: Understanding the flow. *Journal of Fluids Engineering*, 127(5):919–928, 2005.

[113] S. Krajnović and L. Davidson. Influence of floor motions in wind tunnels on the aerodynamics of road vehicles. *Journal of Wind Engineering and Industrial Aerodynamics*, 92(5):677–696, 2005.

[114] S. Dahlström and L. Davidson. Large eddy simulation applied to a high-Reynolds flow around an airfoil close to stall. AIAA paper 2003-0776, 2003.

[115] S. Dahlström. *Large Eddy Simulation of the Flow Around a High-Lift Airfoil*. PhD thesis, Dept. of Thermo and Fluid Dynamics, Chalmers University of Technology, Göteborg, Sweden, 2003.

[116] J. Ask and L. Davidson. Flow and dipole source evaluation of a generic SUV. *Journal of Fluids Engineering*, 132(051111), 2010.

[117] H. Hemida and S. Krajnović. LES study of the impact of the wake structures on the aerodynamics of a simplified ICE2 train subjected to a side wind. In *Fourth International Conference on Computational Fluid Dynamics (ICCFD4)*, 10-14 July, Ghent, Belgium, 2006.

[118] H. Hemida and S. Krajnović. Numerical study of the unsteady flow structures around train-shaped body subjected to side winds. In *ECCOMAS CFD 2006*, 5-8 September, Egmond aan Zee, The Netherlands, 2006.

[119] S. Krajnović. Numerical simulation of the flow around an ICE2 train under the influence of a wind gust. In *International Conference on Railway Engineering 2008 (IET ICRE2008)*, 25-28 March, Hong Kong, China, 2008.

[120] S.-H. Peng and L. Davidson. On a subgrid-scale heat flux model for large eddy simulation of turbulent thermal flow. *International Journal of Heat and Mass Transfer*, 45:1393–1405, 2002.

[121] S.-H. Peng and L. Davidson. Large eddy simulation for turbulent buoyant flow in a confined cavity. *International Journal of Heat and Fluid Flow*, 22:323–331, 2001.

[122] S.-H. Peng. *Modeling of Turbulent flow and Heat Transfer for Building Ventilation*. PhD thesis, Dept. of Thermo and Fluid Dynamics, Chalmers University of Technology, Göteborg, 1998.

[123] D. G. Barhaghi and L. Davidson. Natural convection boundary layer in a 5:1 cavity. *Physics of Fluids*, 19(125106), 2007.

[124] D. Barhaghi. *A Study of Turbulent Natural Convection Boundary Layers Using Large-Eddy Simulation*. PhD thesis, Div. of Fluid Dynamics, Dept. of Applied Mechanics, Chalmers University of Technology, Göteborg, Sweden, 2007.

[125] D. G. Barhaghi, L. Davidson, and R. Karlsson. Large-eddy simulation of natural convection boundary layer on a vertical cylinder. *International Journal of Heat and Fluid Flow*, 27(5):811–820, 2006.

[126] D. G. Barhaghi and L. Davidson. Les of mixed convection boundary layer between radiating parallel plates. In *5th International Symposium on Turbulence, Heat and Mass Transfer*, September 25-29, 2006, Dubrovnik, Croatia, 2006.

[127] S. R. Robinson. Coherent motions in the turbulent boundary layer. *Annual Review of Fluid Mechanics*, 23:601–639, 1991.

[128] L. Davidson. Large eddy simulations: how to evaluate resolution. *International Journal of Heat and Fluid Flow*, 30(5):1016–1025, 2009.

[129] L. Davidson. How to estimate the resolution of an LES of recirculating flow. In M. V. Salvetti, B. Geurts, J. Meyers, and P. Sagaut, editors, *ERCOFTAC*, volume 16 of *Quality and Reliability of Large-Eddy Simulations II*, pages 269–286. Springer, 2010.

[130] L. Davidson. Inlet boundary conditions for embedded LES. In *First CEAS European Air and Space Conference*, 10-13 September, Berlin, 2007.

[131] L. Davidson, D. Cokljat, J. Fröhlich, M. A. Leschziner, C. Mellen, and W. Rodi, editors. *LESFOIL: Large Eddy Simulation of Flow Around a High Lift Airfoil*, volume 83 of *Notes on Numerical Fluid Mechanics*. Springer Verlag, 2003.

[132] C. P. Mellen, J. Fröhlich, and W. Rodi. Lessons from LESFOIL project on large eddy simulation of flow around an airfoil. *AIAA Journal*, 41(4):573–581, 2003.

[133] S. Johansson, L. Davidson, and E. Olsson. Numerical simulation of vortex shedding past triangular cylinders at high reynolds numbers using a $k - \varepsilon$ turbulence model. *International Journal for Numerical Methods in Fluids*, 16:859–878, 1993.

[134] S. Perzon and L. Davidson. On CFD and transient flow in vehicle aerodynamics. In *SAE Technical Paper 2000-01-0873, Detroit*, 2000.

[135] S. Perzon and L. Davidson. On transient modeling of the flow around vehicles using the Reynolds equation. In J.-H. Wu, Z.-J. Zhu, F.-P. Jia, X.-B. Wen, and W. Hu, editors, *ACFD 2000*, Bejing, 2000.

[136] T. H. Shih, J. Zhu, and J. L. Lumley. A realizable Reynolds stress algebraic equation model. Technical memo 105993, NASA, 1993.

[137] P. Spalart and S. Allmaras. A one equation turbulence model for aerodynamic flows. AIAA paper 92-0439, Reno, NV, 1992.

[138] P. R. Spalart, W.-H. Jou, M. Strelets, and S. R. Allmaras. Comments on the feasability of LES for wings and on a hybrid RANS/LES approach. In C. Liu and Z. Liu, editors, *Advances in LES/DNS, First Int. conf. on DNS/LES*, Louisiana Tech University, 1997. Greyden Press.

[139] F. R. Menter, M. Kuntz, and R. Bender. A scale-adaptive simulation model for turbulent flow prediction. AIAA paper 2003–0767, Reno, NV, 2003.

[140] A. K. Travin, M. Shur, , M. Strelets, and P. R. Spalart. Physical and numerical upgrades in the detached-eddy simulations of complex turbulent flows. In R. Friederich and W.Rodi, editors, *Fluid Mechanics and its Applications. Advances in LES of Complex Flows*, volume 65 of *Euromech Colloquium 412*.

Fluid Mechanics and its Applications. Advances in LES of Complex Flows, pages 239–254. Academic Publishers, Dordrecht, 2002.

[141] C. De Langhe, B. Merci, K. Lodefier, and E. Dick. Hybrid RANS-LES modelling with the renormalization group. In K. Hanjalić, Y. Nagano, and M. J. Tummers, editors, *Turbulence Heat and Mass Transfer 4*, pages 697–704, New York, Wallingford (UK), 2003. begell house, inc.

[142] J. C. Kok, H. S. Dol, B. Oskam, and H. van der Ven. Extra-large eddy simulation of massively separated flows. AIAA paper 2004-264, Reno, NV, 2004.

[143] J. Yan, C. Mocket, and F. Thiele. Investigation of alternative length scale substitutions in detached-eddy simulation. *Flow, Turbulence and Combustion*, 74:85–102, 2005.

[144] S. S. Girimaji. Partially-averaged Navier-Stokes model for turbulence: A Reynolds-averaged Navier-Stokes to direct numerical simulation bridging method. *ASME Journal of Applied Mechanics*, 73(2):413–421, 2006.

[145] J. Ma, S.-H. Peng, L. Davidson, and F. Wang. A low Reynolds number variant of Partially-Averaged Navier-Stokes model for turbulence. *International Journal of Heat and Fluid Flow*, 32(3):652–669, 2011. 10.1016/j.ijheatfluidflow.2011.02.001.

[146] R. Schiestel and A. Dejoan. Towards a new partially integrated transport model for coarse grid and unsteady turbulent flow simulations. *Theoretical and Computational Fluid Dynamics*, 18(6):443–468, 2005.

[147] L. Davidson. Zonal PANS: evaluation of different treatments of the RANS-LES interface. *Journal of Turbulence*, 17(3):274–307, 2016.

[148] P. Batten, U. Goldberg, and S. Chakravarthy. Interfacing statistical turbulence closures with large-eddy simulation. *AIAA Journal*, 42(3):485–492, 2004.

[149] U. Piomelli, E. Balaras, H. Pasinato, K. D. Squire, and P. R. Spalart. The inner-outer layer interface in large-eddy simulations with wall-layer models. *International Journal of Heat and Fluid Flow*, 24:538–550, 2003.

[150] L. Davidson and S. Dahlström. Hybrid LES-RANS: An approach to make LES applicable at high Reynolds number. *International Journal of Computational Fluid Dynamics*, 19(6):415–427, 2005.

[151] J. Larsson, F. S. Lien, and E. Yee. The artificial buffer layer and the effects of forcing in hybrid LES/RANS. *International Journal of Heat and Fluid Flow*, 28(6):1443–1459, 2007.

[152] F. R. Menter and M. Kuntz. Adaption of eddy-viscosity turbulence models to unsteady separated flows behind vehicles. In Rose McCallen, Fred Browand, and James Ross, editors, *The Aerodynamics of Heavy Vehicles: Trucks, Buses, and Trains*, volume 19 of *Lecture Notes in Applied and Computational Mechanics*. Springer Verlag, 2004.

[153] M. Strelets. Detached eddy simulation of massively separated flows. AIAA paper 2001–0879, Reno, NV, 2001.

[154] P. R. Spalart. Strategies for turbulence modelling and simulations. *International Journal of Heat and Fluid Flow*, 21:252–263, 2000.

[155] N. V. Nikitin, F. Nicoud, B. Wasistho, K. D. Squires, and P. Spalart. An approach to wall modeling in large-eddy simulations. *Physics of Fluids*, 12(7):1629–1632, 2000.

[156] F. R. Menter and Y. Egorov. Revisiting the turbulent length scale equation. In *IUTAM Symposium: One Hundred Years of Boundary Layer Research*, Göttingen, 2004.

[157] F. R. Menter, M. Kuntz, and R. Bender. A scale-adaptive simulation model for turbulent flow predictions. AIAA-2003-0767, Reno, 2003.

[158] J. C. Rotta. *Turbulente Strömungen*. Teubner Verlag, Stuttgart, 1972.

[159] F. R. Menter and Y. Egorov. A scale-adaptive simulation model using two-equation models. AIAA paper 2005–1095, Reno, NV, 2005.

[160] L. Davidson. Evaluation of the SST-SAS model: Channel flow, asymmetric diffuser and axi-symmetric hill. In *ECCOMAS CFD 2006*, September 5-8, 2006, Egmond aan Zee, The Netherlands, 2006.

[161] S. S. Girimaji. Partially-averaged Navier-Stokes model for turbulence: A Reynolds-averaged Navier-Stokes to direct numerical simulation bridging method. *ASME Journal of Applied Mechanics*, 73(2):413–421, 2006.

[162] S. S. Girimaji and K. S. Abdul-Hamid. Partially-Averaged Navier-Stokes model for turbulence: Implementation and Validation. AIAA paper 2005-0502, Reno, N.V., 2005.

[163] M. L. Shur, P. R. Spalart, M. Kh. Strelets, and A. K. Travin. A hybrid RANS-LES approach with delayed-DES and wall-modelled LES capabilities. *International Journal of Heat and Fluid Flow*, 29:1638–1649, 2008.

[164] J. Ma, S.-H. Peng, L. Davidson, and F. Wang. A low Reynolds number partially-averaged Navier-Stokes model for turbulence. In *8th International ERCOFTAC Symposium on Engineering Turbulence, Modelling and Measurements*, Marseille, France, 9-11 June, 2010.

[165] L. Davidson. The PANS $k-\varepsilon$ model in a zonal hybrid RANS-LES formulation. *International Journal of Heat and Fluid Flow*, 46:112–126, 2014.

[166] S. S. Girimaji and S. Wallin. Closure modeling in bridging regions of variable-resolution (VR) turbulence computations. *Journal of Turbulence*, 14(1):72 – 98, 2013.

[167] S. Kenjeres and K. Hanjalic. LES, T-RANS and hybrid simulations of thermal convection at high ra numbers. *International Journal of Heat and Fluid Flow*, 27:800–810, 2006.

[168] H. Foroutan and S. Yavuzkurt. A partially-averaged Navier-Stokes model for the simulation of turbulent swirling flow with vortex breakdown. *International Journal of Heat and Fluid Flow*, 50:402–416, 2014.

[169] L. Davidson and C. Friess. A new formulation of f_k for the PANS model. *Journal of Turbulence*, pages 1–15, 2019.

[170] Ch. Friess, R. Manceau, and T.B. Gatski. Toward an equivalence criterion for hybrid RANS/LES methods. *International Journal of Heat and Fluid Flow*, 122:233–246, 2015.

[171] B. Chaouat and R. Schiestel. A new partially integrated transport model for subgrid-scale stresses and dissipation rate for turbulent developing flows. *Physics of Fluids*, 17(065106), 2005.

[172] L. Davidson. Using isotropic synthetic fluctuations as inlet boundary conditions for unsteady simulations. *Advances and Applications in Fluid Mechanics*, 1(1):1–35, 2007.

[173] L. Davidson and S.-H. Peng. Embedded large-eddy simulation using the partially averaged Navier-Stokes model. *AIAA Journal*, 51(5):1066–1079, 2013.

[174] A. Travin, M. Shur, M., Strelets, and P. Spalart. Detached-eddy simulations past a circular cylinder. *Flow, Turbulence and Combustion*, 63:293–313, 2000.

[175] F. Hamba. Analysis of filtered Navier-Stokes equation for hybrid RANS/LES simulation. *Physics of Fluids A*, 23(015108), 2011.

[176] S. Arvidson, L. Davidson, and S.-H. Peng. Hybrid RANS-LES modeling based on a low-Reynolds-number $k - \omega$ model. *AIAA Journal*, 54(12):4032–4037, 2016.

[177] S. Arvidson, L. Davidson, and S.-H. Peng. Interface methods for grey-area mitigation in turbulence-resolving hybrid RANS-LES. *International Journal of Heat and Fluid Flow*, 73:236–257, 2018.

[178] L. Davidson. Two-equation hybrid RANS-LES models: A novel way to treat k and ω at inlets and at embedded interfaces. *Journal of Turbulence*, 18(4):291–315, 2017.

[179] S. Arvidson. *Methodologies for RANS-LES interfaces in turbulence-resolving simulations*. PhD thesis, Div. of Fluid Dynamics, Dept. of Mechanics and Maritime Sciences, Chalmers University of Technology, Göteborg, Sweden, 2017.

[180] L. Davidson. Hybrid LES-RANS: Inlet boundary conditions for flows including recirculation. In *5th International Symposium on Turbulence and Shear Flow Phenomena*, volume 2, pages 689–694, 27-29 August, Munich, Germany, 2007.

[181] N. Jarrin, S. Benhamadouche, D. Laurence, and R. Prosser. A synthetic-eddy-method for generating inflow conditions for large-eddy simulations. *International Journal of Heat and Fluid Flow*, 27(4):585–593, 2006.

[182] M. Billson. *Computational Techniques for Turbulence Generated Noise*. PhD thesis, Dept. of Thermo and Fluid Dynamics, Chalmers University of Technology, Göteborg, Sweden, 2004.

[183] M. Billson, L.-E. Eriksson, and L. Davidson. Jet noise prediction using stochastic turbulence modeling. AIAA paper 2003-3282, 9th AIAA/CEAS Aeroacoustics Conference, 2003.

[184] L. Davidson. Hybrid LES-RANS: Inlet boundary conditions. In B. Skallerud and H. I. Andersson, editors, *3rd National Conference on Computational Mechanics – MekIT'05 (invited paper)*, pages 7–22, Trondheim, Norway, 2005.

[185] L. Davidson. Hybrid LES-RANS: Inlet boundary conditions for flows with recirculation. In *Second Symposium on Hybrid RANS-LES Methods*, Corfu island, Greece, 2007.

[186] J. R. Welty, C. E. Wicks, and R. E. Wilson. *Fundamentals of Momentum, Heat, and Mass Transfer*. John Wiley & Sons, New York, 3 edition, 1984.

[187] L. Davidson. HYBRID LES-RANS: Inlet boundary conditions for flows with recirculation. In *Advances in Hybrid RANS-LES Modelling*, volume 97 of *Notes on Numerical Fluid Mechanics and Multidisciplinary Design*, pages 55–66. Springer Verlag, 2008.

[188] M. Billson, L.-E. Eriksson, and L. Davidson. Modeling of synthetic anisotropic turbulence and its sound emission. The 10th AIAA/CEAS Aeroacoustics Conference, AIAA 2004-2857, Manchester, United Kindom, 2004.

[189] R. D. Moser, J. D. Kim, and N. N. Mansour. Direct numerical simulation of turbulent channel flow up to $Re_\tau = 590$. *Physics of Fluids*, 11(4):943–945, 1999.

[190] L. Davidson. Python and Matlab scripts for synthetic fluctuations.

[191] Lars Davidson and Shia-Hui Peng. Hybrid LES-RANS: A one-equation SGS model combined with a $k - \omega$ for predicting recirculating flows. *International Journal for Numerical Methods in Fluids*, 43(9):1003–1018, 2003.

[192] F. R. Menter and Y. Egorov. The scale adaptive simulation method for unsteady turbulent flow predictions. Part 1: Theory and description. *Flow, Turbulence and Combustion*, 85:113–138, 2010.

[193] Y. Egorov, F. R. Menter, R. Lechner, and D. Cokljat. The scale adaptive simulation method for unsteady flow predictions. Part 2: Application to complex flows. *Flow, Turbulence and Combustion*, 85:139–165, 2010.

[194] J. Fröhlich and D. von Terzi. Hybrid LES/RANS methods for the simulation of turbulent flows. *Progress in Aerospace*, 44(5):349–377, 2008.

[195] A. Travin, M. Shur, M. Strelets, and P. Spalart. Detached-eddy simulations past a circular cylinder. *Flow Turbulence and Combustion*, 63(1/4):293–313, 2000.

[196] L. Davidson and B. Farhanieh. CALC-BFC: A finite-volume code employing collocated variable arrangement and cartesian velocity components for computation of fluid flow and heat transfer in complex three-dimensional geometries. Rept. 95/11, Dept. of Thermo and Fluid Dynamics, Chalmers University of Technology, Gothenburg, 1995.

[197] B. P. Leonard. A stable and accurate convective modelling based on quadratic upstream interpolation. *Computational Methods in Applied Mechanical Engineering*, 19:59–98, 1979.

[198] M. Breuer, N. Peller, Ch. Rapp, and M. Manhart. Flow over periodic hills – numerical and experimental study in a wide range of Reynolds numbers. *Computers & Fluids*, 38:433–457, 2009.

[199] F. Eriksson. *Flerdimensionell analys (in Swedish)*. Studentlitteratur, Lund, Sweden, 4 edition, 1977.

[200] S.B. Pope. Ten questions concerning the large-eddy simulations of turbulent flows. *New Journal of Physics*, 6(35):1–24, 2004.

[201] R. L. Panton. *Incompressible Flow*. John Wiley & Sons, New York, 1984.

[202] M. Mirzaei, L. Davidson, A. Sohankar, and F. Innings. The effect of corrugation on heat transfer and pressure drop in channel flow with different Prandtl numbers. *International Journal of Heat and Mass Transfer*, 66:164–176, 2013.

[203] B. J. Daly and F. H. Harlow. Transport equation in turbulence. *Physics of Fluids*, 13:2634–2649, 1970.

[204] S. M. El-Behery and M. H. Hamed. A comparative study of turbulence models performance for separating flow in planar asymmetric diffuser. *Computers & Fluids*, 44(1):248–257, 2011.

[205] C .U. Buice and J. K. Eaton. Experimental investigation of flow through an asymmetric plane diffuser. *Journal of Fluids Engineering*, 122:433–435, 2000.

[206] L. Davidson. Large eddy simulation of heat transfer in boundary layer and backstep flow using PANS (corrected version can be downloaded at `http://www.tfd.chalmers.se/~lada/`). In *Turbulence, Heat and Mass Transfer, THMT-12*, Palermo, Sicily/Italy, 2012.

[207] L. Davidson and S.-H. Peng. Embedded LES with PANS. In *6th AIAA Theoretical Fluid Mechanics Conference, AIAA paper 2011-3108*, 27-30 June, Honolulu, Hawaii, 2011.

[208] F. Nicoud and F. Ducros. Subgrid-scale stress modelling based on the square of the velocity gradient tensor. *Flow, Turbulence and Combustion*, 62(3):183–200, 1999.

[209] L. Davidson. Zonal detached eddy simulation coupled with steady RANS in the wall region. In *ECCOMAS MSF 2019 Thematic Confernence, Minisyposium "Current trends in simulation and modelling of turbulent flows. MS devoted to 80th birthday of Prof. Kemo Hanjalic"*, Sarajevo, Bosnia and Herzegovina, 2019.

[210] L. Davidson. Non-zonal detached eddy simulation coupled with a steady RANS solver in the wall region. ERCOFTAC Bullentin 89, Special Issue on *Current trends in RANS-based scale-resolving simulation methods*, 2019.

[211] A. Mehdizadeh and A. Sadiki. A zonal hybrid turbulence model based on Rotta integral length scale transport equation. In *Turbulence, Heat and Mass Transfer, THMT-12*, Palermo, Sicily/Italy, 2012.

[212] Siavash Toosi and Johan Larsson. Anisotropic grid-adaptation in large eddy simulations. *Computers & Fluids*, 156:146–161, 2017.

[213] J. Larsson. private communication. Department of Mechanical Engineering, University of Maryland, 2019.

[214] D. Greenblatt, K. B. Paschal, C.-S. Yao, J. Harris, N. W. Schaeffler, and A. E. Washburn. A separation control CFD validation test case. Part 1: Baseline & steady suction. AIAA-2004-2220, 2004.

[215] D. Greenblatt, K. B. Paschal, C.-S. Yao, and J. Harris. A separation control CFD validation test case Part 1: Zero efflux oscillatory blowing. AIAA-2005-0485, 2005.

[216] B. van Leer. Towards the ultimate conservative difference scheme. Monotonicity and conservation combined in a second order scheme. *Journal of Computational Physics*, 14(4):361–370, 1974.

[217] S. Dahlström and L. Davidson. Large eddy simulation of the flow around an Aerospatiale A-aerofoil. In *ECCOMAS 2000, European Congress on Computational Methods in Applied Sciences and Engineering, 11-14 September*, Barcelona, Spain, 2000.

[218] L. Davidson and C. Friess. The PANS and PITM model: a new formulation of f_k. In *Proceedings of 12th International ERCOFTAC Symposium on Engineering Turbulence Modelling and Measurements (ETMM12), Montpelier, France 26-28 September*, 2018.

[219] B. Basara, S. Krajnović, S. Girimaji, and Z. Pavlović. Near-wall formulation of the Partially Averaged Navier Stokes turbulence model. *AIAA Journal*, 49(12):2627–2636, 2011.

[220] L. Davidson. A new approach of zonal hybrid RANS-LES based on a two-equation $k - \varepsilon$ model. In *ETMM9: 9th International ERCOFTAC Symposium on Turbulence Modelling and Measurements*, Thessaloniki, Greece, 2012.

[221] S-H Peng, L. Davidson, and S. Holmberg. A modified low-Reynolds-number $k - \omega$ model for recirculating flows. *Journal of Fluids Engineering*, 119:867–875, 1997.

[222] A. Zarmehri. Aerodynamic analysis of wind turbine. MSc Thesis 2012:58, Division of Fluid Dynamics, Department of Applied Mechanics, Chalmers University of Technology, Göteborg, Sweden, 2012.

[223] O. Brander. *Vektoranalys (in Swedish)*. Studentlitteratur, Lund, Sweden, 2007.